TRANSPORT AND CHEMICAL RATE PHENOMENA

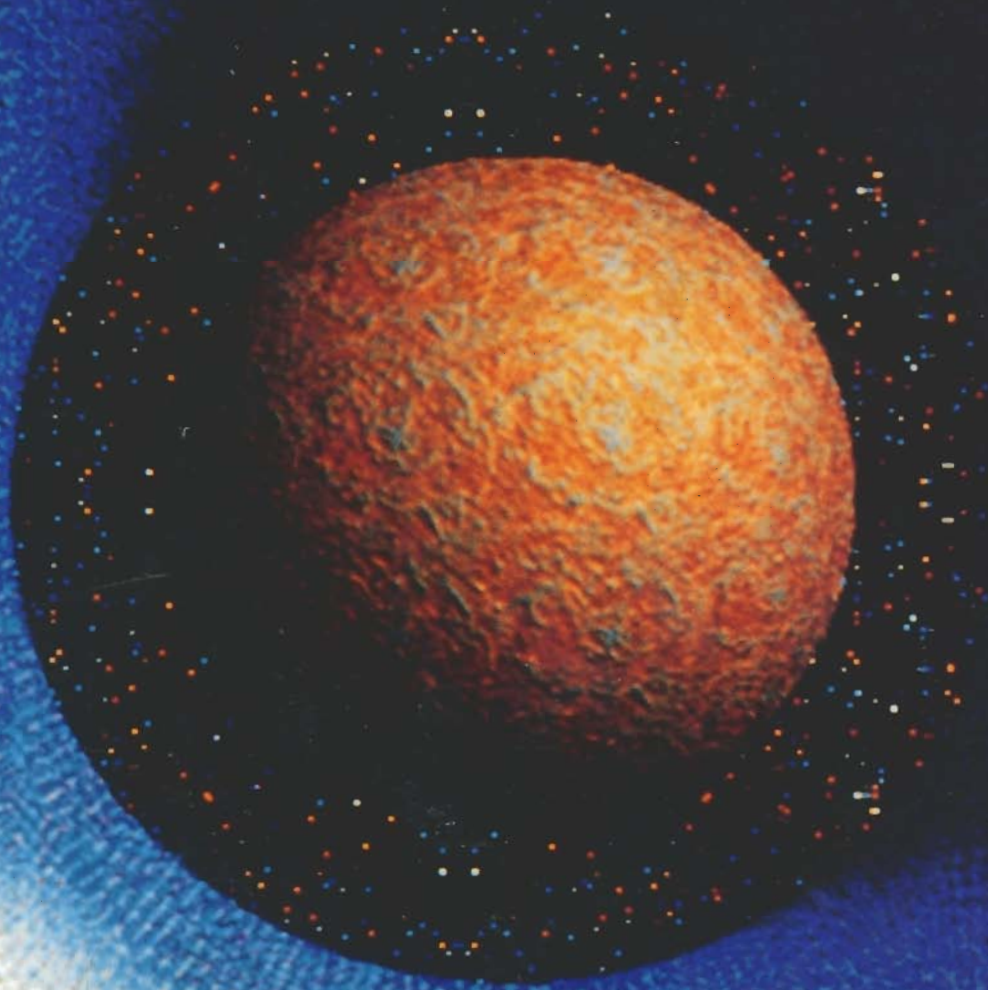

NICKOLAS J. THEMELIS

GORDON AND BREACH
PUBLISHERS

Transport and Chemical Rate Phenomena

Transport and Chemical Rate Phenomena

Nickolas J. Themelis

Department of Chemical Engineering, Materials Science and Mining Engineering
Columbia University in the City of New York

CONTENTS

PREFACE

In the early seventies, Professor Julian Szekely of M.I.T. and I published a pioneer textbook on the application of transport phenomena in the processing of minerals and metals. The title of that book was *Rate Phenomena in Process Metallurgy* (Wiley, 1971), and the first edition went out of print by 1980. Meanwhile, I spent another ten years in industrial research at Noranda Inc. and later as vice president of technology at Kennecott Corporation before joining the Henry Krumb School of Mines of Columbia University in 1980. At Columbia, I teach rate phenomena and process design to students in chemical engineering, materials science, and mining engineering. Also, during the last decade, I have presented short, intensive courses on the same subjects to graduate students and practicing engineers at several universities.

On the basis of this combination of industrial research and teaching experience, I concluded that there is a need for a textbook that integrates the elements of transport phenomena and chemical rate theory with numerical examples of their application in the chemical processing of minerals and other primary materials. The word "minerals" is used because most of the materials we use originate in the mineral wealth of our planet. The oldest materials used by mankind were stones and metals, and the same materials in improved forms are the bones, muscles, and skin of our present-day civilization.

Each of the transport phenomena, for example fluid flow or heat conduction, is complex enough to warrant one or more textbooks of its own; however, there is a common thread that runs through transport phenomena and heterogeneous reactions and deserves to be followed up in a single course. Differential and overall material and energy balances, dimensions, units, physical properties, engineering concepts, and correlations can be one thousand pieces of a puzzle or an admirable picture of the simplicity of the laws of nature. I have tried to follow that common thread and to write a book that is, to borrow a term of the computer age, "user-friendly" to teachers and students alike.

This book is designed as a basic course in rate phenomena for all engineering or applied science students interested in the chemical processing of materials. Additional courses in transport theory or in chemical kinetics may then be taken in specialized fields, such as advanced transport theory for chemical engineers and solid-state diffusion for materials scientists.

In my travels and lectures outside the U.S., it has become obvious that professors and students of engineering around the world refer frequently to English-language textbooks. Indeed, the earlier book on rate phenomena with Professor Szekely has made friends and opened doors for us throughout the world. In recognition of this special role, I have tried to simplify the language and standardize the nomenclature and units used in this textbook.

In the eighties, the exorbitant claim was made in the press that "mining is dead" and other heavy industries, such as steelmaking, were practically written off. Subsequent events have shown that such notices were premature. Humanity cannot progress or even maintain present standards without the intelligent utilization of mineral resources and recycled materials. In recent years, "advanced materials" have become the focus of government research funding; yet, if one looks at the "bottom line" of materials-producing companies around the globe, it is

clear that the bulk of the revenues and profits are still derived from primary materials. In the foreseeable future, chemical, metallurgical, mineral, and mining engineers, as well as materials scientists, will be needed in order to cope with dwindling natural resources, environmental concerns, and the aspirations of underdeveloped nations for a better standard of living.

It is said that imitation is the sincerest form of flattery. In our 1971 textbook we adapted much from chemical engineering literature and from technical papers of numerous authors. Later on, we were flattered to see parts of our book in other textbooks on process metallurgy. In this book, I have also adapted suitable material from books by Geiger and Poirier (*Transport Phenomena in Metallurgy*, 1973); Szekely (*Fluid Flow in Metals Processing*, 1979); Cheremisinoff and Gupta (*Handbook of Fluids in Motion*, 1983); Rohsenow et al. (*Handbook of Heat Transfer*, 1985); Rosner (*Transport Processes in Chemically Reacting Flow Systems*, 1986); Guthrie (*Engineering in Process Metallurgy*, 1987); Evans and De Jonghe (*Production of Inorganic Materials*, 1991); and others mentioned in the references.

I am greatly indebted to Professor Szekely for the parts of *Rate Phenomena in Process Metallurgy* that have been adapted in this book and regret that circumstances did not allow us to collaborate again. The contributions of Professor Szekely and his former students to the understanding of transport phenomena in materials processing are towering.

I thank Professor James W. Evans of the University of California (Berkeley) for critically reviewing an early draft of this book and making many invaluable suggestions for improving the material. Professor Paul Duby of Columbia University kindly reviewed the electrochemical examples. My doctoral students at Columbia have assisted along the way; in particular, the outstanding work of Baozhong Zhao on the illustrations and the review of numbers in the final manuscript by Roger Westcott are most gratefully acknowledged.

Financial support over the years of my research at Columbia by the Mining and Mineral Resources Research Institutes program of the U.S. Bureau of Mines, National Science Foundation, Environmental Protection Agency, Noranda Technology, Outokumpu Research, Boliden Metall, and others was essential. In particular, I would like to express my gratitude to Peter Tarassoff, Phillip Mackey, John Peacey, Dan Poggi, Keith Brimacomb, Jyrki Juusela, Juho Makinen, Jussi Asteljoki, Theo Lehner, Ivan Gorup, and Milton Ward for their support of my academic endeavors over the years.

Two professors who shaped my academic career are Bill Gauvin, the unforgettable chemical engineering teacher at McGill University, and Herbert Kellogg, who opened the way to Columbia University.

This book was completed in large part while I was visiting professor at the Institute for Advanced Materials Processing (Sozaiken) of Tohoku University in Sendai, Japan. Thanks are due to my hosts, Professors Tokuda and Waseda, for their wonderful hospitality, and to Professors Itagaki, Omori, and Yazawa for introducing me to Japanese culture.

Lastly, I want to thank Liliana Nikolich Themelis for her contribution in the word processing of this book and my entire family for their moral support and encouragement over the years.

ONE

Introduction

Chemicals, metals and other materials are produced by means of a series of unit operations each of which involves a number of simultaneous, or sequential, phenomena: the transfer of momentum or kinetic energy, the transfer of heat and mass, and chemical reactions between different phases. In general, such processes involve a number of physical and chemical transformations. The rate of these transformations determines, by and large, the cost of production of such materials.

For example, in the production of chemicals and metals by the leaching of mineral particles, a solution is pumped to a reactor where a slurry of the particles is maintained in a state of agitation by air injection or other means. Fluid flow phenomena determine the energy required to pump the solution in and out of the tank and to maintain the particles in suspension. The tank is controlled at the proper operating temperature by means of heat transfer. The rate of leaching depends on the rates of mass transfer between the solution and the particles, diffusion through each particle and chemical reaction at the interface of the unreacted core. After the leaching solution leaves the tank, various other unit operations, such as solvent extraction, precipitation, settling, filtration, and electrowinning may be required to produce a final marketable material.

As another example, in the production of steel by injecting an oxygen jet through a bath of high-carbon iron, the momentum of the rising gas bubbles is transferred to the liquid and mixes the bath; the gas bubbles are heated by heat transfer from the metal; there is mass transfer of carbon from the melt to the gas bubbles, through the gas/liquid interface, and chemical reaction between carbon atoms and oxygen molecules.

The effectiveness and cost of an industrial unit operation are very much related to the rate at which such phenomena take place within it. Phenomena which are beneficial to the process should be speeded up as much as possible while others, of an adverse effect, need to be slowed down. For instance, in the production of cement, an *increase* in the heat transfer rate between the rolling bed of limestone and the combustion gases above it will increase the productivity of a rotary kiln. On the other hand, a *decrease* in heat transfer by conduction through the kiln wall, by means of improved insulation, will reduce heat loss and also be beneficial.

1.1. CLASSES OF RATE PHENOMENA

The rate phenomena involved in materials processing can be divided into two broad classes:

- Transport phenomena involve the transfer of momentum (kinetic energy), heat (thermal energy), and mass;

- Chemical or physicochemical phenomena (e.g., combustion, absorption, desorption, electrodeposition) involve transformation of a species and interaction between various chemical species and phases.

1.2. "MICRO-SCALE" AND "MACRO-SCALE" STUDY OF RATE PHENOMENA

Momentum transport theory allows us to define the "fine structure of flow," that is to determine the velocity distribution in a fluid, especially in the vicinity of a solid surface. For instance, if we want to understand the rate of heat or mass transfer between a reacting iron oxide particle and the hydrogen gas around it, we must attempt to quantify the effect of flow conditions on the thickness of the gaseous "boundary layer" around the particle and the rate of diffusion of hydrogen through this gas film. One of the strong motivating forces behind the study of transport phenomena is the need to understand better the nature of these boundary layers and use this knowledge to control the processing conditions for a particular product.

An understanding of fluid flow phenomena (i.e., the transport of momentum) is also needed to establish the energy, or power, requirements to move a fluid at a specified flow rate. For example, one may have to calculate the size of the pump and of the pipe diameter required to move a given flow rate of a liquid from one point to another; or it may be necessary to calculate the mixing energy to be provided in a leaching tank in order to keep the particles in suspension and provide a certain rate of interaction between them and the enveloping liquid.

Therefore, we need to study the momentum transport phenomena both in "micro-scale," where we focus on what is happening to an infinitely small fluid element; and in "macro-scale," where we treat a large section of the vessel under investigation, or even the entire vessel, as a "black box" and we examine the inputs and outputs from the box, by means of overall energy and material balances.

1.3. COUPLING OF RATE PHENOMENA

The flow of a fluid through a heat exchanger can be controlled by the size of the pump used to move the fluid and is independent of the rate of heat transfer through the pipe wall. However, the flow of air rising from a room heater is very much dependent on the rate of heat transfer from the heater to the surrounding air. In the latter case, momentum and heat transfer are said to be *coupled.*

Also, the surface area of a solid particle does not depend on the forces acting on it; while the size and shape of gas bubbles injected in a liquid will depend on pressure and temperature and other factors. Therefore, in order to determine the heat or mass transfer between a gas and a liquid, it is necessary to first estimate the interface area by considering the forces acting on the system. The coupling of transport phenomena in such a case is evident.

1.4. TOOLS USED IN STUDY OF TRANSPORT PHENOMENA

The main tools used in the study of transport phenomena are:

a. The phenomenological (i.e., experimentally derived) relationships expressing the proportionality between:

- momentum flux and velocity gradient (*Newton's law of viscosity*),

Table 1.1. Analogies in Transport Phenomena

	Transport of		
	Momentum	Heat	Mass
Flux	$\tau_{y,x}$	q_y	$N_{A,y}$
Driving force	$\partial u_x/\partial y$ Velocity gradient	$\partial T/\partial y$ Temperature gradient	$\partial c_A/\partial y$ Concentration gradient
Transport property	μ	k	D_{AB}
Analogous transport properties	$\nu = \mu/\rho$	$\alpha = k/\rho C_p$	D_{AB}
Analogous laws	$\tau_{y,x} = -\nu[\partial(\rho u_x)/\partial y]$ Newton's law of viscosity*	$q_y = -\alpha[\partial(\rho C_p T)/\partial y]$ Fourier's law of conduction*	$N_{A,y} = -D_{AB}[\partial c_A/\partial y]$ Fick's law of diffusion*

*For constant values of material properties.

- heat flux and temperature gradient (*Fourier's law of conduction*),
- mass flux and concentration gradient (*Fick's first law of diffusion*).

b. The basic mass and energy conservation equations:

- the differential mass balance (conservation of mass),
- the differential momentum balance (*Newton's law of conservation of energy*),
- the differential heat balance (conservation of thermal energy).

c. Semi-empirical correlations derived by experimentation on the actual system or from appropriate physical or mathematical model.

d. Chemical rate theory and thermodynamics.

1.5. ANALOGIES BETWEEN TRANSPORT PHENOMENA

Although there are differences between momentum, which is a vectorial quantity (magnitude and direction), and heat and mass, which are scalar (magnitude only), there are also important similarities. These similarities, or analogies, help us to understand the various transport phenomena and allow us to use analytical solutions, correlations, and computer programs developed for one type of transport in problems related to the other two. For example, the transport of momentum within a fluid depends on the fluid viscosity and velocity gradients; similarly, the transfer of heat by conduction within a material depends on its thermal conductivity and the existing temperature gradients. Table 1.1 illustrates the principal analogies between momentum, heat and mass transfer; these and other useful analogies will be discussed in detail throughout this book.

1.6. DIFFUSIVE AND CONVECTIVE COMPONENTS OF TRANSPORT

Mass and heat can be transported through fluids in two ways:

a. By diffusion/conduction through a stagnant layer of fluid; for example, hot molecules in a liquid film will transfer heat by conduction to adjacent cooler molecules. This type of mass/heat transfer is called **diffusive transport.**

b. By movement of fluid elements from one location to another; for example, air heated by contact with a room heater will rise and heat other parts of the room. This type of heat/mass transfer is called **convective transport.**

1.7. SEMI-EMPIRICAL CORRELATIONS

The theory of transport phenomena is essential in trying to understand and control the reactions involved in the processing of materials. However, the complexity of many processing systems does not allow for a purely theoretical description of the occurring phenomena.

This has necessitated the development of derivative semi-empirical concepts (i.e., based partly on experimentation) which are also described in this book. Examples of such engineering correlations are the concepts of the friction factor, which is used extensively in fluid flow calculations, and of the heat and mass transfer coefficients.

Of course, there can also be totally empirical correlations, such as are developed by so-called factorial experiments at the end of which variable Y is related to variables X, W, and Z solely on the basis of the experiments. However, the semi-empirical approach is preferable because it requires a basic understanding of the fundamentals of the system. As will be seen throughout this text, many of the problems facing process engineers in fluid flow, heat transfer, mass transfer and chemical reaction can be solved by means of semi-empirical correlations.

Some engineering problems are relatively old, such as the flow of fluids through conduits; therefore, the corresponding correlations have been honed to perfection and are available in the form of equations, plots or tables where one has only to look to find the answer to a specific question. There are other systems, for instance the flow of a gas jet injected into a liquid, where correlations are still being tested; and there are many other systems where, as of yet, there are no available correlations. It is hoped that readers of this text, by combining their knowledge of theory with experimentation and analysis, will find opportunities to develop such correlations and thus advance further the technology of materials processing.

1.8. PROCESSING OF ADVANCED MATERIALS

In recent years, metallurgical engineering departments, and many mineral resource companies, have broadened their base of operations to encompass inorganic materials in general. An example of this trend is the renaming of the Metallurgical Society in the U.S. to the Minerals, Metals and Materials Society. Also, there has been much development of novel advanced materials which may consist of metals, ceramics, plastics or composites. At some stage of the production of such materials, the primary materials or the reagents are in a fluid state; understanding and controlling the rate phenomena in the liquid or gaseous state may have a profound effect on the properties and quality of the final product.

Examples of such processes are the rapid solidification of molten droplets and films, crystal growing from a melt, chemical vapor deposition, plasma spraying and similar processes. In such cases, the structure of a solid product depends on the processing operations which involve fluid flow, heat and mass transfer. In general, the efficient production of

advanced materials, such as semiconductors and superconductors, rapidly solidified ribbons for magnetic applications, and high-strength alloys, depends on the intelligent application of transport phenomena in the design and control of processes.

1.9. SCOPE OF THIS BOOK

This book is an introduction to the application of transport and chemical rate theory for solving problems encountered in the chemical processing of materials. On the basis of the teaching experience of the author, the material has been designed for presentation in about sixty hours of lectures to engineering students and also to graduate students who have moved to chemical processing from other disciplines. The text has also been written with the idea of serving practicing engineers as a quick reference to the theory and application of rate phenomena.

The advanced mathematical aspects of transport theory, such as three-dimensional energy and mass transfer and the modeling of turbulent flow are introduced. However, for a more advanced treatise of a particular transport phenomenon, the reader is referred throughout the text to more specialized textbooks.The emphasis of this text is on how easily one can use transport and chemical rate theory and the relevant properties of materials to solve the kind of problems that are most frequently encountered in the chemical processing of minerals and materials.

Following this introduction, the text continues with a description of fluid flow and momentum transfer, heat transfer by conduction, convection and radiation, and mass transfer by diffusion and convection. The final chapters discuss the basic aspects of chemical thermodynamics and kinetics and some applications of rate theory in the analysis of heterogeneous reaction systems which involve a combination of transport and chemical rate phenomena.

It is evident that the application of transport theory is not limited to a particular class of materials. Thus, this book is designed for chemical and metallurgical engineers who are interested in the efficient processing of materials; and for mineral and mining engineers who are concerned principally with the processing of mineral resources. The common thread is that most systems of concern in the chemical processing of minerals, metals and other materials are of a heterogeneous nature, that is they involve interphase reactions.

TWO

Dimensions and Units of Measurement

In applying transport theory to the solution of engineering problems, we have to use a multiplicity of principles, laws and relationships; these are derived from mathematics, physics and chemistry as well as from experimentation. It is not enough to know the particular laws and equations that apply to a particular case. In order to obtain a specific solution to a particular problem, we must be able to deal effectively with the numbers underlying the various equations. The solution of a problem involves four steps: a) identifying the appropriate controlling equations; b) ensuring that these equations are dimensionally consistent; c) ensuring that the units used in the equations are homogeneous; d) performing the required numerical calculations.

In this chapter, we will discuss steps b) and c) which are common to all rate phenomena.

2.1. THE DIMENSIONS OF PHYSICAL SYSTEMS

We know from elementary geometry that the volume of a rectangular box is expressed in terms of three linear measurements: length, width and height. Therefore, if the *dimension of distance* is denoted by $\mathbf{L}$, the dimensions of surface area are $\mathbf{L}^2$ and of volume $\mathbf{L}^3$. Let us now define the *dimension of time* by $\mathbf{t}$ and the *dimension of mass* by $\mathbf{M}$. Then, from elementary physics, the dimensions of velocity must be $\mathbf{Lt}^{-1}$ and of acceleration $\mathbf{Lt}^{-2}$. Also, since force is equal to mass times acceleration, the dimensions of force are $\mathbf{MLt}^{-2}$.

In physics, work is defined as the product of force times the distance over which the force is applied. Therefore, the dimensions of work are $\mathbf{ML}^2\mathbf{t}^{-2}$. Kinetic, potential, and other forms of energy have the same dimensions as work. Finally, the power used in doing work, that is the rate of expending energy, is the ratio of work done per unit time. Accordingly, the dimensions of power are $\mathbf{ML}^2\mathbf{t}^{-3}$.

In problems involving the generation or transfer of heat, we must introduce the *dimension of temperature*, $\mathbf{T}$. The dimensions of thermal energy are the same as for all other kinds of energy we discussed above, i.e., $\mathbf{ML}^2\mathbf{t}^{-2}$. However, since heat is usually expressed in heat units (e.g., Joules or calories) and usually appears in all terms of a thermal energy balance, it is convenient to represent it by the composite *dimension of heat*, $\mathbf{Q}$. Accordingly, the dimensions of heat transfer rate are $\mathbf{Qt}^{-1}$ and of the specific heat capacity of a material $\mathbf{QM}^{-1}\mathbf{T}^{-1}$.

In this book, we shall discuss equations that contain the above parameters and also others which may be more complex. Since apples cannot be added to oranges, it is obvious that all separate terms in an algebraic or differential equation describing a physical or chemical phenomenon must have the same dimensions. In other words, all such equations must be **dimensionally homogeneous**. This is examined by writing the dimensions of all

terms in the equation and ensuring, by algebraic manipulation, that the dimensions of all terms, on both sides of the equation, are the same.

Whenever possible, it is most convenient to express mathematical correlations and other equations in **dimensionless** form. This has led to the development of groupings of various parameters in a system, called **dimensionless numbers**. For example, the well known *Mach number* in aerodynamics is the ratio of the actual velocity of flow in a particular system divided by the velocity of sound in the same fluid.

2.2. UNITS OF MEASUREMENT

In applying transport theory to the solution of engineering problems, the ultimate objective is to calculate a specific number which can be used for designing or operating a process; for example, we may wish to calculate the required gas flow rate in a heat-treating furnace or the power rating of a compressor needed to do a certain job. In order to do this, we must ensure that the **units of measurement** in all terms of the equation, or in a system of equations, have been expressed homogeneously.

Unfortunately, in many problems the engineer is faced with material properties and other parameters which may be expressed in various units, such as grams, kilograms and tons, for the dimension of mass, or in microns, centimeters, and meters, for the dimension of length. The situation is worse in the US, the last nation in the world still dealing in ounces, pounds, short tons, inches and feet; an operating problem may be stated in such "British" units, while the material properties in the available handbooks are in metric.

It is therefore essential, before proceeding with numerical calculations in a certain problem, to ensure that the equations used are consistent in terms of the units used for the various constants and variables. The use of the **unit equation** for replacing non-homogeneous units in a equation will be demonstrated in examples throughout this book. Here is an illustration of a very simple conversion of velocity units from cm/h to m/s:

$$7200\,\frac{\mathrm{cm}}{\mathrm{h}} = ?\,\frac{\mathrm{m}}{\mathrm{s}}.$$

$$7200\,\frac{\cancel{\mathrm{cm}}}{\cancel{\mathrm{h}}} \times \left(\frac{\mathrm{m}}{\cancel{\mathrm{cm}}} \times \frac{1}{100}\right) \times \left(\frac{\cancel{\mathrm{h}}}{\mathrm{s}} \times \frac{1}{3600}\right) = 0.02\,\frac{\mathrm{m}}{\mathrm{s}}.$$

It can be seen that the ratios 1/100 and 1/3600 introduced in the left-hand side of the second equation are the numerical equivalents of the unit conversion ratios of m/cm and h/s which were used in order to make the required conversion.

In the **metric** system of units, length is expressed in centimeters (cm), mass in grams (g) and time in seconds (s). This system is much more rational than the "British" system of units (foot-pound-second) which is used in the US. However, in 1960, an even more rationalized system was introduced: the **SI system** (Système International des Unités). The SI unit of length is the meter (m), of mass the kilogram (kg), and of time the second (s). The SI units have been accepted nearly universally and are used predominantly in this book.

To make things a bit easier for the reader, Table A1 in Appendix A at the end of the book shows the SI units of nearly all the parameters to be used in this text. The same tabulation shows the numerical conversion factors necessary for converting units from other systems to the SI system. Also for convenience, Table A2 in the Appendix shows the values of the physical constants to be used in the following chapters.

2.3. DIMENSIONLESS NUMBERS

As will be discussed in later chapters, engineering correlations and graphs are best presented in dimensionless form; they are then of more general use and independent of a particular system of units. For example, a given length, L, in a conduit can be made dimensionless by expressing it as a ratio of L/d_c, where d_c is the diameter of the conduit. Also, the rising temperature, T, of a metal piece inserted in a furnace can be made dimensionless by expressing it as the ratio of $(T - T_i)/(T_f - T_i)$, where T_i is the initial temperature of the metal and T_f the furnace temperature; expressed in this way, the temperature change will range from 0 to 1.

It is equally convenient to express more complex quantities, such as velocities, forces and energy terms in dimensionless form. We already mentioned the use of the *Mach number* in aerodynamics to express the velocity of a body moving through a fluid by means of the ratio u/u_s, where u_s is the velocity of sound in the fluid. A number of such **dimensionless groups** will be introduced in later chapters. A tabulation of the most important dimensionless groups in rate phenomena is presented in Table 2.1.

Throughout the text, reference is made to the numerical values of transport properties, such as viscosity, thermal conductivity and molecular diffusivity. Because of the paramount importance of numbers in engineering, the emphasis in the examples presented in this book will be on the correct manipulation of numbers. It is evident that when the numbers are not right the best of theories is of little practical use.

Table 2.1. Dimensionless Groups in Rate Phenomena

Dimensionless group	Symbol	Definition		Ratio represented
Fluid flow				
Reynolds number	Re	$\frac{Lu\rho}{\mu}$	L: Characteristic length u: Fluid velocity ρ: Fluid density μ: Fluid viscosity	$\frac{\text{inertial force}}{\text{viscous force}}$
Drag coefficient	C_D	$\frac{F_d}{\left(\frac{1}{2}\rho u_p^2\right)\left(\frac{\pi}{4}d_p^2\right)}$	F_d: Drag force u_p: Particle velocity d_p: Particle diameter	$\frac{\text{drag force}}{\text{inertial force}}$
Friction factor	f_{fr}	$\frac{d}{L}\frac{\Delta P}{2\rho u^2}$	d: Pipe diameter L: pipe length ΔP: Pressure drop	$\frac{\text{friction loss}/L}{\text{kinetic energy of fluid}}$
Mach number	Ma	$\frac{u}{u_s}$		$\frac{\text{fluid velocity}}{\text{velocity of sound}}$
Weber number	We	$\frac{\rho L u^2}{\sigma}$	σ: Surface tension	$\frac{\text{inertial force}}{\text{surface tension force}}$
Heat transfer				
Biot number	Bi	$\frac{hr_0}{k}$	r_0: Radius or half thickness of body	$\frac{\text{internal conductive resistance}}{\text{boundary layer resistance}}$
Fourier number	Fo	$\frac{kt}{\rho C_p r_0^2} = \frac{\alpha t}{r_0^2}$	α: Thermal diffusivity	$\frac{\text{time elapsed}}{\text{time to temperature equilibrium}}$
Grashof number	Gr	$\frac{L^3 g\rho^2\beta\Delta T}{\mu^2}$	β: coefficient of expansion ΔT: Temperature difference L: Height of surface	$\frac{\text{buoyancy forces}}{\text{viscous forces}}$

cont'd

Dimensionless group	Symbol	Definition		Ratio represented
Nusselt number	Nu	$\frac{hL}{k}$	h: Heat transfer coefficient k: Thermal conductivity L: Characteristic length	$\frac{\text{total heat transfer}}{\text{conductive heat transfer}}$
Prandtl number	Pr	$\frac{C_p\mu}{k}$	C_p: Heat capacity	$\frac{\text{momentum diffusivity}}{\text{thermal diffusivity}}$
Peclet number for heat transfer	Pe	$\frac{\rho u L C_p}{k} = \text{Re} \cdot \text{Pr}$		$\frac{\text{bulk heat transport}}{\text{conductive heat transport}}$
Rayleigh number	Ra	$(L^3 g \rho^2 \beta \Delta T C_p)/(\mu k) = \text{Gr} \cdot \text{Pr}$		$\frac{\text{natural bulk heat transport}}{\text{conductive heat transport}}$
Stanton number	St	$\frac{h}{\rho u C_p} = \text{Nu} \cdot \text{Re}^{-1} \cdot \text{Pr}^{-1}$		$\frac{\text{heat transferred}}{\text{thermal capacity of fluid}}$
J factor for heat transfer	j_H	$\frac{h}{\rho u C_p}\left(\frac{C_p\mu}{k}\right)^{2/3}$		$\text{Nu} \cdot \text{Re}^{-1} \cdot \text{Pr}^{-1/3}$
Mass transfer				
Concentration Grashof number	Gr′	$\frac{L^3 g \beta'(X_s - X_b)}{\nu^2}$	β′: Coefficient of fractional expansion	$\frac{\text{buoyancy forces}}{\text{viscous forces}}$
Sherwood number	Sh	$\frac{k_d L}{D_{AB}}$	k_d: Mass transfer coefficient D_{AB}: Molecular diffusivity	$\frac{\text{total mass transfer}}{\text{diffusive mass transfer}}$
Schmidt number	Sc	$\frac{\mu}{\rho D_{AB}}$		$\frac{\text{momentum diffusivity}}{\text{molecular diffusivity}}$
Peclet number for mass transfer	Pe	$\frac{Lu}{D_{AB}} = \text{Re} \cdot \text{Sc}$		$\frac{\text{bulk mass transport}}{\text{diffusive mass transport}}$
J factor for mass transfer	j_D	$\frac{k_d}{u}\left(\frac{\mu}{\rho D_{AB}}\right)^{2/3}$		$\text{Sh} \cdot \text{Re}^{-1} \cdot \text{Sc}^{-1/3}$

THREE

The Concept of Viscosity

Fluid flow plays a very important part in the processing of materials. Most processes are based on the use of fluids either as raw materials, reagents, or heat transfer media. In this book, we will see many examples of processes where the rates of heat transfer, mass transfer and chemical reaction between two phases depend on the fluid flow phenomena in the system. It is therefore necessary to start our study of rate phenomena in processing systems by examining the motion of fluids.

3.1. DEFINITION AND MEASUREMENT OF VISCOSITY

The behavior of a fluid in flow is very much related to two intrinsic properties of the fluid: **density** and **viscosity**. For example, a solid body moving through a gas has to overcome a certain resistance which depends on the relative velocity between fluid and solid, the shape of the solid, the density of the gas and its viscosity. The power required to move a fluid through a conduit is a function of the fluid velocity, the diameter of the conduit and the fluid density and viscosity.

The existence and nature of viscosity can be demonstrated by suspending two horizontal, parallel plates in a liquid so that they are separated by a very small distance, Y (Fig. 3.1). Now, if the upper plate is kept stationary while the lower plate is set to motion with a velocity u_0, the layer of liquid right next to this plate will also start to move. With time, the motion of the bottom layer of fluid will cause the fluid layers higher up to also move.

As shown in Fig. 3.1, when steady-state conditions are established, the velocity of the uppermost layer, which is in contact with the stationary plate, will also be zero, while the bottom layer, in contact with the moving plate, will be moving with velocity u_0. If we measure the velocity distribution across the intermediate fluid layers, we find that velocity changes linearly with distance y from the stationary plate:

$$u_x = u_0 \frac{y}{Y}. \tag{3.1.1}$$

Assume that we can measure, e.g., by means of a calibrated spring or transducer, the horizontal force ($-F_x$, Fig. 3.1) which must be applied, in the opposite direction to u_0, to maintain the upper plate at rest; if we divide this force by the surface area of the plate, A, we find that this ratio, called the **shear stress**, is proportional to the velocity of the lower plate, u_0, and inversely proportional to distance Y between the two plates

$$\frac{\text{force}}{\text{area}} = \text{shear stress} \propto \frac{u_0}{Y} = \mu \frac{u_0}{Y}. \tag{3.1.2}$$

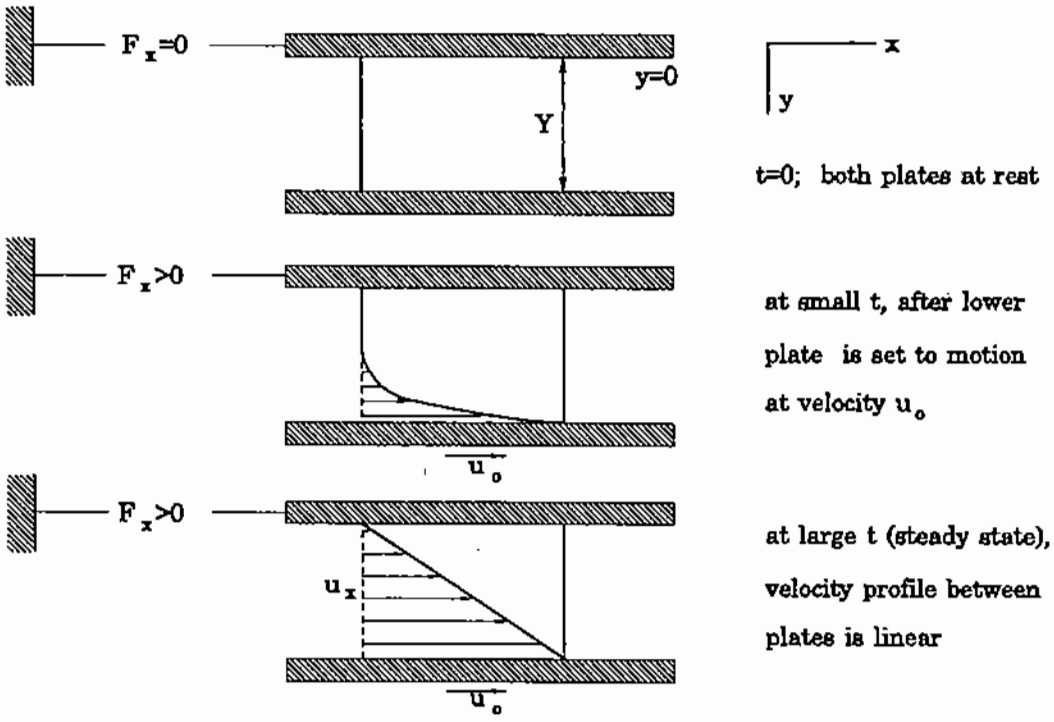

Figure 3.1. Change of velocity profile with time (upper plate stationary, lower plate velocity: u_0).

As shown in (3.1.2), the proportionality constant between shear stress and the velocity gradient u_0/Y is called the **viscosity** of the liquid, μ. Since at steady state conditions the velocity profile between the two plates is linear, every infinitesimal segment of the line is represented by the same relationship. Therefore, (3.1.2) can be expressed in differential form:

$$\text{shear stress} = \tau_{y,x} = -\mu \frac{du_x}{dy}. \tag{3.1.3}$$

The first subscript of the shear stress denotes the *area* on which the shear stress acts (here, an area perpendicular to the y-axis and at distance y from the origin); the second subscript represents the *direction* in which the shear stress acts (here, in the direction of velocity, x). The negative sign expresses the fact that the shear stress is applied from a region of higher velocity to a lower one (i.e., $u_{x,2} < u_{x,1}$ and $du_x < 0$).

Equation (3.1.3) is called the **Newton's law of viscosity** and states that *the shear stress between adjacent fluid layers is proportional to the negative value of the velocity gradient between the two layers.*

An alternative interpretation can be given to (3.1.3) by noting, from elementary physics, that

force = mass × acceleration = mass × change in velocity/time = change in momentum/time.

Therefore, (3.1.3) also states that *the rate of momentum transfer per unit area* (i.e., the shear stress) *between two adjacent layers of fluid is proportional to the negative value of the velocity gradient between them.*

In transport theory, the *transport rate per unit surface area* of a certain quantity (e.g., of mass, momentum, heat) is called **flux**; for example, the dimensions of mass flux are

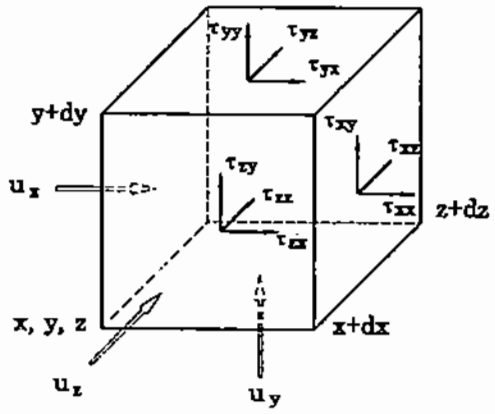

Figure 3.2. Tangential and normal stresses acting on three "visible" sides of a cubical element (an additional nine stresses are acting on the other three sides).

$Mt^{-1}L^{-2}$. Also, the change of a certain quantity with distance is called **gradient**; for example, the dimensions of the mass gradient are ML^{-1}.

If we now divide and multiply the second term of (3.1.3) by the fluid density, we obtain

$$\tau_{y,x} = -\frac{\mu}{\rho}\left(\frac{\rho du_x}{dy}\right) = -\nu\left(\frac{\rho du_x}{dy}\right), \tag{3.1.4}$$

and for an incompressible flow:

$$\tau_{y,x} = -\nu\,\frac{d(\rho u_x)}{dy}, \tag{3.1.5}$$

which expresses the fact that *the momentum flux is proportional to the negative value of the gradient of mass flux.*

In the above equation, we have introduced a new term, the ratio of fluid viscosity to density, μ/ρ. This ratio is called the **kinematic viscosity** of a fluid, ν, and has the dimensions of $L^2\ t^{-1}$. As we shall see later, the properties of *thermal diffusivity* (Chapter 10) and *molecular diffusivity* (Chapter 14) have the same dimensions. Therefore, by analogy, the kinematic viscosity is also referred to as the **momentum diffusivity** of the fluid, i.e., the ability of the fluid to transport momentum.

The above discussion was based on unidirectional flow. However, it also applies for the general case of flow in all three directions, x, y, and z, as illustrated in Fig. 3.2. The stresses

$$\tau_{y,x},\ \tau_{y,z},\ \tau_{x,y},\ \tau_{x,z},\ \tau_{z,x},\ \tau_{z,y}$$

are called *shear* or *tangential* stresses. The stresses $\tau_{x,x}$, $\tau_{y,y}$, and $\tau_{z,z}$ are called *normal* stresses and can be either *compressive* (+) or *tensile* (-).

By substituting the dimensions of force, area, length and velocity into (3.1.3) we find that the dimensions of viscosity are $M\ L^{-1}\ t^{-1}$. In the metric system, the unit of viscosity is the Poise ($1\ P = 1\ g\ cm^{-1}\ s^{-1}$), which is subdivided into 100 centipoise (cP).

In the SI system, viscosity is expressed in $kg\ m^{-1}\ s^{-1}$; however, sometimes viscosity values are shown in terms of the equivalent units of $N\ m^{-2}$ s or Pa s, where the Pascal (Pa)

Table 3.1. Comparative Values of Viscosity of Some Gases and Liquids

Fluid	Temperature, °C	Density kg m^{-3}	Viscosity kg s^{-1} m^{-1}	Momentum diffusivity, m^2 s^{-1}
Hydrogen	0	8.93×10^{-2}	8.40×10^{-6}	9.41×10^{-5}
	20.7	8.30×10^{-2}	8.80×10^{-6}	1.06×10^{-4}
	229	4.86×10^{-2}	1.26×10^{-5}	2.59×10^{-4}
	490	3.19×10^{-2}	1.67×10^{-5}	5.24×10^{-4}
	825	2.22×10^{-2}	2.14×10^{-5}	9.64×10^{-4}
Air	0	1.30×10^{0}	1.71×10^{-5}	1.32×10^{-5}
	18	1.22×10^{0}	1.83×10^{-5}	1.50×10^{-5}
	229	7.08×10^{-1}	2.64×10^{-5}	3.73×10^{-5}
	409	5.21×10^{-1}	3.41×10^{-5}	6.55×10^{-5}
	810	3.28×10^{-1}	4.42×10^{-5}	1.35×10^{-4}
	1134	2.53×10^{-1}	5.21×10^{-5}	2.06×10^{-4}
Water	0	1.00×10^{3}	1.79×10^{-3}	1.79×10^{-6}
	20	9.98×10^{2}	1.01×10^{-3}	1.01×10^{-6}
	60	9.83×10^{2}	4.69×10^{-4}	4.77×10^{-7}
	100	9.58×10^{2}	2.84×10^{-4}	2.96×10^{-7}
Molten iron	1550	7.21×10^{3}	6.70×10^{-3}	9.29×10^{-7}
	1600	7.16×10^{3}	6.10×10^{-3}	8.52×10^{-7}
	1700	7.06×10^{3}	5.60×10^{-3}	7.93×10^{-7}
	1800	6.96×10^{3}	5.30×10^{-3}	7.61×10^{-7}
High-iron slag	1200	4.50×10^{3}	3.50×10^{-1}	7.78×10^{-5}
Low-iron slag	1500	3.50×10^{3}	5.00×10^{-1}	1.43×10^{-4}

is the SI unit of pressure and is equal to 1 Newton per square meter (Table A1). The SI unit of viscosity is equal to 10 Poise or 1000 centipoise.

All gases and most simple liquids, including liquid metals and other high-temperature melts, obey Newton's law of viscosity and are accordingly called Newtonian fluids. On the other hand, polymer solutions, slurries, pastes, and paints are frequently "non-Newtonian": their viscosity depends on the applied shear and, for some fluids, also on the rate at which a given shear is applied [1]. The viscosities and momentum diffusivities of some gases and liquids of interest in the chemical processing of materials are compared in Table 3.1.

3.2. FACTORS AFFECTING VISCOSITY

The viscosity of Newtonian fluids is affected by temperature, pressure, and, in the case of solutions and mixtures, by composition. The effect of pressure and temperature on the viscosity of gases is illustrated in Fig. 3.3 which shows the viscosity of carbon dioxide as a function of pressure and temperature [14]. The lowest viscosity is reached (Fig. 3.3) at

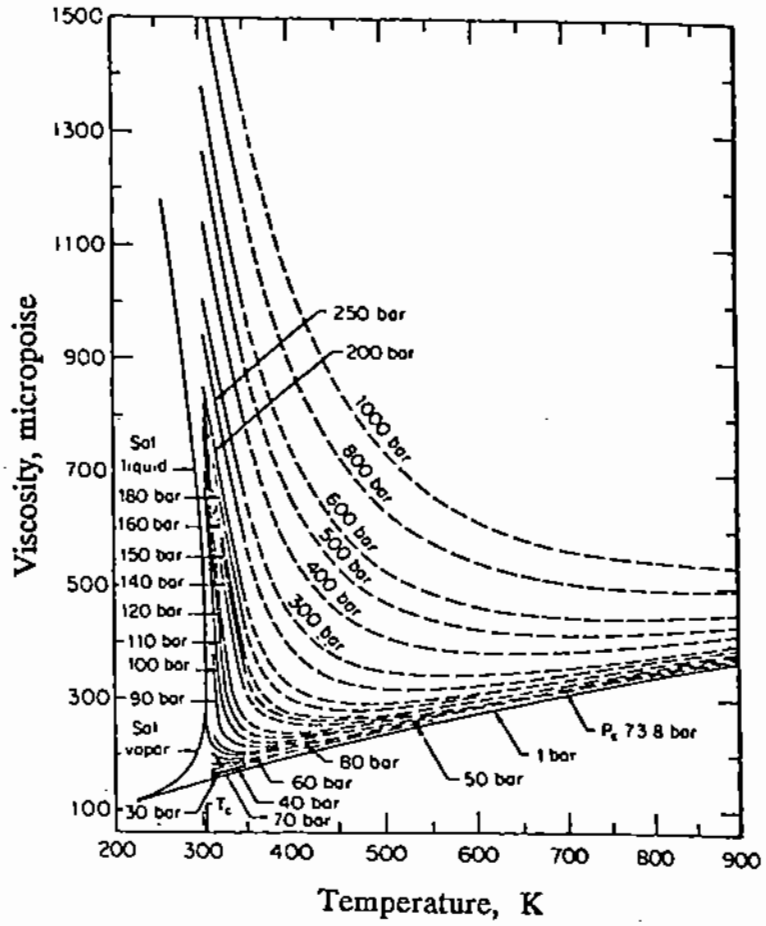

Figure 3.3. Viscosity of carbon dioxide as a function of pressure temperature and pressure [14].

the *critical temperature* of carbon dioxide ($T_c = 304.1$ K). This is the highest temperature at which a gaseous substance can exist in liquid form regardless of the pressure; the corresponding *critical pressure* (P_c) for CO_2 is 73.8 bar (72.9 atm). As indicated in Fig. 3.3, at high ratios of T/T_c, pressure has little effect and the gas viscosity increases with temperature. The plot of Fig. 3.3 is typical of the viscosity plots for other gases. The critical temperatures and pressures of other compounds and elements can be found in the *Chemical Engineers' Handbook* [4] and other reference books.

3.2.1. Estimation of Gas Viscosities

When experimental data on the viscosity of a particular gas are not available, its viscosity may be estimated from theoretical models. This topic has been extensively treated in other texts, the most recent of which is *The Properties of Gases and Liquids* by Reid et al. [2]. In general, the molecular theory of gases is sufficiently developed to allow the prediction of transport properties. Therefore, the viscosity of gases may be estimated with an accuracy sufficient for most engineering calculations, e.g., by using the following correlation for the viscosity of quasi-spherical molecules [1,2]:

$$\mu = 26.7 \times 10^{-6} \frac{(MT)^{1/2}}{\sigma_c^2 \Omega_\mu}. \tag{3.2.1}$$

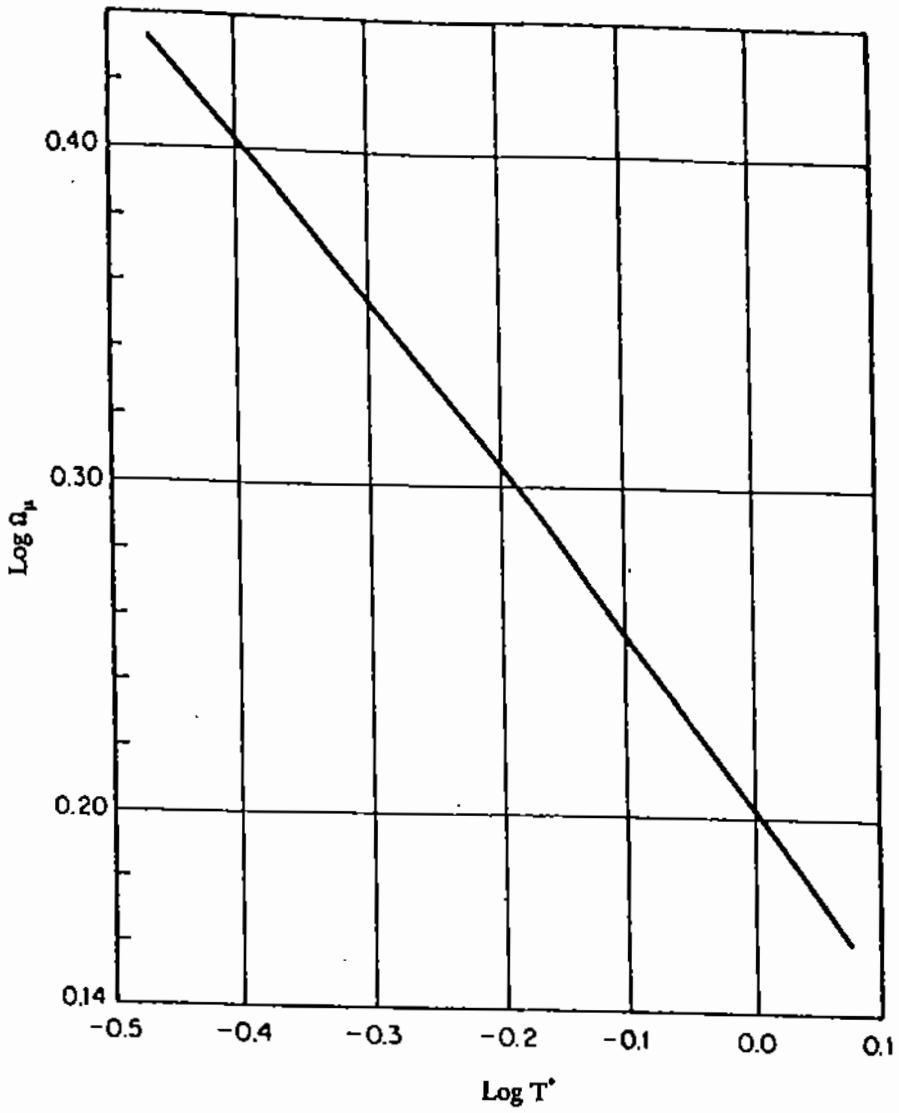

Figure 3.4. Effect of temperature on collision integral [2].

where μ is the gas viscosity, Poise; M is the molecular weight, grams; T is absolute temperature, K; σ_c is the collision diameter, Å; Ω_μ is the collision integral (equal to 1 for noninteracting molecules).

As shown in Fig. 3.4 [2], the value of Ω_μ is a function of the group:

$$T^* = \frac{kT}{\varepsilon}, \tag{3.2.2}$$

where k is Boltzmann's constant (1.38×10^{-23} joules molecule^{-1} K^{-1}, Table A2), and ε is an energy parameter for interaction between molecules (units: kg m^2 s^{-2} molecule^{-1}). Numerical values of σ_c and ε are available in the literature for most common gases; otherwise, the following empirical formulae may be used for estimating these quantities:

$$\varepsilon/k = 1.92T_m \text{ and } \sigma_c = 1.222V_m^{1/3}, \tag{3.2.3}$$

$$\varepsilon/k = 1.15T_b \text{ and } \sigma_c = 1.166V_b^{1/3}, \tag{3.2.4}$$

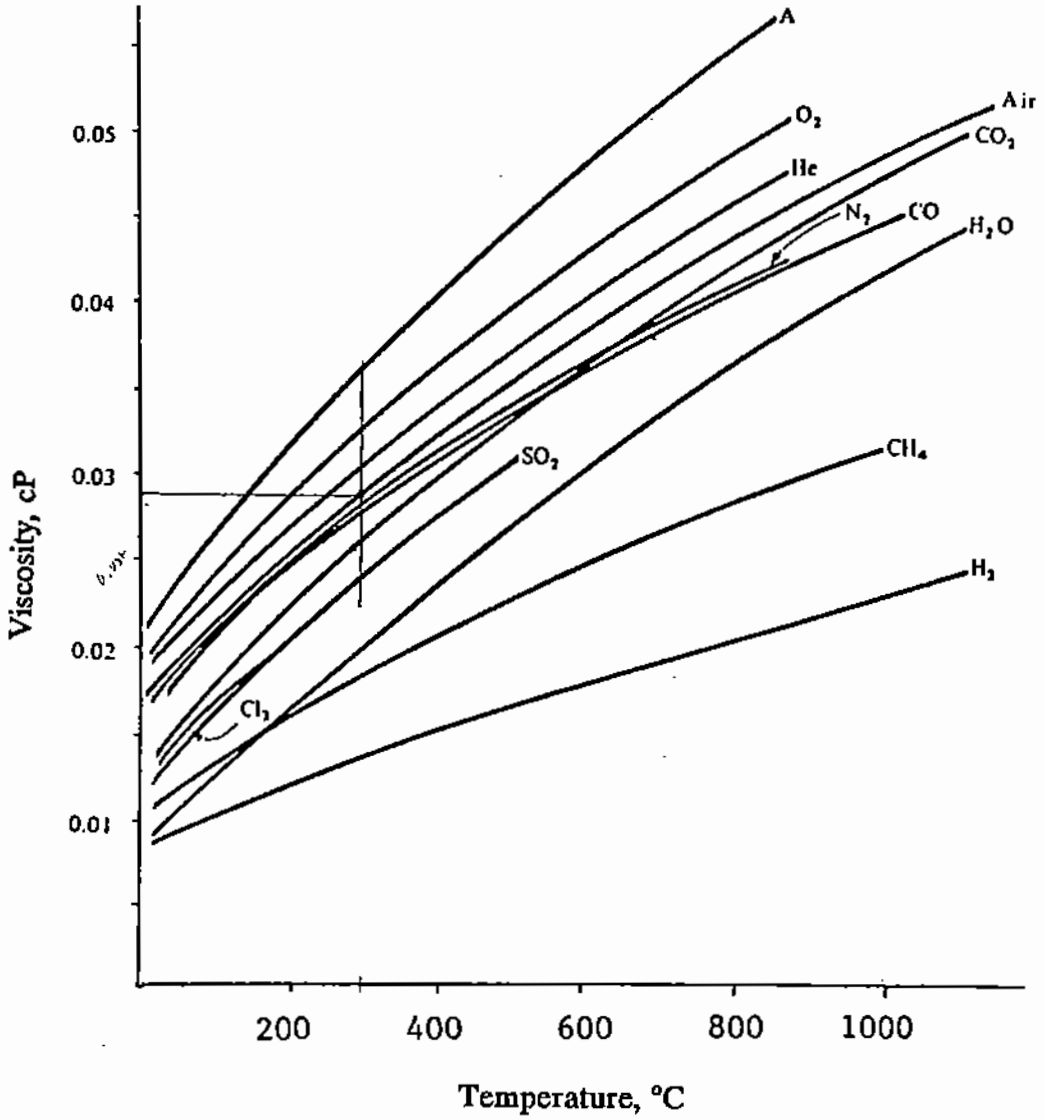

Figure 3.5. Viscosities of common gases as a function of temperature (after [6]).

where T_m and T_b are the melting and boiling points of the substance in K; V_m is the molar volume of the species at the melting point (solid), and V_b its molar volume at the boiling point (liquid), both expressed in $cm^3\ mol^{-1}$. The molecular volumes of some liquid metals are shown in Table 14.3 (Chapter 14).

The effect of temperature on the viscosity of some commonly used gases is shown in Fig. 3.5 [6]. With regard to the viscosity of mixtures of gases, the following semi-empirical equation can be used to represent with reasonable accuracy the viscosity of a gas mixture at low or moderate pressures:

$$\mu_{\text{mix}} = \frac{\sum X_i \mu_i (M_i)^{1/2}}{\sum X_i (M_i)^{1/2}}, \tag{3.2.5}$$

where X_i is the mole fraction of component i of viscosity μ_i, and M_i is the molecular weight of component i.

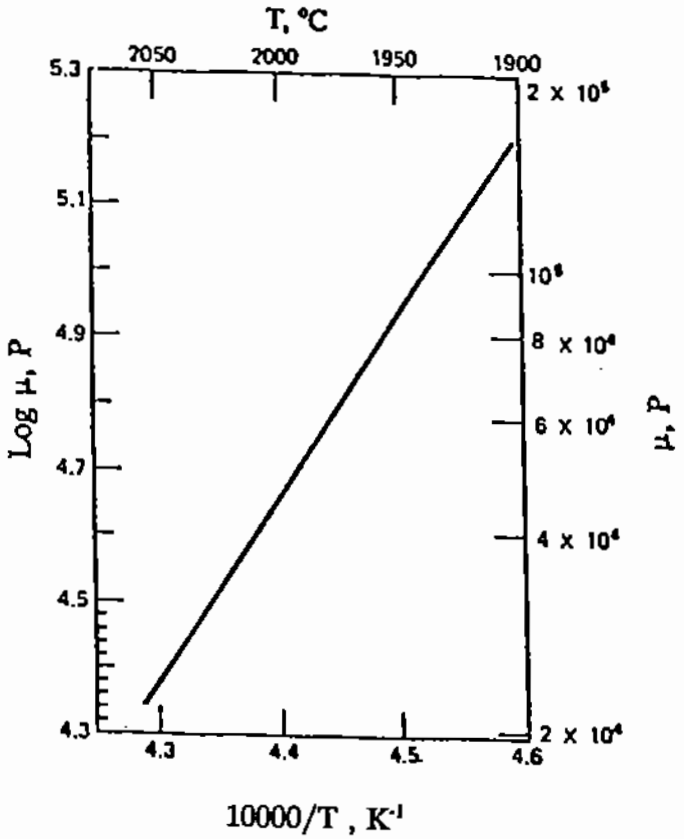

Figure 3.6. Effect of temperature on viscosity of silica [5].

The use of such equations for predicting the viscosity is illustrated in the following example.

Example 3.2.1

Let us estimate the viscosity of a gas mixture consisting of 20% Zn vapor, 50% N_2, and 30% CO at 1000°C.

The density of zinc at its melting point ($T_m = 692$ K) is approximately 7.14 g cm^{-3}. Therefore, its molar volume at that temperature is calculated to be = 65.38/7.14 = 9.16 cm^3/mole and the corresponding $\sigma_c = 2.56$ Å (see (3.2.3)). Also from (3.2.3) we obtain $\varepsilon/k = 1.92 \times 692 = 1329$. Therefore, at a given temperature of 1273 K, the value of T^* is calculated to be equal to 0.958, and $\log T^* = -0.019$. From Fig. 3.4, the corresponding value of $log\Omega_\mu$ is approximately 0.21, and $\Omega_\mu = 1.63$. By introducing the calculated values of σ_c and Ω_μ in (3.2.1), we obtain the viscosity of zinc:

$$\mu_{Zn} = \frac{26.7 \times 10^{-6}(65.37 \times 1273)^{0.5}}{2.55^2 \times 1.63} = 727 \times 10^{-6} \text{ Poise.}$$

Also, from the available compilations for gas viscosities, we obtain

$$\mu_{N_2} = 500 \times 10^6 \text{ P} \quad \mu_{CO} = 480 \times 10^{-6} \text{ P.}$$

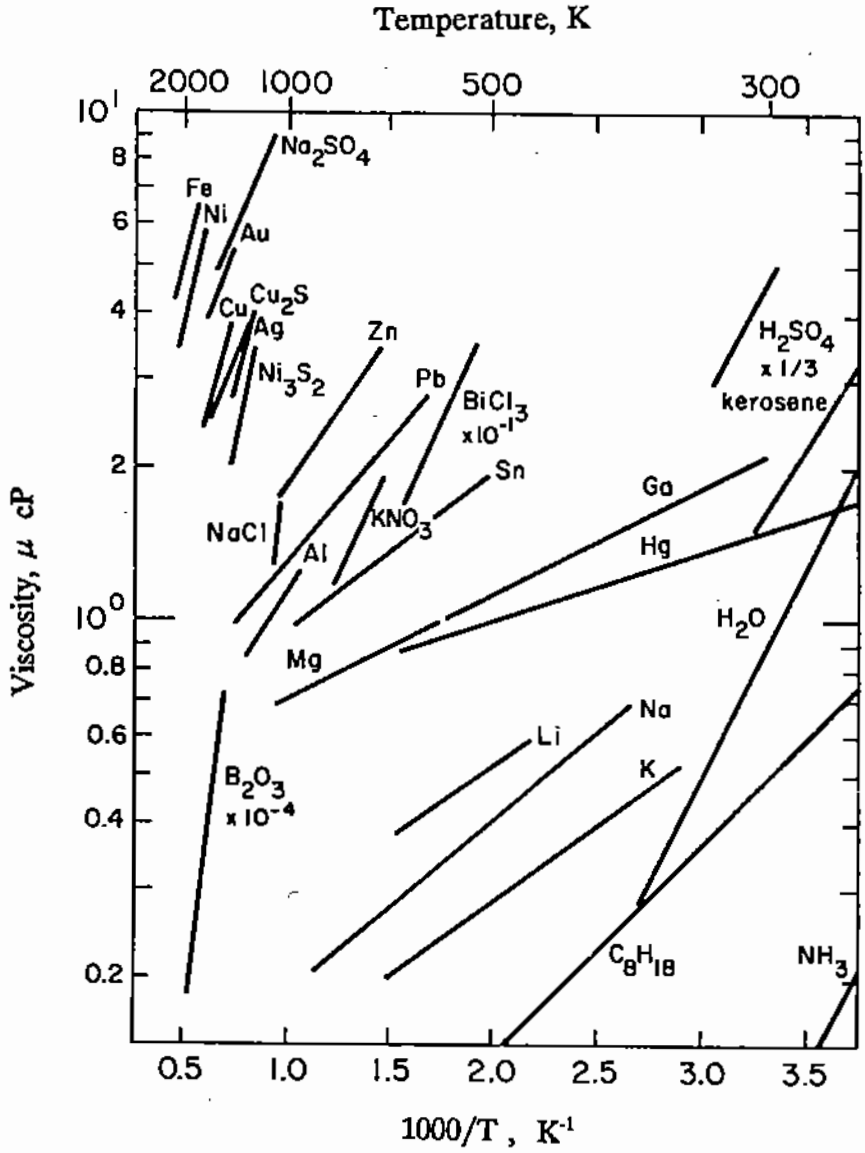

Figure 3.7. Viscosity of various liquids [17].

We can now set up the following table and use (3.2.5), to calculate the viscosity of the gas mixture:

$$\mu_{\text{mix}} = \frac{3262 \times 10^{-6}}{5.85} = 558 \times 10^{-6} \text{ P}.$$

Species	Mole fraction	M	μ_i, P	$X_i M_i^{1/2}$	$X_i M_i^{1/2} \mu_i$
Zn	0.2	65.37	727×10^{-6}	1.62	1178×10^{-6}
N_2	0.5	28.02	500×10^{-6}	2.65	1323×10^{-6}
CO	0.3	28.00	480×10^{-6}	1.59	761×10^{-6}
Σ				5.85	3262×10^{-6}

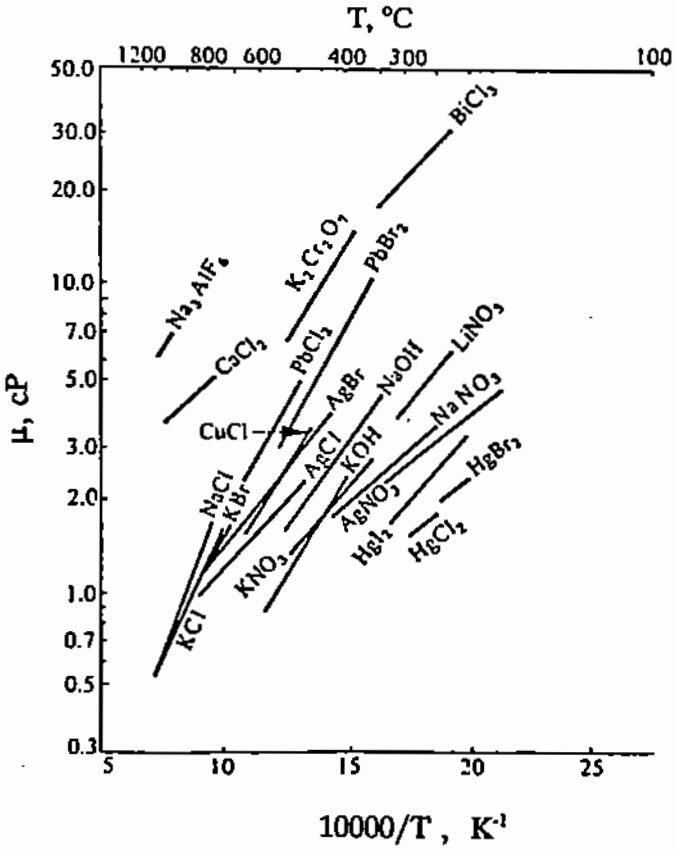

Figure 3.8. Viscosity of molten salts [13].

3.2.2. Estimation of Liquid Viscosities

Models for predicting liquid viscosities are much less developed than for gases and their use is limited to a qualitative description of observed behavior. The behavior of liquids is markedly different from gases in that the viscosity *decreases* with increasing temperature; the relationship can be expressed in the form of an Arrhenius-type equation

$$\mu = \mu_0 e^{E_\mu / RT}, \tag{3.2.6}$$

where μ_0 is the viscosity at some reference temperature, and E_μ is the temperature coefficient for viscosity.

The viscosity temperature coefficient, E_μ, has the physical significance of activation energy (ΔG_μ is the Gibbs free energy, Chapter 18), so that the mobility ($1/\mu$) of liquid molecules is a temperature-activated process while that of gas molecules is not. An example of the Arrhenius-type dependence of viscosity on temperature is given in Fig. 3.6 for pure silica [5]. Figures 3.7 [17] and 3.8 [13] show a similar behavior for a large number of metals, fused salts, and other liquids of interest in materials processing.

The dependence of viscosity on the composition of liquid solutions is illustrated by Fig. 3.9 for molten zinc/aluminum solutions [7]; and by Fig. 3.10 for iron-carbon alloys [8]. It can be seen that the behavior of molten alloys cannot be described by simple addition rules.

In many materials processing systems, it is of considerable importance to maintain liquid viscosities at a sufficiently low level so as to ensure satisfactory mass transfer rates and to facilitate charging and discharging of liquid materials. In the case of some liquids,

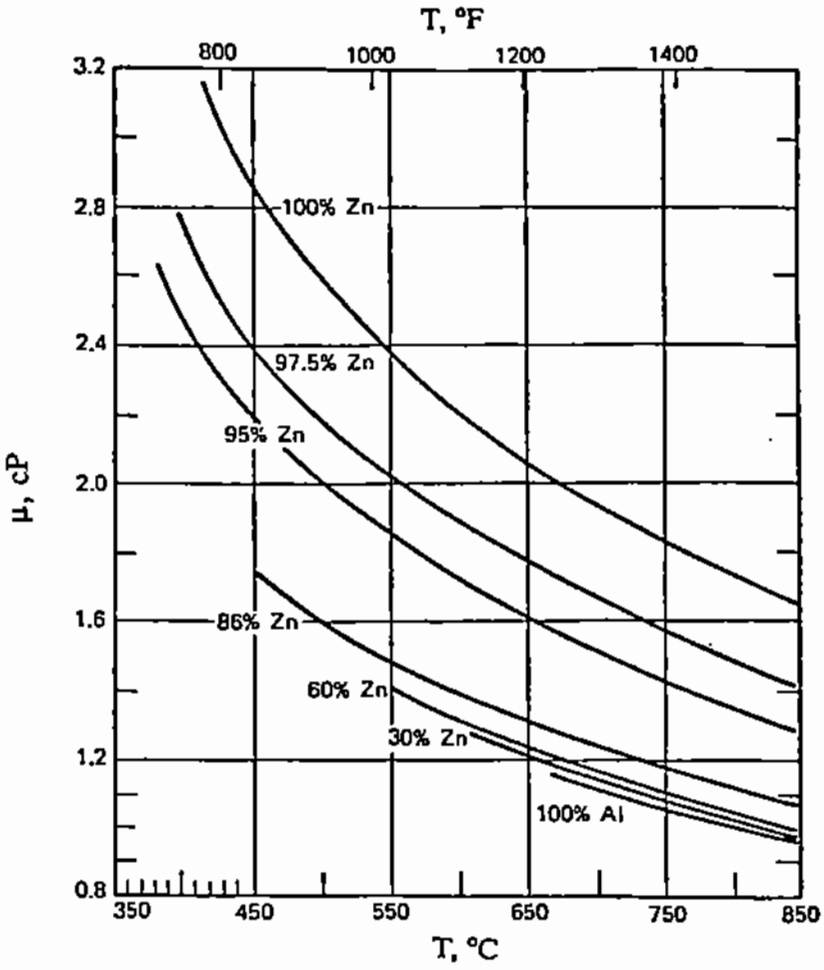

Figure 3.9. Viscosity of zinc–aluminum liquid solutions [7].

such as metal oxide and silica solutions (slags), this minimum viscosity may exist only over a very narrow composition range so that very careful control may be required.

In the pyrometallurgical production of metals, the unwanted components in the raw feed are driven off either as gaseous components (e.g., SO_2 or CO_2) or in the form of a liquid silicate solution ("slag"). Because of the importance of slag fluidity in metallurgical processes, there have been many experimental investigations of slag viscosity. In addition to SiO_2, steelmaking slags contain CaO, MgO, Al_2O_3 and other compounds in smaller concentrations. Pure silica has a very high viscosity (Fig. 3.6) but the addition of other metal oxides, with the exception of Al_2O_3, decreases the slag viscosity. At low alumina concentrations, Al_2O_3 is equivalent to SiO_2 but at $X_{Al_2O_3}$ (mole fraction of alumina in solution) above 0.05, its effect depends on the molar ratio of Al_2O_3/(CaO + MgO) present in the slag (Fig. 3.11, [9]). Once the effective concentration of $X_{Al_2O_3,eq}$ is established, it can be added to the X_{SiO_2} content of the slag and Fig. 3.12 [9] can be used to determine the viscosity of a particular slag.

Example 3.2.2

A blast furnace slag at 1500°C contains 39.8% CaO, 2.5% MgO, 15.2% Al_2O_3 and 40.7% SiO_2 (by weight). Use the plots of Figs. 3.11 and 3.12 to estimate slag viscosity.

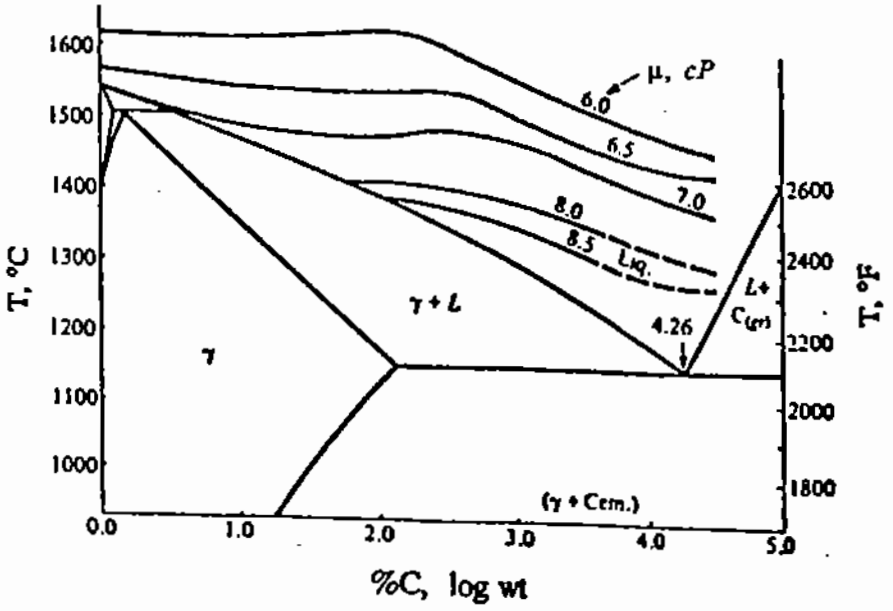

Figure 3.10. Viscosity of iron–carbon alloys [8].

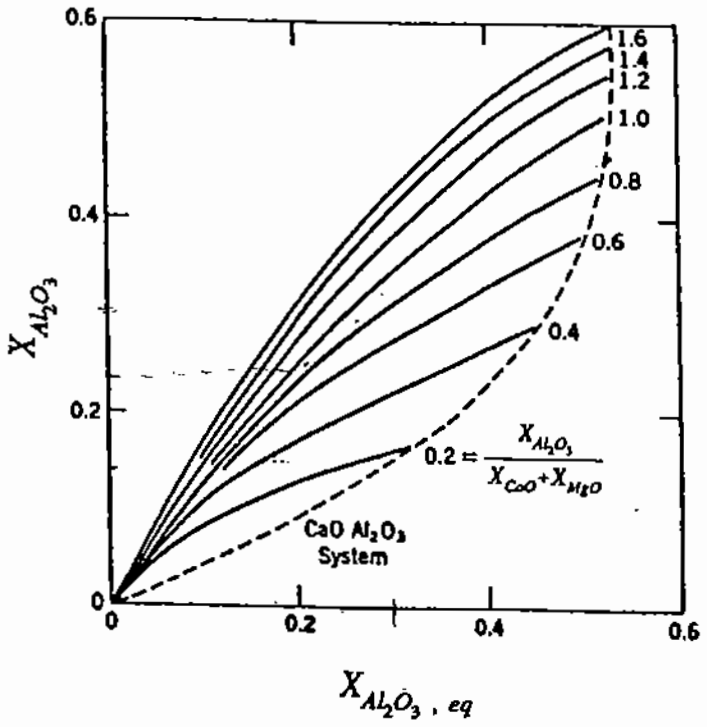

Figure 3.11. Silica equivalence of alumina in CaO-Al_2O_3-SiO_2, melts, 1500-1800°C [9].

From the given composition, we calculate the molar composition of the slag to be as follows:

$$X_{CaO} = 0.44,\ X_{MgO} = 0.04,\ X_{Al_2O_3} = 0.09,\ X_{SiO_2} = 0.42.$$

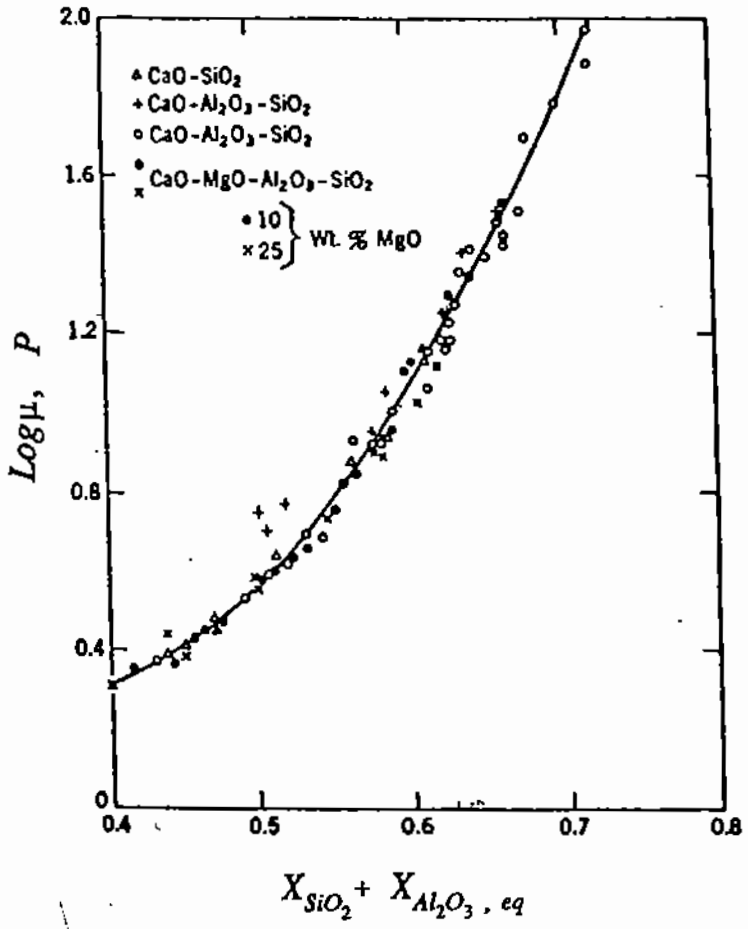

Figure 3.12. Effect of composition on viscosity of CaO–MgO–Al_2O_3–SiO_2, melts, 1500°C–1800°C [9].

Also, we calculate the ratio $X_{Al_2O_3}/(X_{CaO}+X_{MgO})$ to be equal to 0.19. Figure 3.11 shows that at this ratio and for $X_{Al_2O_3}$ = 0.09, the value of $X_{Al_2O_3,eq}$ is about 0.14; reference to Fig. 3.12 shows that the viscosity of the slag containing $X_{SiO_2} + X_{Al_2O_3,eq} = 0.56$ is approximately 7 Poise.

In contrast to slags produced in the ironmaking process, slags from non-ferrous smelting (production of Cu, Pb, Zn, Ni, etc.) contain a large amount of iron as FeO and Fe_3O_4 and are usually more fluid than steelmaking slags; the iron content of copper smelting slags is in the range of 30 to 45% Fe.

Work by Johannsen and Wiese [10] on synthetic copper smelting slags has shown that FeO, CaO, MgO, and Fe_3O_4 have an equivalent effect on viscosity; also, in the concentration range encountered in copper production, the effects of silica and alumina are additive. These data were correlated [11] by means of a "viscosity modulus," K_ν, which was defined as follows:

$$K_\nu = \frac{\%FeO + \%Fe_3O_4 + \%CaO + \%MgO}{\%SiO_2 + \%Al_2O_3}. \tag{3.2.7}$$

The resulting plot is shown in Fig. 3.13 [11], which also shows the wide variation between the viscosity of synthetic slags and industrial slags which contain other impurities [10]. Other metal oxides, such as copper and zinc, may be included in the numerator of the

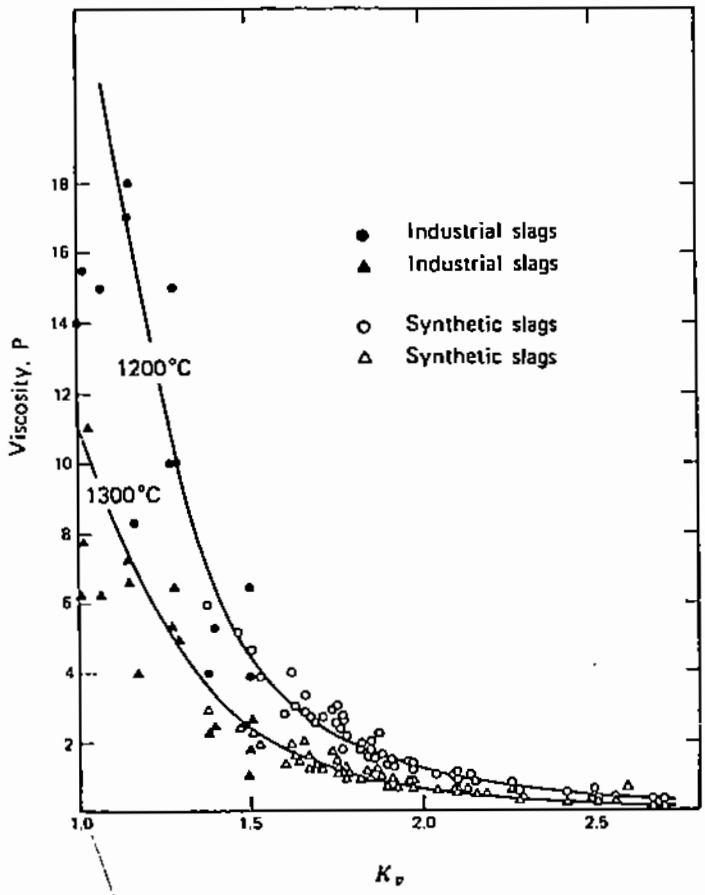

Figure 3.13. Effect of temperature on slag viscosity [11].

(3.2.7). Manganese and chromium oxides may be assumed to act as Al_2O_3 and be included in the denominator. A recent study by Battle and Hager [12] has confirmed the usefulness of a similar slag modulus for estimating the viscosity of lead and zinc smelting slags (Fig. 3.14).

REFERENCES

1. R.B. Bird, W.E. Stewart, and E.N. Lightfoot, *Transport Phenomena*, Wiley, New York (1960).
2. R.C. Reid, J.M Pransuitz, and B.E. Poling, *The Properties of Gases and Liquids*, McGraw-Hill, New York (1987).
3. J. Szekely, *Fluid Flow Phenomena in Metals Processing*, Academic Press, New York (1979).
4. R.H. Perry and D. Green, eds., *Chemical Engineers' Handbook*, 6th ed., McGraw-Hill, New York (1984).
5. J.F. Elliot, M. Gleiser, and V. Ramakrishna, *Thermochemistry for Steelmaking*, Addison-Wesley, Reading, MA (1963).
6. G.H. Geiger and D.R. Poirier, *Transport Phenomena in Metallurgy*, Addison-Wesley, Reading, MA (1973).
7. W.R.D. Jones and W.L. Bartlett, *J. Inst. Metals*, **81**, 145 (1952–53).
8. R.N. Barfield and J.A. Kitchener, *J.Iron and Steel Inst.*, **180**, 324 (1955).
9. E. T. Turkdogan and P.M. Bills, *Am. Ceram. Soc. Bull.*, **39**, 682–687 (1960).
10. F. Johannsen and W. Weise, *Erzmetal*, **11**, 13–15 (1958).
11. J.M. Toguri, N.J. Themelis, and P.H. Jennings, *Can. Met. Quart.*, **3**, 197–219 (1964).
12. T.P. Battle and J.P. Hager, *Metallurgical Transactions B*, **21B**, 501–510 (1990).

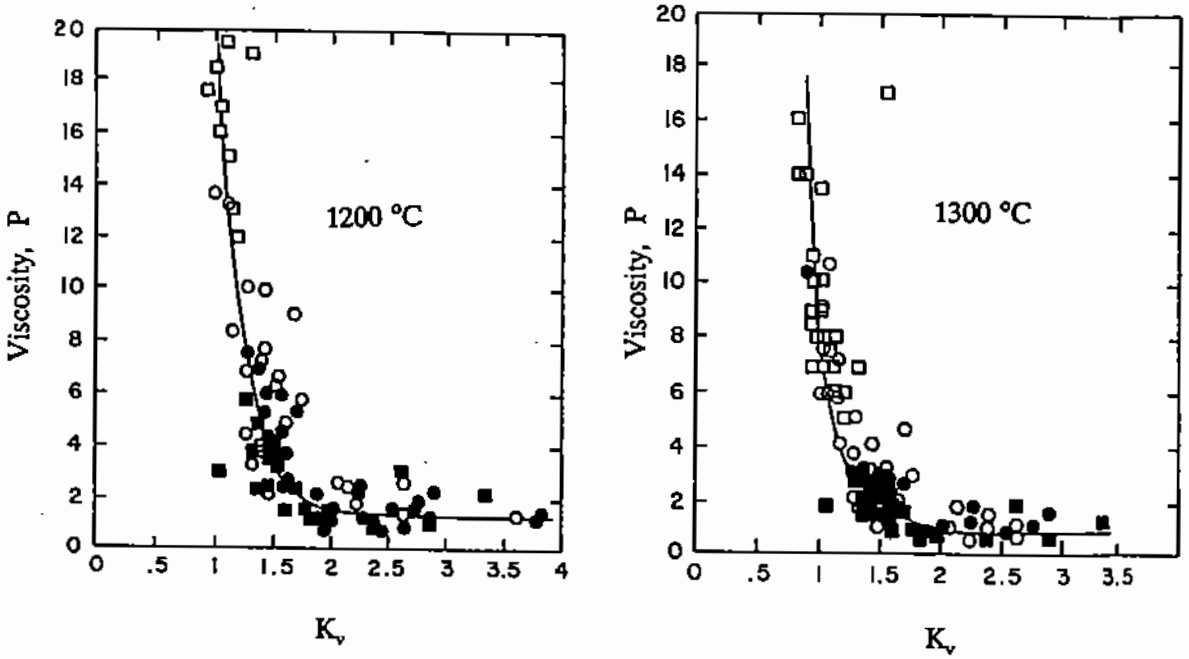

$$K_v = \frac{\%FeO + \%Fe_3O_4 + \%CaO + \%MgO + \%ZnO + \%PbO + \%CuO + \%CaS}{\%SiO_2 + \%Al_2O_3}$$

Figure 3.14. The effect of composition (weight%) on the viscosity of copper slags [11].

13. J.C. Smithells, *Metals Reference Book*, 4th ed., Vol. 1, Plenum Press, New York (1967).
14. K. Stephan and K. Lucas, *Viscosity of Dense Fluids*, Plenum, New York (1979).
15. S. Levy and J.W. Mausteller, eds., *Liquid Metals Handbook*, Atomic Energy Commission, TID 5277 (1955).
16. T.W. Chapman, *A.I.Ch.E.J.*, **12**, 395–400 (1966).
17. D.F. Rosner, *Transport Processes in Chemically Reacting Flow Systems*, Butterworths, Boston (1986).

FOUR

Steady-State Unidirectional Flow

In this chapter, we shall examine how to use Newton's law of viscosity (equation (3.1.3)) to determine velocities in steady-state flow of an incompressible fluid (i.e., of constant density) in the direction x. To simplify matters further, we will consider conduits of constant cross sectional area, such as pipes.

4.1. GENERAL APPROACH

The general strategy is similar to the one we will use in Chapter 5 for more complex problems: We consider an infinitesimal volume element of the fluid and apply to it *Newton's law of the conservation of energy*:

$$\begin{aligned} &\text{rate of momentum accumulation in element} \\ &\quad = \text{transport rate of momentum in} \\ &\quad - \text{transport rate of momentum out} \\ &\quad + \text{sum of forces acting on element.} \end{aligned} \tag{4.1.1}$$

Since we are concerned with steady state flow, the rate of momentum accumulation is zero and the energy balance of (4.1.1) becomes:

$$\begin{aligned} &\text{transport rate of momentum out} \\ &\quad - \text{transport rate of momentum in} \\ &\quad = \text{sum of forces acting on element.} \end{aligned} \tag{4.1.2}$$

In order to express this balance mathematically for a volume element of the fluid, we need to express the transport rates of momentum, in and out of the element, in terms of the *momentum flux* acting on a particular surface of the volume element times the area of the surface on which the flux is acting.

Since we are considering a conduit of constant cross section and the fluid is incompressible, there can be no change in the velocity profile along the direction x of flow (Fig. 4.1). Therefore, the momentum carried by the fluid entering the differential volume element at location x must be equal to the momentum of the fluid going out at location $x + dx$. Consequently, the only *net* momentum flux in and out of the element is that due to the

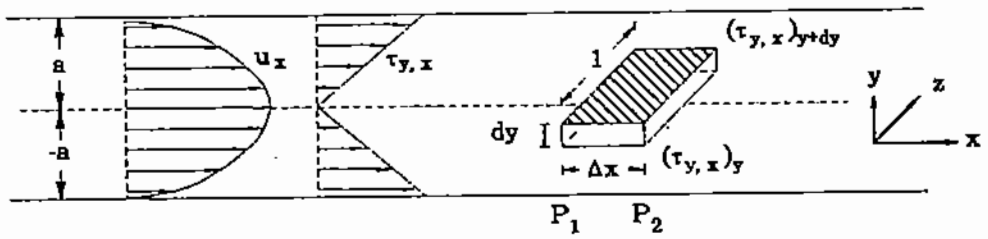

Figure 4.1. Velocity profile in flow between parallel plates.

viscous shear stress, $\tau_{y,x}$, acting between adjacent layers of fluid in the direction y, due to the gradient of the velocity u_x with respect to y.

To calculate the *transport rate of momentum* which we need for (4.1.2), we must multiply the momentum flux due to shear stress by the area over which the shear stress acts, here the sides $dx \cdot dz$ of the volume element.

Also, let us assume that the force acting on the fluid element and in the x-direction, F_x, is a *body force* such as gravity which is proportional to the mass of the element; therefore, it is expressed in terms of *force/unit volume*.

By substituting the above mathematical expressions in the statement of (4.1.2) we obtain the following momentum balance for the differential volume element $dx \cdot dy \cdot dz$:

$$[(\tau_{y,x})_{y+dy} - (\tau_{y,x})_y]\,(dx\,dz) = F_x(dx\,dy\,dz). \tag{4.1.3}$$

However, by mathematical definition,

$$(\tau_{y,x})_{y+dy} = (\tau_{y,x})_y + \frac{d\tau_{y,x}}{dy}\,dy. \tag{4.1.4}$$

By substituting from the above identity in (4.1.3), eliminating the two redundant terms and dividing both sides of the equation by $dx \cdot dy \cdot dz$, we obtain the following equation:

$$\frac{d\tau_{y,x}}{dy} = F_x, \tag{4.1.5}$$

and by replacing the shear stress by Newton's law of viscosity (3.1.3), we obtain

$$-\mu\frac{d^2u_x}{dy^2} = F_x. \tag{4.1.6}$$

The solution of the above second-order ordinary differential equation requires two boundary conditions. Therefore, it is necessary to specify the velocity or the velocity gradient at two of the appropriate bounding surfaces. In the simple problems to be discussed in this chapter, the only forces acting on the control volume element are the *gravity force* acting on its volume and the *pressure force* acting on some of its surfaces.

It must be noted that the formulations and solutions to be presented in this section are valid only for situations where the flow is **laminar**. The differences between laminar and **turbulent** flows will be discussed in Chapter 7.

4.2. LAMINAR FLOW BETWEEN PARALLEL PLATES

We first consider the simplest possible case of unidirectional fluid flow, in the x-direction, between two horizontal infinite parallel plates separated by a distance $2a$ (Fig. 4.1). For convenience, in this case we select the control volume to be of unit width (i.e., $dz = 1$), of a small finite length Δx (in the x direction), and of infinitesimal height dy (in the y direction).

Since the fluid flow is in the horizontal direction, the only force acting on the fluid in this case is due to the pressure differential $P_1 - P_2$ (i.e., $-\Delta P$) across the length Δx of the control volume. Pressure has the dimensions of force/area and the *net pressure force* (literally the force due to pressure) acting on the control volume of Fig. 4.1 is obtained by multiplying the pressure difference, $-\Delta P$, by the surface area over which $-\Delta P$ acts, i.e., the sides $1 \cdot dy$ of the control element which are perpendicular to the direction of flow:

$$\text{net force} = -\Delta P(1 \cdot dy). \tag{4.2.1}$$

As discussed in §4.1, the change of rate of momentum within the control volume is equal to momentum flux leaving the control volume across the $y + dy$ plane minus the momentum entering the control volume at the y plane times the area of the sides $1 \cdot \Delta x$ of the control volume. By equating this change in rate of momentum to the pressure force (see (4.1.3)) we obtain

$$\left[(\tau_{y,x})_{y+dy} - (\tau_{y,x})_y\right](1 \cdot \Delta x) = -\Delta P(1 \cdot dy), \tag{4.2.2}$$

which, on the basis of (4.1.4), can be simplified to

$$\frac{d\tau_{y,x}}{dy} = -\frac{\Delta P}{\Delta x}. \tag{4.2.3}$$

Finally, by substituting for the shear stress from Newton's law of viscosity (see (3.1.3)) we obtain an equation which relates the velocity distribution between the two plates to the fluid viscosity and the net force acting on the fluid:

$$\mu \frac{d^2 u_x}{dy^2} = \frac{\Delta P}{\Delta x}. \tag{4.2.4}$$

In order to solve this differential equation, we need two boundary conditions. These are supplied by considering that the fluid velocity next to the two plates is zero:

$$u_x = 0 \text{ at } y = \pm a.$$

By integrating (4.2.4) for the above boundary conditions we obtain

$$u_x = -\frac{1}{2\mu} \frac{\Delta P}{\Delta x}(a^2 - y^2). \tag{4.2.5}$$

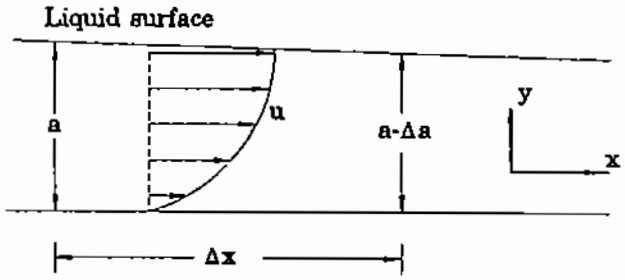

Figure 4.2. Velocity profile in open channel flow.

The parabolic velocity profile expressed by (4.2.5) is plotted in Fig. 4.1. It can be seen that the velocity has its maximum value at $y = 0$ and at that point, $du_x/dy = 0$.

4.3. FLOW IN AN OPEN CHANNEL

We now consider fluid flow in a section of a horizontal open channel (Fig. 4.2) of liquid depth a, and of sufficient width (in the z direction, $\Delta z = 1$) so that edge or corner effects may be neglected. In this case, flow occurs because liquid is added at one end of the channel (left of Fig. 4.2) and removed, at the same rate, at the other end; thus, a surface level gradient is established across the length of the channel and causes flow. By equating the change of momentum to the net driving force, as in the previous example, we obtain

$$\mu \frac{d^2 u_x}{dy^2} = \rho g \frac{\Delta a}{\Delta x}, \tag{4.3.1}$$

where $\Delta a/\Delta x$ is the change in liquid depth with distance x along the length of the channel. In this case, the boundary conditions are obtained from consideration of the following physical facts:

a. The velocity is zero at the bottom surface of the channel, i.e., $u_x = 0$ at $y = 0$.
b. Because the air viscosity, above the liquid surface, is negligible in comparison to that of the liquid, the shear stress transmitted at the free surface of the channel can be neglected; therefore

$$\frac{du_x}{dy} = 0 \text{ at } y = 1$$

By integrating (4.3.1) for the above boundary conditions, we obtain

$$u_x = -\frac{\rho g}{2\mu} \frac{\Delta a}{\Delta x}(2ay - y^2). \tag{4.3.2}$$

As illustrated in Fig. 4.2, the resulting velocity profile is parabolic and the maximum velocity occurs at the free surface of the liquid.

4.4. FLOW OF A FLUID ON AN INCLINED PLATE

We now consider the flow of a fluid under the force of gravity, along an inclined flat plate placed at an angle to the horizontal plane (Fig. 4.3). The only force acting on the fluid, in

this case, is gravity. By establishing a control volume, $1 \cdot \Delta x \cdot dy$, as in the previous two examples, we obtain

$$[(\tau_{y,x})_{y+dy} - (\tau_{y,x})_y](1 \cdot \Delta x) = \rho g \sin\alpha (1 \cdot \Delta x\, dy), \tag{4.4.1}$$

$$\therefore \quad \frac{d\tau_{y,x}}{dy} = \rho g \sin\alpha, \tag{4.4.2}$$

where $\rho g \sin\alpha$ represents the gravitational force in the direction x parallel to the plate. By substituting from Newton's law of viscosity (equation (3.1.3)), we obtain

$$-\mu \frac{d^2 u_x}{dy^2} = \rho g \sin\alpha. \tag{4.4.3}$$

The boundary conditions for this equation are: $u_x = 0$ at $y = 0$ (zero velocity of fluid at the plate surface) and

$$\frac{du_x}{dy} = 0 \text{ at } y = a,$$

i.e., the velocity gradient at the surface of the liquid ($y = a$) is zero. Integration of (4.4.3) for these boundary conditions yields:

$$u_x = \frac{\rho g \sin\alpha}{2\mu}(2ay - y^2), \tag{4.4.4}$$

which shows that the maximum fluid velocity occurs at $y = a$ and its value is

$$u_{\max} = \frac{\rho g \sin\alpha}{2\mu} a^2. \tag{4.4.5}$$

Since the flow is assumed to be unidirectional, the average velocity over the depth of the film is expressed as follows:

$$u_{\text{ave}} = \frac{1}{a} \int_{y=0}^{y=a} u_x\, dy, \tag{4.4.6}$$

and by substituting for u_x from (4.4.4) and integrating:

$$u_{\text{ave}} = \frac{\rho g \sin\alpha}{3\mu} a^2. \tag{4.4.7}$$

The average thickness of the film, a, will depend on the flow rate of liquid per unit width at the top of the inclined plate. Its value can be obtained by dividing the volumetric flow rate per unit width of the plate by the average flow velocity (equation (4.4.7)). Alternatively, if

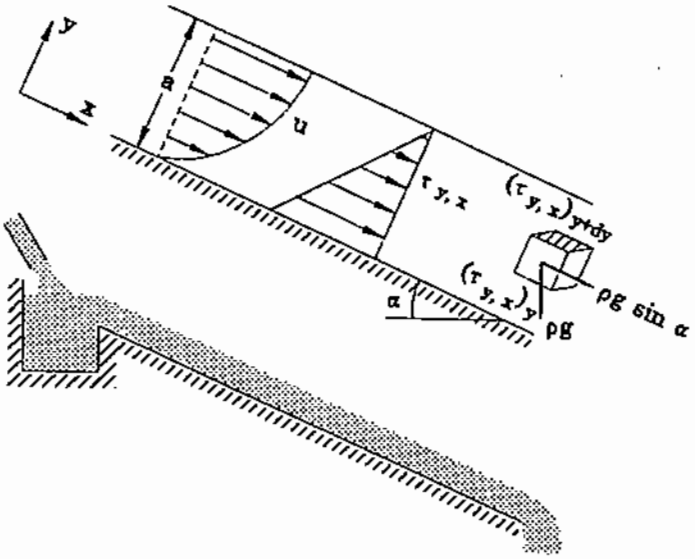

Figure 4.3. Velocity profile in flow over an inclined plate.

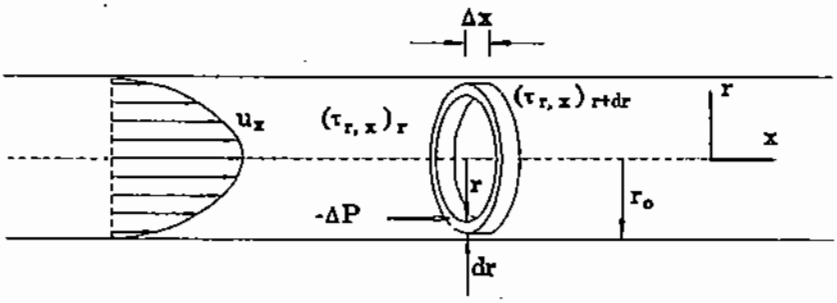

Figure 4.4. Velocity profile in a cylindrical conduit.

the thickness of the film can be measured, the volumetric flow rate and the average velocity can be calculated from it.

4.5. FLOW THROUGH A CYLINDRICAL CONDUIT

We now consider the laminar flow of a fluid through a horizontal cylindrical tube of radius r_0. In this case, the control volume is assumed to be a cylindrical shell of radius r, of infinitesimal thickness dr and of finite length Δx (Fig. 4.4). As in the previous cases, the differential change of momentum is expressed by the product of the shear stress times the surface area over which this stress acts:

$$d\left[\tau_{r,x}(2\pi r\,\Delta x)\right].$$

Also, the net force acting on the control volume is pressure difference $-\Delta P$ along finite length Δx times the cross-sectional area of the element perpendicular to the direction of flow:

$$-\Delta P\,(2\pi r\,dr).$$

By equating the change of transport rate of momentum to the net acting force, we obtain

$$d(r\tau_{r,x})(2\pi\,\Delta x) = -\Delta P(2\pi r\,dr). \tag{4.5.1}$$

or

$$\frac{d(r\tau_{r,x})}{dr} = -\frac{\Delta P}{\Delta x}\,r. \tag{4.5.2}$$

We now replace the shear stress in the above equation by Newton's law of viscosity (see (3.1.3))

$$\tau_{r,x} = -\mu\,\frac{du_x}{dr} \tag{4.5.3}$$

to obtain

$$\frac{d}{dr}\left(r\mu\,\frac{du_x}{dr}\right) = \frac{\Delta P}{\Delta x}\,r, \tag{4.5.4}$$

which is then integrated to yield

$$\frac{du_x}{dr} = \frac{1}{2\mu}\,\frac{\Delta P}{\Delta x}r + \frac{C_1}{\mu r}, \tag{4.5.5}$$

and

$$u_x = \frac{1}{4\mu}\,\frac{\Delta P}{\Delta x}r^2 + \frac{C_1}{\mu}\ln r + C_2, \tag{4.5.6}$$

where C_1 and C_2 are integration constants. Their values can be determined on the basis of the following considerations:

a. velocity is zero at the wall of the conduit, i.e., $u_x = 0$ at $r = r_0$;
b. as in the case of flow between parallel plates (§4.2), the velocity has its maximum value at the center; therefore $du_x/dr = 0$ at $r = 0$ and $C_1 = 0$ (see (4.5.5)).

From (4.5.6) and boundary condition a, we also conclude that

$$C_1 = 0 \text{ and } C_2 = -\frac{r_0^2}{4\mu}\,\frac{\Delta P}{\Delta x}.$$

Therefore, the velocity profile in a cylindrical conduit is expressed by

$$u_x = -\frac{1}{4\mu}\,\frac{\Delta P}{\Delta x}(r_0^2 - r^2). \tag{4.5.7}$$

It can be seen that the velocity profile is parabolic with distance from the center of the conduit and that the maximum velocity occurs at the center ($r = 0$):

$$u_{x,\max} = -\frac{r_0^2}{4\mu}\,\frac{\Delta P}{\Delta x}. \tag{4.5.8}$$

The volumetric flow rate in the conduit can be calculated by integrating the product of the velocity (equation (4.5.7)) and the differential cross-sectional area of flow corresponding to dr:

$$\dot{v} = \int_0^{r_0} u_x(2\pi r\,dr) = -\frac{\pi r_0^4}{8\mu}\,\frac{\Delta P}{\Delta x}. \tag{4.5.9}$$

The above equation is frequently referred to as the *Hagen-Poiseuille equation.*

The average velocity in the conduit is obtained by dividing the volumetric flow rate by the cross-sectional area available for flow:

$$u_{\text{ave}} = \frac{\dot{v}}{\pi r_0^2} = -\frac{r_0^2}{8\mu}\frac{\Delta P}{\Delta x}. \tag{4.5.10}$$

As noted above, finite pressure gradient $-\Delta P/\Delta x$ in the above equations represents the change in pressure along length L of the conduit:

$$-\frac{\Delta P}{\Delta x} = \frac{P_1 - P_2}{L},$$

where P_1 and P_2 are the corresponding pressures at the beginning and end of L.

FIVE

The Differential Equations of Flow

In Chapter 4, we used Newton's law of conservation of energy and the definition of viscosity to determine the velocity distribution in steady-state, unidirectional flow through a conduit. In this chapter, we shall examine the application of the same laws in the general case of three-dimensional, unsteady state flow. We will do so by developing and solving the *differential equations of flow*. These equations are very useful when detailed information on a flow system is required, such as the velocity, temperature and concentration profiles.

The differential equations of flow are derived by considering a differential volume element of fluid and describing mathematically

a. the conservation of mass of fluid entering and leaving the control volume; the resulting mass balance is called the **equation of continuity**.
b. the conservation of momentum entering and leaving the control volume; this energy balance is called the **equation of motion**.

In describing the momentum of a fluid, we should note that in the case of a solid body, its mass is readily defined and has the dimension M; the same is true for its momentum which has the dimensions of M L t^{-1}. However, in the case of a fluid, we are dealing with a continuum and the only way to define mass at any given location is in terms of **mass flux**, i.e., mass transport rate per unit cross-sectional area through which flow occurs. This quantity is equal to the product of density of the fluid times its velocity (ρu) and has the dimensions of M t^{-1} L^{-2}. For the same reasons, the momentum of a fluid is expressed in terms of **momentum flux** ($\rho u\, u$), i.e., the transport rate of momentum per unit cross-sectional area (M t^{-2} L^{-1}).

In three-dimensional flow, the mass flux has three components (x, y, and z) and the velocity also three (u_x, u_y, and u_z); therefore, in order to express momentum, we need to consider a total of nine terms.

5.1. THE EQUATION OF CONTINUITY

We consider an infinitesimal cubical element $dx \cdot dy \cdot dz$ (Fig. 5.1) in the three-dimensional flow of a fluid in a vessel. The mass conservation of fluid passing through this element is stated as follows:

$$\begin{aligned} &\text{rate of mass accumulation within element} \\ &\quad = \text{transport rate of mass in} \\ &\quad - \text{transport rate of mass out.} \end{aligned} \tag{5.1.1}$$

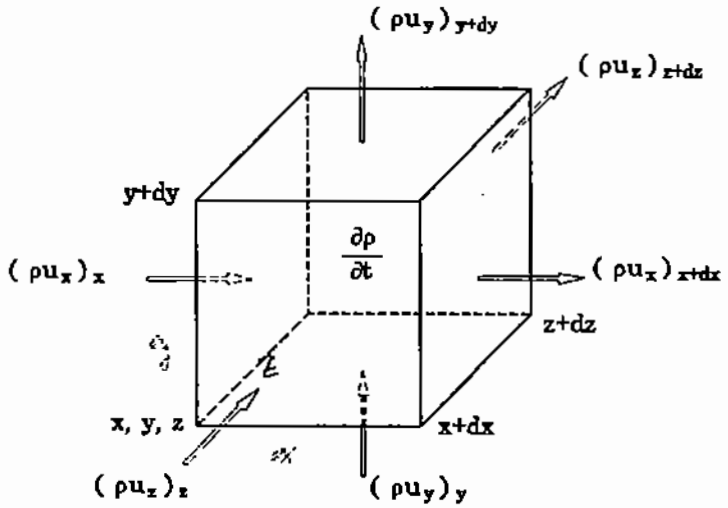

Figure 5.1. Material balance on a cubical control element.

The transport rate of mass into the element at location x and through the face $dy \cdot dz$ of the element is equal to

$$\text{mass flux of fluid in } x\text{-direction} \times \text{surface area of face } dy \cdot dz,$$

i.e.,

$$(\rho u_x)_x (dy\, dz). \tag{5.1.2}$$

Similarly, the transport rate of mass out of the element at location $x + dx$ and through face $dy \cdot dz$ is expressed by

$$(\rho u_x)_{x+dx}(dy\, dz) \equiv \left[(\rho u_x)_x + \frac{\partial \rho u_x}{\partial x}\, dx\right] (dy\, dz). \tag{5.1.3}$$

The only way that mass can be accumulated (or depleted) within the control volume is by a corresponding change in the fluid density. Mathematically, the rate of accumulation is expressed as follows:

$$\frac{\partial \rho}{\partial t}(dx\, dy\, dz). \tag{5.1.4}$$

By substituting from (5.1.2)–(5.1.4) into conservation equation (5.1.1) and eliminating redundant terms, we obtain

$$\frac{\partial \rho}{\partial t} = -\frac{\partial \rho u_x}{\partial x}. \tag{5.1.5}$$

In the above derivation, we used partial differentials because we dealt only with the x-component of velocity. Of course, the same considerations apply to the y- and z-components. Therefore, the *general equation of continuity* in three-dimensional flow is expressed as follows:

$$\frac{\partial \rho}{\partial t} = -\left(\frac{\partial \rho u_x}{\partial x} + \frac{\partial \rho u_y}{\partial y} + \frac{\partial \rho u_z}{\partial z}\right), \tag{5.1.6}$$

or in abbreviated vector notation

$$\frac{\partial \rho}{\partial t} = -\nabla \cdot \rho u, \tag{5.1.7}$$

where $\boldsymbol{u}$ is the velocity vector and $\nabla \cdot \rho\boldsymbol{u}$ is called the divergence of quantity $\rho\boldsymbol{u}$.

By differentiating the product terms on the right-hand side of (5.1.6) and then collecting all derivatives of density on the left-hand side, we obtain:

$$\frac{\partial \rho}{\partial t} + u_x\frac{\partial \rho}{\partial x} + u_y\frac{\partial \rho}{\partial y} + u_z\frac{\partial \rho}{\partial z} = -\rho\left(\frac{\partial u_x}{\partial x} + \frac{\partial u_y}{\partial y} + \frac{\partial u_z}{\partial z}\right). \tag{5.1.8}$$

The left side of (5.1.8) is called the **substantial time derivative** of density. In a physical sense, the substantial time derivative of a quantity designates its time derivative (i.e., rate of change) evaluated along a path that follows the motion of the fluid (*streamline*, Chapter 6). In general terms, the substantial time derivative of a variable w is defined by the following expression:

$$\frac{D(w)}{Dt} = \frac{\partial w}{\partial t} + u_x\frac{\partial w}{\partial x} + u_y\frac{\partial w}{\partial y} + u_z\frac{\partial w}{\partial z}. \tag{5.1.9.}$$

Therefore, (5.1.8) can be expressed in abbreviated vector notation as follows:

$$\frac{D\rho}{Dt} = -\rho\nabla \cdot \boldsymbol{u}. \tag{5.1.10}$$

Equations (5.1.8) and (5.1.10) describe the rate of change of density as observed by someone who is moving along with the fluid. For steady state conditions, there is no mass accumulation and the equation of continuity becomes

$$\frac{\partial \rho u_x}{\partial x} + \frac{\partial \rho u_y}{\partial y} + \frac{\partial \rho u_z}{\partial z} = 0, \tag{5.1.11}$$

and for an incompressible fluid (i.e., for negligible variation in density of fluid)

$$\frac{\partial u_x}{\partial x} + \frac{\partial u_y}{\partial y} + \frac{\partial u_z}{\partial z} = 0. \tag{5.1.12}$$

5.2. THE EQUATION OF MOTION

To develop the equation of motion, we start from Newton's law of conservation of energy:

$$\begin{aligned} &\text{rate of momentum accumulation} \\ &\quad = \text{transport rate of momentum in} \\ &\quad - \text{transport rate of momentum out} \\ &\quad + \text{sum of forces acting on element.} \end{aligned} \tag{5.2.1}$$

In order to express this equation mathematically, we must consider that momentum is transported in and out of the element in two ways:

a. *convective transport of momentum* is by means of the kinetic energy of the fluid mass moving in and out of the six faces of our cubical element. Thus, the convective transport of momentum in the x-direction (x-momentum) consists of three terms:

$$(\rho u_x)u_x,\ (\rho u_y)u_x,\ (\rho u_z)u_x.$$

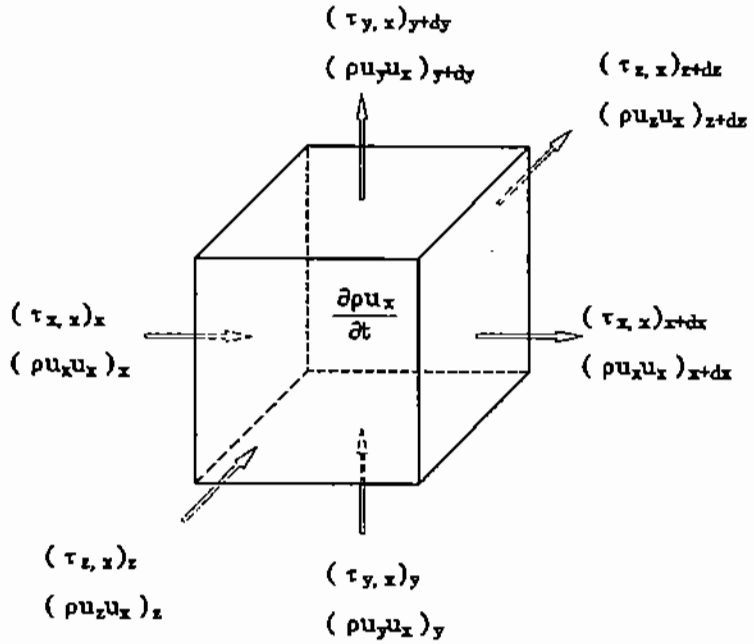

Figure 5.2. Mechanical energy balance on a cubical control element.

The **net** convective transport of x-momentum through the faces $dy \cdot dz$ of the cubical element $dx \cdot dy \cdot$ dz (Fig. 5.2) is

$$[(\rho u_x)u_x - (\rho u_x)u_{x+dx}]\,(dy\,dz) = -\frac{\partial \rho u_x u_x}{\partial x}\,(dx\,dy\,dz). \tag{5.2.2}$$

Similarly, the net convective transport of x-momentum through the faces $dx \cdot dz$ and $dx \cdot dy$ of the element is represented by terms

$$-\frac{\partial \rho u_y u_x}{\partial y}(dx\,dy\,dz), \tag{5.2.3}$$

$$-\frac{\partial \rho u_z u_x}{\partial z}(dx\,dy\,dz), \tag{5.2.4}$$

Of course, there are six more symmetrical terms for convective transport of momentum in the y- and z-directions of flow.

b. *diffusive transport of momentum* also takes place at the six surfaces of the cubical element (Fig. 5.2) by means of the viscous shear stresses. Thus, the *net* diffusive transport of momentum in the x-direction through the faces $dy \cdot dz$ of the element is

$$[(\tau_{x,x})_x - (\tau_{x,x})_{x+dx}]\,(dy\,dz) = -\frac{\partial \tau_{x,x}}{\partial x}(dx\,dy\,dz). \tag{5.2.5}$$

Similarly, the net diffusive transport of momentum in the x-direction through the faces $dx \cdot dz$ and $dx \cdot dy$ is expressed by terms

$$-\frac{\partial \tau_{y,x}}{\partial y}(dx\,dy\,dz), \tag{5.2.6}$$

$$-\frac{\partial \tau_{z,x}}{\partial z}(dx\,dy\,dz). \tag{5.2.7}$$

There are six more symmetrical terms for diffusive transport of momentum in the y- and z-directions of flow.

We now consider the forces acting on the control volume of Fig. 5.2. The *net* pressure force acting on the faces $dy \cdot dz$ of the element (i.e., the faces normal to the x-direction) is

$$(P_x - P_{x+dx})(dy\,dz) = -\frac{\partial P}{\partial x}(dx\,dy\,dz). \tag{5.2.8}$$

There are two more symmetrical terms for the pressure on the faces $dx \cdot dz$ and $dx \cdot dy$ of the element.

The other force acting on the element is gravity; this is a *body force* and is equal to the density of the fluid times the volume of the element (i.e., its mass) times the gravitational acceleration. In the x-direction, the gravity force is expressed as follows:

$$(\rho g_x)(dx\,dy\,dz), \tag{5.2.9}$$

where g_x is the component of the gravitational acceleration in the x-direction. There are two more symmetrical terms for the g_y and the g_z components of gravity.

In developing equation of continuity (5.1.6), we showed that the rate of accumulation of mass in the control element was equal to the time differential of density times the volume of the element. Similarly, the rate of accumulation of momentum in the x-direction is expressed by

$$\frac{\partial \rho u_x}{\partial t}(dx\,dy\,dz). \tag{5.2.10}$$

There are two more symmetrical terms for the y- and z-directions of momentum.

We now have mathematical expressions for all the terms of (5.2.1). By substitution and elimination of redundant terms, we obtain the following equation for the equation of motion in the x-direction of momentum:

$$\begin{aligned}\frac{\partial \rho u_x}{\partial t} = &-\left(\frac{\partial \rho u_x u_x}{\partial x} + \frac{\partial \rho u_y u_x}{\partial y} + \frac{\partial \rho u_z u_x}{\partial z}\right) \\ &-\left(\frac{\partial \tau_{x,x}}{\partial x} + \frac{\partial \tau_{y,x}}{\partial y} + \frac{\partial \tau_{z,x}}{\partial z}\right) - \frac{\partial P}{\partial x} + \rho g_x;\end{aligned} \tag{5.2.11}$$

in the y-direction of momentum:

$$\begin{aligned}\frac{\partial \rho u_y}{\partial t} = &-\left(\frac{\partial \rho u_x u_y}{\partial x} + \frac{\partial \rho u_y u_y}{\partial y} + \frac{\partial \rho u_z u_y}{\partial z}\right) \\ &-\left(\frac{\partial \tau_{x,y}}{\partial x} + \frac{\partial \tau_{y,y}}{\partial y} + \frac{\partial \tau_{z,y}}{\partial z}\right) - \frac{\partial P}{\partial y} + \rho g_y,\end{aligned} \tag{5.2.12}$$

and in the z-direction of momentum:

$$\begin{aligned}\frac{\partial \rho u_z}{\partial t} = &-\left(\frac{\partial \rho u_x u_z}{\partial x} + \frac{\partial \rho u_y u_z}{\partial y} + \frac{\partial \rho u_z u_z}{\partial z}\right) \\ &-\left(\frac{\partial \tau_{x,z}}{\partial x} + \frac{\partial \tau_{y,z}}{\partial y} + \frac{\partial \tau_{z,z}}{\partial z}\right) - \frac{\partial P}{\partial z} + \rho g_z.\end{aligned} \tag{5.2.13}$$

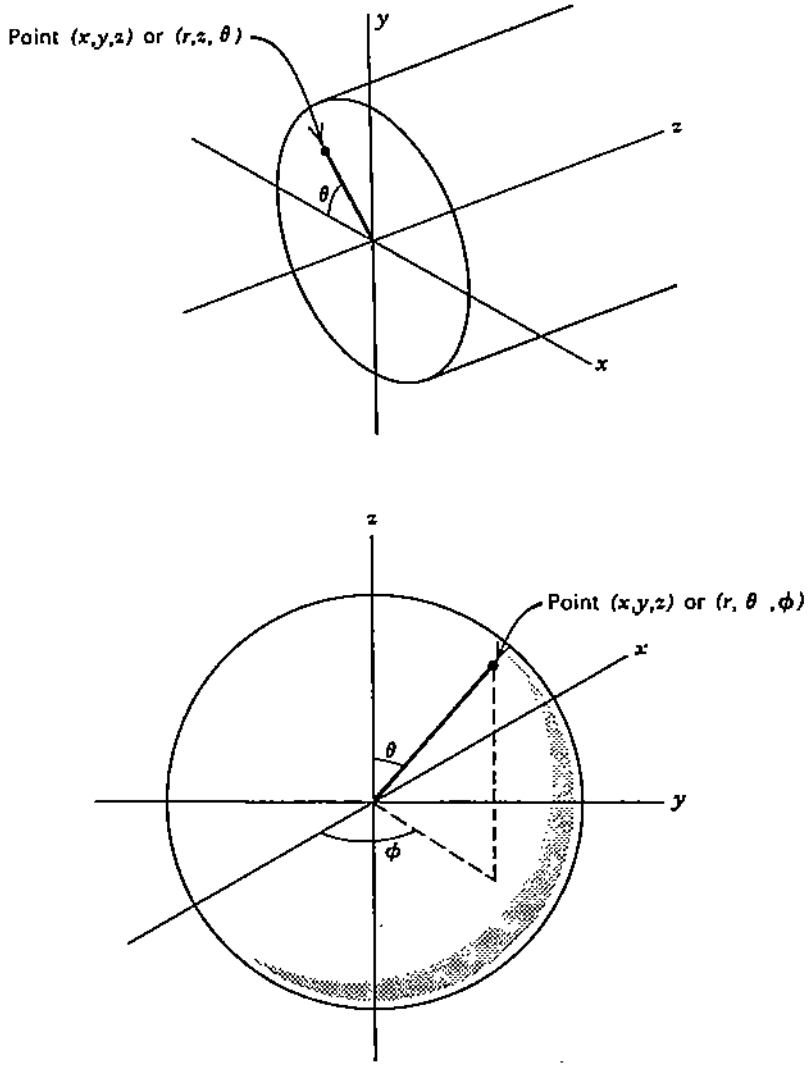

Figure 5.3. Cylindrical and spherical coordinates.

The above equations of motion can be expressed more conveniently in vector notation as

$$\frac{\partial \rho \boldsymbol{u}}{\partial t} = -\nabla \cdot \rho \boldsymbol{u}\boldsymbol{u} - \nabla \cdot \boldsymbol{\tau} - \nabla P + \rho \boldsymbol{g}, \tag{5.2.14}$$

where the bold type indicates vector quantities. It should be noted that if, in addition to gravity, there were other "body" forces acting on the fluid (e.g., an electromagnetic force), their effect would be added to the gravitational components.

The vectorial shear stress in (5.2.14) represents six **shear stresses** (i.e., acting in the direction of flow) and three **normal stresses** (i.e., compressive or tensile stresses normal to the direction of flow). Mathematically, these stresses are expressed as follows (3):

Shear stresses:

$$\tau_{x,y} = \tau_{y,x} = -\mu\left(\frac{\partial u_x}{\partial y} + \frac{\partial u_y}{\partial x}\right),$$
$$\tau_{y,z} = \tau_{z,y} = -\mu\left(\frac{\partial u_y}{\partial z} + \frac{\partial u_z}{\partial y}\right),$$
$$\tau_{z,x} = \tau_{x,z} = -\mu\left(\frac{\partial u_z}{\partial x} + \frac{\partial u_x}{\partial z}\right).$$

Normal stresses:

$$\tau_{x,x} = -\mu\left(2\frac{\partial u_x}{\partial x} - \frac{2}{3}\nabla \cdot \boldsymbol{u}\right),$$
$$\tau_{y,y} = -\mu\left(2\frac{\partial u_y}{\partial y} - \frac{2}{3}\nabla \cdot \boldsymbol{u}\right), \tag{5.2.15}$$
$$\tau_{z,z} = -\mu\left(2\frac{\partial u_z}{\partial z} - \frac{2}{3}\nabla \cdot \boldsymbol{u}\right).$$

For an *incompressible* flow (i.e., when changes in density are negligible), we can differentiate each component of convective momentum in the equation of motion (5.2.11)–(5.2.13) as follows:

$$\frac{\partial \rho u_x u_y}{\partial x} = \rho u_x \frac{\partial u_y}{\partial x} + \rho u_y \frac{\partial u_x}{\partial x}. \tag{5.2.16}$$

By eliminating the following terms (see (5.1.12))

$$\rho u_y \left(\frac{\partial u_x}{\partial x} + \frac{\partial u_y}{\partial y} + \frac{\partial u_z}{\partial z}\right) = 0,$$

and moving the remaining convective momentum terms to the left-hand side of (5.2.11)–(5.2.13), we obtain the following simplified equation for the x-momentum balance:

$$\rho\left(\frac{\partial u_x}{\partial t} + u_x\frac{\partial u_x}{\partial x} + u_y\frac{\partial u_x}{\partial y} + u_z\frac{\partial u_x}{\partial z}\right) = -\left(\frac{\partial \tau_{x,x}}{\partial x} + \frac{\partial \tau_{y,x}}{\partial y} + \frac{\partial \tau_{z,x}}{\partial z}\right) - \frac{\partial P}{\partial x} + \rho g_x. \tag{5.2.17}$$

The left-hand side of (5.2.17) will be recognized by the reader as the *substantial time derivative of velocity*, as defined earlier (equation (5.1.8)). Therefore, (5.2.17) for all three dimensions is expressed as follows in vector notation:

$$\rho\frac{D\boldsymbol{u}}{Dt} = -\nabla \cdot \boldsymbol{\tau} - \nabla P + \rho \boldsymbol{g}. \tag{5.2.18}$$

Table 5.1 shows the general equations of motion for incompressible flow in the three principal coordinate systems: rectangular, cylindrical and spherical. The angles shown in the last two systems are defined in Fig. 5.3. It can be seen that the complexity of these equations increases from rectangular to spherical coordinates. The reason is obvious: In rectangular coordinates, the cross-sectional area of flow does not change in all three dimensions; in cylindrical coordinates, this area does not change in the z-dimension; and in spherical, the cross-sectional area of flow changes in all three dimensions.

Table 5.1. General Equations of Motion

Rectangular coordinates, (x, y, z):

$$\rho\left(\frac{\partial u_x}{\partial t}+u_x\frac{\partial u_x}{\partial x}+u_y\frac{\partial u_x}{\partial y}+u_z\frac{\partial u_x}{\partial z}\right)=-\left(\frac{\partial \tau_{x,x}}{\partial x}+\frac{\partial \tau_{y,x}}{\partial y}+\frac{\partial \tau_{z,x}}{\partial z}\right)-\frac{\partial P}{\partial x}+\rho g_x,$$

$$\rho\left(\frac{\partial u_y}{\partial t}+u_x\frac{\partial u_y}{\partial x}+u_y\frac{\partial u_y}{\partial y}+u_z\frac{\partial u_y}{\partial z}\right)=-\left(\frac{\partial \tau_{x,y}}{\partial x}+\frac{\partial \tau_{y,y}}{\partial y}+\frac{\partial \tau_{z,y}}{\partial z}\right)-\frac{\partial P}{\partial y}+\rho g_y,$$

$$\rho\left(\frac{\partial u_z}{\partial t}+u_x\frac{\partial u_z}{\partial x}+u_y\frac{\partial u_z}{\partial y}+u_z\frac{\partial u_z}{\partial z}\right)=-\left(\frac{\partial \tau_{x,z}}{\partial x}+\frac{\partial \tau_{y,z}}{\partial y}+\frac{\partial \tau_{z,z}}{\partial z}\right)-\frac{\partial P}{\partial z}+\rho g_z,$$

Cylindrical coordinates, (r, θ, z):

$$\rho\left(\frac{\partial u_r}{\partial t}+u_r\frac{\partial u_r}{\partial r}+\frac{u_\theta}{r}\frac{\partial u_r}{\partial \theta}-\frac{u_\theta^2}{r}+u_z\frac{\partial u_r}{\partial z}\right)=-\left(\frac{1}{r}\frac{\partial(r\tau_{r,r})}{\partial r}+\frac{1}{r}\frac{\partial \tau_{r,\theta}}{\partial \theta}-\frac{\tau_{\theta,\theta}}{r}+\frac{\partial \tau_{r,z}}{\partial z}\right)-\frac{\partial P}{\partial r}+\rho g_r,$$

$$\rho\left(\frac{\partial u_\theta}{\partial t}+u_r\frac{\partial u_\theta}{\partial r}+\frac{u_\theta}{r}\frac{\partial u_\theta}{\partial \theta}+\frac{u_r u_\theta}{r}+u_z\frac{\partial u_\theta}{\partial z}\right)=-\left(\frac{1}{r^2}\frac{\partial(r^2\tau_{r,\theta})}{\partial r}+\frac{1}{r}\frac{\partial \tau_{\theta,\theta}}{\partial \theta}+\frac{\partial \tau_{\theta,z}}{\partial z}\right)-\frac{1}{r}\frac{\partial P}{\partial \theta}+\rho g_\theta,$$

$$\rho\left(\frac{\partial u_z}{\partial t}+u_r\frac{\partial u_z}{\partial r}+\frac{u_\theta}{r}\frac{\partial u_z}{\partial \theta}+u_z\frac{\partial u_z}{\partial z}\right)=-\left(\frac{1}{r}\frac{\partial(r\tau_{r,z})}{\partial r)}+\frac{1}{r}\frac{\partial \tau_{\theta,z}}{\partial \theta}+\frac{\partial \tau_{z,z}}{\partial z}\right)-\frac{\partial P}{\partial z}+\rho g_z.$$

Spherical coordinates, (r, θ, ϕ):

$$\rho\left(\frac{\partial u_r}{\partial t}+u_r\frac{\partial u_r}{\partial r}+\frac{u_\theta}{r}\frac{\partial u_r}{\partial \theta}+\frac{u_\phi}{r\sin\theta}\frac{\partial u_r}{\partial \phi}-\frac{u_\theta^2+u_\phi^2}{r}\right)$$

$$=-\left(\frac{1}{r^2}\frac{\partial}{\partial r}(r^2\tau_{r,r})+\frac{1}{r\sin\theta}\frac{\partial}{\partial \theta}(\tau_{r\theta}\sin\theta)+\frac{1}{r\sin\theta}\frac{\partial \tau_{r,\phi}}{\partial \phi}-\frac{\tau_{\theta,\theta}+\tau_{\phi,\phi}}{r}\right)-\frac{\partial P}{\partial r}+\rho g_r,$$

$$\rho\left(\frac{\partial u_\theta}{\partial t}+u_r\frac{\partial u_\theta}{\partial r}+\frac{u_\theta}{r}\frac{\partial u_\theta}{\partial \theta}+\frac{u_\phi}{r\sin\theta}\frac{\partial u_\theta}{\partial \phi}+\frac{u_r u_\theta}{r}-\frac{u_\phi^2\cot\theta}{r}\right)$$

$$=-\left(\frac{1}{r^2}\frac{\partial}{\partial r}(r^2\tau_{r,\theta})+\frac{1}{r\sin\theta}\frac{\partial}{\partial \theta}(\tau_{\theta,\theta}\sin\theta)+\frac{1}{r\sin\theta}\frac{\partial \tau_{\theta,\phi}}{\partial \phi}+\frac{\tau_{r,\theta}}{r}-\frac{\cot\theta}{r}\tau_{\phi,\phi}\right)-\frac{1}{r}\frac{\partial P}{\partial \theta}+\rho g_\theta,$$

$$\rho\left(\frac{\partial u_\phi}{\partial t}+u_r\frac{\partial u_\phi}{\partial r}+\frac{u_\theta}{r}\frac{\partial u_\phi}{\partial \theta}+\frac{u_\phi}{r\sin\theta}\frac{\partial u_\phi}{\partial \phi}+\frac{u_\phi u_r}{r}+\frac{u_\theta u_\phi\cot\theta}{r}\right)$$

$$=-\left(\frac{1}{r^2}\frac{\partial}{\partial r}(r^2\tau_{r,\phi})+\frac{1}{r}\frac{\partial \tau_{\theta,\phi}}{\partial \phi}+\frac{1}{r\sin\theta}\frac{\partial \tau_{\phi,\phi}}{\partial \phi}+\frac{\tau_{r,\phi}}{r}+\frac{2\cot\theta}{r}\tau_{\theta,\phi}\right)-\frac{1}{r\sin\theta}\frac{\partial P}{\partial \phi}+\rho g_\phi.$$

For incompressible Newtonian fluids at constant viscosity, the general equations of motion can be simplified further by replacing the shear stress functions by Newton's law of viscosity. Thus, (5.2.17) becomes

$$\rho\left(\frac{\partial u_x}{\partial t}+u_x\frac{\partial u_x}{\partial x}+u_y\frac{\partial u_x}{\partial y}+u_z\frac{\partial u_x}{\partial z}\right)= \mu\left(\frac{\partial^2 u_x}{\partial x^2}+\frac{\partial^2 u_x}{\partial y^2}+\frac{\partial^2 u_x}{\partial z^2}\right)-\frac{\partial P}{\partial x}+\rho g_x. \tag{5.2.19}$$

This equation, and the symmetric equations for the y- and z-components of momentum, are called the *Navier–Stokes equations* of flow. In vector notation, they are expressed as:

$$\rho\frac{D\boldsymbol{u}}{Dt}=\mu\nabla^2\boldsymbol{u}-\nabla P+\rho\boldsymbol{g}. \tag{5.2.20}$$

In cases where the viscous effects can be considered to be negligible, the Navier–Stokes equations may be written as follows:

$$\rho\frac{D\boldsymbol{u}}{Dt}=-\nabla P+\rho\boldsymbol{g}. \tag{5.2.21}$$

This equation is known as the *Euler equation*. In the case of very slow motion, such as the flow of glass in a melting furnace, the inertia terms in the Navier–Stokes equations may be neglected to yield:

$$\nabla P=\mu\nabla^2\boldsymbol{u}+\rho\boldsymbol{g}. \tag{5.2.22}$$

In the following chapter we illustrate the manner in which the differential equations of flow can be solved to provide detailed information on the microstructure of flow systems.

REFERENCES

1. R.B. Bird, W.E. Stewart, and E.N. Lightfoot, *Transport Phenomena*, Wiley, New York (1960).
2. N.P. Cheremisinoff and R. Gupta, eds., *Handbook of Fluids and Motion*, Butterworths, Boston (1983).
3. H. Schlichting, *Boundary Layer Theory*, Pergamon Press, 1st ed., p. 48 (1955).

SIX

Applications of the Differential Equations of Flow

In this chapter, we discuss some applications of the differential equations of continuity and motion which were developed in Chapter 5.

6.1. FLOW IN IDEAL FLUIDS

All fluids have a certain viscosity. However, in some cases of fluid flow, the effect of viscosity on fluid flow may be considered to be negligible in comparison to other forces. Also, if the variation in the density of a fluid within the region of interest is very small, the fluid may be considered to be **incompressible**. Incompressible fluids, under circumstances where the viscous effects are negligible, are said to behave as **ideal fluids**. For example, the assumption of ideality may be made in cases where the region of interest is away from boundary surfaces and in the absence of recirculating flows.

In chemical and metal processing, the flow of liquids through nozzles and of liquid jets impinging on flat surfaces are examples of near-ideal fluid behavior. The assumption of ideal flow can simplify considerably the solution of the Navier–Stokes equations.

6.1.1. The Concept of Vorticity

In some cases of fluid flow, it is convenient to introduce the concept of **vorticity**, which is a measure of the rotation or angular velocity of a fluid element. For instance, let us imagine a small, frictionless paddle wheel which is placed in a flow field of uniform velocity, away from wall surfaces that create shear stresses. As illustrated in Fig. 6.1a, under these circumstances, all paddle surfaces across the fluid flow would be exposed to the same velocity and the wheel would not turn. On the other hand, if the paddle wheel were placed in flow through an open channel, where a velocity distribution exists (Fig. 6.1b), different paddles would be exposed to different flow velocities and the wheel would rotate.

The first kind of flow is called **irrotational**. An interesting parallel of such motion is that followed by the gondolas on a ferris wheel: each gondola follows a circular path as the wheel turns but the gondola does not rotate with respect to the earth.

For a fluid moving in the x-direction, the vorticity or angular velocity about the x-axis is defined as the average rate of twisting of a fluid element in the y and z planes. Mathematically, this angular velocity is expressed as follows:

$$\omega_x = \frac{1}{2}\left(\frac{\partial u_z}{\partial y} - \frac{\partial u_y}{\partial z}\right). \tag{6.1.1}$$

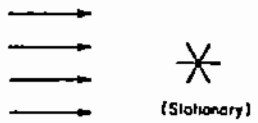

(a)

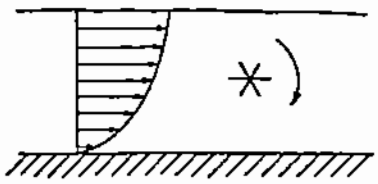

(b)

Figure 6.1. Illustration of irrotational (a) and rotational (b) flow.

In three-dimensional flow, the degree of rotation of a fluid element is expressed as follows:

$$2\omega = i\left(\frac{\partial u_z}{\partial y} - \frac{\partial u_y}{\partial z}\right) + j\left(\frac{\partial u_x}{\partial z} - \frac{\partial u_z}{\partial x}\right) + k\left(\frac{\partial u_y}{\partial x} - \frac{\partial u_x}{\partial y}\right), \tag{6.1.2}$$

where i, j, and k are unit vectors in the x-, y-, and z-directions, respectively.

It should be noted that the angular velocity components are related only to the viscosity terms of the Navier–Stokes equations. Therefore, away from the boundary layers which are formed near surfaces, the bulk flow in many systems may be assumed to be irrotational, i.e.,

$$\boldsymbol{\omega} = \omega_x + \omega_y + \omega_z = 0. \tag{6.1.3}$$

6.1.2. The Concept of the Stream Function

As discussed earlier, the velocity field in the general case of three-dimensional flow can be represented by means of the velocity components, u_x, u_y, and u_z. In flow that can be represented adequately in two dimensions, e.g., flow in an axisymmetric, cylindrical system, it is sometimes convenient to use an alternative representation of the velocity field. This is done by means of the **stream function** which is defined as the function of u_x and u_y that satisfies the continuity equation for a two-dimensional system, i.e.,

$$\frac{\partial u_x}{\partial x} + \frac{\partial u_y}{\partial y} = 0 \tag{6.1.4}$$

As can be seen by substitution into the above equation, the higher-order function, ψ, that will satisfy the continuity equation is expressed by the following equations:

$$u_x = -\frac{\partial \psi}{\partial y}, \quad u_y = +\frac{\partial \psi}{\partial x}. \tag{6.1.5}$$

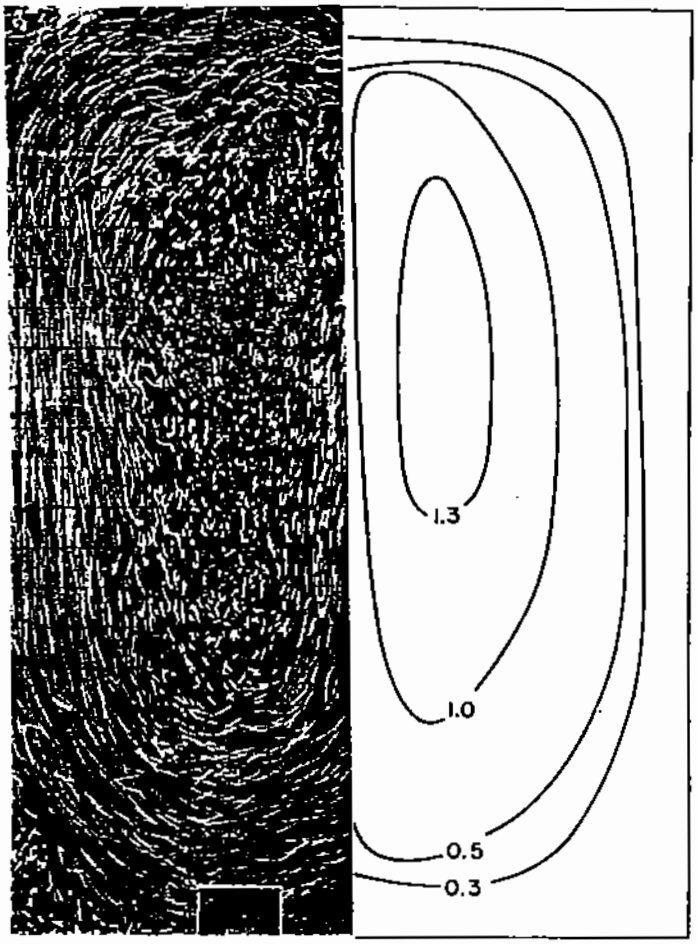

Figure 6.2. Photograph of tracer particles (left) and computed streamlines (right) in a bottom-injected flow model [1].

If we now consider the case of **irrotational**, two-dimensional flow (no z terms) and express u_x and u_y in (6.1.3) in terms of the stream function, we obtain:

$$\frac{\partial u_y}{\partial x} - \frac{\partial u_x}{\partial y} = \frac{\partial}{\partial x}\left(\frac{\partial \psi}{\partial x}\right) - \frac{\partial}{\partial y}\left(-\frac{\partial \psi}{\partial y}\right) = 0,$$

$$\therefore \frac{\partial^2 \psi}{\partial x^2} + \frac{\partial^2 \psi}{\partial y^2} = 0. \tag{6.1.6}$$

The above equation satisfies the continuity equation and also the criterion for irrotational, two-dimensional flow. It has the form of the **Laplace equation**, which will be discussed further in §6.1.3.

The stream function has an important physical significance: In a two-dimensional flow field, a **streamline** is defined as a line connecting locations where the stream function, ψ, is constant. At steady-state conditions, the streamlines are identical to the path lines (or "streak lines") followed by particles of the fluid as they move through the flow system.

For example, Fig. 6.2 [1] is a time-lapse photograph of tracer particles following the recirculating flow of liquid in a water tank due to injection of gas at the bottom of the tank (left side of illustration); the computed streamlines for the same system are shown on the

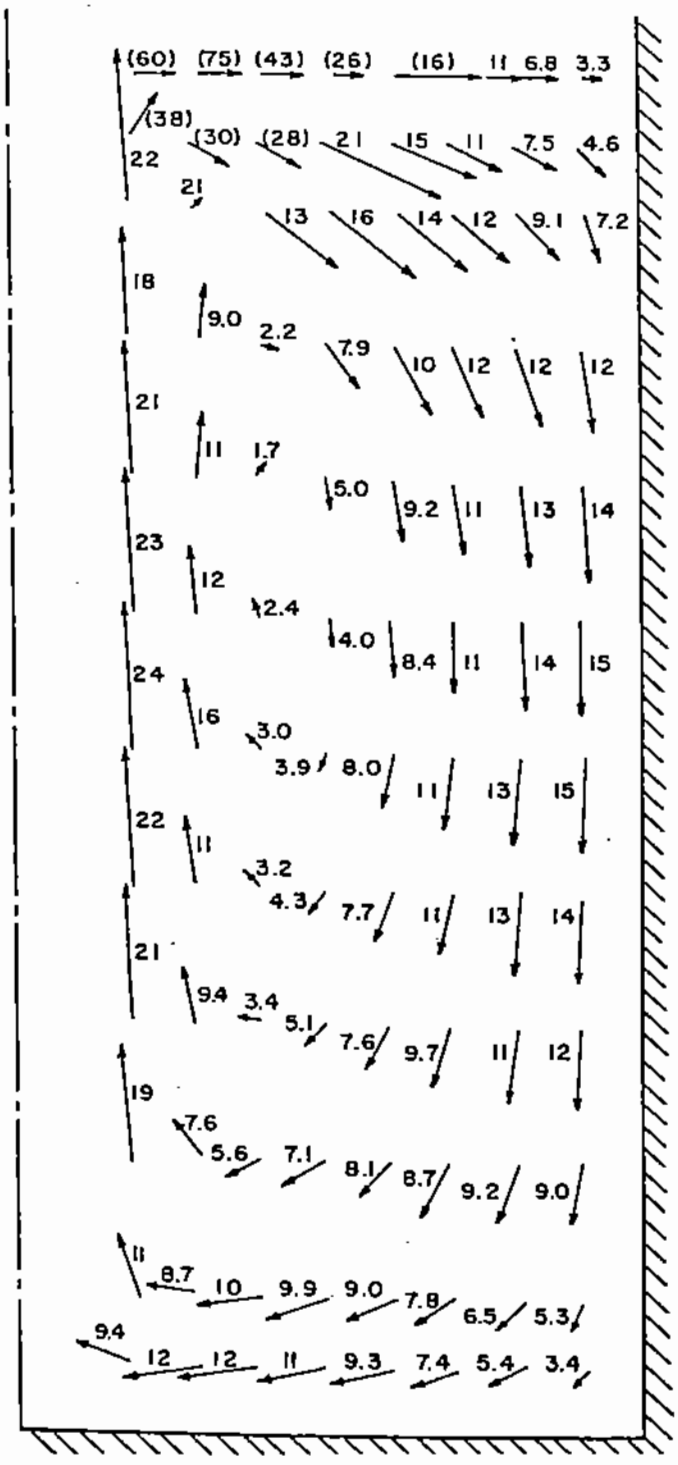

Figure 6.3. Computed velocities corresponding to the streamlines of Fig. 6.2 [1].

right side of Fig. 6.2. Figure 6.3 [1] shows the calculated velocities corresponding to the streamlines of Fig. 6.2. Inspection of Figs. 6.2 and 6.3 shows that the regions where the streamlines are closer together correspond to the higher velocities of the fluid particles.

Figure 6.4 is a time-lapse photograph of the fluid streamlines observed [2] in a water model of a copper converter; in the model an air jet was injected through a side orifice,

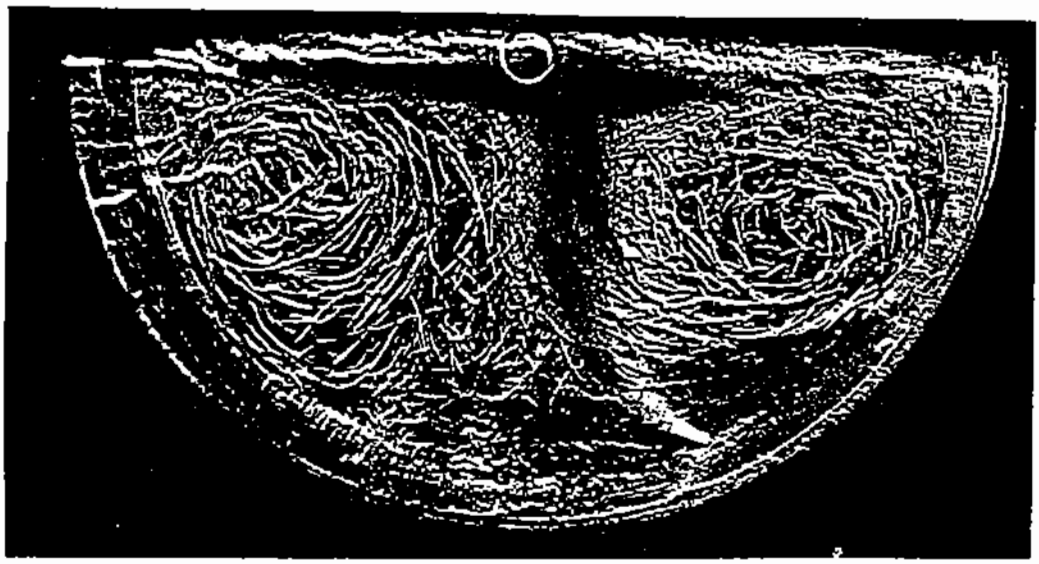

Figure 6.4. Streamlines in a water model of a gas-injected copper converter [2].

representing a tuyere, into the water bath representing copper. Polystyrene particles were used as the tracer element.

6.1.3. The Concept of Velocity Potential

For ideal flow behavior, the Navier–Stokes equations can be written for the x-component of velocity as follows:

$$\rho\left(\frac{\partial u_x}{\partial t}+u_x\frac{\partial u_x}{\partial x}+u_y\frac{\partial u_x}{\partial y}+u_z\frac{\partial u_x}{\partial z}\right)=-\frac{\partial P}{\partial x}+\rho F_x, \tag{6.1.7}$$

and in vector notation for all three components of velocity:

$$\rho\frac{Du}{Dt}=-\nabla P+\rho F. \tag{6.1.8}$$

The above equation is referred to as the **Euler equation** and must be solved in conjunction with equation of continuity (5.1.11).

We now define a new function, to be called the **velocity potential**, $\phi(x,y,z)$, which is related to the velocity components by means of the following equations:

$$\frac{\partial\phi}{\partial x}=u_x,\quad \frac{\partial\phi}{\partial y}=u_y,\quad \frac{\partial\phi}{\partial z}=u_z. \tag{6.1.9}$$

Introduction of the velocity potential function in the continuity equation for incompressible fluids at steady state (5.1.12) yields

$$\frac{\partial^2\phi}{\partial x^2}+\frac{\partial^2\phi}{\partial y^2}+\frac{\partial^2\phi}{\partial z^2}=0, \tag{6.1.10}$$

or in vector notation

$$\nabla^2\phi=0. \tag{6.1.11}$$

Equation (6.1.10), like (6.1.6) for the stream function, is in the form of the renown Laplace equation which also describes the flow of electricity due to an electric voltage gradient, the flow of heat by conduction under a temperature gradient, and the flow of mass by diffusion under a concentration gradient. It is therefore possible to use solutions of the Laplace equation developed for other phenomena (e.g., equations or computer programs) to determine the velocity distribution in an ideal, incompressible flow system. Because of this similarity, one can also use electric analogue models of flow, such as graphite conductive paper or a shallow bath of electrolyte to simulate a flow system and measure "velocities," by measuring the voltage distribution in the electric analogue.

If we now consider the velocity potential function for a two-dimensional, incompressible flow system, we can develop a relationship between ϕ and the stream function ψ in a flow system. It is evident that for a line of constant ϕ,

$$d\phi = 0 = \frac{\partial \phi}{\partial x} dx + \frac{\partial \phi}{\partial y} dy, \tag{6.1.12}$$

and by substituting for the potential function differentials from (6.1.9):

$$0 = u_x dx + u_y dy. \tag{6.1.13}$$

Finally, by algebraic manipulation of the above equation and replacing u_x and u_y by the corresponding definitions of the stream function (equation (6.1.5)), we obtain the following relationship:

$$\left(\frac{dy}{dx}\right)_{\phi,\text{const}} = -\frac{u_x}{u_y} = -\frac{(-\partial\psi/\partial y)}{(\partial\psi/\partial x)} = \frac{1}{(dy/dx)_{\psi,\text{const}}}. \tag{6.1.14}$$

The above equation expresses the fact that the ϕ and ψ lines at any particular location must be perpendicular to each other. Therefore, one can deduce the location of the streamlines (constant ψ) on the basis of the isopotential lines (constant ϕ) and vice versa. Figure 6.5 [3] is an example of the orthogonal flownet of streamlines and velocity potential lines for the flow of an ideal fluid through a slot.

Example 6.1.1. Flow from a Source Point

We now consider the two-dimensional (x, y) flow of water introduced at a central point (source) in a large, shallow reservoir (Fig. 6.6). The solution of the velocity potential and streamline equations (6.1.6) and (6.1.11) for this situation yields [5] the following expressions for the velocity potential and for the stream function in terms of the flow of water in the reservoir at the coordinates x and y from the entry point:

$$\phi = \frac{v'}{2\pi} \ln(x^2 + y^2)^{1/2}, \tag{6.1.15}$$

and

$$\psi = \frac{v'}{2\pi} \tan^{-1}\left(\frac{y}{x}\right), \tag{6.1.16}$$

where v' is the volumetric flow rate of water into the reservoir, in m^3/s of flow per m of depth of the reservoir. A plot of the above two equations is shown in Fig. 6.6 [5]. The

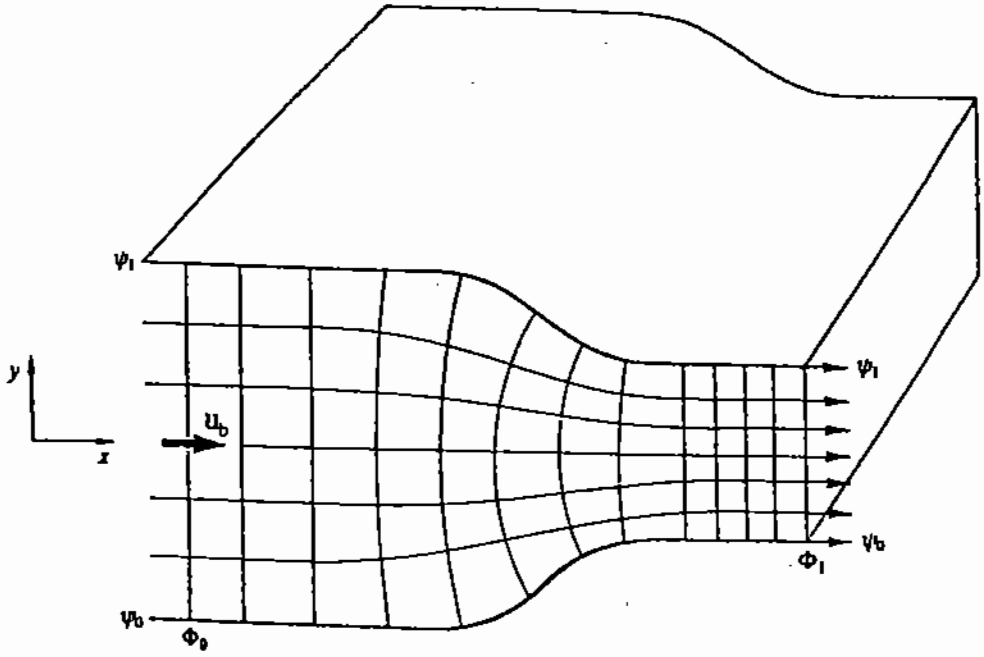

Figure 6.5. Streamlines and velocity potential lines through a slot [3].

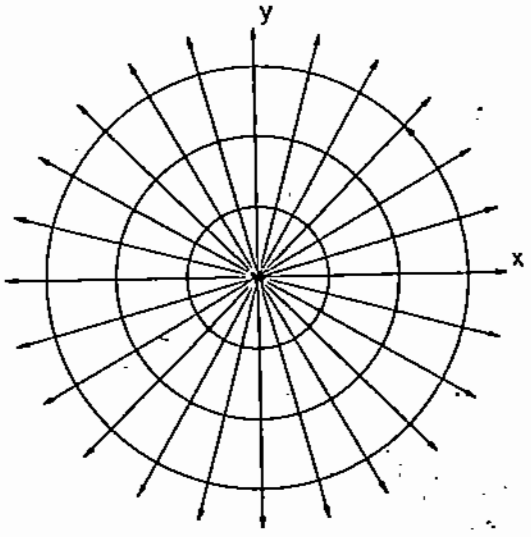

Figure 6.6. Streamlines and iso-potential lines for flow from a source in a reservoir.

lines radiating outward from the source point are the streamlines and the circles represent the isopotential lines.

To obtain the x and y-components of velocity, we can now use Equations (~~10~~) and (~~11~~) and the definitions of streamline and flow potential presented earlier. By differentiation, we obtain

$$u_x = \frac{\partial \phi}{\partial x} = \frac{\partial \psi}{\partial y} = \frac{v'}{2\pi}\left(\frac{x}{x^2+y^2}\right), \tag{6.1.17}$$

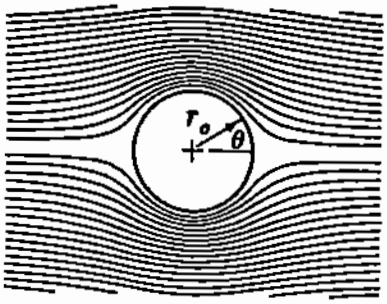

Figure 6.7. Streamlines around a sphere [3].

and

$$u_y = \frac{\partial \phi}{\partial y} = -\frac{\partial \psi}{\partial x} = \frac{v'}{2\pi}\left(\frac{y}{x^2+y^2}\right). \tag{6.1.18}$$

The absolute value of the velocity at any location x, y from the point of entry is given by the vector sum of the above two components:

$$|u| = \left(u_x^2 + u_y^2\right)^{1/2} = \frac{v'}{2\pi r}, \tag{6.1.19}$$

where $r = (x^2 + y^2)^{1/2}$ is the radial distance from the source.

Example 6.1.2. Flow Around a Sphere

The solutions of the stream and velocity potential functions around a sphere (Fig. 6.7 [3]), yield the following relationships for the radial and tangential velocity components:

$$u_r = u_b \cos\theta \left(1 - \frac{r_0^3}{r^3}\right), \tag{6.1.20}$$

$$u_\theta = \frac{1}{2} u_b \sin\theta \left(2 + \frac{r_0^3}{r^3}\right), \tag{6.1.21}$$

where r_0 is the radius of the sphere, r is the radial distance into a fluid which is flowing in the horizontal direction (Fig. 6.7) at a bulk velocity of u_b, and θ is the angle from the forward point of the sphere into the flowing stream. The velocity equations show that the tangential velocity (u_θ) ranges from 0 at the forward (stagnation) point to a maximum of $1.5u_b$ at $\theta = 90°$. Experimental measurements at high velocities past a sphere are in agreement with the above equations except towards the rear of the sphere where turbulent eddies are formed (Chapter 7).

As another illustration, Fig. 6.8 [3] shows the streamlines for the idealized flow of a fluid stream, traveling downward at an initially uniform bulk velocity of $u_{z,b}$, which is directed against a flat surface at plane x, y. In this case, the ideal flow velocity components on the plane x, y are expressed as follows [3]:

$$u_x = u_{z,b}\frac{x}{L}, \quad u_y = u_{z,b}\frac{y}{L}, \tag{6.1.22}$$

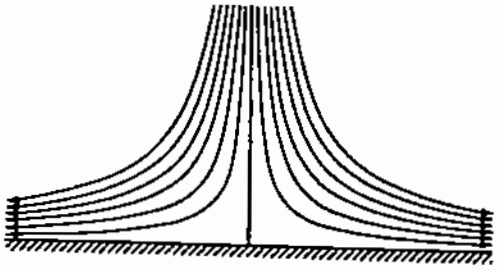

Figure 6.8. Streamlines for flow against a flat surface [3].

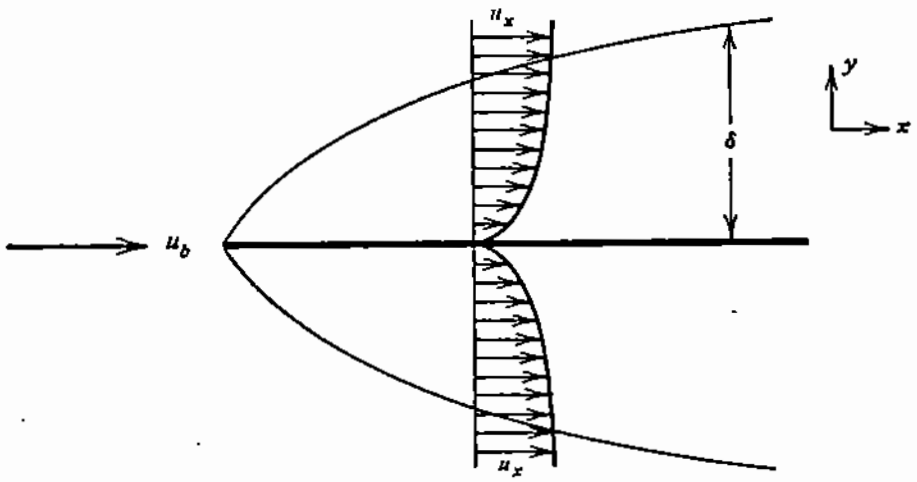

Figure 6.9. Boundary layer formation along a flat plate.

where L is a reference length.

6.2. THE CONCEPT OF THE BOUNDARY LAYER

In our discussion of velocity potential, we considered fluid systems where the viscous terms in the Navier–Stokes equations were negligible in comparison to the kinetic terms. However, in the flow region close to a surface, viscosity effects have a pronounced effect on the fluid velocity. It can be shown experimentally that as a fluid approaches a stationary flat plate with a "free stream" or "bulk" velocity u_b, the layers of fluid close to the plate are gradually retarded and the fluid layer in contact with the stationary plate is also at rest (Fig. 6.9). The flow region which is affected by the presence of the plate is called the **boundary layer** [6]. Its thickness is a function of the fluid properties and velocity and of the distance x and y from the leading edge of the plate.

The presence of the boundary layer is of importance not only in fluid flow problems but also in heat and mass transfer. As we shall show in this section, the thickness of the boundary layer in laminar flow can be calculated from the differential equations of continuity and motion. However, as will be discussed in Chapters 12 and 17, in many engineering problems the boundary layer thickness can be "rolled into" semi-empirical factors which are called *heat transfer and mass transfer coefficients.*

6.2.1. Velocity Profiles in the Boundary Layer

We now consider the flow of an incompressible fluid over a horizontal thin plate (Fig. 6.9). Flow is in the x-direction and at **bulk velocity** (i.e., main stream velocity) u_b; however, due to viscosity, in the vicinity of the plate there is transport of momentum in the y-direction and this results in a u_y component of velocity. There are no velocity components in the z-direction and the system can be considered as two-dimensional. From Table 5.1, the corresponding equations of continuity and motion at steady state are:

$$\frac{\partial u_x}{\partial x} + \frac{\partial u_y}{\partial y} = 0, \tag{6.2.1}$$

$$u_x \frac{\partial u_x}{\partial x} + u_y \frac{\partial u_x}{\partial y} = -\frac{1}{\rho}\frac{\partial P}{\partial x} + \frac{\mu}{\rho}\left(\frac{\partial^2 u_x}{\partial x^2} + \frac{\partial^2 u_x}{\partial y^2}\right), \tag{6.2.2}$$

$$u_x \frac{\partial u_y}{\partial x} + u_y \frac{\partial u_y}{\partial y} = -\frac{1}{\rho}\frac{\partial P}{\partial y} + \frac{\mu}{\rho}\left(\frac{\partial^2 u_y}{\partial x^2} + \frac{\partial^2 u_y}{\partial y^2}\right). \tag{6.2.3}$$

These equations can be simplified further on the basis of the following considerations:

a. The flow over the plate is obviously created by a pressure gradient in the x-direction. However, the immediate pressure gradients in the vicinity of the surface are negligible in comparison to the interchange between kinetic and viscous forces.
b. The *gradient* of the x-component of velocity in the y-direction, $\partial u_x/\partial y$, is large; however, the y-component of velocity, u_y, is very small in comparison to u_x. Therefore, the momentum components associated with changes in u_y (i.e., (6.2.3)) can be assumed to be negligible and the equation of motion can be represented only by (6.2.2) for the x-component [7].
c. The transport of momentum in the x-direction is principally by *convection*, i.e., by the flow of the fluid in the x-direction; therefore the *diffusive* term $(\mu/\rho)\partial^2 u_x/\partial x^2$ in (6.2.2) is much smaller than the *convective* term $u_x \partial u_x/\partial x$ and can be neglected.

On the basis of the above considerations, the equations of motion simplify to the following two equations:

$$\frac{\partial u_x}{\partial x} + \frac{\partial u_y}{\partial y} = 0, \tag{6.2.4}$$

$$u_x \frac{\partial u_x}{\partial x} + u_y \frac{\partial u_x}{\partial y} = \frac{\mu}{\rho}\frac{\partial^2 u_x}{\partial y^2}. \tag{6.2.5}$$

By integrating (6.2.4) for u_y, for the boundary condition specified by Newton's law of viscosity, i.e., $u_y = 0$ at $y = 0$, and substituting in (6.2.5) we obtain the following equation:

$$u_x \frac{\partial u_x}{\partial x} - \left(\int_0^y \frac{\partial u_x}{\partial x}\, dy\right) \frac{\partial u_x}{\partial y} = \frac{\mu}{\rho}\frac{\partial^2 u_x}{\partial y^2}. \tag{6.2.6}$$

The boundary conditions for the above equation are:

$u_x = 0$, $u_y = 0$ at $y = 0$ (plate surface),

$u_x = u_b$, $u_y = 0$ at $y \to \infty$ (i.e., far from the plate surface),

$u_x = u_b$ at $x = 0$ for all y.

To solve (6.2.6), we start by assuming that the fluid velocity is affected by the presence of the surface only within a certain *boundary layer thickness*, δ_x; beyond this layer, the fluid velocity is u_b. Furthermore, we assume that the dimensionless velocity profiles, u_x/u_b, have a similar shape which is a function, f, of the ratio y/δ_x which is called transform variable η:

$$\frac{u_x}{u_b} = f\left(\frac{y}{\delta_x}\right) = f(\eta), \tag{6.2.7}$$

where y is the distance above the plate and δ_x is the thickness of the boundary layer at distance x from the leading edge of the plate. On the basis of these two assumptions, the derivatives in (6.2.6) can be expressed as follows [7]:

$$\frac{\partial u_x}{\partial x} = u_b f'\left(-\frac{\eta}{\delta_x}\right)\frac{d\delta_x}{dx}, \tag{6.2.8}$$

$$\frac{\partial u_x}{\partial y} = u_b f'\left(\frac{1}{\delta_x}\right), \tag{6.2.9}$$

$$\frac{\partial^2 u_x}{\partial y^2} = u_b f''\left(\frac{1}{\delta_x^2}\right), \tag{6.2.10}$$

where f' and f'' signify differentiation of the function f with respect to η. By substituting from (6.2.8)–(6.2.10) in (6.2.6) and integrating with respect to η, we obtain [7]

$$(B - A)\delta_x \frac{d\delta_x}{dx} = \frac{\mu}{\rho u_b} C = \frac{\nu}{u_b} C, \tag{6.2.11}$$

where

$$A = \left(\int_0^1 f f' \, d\eta\right), \tag{6.2.12}$$

$$B = \int_0^1 f'\left(\int_0^\eta f' \eta \, d\eta\right) d\eta = -A + \left(\int_0^1 f' \eta \, d\eta\right), \tag{6.2.13}$$

$$C = \left(\int_0^1 f'' \, d\eta\right) = f'\Big|_0^1 \tag{6.2.14}$$

Integrating (6.2.11) for the boundary condition of $\delta_x = 0$ at $x = 0$ yields [7]:

$$\delta_x = \sqrt{2\left(\frac{C}{B - A}\right)\frac{\nu x}{u_b}}. \tag{6.2.15}$$

Equation (6.2.15) shows that the thickness of the boundary layer is proportional to the square root of the distance from the leading edge, x, and inversely proportional to the square root of the free stream velocity, u_b.

An exact solution of (6.2.15) can be obtained by a numerical technique and the use of a computer, as will be discussed in Chapter 11 for the solution of the unsteady state

conduction equation. To proceed further with the analytical solution, it is necessary at this point to select a reasonable velocity profile to represent the function $f(\eta)$ of (6.2.7). For example, as a first approximation one can assume that u_x increases linearly from 0 at $y = 0$ to u_b at $y = \delta$. However, the following simple algebraic equation was found [7] to represent better the shape of velocity profile observed in experiments:

$$f(\eta) = \frac{u_x}{u_b} = \frac{3}{2}\eta - \frac{1}{2}\eta^3. \tag{6.2.16}$$

On the basis of (6.2.16), parameters A, B, and C have been estimated [7] from (6.2.12)–(6.2.14) to be

$$A = \frac{9}{35}, \quad B = \frac{33}{280}, \quad C = -\frac{3}{2}. \tag{6.2.17}$$

By inserting these numbers in (6.2.15), the boundary layer thickness is expressed as follows:

$$\delta_x = \sqrt{\frac{280}{13}\frac{\nu x}{u_b}} = 4.64\sqrt{\frac{\nu x}{u_b}}. \tag{6.2.18}$$

Substituting now for $\eta = y/\delta_x$ from (6.2.18) into (6.2.16), we obtain the velocity distribution in the boundary layer as a function of x and y:

$$\frac{u_x}{u_b} = \frac{3}{2}\left(\frac{y}{4.64\sqrt{\frac{\nu x}{u_b}}}\right) - \frac{1}{2}\left(\frac{y}{4.64\sqrt{\frac{\nu x}{u_b}}}\right)^3 \quad \text{for } 0 \le y \le \delta_x. \tag{6.2.19}$$

The validity of this equation has been tested by calculating the *drag force* (shear stress due to viscous force times surface area affected, Chapter 8) exerted by a fluid on the upper and bottom surface of a plate of width W and over distance L from the leading edge of the plate:

$$F_x = 2\int_0^W \int_0^L \left(\mu \frac{\partial u_x}{\partial y}\right)_{y=0} dx\, dz = 1.292\sqrt{\rho\mu L W^2 u_b^3}. \tag{6.2.20}$$

It should be noted that an exact solution of (6.2.6), obtained by Blasius [10] long before the advent of computers, has the same form as (6.2.20) with the exception that the constant is 1.328 instead of 1.292; this confirms the validity of the assumptions made in deriving the above analytical solution.

The solution of (6.2.6) is shown in graphical form, in terms of the dimensionless functions of u_x, u_y, and x, in Fig. 6.10; it can be seen that u_x approaches u_b asymptotically. The **boundary layer** thickness, δ_x, is assumed to be the distance from the wall where the fluid velocity is within 1% of the bulk velocity of the fluid; in other words, the perpendicular distance from the plate surface at which

$$\frac{u_x}{u_b} = 0.99. \tag{6.2.21}$$

On the basis of this definition, we can obtain from the data of Fig. 6.10 the following expression for the thickness of the boundary layer:

$$\delta_x \approx 5.0\left(\frac{\nu x}{u_b}\right)^{1/2}, \tag{6.2.22}$$

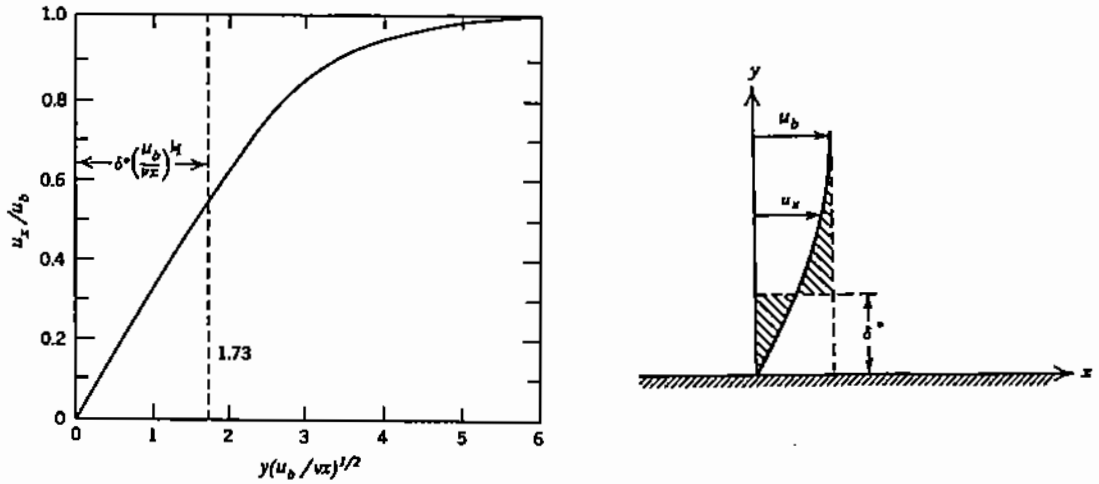

Figure 6.10. Velocity profile in the boundary layer along a flat plate and illustration of displacement thickness.

where δ_x is the thickness of the boundary layer at distance x from the leading edge of the plate. A more useful, and physically more significant, measure of the boundary layer thickness is in terms of the **displacement thickness** which is defined mathematically as follows:

$$\delta^* = \int_0^\infty \left(\frac{u_b - u_x}{u_b}\right) dy. \tag{6.2.23}$$

The form of (6.2.23) shows that the displacement thickness is an averaged expression of the boundary layer thickness. In physical terms, the product of the displacement thickness and the bulk velocity of the fluid over the plate (i.e., $\delta^* u_b$) is equal to the volumetric flow rate, per unit width of the plate, at which the fluid stream is retarded because of the presence of the surface. Looking at the same situation in a different way, if the plate were moving in a stationary fluid, the product of the plate velocity and the boundary layer displacement thickness would represent the volume of fluid carried over with the plate, per unit width of plate.

The actual value of the integral representing the displacement thickness (see equation (6.2.23)) can be obtained graphically from Fig. 6.10 and is expressed by the following equation:

$$\delta^* \approx 1.73 \left(\frac{\nu x}{u_b}\right)^{1/2}. \tag{6.2.24}$$

It must be noted that the above equations apply to laminar flow which, for flow over a flat plate is in the region of Reynolds numbers (Chapter 7) of

$$\mathrm{Re} = \frac{u_b x}{\nu} < 10^5. \tag{6.2.25}$$

The above definition of the displacement thickness of the boundary layer can be useful in situations where it is necessary to estimate the volume of fluid entrained by a solid or liquid body moving through a fluid. Examples are the entrainment of oxygen by liquid

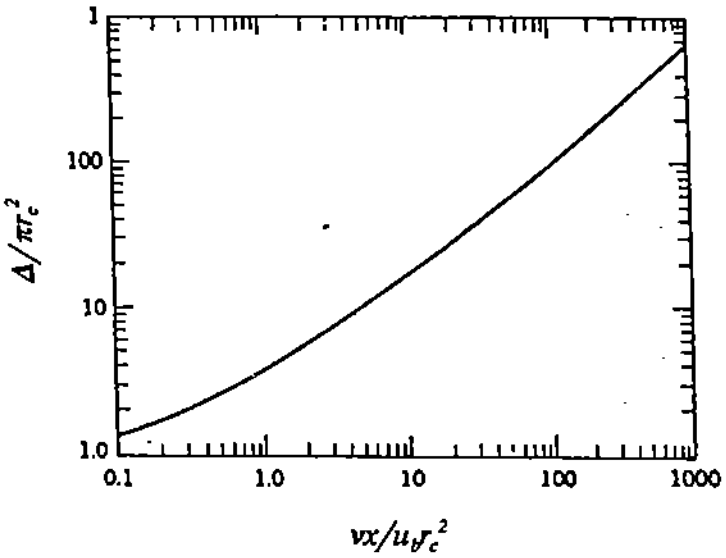

Figure 6.11. Displacement thickness for thin cylindrical bodies.

streams during tapping and casting and the coating of plates and wires by immersion into a liquid bath.

It has been determined [4] that the concept of the displacement thickness, which was originally developed for flat plates, can also be applied to cylindrical bodies with fluid flow parallel to their axis provided that the radius of the cylinder, r_c, is much larger than the value of δ^*. In such cases, the volumetric flow rate of entrained fluid is expressed by the product of the plate velocity relatively to the fluid and the cross-sectional area of an annulus of width δ^*, i.e.,

$$\dot{v} = u_b \pi \left[(\delta^* + r_c)^2 - r_c^2 \right] \equiv u_b \Delta, \tag{6.2.26}$$

where Δ is the cross-sectional area of the fluid annulus. In cases where the displacement thickness is large in relation to the radius of the cylindrical body, Glauert and Lighthill [4] recommended the use of Fig. 6.11 which gives the value of the cross-sectional area of the fluid annulus (expressed as a fraction of the cross-sectional area of the cylinder) as a function of the dimensionless group

$$\frac{\mu x}{\rho u_b r_c^2} \text{ or } \frac{\nu x}{u_b r_c^2}.$$

Equations (6.2.24) and (6.2.26) can be used to calculate the volume of gas carried along by a cylindrical body moving through a stationary gas. Such a case is illustrated in Fig. 6.12 which shows a stream of molten metal flowing through a nozzle at the bottom of a ladle, through the atmosphere and into a mold, during casting. In this kind of problem, it is convenient to calculate the mass of gas entrained per mass of falling metal stream (e.g., parts per million of gas entrainment). Therefore, we need to compute

$$\frac{\text{mass of gas entrained}}{\text{mass of cylinder}} = \frac{\text{B.L. cross-section} \times \text{gas density}}{\text{cylinder cross-section} \times \text{its density}}.$$

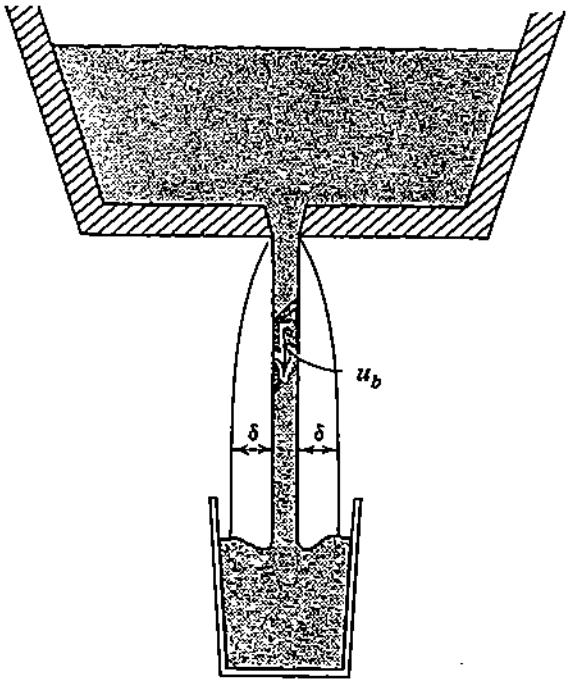

Figure 6.12. Entrainment of gas by a liquid metal stream.

If the above ratio is denoted by R_m, by combining (6.2.24) and (6.2.26) we obtain

$$R_m = \frac{\rho_g}{\rho_c r_c^2}\left[\frac{3\nu x}{u_b} + 3.46 r_c \left(\frac{\nu x}{u_b}\right)^{1/2}\right], \tag{6.2.27}$$

where ρ_g is the density of the entrained gas, calculated at the "film" temperature (assumed to be equal to the arithmetic mean of the temperatures of the cylinder and the bulk temperature of the enveloping gas) and ρ_c is the density of the cylinder.

Equation (6.2.26) can be used in cases where the liquid stream is relatively short and behaves like a cylinder, rather than breaks up. For thin cylindrical bodies, instead of using (6.2.26), Fig. 6.11, which was experimentally derived, should be used to determine the mass ratio of entrained gas from the following equation:

$$R_m = \frac{\rho_g}{\rho_c}\left(\frac{\Delta}{\pi r_c^2}\right). \tag{6.2.28}$$

Example 6.2.1

In a continuous casting operation, a stream of molten steel issues from a 2.0 cm diameter orifice at the bottom of a tundish and falls through air into a mold below (Fig. 6.12). The surface of the metal in the mold is 20 cm below the orifice, the metal temperature is 1560°C and the "film" temperature 790°C ($\rho_g = 3.31 \times 10^{-4}$ g cm^{-3}; $\mu_g = 4.34 \times 10^{-4}$ g s^{-1} cm^{-1}). If the casting rate is 250 kg/min, calculate the amount of oxygen entrained in the metal stream during its fall, using the data of Fig. 6.11.

First, from the casting rate, the orifice diameter and the assumed metal density of 7.9 g cm^{-3}, the stream velocity is calculated to be $u_b = 168$ cm/s. We then calculate the value of the group

$$\frac{\nu_g x}{u_b r_c^2} = 0.156,$$

and from Fig. 6.11 we find that the corresponding value of the film annulus to be

$$\frac{\Delta}{\pi r_c^2} = 1.55.$$

Finally, from (6.2.28) we calculate that the ratio of mass of air entrained per unit mass of steel as

$$R_m = 64.9 \times 10^{-6}.$$

If it is assumed that all the oxygen content in the entrained air (23% O_2 by weight) is absorbed in the liquid metal, the calculated pickup of oxygen is

$$0.23 \times 64.9 \times 10^{-6} = 14.9 \text{ ppm}.$$

Example 6.2.2

It was reported in [8] that the oxygen content of a liquid steel stream flowing through a 3.86 cm orifice at the bottom of a ladle to a casting machine below the ladle decreased by 9 ppm when a protective atmosphere of argon was provided around the falling stream. The rate of flow was reported to be 1.21 tons/min. and the height of fall between orifice and surface of melt in tundish of casting machine was 40.5 cm. Compare the reported data with the calculated value for oxygen entrainment when the steel stream falls through air instead of argon.

As in the previous example, we calculate the stream velocity to be 218 cm/s and the ratio

$$\frac{\nu_g x}{u_b r_c^2} = 0.0654$$

to be much less than 1. Therefore, in this case we are justified in using (6.2.27) to calculate the pickup of oxygen when the stream falls through air (23% O_2 by weight):

$$R_{m,\text{air}} = 45.3 \text{ ppm}, \quad \text{and} \quad R_{m,\text{ox}} = 10.4 \text{ ppm}.$$

The calculated value is close to the reported reduction in ppm of oxygen pickup, when the argon shroud was used around the stream of molten metal.

REFERENCES

1. J. Szekely, *Fluid Flow Phenomena in Metals Processing*, Academic Press, New York (1979).
2. P. Tarassoff, Private communication, in J. Szekely, *Fluid Flow Phenomena in Metals Processing*, Academic Press, New York (1979).
3. R.I.L. Guthrie, *Engineering in Process Metallurgy*, Clarendon Press, Oxford (1989).
4. M.B. Glauert and M.J. Lighthill, *Proc. Royal Soc., London, Ser. A*, **204**, 188 (1954).
5. J. Szekely and N.J. Themelis, *Rate Phenomena in Process Metallurgy*, Wiley, New York (1971).
6. H. Schlichting, *Boundary Layer Theory*, Pergamon, London (1955).
7. R.B. Bird, W.E. Stewart, and E.N. Lightfoot, *Transport Phenomena*, Wiley. New York (1960).
8. W.H. Ray and J. Szekely, *Process Optimization with Applications in Metallurgy and Chemical Engineering*, Wiley, New York (1973).
9. W. Wilson, in: Proc. Vacuum Metal. Conference, New York, p. 235, 1960.
10. H. Blasius, Z. *Math. Phys.*, **56**, 1–37 (1908); or NASA Tech. Memorandum No. 1256.

SEVEN

Turbulent Flow

Throughout our earlier discussion of Newton's law of viscosity and the differential equations of motion, it was assumed that the flow was **laminar**. Reynolds [1] was the first known experimenter to demonstrate that under certain conditions of flow velocity, pipe diameter and fluid properties, a tracer dye introduced in the center of the flow in the pipe does not mix with adjacent layers and travels in a line parallel to the axis of the pipe (Fig. 7.1). However, when the flow rate through the pipe is gradually increased, at some critical velocity of flow the dye is quickly dispersed throughout the pipe, as illustrated in Fig. 7.1b.

7.1. CHARACTERISTICS OF LAMINAR AND TURBULENT FLOW

The first regime of flow (Fig. 7.1.a) where the layers of fluid slide over each other without mixing and where the velocity at any location in the pipe remains constant, is called **laminar** flow. The second regime of flow, which entails mixing between adjacent layers by means of **eddies** or "curls" (Fig. 7.2) is called **turbulent**.

To visualize eddy formation, consider a smooth pipe through which there is laminar flow of a fluid. Let us assume that this flow comes to a zone of the pipe where the wall is slightly rough. This roughness may cause particles of fluid to be torn away from the outer layers of the laminar flow and forced into the core of the flow where their momentum may cause other particles to move out of laminar flow and so on.

The above is only an illustration because, at sufficiently high flow velocities, there will be **eddy** formation and turbulence even in flow through perfectly smooth conduits: Eddies start to form near the wall and the turbulent boundary layer soon grows to occupy the entire cross-section of flow. Depending on the flow system, eddies can be as large as the characteristic length of the system but generally larger eddies break down to smaller ones. The size of eddies is usually represented by the **Prandtl mixing length**, which is considered to be the distance that an eddy can travel before colliding with another. Figure 7.3 [2] shows the variation in mixing length, l (expressed as the dimensionless ratio l/r_0, where r_0 is the radius of the pipe), with vertical distance from the surface of the pipe (also expressed in dimensionless form as y/r_0).

The transition from laminar to turbulent flow depends on the ratio of inertial to viscous forces in a flow system and can be quantified by means of the dimensionless **Reynolds number**, Re, which is defined as follows:

$$\mathrm{Re} = \frac{L\bar{u}\rho}{\mu} = \frac{L\bar{u}}{\nu}, \tag{7.1.1}$$

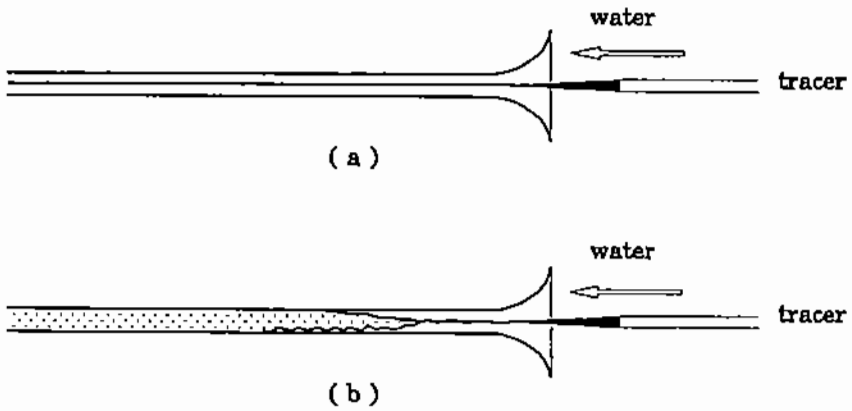

Figure 7.1. Experiment of Reynolds on dispersion of dye tracer in water in (*a*) laminar and (*b*) turbulent flow.

Figure 7.2. Eddy formation in turbulent flow through a channel.

where L is the characteristic length of the flow system, m; $\overline{u}$ is the average fluid velocity, m s^{-1}; ρ is the fluid density, kg m^{-3}; μ is the fluid viscosity, kg s^{-1} m^{-1}; ν is the momentum diffusivity, m^2 s^{-1}.

As shown by (7.1.1), the Reynolds number is the ratio of the inertial force in the system (represented by the product of the characteristic length, the flow velocity, and the density of the fluid) to the viscous force (represented by the viscosity of the fluid).

For flow through pipes and conduits, the characteristic length L is taken to be the diameter or equivalent diameter of the conduit. The transition from laminar to turbulent flow in pipes starts at about Re > 2100 and is considered to become fully turbulent at Re > 4000 (Chapter 8). For flow around a spherical particle, the characteristic length is the particle diameter and transition occurs at Re > 200. The transition Reynolds number for other systems will be discussed in later chapters.

In addition to the visually observed differences between laminar and turbulent flow, there are other physical manifestations of turbulence. Thus, as discussed in Chapter 4, in laminar flow the pressure drop over a certain length of conduit is linearly proportional to the average velocity; on the other hand, it has been shown experimentally that at flow velocities

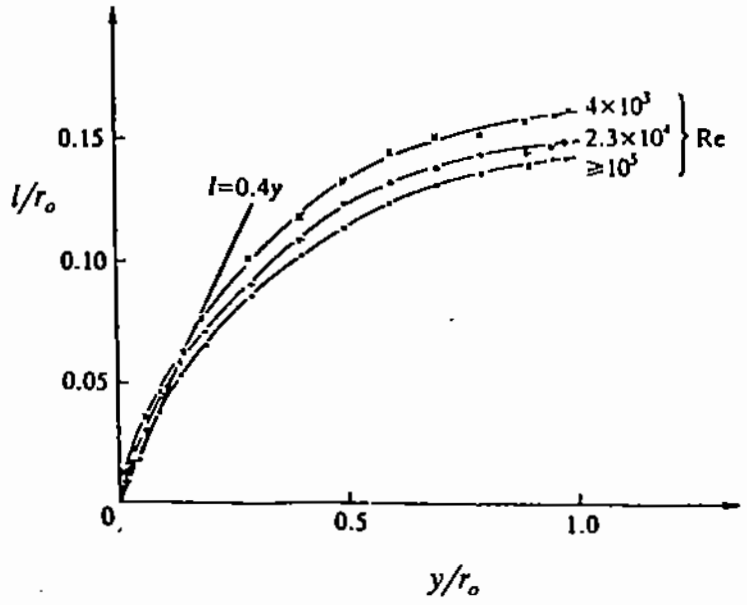

Figure 7.3. Eddy mixing length as a function of distance from wall of pipe [2].

above the critical Reynolds number, there is an abrupt increase in the slope of the plot of pressure drop against velocity and the pressure drop becomes proportional to $u^{1.8} - u^{2.0}$.

It was also shown in Chapter 4 that the velocity profile for laminar flow in a pipe is parabolic with distance from the center of flow and the following relationships apply:

$$\frac{u}{u_{\max}} = 1 - \left(\frac{r}{r_0}\right)^2, \tag{7.1.2}$$

$$\frac{\overline{u}}{u_{\max}} = \frac{1}{2}. \tag{7.1.3}$$

In contrast, in turbulent flow, because of the transfer of momentum by the eddies, the velocity profile across the pipe is flatter. The corresponding relationships can be expressed approximately as follows:

$$\frac{u}{u_{\max}} \approx \left(1 - \frac{r}{r_0}\right)^{1/7}, \tag{7.1.4}$$

$$\frac{\overline{u}}{u_{\max}} \approx 0.875. \tag{7.1.5}$$

The difference between laminar and turbulent velocity profiles is illustrated in Fig. 7.4.

7.2. FLUCTUATING COMPONENTS OF VELOCITY

If a hot-wire anemometer (Fig. 7.5), or other sensitive velocity-measuring instrument, is used to measure the instantaneous velocity at a fixed point in a turbulent flow field, it will be found that although the average velocity at that location is constant, there is a fluctuation of instantaneous velocity with time (Fig. 7.6).

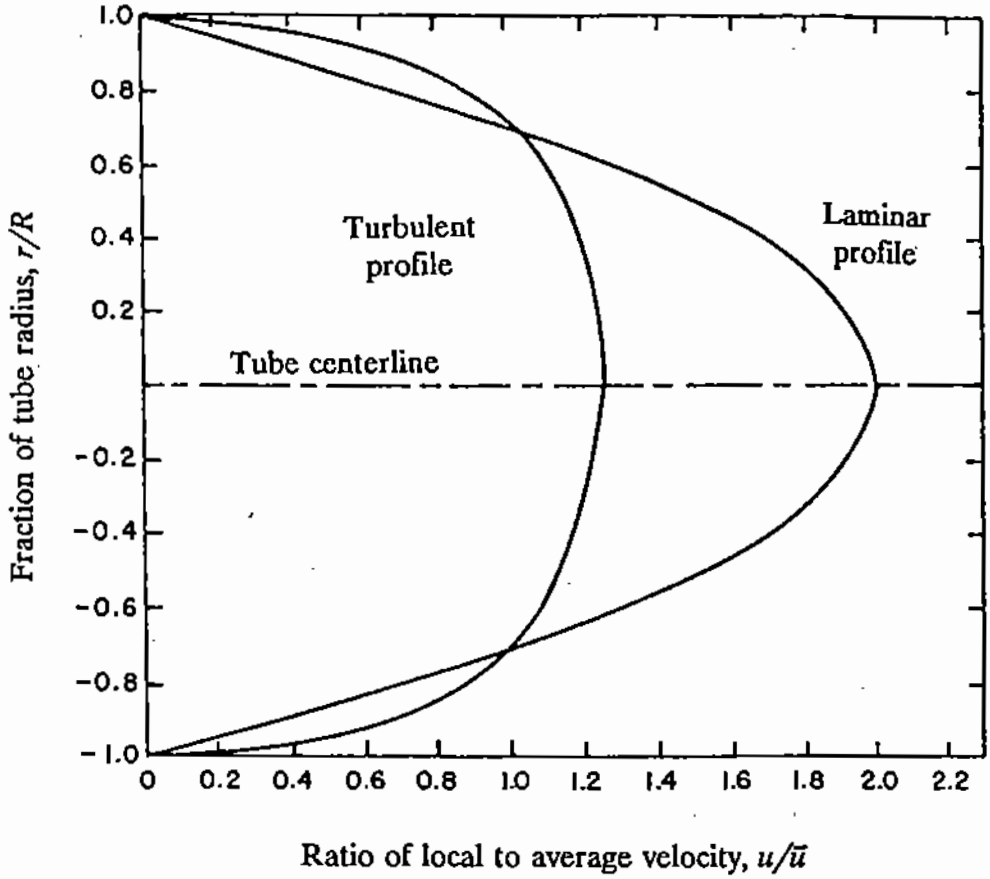

Figure 7.4. Comparison of laminar and turbulent velocity profiles at same average velocity and Reynolds number.

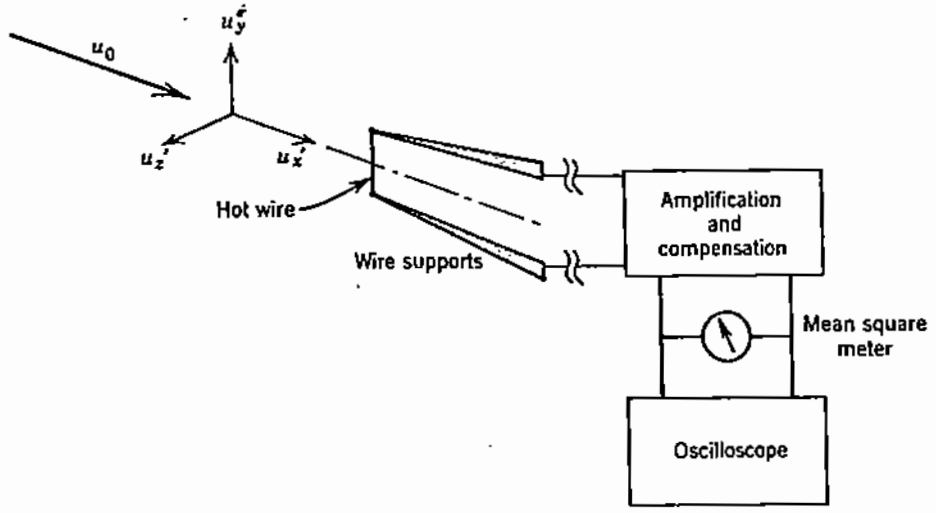

Figure 7.5. Hot wire anemometer for measuring intensity of turbulence.

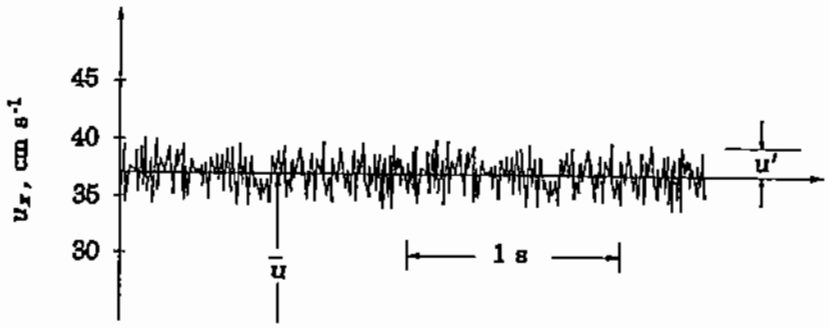

Figure 7.6. Time-averaged and fluctuating velocity components in turbulent flow.

The actual velocity at any particular time, u_x, may be expressed as the sum of the time-averaged velocity and the fluctuating component u'_x, i.e.,

$$u_x = \overline{u}_x + u'_x. \tag{7.2.1}$$

The same considerations apply to the velocity components in the other two directions, i.e., u_y and u_z. Similarly, the pressure at any point and at any particular instant can be expressed as the sum of a time-averaged pressure plus a fluctuating component P':

$$P = \overline{P} + P'. \tag{7.2.2}$$

The time-averaged velocity in the direction x over time interval t_c is expressed mathematically as follows:

$$\overline{u_x} = \frac{1}{t_c} \int_0^{t_c} u_x \, dt. \tag{7.2.3}$$

By definition, the time-averaged values of the fluctuating components

$$\overline{u'_x}, \ \overline{u'_y}, \ \overline{u'_z}, \ \overline{P'}$$

are equal to zero. However, the time-averaged value of the *square* of a fluctuating component is not equal to zero:

$$\overline{u'^2_x} = \left(\frac{1}{t_c}\right) \int_0^{t_c} (u'_x)^2 \, dt \neq 0. \tag{7.2.4}$$

Therefore, the degree of turbulence in a flow system may be expressed either in terms of the **root mean square of the fluctuating velocity components**, i.e.,

$$\overline{(u'^2_x)}^{1/2}, \ \overline{(u'^2_y)}^{1/2} \ \overline{(u'^2_z)}^{1/2}, \tag{7.2.5}$$

or in terms of the ratios of the above quantities to the corresponding time- averaged velocity components:

$$\frac{\overline{(u'^2_x)}^{1/2}}{\overline{u_x}}, \ \frac{\overline{(u'^2_y)}^{1/2}}{\overline{u_y}}, \ \frac{\overline{(u'^2_z)}^{1/2}}{\overline{u_z}}. \tag{7.2.6}$$

The ratios of (7.2.6) are called the **intensity of turbulence**. Their values range from 0.02 to 0.1 for flow through a pipe but can be much higher in highly mixed systems, such as, for example, a gas-injected liquid bath.

The equations of continuity and motion for laminar flow, can also be adapted to turbulent flow systems by taking into consideration both the time-averaged and the fluctuating components of velocity. However, the solution of the differential equations of motion for turbulent systems presents much greater complexity than for laminar systems.

The principal difference is that in laminar flow there is a unique relationship between the shear stress in the fluid and the velocity gradient, in terms of the molecular viscosity of the fluid. There is no such relationship in turbulent flow: the value of the proportionality constant between shear stress and the averaged velocity gradient in a turbulent system depends both on the fluid properties and the actual flow conditions in the system.

By substituting from (7.2.1) into the equations of continuity and motion presented earlier (see (5.1.6) and (5.2.18)), it can be shown that the form of the continuity equation remains the same. However, because of the presence of the fluctuating components, six new terms appear in the equation of motion:

$$\begin{aligned} &\overline{\rho u_x' u_x'},\ \overline{\rho u_x' u_y'},\ \overline{\rho u_x' u_z'}, \\ &\overline{\rho u_y' u_y'},\ \overline{\rho u_y' u_z'},\ \overline{\rho u_z' u_z'}. \end{aligned} \tag{7.2.7}$$

The above terms are usually called *Reynolds stresses*.

7.3. THE CONCEPT OF EDDY VISCOSITY

Boussinesq [3] related the magnitude of the Reynolds stresses (see (7.2.7)) to the velocity gradient in a turbulent fluid by means of the following equation:

$$\tau_{y,x}' = \overline{\rho u_x' u_y'} = -\mu_e \frac{d\overline{u}_x}{dy}, \tag{7.3.1}$$

where μ_e is defined as the **eddy viscosity**, or *apparent turbulent viscosity*, of the fluid system and is dependent on location. For instance, close to a wall μ_e may be insignificant in comparison to the molecular viscosity of the fluid, but in the bulk of a highly mixed fluid the eddy viscosity can be orders of magnitude greater.

In accordance with the Boussinesq concept, the total shear stress in a fluid consists of the sum of the laminar and turbulent components:

$$\tau_{y,x} + \tau_{y,x}' = -(\mu + \mu_e) \frac{d\overline{u}_x}{dy}. \tag{7.3.2}$$

The above equation expresses elegantly the contribution of turbulence to the shear stress in a system but it is of little practical use unless one can assign specific values to the eddy viscosity at each location. In order to do so, Prandtl [4] assumed that eddies move in the fluid in the same way as molecules in a gas. Accordingly, a **mixing length** was defined which is equivalent to the mean free path in the molecular representation of gas viscosity. This assumption led to the following equation for eddy viscosity:

$$\mu_e = \rho l_m^2 \frac{du_x}{dy}. \tag{7.3.3}$$

Prandtl suggested that the size of the mixing length, l_m, was proportional to the distance from the wall, y. For flow in a pipe of radius r_0, the mixing length is related as follows to the pipe radius (see Fig. 7.3):

$$l_m \approx 0.4y \text{ for } y \geq 0.2r_0. \tag{7.3.4}$$

Subsequent studies have shown that the mixing length hypothesis can describe well the effects of turbulence near the wall of a conduit. However, the Prandtl model cannot describe adequately turbulent flow in complex two-dimensional or three-dimensional systems, such as in chemical and metallurgical reactors.

7.4. THE $k-\varepsilon$ MODEL OF TURBULENCE

It is now generally accepted that a very useful way of characterizing turbulent flows is by means of the *kinetic energy of turbulence*, k, per unit mass of fluid. This is defined as the following function of the fluctuating components of velocity:

$$k = \frac{1}{2}\left(\overline{u_x'^2} + \overline{u_y'^2} + \overline{u_z'^2}\right). \tag{7.4.1}$$

For **isotropic turbulence**, which represents most of the turbulent energy in bulk flows, we have

$$\overline{u_x'^2} = \overline{u_y'^2} = \overline{u_z'^2}. \tag{7.4.2}$$

Therefore, the kinetic energy of turbulence (see (7.4.1)) can be expressed as follows:

$$k = \frac{3}{2}\overline{u_x'^2}, \tag{7.4.3}$$

and its dimensions are $L^2\ t^{-2}$. One of the most prominent mathematical models for describing turbulence in bulk flows is the $k-\varepsilon$ model developed by Spalding and co-workers [5]. This model assumes that the *rate of change of turbulent energy*, k, in a fluid element is a function of the turbulence energy and velocity gradients in the fluid minus a function ε which is defined as the *rate of dissipation of turbulent energy*. If we use the index notation of i and j to represent the dyadic products of the three components of velocity, u_x, u_y, and u_z, the corresponding energy balance is expressed as follows:

$$\frac{\partial k}{\partial t} + u_i\frac{\partial k}{\partial x_i} = \frac{\partial}{\partial x_i}\left(\frac{\nu_t}{\sigma_k}\frac{\partial k}{\partial x_i}\right) + \nu_t\left(\frac{\partial u_i}{\partial x_j} + \frac{\partial u_j}{\partial x_i}\right)\frac{\partial u_i}{\partial x_j} - \varepsilon, \tag{7.4.4}$$

where σ_k is a constant and ν_t is the effective turbulent momentum diffusivity (or turbulent kinematic viscosity) and is defined as follows:

$$\nu_t = \nu + \nu_e = \frac{\mu + \mu_e}{\rho} = \frac{\mu_t}{\rho}. \tag{7.4.5}$$

apparent

The $k-\varepsilon$ model assumes that the ~~effective~~ turbulent kinematic viscosity is related to the kinetic energy of turbulence by the following equation:

$$\nu_e = \frac{C_D k^2}{\varepsilon}, \tag{7.4.6}$$

where $C_D = 0.09$ [6].

The $k-\varepsilon$ model also assumes that the rate of change of the function ε in a fluid element is represented by the following equation:

$$\frac{\partial \varepsilon}{\partial t} + u_i \frac{\partial \varepsilon}{\partial x_i} = \frac{\partial}{\partial x_i}\left(\frac{\nu_t}{\sigma_\varepsilon}\frac{\partial \varepsilon}{\partial x_i}\right) + C_1 \nu_e \left[\frac{\partial}{\partial x_i}\left(\frac{\partial u_i}{\partial x_j}\right)\right]\frac{\varepsilon}{k} - C_2\frac{\varepsilon^2}{k}, \tag{7.4.7}$$

where σ_ε, C_1, and C_2 are constants.

It can be seen that the left sides of (7.4.4) and (7.4.7) correspond to the substantial time derivatives of k and ε, respectively. As we discussed in Chapter 5 (see (5.1.8)), these derivatives describe the rate of change of k and ε as observed by someone moving with the fluid element. In the case of non-isothermal flow, the $k-\varepsilon$ model includes one more equation and additional terms to account for the effect of buoyancy forces in the fluid (Chapter 12).

The value of the "constants" σ_k, σ_ε, C_1, and C_2 in (7.4.4)–(7.4.7) to a certain extent depends on the geometry of the flow system (curvature, near-wall effects, etc. However, for most cases, the following values were recommended by Jones and Launder [7] and are generally used:

$$\sigma_k = 1.0,\ \ \sigma_\varepsilon = 1.3,\ \ C_1 = 1.44,\ \ C_2 = 1.92,\ \ C_D = 0.09.$$

Equations (7.4.4) and (7.4.7) are coupled and must be solved simultaneously by means of numerical techniques. The FIDAP fluid dynamics program [9] is one of the commercially available packages which facilitate greatly the solution of the differential equations for turbulent flow. This program uses the finite element method of numerical analysis. Examples of this technique in heat transfer problems will be presented in later chapters.

Example 7.4.1

Sahai and Guthrie [8] developed the following equation for the effective turbulent viscosity of a metal bath contained in a ladle stirred by means of gas injection through a bottom orifice (Fig. 7.7):

$$\mu_t = 5.5 \times 10^{-3} \rho_m L \left[\frac{(1-\alpha) g \dot{v}}{d_l}\right]^{1/3}, \tag{7.4.8}$$

where ρ_m is the density of liquid metal, 7500 kg/m^3; L is the depth of metal above point of injection, m; α is the gas fraction in the "plume" rising above the point of injection; $\dot{v}$ is the gas injection rate, m^3/s; d_l is the ladle diameter, m.

Calculate the effective turbulent viscosity of the bath in a 250-ton steel refining ladle (1600°C) under the following operating conditions:

Ladle diameter = 3.6 m.

Depth of liquid bath = 2.4 m.

Injection gas flow rate = 1.07 Nm^3/min.

Estimated gas volume fraction in plume = 0.2.

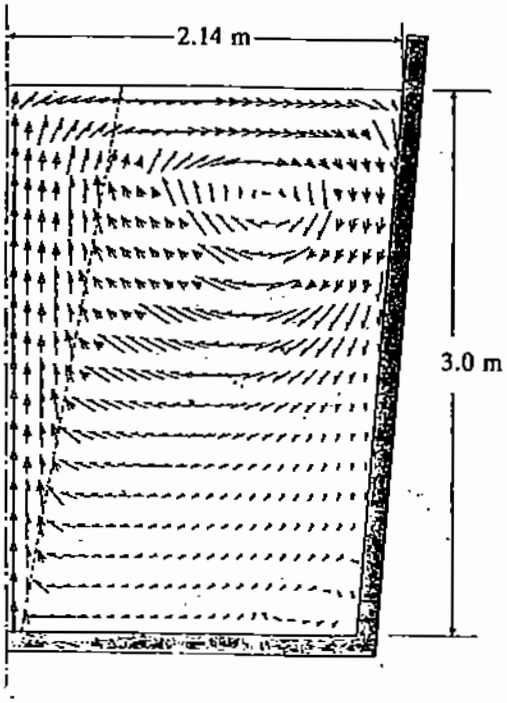

Figure 7.7. Plume formation and recirculating flow in a gas-injected metal bath (injection orifice at centerline of vesssel).

First we calculate the volumetric rate of gas injection at 1600°C and at an average pressure equal to half the metal depth:

$$\dot{v} = \frac{1.07}{60} \times \frac{(1600 + 273)}{273} \times \frac{101300}{(101300 + \frac{2.4}{2} \times 7500 \times 9.807)} = 0.065 \frac{\text{m}^3}{\text{s}}.$$

Then, by substituting the given numerical values in (7.4.8), we find that the effective turbulent viscosity is

$$\mu_t = 5.5 \times 10^{-3} \times 7500 \times 2.4 \times \left(\frac{9.807 \times 0.061}{3.6}\right)^{1/3} = 51.6 \text{ kg s}^{-1} \text{ m}^{-1}. \quad (51.6)$$

It can be seen that this value is much larger than the molecular viscosity of molten steel ($\mu = 6$ cP $= 6 \times 10^{-3}$ kg s^{-1} m^{-1}).

Example 7.4.2

Sahai and Guthrie proposed [8,2] the following correlations for calculating the velocity of the rising plume (u_p) and the average recirculation velocity (u_{ave}) in a liquid steel bath in which gas is injected through an orifice at the bottom of the bath (Fig. 7.7):

$$u_p = \frac{4.4 L^{0.25} \dot{v}^{0.33}}{R^{0.33}}, \quad (7.4.9)$$

$$u_{\text{rec}} = \frac{0.18 u_p}{R^{0.33}}, \quad (7.4.10)$$

where L is the depth of the orifice below the bath surface, m; $\dot{v}$ is the gas flow rate through the orifice, m^3/s, at actual conditions; R is the radius of the ladle containing the liquid, m.

Gas is injected through the bottom of a ladle containing liquid metal (Fig. 7.7) at the flow rate of 0.4 $Nm^3\ s^{-1}$ (1.65 $m^3\ s^{-1}$ at the actual conditions of 1200°C and 1.3 atm in the molten bath). The injection orifice is located 1 m below the surface of the bath. If it is assumed that the equivalent radius of the molten bath, i.e., the radius of the zone affected by the rising "plume" of gas (Fig. 7.7) is 1 m, calculate: a) the "plume" velocity; b) the average residence time of the injected gas in the melt; and c) the recirculating velocity of the melt in the zone around the plume.

From (7.4.9), the "plume" velocity is calculated to be 5.2 m s^{-1}. Accordingly, the residence time of the gas in the melt is approximately $1/5.2 = 0.19$ seconds. The recirculating velocity is calculated from (7.4.10) to be 0.94 m s^{-1}.

REFERENCES

1. O. Reynolds, *Phil. Trans. Roy. Soc., London*, **174A**(3), 935 (1883).
2. R.I.L. Guthrie, *Engineering in Process Metallurgy*, Clarendon Press, Oxford, p. 118 (1989).
3. T.V. Boussinesq, *Mem. Pres. Div. Sav., Paris*, **23** (1877).
4. L. Prandtl, Z *Angew. Math. Mech.*, **5**, 136 (1925).
5. B.E. Launder and D.B. Spalding, *Lectures in Mathematical Models of Turbulence*, Academic Press, New York (1972).
6. Patterson, "Turbulent Mixing and its Measurement," in *Handbook of Fluids and Motion*, eds. Cheremisinoff and Gupta, Butterworths, Boston, pp. 96–97 (1983).
7. W.P. Jones and B.E. Launder, *Int. J. Heat and Mass Transfer*, **16**, 119 (1973).
8. Y. Sahai and R.I.L. Guthrie, *Metallurgical Trans. B*, **13B**, 193–202 (1982).
9. *FIDAP Program*, Version 7, Fluid Dynamics International, Evanston, IL (1993).

EIGHT

Overall Material and Energy Balance in Fluid Flow

In Chapters 4 through 7, we developed the equations of continuity and motion and discussed some of their applications. In their general form, these equations are highly complex; however, we showed that by making certain simplifying assumptions, they can be solved to provide the velocity profiles resulting from the forces acting on the flow system.

The principal advantage of the differential equations of flow is that they can provide information on the fine structure of flow. However, in many engineering problems we are not concerned with the "microstructure" of flow but with the overall relationship between the forces acting on a flow system, such as pressure and gravity, and the flow rate of fluids through it.

Examples of problems on the "macrostructure" of flow are: the size of a pump needed to move a fluid between two points; the time required to empty a vessel containing liquid through an orifice; the design of an orifice meter to measure flow velocities through a conduit, and so forth.

Such problems are quite common in the design and operation of processes. They can be solved by establishing the overall energy and material balances between an "inlet" and an "outlet" point of the system; and then solving the resulting equations for the inlet and outlet boundary conditions. The difference between the "microstructure" and the "macrostructure" approaches to fluid flow problems is illustrated in Fig. 8.1.

In general, the overall balances result in algebraic equations for steady-state systems and in first order differential equations for unsteady-state, or time-dependent systems. Such equations are much easier to solve than the differential equations of flow but, of course, provide less information on the flow phenomena within the system.

In dealing with the fine structure of flow, we had to introduce the phenomenological factor of viscosity which relates the shear stress to the velocity gradient (Newton's law of viscosity). In the same way, in developing the overall energy equations we need to establish various relationships between the parameters involved. In general, such correlations are "semi-empirical," i.e., they are based both on theoretical considerations and on experimentally developed constants.

8.1. THE OVERALL MATERIAL BALANCE

To construct the overall material balance for flow in the vessel shown in Fig. 8.2, we will consider the whole vessel as the control volume. Since material enters only through surface

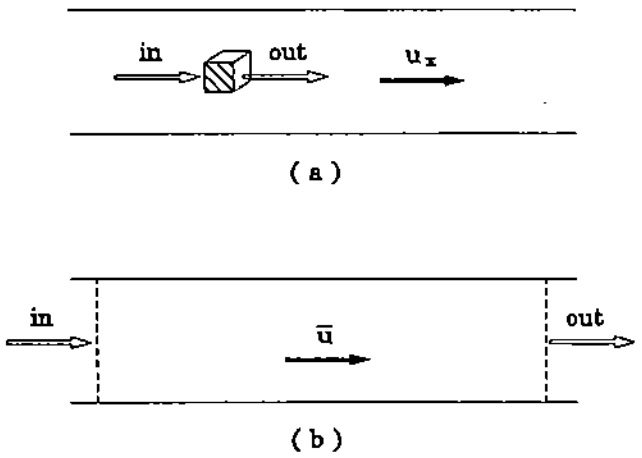

Figure 8.1. Illustration of (*a*) "microscale" and (*b*) "macroscale" balances in a conduit.

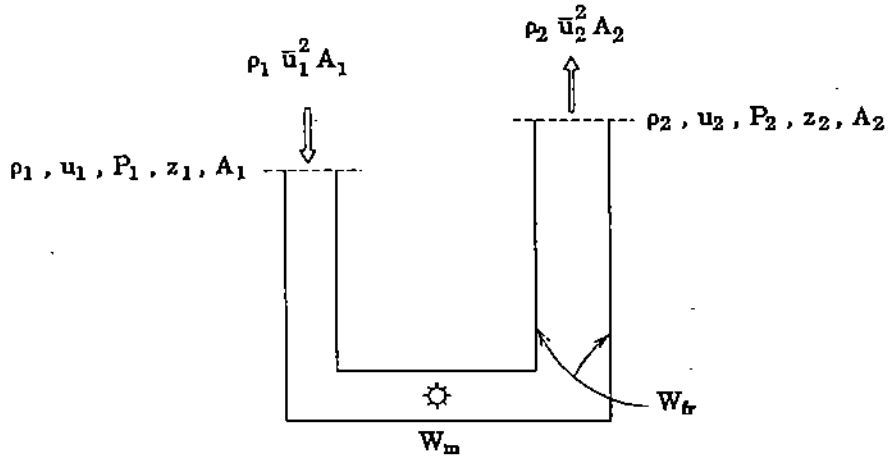

Figure 8.2. Overall momentum balance in a flow system.

A_1 and leaves through surface A_2, the conservation of mass in the control volume can be expressed algebraically as follows:

$$\begin{aligned}&\text{rate of material accumulation within the system}\\&= \text{mass flow rate in} - \text{mass flow rate out.}\end{aligned} \tag{8.1.1}$$

Under steady state conditions, there is no accumulation or depletion of mass in the control volume and the above equation simplifies to:

$$\text{mass flow rate in} = \text{mass flow rate out} \tag{8.1.2}$$

$$\rho A\bar{u} = \rho_1 A_1 \bar{u}_1 = \rho_2 A_2 \bar{u}_2, \tag{8.1.3}$$

where ρ represents the density and $\bar{u}$ the average velocity of the fluid at locations *1* and *2*.

8.2. THE OVERALL MECHANICAL ENERGY BALANCE

In the following discussion, we shall consider only the mechanical energy terms of the energy balance, that is kinetic, pressure and potential (e.g., gravity) energy; a more general statement of the conservation of energy, i.e., the first law of thermodynamics, must include thermal effects such as the generation of heat due to the viscous force. The equations to be developed in this chapter apply to systems which can be assumed to be isothermal. This assumption is reasonable for most engineering systems, since the heat produced by friction is relatively small and can not affect the temperature of the flow system appreciably. For high friction systems, e.g., in certain problems of lubrication, provision must be made in the system design to remove the heat produced (e.g., by air or water cooling) and maintain the system essentially isothermal.

The overall mechanical energy balance is established in a similar way as was done in Chapter 5 for developing the equation of motion; however, in this case, the differential volume element is replaced by the volume of the entire system, as illustrated in Fig. 8.2:

$$\begin{aligned}&\text{rate of accumulation of energy within the control volume}\\&\quad=\text{net transport rate of kinetic energy}\\&\qquad+\text{net transport rate of potential energy}\\&\qquad+\text{net transport rate of pressure energy}\\&\qquad+\text{rate of mechanical work done}\\&\qquad+\text{rate of work done against friction}\end{aligned}\tag{8.2.1}$$

The word *net* is used in (8.2.1) to indicate *input minus output* to the control volume. The words *transport rate* are used to indicate that kinetic, potential, and pressure energy are associated with a particular *mass flow rate*; e.g., as the fluid moves from a high level to a lower one its potential energy content decreases. The terms *rate of work* are used in the last two terms of (8.2.1) to indicate that this work is also due to a particular mass flow rate.

At steady state conditions, there is no change in the kinetic and potential energy within the control volume. Therefore, the left side of (8.2.1) becomes zero. This equation is then expressed in algebraic form as follows:

$$\begin{aligned}&\frac{1}{2}\left[(\rho_2 A_2\overline{u}_2)\,\overline{u}_2^2-(\rho_1 A_1\overline{u}_1)\,\overline{u}_1^2\right]\\&+\left[(\rho_2 A_2\overline{u}_2)\,gz_2-(\rho_1 A_1\overline{u}_1)\,gz_1\right]+\int_1^2 d(PA\overline{u})+W_m+W_{\mathrm{fr}}=0.\end{aligned}\tag{8.2.2}$$

In (8.2.2), the pressure term is expressed as an integral of $d(PA\overline{u})$ to include the case of compressible flow where density is a function of pressure. The rate of "mechanical work," W_m, refers to the rate at which the system performs mechanical work, e.g., work done *by* the fluid in turning a turbine; it is preceded by a minus sign if it represents mechanical work done *on* the system, e.g., by an internal pump. The term "work done against friction," W_{fr}, represents the rate at which mechanical energy in the fluid is used up because of the viscous forces in the fluid.

For steady-state conditions, the mass flow rate through the control volume does not change (see (8.1.3)). By dividing all terms of (8.2.2) by the mass flow rate of (8.1.3), we obtain

$$\frac{1}{2}\left(\overline{u}_2^2 - \overline{u}_1^2\right) + g(z_2 - z_1) + \int_1^2 \frac{d(PA\overline{u})}{\rho A\overline{u}} + W'_m + W'_{\text{fr}} = 0, \tag{8.2.3}$$

and for a conduit of constant cross-section, where $A\overline{u} = A_1\overline{u}_1 = A_2\overline{u}_2$,

$$\frac{1}{2}\left(\overline{u}_2^2 - \overline{u}_1^2\right) + g\left(z_2 - z_1\right) + \int_1^2 \frac{dP}{\rho} + W'_m + W'_{\text{fr}} = 0. \tag{8.2.4}$$

The term W'_m represents the rate of mechanical work done on the system (e.g., turning an impeller), or by the system on the fluid (e.g., a pump within the conduit); the term W'_{fr} represents the rate of work to overcome frictional forces; they are both expressed per unit mass of fluid through the system in order to be consistent with the rest of the terms in this equation. Thus, all the terms in (8.2.3) have the dimensions of *energy (or work) per unit mass*, i.e., $\text{L}^2\ \text{t}^{-2}$.

Equation (8.2.3) represents the conservation of mechanical energy for steady state systems and is sometimes referred to as the **Bernoulli equation** for engineering systems. This equation is very useful in providing a relationship between the initial and terminal values of u, z, and P and the work terms W'_m and W'_{fr}.

In the following section, we shall discuss some cases of flow where there is no work done on the surroundings and where the frictional term may be assumed to be negligible. Such problems can be solved using (8.2.3) without needing to resort to any semi-empirical relationships.

8.3. MEASUREMENT OF VELOCITY

8.3.1. The Pitot and Venturi Meters

An important application of the Bernoulli equation is in measuring the velocity of fluids. An instrument used for this purpose and also for measuring the speed of vehicles through air (e.g., airplanes) is the Pitot tube shown in Fig. 8.3. It consists of two concentric tubes which are sealed together at the front annulus and at the other end are connected to each side of a manometer or other pressure measuring device; at the front end of the Pitot tube, the inner tube measures the "impact" pressure of the flow stream while the outer tube, through a downstream opening on the side, measures the "static" pressure at the same location (Fig. 8.3).

At point *1* where the gas flow impacts on the tip of the Pitot tube, the gas velocity, $\overline{u}_1$, becomes zero; at the downstream point 2, the gas flows past the tube at the average velocity of the stream, $\overline{u}_2$. It is evident that the kinetic energy of the stream is converted to pressure energy and therefore $P_1 > P_2$. If we assume that the compressibility effects are negligible and there is no loss of energy between sections *1* and 2, (8.2.4) yields

$$\frac{1}{2}\left(\overline{u}_2^2 - \overline{u}_1^2\right) = -\int_1^2 \frac{dP}{\rho} = -\frac{(P_2 - P_1)}{\rho}. \tag{8.3.1}$$

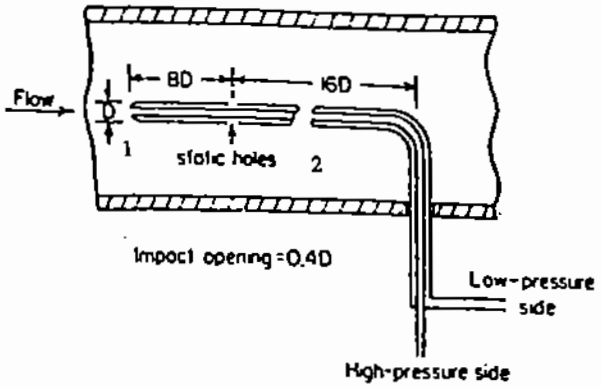

Figure 8.3. Pitot tube for measuring fluid velocity.

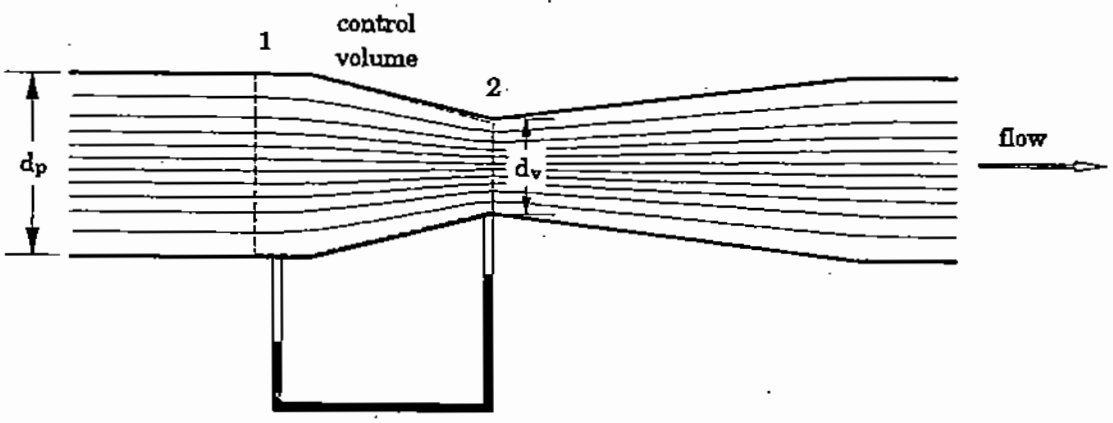

Figure 8.4. Streamlines through venturi tube.

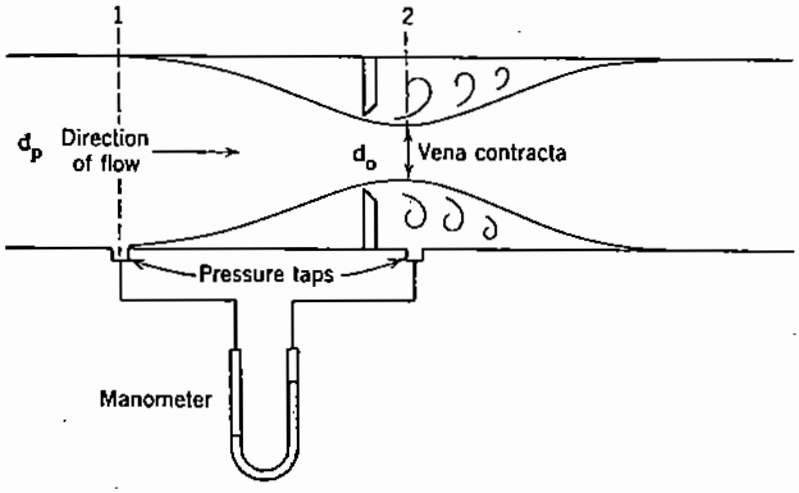

Figure 8.5. Orifice plate meter for measuring flow velocity.

Since $\overline{u}_1 = 0$, the stream velocity $\overline{u}_2$ can be calculated from the measured pressure differential as follows:

$$\overline{u}_2 = \left[\frac{2(P_1 - P_2)}{\rho}\right]^{0.5}. \tag{8.3.2}$$

Another instrument used to measure total flow through a tube is the **venturi meter**, where the cross-sectional area for flow is first reduced and then expanded (Fig. 8.4). If we measure the pressures at points *1* and 2, we find that $P_1 > P_2$. The reason is that the constriction in area between points *1* and *2* has resulted in a higher velocity at point 2; thus, the kinetic energy of the fluid has increased at the expense of the pressure energy. By using (8.3.1) and also the overall material balance of (8.1.3) for negligible change in density of the fluid between point *1* (where the diameter of the pipe is d_p) and at the "throat" of the venturi (point 2, diameter = d_v), we derive the following equation for the fluid velocity at the "throat" of the venturi:

$$\overline{u}_2 = \left[\frac{2(P_1 - P_2)}{\rho\,(1 - A_2^2/A_1^2)}\right]^{0.5}. \tag{8.3.3}$$

Once the velocity is calculated, the volumetric flow rate can be determined from the product $\overline{u}_2 A_2$.

It should be noted that venturi meters provide for gradual and relatively smooth contraction and expansion of the conduit, in order to minimize friction loss in the venturi. However, in practice there is some energy loss and to account for it the **venturi coefficient**, C_v, is introduced in (8.3.3); typical values of this coefficient range from 0.98 to 1.0. Thus, a more general form of (8.3.3) for the cylindrical venturi of Fig. 8.4 is as follows:

$$\overline{u}_t = C_v \left[\frac{2(P_1 - P_2)}{\rho\,(1 - d_v^4/d_p^4)}\right]^{0.5}, \tag{8.3.4}$$

where $\overline{u}_t$ is the velocity at the venturi throat, d_v the throat diameter, and d_p the diameter at the entry to the venturi.

8.3.2. The Orifice Plate Meter

A very useful device for measuring flow in cylindrical conduits is the **orifice meter** shown in Fig. 8.5. The fluid approaches the orifice with a velocity u_1 and at pressure P_1. At the orifice plate, the cross-sectional area of flow is restricted suddenly from A_1 to A_2 and the velocity is therefore increased to u_2. Therefore, the principle of operation is the same as for the venturi meter but, because of the sudden contraction and expansion of the flow area, the frictional loss in this case is appreciable.

It is therefore necessary to introduce a correction factor in the balance between kinetic and pressure energy, as we did in the case of the venturi meter. However, this **orifice coefficient**, C_o is considerably smaller than 1 and depends on the design of the orifice plate, the ratio of orifice diameter to pipe diameter, and the location of the pressure measuring taps (Fig. 8.6). For a cylindrical conduit of diameter d_p and orifice plate diameter d_o (Fig. 8.5), the orifice meter equation is similar to (8.3.4) for the venturi meter:

$$\overline{u}_2 = C_o \left[\frac{2(P_1 - P_2)}{\rho(1 - d_o^4/d_p^4)}\right]^{0.5}. \tag{8.3.5.}$$

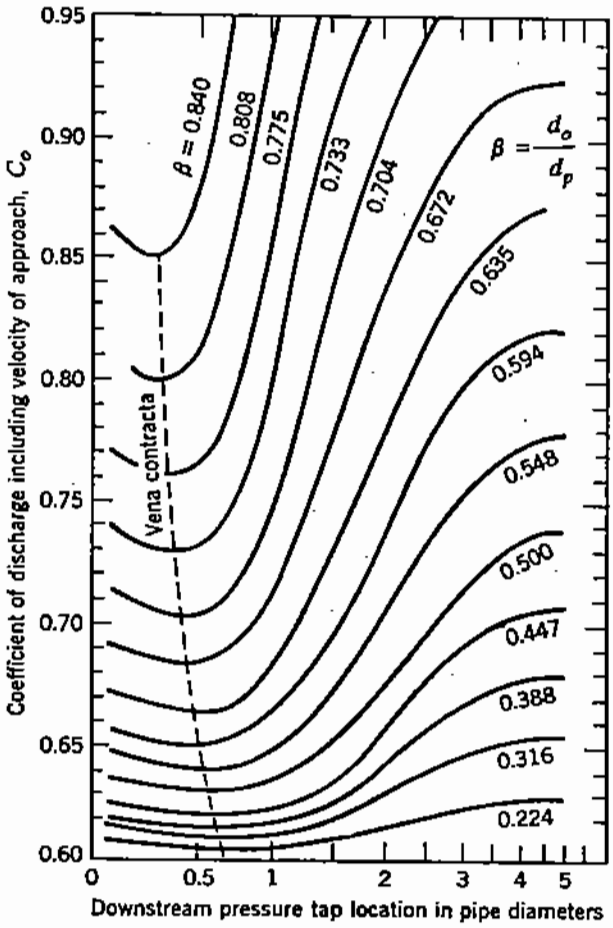

Figure 8.6. Discharge coefficients for square-edged circular orifices.

Let us now develop an expression equivalent to (8.3.5) for the case of a **compressible** fluid in isothermal flow through an orifice; for isothermal flow, the ideal gas law yields:

$$PV = P_1V_1 = P_2V_2 = nRT, \tag{8.3.6}$$

where V is the volume of n moles of gas, and R the universal gas constant (Table A2). By combining (8.3.6) with the pressure integral of (8.3.1), we obtain:

$$-\int_1^2 \frac{dP}{\rho} = -\int_1^2 V\,dP = -\int_1^2 P_1V_1\,\frac{dP}{P} = P_1V_1 \ln\left(\frac{P_1}{P_2}\right). \tag{8.3.7}$$

Therefore, on the basis of the same assumptions as we made in the derivation of (8.3.5), we obtain the following equation for the velocity of compressible flow through an orifice of diameter d_o:

$$\overline{u}_2 = C_o \left[\frac{2P_1V_1 \ln \frac{P_1}{P_2}}{\left(1 - \frac{d_o^4 P_2^2}{d_p^4 P_1^2}\right)}\right]^{0.5}. \tag{8.3.8}$$

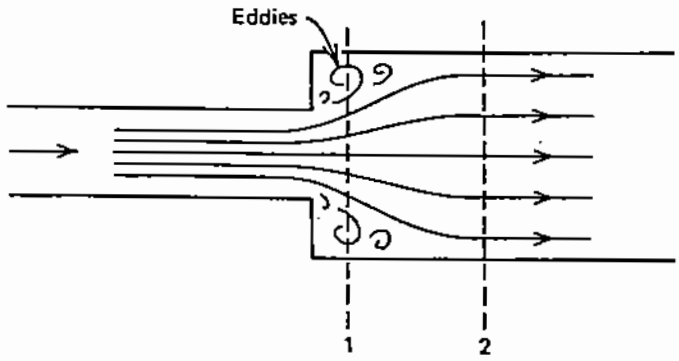

(a)

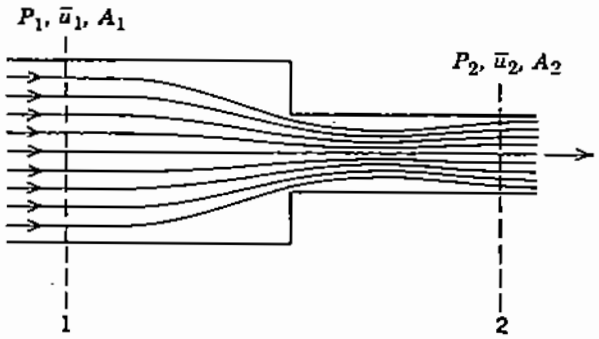

(b)

Figure 8.7. Streamlines for (*a*) sudden expansion and (*b*) sudden contraction of flow.

8.4. FRICTIONAL LOSS IN SUDDEN EXPANSION AND CONTRACTION

When a fluid flows through a sudden expansion in a pipe (Fig. 8.7a), the increase in cross-sectional area results in a gradual decrease in the fluid velocity. Thus, fluid with a relatively high velocity is suddenly injected into a fluid moving more slowly. This results in eddies and energy loss between the planes *1* and *2*. The frictional loss due to this phenomenon can be expressed by

$$W'_{\mathrm{fr,e}} = k_{\mathrm{e}} \left(\frac{\overline{u}_1^2}{2} \right), \tag{8.4.1}$$

where k_e is the expansion loss coefficient. For turbulent flow, k_e is related to the initial and final diameters as follows [1]:

$$k_{\mathrm{e}} = \left(1 - \frac{d_1^2}{d_2^2} \right)^2, \tag{8.4.2}$$

where d_1 and d_2 are the diameters of the small and the larger pipes, respectively.

In contrast, Fig. 8.7b shows the flow through a pipe, the diameter of which is suddenly reduced from d_1 to d_2. The reduction in effective area for flow continues for a short distance beyond the actual constriction, forming a "vena contracta" similar to that observed in orifice plates. After passing through the vena contracta, the flow area gradually expands to fill the cross-sectional area of the pipe. As the fluid moves towards the vena contracta, its velocity

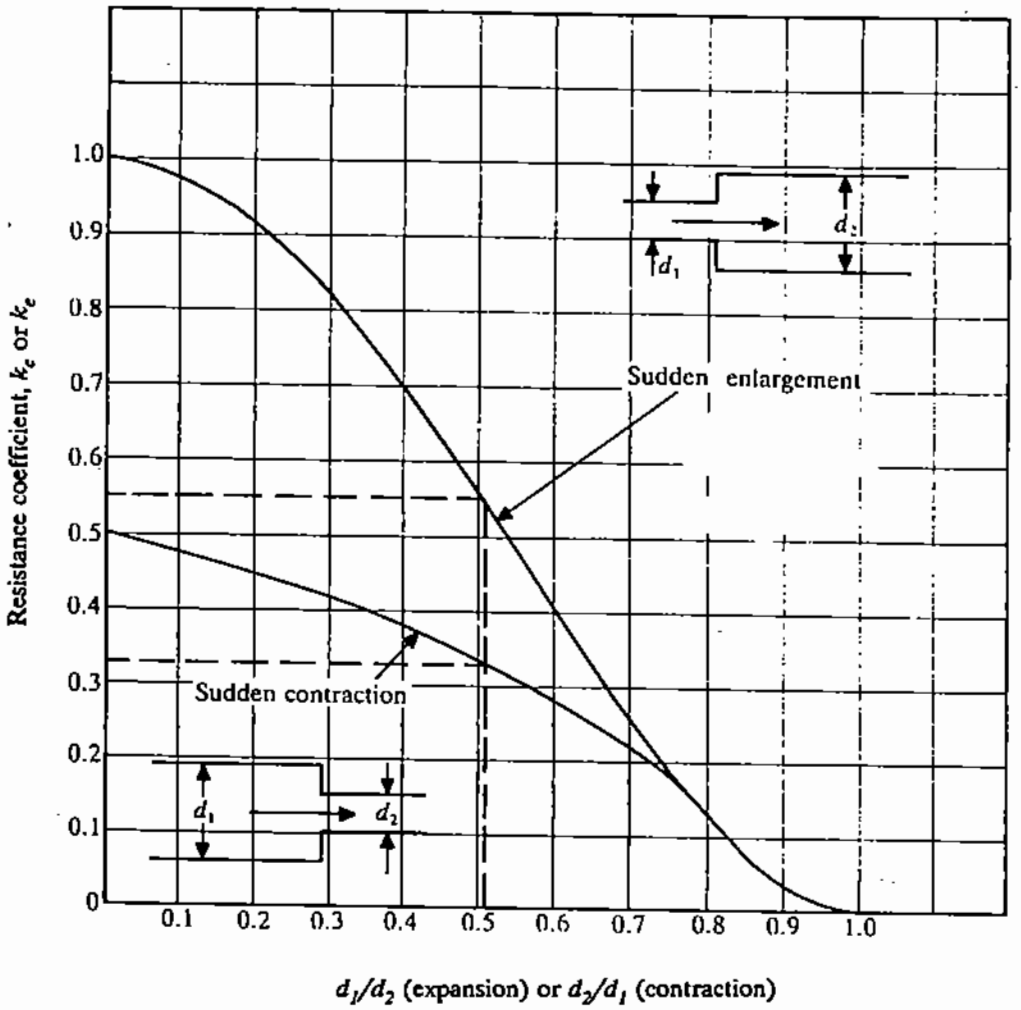

Figure 8.8. Coefficients of expansion and contraction in turbulent flow [10].

increases and some of the pressure energy is converted to kinetic energy; this process does not result in eddy formation. On the other hand, the expansion of the fluid after passing through the vena contracta is similar to the case of sudden expansion and results in the formation of energy-consuming eddies. The energy loss in this case can be expressed as follows:

$$W'_{\mathrm{fr,c}} = k_c \left(\frac{\overline{u}_2^2}{2}\right), \tag{8.4.3}$$

where, for turbulent flow, the contraction loss coefficient k_c is expressed by the following equation [1]:

$$k_c = 0.42 \left(1 - \frac{d_2^2}{d_1^2}\right)^2 \quad \text{for } 0.4 \leq \frac{d_2}{d_1} \leq 0.76. \tag{8.4.4}$$

As shown in the empirical plot of Fig. 8.8 [1], at the value of $d_2/d_1 = 0.76$ the sudden contraction curve merges with the sudden expansion curve. Therefore, (8.4.2) can be used to determine the value of k_c at $d_2/d_1 > 0.76$, by reversing the definitions of d_1 and d_2.

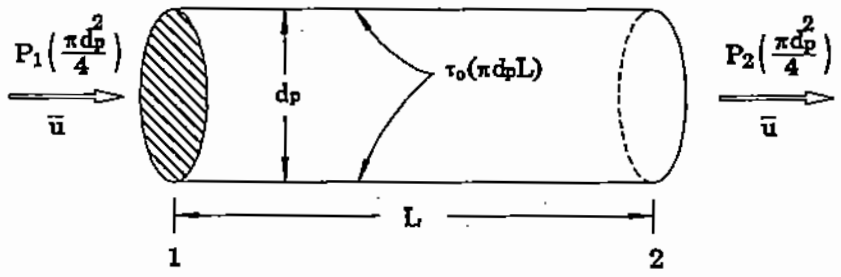

Figure 8.9. Balance of viscous shear stress and pressure forces in a conduit.

Also, Fig. 8.8 shows that in the case of very large contraction in flow ($d_2/d_1 \to 0$), the limiting value of k_c is 0.5 and the energy loss of (8.4.3) becomes

$$W'_{\mathrm{fr,c}} = 0.25\,\bar{u}_2^2. \tag{8.4.5}$$

8.5. THE FRICTION FACTOR

In the applications of the overall energy balance discussed in §8.3, the friction force acting on the surface on the conduit was assumed to be negligible. However, in most engineering problems, such an assumption would not be realistic. Therefore, we need to find a correlation between the frictional loss, W'_{fr}, and the measurable characteristics of the flow system.

Let us consider the flow of an incompressible fluid at an average velocity ($\bar{u}$) through a horizontal pipe of length L and diameter d_p (Fig. 8.9). Under these conditions, there is no change in the potential energy and kinetic energy contents of the fluid and also there is no mechanical work done. Therefore, under steady state conditions, the overall energy balance yields

$$-\int_{P_1}^{P_2} \frac{dP}{\rho} = \frac{P_1 - P_2}{\rho} = W'_{\mathrm{fr}}. \tag{8.5.1}$$

This equation expresses the fact that between points *1* and *2*, the fluid loses a certain amount of pressure energy by doing work against friction. However, (8.5.1) is of little practical use for calculating the pressure drop, unless we have a way of expressing the frictional loss in terms of some of the other known parameters of the flow system.

Such a correlation can be obtained by introducing the **friction factor**, f_{fr}, a dimensionless number which is defined as the ratio of the shear stress at the surface of a conduit (or *drag force* per unit surface area of conduit wall) to the kinetic energy per unit mass flow of the fluid:

$$f_{\mathrm{fr}} = \frac{\tau_0}{\left(\frac{\rho \bar{u}^2}{2}\right)}. \tag{8.5.2}$$

Since the only forces acting in the horizontal pipe between points *1* and *2* are due to friction and pressure (since there is no change in the kinetic and potential energies), a balance between these two forces (Fig. 8.9) yields

$$F_{\mathrm{fr}} = \tau_0(\pi d_p L) = (P_1 - P_2)\left(\frac{\pi d_p^2}{4}\right). \tag{8.5.3}$$

Table 8.1. Typical Values of Material Roughness

Material	e, cm
Copper tubing	1.0×10^{-3}
Finished concrete	4.6×10^{-3}
Unfinished concrete	1.2×10^{-2}
Cast iron	1.8×10^{-2}
Refractory	2.7×10^{-2}
Riveted steel	4.6×10^{-2}
Corrugated metal	2.1×10^{-1}

By solving for τ_0 from (8.5.3) and substituting in (8.5.2), we obtain the following equation for the friction factor:

$$f_{\text{fr}} = \frac{d_p(P_1 - P_2)}{2\,L\rho\bar{u}^2}. \tag{8.5.4}$$

Alternatively, the above equation can be expressed as a statement that the ratio of pressure loss due to friction to the kinetic energy of the stream is proportional to the friction factor:

$$\frac{(P_1 - P_2)}{\frac{1}{2}\rho\bar{u}^2} = \frac{4L}{d_p} f_{\text{fr}}. \tag{8.5.5}$$

Numerous experimental studies have shown that the friction number depends only on the Reynolds number and the *roughness* of the pipe wall, e (Table 8.1); the latter is usually expressed as the ratio of the actual surface roughness (i.e., the height of protrusions from surface) divided by the inner diameter of the pipe (relative roughness = e/d_p).

A plot of f_{fr} against the Reynolds number, which summarizes a very large number of experimental data, is shown in Fig. 8.10 [2]. This plot can be divided into four regions:

a. For Re < 2100, the experimental data are represented by a single line:

$$f_{\text{fr}} = \frac{16}{\text{Re}}. \tag{8.5.6}$$

This region corresponds to **laminar** flow, and the relationship of pressure drop versus flow velocity (Fig. 8.10) is identical to the theoretically derived Hagen–Poiseuille equation (Chapter 4, equation (4.5.9)).

b. Region $2100 <$ Re < 4000 represents the **transition** between laminar and turbulent flow; it is difficult to obtain reproducible data in this region and, in general, the values of f_{fr} are higher than indicated by the dashed line extension of the line for the laminar region (Fig. 8.10).

c. Region Re > 4000 corresponds to **turbulent** flow of the fluid; in this region, the friction factor is a function of both the Reynolds number and the relative roughness of the pipe.

d. Finally, for each pipe roughness curve, a value of Re is reached where f_{fr} becomes nearly independent of the Reynolds number and is only a function

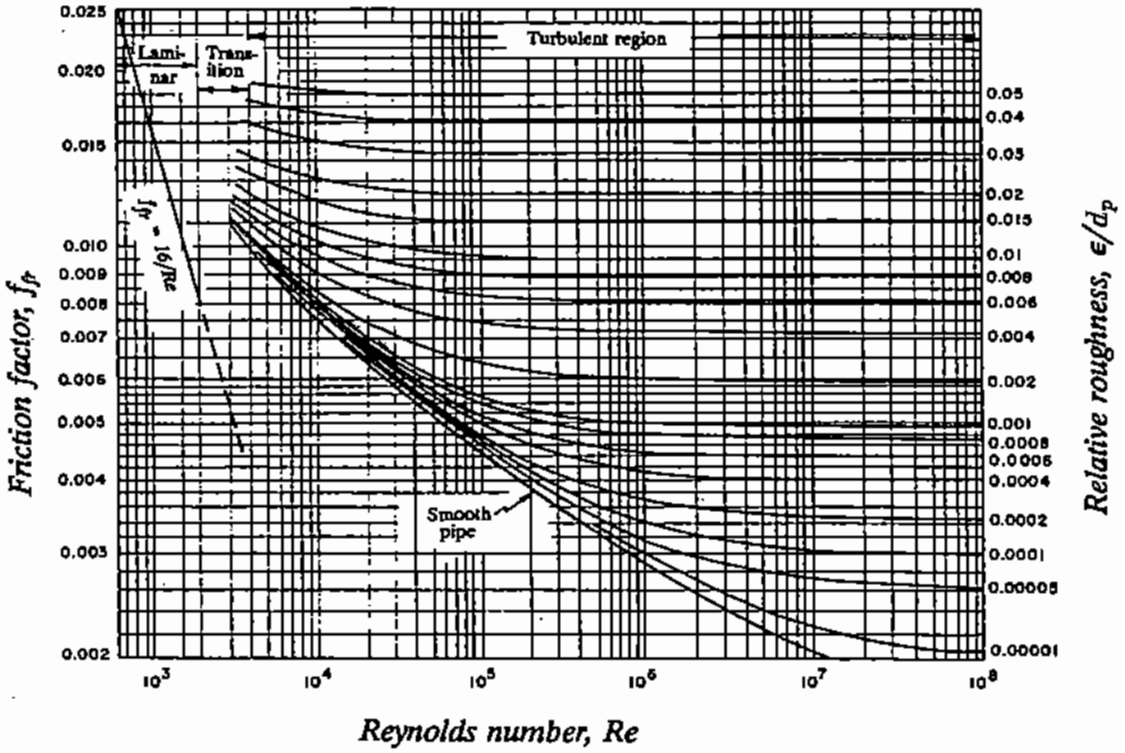

Figure 8.10. Friction factor as a function of Reynolds number and relative roughness of pipe (e/dp, [2]).

of the pipe roughness. Figure 8.11 [2] is a nomograph of relative roughness and friction factor in this region of complete turbulence.

It should be noted that the friction factor correlation is applicable for fully developed flow, which is usually assumed to exist after the fluid has travelled a distance of over fifty pipe diameters ($L/d_p > 50$). It cannot be used for short pipes where entrance effects can be very important.

From the above discussion, it can be concluded that, for pipe flow, the work expended to overcome friction in the overall energy balance (see (8.2.3)) can be expressed in terms of the friction factor as follows:

$$W'_{\mathrm{fr}} = 2 f_{\mathrm{fr}} \overline{u}^2 \frac{L}{d_p}. \tag{8.5.7}$$

In summary, the definition of the friction factor provides a very convenient and reliable tool for engineering calculations. It can serve as a model of the ingenuity and simplicity that are essential in the development of lasting engineering correlations. Some examples of the use of the friction factor are presented below.

Example 8.5.1

On the basis of the definition of the friction factor and Fig. 8.10, it is required to derive a relationship between the flow velocity in a pipe and the pressure difference along the length L of the pipe.

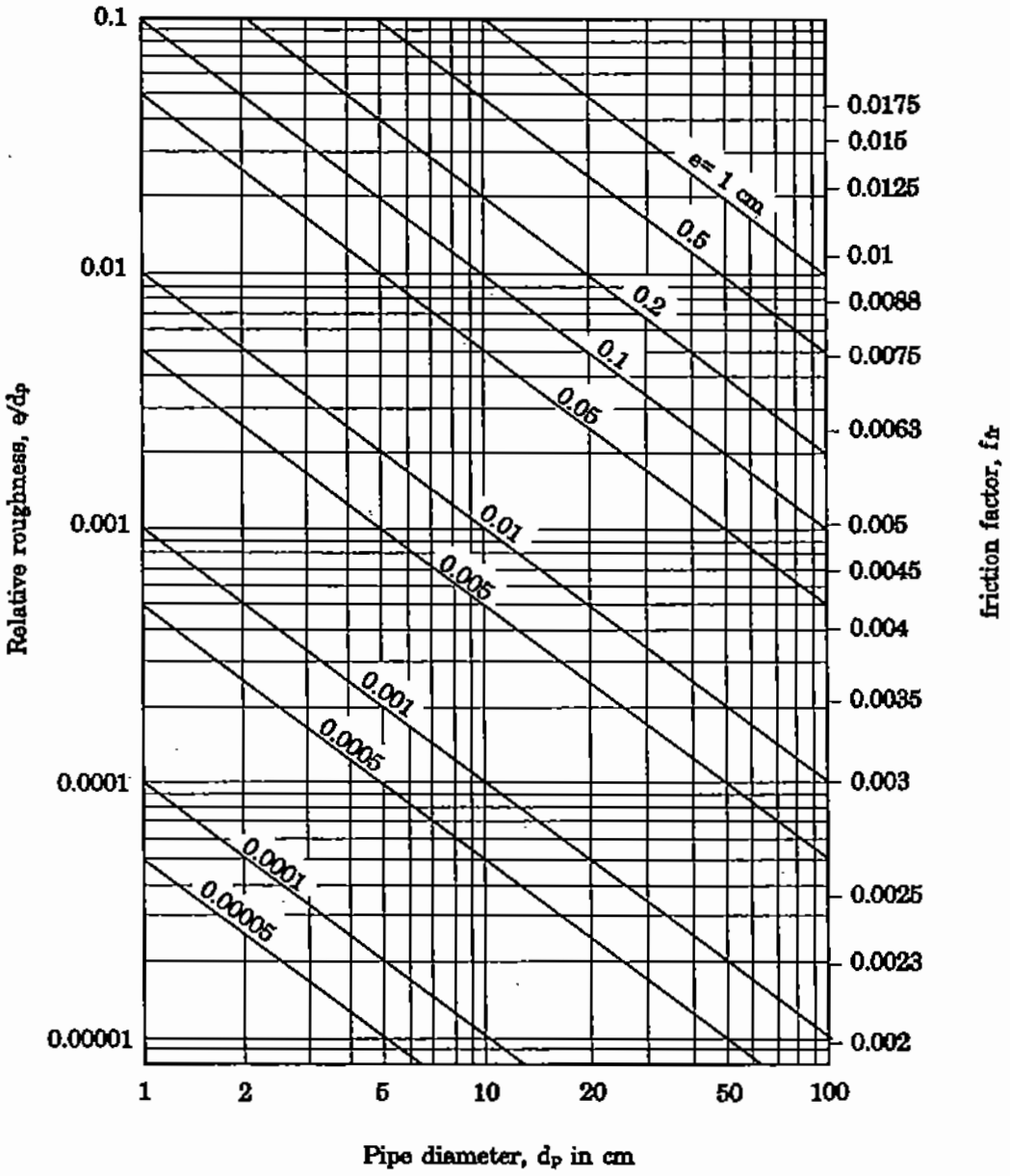

Figure 8.11. Plot of friction factor for fully turbulent flow in pipes [2].

From Fig. 8.10 and also from the definition of the friction factor (see (8.5.4)), we obtain the following two equations for f_{fr}:

$$f_{\text{fr}} = \frac{16}{\text{Re}} = \frac{16\mu}{d_p \overline{u} \rho}, \tag{8.5.6}$$

$$f_{\text{fr}} = \frac{d_p(P_1 - P_2)}{2\rho L \overline{u}^2}. \tag{8.5.8}$$

Combining these equations and eliminating f_{fr} yields the following equation for the velocity in the pipe:

$$\overline{u} = \frac{(P_1 - P_2)d_p^2}{32\mu L}. \tag{8.5.9}$$

This equation is identical to (4.5.10) (Chapter 4) which was derived analytically from the differential momentum balance.

Example 8.5.2

Cooling water ($T = 21°C$; $\rho = 1000$ kg m^{-3}; $\mu = 1$ cP $= 0.001$ kg m^{-1} s^{-1}) is pumped through a pipe with an internal diameter of 0.05-m and 90 m long (wall roughness, $e = 4.5\times10^{-5}$ m) at a rate of 15 m^3 h^{-1}. Calculate the pressure difference and the corresponding theoretical power requirement (i.e., at 100% electromechanical efficiency of the pump) to maintain this flow.

a. Calculated velocity corresponding to flow of 15 m^3 h^{-1} = volumetric flow rate/cross-sectional area of pipe = 2.12 m s^{-1}.
b. Calculated Reynolds number for water at 21°C:

$$\mathrm{Re} = \frac{d_p \overline{u} \rho}{\mu} = \frac{0.05 \times 2.12 \times 1000}{1 \times 10^{-3}} = 106,000.$$

c. Estimate of friction factor: For Re = 106000 and relative roughness (e/d_p) of $4.5 \times 10^{-5}/0.05 = 0.0009$, we obtain from the friction factor plot of Fig. 8.10

$$f_{\mathrm{fr}} = 0.0055.$$

Since by the definition of the problem there is no change in velocity of flow or elevation of the pipe between the inlet and outlet points, the change in pressure energy between the inlet and outlet points must be equal to the energy used to overcome the frictional forces along the length of the pipe. Therefore, from (8.5.5):

$$\begin{aligned} P_1 - P_2 &= 2 f_{\mathrm{fr}} \rho \overline{u}^2 L/d_p = 2 \times 0.0055 \times 1000 \times 2.12^2 \times 90/0.05 \\ &= 89000 \text{ kg m}^{-1} \text{ s}^{-2} = 89000 \text{ Pa}. \end{aligned}$$

The theoretical power requirement can be calculated by multiplying the pressure drop along the length of the pipe by the cross-sectional area of the pipe and by the flow velocity, i.e.,

$$\begin{aligned} &\text{force/area} \times \text{area} \times \text{distance/time} \\ &\quad = \text{force} \times \text{distance/time} = \text{work/time} = \text{power}; \\ &\text{power} = 89000 \times \pi d_p^2/4 \times 2.12 \\ &\quad = 370 \text{ kg m}^2 \text{ s}^{-3} = 370 \text{ J/s} = 370 \text{ W} = 0.37 \text{ kW}. \end{aligned}$$

8.5.1. Friction Factors for Noncircular Conduits

The friction factor correlations developed for circular pipes may also be used for conduits of noncircular section, provided that a hydraulic mean diameter (d_h) is used, which is defined by the following equation:

$$d_h = \frac{4(\text{cross-sectional area})}{\text{wetted perimeter}}. \tag{8.5.10}$$

It can be seen that for a cylindrical conduit the above equation yields

$$d_h = \frac{\left(\frac{4\pi d_p^2}{4}\right)}{\pi d_p} = d_p,$$

and for a duct of rectangular cross-section l_1 by l_2:

$$d_h = \frac{4l_1l_2}{2(l_1 + l_2)} = \frac{2l_1l_2}{l_1 + l_2}. \tag{8.5.11}$$

Example 8.5.3

Combustion gases at an average temperature of 700°C are exhausted through a rectangular duct (0.6-m × 0.3-m cross-section × 50-m long) at the rate of 1.2 $m^3\ s^{-1}$. Calculate the pressure drop through the duct if the flow is assumed to be isothermal and incompressible (i.e., negligible density variation through duct):

$$\rho = 0.24\ \text{kg/m}^3; \quad \mu = 0.05\ \text{cP};$$

$$\text{relative roughness of duct wall} = 0.0005.$$

a. Average gas velocity: $1.2/(0.6 \times 0.3) = 6.67\ \text{m s}^{-1}$.
b. Hydraulic diameter of duct: $2 \times 0.6 \times 0.3/(0.6 + 0.3) = 0.4$ m.
c. Reynolds number $= 0.4 \times 6.67 \times 0.24/0.00005 = 12800$.
d. Friction factor for Re = 12800, $e/d = 0.0005$: $f_{fr} = 0.0075$.
e. Calculated pressure drop through duct: 20.0 Pascal.

Example 8.5.4: Flow Through a Curved Pipe

For fluid flow through curved pipes and coils, the friction loss per unit length is higher than for straight conduits. Also, the critical Reynolds number for the coil (Re_c), i.e., where transition occurs from laminar to turbulent flow, in the range of $15 < d_c/d_p < 860$ is expressed as follows [4]:

$$Re_c \leq 20000\left(\frac{d_p}{d_c}\right)^{0.32}, \tag{8.5.12}$$

where d_c and d_p are the coil and pipe diameters, respectively.

It has also been shown [4] that for turbulent flow in coils, the friction factor, $f_{fr,c}$, is related to the friction factor in straight pipes, f_{fr}, by the following correlation:

$$\frac{f_{fr,c}}{f_{fr}} = \left(Re\frac{d_p^2}{d_c^2}\right)^{0.05}. \tag{8.5.13}$$

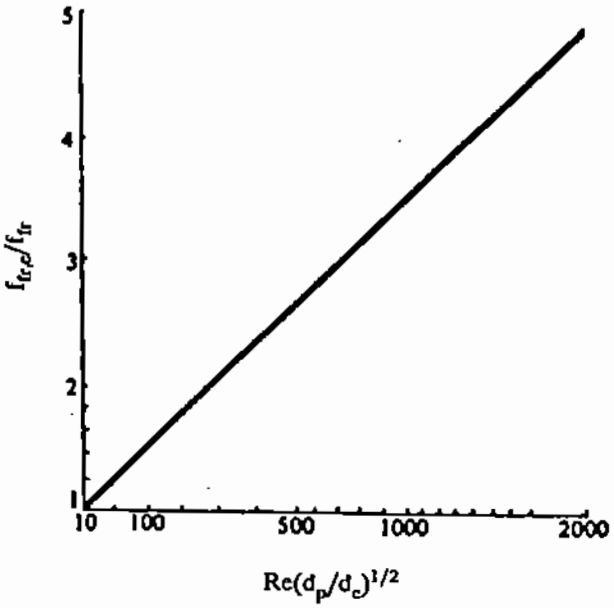

Figure 8.12. Correction of friction factor for coiled pipes.

This correlation is plotted in Fig. 8.12.

In the design of a melting furnace, it is necessary to use an induction coil consisting of 20 turns of 0.3-m diameter coil. The copper tube to be used has a 0.01-m internal diameter and, in order to maintain adequate cooling of the coil during operation, the average flow velocity through the coil must be maintained at 2 m s^{-1}. We need to calculate the required water supply pressure to provide this flow. The Reynolds number for the pipe is

$$\mathrm{Re}_p = \frac{d_p \overline{u} \rho}{\mu} = \frac{0.01 \times 2.0 \times 1000}{0.001} = 20,000$$

$$\rho = \frac{1000\,\mathrm{kg}}{\mathrm{m}^3}, \quad \mu = 0.01\,\mathrm{P} = 0.001\,\mathrm{kg\,s^{-1}\,m^{-1}}.$$

By introducing numerical values in (8.5.12), we find that the flow is turbulent. Therefore, from (8.5.13)

$$\frac{f_{\mathrm{fr,c}}}{f_{\mathrm{fr}}} = \left[20000 \times \left(\frac{0.01}{0.3}\right)^2\right]^{0.05} = 1.168.$$

We now obtain f_{fr} for flow through the pipe from the friction factor plot (Fig. 8.10):

$$f_{\mathrm{fr}} = 0.0068.$$

Therefore,

$$f_{\mathrm{fr,c}} = 1.168 \times 0.0068 = 0.0079.$$

Finally, we use the equation relating the pressure drop through the coil to the friction factor (see (8.5.4)) to obtain

$$(P_1 - P_2) = 2 \times 0.0079 \times \left(\frac{20 \times \pi \times 0.3}{0.01}\right) \times 1000 \times 2.0^2 = 119070\,\mathrm{Pascal} = 1.178\,\mathrm{atm}.$$

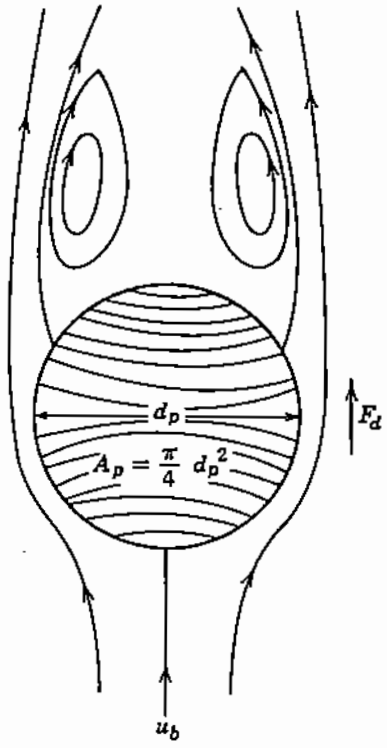

Figure 8.13. Drag force acting on a spherical particle in relative motion to fluid (streamlines shown at $\mathrm{Re}_p = 200$).

8.6. THE DRAG COEFFICIENT

Flow around solid objects is of interest in many materials processing systems, such as fluid bed reactors, flash reactors, metal atomizing processes, spray coating and many others. When a particle is in relative motion to an enveloping fluid, a **drag force** is exerted on the particle (Fig. 8.13). This force is due to the shear stress exerted in the boundary layer of the fluid next to the surface of the particle. As in the case of flow through a conduit, this shear stress is due to the viscosity of the fluid and the velocity gradient between fluid and particle.

Experimental work has shown that this drag force is a function of the particle size, the *relative velocity* between fluid and particle and the kinematic viscosity of the fluid. On the basis of an energy balance, similar to that carried out in §8.5 for flow through a conduit, it has been shown that the drag force can be expressed as follows:

$$F_d = C_d A_p \left(\frac{\rho u_p^2}{2} \right), \tag{8.6.1}$$

where C_d is the dimensionless drag coefficient; A_p is the cross-sectional area of particle projected on a plane perpendicular to direction of flow; ρ is the fluid density; u_p is the relative velocity between particle and bulk velocity of fluid.

It has been found experimentally that the drag coefficient, C_d, is a function of the particle shape, surface roughness and Reynolds number, which is defined as

$$\mathrm{Re}_p = \frac{d_p u_p \rho}{\mu}. \tag{8.6.2}$$

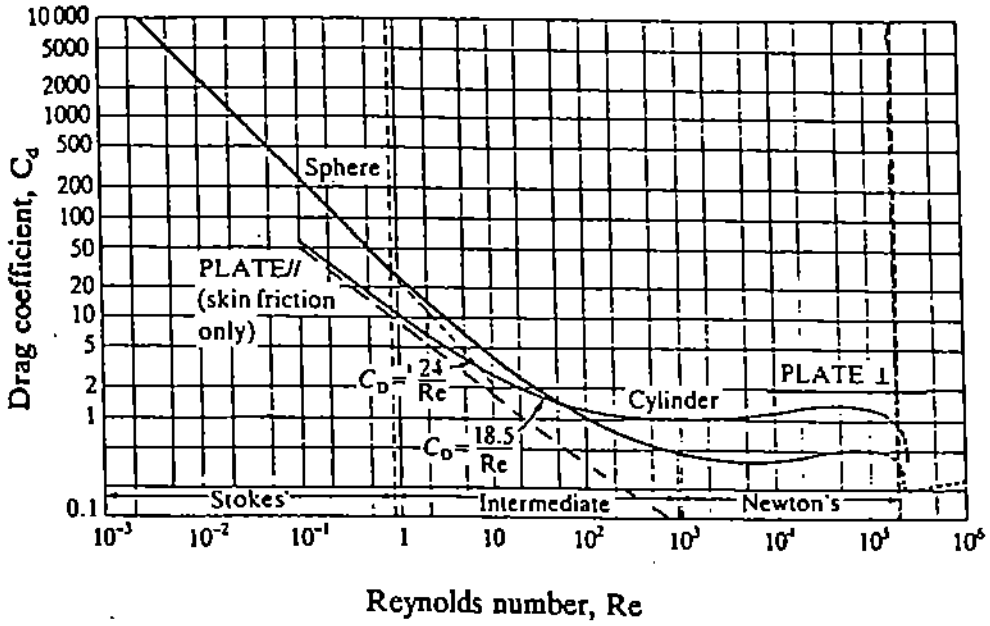

Figure 8.14. Drag coefficient for spheres, cylinders and plates as a function of Reynolds number [5].

The similarity between the drag coefficient, for flow around solids, and the friction factor, for flow in conduits, is evident.

Figure 8.14 [5] is a logarithmic plot of experimentally determined values of the drag coefficient plotted against Re_p for spherical particles. As indicated on the graph, this plot may be conveniently divided into at least three regions of flow:

a. **Creeping flow**: $10^{-10} < \mathrm{Re}_p < 2$. In this region, the drag coefficient is proportional to the Reynolds number and can be expressed as

$$C_d = \frac{24}{\mathrm{Re}}. \tag{8.6.3}$$

By substituting for C_d from the above equation in (8.6.1) for a spherical particle of cross-sectional area $A_p = \pi d_p^2/4$, we obtain the following equation for the drag force acting on the particle:

$$F_d = 3\pi d_p u_p \mu. \tag{8.6.4}$$

This equation is called the Stokes law in honor of Stokes, who derived it by integrating the Navier–Stokes equations for the case of creeping flow.

b. **Intermediate Region**: $2 < \mathrm{Re}_p < 500$. The experimental data in this region may be represented by the following approximation:

$$C_d \approx \frac{18.5}{\mathrm{Re}_p^{0.6}}. \tag{8.6.5}$$

The drag force acting on a spherical particle in this region is expressed by

$$F_d = \frac{2.31\pi d_p^2 \rho u_p^2}{\mathrm{Re}_p^{0.6}}. \tag{8.6.6}$$

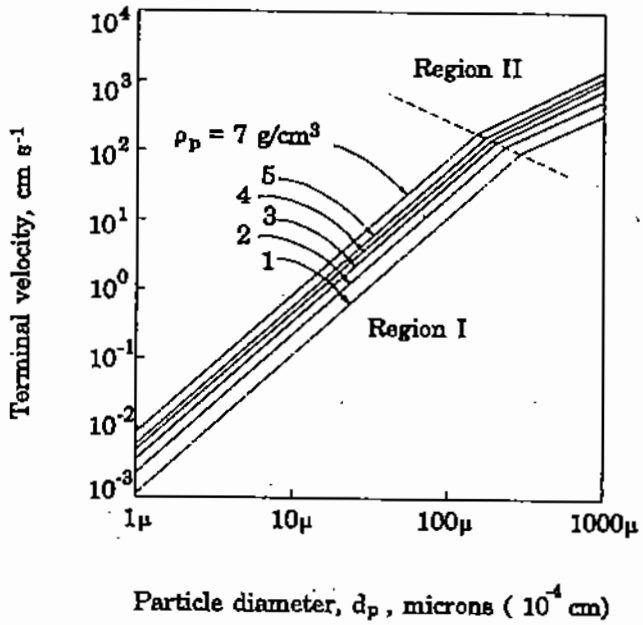

Figure 8.15. Terminal velocity of spherical particles of different densities falling through air at 900°C.

c. **Newton's Law Region**: $500 < \mathrm{Re}_p < 2 \times 10^5$. In this region, the drag coefficient remains approximately constant and independent of the Reynolds number:

$$C_d \approx 0.44. \tag{8.6.7}$$

The corresponding drag force on a spherical particle is

$$F_d = 0.055\pi d_p^2 \rho u_p^2. \tag{8.6.8}$$

Inspection of the above equations for the drag forces acting on a particle shows that the viscosity appears in the first and second regions but not in the third. The physical reason for this is that the total force acting on the particle is made up of two components: one due to viscous forces and the other due to inertia forces. At low velocities and Reynolds numbers, the viscous forces are predominant while the reverse is true at high velocities.

8.6.1. Terminal Falling Velocity of a Particle

As a particle starts falling through a fluid, it will accelerate until the force of gravity producing this motion is exactly balanced by the drag force which resists it. From this point onward, the particle will move at a constant speed, usually termed the **terminal falling velocity**. The terminal falling velocity can be determined by equating the force of gravity, acting on the particle, to the drag force. Thus, for the creeping flow region we have

$$F_g = \frac{\pi d_p^3}{6}(\rho_p - \rho_f)g = F_d = 3\pi d_p u_t \mu, \tag{8.6.9}$$

and therefore

$$u_t = \frac{d_p^2 g(\rho_p - \rho_f)}{18\mu}, \tag{8.6.10}$$

where u_t is the terminal velocity, and ρ_p and ρ_f are the densities of the particle and the fluid.

Figure 8.15 shows the terminal velocities of particles of various densities falling through air at 900°C.

Example 8.6.1

Determine the terminal falling velocity of a 100-micron matte (30% Cu) droplet settling through a 38% SiO_2/33% Fe molten slag at 1150°C.

Data:

matte density = 4.1 g cm^{-3},

slag density = 3.5 g cm^{-3},

slag viscosity = 2.0 P = 2.0 g cm^{-1} s^{-1},

gravitational acceleration = 980 cm s^{-2}.

Let us assume that the liquid matte flow past the particle is in region a, i.e., $Re_p < 2$; then, from (8.6.10),

$$u_t = \frac{d_p^2 g(\rho_m - \rho_s)}{18\mu} = \frac{(100 \times 10^{-4})^2 \times 980.7 \times (4.1 - 3.5)}{18 \times 2}$$
$$= 0.0016\,\mathrm{cm\,s^{-1}} = 5.8\,\mathrm{cm\,h^{-1}}.$$

We can now calculate the Reynolds number of the falling droplet:

$$\mathrm{Re} = \frac{100 \times 10^{-4} \times 0.0016 \times 3.5}{2} = 2.8 \times 10^{-5}.$$

We can see that our preliminary assumption that $Re_p < 2$ was correct.

REFERENCES

1. L.L. Simpson, *Chem.Eng.*, **76**(8), 167–181 (1969).
2. L.F. Moody, *Trans. ASME*, **66**, 671 (1944).
3. G.H. Geiger and D.R. Poirier, *Transport Phenomena in Metallurgy*, Addison-Wesley, Reading, MA (1973).
4. H. Ito, *Trans. ASME*, Ser. D, **82**, 123–134 (1959).
5. R.I.L. Guthrie, *Engineering in Process Metallurgy*, Clarendon Press, Oxford (1989).
6. R.S. Brodkey and H.C. Hershey, *Transport Phenomena: A Unified Approach*, McGraw-Hill, NY (1988).

NINE

Applications of the Overall Energy Balance

The overall energy balance developed in Chapter 8 can be applied to a wide variety of processing problems. However, it is very important to select properly the *control volume* across which the balance will be made so that it represents accurately the physical problem under consideration. Also, in the case of complex physical systems, engineering judgment must be used to decide on the simplifying assumptions to be made, in order to provide the desired balance between ease of solution and degree of accuracy required in the solution.

Some examples are presented in the following sections. It should be noted that all velocity terms (u_1, u_2, etc.) shown from now on represent average velocities at a particular location and the overline marker is omitted.

9.1. PROBLEMS IN INCOMPRESSIBLE FLOW

Example 9.1.1

Figure 9.1 is a schematic diagram of a 0.05-m i.d. pipeline ($e/d = 0.001$) through which an aqueous solution is pumped at a rate of 11 $m^3\ h^{-1}$. The conduit consists of a 91-m long horizontal section, containing a gate valve; this leads into a 90° elbow bend and an 18-m elevation to a second horizontal section (24-m long) and a third elbow bend through which water is discharged on the surface of an ore vat. The density and viscosity of the solution may be assumed to be 1 g cm^{-3} and 1 cP, respectively. It is required to calculate the pressure required at the bottom end of the conduit to maintain this flow.

In this case, the control volume lies between planes 1 and 2 (Fig. 9.1). As the fluid passes between these two planes, its potential energy changes because of the 18-m elevation; furthermore, work is done to overcome the frictional forces in the conduit, orifice, elbow bends, and gate valve. Since the fluid is incompressible and the pipe diameter at the inlet and exit points of the control volume is the same, the kinetic energy term is negligible ($u_1 = u_2$).

For the purposes of such calculations, it is convenient to represent the frictional loss through each fitting in the pipe by assigning to it an equivalent pipe length. Table 9.1 is a typical tabulation of equivalent lengths for a number of pipe fittings; for convenience, such lengths are expressed in terms of "number of pipe diameters." In this case, the equivalent lengths of the various fittings are found to add up to about 10 m. Accordingly, the conduit may be assumed to be consisting of a total pipe length of

$$L = (91 + 18 + 24 + 10)\,\text{m} = 143\,\text{m}.$$

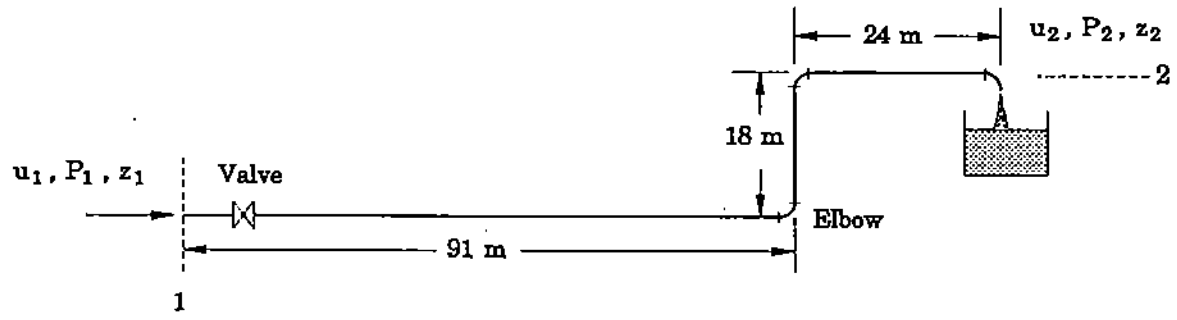

Figure 9.1. Illustration of Example 9.1.1.

Table 9.1. Equivalent Length of Pipe Fittings

Fitting	Pipe diameters
45° elbows	15
90° elbows (standard radius)	30–40
90° square elbows	60
Entry from leg of T-piece	60
Entry into leg of T-piece	90
Unions and couplings	generally very small
Globe valves fully open	60–300
Gate valves: fully open	7
3/4 open	40
1/2 open	200
1/4 open	800

As discussed in the previous chapter, for steady state conditions, the mechanical energy balance is

$$\frac{1}{2}\left(u_2^2 - u_1^2\right) + g(z_2 - z_1) + \int_1^2 \frac{dP}{\rho} + W'_m + W'_{\text{fr}} = 0. \tag{9.1.1}$$

Since there is no work done by the fluid, $W'_m = 0$. Furthermore, for an incompressible fluid

$$\int_1^2 \frac{dP}{\rho} = \frac{P_2 - P_1}{\rho}. \tag{9.1.2}$$

Also, there is no change in the diameter of the conduit so that $u_2 = u_1$; finally, W'_{fr} can be expressed in terms of the friction factor, as defined in Chapter 8 (see (8.5.7)). Therefore, (9.1.1) can be written as follows:

$$P_1 - P_2 = \rho\left[2f_{\text{fr}}\frac{L}{d}u_1^2 + g(z_2 - z_1)\right]. \tag{9.1.3}$$

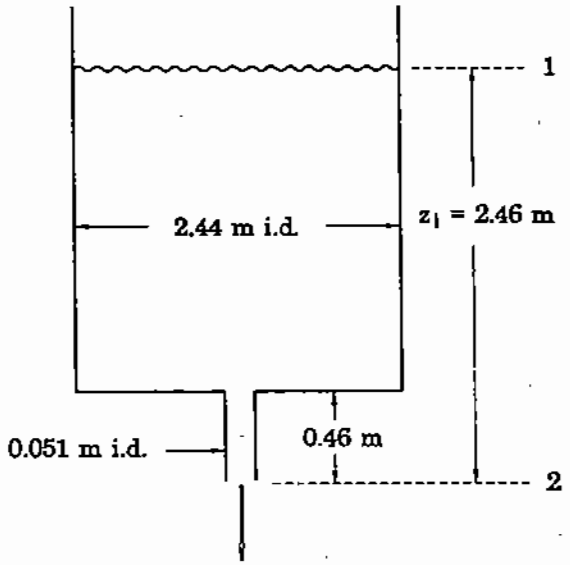

Figure 9.2. Illustration of Example 9.1.2.

Next, on the basis of the stated volumetric flow and the pipe diameter, the flow velocity in the pipe is calculated to be 1.56 m s^{-1}. We now know all the quantities on the right-hand side of (9.1.3), with the exception of f_{fr}, which must be obtained from a friction factor chart. To do so, we need to calculate the Reynolds number:

$$\mathrm{Re} = \frac{du_1\rho}{\mu} = \frac{0.05 \times 1.56 \times 1000}{1 \times 10^{-3}} = 78,000.$$

From Fig. 8.10, for Re = 78,000 and $e/d = 0.001$, we find that $f_{fr} = 0.0058$. Substitution of this value into (9.1.3) yields

$$\begin{aligned} P_1 - P_2 &= 80,700\,\mathrm{N\,m^{-2}}\,(\text{frictional loss}) \\ &\quad + 176,400\,\mathrm{N\,m^{-2}}(\text{ potential energy change}) \\ &= 257,100\,\mathrm{N\,m^{-2}} = 2.54\,\text{atm}. \end{aligned}$$

Example 9.1.2.

In a continuous vacuum degassing operation, molten steel is discharged from a nozzle at the bottom of a ladle into a vacuum chamber (Fig. 9.2). Develop a relationship between the flow rate of metal and time after the nozzle is opened which a) neglects frictional losses, and b) allows for frictional losses in the nozzle.

Data:

ladle diameter, $d_l = 2.44m$,

initial level of metal in ladle, $z_0 = 2.0$ m,

internal diameter of nozzle, $d_n = 0.051$ m,

length of nozzle, $L = 0.46$ m (relative roughness: 0.01),

density of steel, $\rho = 7100$ kg m^{-3},

viscosity of steel, $\mu = 1.5$ cP = 0.0015 kg

In this case, the control volume is established between reference plane *1*, corresponding to the surface of the metal bath to the metal level in the ladle at any time t, and plane *2* at the discharge end of the nozzle (Fig. 9.2). Since the metal level in the ladle, z, is clearly a function of time (as are u_1, u_2, and possibly W'_{fr}), one may ask whether it is appropriate to use the steady-state energy balance of (9.1.1). However, it should be noted that this equation is expressed on the basis of unit mass of fluid flowing, so that the total amount of steel present in the ladle does not enter into the energy balance, apart from affecting the value of the metal level z.

Equation (9.1.1) is simplified by considering that $P_1 = 1$ atm (above the metal bath) $P_2 = 0$ (in the vacuum chamber) and that $u_2 \gg u_1$, since the diameter of the ladle is much larger than that of the nozzle. Furthermore, we may select the reference level for the potential energy so that $z_2 = 0$, at the bottom of the orifice. It is noted that, in this case, the frictional loss, W'_{fr}, consists of two terms: the sudden contraction at the entrance to the nozzle which, from (8.4.5) (Chapter 8), is equal to $0.25u_2^2$, and the frictional loss through the nozzle (stated in terms of the friction factor equation). Accordingly, the energy balance is expressed as follows:

$$\frac{u_2^2}{2} - gz - \frac{P_1}{\rho} + \left(2f_{\text{fr}}\frac{L}{d_n}u_2^2 + 0.25u_2^2\right) = 0. \tag{9.1.4}$$

a. **Neglecting Frictional Effects**. If frictional effects are assumed to be negligible, $W'_{\text{fr}} = 0$, and the above equation simplifies to

$$u_2 = \sqrt{2}\left(gz + \frac{P_1}{\rho}\right)^{1/2}. \tag{9.1.5}$$

The volumetric flow rate through the nozzle is related to the nozzle velocity and cross-sectional area and also to the rate of change of metal depth in the ladle:

$$\dot{v} = u_2\frac{\pi d_n^2}{4} = -\frac{dz}{dt}\frac{\pi d_l^2}{4} \quad \text{for } 2.46\,\text{m} > z > 0.46\,\text{m}. \tag{9.1.6}$$

By combining (9.1.5) and (9.1.6), we obtain

$$-\frac{dz}{dt} = \sqrt{2}\frac{d_n^2}{d_l^2}\left(gz + \frac{P_1}{\rho}\right)^{1/2}, \tag{9.1.7}$$

where d_n and d_l are the diameters of the nozzle and the ladle. Equation (9.1.7) is a first-order differential equation which can be integrated to yield

$$t = C_1 - \frac{\sqrt{2}}{g}\frac{d_l^2}{d_n^2}\left(gz + \frac{P_1}{\rho}\right)^{1/2}. \tag{9.1.8}$$

Substituting the boundary condition, $z = z_0$ at $t = 0$, we obtain the value of the integration constant C_1:

$$C_1 = \frac{\sqrt{2}}{g}\frac{d_l^2}{d_n^2}\left(gz_0 + \frac{P_1}{\rho}\right)^{1/2}, \tag{9.1.9}$$

and by substituting in (9.1.8)

$$t = \frac{\sqrt{2}}{g}\frac{d_l^2}{d_n^2}\left[\left(gz_0 + \frac{P_1}{\rho}\right)^{1/2} - \left(gz + \frac{P_1}{\rho}\right)^{1/2}\right]. \tag{9.1.10}$$

Equation

If necessary, (9.1.10) [illegible] provide an explicit relationship between the time of metal discharge from the ladle and the liquid depth in the ladle. From (9.1.10), we can calculate the time required to empty the ladle for the given values of $z_0 = 2.46$ m, $z_f = 0.46$ m, $P_1 = 1$ atm = 101,325 N m^{-2} and $P_1/\rho = 14.27$ m^2 s^{-2}:

$$t = \frac{\sqrt{2}}{9.81} \times \frac{2.44^2}{0.051^2}\left[(9.81 \times 2.46 + 14.27)^{1/2} - (9.81 \times 0.46 + 14.27)^{1/2}\right] = 615\,\text{s}.$$

The above simplified treatment allows us to make a rough estimate of the time required to empty the ladle and also of the nozzle velocity, which can be used in the following calculation of the effect of friction on the time to empty the ladle.

b. **Allowance for Frictional Effects.** The appropriate form of (9.1.1) for this case is

$$\frac{u_2^2}{2} - gz - \frac{P_1}{\rho} + \left(2f_{\text{fr}}\frac{L}{d_n}u_2^2 + 0.25u_2^2\right) = 0, \tag{9.1.11}$$

where L is the length of the nozzle. We proceed, as previously, to express u_2 in terms of the other variables:

$$u_2 = \left[\frac{gz + \frac{P_1}{\rho}}{0.75 + 2f_{\text{fr}}\frac{L}{d_n}}\right]^{1/2}, \tag{9.1.12}$$

and by substituting for u_2 from (9.1.6), as before

$$-\frac{dz}{dt} = \frac{d_n^2}{d_l^2}\left[\frac{gz + \frac{P_1}{\rho}}{0.75 + 2f_{\text{fr}}\frac{L}{d_n}}\right]^{1/2}. \tag{9.1.13}$$

As in the previous case, the boundary condition is $z = z_0$ at $t = 0$. If we assume that the flow is highly turbulent, so that the friction factor is nearly constant with Reynolds number (Fig. 8.10), the above equation can be integrated for the boundary condition $z = z_0$ at $t = 0$ to yield

$$t = \frac{2}{g}\frac{d_l^2}{d_n^2}\left(0.75 + 2f_{\text{fr}}\frac{L}{d_n}\right)^{1/2}\left[\left(gz_0 + \frac{P_1}{\rho}\right)^{1/2} - \left(gz + \frac{P_1}{\rho}\right)^{1/2}\right]. \tag{9.1.14}$$

This equation has been put in the same form as (9.1.10) to indicate the similarities between the two equations. A first estimate of the friction factor may be made by considering the range of nozzle velocities, and hence the corresponding Reynolds numbers, for the frictionless case. Thus, from (9.1.5), the initial velocity at the nozzle, for $z = 2.46$, is

$$u_{2,i} \approx \sqrt{2} \times (9.81 \times 2.46 + 14.27)^{1/2} = 8.77\,\text{m s}^{-1}.$$

Similarly, the final velocity, for $z_f = 0.46$ m, is

$$u_{2,f} \approx 6.13\,\mathrm{m\,s^{-1}}.$$

The corresponding values of the Reynolds numbers are calculated to be 2.12×10^6 and 1.48×10^6, respectively.

The friction factor chart of Fig. 8.10 shows that for the given relative roughness of 0.01, the friction factor is about 0.0095 for both of these velocities. Also, it can be seen that even a tenfold reduction in the linear velocity would not result in any significant change in the friction factor at these very high Reynolds numbers. Therefore, the assumption that f_{fr} is constant is reasonable for this case. However, if f_{fr} were a function of velocity, (9.1.13) could be solved by trial and error, e.g., using Lotus 1-2-3.

Inspection of (9.1.10) and (9.1.14) shows that the time of metal flow in the presence of frictional effects can be determined either by substitution of the numerical values in (9.1.14) or by introducing the friction factor correction in the estimated time from (9.1.10), i.e.,

$$t = 614 \times \frac{2}{\sqrt{2}} \left(0.75 + 2 f_{\mathrm{fr}} \frac{L}{d_n}\right)^{1/2} = 614 \times \frac{2}{\sqrt{2}} \left(0.75 + 2 \times 0.0095 \times \frac{0.46}{0.051}\right)^{1/2}$$
$$= 833 \text{ seconds}.$$

It can be seen that the neglect of the frictional effects in case a resulted in an appreciable error.

9.2. PROBLEMS IN COMPRESSIBLE FLOW

The previous examples dealt with incompressible fluids, such as water and molten metals, where the density of the fluid could be assumed to be constant. In the case of flow of gases, which are compressible, the use of the Bernoulli equation is somewhat more complex, as illustrated in the following examples.

9.2.1. Isothermal Gas Flow

At steady state conditions in a horizontal pipe ($\Delta z = 0$) and for $W'_m = 0$, the overall energy balance may be written in differential form as follows:

$$d\left(\frac{u^2}{2}\right) + \frac{dP}{\rho} + \frac{2 f_{\mathrm{fr}}}{d_p}\, dx\, u^2 = 0, \tag{9.2.1}$$

where dx is a differential element of the total length, L, of the pipe. In order to integrate this equation, it is convenient to introduce the mass flux of the fluid, G (dimensions: M t^{-1} L^{-2}), which for a conduit of constant cross-section, as in this case, does not change with x:

$$G = \rho u = \frac{u}{V}, \tag{9.2.2}$$

where $V = 1/\rho$ is the specific volume of the gas in $\mathrm{cm^3\ g^{-1}}$. By replacing u in (9.2.1) by G, we obtain

$$G^2 V\, dV + V\, dP + \frac{2 f_{\mathrm{fr}}}{d_p} G^2 V^2\, dx = 0, \tag{9.2.3}$$

and by dividing all terms of the above equation by V^2 and integrating over the length of the pipe, L:

$$G^2 \ln \frac{V_2}{V_1} + \int_1^2 \frac{dP}{V} + \frac{2f_{\text{fr}}}{d_p} G^2 L = 0, \tag{9.2.4}$$

where the subscripts 1 and 2 denote the beginning and the end of the pipe length L. In the above integration, it was tacitly assumed that the Reynolds number is high enough so that f_{fr} is constant over length L of the pipe (see Fig. 8.10). If this is not so, the friction term in the above equation must be replaced by an integral:

$$\frac{2G^2}{d_p} \int_1^2 f_{\text{fr}}\, dx,$$

and the equation integrated by a numerical method.

Returning to (9.2.4), all the terms are known with the exception of the pressure integral. However, for isothermal flow of gas, the ideal gas law yields:

$$PV = P_1 V_1. \tag{9.2.5}$$

Therefore,

$$\int_1^2 \frac{dP}{V} = \int_1^2 \frac{P\,dP}{P_1 V_1} = \frac{P_2^2 - P_1^2}{2P_1 V_1}. \tag{9.2.6}$$

Also, from the ideal gas law

$$\frac{V_2}{V_1} = \frac{P_1}{P_2}, \tag{9.2.7}$$

and

$$P_1 V_1 = nRT = \frac{1}{M} RT = \frac{RT}{M}, \tag{9.2.8}$$

where n is the number of moles (here $n = 1/M$), T is the absolute temperature of the gas, R is the universal gas constant (Table 2.2), and M is the molecular weight of the gas. By combining (9.2.4) and (9.2.6)–(9.2.8), we obtain:

$$G^2 \ln \frac{P_1}{P_2} + \frac{(P_2^2 - P_1^2)}{2P_1 V_1} + \frac{2f_{\text{fr}} L}{d_p} G^2 = 0, \tag{9.2.9}$$

or

$$G^2 \ln \frac{P_1}{P_2} + \frac{(P_2^2 - P_1^2)M}{2RT} + \frac{2f_{\text{fr}} L}{d_p} G^2 = 0. \tag{9.2.10}$$

Either of the above two equations can be used to compute the required pressure for providing a certain mass flux G in isothermal gas flow.

9.2.2. Adiabatic Flow of an Ideal Gas

Let us now develop the approximate equivalent of (9.2.9) for the *adiabatic* expansion of an ideal gas, i.e., without gain or loss of heat during the change from P_1 to P_2. Here we start with (9.2.4):

$$G^2 \ln \frac{V_2}{V_1} + \int_1^2 \frac{dP}{V} + \frac{2f_{fr}}{d_p} G^2 L = 0. \tag{9.2.4}$$

For adiabatic conditions, the P–V relationship needed for evaluation of the pressure integral may be approximated as follows:

$$PV^\gamma = P_1 V_1^\gamma, \tag{9.2.11}$$

where

$$\gamma = \frac{C_p}{C_v} = \frac{\text{heat capacity of gas at constant pressure}}{\text{heat capacity of gas at constant volume}}.$$

Therefore,

$$\ln \frac{V_2}{V_1} = \frac{1}{\gamma} \ln \frac{P_1}{P_2}, \tag{9.2.12}$$

and

$$\int_1^2 \frac{dP}{V} = -\int_1^2 \frac{P^{1/\gamma} dP}{P_1^{1/\gamma} V_1} = \left(\frac{\gamma}{\gamma+1}\right) \frac{P_1}{V_1} \left[\left(\frac{P_2}{P_1}\right)^{(\gamma+1)/\gamma} - 1\right]. \tag{9.2.13}$$

By combining (9.2.4), (9.2.12), and (9.2.13), we obtain

$$\frac{G^2}{\gamma} \ln \frac{P_1}{P_2} + \left(\frac{\gamma}{\gamma+1}\right) \frac{P_1}{V_1} \left[\left(\frac{P_2}{P_1}\right)^{(\gamma+1)/\gamma} - 1\right] + \frac{2f_{fr}}{d_p} G^2 L = 0. \tag{9.2.14}$$

From this equation we can evaluate the mass flux through the conduit, if P_1 and P_2 are known; alternatively, if P_2 and G are given, P_1 can be computed by trial and error.

9.3. SONIC VELOCITY AND SUPERSONIC JETS

In some processes for metal refining, such as the basic oxygen converter for steelmaking, a high-velocity gas jet is injected in the reactor through a lance. Equation (9.2.9) can be used to examine how changes in the downstream pressure, P_2, affect the mass flux G of a gas flowing through a nozzle.

By rearranging (9.2.9) for isothermal flow we obtain the following expression for G:

$$G^2 = \frac{-\left(P_2^2 - P_1^2\right)}{\left[\ln \frac{P_1}{P_2} + 2f_{fr}\frac{L}{d_p}\right] 2P_1 V_1}. \tag{9.3.1}$$

Equation (9.3.1) shows that for $P_2 = P_1$ and also for $P_2 = 0$, G must be equal to zero. It follows that at some intermediate value of P_2, G must have a maximum value. For a

fixed value of P_1, this maximum will occur at $dG/dP_2 = 0$. It has been shown that at this maximum mass flux, the fluid velocity is expressed as follows:

$$u_s^2 = \frac{P}{\rho}, \tag{9.3.2}$$

and for an ideal gas in isothermal flow:

$$u_s^2 = \frac{P}{\rho} = \left(\frac{dP}{d\rho}\right)_T = \frac{RT}{M}. \tag{9.3.3}$$

It can be shown that u_s in the above equations corresponds to the velocity of sound in the fluid and it is the speed at which a pressure wave propagates through the fluid. Physically, this means that if the downstream pressure were to be reduced below a critical value, which depends on the upstream pressure and on the properties of the fluid, the flow of the fluid would be faster than the rate of propagation of the pressure wave; in other words, the upstream end of the pipe or nozzle "would not know" that the downstream pressure has been decreased to a value below the critical value.

The physical result of reducing the downstream pressure below the critical value of P results in a discontinuity, called a **shock wave.**

It should be noted that in describing the propagation of the pressure wave, we assumed isothermal flow. However, in practice, it would be extremely difficult to maintain isothermal conditions and, in most cases, the flow would be adiabatic and the speed of propagation of the pressure wave would be expressed as follows:

$$u_s^2 = \gamma \frac{P}{\rho}. \tag{9.3.4}$$

In view of the above, sonic velocities may not be exceeded in a pipe of constant cross-section. However, as discussed in the following section, it is possible to achieve supersonic velocities by the use of a convergent-divergent nozzle.

9.3.1. The Convergent-Divergent Nozzle

For gas flow through a short length of pipe or nozzle, the potential energy, friction and work terms in the energy balance equation may be assumed to be negligible and it can be written as follows:

$$\frac{u_2^2 - u_1^2}{2} + \int_1^2 V dP = 0. \tag{9.3.5}$$

For an adiabatic system, the pressure integral can be evaluated by substituting for V from (9.2.11) (§9.2.2) and integrating to yield

$$\frac{u_2^2 - u_1^2}{2} = \int_1^2 P_1^{1/\gamma} V_1 \frac{dP}{P^{1/\gamma}} = P_1 V_1 \left(\frac{\gamma}{\gamma - 1}\right) \left[1 - \left(\frac{P_2}{P_1}\right)^{(\gamma-1)/\gamma}\right], \tag{9.3.6}$$

or the equivalent expression

$$\frac{u_2^2 - u_1^2}{2} = -P_2 V_2 \left(\frac{\gamma}{\gamma - 1}\right) \left[1 - \left(\frac{P_1}{P_2}\right)^{(\gamma-1)/\gamma}\right]. \tag{9.3.7}$$

Equations (9.3.6) and (9.3.7) express the conservation of the sum of kinetic and pressure energies for the frictionless, adiabatic flow of an ideal gas. This equation is valid for both subsonic and sonic velocities.

Let us now consider how changes in the cross-sectional area of a conduit may affect the velocity. Since the potential energy and frictional terms are assumed to be negligible, the energy balance equation can be written in differential form as

$$udu + VdP \equiv udu + \frac{dP}{\rho} = 0. \tag{9.3.8}$$

Since the mass flow rate through a conduit remains constant:

$$\dot{m} = \rho u A, \tag{9.3.9}$$

we can differentiate (9.3.9) and then divide each term by the mass flow rate to obtain

$$\frac{du}{u} + \frac{d\rho}{\rho} + \frac{dA}{A} = 0, \tag{9.3.10}$$

which can be rewritten as

$$\frac{du}{u} + \frac{d\rho}{dP}\left(\frac{dP}{\rho}\right) + \frac{dA}{A} = 0. \tag{9.3.11}$$

Finally, by combining (9.3.3), (9.3.8), and (9.3.11), we obtain

$$\frac{du}{u}\left(\frac{u^2}{u_s^2} - 1\right) = \frac{dA}{A}. \tag{9.3.12}$$

By definition, the ratio of velocity in a fluid to the velocity of sound under the same conditions, u/u_s, is called the *Mach number* and is denoted by Ma. Therefore, (9.3.12) may be written as

$$\frac{du}{u} = \left(\frac{1}{\mathrm{Ma}^2 - 1}\right)\left(\frac{dA}{A}\right). \tag{9.3.13}$$

Inspection of (9.3.13) shows that when the velocity is **subsonic** ($\mathrm{Ma} < 1$ and $\mathrm{Ma}^2 - 1 < 0$), an *increase* in the cross- sectional area of the conduit will result in a *decrease* in the fluid velocity; this behavior is the same as discussed earlier for the flow of incompressible

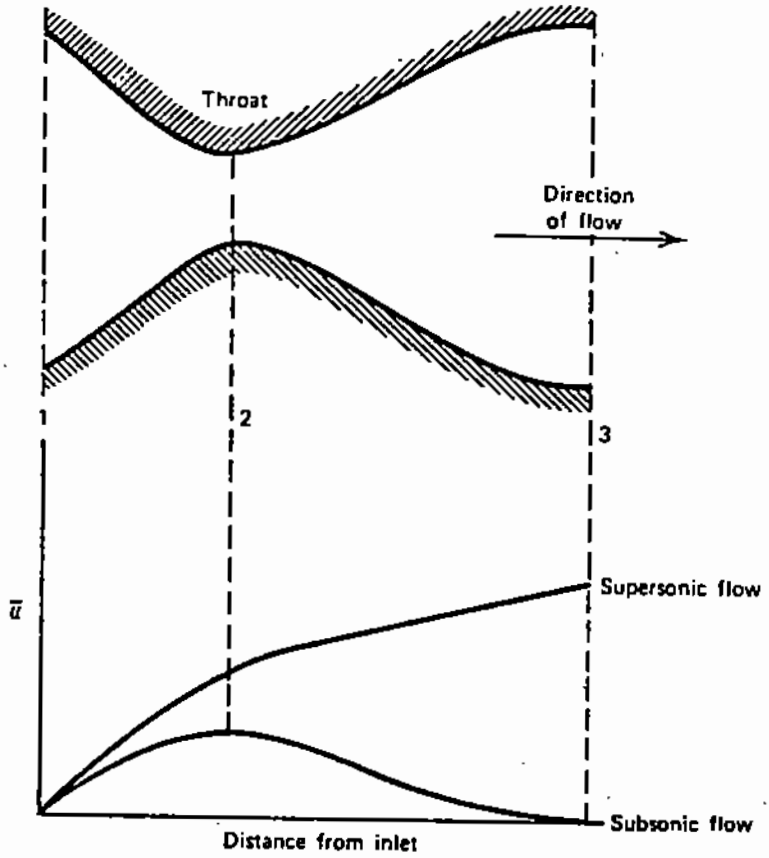

Figure 9.3. Velocity profiles in a convergent-divergent nozzle.

fluids. However, when the velocity is **supersonic** (Ma > 1 and $Ma^2 - 1 > 0$), an *increase* in the cross-sectional area will lead to an **increase** in the fluid velocity.

Therefore, a gas may be accelerated to supersonic velocities by using a convergent-divergent nozzle of the type shown in Fig. 9.3. In this nozzle, the flow is initially subsonic in the convergent part of the nozzle (plane *1*, Fig. 9.3) and is accelerated to sonic velocity at the "throat" (plane 2). Then, further acceleration to supersonic speed is possible in the divergent part of the nozzle.

Figure 9.3 also shows that, in accordance with (9.3.13), if sonic speed is not reached at the "throat" of the nozzle, the velocity will be decreased rather than increased in the divergent passage of the nozzle. The criterion for achieving sonic velocity at the "throat" ($u_2 = u_s$) can be established in the following way: By establishing an energy balance between planes 1 and the throat of the nozzle (Fig. 9.3), we obtain for adiabatic expansion conditions (see (9.3.7)):

$$\frac{u_s^2 - u_1^2}{2} = P_2 V_2 \left(\frac{\gamma}{\gamma - 1}\right) \left[\left(\frac{P_1}{P_2}\right)^{(\gamma-1)/\gamma} - 1\right]. \tag{9.3.14}$$

By noting from (9.3.4) that the sonic velocity u_s is expressed by

$$u_s^2 = \frac{\gamma P}{\rho} = \gamma P_2 V_2, \tag{9.3.15}$$

and assuming that $u_1^2 \ll u_s^2$ and can be neglected from (9.3.14), combining (9.3.14) and (9.3.15) results in the following criterion for the establishment of sonic velocity at the "throat" of the nozzle (plane 2):

$$\frac{u_2^2}{u_s^2} = M_a^2 = 1 = \frac{2}{\gamma - 1}\left[\left(\frac{P_1}{P_2}\right)^{(\gamma-1)/\gamma} - 1\right]. \tag{9.3.16}$$

It can be seen that the criterion for the establishment of sonic velocity at the throat is defined in terms of γ, which is a property value of the gas, and the ratio P_1/P_2. The value of this critical ratio can be obtained from (9.3.16):

$$\left(\frac{P_2}{P_1}\right)_{\text{crit}} = \left(\frac{2}{\gamma+1}\right)^{\gamma/(\gamma-1)}. \tag{9.3.17}$$

The critical pressure ratio of (9.3.17) must be provided in order for the flow to become supersonic in a converging-diverging nozzle at the throat. If the ratio P_2/P_1 is larger than the critical ratio, the flow will be subsonic, and will remain so, independently of the design of the diverging section of the nozzle. At room temperature, the critical pressure ratio for most gases of interest is in range 0.49–0.55.

The velocity at the end of the divergent section may be evaluated by applying (9.3.6) between planes 2 and 3 of the nozzle (Fig. 9.3). In this way, we obtain:

$$\frac{u_3^2}{2} = \frac{u_2^2}{2} + P_2 V_2 \left(\frac{\gamma}{\gamma - 1}\right)\left[1 - \left(\frac{P_3}{P_2}\right)^{(\gamma-1)/\gamma}\right]. \tag{9.3.18}$$

TEN

Thermal Conductivity and Steady State Conduction

10.1. INTRODUCTION TO HEAT TRANSFER

The processing of materials is usually carried out above atmospheric temperature. Before they can react, the feed materials and reagents must be heated to the processing temperature and, ultimately, the products have to be cooled to the temperature of the environment. Thus, at various stages in the processing sequence, heat has to be supplied to or removed from the reaction system.

The steelmaking process (Fig. 10.1) is a good illustration: Starting with iron ore concentrates, pellets are formed and then sintered. In the sintering process, pellets are heated to about 1100°C and then cooled prior to their introduction into the blast furnace. In the furnace, the iron oxides are reduced to produce liquid iron which is tapped at about 1400°C and transferred in ladles to the steelmaking converter.

In the subsequent refining of high-carbon iron to steel, carbon and other elements are removed by means of oxygen injection and the heat of oxidation increases the temperature of the steel to about 1550°C. The furnace is than tapped and the metal is transferred in ladles to a casting bay, where it may be cast to ingots.The ingots lose heat to the atmosphere until they are moved to a reheating furnace where they are heated to a uniform temperature before they are rolled to a final product in a rolling mill. It can be seen that the rate of heat transfer plays a prominent role throughout the processing sequence.

For the ideal case, where the heat losses of the system are negligible, the heat requirements at each stage of a process can be determined on the basis of thermodynamics. However, in order to determine the *rate* at which these heat requirements can be added or removed from the system, and also the rate of the inevitable heat losses, we must use the heat transfer theory which is the subject of this chapter and Chapters 11–13.

Heat is transferred by the following three mechanisms:

a. **Conduction**: Conduction is the transfer of thermal energy from a higher to a lower temperature zone in a material (Fig. 10.2). In fluids, conduction takes place at the molecular level with the more energetic molecules passing energy to their lower temperature neighbors. In solids which are not conductors of electricity (*dielectric materials*), conduction takes place by means of the oscillation of atoms which creates lattice waves; in good conductors of electricity, conduction occurs mostly by the motion of free electrons which move about similarly to molecules in a gas. The same is true in liquid metals, which have a relatively high electric conductivity.

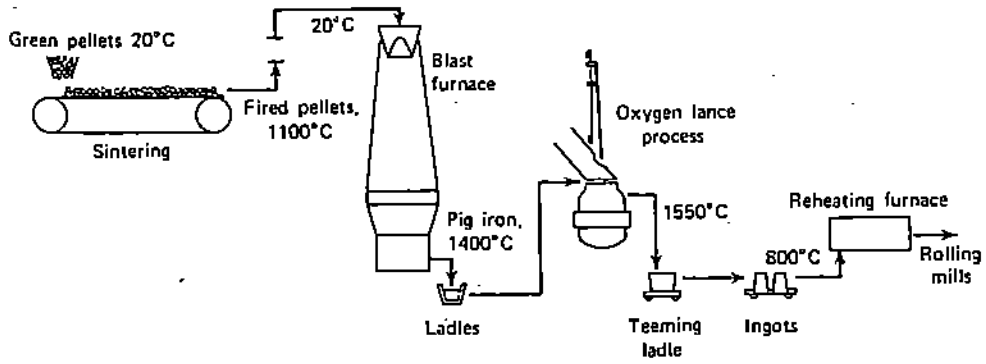

Figure 10.1. Temperature changes in the production of steel.

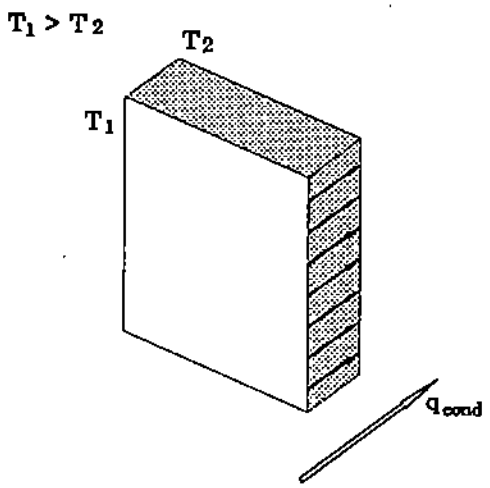

Figure 10.2. Heat transfer by conduction.

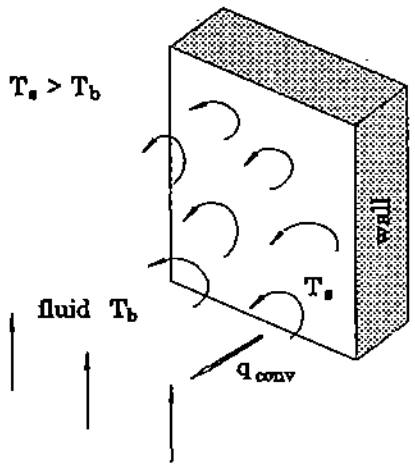

Figure 10.3. Heat transfer by convection.

b. **Convection**: In this case, thermal energy is moved from one part of the system to another as a result of the bulk motion of a fluid. This is illustrated

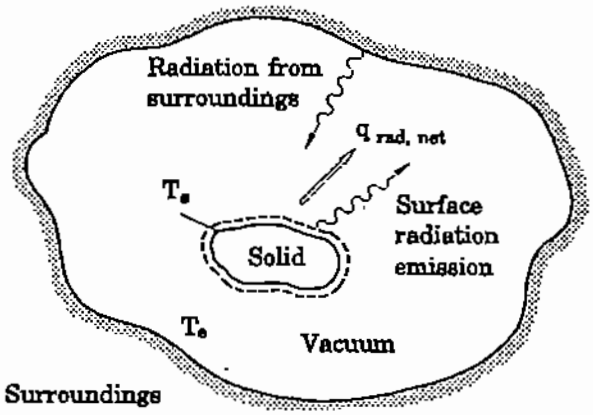

Figure 10.4. Heat transfer by radiation.

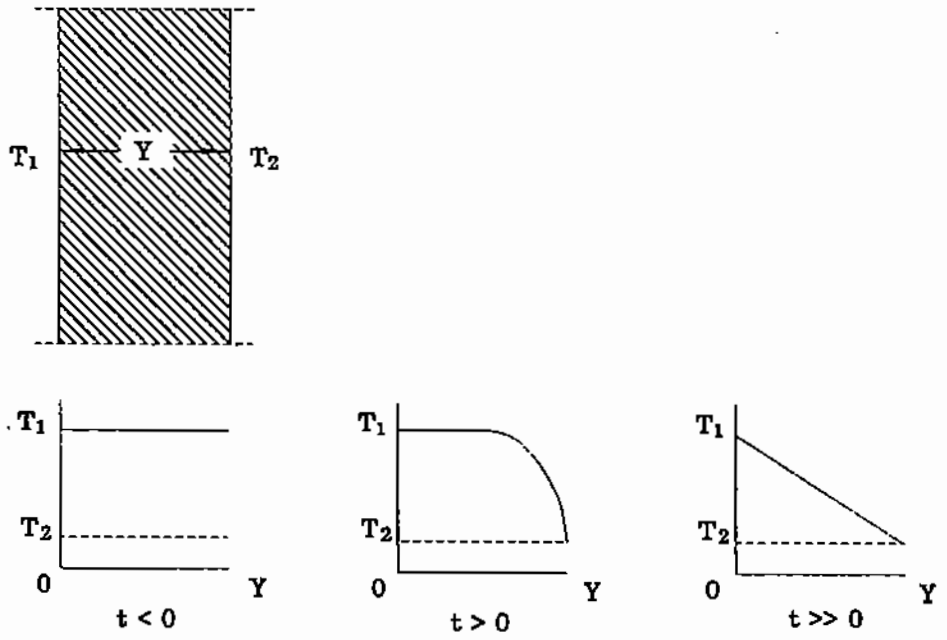

Figure 10.5. Temperature profiles across a plate at time t after cooling lower surface from T_1 to T_2.

in Fig. 10.3, which shows a fluid of bulk temperature T_b flowing past a solid surface at a higher temperature T_s; heat is transferred from the surface by elements of fluid which travel from the bulk and remain close to the solid surface for a short period of time.

c. **Radiation**: Both the conductive and convective transmission of thermal energy require the presence of an intervening medium (e.g., the solid body in the case of conduction, and the fluid in the case of convection). On the other hand, radiation between two surfaces occurs by the transmission of photons or electromagnetic waves through space and does not require the presence of an intervening medium (Fig. 10.4).

10.2. THE CONCEPT OF THERMAL CONDUCTIVITY

The nature of heat conduction may be illustrated by the following experiment (Fig. 10.5): A thin plate of thickness Y is initially at the uniform temperature T_1. At time $t = 0$, surface 2 of the plate is cooled to the temperature T_2 (e.g., by spraying with water) while the surface 1 is maintained at T_1 (e.g., by means of an electric heater). Experiments have shown that the sudden change in temperature of the lower surface will gradually affect the temperature profile throughout the thickness of the slab, as illustrated in Fig. 10.5. After a sufficiently long period of time for steady state conditions to prevail, a linear temperature profile is established across the plate; if we measure the heat flow from surface 1 to surface 2 (e.g., by measuring the temperature increase of the cooling water), we find that it is represented by the following equation:

$$Q_y = kA\frac{(T_1 - T_2)}{Y}. \tag{10.2.1}$$

where Q_y is the heat transferred in the direction y through the plate per unit time, and A is the surface area of the plate. The proportionality constant k is defined as the **thermal conductivity** of the material of the plate.

Since the temperature profile across the slab is linear, every infinitesimal segment of the line is represented by the same relationship. Therefore, (10.2.1) can be expressed in differential form as follows:

$$q_y = \frac{Q_y}{A} = -k\frac{dT}{dy}, \tag{10.2.2}$$

where q_y is the **heat flux** in the y direction, i.e., the rate of heat transfer per unit cross-sectional area of the plate. The negative sign reflects the fact that heat is always conducted from a higher to a lower temperature (i.e., $T_2 < T_1$ and $dT < 0$). Equation (10.2.2) can be generalized for heat conduction in all three dimensions as follows:

$$q_x = -k\frac{\partial T}{\partial x}, \quad q_y = -k\frac{\partial T}{\partial y}, \quad q_z = -k\frac{\partial T}{\partial z}, \tag{10.2.3}$$

and in vector notation:

$$q = -k\nabla T, \tag{10.2.4}$$

where $q = q_x + q_y + q_z$.

Equation (10.2.2), and the corresponding (10.2.3)–(10.2.4), are called the *Fourier law of conduction*. This law expresses the phenomenological observation that *the heat flux by conduction is proportional to the negative value of the temperature gradient in the direction of heat flow*.

In (10.2.3)–(10.2.4), by using the same value of k for all three directions of heat flow, we assumed that the material is **isotropic**. This assumption is valid for most homogeneous materials but does not hold for some crystalline structures with preferred orientation or for laminated and composite materials.

10.2.1. The Dimensions of Thermal Conductivity

The dimensions of the quantities appearing in (10.2.2) are:

q (heat flux: energy time^{-1} area^{-1}): Q t^{-1} L^{-2},

$\partial T/\partial y$ (temperature gradient): T L^{-1}.

Therefore, the dimensions of the thermal conductivity k are:

$$\text{(heat flux)} \cdot \text{(temperature gradient)}^{-1} = \text{Q t}^{-1}\ \text{L}^{-1}\ \text{T}^{-1}.$$

In the SI system, the unit of thermal and all other kinds of energy is the Joule. Since, by definition, 1 J s^{-1} = 1 W (watt: energy per unit time) the SI units of thermal conductivity are W m^{-1} K^{-1}. In the metric system, the unit of heat is the calorie, distance is measured in centimeters and temperature in degrees centigrade. Therefore, the units of k are: cal s^{-1} cm^{-1} $°C^{-1}$. The conversion factors between these two kinds of units and also to the "British" system unit (BTU) are

$$1\ \text{W m}^{-1}\ \text{K}^{-1} = 2.388 \times 10^{-3}\ \text{cal s}^{-1}\ \text{cm}^{-1}\ °\text{C}^{-1} = 0.578\ \text{BTU h}^{-1}\ \text{ft}^{-1}\ °\text{F}^{-1}.$$

10.3. ANALOGY BETWEEN MOMENTUM AND HEAT TRANSFER BY CONDUCTION

As noted in Chapter 1, there is a close analogy between the concept of viscosity (Chapter 3) and that of thermal conductivity: In the case of fluid flow, viscosity is the proportionality constant between the rate of momentum transfer and the driving force of the velocity gradient. In a similar way, thermal conductivity relates the conduction of heat to the driving force of the temperature gradient. This analogy becomes more evident in the case where the density, ρ, and specific heat, C_p, are constant with y so that we can rewrite (10.2.2) as follows:

$$q_y = -k\frac{\partial T}{\partial y} = -\frac{k}{\rho C_p}\frac{\partial(\rho C_p T)}{\partial y} = -\alpha\frac{\partial(\rho C_p T)}{\partial y}, \tag{10.3.1}$$

where k is the thermal conductivity, ρ the density, C_p the specific heat, and $\alpha = k/\rho C_p$, the **thermal diffusivity** of the material.

The corresponding equations are:

a. For momentum flux:

$$\tau_{y,x} = -\nu\frac{\partial(\rho u_x)}{\partial y}. \tag{10.3.2}$$

b. For heat flux:

$$q_y = -\alpha\frac{\partial(\rho C_p T)}{\partial y}. \tag{10.3.3}$$

The momentum diffusivity and the thermal diffusivity have the same dimensions, L^2 t^{-1}. In the SI system, the units of momentum and thermal diffusivity are m^2 s^{-1} and in the metric system cm^2 s^{-1}.

As will be discussed in Chapter 12, the ratio of the momentum and thermal diffusivities plays an important role in the *convection* of heat and is defined as the dimensionless **Prandtl number**:

$$\text{Pr} = \frac{\nu}{\alpha} = \frac{C_p\mu}{k}. \tag{10.3.4}$$

Table 10.1. Thermal Conductivity of Some Solid Materials

Material	Temperature, °C	k, W m^{-1} K^{-1}
Aluminum metal	500	222
Alumina (Al_2O_3) ceramic	500	10
Magnesite refractory	200	3.8
(87%MgO, 6.3%Fe_2O_3, 3%CaO, 3.7%SiO_2)	650	2.8
" "	1200	1.9
Silicon carbide refractory	600	18.5
" "	800	16.1
" "	1000	13.8
" "	1200	12.1
" "	1400	10.9
Chrome magnesite refractory	200	1.16
" "	650	1.47
" "	1300	1.73
Insulating brick (high porosity)	200	0.09
" "	760	0.02
Graphite brick	800	53.6
Copper metal	–263	19000
" "	900	345

Table 10.2. Thermal Conductivity of Some Common Gases
(k, W m^{-1} K^{-1}; at 1 atm pressure)

Temp, °C	Hydrogen	Air	Carbon monoxide	Carbon dioxide
25	0.182	0.027	0.025	0.017
175	0.251	0.037	0.044	0.029
525	0.384	0.058		
825	0.464		0.072	
1060	0.519			
1425		0.096		

10.4. VALUES OF THERMAL CONDUCTIVITY

The thermal conductivity of some solid materials at various temperatures is shown in Table 10.1. The conductivity of some common gases is shown in Table 10.2.

The thermal conductivity of materials is affected by temperature, pressure and composition. As in the case of viscosity, at low to moderate pressures the thermal conductivity of gases increases with temperature. The reverse behavior is observed with non-metallic materials, while metals exhibit a mixed behavior. The conductivities of various metals, minerals and other materials are shown in Figs. 10.6 [6] and 10.7 [1].

10.5. STEADY-STATE UNIDIRECTIONAL HEAT CONDUCTION

In this section we shall examine the use of the Fourier law of heat conduction for determining the temperature distribution and the rate of unidirectional heat conduction under steady-state conditions.

Let us consider an infinitesimal cubical element of volume $dx \cdot dy \cdot dz$ in a material of density ρ and specific heat C_p (Fig. 10.8). Heat is transferred in and out of the surfaces $dy \cdot dz$ of the element and also some heat is generated throughout the volume of the element, e.g., by chemical reaction or electric heating.

At steady state, the thermal energy balance for the control volume element of Fig. 10.8 is stated as follows:

heat in by conduction − heat out by conduction
+ heat generation in element = 0.

On the basis of the Fourier law of conduction (see (10.2.2)), the above statement can be expressed mathematically as

$$\frac{d}{dy}\left(k\frac{dT}{dy}\right) + \dot{q} = 0, \tag{10.5.1}$$

where $\dot{q}$ is the rate of heat generation per unit volume of the material. The above equation represents the thermal energy balance for steady-state unidirectional conduction. In the following section, we will examine its application in the solution of some simple heat conduction problems.

10.5.1. Heat Conduction through a Plane Wall

a. Known boundary conditions: two temperatures. Let us consider the very simple problem of heat conduction through a plane wall of thickness Y and constant thermal conductivity, k. The temperature at $y = 0$ is maintained at T_0 and at $y = Y$ is T_Y, where $T_0 > T_Y$. In this case, there is no generation of heat ($\dot{q} = 0$) and (10.5.1) simplifies to

$$k\frac{d^2T}{dy^2} = 0. \tag{10.5.2}$$

The boundary conditions for this second order equation are:

$$T = T_0 \text{ at } y = 0, \text{ and } T = T_Y \text{ at } y = Y.$$

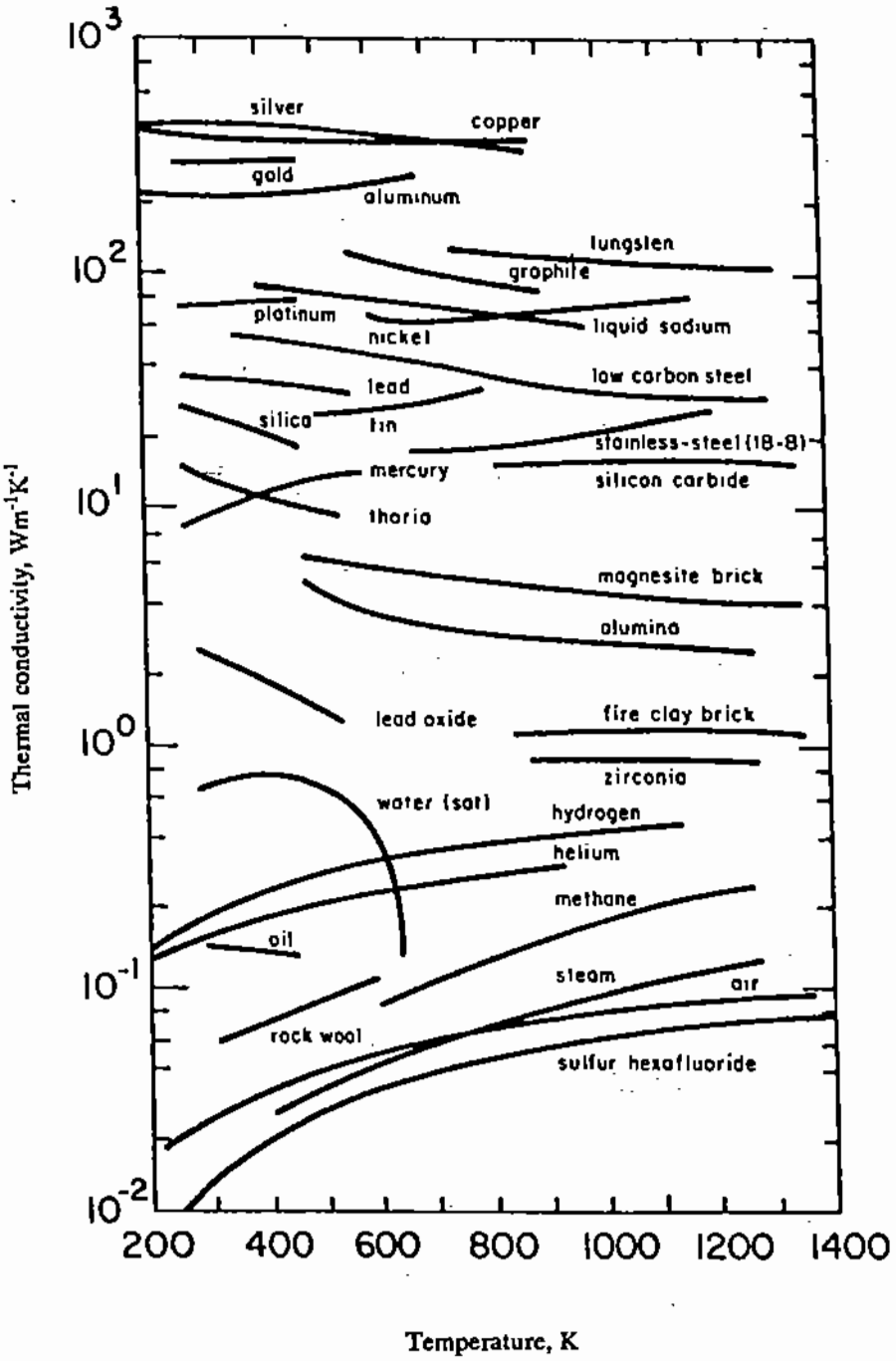

Figure 10.6. Thermal conductivity of metals and other materials [6].

By integrating (10.5.2) twice, we obtain

$$T = C_2 + C_1 y, \tag{10.5.3}$$

where C_1 and C_2 are integration constants. Solving for the integration constants on the basis of the above boundary conditions, we obtain

$$C_2 = T_0 \text{ and } C_1 = \frac{T_Y - T_0}{Y}.$$

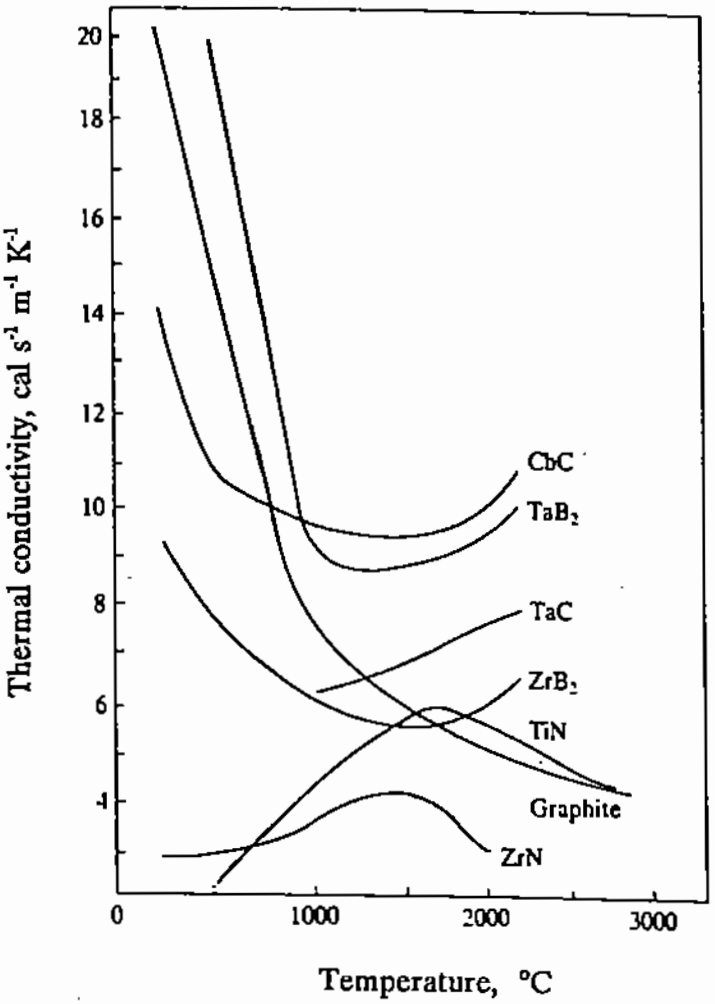

Figure 10.7. Thermal conductivity of refractory materials [1].

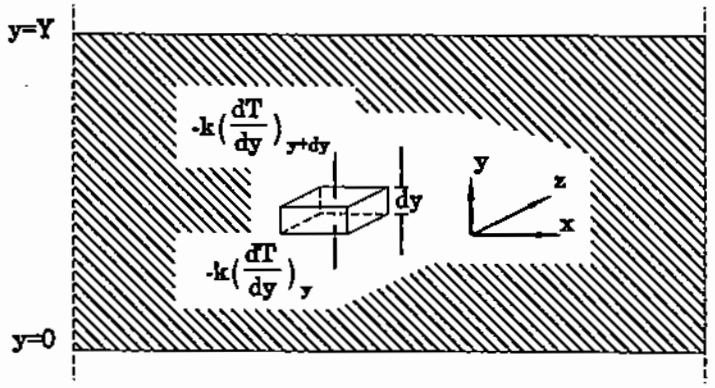

Figure 10.8. Control volume element in heat conduction.

Therefore, the temperature distribution across the wall thickness is:

$$T = T_0 + (T_Y - T_0)\frac{y}{Y}. \tag{10.5.4}$$

The heat flux through the wall can be obtained from the first derivative of the above temperature distribution:

$$q_y = -k\frac{dT}{dy} = k\frac{(T_0 - T_Y)}{Y}. \tag{10.5.5}$$

Example 10.5.1

A furnace wall is 18 cm thick; the temperature of the inside surface is 550°C and the outside surface is kept at 30°C. If the thermal conductivity of the wall is 3.0 W m^{-1} K^{-1}, calculate the heat loss per unit surface of furnace wall.

Solution: The required heat loss is equal to the heat flux by conduction through the wall and is calculated as follows:

$$q_y = \frac{3}{0.18}(550 - 30) = 8867\,\mathrm{W\,m^{-2}} = 2070\,\mathrm{cal\,s^{-1}\,m^{-2}}.$$

b. **Known boundary conditions: temperature and heat flux.** Let us now consider a similar case of heat conduction through a wall of a furnace where the inside temperature is known but not the outside one; instead, we know that the heat loss from the outside surface of the wall is expressed by a given function of the outside temperature. The boundary conditions in such a case are:

$$T = T_0 \text{ at } y = 0,$$

and

$$\text{heat flux through wall} = \text{heat loss from outside surface},$$

i.e.,

$$q_y = -k\frac{dT}{dy} = \frac{k(T_0 - T_Y)}{Y} = h(T_Y - T_a) \text{ at } y = Y, \tag{10.5.6}$$

where T_Y is the outside surface temperature, T_a is the temperature of the atmosphere around the furnace, and h is the heat transfer coefficient for convection from the outside surface to the environment (heat convection will be discussed in detail in Chapter 12).

On the basis of the above boundary conditions, and by using (10.5.6) to eliminate the intermediate temperature T_Y, the solutions for the integration constants C_1 and C_2 of (10.5.3) are now

$$C_2 = T_0, \text{ and } C_1 = \frac{T_Y - T_0}{Y} = \frac{h(T_a - T_0)}{k + hY}.$$

Accordingly, the temperature distribution of (10.5.3) is expressed as follows:

$$T = T_0 + \frac{h(T_a - T_0)}{k + hY}y, \tag{10.5.7}$$

or

$$T = T_0 + \frac{(T_a - T_0)\frac{y}{Y}}{1 + \frac{k}{hY}}. \tag{10.5.8}$$

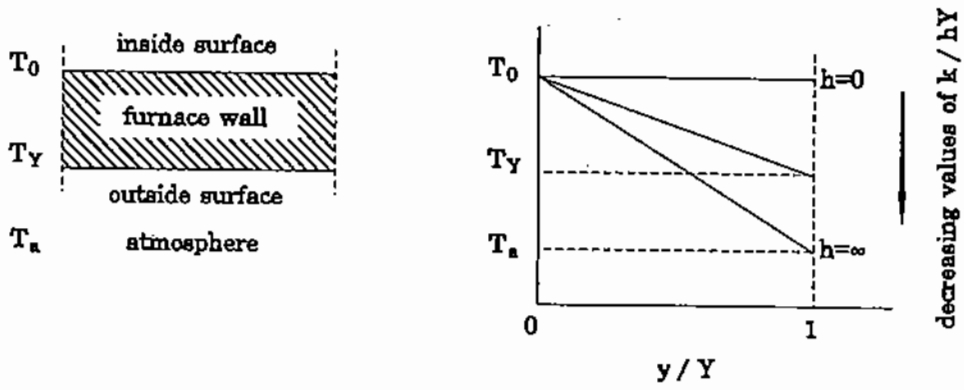

Figure 10.9. Temperature profiles through wall at increasing heat loss by convection from outside surface.

The temperature profile is shown in Fig. 10.9. It can be seen that as the ratio k/hY decreases, the outside wall temperature (at $y = Y$) approaches that of the environment.

Example 10.5.2

The inside wall temperature (T_0) of a furnace under design is to be 1500°C. Calculate the minimum wall thickness (Y) required if the temperature of the outside surface (T_Y) is not to exceed 200°C. The average thermal conductivity of the refractory wall may be taken as 0.6 W m^{-1} K^{-1}. The environment temperature is 20°C and the heat loss from the outside surface to the environment is expressed by the following empirical relationship:

$$q = 2.8(T_Y - T_a)^{1.25},$$

where T_a is the temperature of the atmosphere around the furnace, °C; T_Y is the outside temperature of the furnace wall, °C; q is the heat flux, W m^{-2}.

We start by equating the heat flux by conduction through the wall to the given equation for heat loss by convection to the environment:

$$\frac{k(T_0 - T_Y)}{Y} = 2.8(T_Y - T_a)^{1.25}.$$

Substituting numerical values and solving for Y, we calculate

$$Y = \frac{0.6(1500 - 200)}{2.8(200 - 20)^{1.25}} = 0.42\,\text{m}.$$

In similar problems, it may be required to determine the outside temperature for a specified wall thickness. In such cases, the heat balance equation must be solved by trial and error.

10.5.2. Heat Conduction in a Sphere

Let us consider a spherical particle of radius R and thermal conductivity k (Fig. 10.10). Heat is generated within the particle, e.g., by induction, at the rate of $\dot{q}$ watts per unit volume

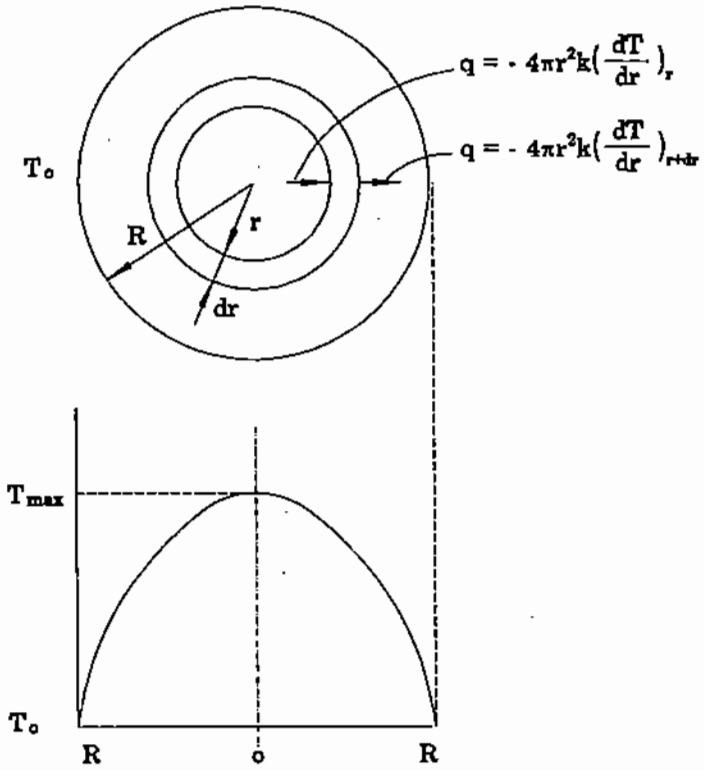

Figure 10.10. Temperature profile in a sphere, with internal heat generation.

of particle. If the outside surface is maintained at a constant temperature T_0, it is required to find the temperature distribution and maximum temperature within the sphere.

To solve this problem, we select as the control volume a spherical shell of thickness dr, as illustrated in Fig. 10.10. A heat balance over this shell yields the following differential equation:

$$d\left(4\pi r^2\, k\frac{dT}{dr}\right) + \dot{q}(4\pi r^2\, dr) = 0$$

or

$$\frac{1}{r^2}\frac{d}{dr}\left(r^2\, k\frac{dT}{dr}\right) + \dot{q} = 0. \tag{10.5.9}$$

By integrating this equation twice, we obtain the following algebraic equation:

$$T = C_2 - \frac{C_1}{r} - \frac{\dot{q}r^2}{6k}. \tag{10.5.10}$$

The integration constants C_1 and C_2 are evaluated from the boundary conditions, one of which was given as $T = T_0$ at $r = R$. Also, by considering that the temperature must have a finite value at all values of r, we deduce that $C_1 = 0$ (otherwise, T would be infinite at $r = 0$). Therefore, the solution of the differential heat balance yields the following temperature profile in the sphere:

$$T = T_0 + \frac{\dot{q}}{6k}(R^2 - r^2). \tag{10.5.11}$$

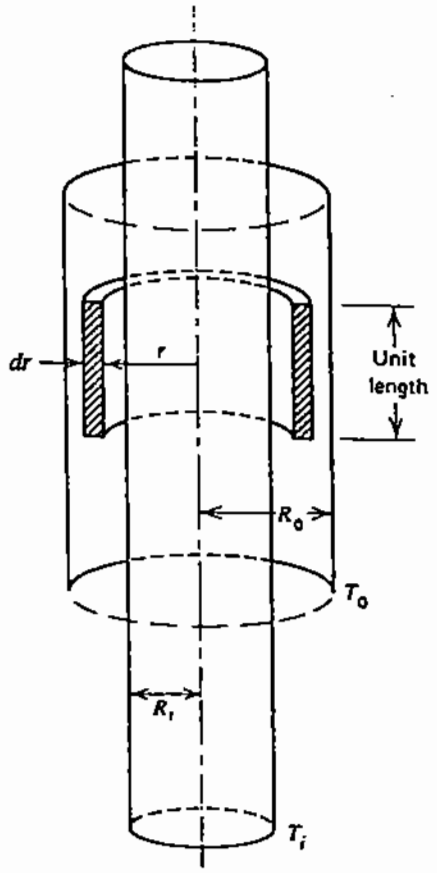

Figure 10.11. Heat conduction in a cylindrical shell.

10.5.3. Heat Conduction in a Hollow Cylinder

A common problem in heat transfer is the conduction of heat through the wall of a hollow cylinder of outer diameter R_0 and inner diameter R_i. To establish the temperature profile across the wall of the cylinder, we select as the control volume a cylindrical shell of radius r, thickness dr and unit length (Fig. 10.11). In the absence of heat generation and for steady state conditions, the differential heat balance in the control volume is

$$\frac{d}{dr}\left(2\pi r \frac{kdT}{dr}\right) = 0 \text{ for } R_i < r < R_0. \tag{10.5.12}$$

The above equation is integrated twice to yield

$$T = C_1 + C_2 \ln r. \tag{10.5.13}$$

The integration constants are evaluated from the boundary conditions which are given as:

$$T = T_i \text{ at } r = R_i \quad \text{and} \quad T = T_0 \text{ at } r = R_0.$$

On the basis of these boundary conditions, the temperature profile across the wall of the cylinder is expressed as follows:

$$T = \frac{T_i \ln \frac{R_0}{r} - T_0 \ln \frac{R_i}{r}}{\ln \frac{R_0}{R_i}}. \tag{10.5.14}$$

The rate of heat flow per length L of the cylinder (dimensions: $Q\,t^{-1}$) is expressed by the following equation:

$$Q = -(2\pi r L)k\frac{dT}{dr} = \frac{2\pi Lk(T_i - T_0)}{\ln \frac{R_0}{R_i}}. \tag{10.5.15}$$

10.6. HEAT CONDUCTION IN COMPOSITE MEDIA

In this section, we shall discuss the solution of simple problems of heat conduction through composite walls.

10.6.1. Planar Geometry

Let us consider a composite wall of thickness L, consisting of three materials arranged in parallel layers (Fig. 10.12). The thickness of the three layers is denoted by Y_1, Y_2, and Y_3, respectively and their corresponding thermal conductivities are k_1, k_2, and k_3. The temperature in each layer will be denoted by the variables T_1, T_2, and T_3, respectively.

The inside surface, corresponding to $y = 0$, is maintained at temperature T_0 and the outside surface, corresponding to $y = L$ ($L = Y_1 + Y_2 + Y_3$), is losing heat by convection to the atmosphere which is at temperature T_a. It is required to develop the equations describing the temperature profile within the system and the heat flux across the composite wall of thickness L.

We proceed by establishing individual control volumes in layers *1*, *2*, and *3*. The differential equations describing the heat flow are

$$\text{layer 1: } \frac{d^2T_1}{dy^2} = 0, \quad 0 \le y \le Y_1, \tag{10.6.1}$$

$$\text{layer 2: } \frac{d^2T_2}{dy^2} = 0, \quad Y_1 \le y \le Y_2, \tag{10.6.2}$$

$$\text{layer 3: } \frac{d^2T_3}{dy^2} = 0, \quad Y_2 \le y \le Y_3. \tag{10.6.3}$$

Six boundary conditions are necessary for the solution of the above equations. The first two conditions are derived from the physical statement that the temperature is specified at $y = 0$, and that there is convective heat transfer at $y = L$:

$$T_1 = T_0 \text{ at } y = 0, \tag{10.6.4}$$

$$-k_3\frac{dT_3}{dy} = h(T_3 - T_a) \text{ at } y = L \quad (L = Y_1 + Y_2 + Y_3). \tag{10.6.5}$$

The remaining four boundary conditions are obtained by reasoning that both the temperature and the heat flux must be continuous functions of distance throughout the composite wall. Therefore, the temperatures and the fluxes in two adjacent phases must be equal at the interface. It should be noted that these conditions are observed only if there is no contact resistance; however, allowance can be made for any contact resistance by introducing into

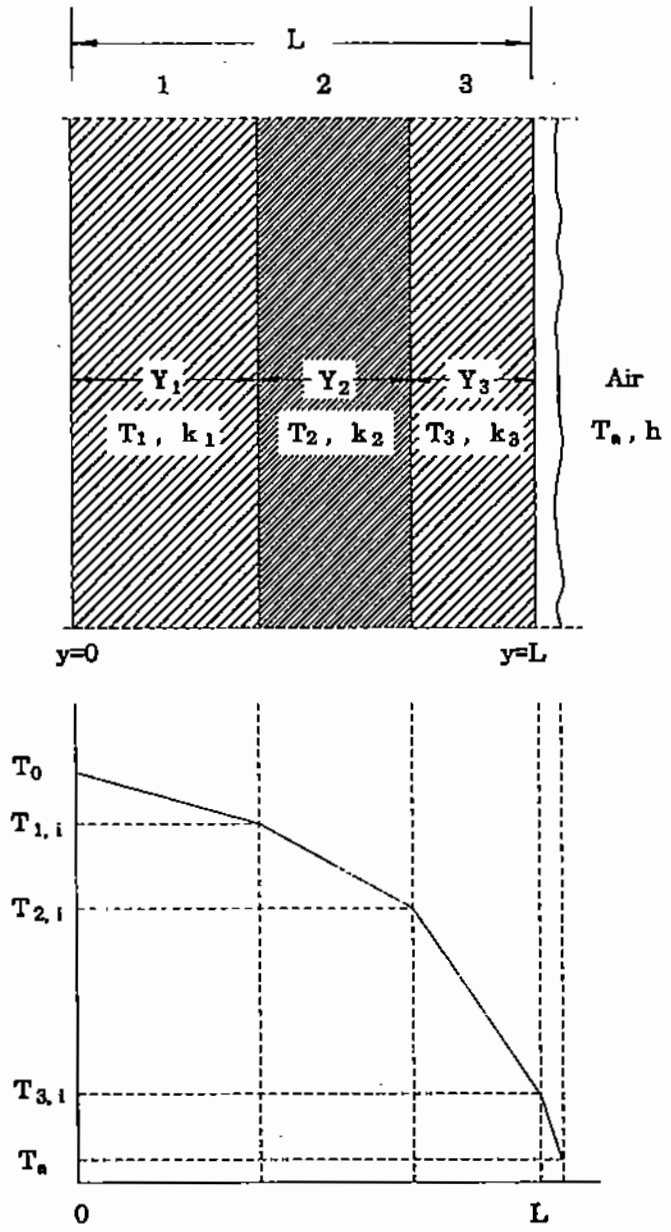

Figure 10.12. Temperature profile in a composite.

the formulation an additional phase of zero thickness. For negligible contact resistance, we have

$$T_1 = T_2 \text{ at } y = Y_1, \tag{10.6.6}$$

$$T_2 = T_3 \text{ at } y = Y_1 + Y_2, \tag{10.6.7}$$

and

$$k_1 \frac{dT_1}{dy} = k_2 \frac{dT_2}{dy} \text{ at } y = Y_1, \tag{10.6.8}$$

$$k_2 \frac{dT_2}{dy} = k_3 \frac{dT_3}{dy} \text{ at } y = Y_1 + Y_2. \tag{10.6.9}$$

The above differential equations and boundary conditions present a complete statement of the problem. An obvious method of solution would be to integrate each of the differential equations and evaluate the six integration constants by substituting the boundary conditions. However, in this case, there is an easier approach: It is obvious that, at steady state, the heat flux through the three layers of the wall and to the atmosphere, q_y, will be constant and the temperature profile in each layer linear. Therefore, if we designate the interface temperatures between successive layers of insulation as $T_{1,i}$, and $T_{2,i}$, and the outside surface temperature $T_{3,i}$, we may write the following system of four equations:

$$q_y = k_1 \frac{T_0 - T_{1,i}}{Y_1} = k_2 \frac{T_{1,i} - T_{2,i}}{Y_2} = k_3 \frac{T_{2,i} - T_{3,i}}{Y_3} = h(T_{3,i} - T_a). \tag{10.6.10}$$

These four equations have four unknowns, $T_{1,i}$, $T_{2,i}$, $T_{3,i}$, and q_y. The intermediate temperatures at the interfaces ($T_{1,i}$, $T_{2,i}$, and $T_{3,i}$) are readily eliminated algebraically to yield the following equation:

$$q_y = \frac{T_0 - T_a}{\frac{Y_1}{k_1} + \frac{Y_2}{k_2} + \frac{Y_3}{k_3} + \frac{1}{h}}. \tag{10.6.11}$$

Equation (10.6.11) provides a relationship between the heat flux and the terminal temperatures. Once q_y is known, the individual temperatures at the interfaces ($T_{1,i}$, $T_{2,i}$, and $T_{3,i}$) are readily obtained by substitution of q_y into (10.6.10).

The numerator in (10.6.11) may be regarded as the overall "driving force" for heat transfer, while the denominator represents the overall resistance to heat flow; the quantities

$$\frac{Y_1}{k_1}, \frac{Y_2}{k_2}, \frac{Y_3}{k_3}, \frac{1}{h},$$

appearing in the denominator may be considered as the individual resistances to the transport of heat; this equation is clearly analogous to Ohm's law for resistances in series, with the heat flux corresponding to current and the temperature difference to voltage difference.

Equation (10.6.11) may be generalized for the case of a composite medium consisting of n layers, as follows:

$$q_y = \frac{T_0 - T_a}{\sum_{j=1}^{n} \frac{Y_j}{k_j} + \frac{1}{h}}. \tag{10.6.12}$$

Example 10.7.1

A furnace wall (Fig. 10.13) consists of three layers, a 20-cm inner layer of refractory (k = 3.8 W m^{-1} K^{-1}), a 9-cm intermediate layer of insulating brick (k = 0.34 W m^{-1} K^{-1}) and a 1-cm steel shell (k = 38 W m^{-1} K^{-1}). The heat losses from the steel plate to the atmosphere can be represented by a combined heat transfer coefficient for convection (Chapter 12) and radiation (Chapter 13) of 14.2 W m^{-2} K^{-1}. If the inside furnace temperature is 1350°C and the atmospheric temperature, T_a = 18°C, calculate the heat loss per unit surface area and the outside temperature of the steel plate, T_s.

To calculate the net heat flow, we substitute the numerical values into (10.6.11):

$$q_y = \frac{1350 - 18}{\frac{0.2}{3.8} + \frac{0.09}{0.34} + \frac{0.01}{38} + \frac{1}{14.2}} = \frac{1332}{0.0526 + 0.2647 + 0.00026 + 0.0704}$$
$$= 3.433\,\text{kW m}^2.$$

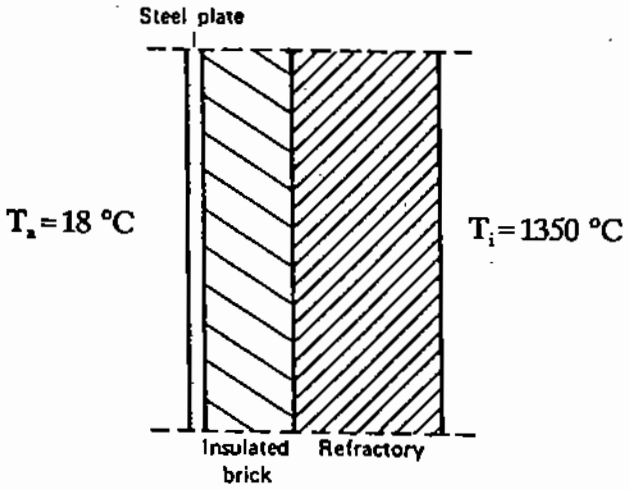

Figure 10.13. Heat conduction through a furnace wall.

It can be seen that the steel plate contributes very little to the overall resistance to the heat flow. The outside temperature of the steel plate, T_s, is calculated by equating the heat flow to the losses from the steel plate:

$$q_y = h(T_s - T_a), \;\; T_s = \frac{3433}{14.2} + 18 = 259.8°\text{C}.$$

The calculated outside temperature would be considered too high for most practical applications and, therefore, a thicker insulating layer, or better insulating material, would be required.

10.6.2. Cylindrical Geometry

Analogous considerations to the plane wall are applied to problems involving composite media of a cylindrical or spherical geometry. We have already presented the differential equation describing the flow of heat across the thickness of a cylindrical shell (see (10.5.15)). In the case of a number of coaxial cylindrical shells, this equation will apply for each layer while the expression of continuity of temperature and heat flux at the interfaces will provide the boundary conditions. The total heat flow for a length L of a multi-layered cylindrical shell, which loses heat to the atmosphere by convection, can be generalized as follows:

$$Q = \frac{2\pi L(T_0 - T_a)}{\sum_{j=1}^{n} \frac{\ln\left(\frac{r_{j+1}}{r_j}\right)}{k_j} + \frac{1}{hr_n}}. \tag{10.6.13}$$

where T_0 is the inside surface temperature, T_a is the atmospheric temperature, r_j is the radius of layer j, h is the heat transfer coefficient for convection, and r_n is the outside radius of the composite cylinder.

Example 10.7.2

Molten lead at 316°C is pumped through a 5-cm internal diameter × 0.32-cm thick steel pipe. The pipe is insulated by a 3-cm thick fiberglass layer (k = 0.08 W m^{-1} K^{-1}) and,

over that, by a 2.5-cm thick glass-wool sleeve ($k = 0.11$ W m^{-1} K^{-1}). If the heat transfer coefficient from the outer surface of the glass-wool sleeve to the atmosphere is 12 W m^{-2} K^{-1}, calculate the heat loss per meter of pipe length (atmospheric temperature= 20°C).

Solution: By substituting the above numerical values in (10.6.13), we obtain:

$$Q = \frac{2 \times 3.142 \times 1 \times (316 - 20)}{\frac{\ln\left(\frac{2.82}{2.6}\right)}{38} + \frac{\ln\left(\frac{5.82}{2.82}\right)}{0.08} + \frac{\ln\frac{8.32}{5.82}}{0.11} + \frac{1}{12 \times 8.32}}$$

$$= 149.97 \text{ W per m of pipe length.}$$

REFERENCES

1. R.I.L. Guthrie, *Engineering in Process Metallurgy*, Clarendon Press, Oxford (1989).
2. W.P. Rohsenow, J.P. Garnett, and E.N. Ganic, eds., *Handbook of Heat Transfer Fundamentals*, McGraw-Hill, New York (1985).
3. G.H. Geiger and D.R. Poirier, *Transport Phenomena in Metallurgy*, Addison-Wesley, Reading, MA (1973).
4. N.P. Cheremisinoff, ed., *Handbook of Heat and Mass Transfer*, Vol. 1: *Heat Transfer Operations*, Gulf Publishing, Houston (1986).
5. W.R. Rohsenow and H. Choi, *Heat, Mass and Momentum Transfer*, Prentice-Hall, New York (1961).
6. D.F. Rosner, *Transport Processes in Chemically Reacting Flow Systems*, Butterworths, Boston (1986).

ELEVEN

Unsteady State Conduction of Heat

In Chapter 10, we introduced the concept of thermal conductivity and used the Fourier law to solve simple problems of steady-state conduction in one direction. In the first part of this chapter, a similar approach will be used to develop the differential equations for three-dimensional unsteady-state conduction. The analytical and numerical methods available for the solution of these equations will be described in the second part.

11.1. THE DIFFERENTIAL EQUATIONS OF HEAT CONDUCTION

To develop the differential energy of heat conduction, we will use an infinitesimal cubical element of volume $dx \cdot dy \cdot dz$ in a material of density ρ and specific heat C_p (Fig. 11.1). Heat is transferred through the element by conduction; also, some heat may be generated within the element, e.g., by resistance or induction heating or by a transformation reaction. The thermal energy balance for this element is stated as follows:

rate of heat accumulation in element
= heat transfer rate in − heat transfer rate out
+ rate of heat generation in element.

On the basis of the Fourier law of conduction (see (10.2.2)), this statement can be expressed mathematically for three-dimensional conduction as follows (Fig. 11.1):

$$\begin{aligned}\frac{\partial(\rho C_p T)}{\partial t}dx\,dy\,dz = &\left[-k_x\left(\frac{\partial T}{\partial x}\right)_x + k_x\left(\frac{\partial T}{\partial x}\right)_{x+dx}\right] dy\,dz \\ &+ \left[-k_y\left(\frac{\partial T}{\partial y}\right)_y + k_y\left(\frac{\partial T}{\partial y}\right)_{y+dy}\right] dx\,dz \\ &+ \left[-k_z\left(\frac{\partial T}{\partial z}\right)_z + k_z\left(\frac{\partial T}{\partial z}\right)_{z+dz}\right] dx\,dy \\ &+ \dot{q}\,dx\,dy\,dz,\end{aligned} \tag{11.1.1}$$

where $\dot{q}$ is the rate of heat generation per unit volume of the material. However, by mathematical definition

$$k_x\left(\frac{\partial T}{\partial x}\right)_{x+dx} = k_x\left(\frac{\partial T}{\partial x}\right)_x + \frac{\partial}{\partial x}\left(k_x\frac{\partial T}{\partial x}\right)dx. \tag{11.1.2}$$

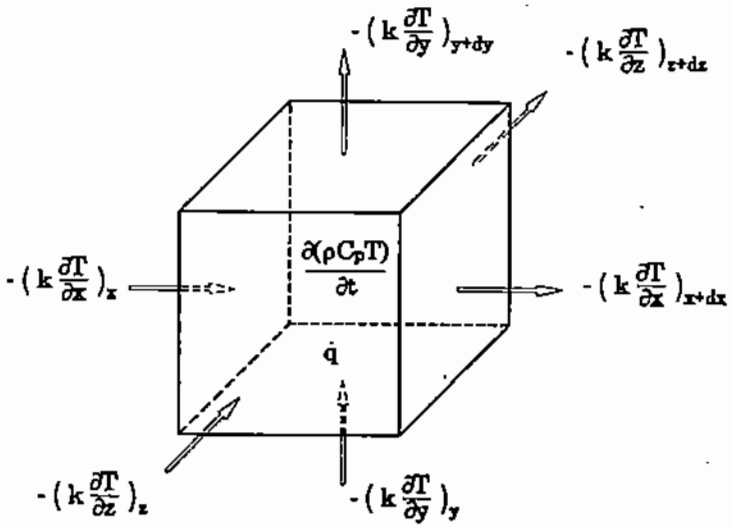

Figure 11.1. Heat balance in a cubical element of volume.

By substituting from the above equation and from the equivalent expressions for y and z in (11.1.1) and eliminating redundant terms, we obtain

$$\frac{\partial(\rho C_p T)}{\partial t} = \frac{\partial}{\partial x}\left(k_x \frac{\partial T}{\partial x}\right) + \frac{\partial}{\partial y}\left(k_y \frac{\partial T}{\partial y}\right) + \frac{\partial}{\partial z}\left(k_z \frac{\partial T}{\partial z}\right) + \dot{q}. \tag{11.1.3}$$

Most materials are **isotropic** in terms of heat conduction, i.e., $k_x = k_y = k_z = k$. Also, if the density, ρ, and the specific heat, C_p, of the material are not strongly temperature-dependent, (11.1.3) can be simplified as follows:

$$\rho C_p \frac{\partial T}{\partial t} = \frac{\partial}{\partial x}\left(k \frac{\partial T}{\partial x}\right) + \frac{\partial}{\partial y}\left(k \frac{\partial T}{\partial y}\right) + \frac{\partial}{\partial z}\left(k \frac{\partial T}{\partial z}\right) + \dot{q}, \tag{11.1.4}$$

and in vector notation

$$\rho C_p \frac{\partial T}{\partial t} = \nabla(k \nabla T) + \dot{q}. \tag{11.1.5}$$

If the change of thermal conductivity with x, y, and z may also be assumed to be negligible, (11.1.4) and (11.1.5) can be simplified further:

$$\frac{\partial T}{\partial t} = \alpha\left(\frac{\partial^2 T}{\partial x^2} + \frac{\partial^2 T}{\partial y^2} + \frac{\partial^2 T}{\partial z^2}\right) + \frac{\dot{q}}{\rho C_p}, \tag{11.1.6}$$

and in vector notation

$$\frac{\partial T}{\partial t} = \alpha \nabla^2 T + \frac{\dot{q}}{\rho C_p}, \tag{11.1.7}$$

where α is the thermal diffusivity:

$$\alpha = \frac{k}{\rho C_p}. \tag{11.1.8}$$

As noted in Chapter 10, the thermal diffusivity has the same dimensions, $L^2\ t^{-1}$ as the momentum diffusivity (or kinematic viscosity, ν) which was discussed in Chapter 3.

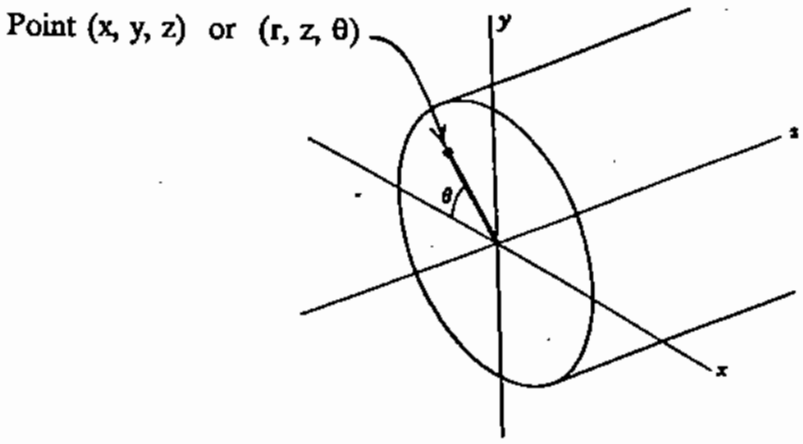

Figure 11.2. Cylindrical coordinates.

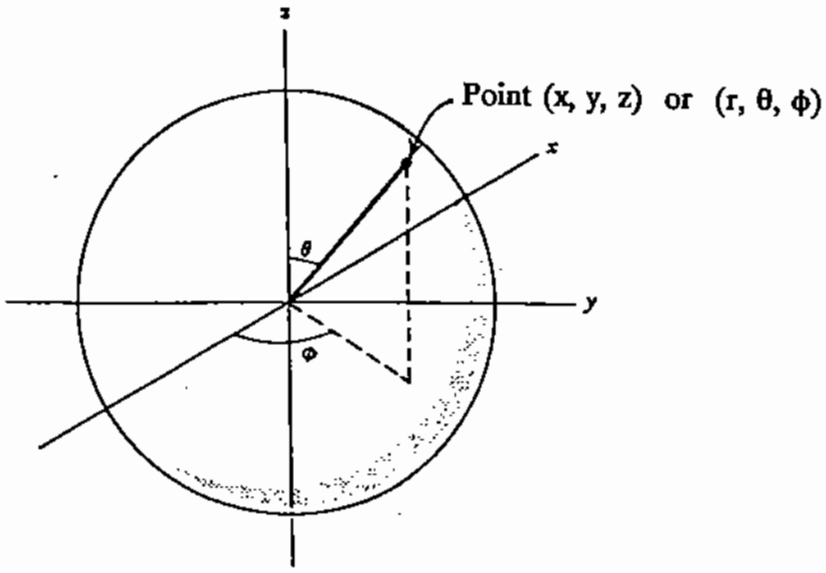

Figure 11.3. Spherical coordinates.

For unsteady state conduction, α represents the capacity of a material to transport heat by conduction better than k, because the product ρC_p accounts for the amount of transferred heat that is retained in the material per degree of temperature increase.

In cylindrical and spherical bodies, it is convenient to use the corresponding forms of the above equations in cylindrical (Fig. 11.2) and spherical (Fig. 11.3) coordinates. The considerations are the same as for the linear coordinate system, with the geometrical complication that the cross-sectional area through which heat is conducted changes with radial distance.

For a cylindrical system, the spatial coordinates are the radial distance from the axis of the cylinder, r, the angle θ around a section of the cylinder, and the axial distance z along the length of the cylinder. These coordinates are related to the linear coordinates x, y, and z as follows (Fig. 11.2):

$$x = r\cos\theta, \quad y = r\sin\theta, \quad z = z. \tag{11.1.9}$$

By substituting the cylindrical coordinates in (11.1.4) we obtain

$$\rho C_p \frac{\partial T}{\partial t} = \frac{1}{r}\frac{\partial}{\partial r}\left(k r \frac{\partial T}{\partial r}\right) + \frac{1}{r^2}\frac{\partial}{\partial \theta}\left(k \frac{\partial T}{\partial \theta}\right) + \frac{\partial}{\partial z}\left(k \frac{\partial T}{\partial z}\right) + \dot{q}, \tag{11.1.10}$$

and for constant k with location

$$\frac{\partial T}{\partial t} = \alpha\left[\frac{1}{r}\frac{\partial}{\partial r}\left(r \frac{\partial T}{\partial r}\right) + \frac{1}{r^2}\frac{\partial^2 T}{\partial \theta^2} + \frac{\partial^2 T}{\partial z^2}\right] + \frac{\dot{q}}{\rho C_p}, \tag{11.1.11}$$

or

$$\frac{\partial T}{\partial t} = \alpha\left(\frac{\partial^2 T}{\partial r^2} + \frac{1}{r}\frac{\partial T}{\partial r} + \frac{1}{r^2}\frac{\partial^2 T}{\partial \theta^2} + \frac{\partial^2 T}{\partial z^2}\right) + \frac{\dot{q}}{\rho C_p}. \tag{11.1.12}$$

Similarly, the spherical system coordinates are related to x, y, and z as follows (Fig. 11.3):

$$x = r\sin\theta\cos\phi, \quad y = r\sin\theta\sin\phi, \quad z = r\cos\theta. \tag{11.1.3}$$

The equation which corresponds to (11.1.4) is

$$\begin{aligned}\rho C_p \frac{\partial T}{\partial t} = {} & \frac{1}{r^2}\frac{\partial}{\partial r}\left(k r^2 \frac{\partial T}{\partial r}\right) + \frac{1}{r^2\sin^2\phi}\frac{\partial}{\partial \theta}\left(k \frac{\partial T}{\partial \theta}\right) \\ & + \frac{1}{r^2\sin\phi}\frac{\partial}{\partial \phi}\left(k\sin\phi \frac{\partial T}{\partial \phi}\right) + \dot{q},\end{aligned} \tag{11.1.14}$$

and for constant k with location

$$\frac{\partial T}{\partial t} = \alpha\left[\frac{1}{r^2}\frac{\partial}{\partial r}\left(r^2 \frac{\partial T}{\partial r}\right) + \frac{1}{r^2\sin^2\phi}\frac{\partial^2 T}{\partial \theta^2} + \frac{1}{r^2\sin\phi}\frac{\partial}{\partial \phi}\left(\sin\phi \frac{\partial T}{\partial \phi}\right)\right] + \frac{\dot{q}}{\rho C_p}, \tag{11.1.15}$$

or

$$\frac{\partial T}{\partial t} = \alpha\left(\frac{\partial^2 T}{\partial r^2} + \frac{2}{r}\frac{\partial T}{\partial r} + \frac{1}{r^2\sin^2\phi}\frac{\partial^2 T}{\partial \theta^2} + \frac{1}{r^2}\frac{\partial^2 T}{\partial \phi^2} + \frac{1}{r^2\tan\phi}\frac{\partial T}{\partial \phi}\right) + \frac{\dot{q}}{\rho C_p}. \tag{11.1.16}$$

The above equations for unsteady state conduction are of first order with respect to time and of second order with respect to the spatial coordinates. To solve them, we need one initial condition for time (i.e., the temperature distribution at $t = 0$) and two boundary conditions for each spatial variable. For example, for unidirectional conduction we need one initial condition and two boundary conditions, while the equivalent expression for an x, y, z system would require $3 \times 2 = 6$ boundary conditions. As in the case of steady-state conduction, which we discussed in Chapter 10, the boundary conditions may be specified in several ways:

a. The temperature may be specified at the boundary surfaces; depending on the nature of the problem, these values of T may be constant or have a specified relationship to time.
b. The heat flux, i.e., the temperature gradient times the thermal conductivity, may be specified at one or more of the boundary surfaces; examples of this situation were given in Chapter 10. In some problems, such heat fluxes may have a specified relationship to time and temperature.

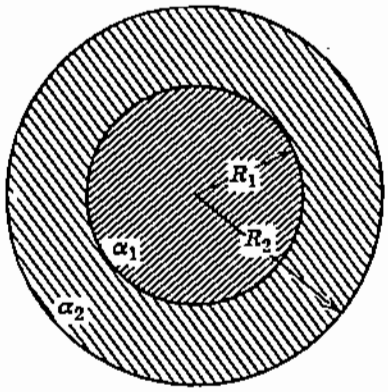

Figure 11.4. Heat conduction in a composite sphere.

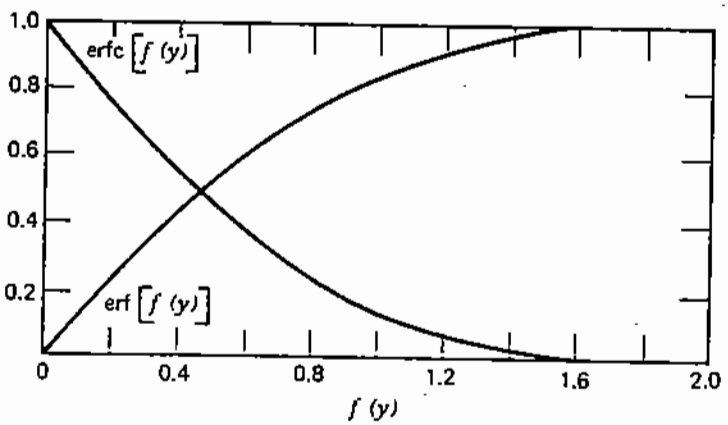

Figure 11.5. Numerical values of the error functions.

c. In the case of composite media, the continuity of temperature and heat flux are generally specified at the phase boundaries. For example, in the case of the composite sphere of Fig. 11.4, the boundary conditions at the interface between the two materials would be

$$T_1 = T_2 \text{ at } r = R_1; \quad k_1 \frac{\partial T_1}{\partial r} = k_2 \frac{\partial T_2}{\partial r} \text{ at } r = R_1, \tag{11.1.17}$$

where R_1 is the radius of the interface between the two materials.

11.2. ANALYTICAL METHODS OF SOLVING THE CONDUCTION EQUATIONS

Differential equations can be solved either by mathematical analysis or by numerical methods. An example of the analytical methods is presented in the following section.

11.2.1. Solution of a Particular Form for a Semi-Infinite Solid

One way to solve a differential equation is by finding a mathematical function that satisfies the equation and its boundary conditions. As an example, let us consider the differential equation for unsteady-state conduction through a solid in the direction y (see (11.1.6)):

$$\frac{\partial T}{\partial t} = \alpha \frac{\partial^2 T}{\partial y^2}. \tag{11.2.1}$$

It has been found that one of the functions that can be a general solution of this equation is as follows:

$$T = A + B\,\mathrm{erfc}\,\frac{y}{2\sqrt{\alpha t}}, \tag{11.2.2}$$

where A and B are constants and $\mathrm{erfc}[f(y)]$ is called the *complementary error function* of $f(y)$. *Error function* $\mathrm{erf}[f(y)]$ and the complementary error function of $f(y)$ are defined mathematically as follows:

$$\mathrm{erf}[f(y)] = \frac{2}{\sqrt{\pi}} \int_0^{f(y)} e^{\zeta^2}\, d\zeta, \tag{11.2.3}$$

$$\mathrm{erfc}[f(y)] = 1 - \mathrm{erf}[f(y)] = \frac{2}{\sqrt{\pi}} \int_{f(y)}^{\infty} e^{-\zeta^2}\, d\zeta, \tag{11.2.4}$$

where ζ is a transform variable.

Plots of the values of $\mathrm{erf}[f(y)]$ and $\mathrm{erfc}[f(y)]$ against $f(y)$ are presented in Fig. 11.5. It can be shown mathematically that the error functions obey the following relationships:

$$\mathrm{erf}(0) = 0,\ \mathrm{erfc}(0) = 1,\ \mathrm{erf}(\infty) = 1,\ \mathrm{erfc}(\infty) = 0,\ \mathrm{erf}(-\infty) = -1,\ \mathrm{erfc}(-\infty) = 2, \tag{11.2.5}$$

and

$$\mathrm{erf}[-f(y)] = \mathrm{erf}[f(y)],\ \ \mathrm{erfc}[-f(y)] = 1 + \mathrm{erf}[f(y)]. \tag{11.2.6}$$

Error functions can be differentiated by using the Leibnitz [1] rule for differentiating integrals:

$$\frac{\partial}{\partial y} \int_{f_1(y)}^{f_2(y)} e^{-\zeta^2}\, d\zeta = \frac{\partial}{\partial y}\left[f_2(y)\right] e^{-f_2^2(y)} - \frac{\partial}{\partial y}\left[f_1(y)\right] e^{-f_1^2(y)}. \tag{11.2.7}$$

Let us now examine whether (11.2.2) is indeed a solution of the differential (11.2.1). By differentiating (11.2.2) with respect to y and applying the Leibnitz rule, we obtain:

$$\frac{\partial}{\partial y}\left[A + B\,\mathrm{erfc}\,\frac{y}{2\sqrt{\alpha t}}\right] = -\frac{2B}{\sqrt{\pi}}\left[\frac{\partial}{\partial y}\left(\frac{y}{2\sqrt{\alpha t}}\right)\right] e^{-y^2/4\alpha t} = -\frac{B}{\sqrt{\pi \alpha t}} e^{-y^2/4\alpha t}. \tag{11.2.8}$$

Therefore, the second derivative with respect to y is

$$\frac{\partial^2}{\partial y^2}\left[A + B\,\mathrm{erfc}\,\frac{y}{2\sqrt{\alpha t}}\right] = \frac{\partial}{\partial y}\left[-\frac{B}{\sqrt{\pi \alpha t}}\, e^{-y^2/4\alpha t}\right] = \frac{By}{2\pi^{1/2}\alpha^{3/2} t^{3/2}}\left(e^{-y^2/4\alpha t}\right). \tag{11.2.9}$$

Finally, by differentiating (11.2.2) with respect to t and applying the Leibnitz rule, we obtain:

$$\frac{\partial}{\partial t}\left[A + B\,\mathrm{erfc}\,\frac{y}{2\sqrt{\alpha t}}\right] = \frac{By}{2\pi^{1/2}\alpha^{1/2} t^{3/2}}\, e^{-y^2/4\alpha t}. \tag{11.2.10}$$

Comparison of the right-hand sides of (11.2.9) and (11.2.10) shows that

$$\frac{\partial}{\partial t}\left[A + B\,\text{erfc}\,\frac{y}{2\sqrt{\alpha t}}\right] = \alpha\frac{\partial^2}{\partial y^2}\left[A + B\,\text{erfc}\,\frac{y}{2\sqrt{\alpha t}}\right], \tag{11.2.11}$$

which proves that the function

$$A + B\,\text{erfc}\,\frac{y}{2\sqrt{\alpha t}}$$

is a solution of the differential (11.2.1).

Example 11.2.1

In unsteady-state heat conduction problems, a *semi-infinite solid* is considered to be one of such thickness that changes in temperature at one side do not reach the other side, within the time reference of the problem. Let us consider such a solid of width or thickness y extending from

$$0 \le y \le \infty,$$

which is initially at temperature T_i. At time $t = 0$, the surface represented by the $y = 0$ plane is suddenly brought up to the temperature T_s. It is required to develop an analytical expression for the temperature profiles within the solid, as a function of time.

The thermal energy balance is the same as (11.2.1):

$$\frac{\partial T}{\partial t} = \alpha\frac{\partial^2 T}{\partial y^2}. \tag{11.2.1}$$

The boundary conditions were stated as follows:

$$T = T_i \text{ at } y > 0 \text{ and } t = 0, \tag{11.2.12}$$

$$T = T_s \text{ at } y = 0 \text{ and } t > 0, \tag{11.2.13}$$

$$T \to T_i \text{ at } y \to \infty \text{ and } t > 0. \tag{11.2.14}$$

The last boundary condition expresses the fact that, for a certain period of time, the temperature at an infinite value of y may be considered to remain at its initial value. On the basis of our earlier discussion, let us examine whether an equation of the form

$$T = A + B\,\text{erfc}\,\frac{y}{2\sqrt{\alpha t}} \tag{11.2.2}$$

satisfies (11.2.1) and the boundary conditions expressed by (11.2.12)–(11.2.14).

From the boundary condition 11.2.14 and the stated fact that $\text{erfc}(\infty) = 0$ (see (11.2.5)), it is concluded that $A = T_i$. Also, by setting $A = T_i$ and $t = 0$, it can be seen that since $\text{erfc}(\infty) = 0$, (11.2.2) also satisfies the boundary condition of (11.2.12). Finally, since $\text{erfc}(0) = 1$, the remaining boundary condition (see (11.2.13)) can be met by setting $B = T_s - T_i$. Therefore, the required solution is:

$$T - T_i = (T_s - T_i)\,\text{erfc}\,\frac{y}{2\sqrt{\alpha t}}. \tag{11.2.15}$$

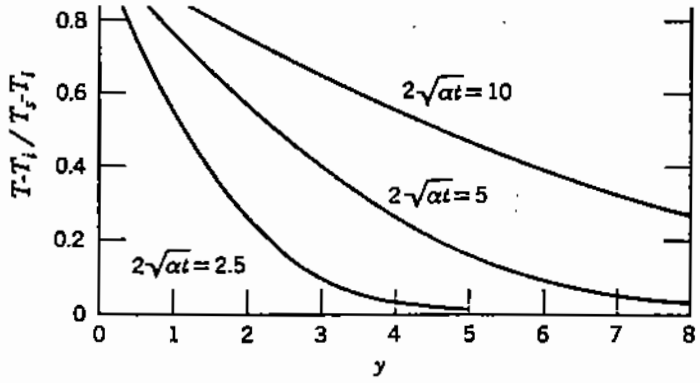

Figure 11.6. Temperature distribution in a semi-infinite plate.

This equation is presented graphically in Fig. 11.6, in the form of the dimensionless temperature ratio of $(T - T_i)/(T_s - T_i)$ against y, for different values of the group $2(\alpha t)^{1/2}$.

In most heat conduction problems, it is necessary to calculate not only the temperature distribution in a body but also the heat flux through it. In the present problem of heat conduction in the y direction, the heat flux is expressed by the Fourier equation for conduction:

$$q_y = -k\frac{\partial T}{\partial y}. \tag{11.2.16}$$

By substituting for T from (11.2.15) and using the expression for the first derivative of erfc$[f(y)]$ presented in (11.2.8), we obtain

$$q_y = +\frac{k(T_s - T_i)e^{-y^2/4\alpha t}}{\sqrt{\pi\alpha t}}. \tag{11.2.17}$$

Therefore, the heat flux at the surface of the solid, i.e., at $y = 0$, is

$$q_{y=0} = \frac{k(T_s - T_i)}{\sqrt{\pi\alpha t}}. \tag{11.2.18}$$

It should be noted that the above equation predicts an infinite heat flux at the exact instant of $t = 0$. It is, of course, impossible to raise the temperature of the surface suddenly by a step value. Let us consider the more practical case of the *average* heat flux over a finite interval, t_c; the average heat flux during this time period is then expressed as follows:

$$\overline{q}_y = \frac{\int_0^{t_c} \frac{k(T_s - T_i)}{\sqrt{\pi\alpha t}} dt}{t_c} = \frac{2k(T_s - T_i)\left(\frac{t_c}{\pi\alpha}\right)^{1/2}}{t_c} = \frac{2k(T_s - T_i)}{\sqrt{\pi\alpha t_c}}. \tag{11.2.19}$$

Example 11.2.2

Molten metal is poured rapidly into a 3-m diameter by 4-m high ladle which is filled to a depth of 2.5 m. If the refractory lining of the ladle (0.3-m thickness) was initially preheated by gas firing to a uniform temperature of 600°C (T_w) and the initial metal temperature is

1600°C (T_i), estimate the heat loss due to conduction into the ladle walls, during the first 15 minutes after the ladle was filled.

Data:

Refractory wall:

$k = 1.2$ W m^{-1} K^{-1} $= 0.287$ cal s^{-1} m^{-1} K^{-1}

$\rho = 2723$ kg m^{-3}

$C_p = 0.3$ cal g^{-1} K^{-1}

$\alpha = 3.1 \times 10^{-7}$ m^2 s^{-1}

Molten metal:

$\rho = 7050$ kg m^{-3}

$C_p = 0.12$ cal g^{-1} K^{-1}

As a first approximation, let us assume that a) the ladle walls act as a semi-infinite solid; b) heat losses from the covered ladle occur only by conduction to the wall across the metal/refractory interface; c) the thermal properties of the system are nearly constant.

On the basis of these assumptions, the problem is formulated as follows:

$$\frac{\partial T}{\partial t} = \alpha \frac{\partial^2 T}{\partial y^2}, \tag{11.2.1}$$

and the boundary conditions are

$$T = T_w\,(600°\text{C})\,\text{at}\,t = 0,\ T \to T_w\,\text{as}\,y \to \infty,\ T = T_i\,(1600°\text{C})\,\text{at}\,y = 0.$$

It should be noted that the last equation introduces another simplifying assumption, i.e., the temperature of the molten steel will remain at 1600°C as heat is conducted into the refractory. The validity of this assumption will be examined later. The above system of equations was solved in Example 11.2.1. For the boundary conditions of this problem, the corresponding temperature distribution is

$$T = T_w + (T_i - T_w)\,\text{erfc}\,\frac{y}{2\sqrt{\alpha t}}. \tag{11.2.20}$$

The corresponding average heat flux over the time interval t_e was shown earlier (see (11.2.19)) to be

$$\overline{q}_y = \frac{2k(T_i - T_w)}{\sqrt{\pi \alpha t_e}}. \tag{11.2.21}$$

The total amount of heat transferred from the metal to the ladle wall over the time period t_e is obtained by multiplying the average heat flux by the time interval and the area of the liquid/wall interface:

$$\begin{aligned} Q_{\text{total}} &= \overline{q}_y t_e A_i = \frac{2k(T_i - T_w)}{\sqrt{\pi \alpha t_e}}\, t_e A_i \\ &= 2k(T_i - T_w)\left(\frac{t_e}{\pi \alpha}\right)^{1/2}\left(\frac{\pi}{4} d_l^2 + \pi d_l h_m\right) \\ &= 2 \times 0.287 \times 1000 \times \left(\frac{900}{\pi \times 3.1 \times 10^{-7}}\right)^{1/2} \times \left(\frac{\pi}{4} \times 3^2 + \pi \times 3 \times 2.5\right) \\ &= 543500 \text{ kcal}, \end{aligned}$$

where t_e is the stated period of 15 minutes (900 seconds), d_i is the inside diameter of the ladle, and h_m is the depth of the metal bath.

The total heat capacity of the melt in the ladle per degree K is

$$\rho C_p \times \text{volume of metal} = 7050 \times 0.12 \times 17.67 = 14948 \text{ kcal K}^{-1}.$$

Therefore, the corresponding decrease in metal temperature during the first 900 seconds is 543500/14948 = 35.8 K. It follows that the initial assumption of a nearly constant temperature at the metal/refractory interface was reasonable.

Let us now also examine the validity of the assumption that the ladle wall acts as a semi-infinite solid. As stated earlier, this assumption is reasonable provided that the region of the temperature gradient is smaller than the characteristic length of the system in which conduction occurs (in this case, the thickness of the refractory wall). We shall define, somewhat arbitrarily, the heat penetration distance as the point which has increased in temperature by less than 5% of the initial metal/wall surface temperature difference (1600–600°C). Thus, from (11.2.20), we are seeking the value of y for which

$$\text{erfc} \frac{y}{2\sqrt{\alpha t_e}} = 0.05.$$

From Fig. 11.5, or any tabulation of error functions, this value of erfc$[f(y)]$ corresponds to $f(y) = y/[2(\alpha t_e)^{1/2}] = 1.4$. Therefore, y is calculated to be 0.046 m.

It can be seen that this depth of penetration in the 15-min interval is small in comparison to the overall thickness of the refractory wall (0.3 m); this justifies the assumption of the refractory wall as a semi-infinite medium. Also, the fact that the distance travelled by the heat in fifteen minutes is very small in comparison to the diameter of the ladle justifies the treatment of the problem in linear rather than in cylindrical coordinates.

11.2.2. Analytical Solutions Available in Graphical Form

The technique of seeking a solution of the differential equation for unsteady-state conduction in the form of an error function is appropriate only for semi-infinite media. Other forms of analytical solutions and mathematical techniques are used for bodies of finite dimensions, as described in detail in the *Handbook of Heat Transfer Fundamentals* [2] and other specialist books on the subject of heat transfer [3,4].

It is important to know that for many cases of practical interest, the equations resulting from such solutions are available in graphical form. Therefore, it is not necessary for one to be a mathematician in order to solve relatively complex problems of heat conduction. Such graphical solutions are included in engineering handbooks and textbooks and are usually presented in terms of the following dimensionless parameters:

- Temperature is expressed relatively to a convenient reference level and is made dimensionless by dividing by the maximum possible temperature difference in the system. Thus, in Example 11.2.1, the dimensionless temperature would be expressed as

$$\frac{T - T_i}{T_s - T_i}.$$

  It can be seen that, expressed in this way, the dimensionless temperature at any point and time has a value between zero and 1.

- Time is made dimensionless by multiplying it by the thermal diffusivity of the medium and dividing by the square of a characteristic length, L, usually taken to be the distance from the center of the body (e.g., radius R of a sphere, half width L of a slab). This grouping is called the **Fourier number**:

$$\text{Fo} = \frac{\alpha t}{L^2}. \tag{11.2.22}$$

  It should be noted that the Fourier number is of the same form as the inverse of the square of the group

$$\frac{y}{\sqrt{\alpha t}},$$

  which we encountered in the error function equations in §11.2.1.
- The effect of heat convection between a fluid and the surface of a body is accounted for by means of the **Biot number** which represents the ratio of fluid thermal resistance (convection) to the internal thermal resistance of the fluid (conduction):

$$\text{Bi} = \frac{h}{k/L} = \frac{hL}{k}, \tag{11.2.23}$$

  where h is the heat transfer coefficient for convection to be discussed in Chapter 12.
- The location of any particular point, x, y, z, in the conducting medium is represented by dimensionless ratios x/L, y/L, and z/L.

There are many such solutions of a graphical form in the literature. Amongst the earliest published plots were the Gurney–Lurie charts [5] which are still included in the Chemical Engineers' Handbook [6]. However, their usefulness is limited to Fourier number values over 0.1. Therefore, Geiger and Poirier [7] recommended the use of the plots shown in Figs. 11.7–11.9 for the most common situations where the geometry is well defined: Heat conduction through a large plate, radial conduction through a long cylinder and conduction through a sphere.

Specialist handbooks, such as that by Rohsenow et al. [2], present similar plots for other situations, such as the heating or cooling of one side of a thick plate while the other side is insulated; the temperature response of reacting solids (e.g., in the presence of thermal decomposition); the two-phase problem of a melting or ablating solid, and other situations of interest in materials processing.

Example 11.2.3

An 8-cm diameter metal sphere is heated to the uniform temperature of 450°C. The sphere is then subjected to cooling by a forced air stream at 25°C. If the heat transfer coefficient from air to sphere is 40 W m^{-2} K^{-1} and the thermal properties of the metal are

Thermal conductivity: $k = 15.6$ W m^{-1} K^{-1},
Specific heat: $C_p = 460$ J kg^{-1} K^{-1},
Density: $\rho = 7600$ kg m^{-3}.

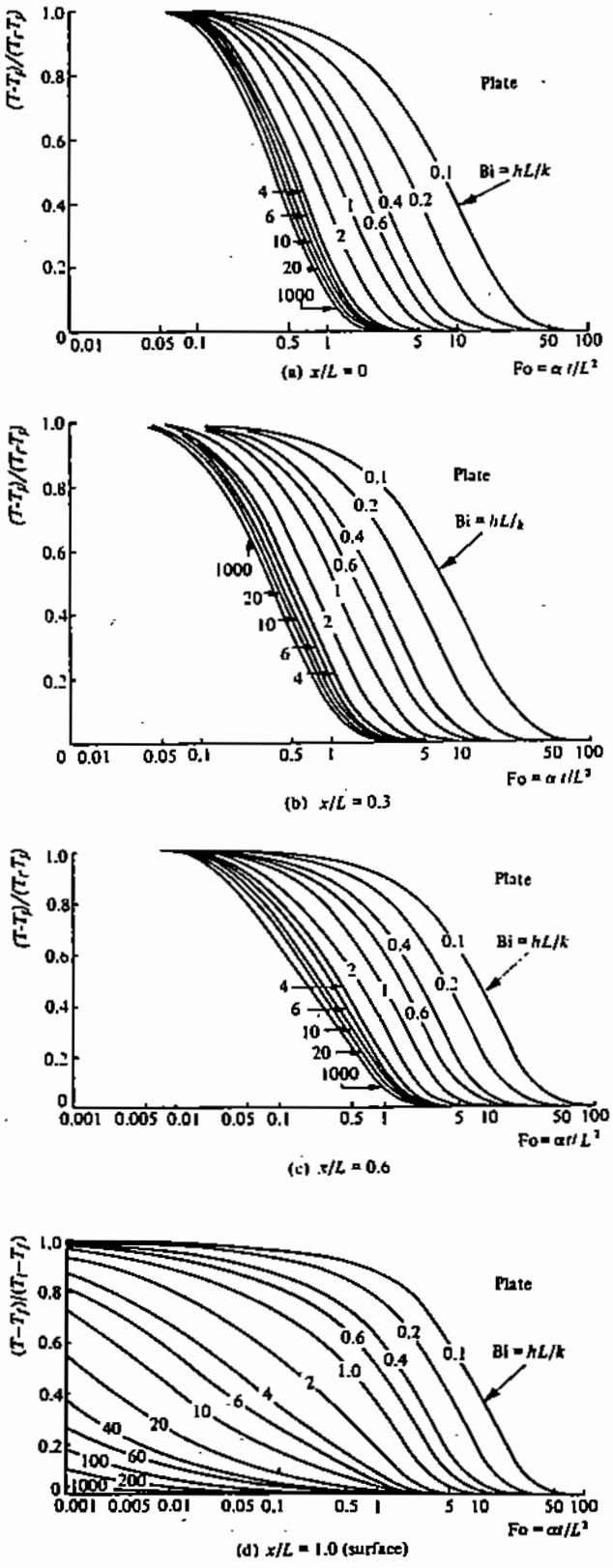

Figure 11.7. Temperature profiles in a large plate of thickness $2L$ initially at T_i, subjected to convective heat transfer from both sides at temperature T_f [7].

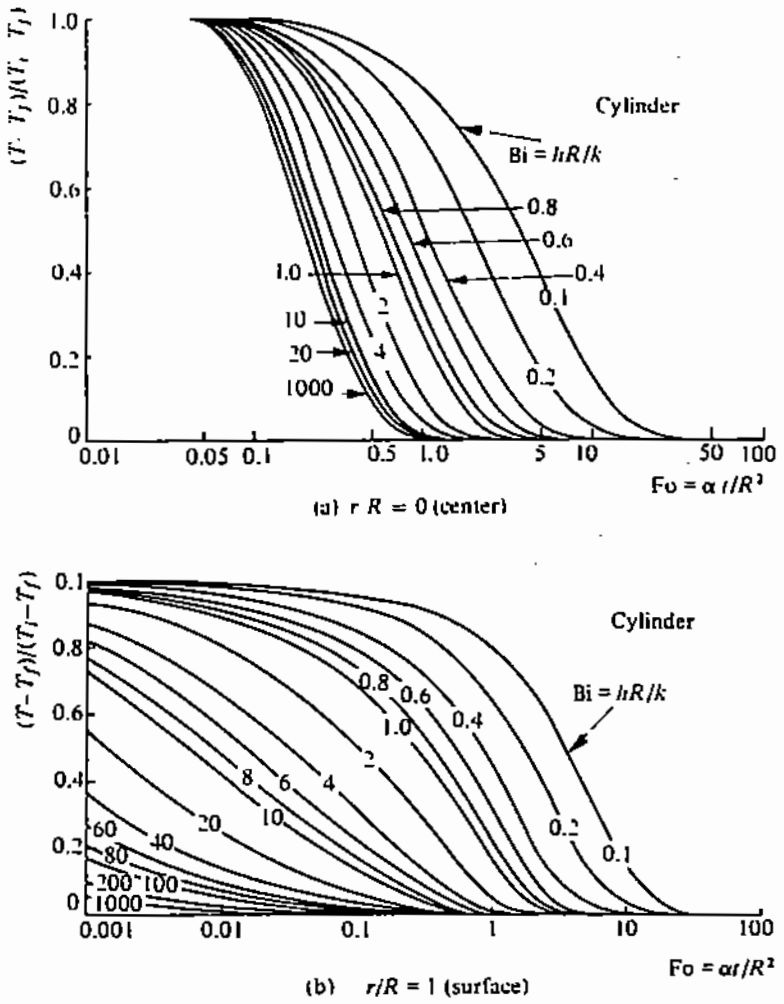

Figure 11.8. Temperature profiles in a long cylinder of diameter $2R$ initially at T_i, subjected to convective heat transfer at temperature T_f [7].

Calculate: a) the time that it takes for the center of the sphere to reach 150°C; b) the time that it will take to cool the center to 150°C, if the sphere is quenched in oil (h=500 W m^{-2} K^{-1}) instead of air; c) the surface temperature of the sphere at time b.

First, we calculate the thermal diffusivity of the metal:

$$\alpha = \frac{k}{\rho C_p} = \frac{15.6}{7600 \times 460} = 4.46 \times 10^{-6}\,\mathrm{m^2\,s^{-1}}.$$

a. The Biot number is

$$h\,R/k = 40 \times 0.04/15.6 = 0.103,$$

and the given temperature of 150°C is expressed in dimensionless form:

$$\theta = \frac{150 - 25}{450 - 25} = 0.29.$$

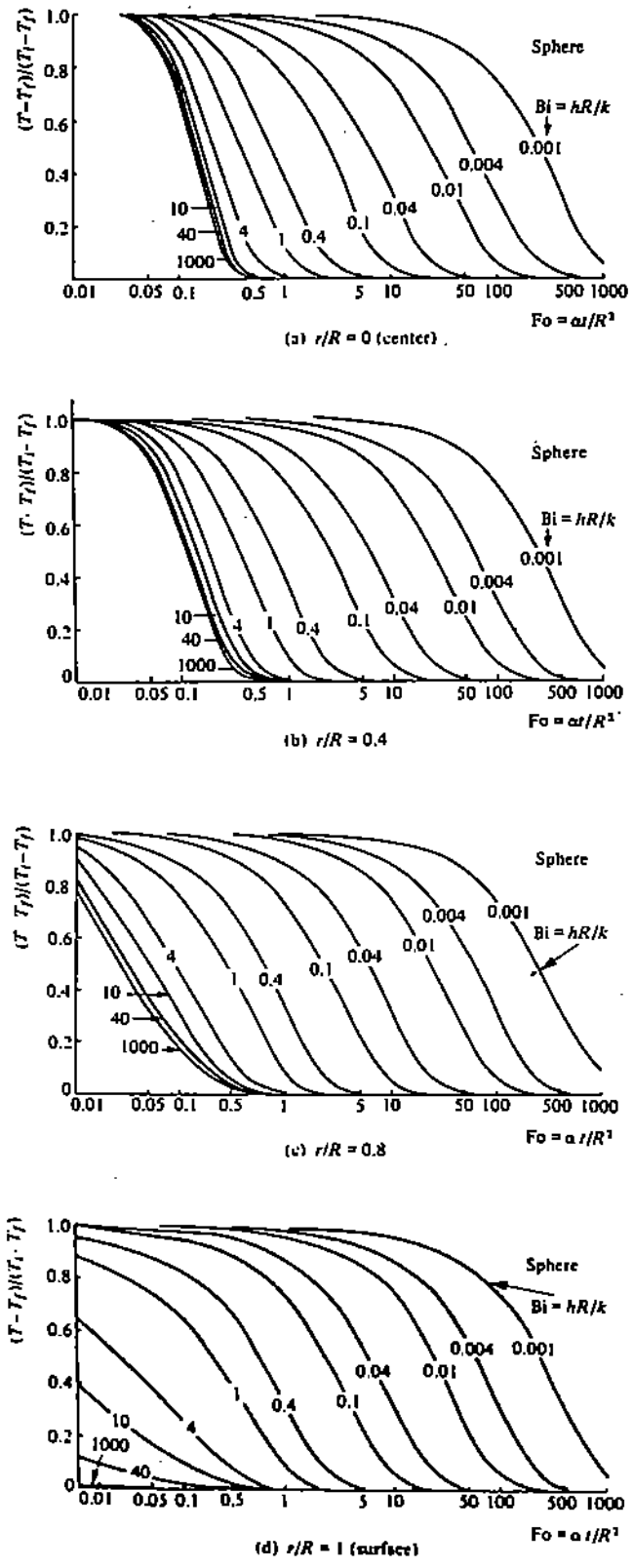

Figure 11.9. Temperature profiles in a sphere of diameter $2R$ initially at T_i, subjected to convective heat transfer at temperature T_f [7].

By referring to the plot for the temperature profiles in the center of a sphere (Fig. 11.9a), we find that at the dimensionless temperature of 0.29 and the Biot number of 0.103, the corresponding Fourier number is approximately 4.5. Therefore, the required time for the center of the sphere to be cooled to 150°C is

$$t = \frac{\mathrm{Fo}\, R^2}{\alpha} = \frac{4.5 \times 0.04^2}{4.45 \times 10^{-6}} = 1618 \text{ seconds.}$$

b. If the sphere is quenched in oil, the heat transfer coefficient for convection is 500 W m^{-1} K^{-1}. Therefore, the Biot number is now 1.28. Referring again to Fig. 11.9a, we find that the Fourier number has now decreased to 0.7 and, therefore, the calculated time for the center of the sphere to reach 150°C is about 250 seconds.

c. To determine the corresponding temperature at the surface of the sphere, 250 seconds after initiating quenching, we use Fig. 11.9d to find that for Bi = 1.28 and Fo = 0.7 the dimensionless temperature at the surface is approximately 0.18. Therefore,

$$\theta = 0.18 = \frac{T - 25}{450 - 25},$$

from which we calculate T to be 102°C.

11.3. NUMERICAL TECHNIQUES AND THE USE OF COMPUTERS

The rapid development and easy availability of computers has, amongst many other things, simplified greatly the solution of differential equations. While, in the past, it was necessary either to develop analytical solutions of such equations or go through very laborious "manual" calculations, computers and commercial software programs have facilitated enormously the use of numerical techniques for solving differential equations.

There are many excellent textbooks on the use of numerical techniques. Here we will present some introductory concepts using as an example the differential equation describing the conduction of heat under non-steady conditions.

Let us consider the case of a metal plate of thickness L which is at the initial uniform temperature of T_i. At time $t = 0$, one side of the plate is suddenly heated, e.g., by contact with an electrically heated surface, to a higher temperature T_s. With time, heat will be conducted through the plate, towards the other side of it. We need to determine how the temperature profiles through the plate will change with time.

In this case, there is no heat generation within the plate and the differential equation for heat conduction through the plate is expressed as follows:

$$\frac{\partial T}{\partial t} = \alpha \frac{\partial^2 T}{\partial y^2} \text{ for } 0 \le y \le L. \tag{11.3.1}$$

The boundary conditions for this equation are:

$$T = T_i \text{ at } 0 \le y \le L \text{ and } t = 0, \tag{11.3.2a}$$

$$T = T_s \text{ at } y = 0 \text{ and } t > 0, \tag{11.3.2b}$$

$$T = T_i \text{ at } y \to \infty. \tag{11.3.2c}$$

A worthwhile first step in all numerical calculations is to express the equations in dimensionless form. In order to do so, let us define the following dimensionless parameters. Dimensionless temperature:

$$\theta = \frac{T - T_i}{T_s - T_i}.$$

Dimensionless length:

$$\beta = \frac{y}{L}.$$

Dimensionless time:

$$\tau = \frac{\alpha t}{L^2}.$$

It can be seen that the temperature was made dimensionless by using as a reference point the initial uniform temperature of the plate, T_i, and dividing by the maximum temperature difference in the system. By using the above dimensionless parameters, the differential equation (11.3.1) and its boundary conditions are written as follows:

$$\frac{\partial \theta}{\partial \tau} = \frac{\partial^2 \theta}{\partial \beta^2} \tag{11.3.3}$$

for $\theta = 0$ at $\tau = 0$ and $0 \leq \beta \leq 1$; $\theta = 1$ at $\beta = 0$ and $\tau > 0$; $\theta = 0$ at $\beta = \infty$ and all τ.

The advantage of the dimensionless representation is that the final solution is more general; also, the numerical range of the dimensionless variables is restricted to $0 \leq \theta \leq 1$ and $0 \leq \beta \leq 1$, so that any computational errors are more easily detected.

Let us now construct a two-dimensional grid (Fig. 11.10), the grid points of which are separated by distances $\Delta\beta$ and $\Delta\tau$ which represent, in dimensionless form, a finite space difference (e.g., 0.1 cm) and a finite time difference (to be discussed later) of our choice on the space and time axes, respectively.

It can be shown, by applying the calculus of finite differences, that the second differential term appearing in (11.3.3) can be expressed in terms of the temperatures at adjacent grid points and the finite space difference between these points, as follows:

$$\left(\frac{\partial^2 \theta}{\partial \beta^2}\right)_m = \frac{(\theta_{m+1} - \theta_m) - (\theta_m - \theta_{m-1})}{(\Delta\beta)^2} = \frac{\theta_{m+1} - 2\theta_m + \theta_{m-1}}{(\Delta\beta)^2}, \tag{11.3.4}$$

where the term

$$\left(\frac{\partial^2 \theta}{\partial \beta^2}\right)_m$$

represents the second derivative of temperature with respect to distance through the plate, at the grid point m, and θ_{m-1}, θ_m, and θ_{m+1} are the dimensionless temperatures at grid points $m - 1$, m, and $m + 1$, respectively (Fig. 11.10).

Similarly, the time derivative at point m is expressed as

$$\frac{\partial \theta}{\partial \tau} = \frac{\theta_m^* - \theta_m}{\Delta\tau}, \tag{11.3.5}$$

where θ_m^* is the temperature at point m after lapse of one time interval $\Delta\tau$.

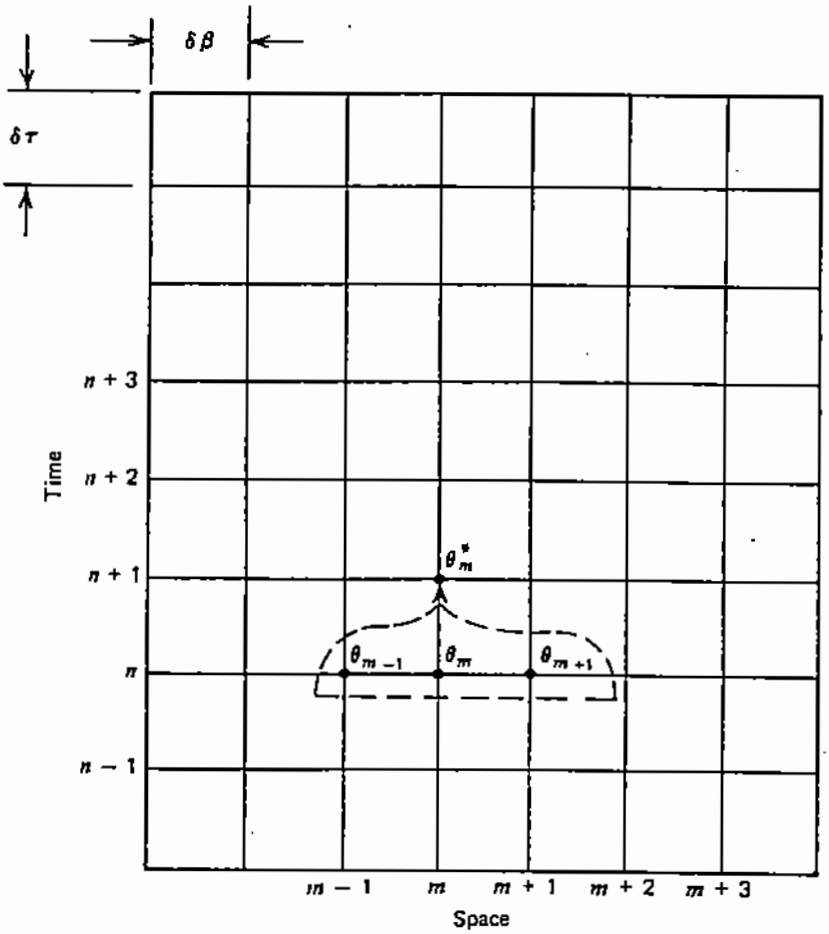

Figure 11.10. Example of two-dimensional time-space grid.

Substituting from (11.3.4) and (11.3.5) in (11.3.3), we obtain

$$\frac{\theta_m^* - \theta_m}{\Delta\tau} = \frac{\theta_{m+1} - 2\theta_m + \theta_{m-1}}{(\Delta\beta)^2}, \tag{11.3.6}$$

and therefore

$$\theta_m^* = \theta_m + \frac{\Delta\tau}{(\Delta\beta)^2}(\theta_{m+1} - 2\theta_m + \theta_{m-1}). \tag{11.3.7}$$

As illustrated in Fig. 11.10, (11.3.8) relates the value of the temperature at a given grid point, at time $\tau + \Delta\tau$, to the values of temperature at the same and adjacent grid points, at time τ. Therefore, if the initial temperature distribution over the whole space domain is known, the temperatures at successive time steps can be evaluated by the repeated application of (11.3.7).

It should be noted that the finite difference representation of differential equations is only approximate and that the accuracy of the results will depend on the number of the grid subdivisions used; in general, the finer the mesh size, the more accurate will be the results, but at the same time, the computing time will increase accordingly. The grid size need not be the same over the whole space domain: A finer grid can be used in the areas where the gradients of temperature, or other driving force, are expected to be greater as, for example, in boundary layers.

It can be shown [8] that in order to satisfy the criteria for convergence, the values of the finite differences for space and time must be selected so that the following ratio is less than 1/2:

$$\frac{\Delta\tau}{(\Delta\beta)^2} < \frac{1}{2} \tag{11.3.8}$$

Inspection of (11.3.7) shows that the actual relationship between θ_m^* and θ_m depends on the numerical value chosen for this ratio; thus, for

$$\frac{\Delta\tau}{(\Delta\beta)^2} = \frac{1}{4},$$

we have

$$\theta_m^* = \frac{1}{4}\left[\theta_{m+1} + 2\theta_m + \theta_{m-1}\right]. \tag{11.3.9}$$

From the definition of dimensionless time and distance, for this particular ratio of $\Delta\tau/(\Delta\beta)^2$ the *real time increment* is related to the *real distance increment* as follows:

$$\Delta t = \frac{\Delta\tau L^2}{\alpha} = \frac{(\Delta\beta)^2}{4}\frac{L^2}{\alpha} = \frac{(\Delta y)^2}{4L^2}\frac{L^2}{\alpha} = \frac{(\Delta y)^2}{4\alpha}. \tag{11.3.10}$$

The use of the above numerical technique is illustrated in the following example.

Example 11.3.1

Compute the change in temperature profile with time, after a "semi-infinite" plate ($\alpha = 0.0128$ cm^2 s^{-1}) of initial temperature T_i is subjected to heating from one side at the temperature T_s. This problem is represented by (11.3.1) and the boundary conditions by (11.3.2a)–(11.3.2c). To solve this equation numerically, we first must decide on the number of grid points that will represent the space and time domains. First, with regard to the space domain, let us consider a thickness of the plate of 0.4 cm. We will estimate the time period for which the temperature at $L = 0.4$ has not yet been affected by the heating of the outside surface of the plate (i.e., while the plate can be considered to be semi-infinite). For simplicity, let us select a length grid of 4 subdivisions, i.e., at every 0.1 cm.

The corresponding size of the allowable time interval in the time domain is then calculated by means of (11.3.10) to be 0.2 s. Let us assign five grid points to the space domain of Fig. 11.10. The first grid point represents the outside surface of the plane (i.e., $y = 0$ and $\beta = 0$), while the fifth represents the location $y = 0.4$ cm. By selecting (see (11.3.8))

$$\frac{\Delta\tau}{(\Delta\beta)^2} = \frac{1}{4},$$

our working equation becomes (11.3.9):

$$\theta_m^* = \frac{1}{4}\left[\theta_{m+1} + 2\theta_m + \theta_{m-1}\right]. \tag{11.3.9}$$

	A	B	C	D	E	F	G
1		Example 11.3.1.					
2				Grid points:			
3			0 cm	0.1 cm	0.2 cm	0.3 cm	0.4 cm
4		Time step	m-1	m	m+1	m+2	m+3
5							
6		1	1	0	0	0	0
7		2	1	0.250	0.000	0.000	0
8		3	1	0.375	0.063	0.000	0
9		4	1	0.453	0.125	0.016	0
10		5	1	0.508	0.180	0.039	0
11		6	1	0.549	0.227	0.064	0
12		7	1	0.581	0.267	0.089	0
13		8	1	0.607	0.301	0.111	0
14		9	1	0.629	0.330	0.131	0
15		10	1	0.647	0.355	0.148	0
		.....					
45		40	1	0.749	0.499	0.249	0

1/4*(C6+2*D6+E6)

Figure 11.11. Use of the Lotus 1-2-3 spreadsheet program to solve a second-order differential equation.

The boundary conditions of this problem specify that at the first grid point, $y = 0$ $(m-1)$ and at any time $t > 0$, the dimensionless temperature has the value of 1; similarly, for a certain period after $t = 0$, the dimensionless temperature at the last grid point, $y = 0.4$, remains constant with time and has the value of 0. At the end of the first time interval, the temperature at $m-1$ will be equal to 1 and zero at all other y points. We must now use (11.3.9) to evaluate the temperature distribution after the second time step and repeat the same calculation for successive time steps, until we have developed a series of temperature profiles as a function of t.

This problem can be expressed in BASICA or FORTRAN and solved by computer. It can also be solved by using a spreadsheet program like Lotus 1-2-3, as illustrated below.

Solution Using a Spreadsheet Program

Using Lotus 1-2-3 [11] or a similar spreadsheet program, we select the columns C to G on the screen (Fig. 11.11) to represent the five grid points of the width of the plate and the rows *6* to *15* to represent the first ten time steps in the calculation. The first column, C, represents the heated surface of the plate; therefore the boundary condition is that the dimensionless temperature is 1 at all values of time. Also, the last column G represents the location 0.4 cm from the surface of the plate which, for a certain period after the outer surface is being heated will remain at $\theta = 0$. We therefore enter these values of the boundary conditions in cells *C6–C16* and *G6–G16* (Fig. 11.11). Finally, in the cells *D6* to *F6*, which correspond to the grid points m, $m+1$, etc., after the first time-step, we place the initial temperature condition of 0; the temperature increase at these grid points cannot be calculated until after

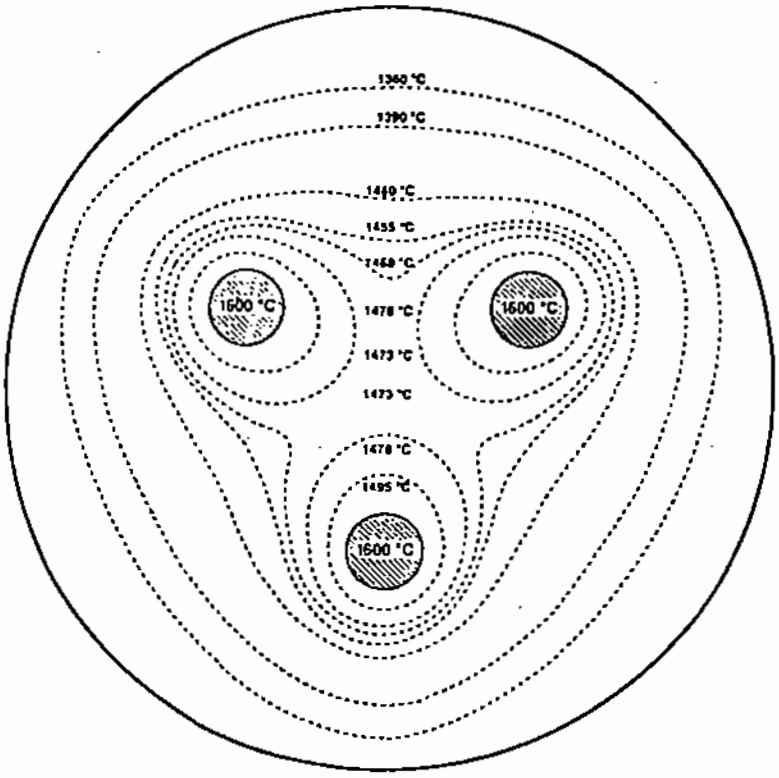

Figure 11.12. Temperature distribution in bath of slag resistance electric furnace, in the absence of natural convection [10].

the first time-step. Now in cell *D7*, i.e., the grid point m at and at time-step 2, we write the formula of (11.3.9), expressed in terms of the neighboring cells in the spreadsheet:

$$\theta_m^* = D7 = \frac{1}{4}\left(C6 + 2 \times D6 + E6\right).$$

We then copy this formula into all the remaining empty cells of our time-space grid (i.e., in cells *D7–F15*). As is shown on the computer screen of Fig. 11.11, the spreadsheet program then automatically calculates the change of temperature profile along the width of the plate for each time step.

It can be seen that this technique allows us to use a very large number of grid points and also to use as short a time interval as we like. Also, the boundary and initial conditions of the problem need not be constant but may be expressed, for example, as a function of heat convection to or from the environment. For example, in the case of a plate of finite length L, the boundary condition at the second surface, $y = L$, could be an equation expressing the heat loss to the atmosphere by convection and radiation as a function of the temperature entered in the cells of the column representing the surface L. In such a case, the boundary conditions of (11.3.1) may be expressed as follows:

$$T = T_i \text{ at } 0 \le y \le R \text{ and } t = 0,$$
$$T = T_s \text{ at } y = 0 \text{ and } t > 0,$$
$$q = 5 \times 10^{-5} T^{1.25} + 1.1 \times 10^{-12} T^4 \text{ at } y = L \text{ and all } t,$$

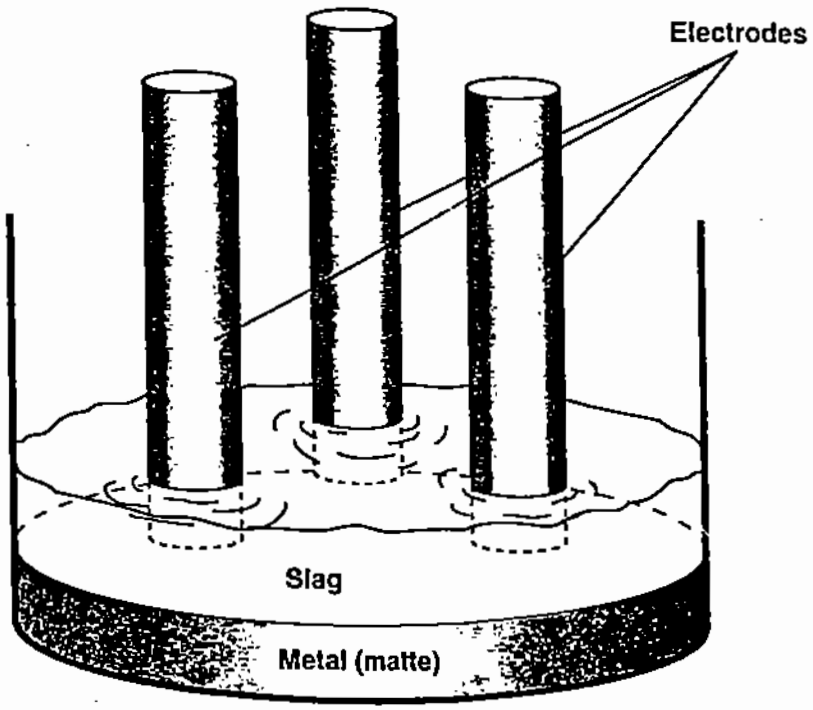

Figure 11.13. Schematic diagram of three-electrode slag resistance furnace [10].

where the last boundary condition expresses the heat losses by convection and radiation, as will be discussed in Chapter 12 and Chapter 13, respectively.

Of course, the above example represents a very simple case of conduction. However, the same principles can be applied to very complex geometries, such as Fig. 11.12 [10] which shows the temperature distribution around the three electrodes in the *slag resistance electric furnace* of Fig. 11.13 (at assumed negligible natural convection). In this case, most of the heat is generated at the three graphite electrodes and is conducted through the slag towards the walls of the furnace.

For additional reading on the mathematical modeling of heat transfer and other problems in materials processing, the [redacted] is referred to Szekely et al. [12].

zeaJez

REFERENCES

1. H.S. Carslaw and J.C. Jaeger, *Conduction of Heat in Solids*, Clarendon Press, Oxford (1959).
2. W.P. Rohsenow, J.P. Garnett, and E.N. Ganic, eds. *Handbook of Heat Transfer Fundamentals*, McGraw-Hill, New York (1985).
3. N.P. Cheremisinoff, ed., *Handbook of Heat and Mass Transfer*, Vol. 1: *Heat Transfer Operations*, Gulf Publishing, Houston (1986).
4. F. Kreith and W.Z. Black, *Basic Heat Transfer*, Harper and Row, New York (1980).
5. Gurney and Lurie, *Ind. Eng. Chem.*, **15**, 1170 (1923).
6. R.H. Perry and D. Green, eds., *Chemical Engineers' Handbook*, 6th ed., McGraw-Hill, New York (1984).
7. G.H. Geiger and D.R. Poirier, *Transport Phenomena in Metallurgy*, Addison-Wesley, Reading, MA (1973).
8. J. Szekely and N.J. Themelis, *Rate Phenomena in Process Metallurgy*, Wiley, New York (1971).

9. B. Gebhart, *Heat Conduction and Mass Diffusion*, McGraw-Hill, New York (1993).
10. Q. Jiao, PhD Thesis, Columbia University, New York (1990).
11. Lotus 1-2-3, Computer Program, Lotus Development Corporation, Cambridge, MA (1983).
12. J. Szekely, J.W. Evans, and J.K. Brimacombe, *Mathematical and Physical Modeling of Primary Metals Processing Operations*, Wiley-Interscience, New York (1988).

TWELVE

Heat Transfer by Convection

In Chapter 11, we developed and solved the differential thermal energy equation by assuming that the only means for heat transport was by **conduction**. However, in the case of heat transfer in fluids, or in fluidized solids, heat is also transported by fluid elements as they move from a higher to a lower temperature zone. For example, the movement of air currents within a room conveys heat from a radiator to other parts of the room. The transport of heat associated with the motion of fluid is called **convection**.

12.1. THE DIFFERENTIAL THERMAL ENERGY BALANCE IN FLUIDS

In Chapter 5, we derived the continuity equation which expresses the conservation of matter:

$$\frac{\partial \rho}{\partial t} = -\nabla \cdot \rho \boldsymbol{u}, \tag{5.1.7}$$

and the equation of motion which expresses the conservation of momentum in a fluid system:

$$\rho \frac{D\boldsymbol{u}}{Dt} = -\nabla \cdot \boldsymbol{\tau} - \nabla P + \rho \boldsymbol{g}. \tag{5.2.18}$$

In non-isothermal fluid systems, we need to consider a third general equation which expresses the conservation of thermal energy in the system:

$$\frac{D(\rho C_p T)}{Dt} - \beta T \frac{DP}{Dt} = \nabla(k \nabla T) + \boldsymbol{\tau} : \nabla \boldsymbol{u} + \dot{q}, \tag{12.1.1}$$

where $D(\rho C_p T)/Dt$ is the substantial derivative (Chapter 5) of $\rho C_p T$, i.e., the heat content per unit volume of the fluid and is defined as follows:

$$\frac{D(\rho C_p T)}{Dt} = \frac{\partial(\rho C_p T)}{\partial t} + u_x \frac{\partial(\rho C_p T)}{\partial x} + u_y \frac{\partial(\rho C_p T)}{\partial y} + u_z \frac{\partial(\rho C_p T)}{\partial z}. \tag{12.1.2}$$

The symbol β in (12.1.1) represents the volume coefficient of thermal expansion (i.e., fractional expansion per degree of temperature); DP/Dt is the substantial derivative of pressure; the term $\boldsymbol{\tau} : \nabla \boldsymbol{u}$ represents the heat generated due to the shear stresses in the fluid and $\dot{q}$ is the rate of heat generation per unit volume of the fluid, e.g., due to electric heating or chemical reaction.

In most heat convection systems, the heat generation associated with friction effects ($\boldsymbol{\tau} : \nabla \boldsymbol{u}$) is very small and can be assumed to be negligible; exceptions are very high velocity flows at low temperatures and certain problems in lubrication. For assumed incompressible

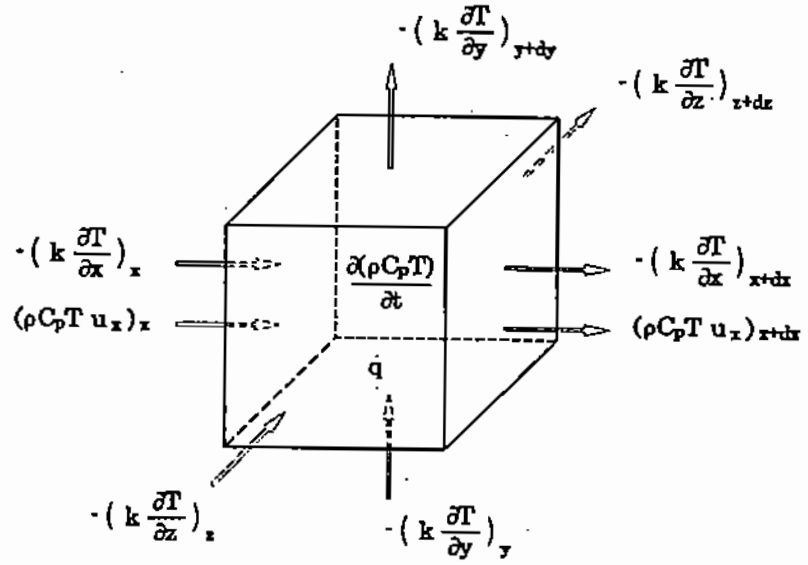

Figure 12.1. Heat energy balance in a cubical element (conveyed heat is shown only in the x-direction).

flow, which is the case for liquids and many gas flow systems, the heat generation associated with expansion and contraction effects is also negligible. Therefore, the pressure derivative and the shear stress terms can be neglected [5] and the thermal energy balance of (12.1.1) is expressed as follows:

$$\frac{D(\rho C_p T)}{Dt} = \nabla(k\nabla T) + \dot{q}. \tag{12.1.3}$$

Equation (12.1.3) can be derived by considering the thermal energy terms in and out of an infinitesimal cubical element of volume $dx \cdot dy \cdot dz$ in a fluid stream (Fig. 12.1). Heat is transferred in and out of the element either by conduction or as heat conveyed by the elements of the fluid; also, there may be heat generation or absorption within the control volume due to a chemical or physical transformation, or due to resistance or induction heating. The thermal energy balance is:

$$\begin{aligned} &\text{rate of heat accumulation in element} \\ &\quad = \text{net heat input rate by conduction} \\ &\quad + \text{net heat input rate by convection} \\ &\quad + \text{rate of heat generation in element.} \end{aligned} \tag{12.1.4}$$

In Chapter 11, we showed that the rate of heat accumulation in a cubical element of volume $dx \cdot dy \cdot dz$ by conduction is:

$$\left(\frac{\partial(\rho C_p T)}{\partial t}\,dx\,dy\,dz\right)_{\text{cond}} = \left[\frac{\partial}{\partial x}\left(k_x\frac{\partial T}{\partial x}\right) + \frac{\partial}{\partial y}\left(k_y\frac{\partial T}{\partial y}\right) + \frac{\partial}{\partial z}\left(k_z\frac{\partial T}{\partial z}\right)\right] dx\,dy\,dz. \tag{12.1.5}$$

If we now consider fluid moving in the x-direction entering and leaving the element $dx \cdot dy \cdot dz$ through the sides $dy \cdot dz$, it is evident that the *heat flux* carried by the fluid is equal to its heat

content per unit volume, $\rho C_p T$, times the fluid velocity, u_x, as shown by the dimensional analysis of this product:

$$\mathrm{ML^{-3}} \times \mathrm{QM^{-1}}T^{-1} \times \mathrm{T} \times \mathrm{Lt^{-1}} = \mathrm{Qt^{-1}L^{-2}}.$$

Therefore, the net heat input rate to the element by convection in the x-direction is

$$[(\rho C_p T u_x)_x - (\rho C_p T u_x)_{x+dx}]\, dy\, dz = -\frac{\partial(\rho C_p T u_x)}{\partial x}\, dx\, dy\, dz, \tag{12.1.6}$$

and the corresponding rate of heat accumulation in the element because of convection in the x-direction is:

$$\left(\frac{\partial(\rho C_p T)}{\partial t}\, dx\, dy\, dz\right)_{\text{conv}} = -\frac{\partial(\rho C_p T u_x)}{\partial x}\, dx\, dy\, dz. \tag{12.1.7}$$

There are two more terms of convective heat in the y- and z-directions of flow.

Finally, the rate of heat accumulation in the element due to heat generation is expressed by the rate of generation per unit volume times the volume of the element:

$$\left(\frac{\partial(\rho C_p T)}{\partial t}\, dx\, dy\, dz\right)_{\dot{q}} = \dot{q}\, dx\, dy\, dz. \tag{12.1.8}$$

We can now add all the terms that contribute to the overall rate of heat accumulation in the element: the net rate of conduction heat (see (12.1.5)), the net rate of convection heat (see (12.1.7) plus two equivalent expressions for flow in the y- and z-directions) and the rate of heat generation (see (12.1.8)). After eliminating redundant terms, we obtain the following equation:

$$\begin{aligned}\frac{\partial(\rho C_p T)}{\partial t} =& \frac{\partial}{\partial x}\left(k_x \frac{\partial T}{\partial x}\right) + \frac{\partial}{\partial y}\left(k_y \frac{\partial T}{\partial y}\right) + \frac{\partial}{\partial z}\left(k_z \frac{\partial T}{\partial z}\right) \\ & - \left(\frac{\partial(\rho C_p T u_x)}{\partial x} + \frac{\partial(\rho C_p T u_y)}{\partial y} + \frac{\partial(\rho C_p T u_z)}{\partial z}\right) + \dot{q},\end{aligned} \tag{12.1.9}$$

and by moving the negative term of this equation to the left side:

$$\begin{aligned}&\frac{\partial(\rho C_p T)}{\partial t} + \frac{\partial(\rho C_p T u_x)}{\partial x} + \frac{\partial(\rho C_p T u_y)}{\partial y} + \frac{\partial(\rho C_p T u_z)}{\partial z} \\ &= \frac{\partial}{\partial x}\left(k_x \frac{\partial T}{\partial x}\right) + \frac{\partial}{\partial y}\left(k_y \frac{\partial T}{\partial y}\right) + \frac{\partial}{\partial z}\left(k_z \frac{\partial T}{\partial z}\right) + \dot{q}.\end{aligned} \tag{12.1.10}$$

If we assume that C_p does not change appreciably with temperature, (12.1.10) can be simplified by first differentiating each of the velocity-temperature terms into two terms; e.g., the x-term is differentiated as follows:

$$\frac{\partial(\rho C_p T u_x)}{\partial x} = C_p T \frac{\partial(\rho u_x)}{\partial x} + u_x \frac{\partial(\rho C_p T)}{\partial x}. \tag{12.1.11}$$

We also note that for incompressible flow the sum of the three partial differentials of velocity represent the equation of continuity (see (5.1.12)) and must be equal to zero:

$$C_pT\left(\frac{\partial(\rho u_x)}{\partial x}+\frac{\partial(\rho u_y)}{\partial y}+\frac{\partial(\rho u_z)}{\partial z}\right)\equiv 0. \tag{12.1.12}$$

By substituting from (12.1.11) and (12.1.12) in (12.1.10) for incompressible flow, we obtain

$$\begin{aligned}&\frac{\partial(\rho C_pT)}{\partial t}+u_x\frac{\partial(\rho C_pT)}{\partial x}+u_y\frac{\partial(\rho C_pT)}{\partial y}+u_z\frac{\partial(\rho C_pT)}{\partial z}\\&\quad=\frac{\partial}{\partial x}\left(k_x\frac{\partial T}{\partial x}\right)+\frac{\partial}{\partial y}\left(k_y\frac{\partial T}{\partial y}\right)+\frac{\partial}{\partial z}\left(k_z\frac{\partial T}{\partial z}\right)+\dot{q}.\end{aligned} \tag{12.1.13}$$

It can be seen that, in vectorial form, the derived equation is identical to (12.1.3).

When the change in thermal conductivity and specific heat with location is negligible, (12.1.13) simplifies further to

$$\frac{\partial T}{\partial t}+u_x\frac{\partial T}{\partial x}+u_y\frac{\partial T}{\partial y}+u_z\frac{\partial T}{\partial z}=\alpha\left(\frac{\partial^2T}{\partial x^2}+\frac{\partial^2T}{\partial y^2}+\frac{\partial^2T}{\partial z^2}\right)+\frac{\dot{q}}{\rho C_p}, \tag{12.1.14}$$

and in vector notation:

$$\frac{DT}{Dt}=\alpha\nabla^2T+\frac{\dot{q}}{\rho C_p}. \tag{12.1.15}$$

As discussed in Chapter 11 on heat conduction, in flow systems of cylindrical and spherical geometry, it is convenient to use the corresponding systems of coordinates. The cylindrical coordinates are the radial distance from the axis of the cylinder, the angle θ around a section of the cylinder, and the axial distance z along the length of the cylinder. The relationships between these coordinates and the linear coordinates x, y, and z are as follows (Fig. 11.2):

$$x=r\cos\theta,\quad y=r\sin\theta,\quad z=z. \tag{11.1.9}$$

By substituting the cylindrical coordinates in (12.1.15), we obtain

$$\frac{\partial T}{\partial t}+u_r\frac{\partial T}{\partial r}+\frac{u_\theta}{r}\frac{\partial T}{\partial\theta}+u_z\frac{\partial T}{\partial z}=\alpha\left(\frac{1}{r}\frac{\partial}{\partial r}\left(r\frac{\partial T}{\partial r}\right)+\frac{1}{r^2}\frac{\partial^2T}{\partial\theta^2}+\frac{\partial^2T}{\partial z^2}\right)+\frac{\dot{q}}{\rho C_p}. \tag{12.1.16}$$

Similarly, the spherical system coordinates are related to x, y, z as follows (Fig. 11.3):

$$x=r\sin\theta\cos\phi,\quad y=r\sin\theta\sin\phi,\quad z=r\cos\theta, \tag{11.1.13}$$

and by substituting in (12.1.14), we obtain the thermal energy balance for a spherical system:

$$\begin{aligned}&\frac{\partial T}{\partial t}+u_r\frac{\partial T}{\partial r}+\frac{u_\theta}{r}\frac{\partial T}{\partial\theta}+\frac{u_\phi}{r\sin\theta}\frac{\partial T}{\partial\phi}\\&=\alpha\left[\frac{1}{r^2}\frac{\partial}{\partial r}\left(r^2\frac{\partial T}{\partial r}\right)+\frac{1}{r^2\sin\theta}\frac{\partial}{\partial\theta}\left(\sin\theta\frac{\partial T}{\partial\theta}\right)+\frac{1}{r^2\sin^2\theta}\frac{\partial^2T}{\partial\phi^2}\right]+\frac{\dot{q}}{\rho C_p}.\end{aligned} \tag{12.1.17}$$

12.1.1. The Boussinesq Approximation

Equation (12.1.3), which was derived in the previous section for incompressible flow systems, can be extended to slightly compressible flows by using the *Boussinesq approximation* [5] of expressing the change of density by means of the following linear equation:

$$\rho = \rho_0 \left[1 - \beta(T - T_0)\right], \tag{12.1.18}$$

where ρ_0 is the density of the fluid at some reference temperature T_0, and β is its coefficient of thermal expansion. In the Boussinesq approximation, the temperature-dependent density, ρ, is used only in the gravity term of the equation of motion and (5.2.18) and (12.1.1) are expressed as follows:

$$\rho_0 \frac{Du}{Dt} = -\nabla \cdot \boldsymbol{\tau} - \nabla P + \rho_0 \beta (T - T_0) \boldsymbol{g}, \tag{12.1.19}$$

and

$$\rho_0 C_p \frac{DT}{Dt} = \nabla \cdot (k \nabla T) + \dot{q}. \tag{12.1.20}$$

When the changes in viscosity and thermal conductivity with location are negligible, the above equations can be simplified as follows:

$$\rho_0 \frac{Du}{Dt} = \mu \nabla^2 \boldsymbol{u} - \nabla P + \rho_0 \beta (T - T_0) \boldsymbol{g}, \tag{12.1.21}$$

and

$$\rho_0 C_p \frac{DT}{Dt} = k \nabla^2 T + \dot{q}, \tag{12.1.22}$$

where P represents the perturbation of the static pressure from the hydrostatic value. The Boussinesq approximation is frequently used for the solution of the differential equations for convection by means of numerical methods. Such methods have been greatly facilitated by the advent of computers. In fact, a number of commercial computer programs, such as the FIDAP program of Fluid Dynamics International [23] are now available where the user can insert specific parameters and boundary conditions and obtain the solutions of fluid flow and heat transfer problems.

12.2. FORCED AND NATURAL CONVECTION OF HEAT

Heat transfer by convection can be divided broadly into two categories: forced convection and natural convection. In **forced convection**, the motion of the fluid is due to externally imposed forces; for example, in the case of heat transfer to a fluid flowing through a heat exchanger tube, the fluid motion is due to a pressure differential imposed by a pump.

In problems of this type, the mechanical and the thermal energy balances can be considered separately: We may start by solving the appropriate equations of continuity and motion to determine the velocity distribution in the system; these results are then incorporated into the thermal energy balance equation to calculate the temperature distribution in the system and the heat flux at any location. Exceptions to this are problems where the density and viscosity are temperature-dependent; in such cases, the velocity distribution in the system cannot be specified without knowledge of the temperature field and the momentum and energy balance equations must be solved simultaneously.

In **natural convection**, the motion of the fluid is due to density variations which in turn are caused either by temperature or concentration gradients in the system; an example of combined thermal and concentration gradients is the natural convection of electrolytic solution in a copper refining cell. Therefore, in natural convection, the equations of motion and thermal energy are coupled and must be solved simultaneously.

12.2.1. Forced Convection in Laminar Flow Between Plates

Let us consider the laminar flow of a liquid in the x-direction between two parallel plates separated by a distance L (Fig. 12.2). The top plate is maintained at a temperature T_2 and the bottom plate at the lower temperature T_1. Let us derive the equations for the fully developed velocity and temperature profiles between the plates, on the assumption that the density and viscosity of the fluid are not temperature-dependent and that the temperature gradient in the direction of flow is negligible (i.e., the term $u_x dT/dx$ is negligible).

From the equation of motion (5-2-18), for steady-state we have (Chapter 4)

$$\frac{\Delta P}{\Delta x} = \mu \frac{d^2 u_x}{dy^2}. \tag{12.2.1}$$

Also, the equation of thermal energy balance (12.1.15) for unidirectional flow reduces to

$$\frac{\partial^2 T}{\partial y^2} = 0. \tag{12.2.2}$$

This is a case of forced convection where the equations of motion and thermal energy can be solved separately. The boundary conditions are:

$$u_x = 0 \text{ at } y = 0 \text{ and } u_x = 0 \text{ at } y = L.$$

Solution of (12.2.1) yields

$$u_x = \frac{(\Delta P/\Delta x)}{2\mu} \left(yL - y^2\right). \tag{12.2.3}$$

Also, for the boundary conditions

$$T = T_1 \text{ at } y = 0 \text{ and } T = T_2 \text{ at } y = L,$$

the solution of (12.2.2) is

$$T = T_1 + (T_2 - T_1)\frac{y}{L}. \tag{12.2.4}$$

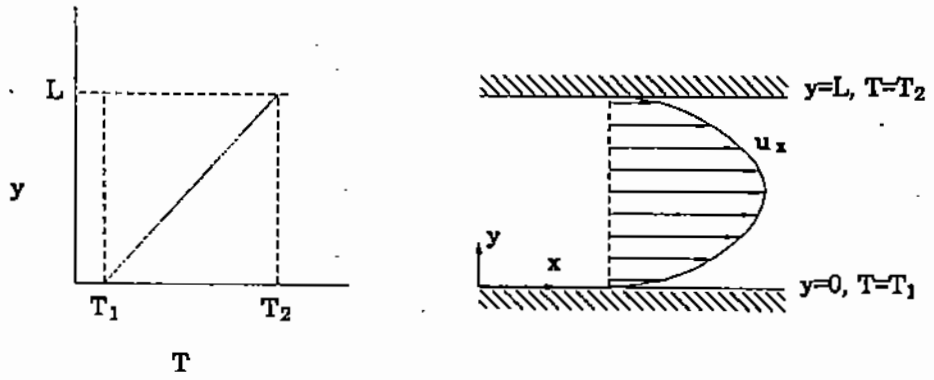

Figure 12.2. Velocity and temperature profiles in flow between parallel plates at steady state conditions.

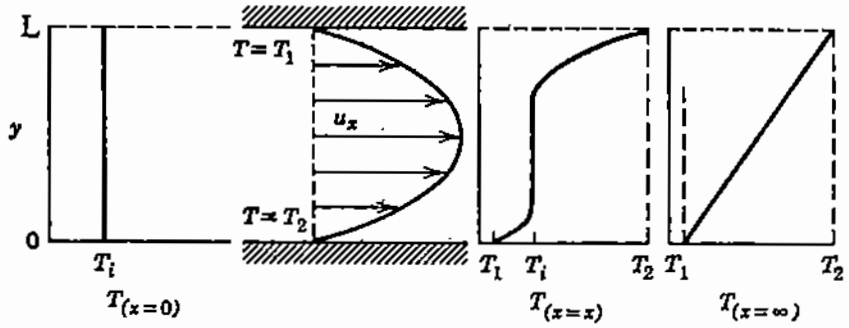

Figure 12.3. Velocity and temperature profiles in flow between parallel plates with fluid initially at T_i.

In deriving (12.2.4), it was assumed that the velocity and temperature profiles were completely independent of each other. Let us now consider the more plausible situation where only the velocity profile is fully developed and the fluid at the inlet to the tube is at a uniform temperature, T_i, which is somewhere between the temperatures of the two plates. As illustrated in Fig. 12.3, the problem is now two-dimensional, since the temperature is a function of both x and y. In this case, at $x = 0$ the temperature of the fluid is uniform at T_i, while at large values of x the temperature profile is represented by (12.2.4). Let us examine what will be the temperature profiles in the y- and x-directions at intermediate values of x.

The velocity profiles in this system are still expressed by (12.2.3). However, the corresponding thermal energy balance, from (12.1.15), is now as follows:

$$u_x \frac{\partial T}{\partial x} = \alpha \left(\frac{\partial^2 T}{\partial x^2} + \frac{\partial^2 T}{\partial y^2} \right). \tag{12.2.5}$$

The corresponding boundary conditions are:

$$T = T_i \text{ at } x = 0; \quad T = T_1 \text{ at } y = 0 \text{ and } x > 0; \quad T = T_2 \text{ at } y = L \text{ and } x > 0.$$

The corresponding temperature profiles now change with distance x, as illustrated in Fig. 12.3.

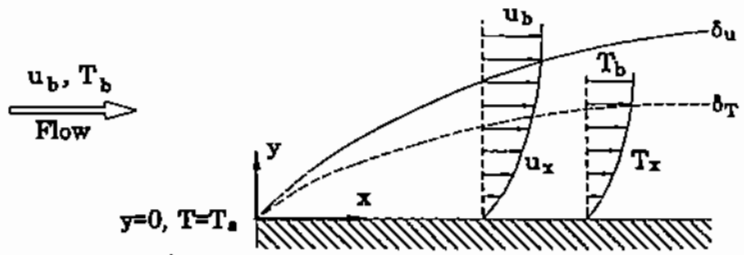

Figure 12.4. Velocity and thermal boundary layers in flow along a flat plate.

12.3. THERMAL BOUNDARY LAYER IN FORCED CONVECTION

Let us now consider a flat plate at the temperature T_s, over which is flowing an incompressible fluid in the x-direction (Fig. 12.4); the velocity of the free stream is u_b ("bulk" velocity) and the fluid is at a higher temperature, T_b. The reader will recall from Chapter 6 that when a free stream flows over a stationary plate, the velocity of the fluid within a *boundary layer* next to the plate is affected because of the viscous force. In the isothermal, laminar flow system which we discussed in Chapter 6, the velocity distribution in the boundary layer was derived from the analytical solution of the equations of motion and was expressed as follows in terms of the free stream velocity, u_b, and the properties of the fluid:

$$\frac{u_x}{u_b} = f(\eta) = \frac{3}{2}\eta - \frac{1}{2}\eta^3, \tag{12.3.1}$$

where

$$\eta = \frac{y}{\delta_x} = \frac{y}{4.64\sqrt{\nu x/u_b}},$$

and δ_x is the thickness of the boundary layer at distance x from the leading edge of the plate; y is the perpendicular distance from the surface of the plate, u_b the bulk fluid velocity and ν the kinematic viscosity (μ/ρ) of the fluid.

In a similar way, we can visualize that in a non-isothermal system, for example the flow of a hot fluid over a cooled surface, the temperature of the layers of the free stream close to the surface will be somewhere between the temperature of the free stream and that of the cooled surface. In Chapter 6, we called the region in which the velocity of the fluid differs from that in the free stream the *velocity boundary layer*. Similarly, the region of the fluid where its temperature is affected by contact with the surface of the solid is called the *thermal boundary layer*.

Let us now write the equations of motion and thermal energy balance for these boundary layers. As discussed in Chapter 6, for incompressible flow in a two- dimensional system, the equations of continuity and motion are

$$\frac{\partial u_x}{\partial x} + \frac{\partial u_y}{\partial y} = 0, \tag{12.3.2}$$

and

$$u_x \frac{\partial u_x}{\partial x} + u_y \frac{\partial u_x}{\partial y} = \frac{\mu}{\rho} \frac{\partial^2 u_x}{\partial y^2}. \tag{12.3.3}$$

The boundary conditions for the above equations are:

$$\begin{aligned} &u_x = 0,\ u_y = 0 \text{ at } y = 0 \text{ (plate surface)} \\ &u_x = u_b,\ u_y = 0 \text{ at } y \to \infty \text{ (away from plate surface)} \\ &u_x = u_b \text{ at } x = 0 \text{ for all } y. \end{aligned} \tag{12.3.4}$$

Also, in this case the thermal energy equation (see (12.1.15)) can be written in the following form:

$$u_x \frac{\partial T}{\partial x} + u_y \frac{\partial T}{\partial y} = \alpha \left(\frac{\partial^2 T}{\partial x^2} + \frac{\partial^2 T}{\partial y^2} \right). \tag{12.3.5}$$

This equation can be simplified further by considering that, in general, the temperature gradient in the direction of flow x is much smaller than the corresponding term in the y-direction; i.e., the transfer of heat in the direction of flow takes place mainly by *convection* rather than by *conduction*. Accordingly, (12.3.5) simplifies to

$$u_x \frac{\partial T}{\partial x} + u_y \frac{\partial T}{\partial y} = \alpha \frac{\partial^2 T}{\partial y^2}. \tag{12.3.6}$$

The boundary conditions for this equation are:

$$\begin{aligned} &T = T_s \text{ at } y = 0, \quad T = T_b \text{ at } y \to \infty, \\ &T = T_b \text{ at } x = 0 \ \forall y. \end{aligned} \tag{12.3.7}$$

Let us now introduce the following dimensionless variable to express temperature:

$$\theta = \frac{T - T_s}{T_b - T_s}; \quad \beta_x = \frac{u_x}{u_b}; \quad \beta_y = \frac{u_y}{u_b},$$

where T_b and T_s are the temperatures of the bulk flow and of the surface, respectively; as stated earlier, in this case $T_b > T_s$.

Restating (12.3.3) in terms of the above dimensionless velocities, we obtain

$$\beta_x \frac{\partial \beta_x}{\partial x} + \beta_y \frac{\partial \beta_x}{\partial y} = \frac{\mu}{\rho u_b} \frac{\partial^2 \beta_x}{\partial y^2}. \tag{12.3.8}$$

The boundary conditions of the above equation are

$$\begin{aligned} &\beta_x = 0,\ \beta_y = 0 \text{ at } y = 0, \quad \beta_x = 1,\ \beta_y = 0 \text{ at } y = \infty \\ &\beta_x = 1 \text{ at } x = 0 \text{ and all } y. \end{aligned} \tag{12.3.9}$$

Similarly, the dimensionless form of (12.3.6) is

$$\beta_x \frac{\partial \theta}{\partial x} + \beta_y \frac{\partial \theta}{\partial y} = \frac{\alpha}{u_b} \frac{\partial^2 \theta}{\partial y^2}, \tag{12.3.10}$$

and the dimensionless boundary conditions are

$$\theta = 0 \text{ at } y = 0 \ \forall x; \quad \theta = 0 \text{ at } x = 0 \ \forall y; \quad \theta = 1 \text{ at } y = \infty. \tag{12.3.11}$$

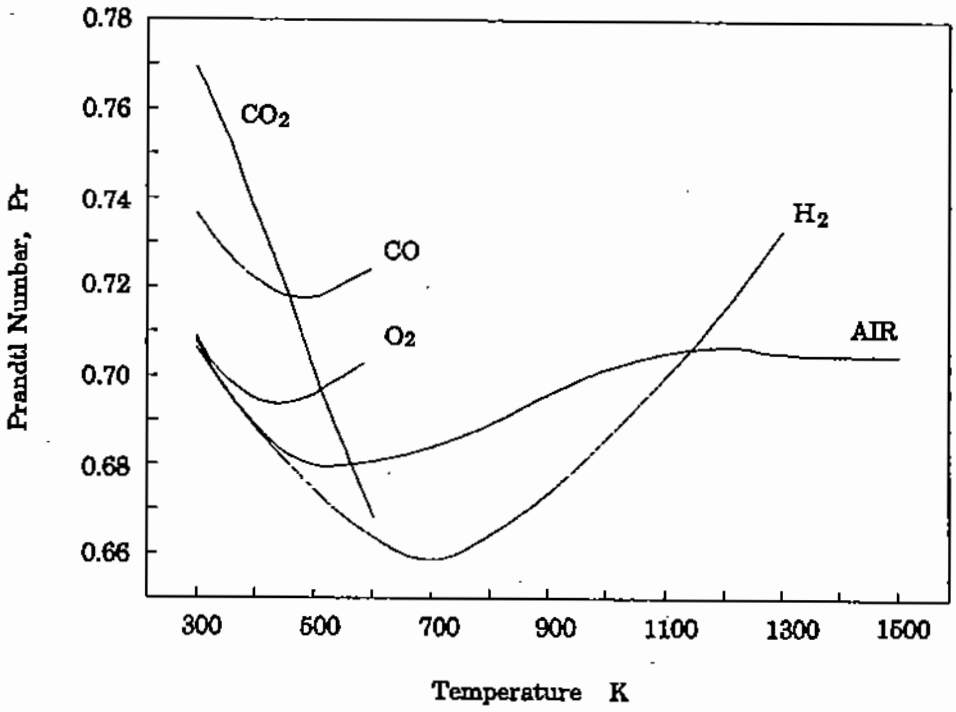

Figure 12.5. Effect of temperature on Prandtl number of some gases.

Since the velocity profiles of u_x and u_y are known from our earlier computation of the velocity boundary layer (Chapter 6, (12.3.1)), we may proceed by substituting these known relationships into the energy (12.3.9) and then integrate this equation by a numerical method. However, it should be noted that the dimensionless (12.3.3) and (12.3.9) are of identical form with the exception of the two coefficients μ/ρ and α. These are, of course, the kinematic viscosity and the thermal diffusivity of the fluid, respectively. As discussed in Chapter 10, their ratio is defined by the dimensionless Prandtl number:

12.3.10

$$\mathrm{Pr} = \frac{\nu}{\alpha} = \frac{C_p \mu}{k}, \tag{12.3.12}$$

which represents the ratio of the rate coefficients for momentum transfer and for heat conduction. At large values of Pr, as in the case of slags, the capacity of the fluid to transport momentum is greater than its capacity to transport thermal energy. In such cases, the distance away from the plate where the fluid velocity is affected will be greater than that for the temperature of the fluid; in other words, the *velocity boundary layer* will be thicker than the *thermal boundary layer*.

On the other hand, for Prandtl numbers much smaller than unity, as in the case of liquid metals where Pr is in the range of 0.01–0.1, the velocity boundary layer is very thin in comparison to the thermal one; we may then consider the velocity gradients to be negligible with regard to calculations of the heat convection between plate and fluid. Finally, when the Prandtl number is close to unity, as in the case with most gases (Fig. 12.5), the velocity and thermal boundary layers coincide.

For Pr close to 1, the solution of the equations of motion and thermal energy balance for gases is simplified. When this assumption cannot be made, (12.3.3) and (12.3.6) can be

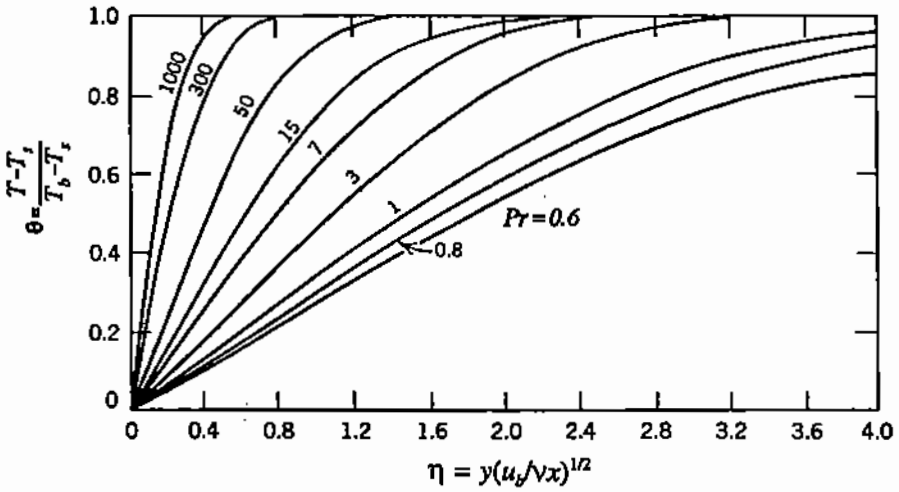

Figure 12.6. Calculated temperature profiles for laminar forced flow along a flat plate.

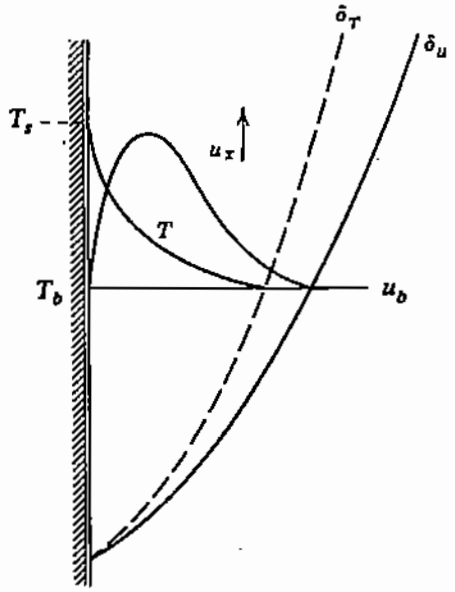

Figure 12.7. Velocity and temperature profiles for natural convection along a vertical wall, at $T_s > T_b$.

solved by introducing the transform variable η as defined earlier in (12.3.1). The transformed equations can be solved by the same numerical method as was used in computing the velocity distribution in the boundary layer (Chapter 6). Figure 12.6 [25] shows the calculated temperatures in a boundary layer as a function of the variable η and the Prandtl number.

12.4. THERMAL BOUNDARY LAYER IN NATURAL CONVECTION

In the previous section, we discussed the forced flow of a fluid past a surface. In such a case, fluid flow is not coupled to heat transfer and the velocity profile can be calculated first and then used to establish the temperature profile and heat flux.

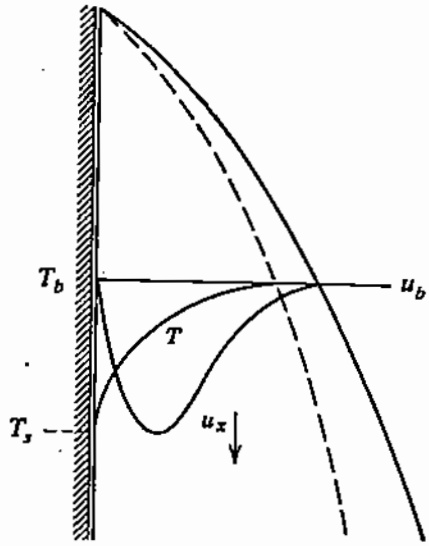

Figure 12.8. Velocity and temperature profiles for natural convection along a vertical wall, at $T_s < T_b$.

In the case of natural convection, the fluid moves because of density differences caused by temperature gradients. Therefore, as noted earlier, the equations of motion and heat transfer are coupled. For example, let us consider a vertical plate of temperature T_s which is immersed in a liquid at a lower bulk temperature T_b, as illustrated in Fig. 12.7. Obviously, the fluid film in contact with the plate will have a temperature of T_s while the adjacent layers of fluid will gradually approach the bulk temperature at some distance away from the plate surface.

The density of the layer of fluid next to the plate will decrease and the buoyancy effect will move the heated fluid upward. Due to the viscous forces, the velocity of the fluid layer in contact with the stationary plate must be zero; it is also zero far away from the heated surface. Therefore, the upward maximum velocity must occur at some intermediate distance from the surface. Figure 12.7 is an illustration of the thermal and velocity boundary layers for a fluid of Prandtl number greater than 1. The reverse situation, where the plate is at a lower temperature than the fluid, is illustrated in Fig. 12.8. In this case, the motion of the cooled boundary layer is downward.

For laminar flow, we can develop the equations for the temperature and velocity profiles near the plate on the basis of the equations of continuity, motion, and thermal energy balance:

$$\text{Equation of continuity:} \quad \frac{\partial u_x}{\partial x} + \frac{\partial u_y}{\partial y} = 0, \tag{12.4.1}$$

$$\text{Equation of motion:} \quad u_x \frac{\partial u_x}{\partial x} + u_y \frac{\partial u_x}{\partial y} = \nu \frac{\partial^2 u_x}{\partial y^2} + g_x \beta (T_s - T), \tag{12.4.2}$$

where g_x is the component of the acceleration due to gravity in the x-direction; β is the coefficient of expansion of fluid with temperature (fractional expansion per degree of temperature); T_s and T_b are the temperatures of the fluid at the surface of plate and in the fluid bulk; T is the temperature of the fluid at distance x from the leading edge and distance y from the surface of plate (Figs. 12.7–12.8).

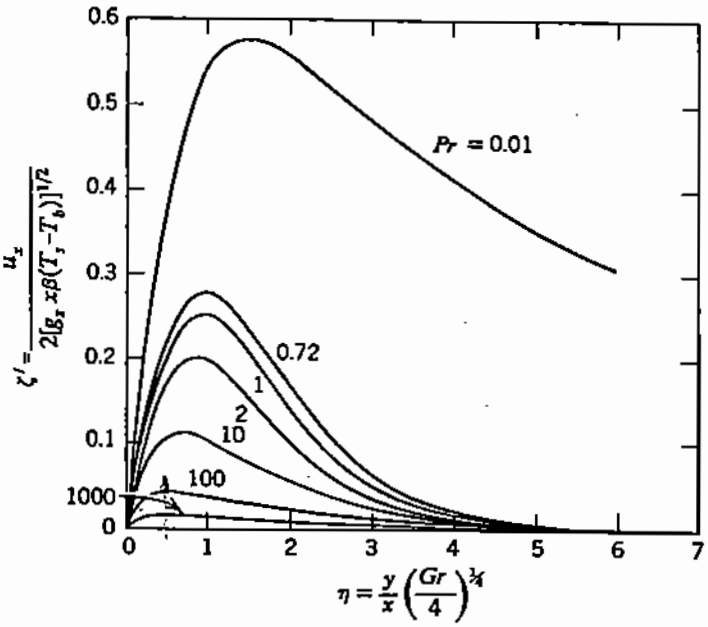

Figure 12.9. Dimensionless velocity profiles for laminar natural convection along a vertical plate.

The gravity term in (12.4.2) represents the buoyancy force in the flow system due to the thermal expansion of the fluid. In view of the assumption that conduction in the x-direction is negligible in comparison to convection, the thermal energy balance equation is expressed as follows:

$$u_x \frac{\partial T}{\partial x} + u_y \frac{\partial T}{\partial y} = \alpha \frac{\partial^2 T}{\partial y^2}. \tag{12.4.3}$$

The boundary conditions for the above equations are:

$$\begin{aligned} &u_x = u_y = 0 \text{ at } y = 0, \quad u_x = 0 \text{ at } y = \infty, \\ &u_x = 0 \text{ at } x = 0, \quad T = T_s \text{ at } y = 0, \\ &T = T_b \text{ at } y = \infty, \quad T = T_b \text{ at } x = 0. \end{aligned} \tag{12.4.4}$$

The above coupled equations are nonlinear and must be solved by numerical techniques. Figures 12.9 and 12.10 [2] show the calculated velocity and temperature profiles, in dimensionless form, for Prandtl numbers ranging from 0.01 to 1000. The quantity appearing on the x-axis is a function of location and of the dimensionless group called the **Grashof number** (Gr, Table 2.1). This group represents the ratio of the buoyancy forces, i.e., those created by density gradients, to the viscous forces in the fluid system. The Grashof number was derived by expressing the solutions of the natural convection equations in dimensionless form and is defined as follows:

$$\mathrm{Gr} = \frac{x^3 g_x \rho^2 \beta (T_s - T_b)}{\mu^2} = \frac{x^3 g_x \beta (T_s - T_b)}{\nu^2}. \tag{12.4.5}$$

The Grashof number for natural convection has a similar function to the Reynolds number for forced flow. Thus, for a vertical plate in a non-confined system, the transition from laminar to turbulent flow has been found to occur at $(\mathrm{Gr}\,\mathrm{Pr}) > 10^9$.

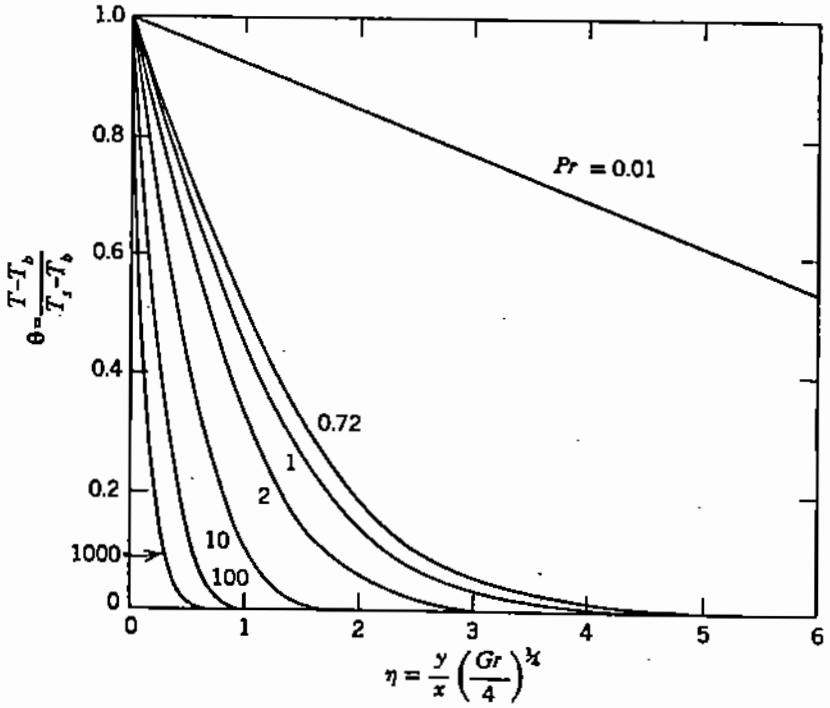

Figure 12.10. Dimensionless temperature profiles for laminar natural convection along a vertical plate.

12.5. THE HEAT TRANSFER COEFFICIENT

In the first part of this chapter, we showed how the differential equations of motion and thermal energy balance can be used to develop the temperature and velocity profiles for heat convection in relatively simple laminar flow systems. However, in most engineering problems, we are not interested in a detailed description of the velocity and temperature distributions but in determining the rate of heat transfer between a fluid and a surface. In principle, this can be done by first establishing the temperature distribution in the boundary layer between surface and fluid and then calculating the heat flux at the heat transfer surface:

$$q_y = -k\left(\frac{dT}{dy}\right)_{y=0}. \tag{12.5.1}$$

However, in many cases, this procedure is not feasible, particularly for turbulent systems or complex geometries where the velocity profiles cannot be determined from first principles. It is therefore necessary to use experimental data. In order to provide a rational framework for correlating and disseminating empirical data on heat transfer, the concept of the *heat transfer coefficient* has been introduced. Let us consider the case of heat transfer from a surface at temperature T_s to a fluid at a lower bulk temperature T_b, under steady state conditions. It can be shown experimentally that the heat flux from the surface to the fluid is proportional to the temperature difference between them:

$$q \propto (T_s - T_b). \tag{12.5.2}$$

In the case of conduction, the proportionality constant between heat flux and temperature difference is equal to the conductivity of the fluid divided by the thickness of the conducting

layer. However, in the case of convection, the thickness of the conducting layer, i.e., the boundary layer, depends on the flow conditions. Therefore, we introduce in (12.5.2) a proportionality constant, h, the value of which must depend on the thermal diffusivity of the fluid as well as on the properties of the flow system:

$$q = h(T_s - T_b). \tag{12.5.3}$$

The proportionality constant h is defined as the **heat transfer coefficient.** Its dimensions can be derived from the form of the above equation and are:

$$\frac{\text{heat flux}}{\Delta T} \equiv \frac{\text{Q}}{\text{t L}^2\,\text{T}}. \tag{12.5.4}$$

The units of the heat transfer coefficient are W m^{-2} K^{-1} in the SI system, and cal s^{-1} cm^{-2} $°C^{-1}$ in the metric system.

By analogy to Ohm's electric resistance law, the temperature difference corresponds to voltage and the heat flux to current; the heat transfer coefficient is then equivalent to the electric conductance (i.e., 1/resistance).

12.5.1. Factors Affecting the Heat Transfer Coefficient

As noted above, the heat transfer coefficient depends both on the thermal properties of the fluid and on the flow conditions in the system. Also, since the properties of the fluid may depend on temperature, h may also be a function of temperature. Table 12.1 [3] shows the range of values of heat transfer coefficients encountered with gases and liquids, in different types of fluid systems.

For fully developed flow, the heat transfer coefficient is independent of position. However, for situations where the boundary layer thickness varies with location, e.g., in flow around a particle, the value of h is also variable. This is illustrated in Fig. 12.11 which shows the interference photograph of a natural convection boundary layer around a horizontal heated tube [4].

12.6. HEAT TRANSFER CORRELATIONS

The heat transfer coefficient for a particular situation can be obtained either by direct measurement or by means of an existing semi-empirical correlation. Such correlations are usually presented in terms of the dimensionless groups introduced earlier (Table 2.1). Thus, the thermal properties of the fluid are represented by the Prandtl number:

$$\text{Pr} = \frac{C_p \mu}{k}. \tag{12.6.1}$$

where C_p is the specific heat of the fluid; μ is the viscosity of the fluid; k is the thermal conductivity of the fluid.

In the case of forced convection, the fluid system is represented by the Reynolds number

$$\text{Re} = \frac{Lu\rho}{\mu}, \tag{12.6.2}$$

where L is the characteristic system length, u the fluid velocity, and ρ the fluid density.

Table 12.1. Typical Values of Heat Transfer Coefficients [3]

	h, W m^{-2} K^{-1}
Natural convection in gases:	
To air around low temperature equipment (K)	3–8
To air around high temperature furnaces (>1000 K)	8–14
Natural convection in liquid metals:	
Molten metals in contact with wall at $\Delta T < 1000$ K	1000–3000
Molten iron in contact with water-cooled plates	7000
Forced convection in gases:	
Air flow in pipes (1–50 m s^{-1})	10–200
Gas flow in packed beds (1000 K)	135
Forced convection in water:	
Turbulent flow in pipes (u= 1 m s^{-1})	1000–8000
Flow through pipes with incipient boiling	5000–10^6
Quenching of hot metal into water or oil	50–500
Metal cooling with water sprays/curtains	3000
Radiation from surfaces:	
Boiling water	10
Clean liquid metals	30–150
High-temperature refractories, slags, oxides and luminous flames	200–500

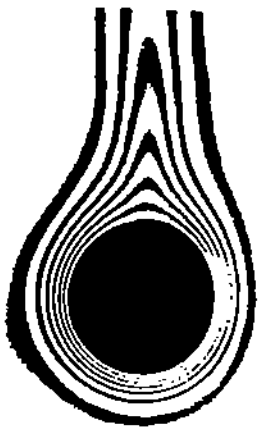

Figure 12.11. Interference photograph showing variation of thickness of natural convection boundary layer around a horizontal heated tube.

In natural convection, the corresponding group is the thermal Grashof number:

$$\mathrm{Gr} = \frac{L^3 \rho^2 g \beta \Delta T}{\mu^2}, \tag{12.6.3}$$

where g is the acceleration due to gravity; β is the thermal expansion coefficient (fractional expansion/degree); ΔT is the temperature difference between surface and bulk fluid.

In general, the correlations for forced convection are of the following form:

$$\mathrm{Nu} = f(\mathrm{Re}, \mathrm{Pr}), \tag{12.6.4}$$

and for natural convection:

$$\mathrm{Nu} = f(\mathrm{Gr}, \mathrm{Pr}), \tag{12.6.5}$$

where Nu is the dimensionless **Nusselt number** (Table 2.1):

$$\mathrm{Nu} = \frac{h}{(k/L)} = \frac{hL}{k}. \tag{12.6.6}$$

As in the case of the Reynolds number, L is the characteristic length of the flow system (e.g., pipe diameter, length of plate, etc). As indicated by the form of (12.6.6), the Nusselt number represents the ratio of convective to conductive heat transfer through the fluid.

In heat transfer correlations, when the temperature for estimating a fluid property is not specified, the value of all properties should be calculated at the *mean film temperature* which is defined as the average of the *bulk flow temperature* of the fluid and the surface temperature:

$$T_{\mathrm{film}} = \frac{T_{\mathrm{bulk}} + T_{\mathrm{surface}}}{2}. \tag{12.6.7}$$

A number of heat transfer correlations of relevance in the processing of materials are described in the following sections. For additional information, the reader is referred to handbooks on heat and mass transfer [5,20,22] and other reference books listed at the end of this chapter. Some correlations are based on a limited number of experimental data; therefore, their validity is limited to a particular geometry and to the range of Reynolds (or Grashof) and Prandtl numbers examined in the original study. Consequently, care must be exercised in extrapolating such correlations beyond the range studied.

Heat transfer correlations for laminar or turbulent flow through pipes and over flat surfaces are quite well established. The same can be said for the correlations to be presented for convective heat transfer to spheres and cylinders. There is less information available on more complex systems, such as stirred or gas-injected liquids, rotary kilns and fluid bed reactors.

12.6.1. Forced Convection Through Pipes and Ducts

For fully developed *laminar* flow through a pipe, the Nusselt number is a function only of the type of boundary condition at the wall surface. Thus, at constant surface temperature

$$\mathrm{Nu} = 3.66. \tag{12.6.8}$$

and at constant heat flux

$$\mathrm{Nu} = 4.36. \tag{12.6.9}$$

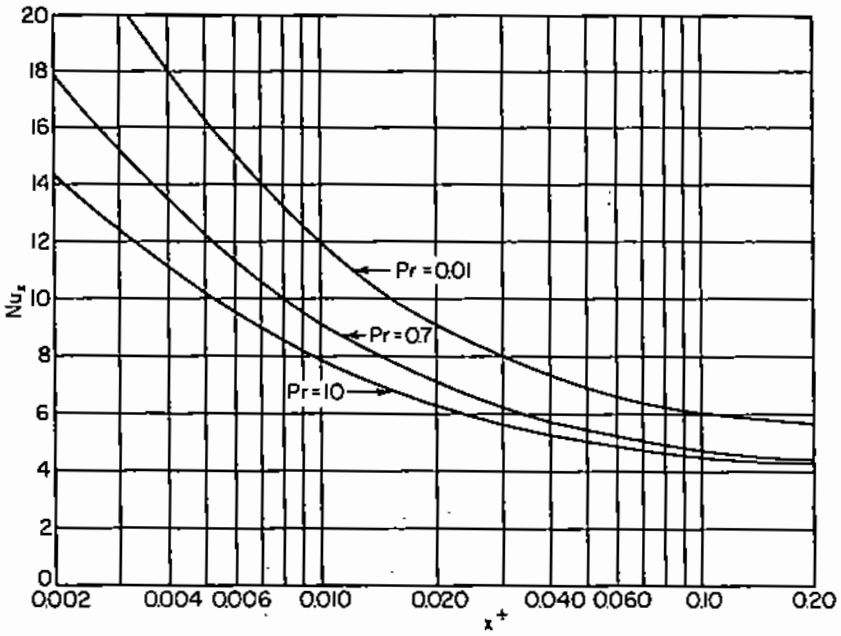

Figure 12.12. Variation of local Nusselt number in the entry region of a tube (laminar flow, constant heat flux, [5]).

However, in the *entrance region* of the pipe, i.e., prior to establishing fully developed flow, the Nusselt number can be considerably higher. The available correlations are shown in graphical form in Fig. 12.12 [5]. In this plot, the distance from the entrance point is expressed in dimensionless form as

$$x^+ = \frac{x}{r_p \mathrm{Re}_x \mathrm{Pr}},$$

where r_p is the pipe radius and Re_x is the Reynolds number at distance x from the entry point. Figure 12.12 shows that the flow becomes fully developed (i.e., Nu reaches a constant value) at values of x^+ of about 0.2.

For *turbulent* flow through pipes, the following correlation was proposed by Dittus and Boelter [6] and has been confirmed by numerous other investigators:

$$\mathrm{Nu} = \frac{h d_p}{k} = 0.023 \mathrm{Re}^{0.8} \mathrm{Pr}^n, \tag{12.6.10}$$

where d_p is the pipe diameter; $n = 0.3$ for $T_s < T_{\text{fluid}}$; $n = 0.4$ for $T_s > T_{\text{fluid}}$.

This correlation is valid for $\mathrm{Re} > 10000$, and for the range $0.7 < \mathrm{Pr} < 100$. It can also be used for non-circular conduits, by substituting the hydraulic mean diameter (d_h), as defined in Chapter 8 (see (8.5.10)), for the diameter of the pipe.

For liquid metals, i.e., at very low Prandtl numbers, Lyon [7] proposed the following correlation for constant net flux at the pipe surface and for values of the **Peclet number**, Pe (Pe = Re Pr) over 100:

$$\mathrm{Nu} = 7 + 0.025 \mathrm{Pe}^{0.8}. \tag{12.6.11}$$

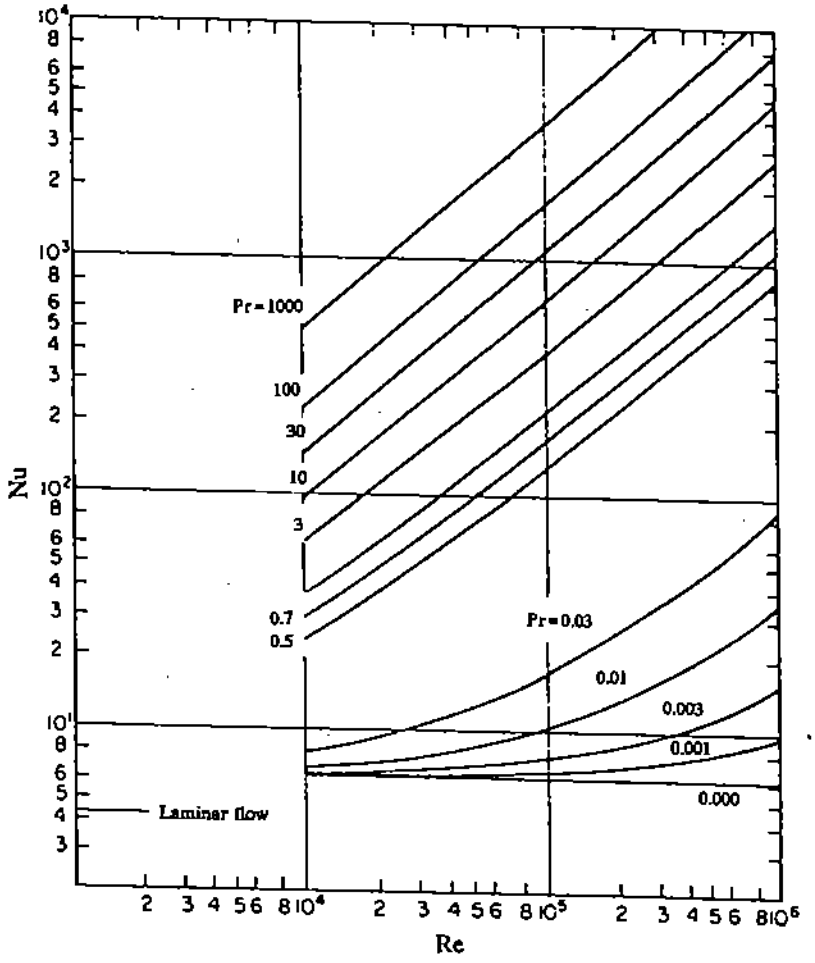

Figure 12.13. Nusselt number as a function of Re for fully developed flow in circular tubes (constant heat flux, [5]).

A similar correlation was proposed by Johnson et al. [8] for the range $200 < \mathrm{Pe} < 10000$:

$$\mathrm{Nu} = 5 + 0.016\mathrm{Pe}^{0.8}, \tag{12.6.12}$$

and by Seban and Shimazaki [9] for heat transfer from a pipe at constant temperature to a liquid metal:

$$\mathrm{Nu} = 4.8 + 0.025\mathrm{Pe}^{0.8}. \tag{12.6.13}$$

Figure 12.13 [5] is a graphical representation of heat transfer correlations for turbulent flow through cylindrical conduits. The low Pr curves on this graph represent heat transfer to liquid metals.

12.6.2. Forced Convection Over Plates

For *laminar* flow over a flat plate, which is defined to extend up to $\mathrm{Re}_x < 10^5$, the following correlation has been derived [10] by solving the appropriate boundary layer equations:

$$\mathrm{Nu}_x = \frac{h_x x}{k} = 0.332\mathrm{Re}_x^{1/2}\mathrm{Pr}^{1/3}, \tag{12.6.14}$$

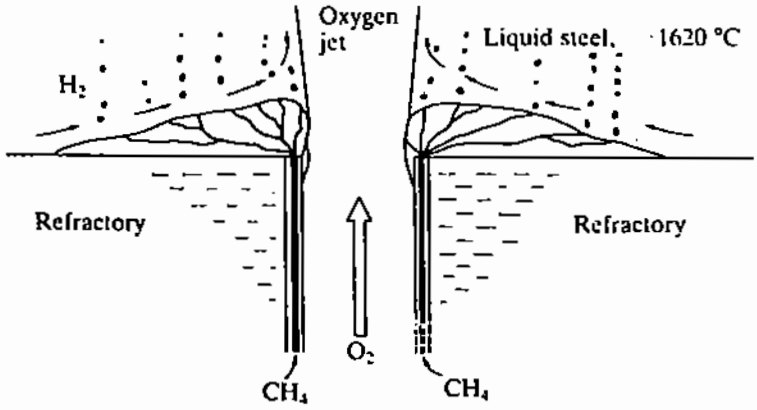

Figure 12.14. "Ring" of protective thermal accretions formed around CH_4-shrouded tuyere for injecting oxygen in liquid steel [3].

where Nu_x, Re_x, and h_x are values of Nu, Re, and h at distance x along the plate. The corresponding average value of the Nusselt number over a plate of length L is

$$\overline{\mathrm{Nu}} = \frac{1}{L}\int_0^L \mathrm{Nu}_x\,dx = 0.664\mathrm{Re}_L^{1/2}\mathrm{Pr}^{1/3}. \tag{12.6.15}$$

Equation (12.6.15) is valid only for $\mathrm{Pr} > 0.7$. For liquid metals, the following relationship has been proposed by Eckert and Drake [16]:

$$\mathrm{Nu}_x = \frac{(\mathrm{Re}_x\,\mathrm{Pr})^{1/2}}{1.55\mathrm{Pr}^{1/2} + 3.09(0.37 - 0.15\mathrm{Pr})^{1/2}}. \tag{12.6.16}$$

For *turbulent* flow over a flat plate, the following equation was recommended [14] for the range of $\mathrm{Re}_L > 10^5$ and $\mathrm{Pr} > 0.7$:

$$\mathrm{Nu}_L = 0.037\mathrm{Re}_L^{0.8}\mathrm{Pr}^{1/3}. \tag{12.6.17}$$

For a *gas jet impinging on a solid surface*, Huang [13] derived experimentally the following correlation:

$$\mathrm{Nu} = \frac{hd_j}{k} = 0.02\mathrm{Re}^{0.87}\mathrm{Pr}^{1/3}, \tag{12.6.18}$$

where

$$\mathrm{Re} = \frac{d_j u_j \rho}{\mu},$$

and h is the mean heat transfer coefficient over the impingement surface; d_j is the diameter of jet at nozzle exit; u_j is the jet average velocity above point of impingement

Example 12.6.1 [3]

The Savard–Lee tuyere for gas injection into metals (Fig. 12.14) consists of two concentric pipes; through the inner pipe flows oxygen and through the outer annulus a hydrocarbon gas, such as methane. The objective of the tuyere is to use the hydrocarbon annular flow to

"shield" the tuyere refractory wall from the oxygen stream, at the entry point to the reactor. The cooling effect is provided by the heating and thermal decomposition of the hydrocarbon gas as it flows through the metal accretion that forms around the tuyere (Fig. 12.14). It is required to calculate the efficiency of utilization of natural gas in the following application of the Savard–Lee tuyere for steelmaking in a bottom-blown converter:

Oxygen flow through central tuyere	1920 Nm^3/h
Methane gas flow through annulus (5% of oxygen flow)	96 Nm^3/h
Diameter of tuyere in operation	0.1 m
Estimated width of metal accretion around tuyere (Fig. 12.14), cm	0.15 m
Estimated average velocity of liquid steel over accretion	0.5 m/s
Steel bath temperature (T_b)	1620°C
Melting point of steel (T_{mp})	1490°C
Decomposition and sensible heat absorbed by CH_4	182248 J/mol
Physical properties of steel at at bath temperature	$\rho = 7000\ kg/m^3$; $\mu = 6.7 \times 10^{-3}\ kg/(m\ s)$; $C_p = 750\ J/(kg\ K)$; $k_{slag} = 41.8\ W/(m\ K)$

First, we calculate the Reynolds and Prandtl numbers for the liquid steel flow over the tuyere accretion, by using the width of the accretion zone, x, as the characteristic length:

$$\mathrm{Re}_x = \frac{xu\rho}{\mu} = \frac{0.15 \times 0.5 \times 7000}{6.7 \times 10^{-3}} = 78360 \quad \mathrm{Pr} = \frac{C_p\mu}{k} = \frac{750 \times 6.7 \times 10^{-3}}{41.8} = 0.12.$$

Then, by using the Eckert correlation (see (12.6.16)) for heat transfer between a liquid metal and a plate of length x, we calculate the heat transfer coefficient between steel bath and the ring of accretion around the tuyere:

$$\begin{aligned}\mathrm{Nu}_x &= \frac{(\mathrm{Re}_x\,\mathrm{Pr})^{0.5}}{1.55\mathrm{Pr}^{0.5} + 3.09(0.37 - 0.15\mathrm{Pr})^{0.5}} \\ &= \frac{(78360 \times 0.12)^{0.5}}{1.55 \times 0.12^{0.5} + 3.09 \times (0.37 - 0.15 \times 0.12)^{0.5}} \\ &= 40.91,\end{aligned}$$

and $h = (\mathrm{Nu}_x k/x) = (40.91 \times 41.8/0.15) = 11.4\ \mathrm{kW\ m^{-2}\ K^{-1}}$. Therefore, the heat transfer rate between liquid and accretion ring is

$$Q = hA(T_b - T_{mp}) = 11.4 \times \frac{\pi}{4} \times (0.25^2 - 0.10^2) \times (1620 - 1490) = 61.11\ \mathrm{kW}.$$

By comparing this amount of heat input to the decomposition and sensible heat absorbed from the tuyere zone by the methane flow, we obtain

$$\text{CH}_4 \text{ cooling capacity} = \frac{96 \times 1000}{22.4 \times 3600} \times 182248 = 216960\,\text{W} = 217\,\text{kW},$$

$$\%\text{ utilization efficiency of CH}_4 = \frac{61.11}{217} \times 100 = 28.2\%.$$

12.6.3. Forced Convection to Spheres and Cylinders

As noted earlier for a cylinder (Fig. 12.11), the local heat transfer coefficient along the surface of a sphere varies with location. The maximum value is attained at the foremost point of the sphere with respect to the direction of flow, where the boundary layer is thinnest. The average coefficient for heat transfer between the surface of a spherical particle and the surrounding fluid can be estimated from the following equation, which was first developed by Frössling [17] and is sometimes called the Ranz-Marshall correlation in honor of the chemical engineers who firmly established its use in heat transfer to droplets [18]:

$$\text{Nu} = 2.0 + 0.6\text{Re}^{1/2}\text{Pr}^{1/3}. \tag{12.6.18}$$

It can be seen that this correlation predicts that at zero relative velocity between sphere and fluid the Nusselt number will be equal to 2. Under these conditions, heat transfer occurs only by conduction through the stagnant gas. Let us examine, from a theoretical point of view, the value of the heat transfer coefficient in the limiting case where there is no relative motion between fluid and particle and at steady state conditions. The rate of heat conduction across a gas shell of differential thickness dr is expressed as

$$Q_c = 4\pi r^2 \left(k \frac{dT}{dr}\right), \tag{12.6.19}$$

where Q_c is the rate of heat transfer by conduction; k is the thermal conductivity of the gas; T is the temperature at distance r from the sphere center.

By integrating the above equation for boundary conditions $T = T_b$ at $r = r_b$ (outer radius of boundary layer) and $T = T_p$ at $r = r_p$ (particle radius), we obtain

$$Q_c = \frac{4\pi k}{\left(\frac{1}{r_p} - \frac{1}{r_b}\right)} (T_b - T_p). \tag{12.6.20}$$

However, by definition, the boundary layer thickness in a stagnant fluid is infinite; consequently, $1/r_b = 0$ and (12.6.20) simplifies to

$$Q_c = 4\pi k r_p (T_b - T_p). \tag{12.6.21}$$

If we now assume the existence of an equivalent heat transfer coefficient, as defined by (12.5.3), we can express Q_c as follows:

$$Q_c = h(4\pi r_p^2)(T_b - T_p), \tag{12.6.22}$$

where h is the heat transfer coefficient between gas and particle.

Comparison of (12.6.21) and (12.6.22) shows that the following identity exists:

$$h r_p \equiv k. \tag{12.6.23}$$

Equation (12.6.23) can be rearranged in terms of the Nusselt group as follows

$$\mathrm{Nu} = \frac{h d_p}{k} = 2, \tag{12.6.24}$$

where d_p (i.e., $2r_p$) is the particle diameter.

Therefore, in the limiting case of a spherical particle in a motionless fluid, the Nusselt number at steady state conditions has the value of 2, as stated in the Frössling and Ranz-Marshall correlations. As will be shown in Chapter 17, similar considerations apply for mass transfer to spherical and cylindrical particles.

A similar correlation to (12.6.18) was derived experimentally by Wait [21] for heat transfer to a sphere immersed in a liquid metal:

$$\mathrm{Nu} = 2 + 0.38(\mathrm{Re}\,\mathrm{Pr})^{0.5}. \tag{12.6.25}$$

For forced flow around a cylinder which is perpendicular to the direction of flow, the following correlation has been proposed [20]:

$$\mathrm{Nu} = a\,\mathrm{Re}^b\,\mathrm{Pr}^{0.33}, \tag{12.6.26}$$

where a and b depend on the range of Reynolds number as shown in the following tabulation:

Re	a	b
0.4–4	0.989	0.330
4–40	0.911	0.385
40–4000	0.683	0.466
4000–40000	0.193	0.618
40000–400000	0.027	0.805

12.6.4. Natural Convection to Vertical Plates

In most correlations for natural convection, the Grashof and Prandtl numbers have the same power exponent. Therefore, some authors have presented their correlations in terms of the **Rayleigh number**, which is equal to the product Gr Pr (Table 2.1). As in the case of other correlations, it is necessary to state whether the expressed heat transfer coefficient is *local*, i.e., at a certain distance x from the point at which natural convection starts, or *average*, i.e., over the entire height of the plate. In local heat transfer correlations, the value of x is

used to calculate Nu and Gr; in averaged correlations, the characteristic length is the height of the plate, L.

As stated earlier, in natural convection over plates, the flow is considered to be laminar when the product $\mathrm{Gr}\,\mathrm{Pr} < 10^9$. For *laminar natural convection to vertical plates*, Eckert [24] proposed the following correlation for the local heat transfer coefficient:

$$\mathrm{Nu}_x = \frac{hx}{k} = \frac{0.508\mathrm{Gr}^{0.25}\mathrm{Pr}^{0.5}}{(0.95+\mathrm{Pr})^{0.25}}, \tag{12.6.27}$$

where x is the distance along the plate. This equation was found to be applicable over a wide range of Prandtl numbers, including liquid metals. A very similar correlation has been proposed [2] for the average heat transfer coefficient in the laminar range of $10^4 < \mathrm{Gr}\,\mathrm{Pr} < 10^9$ and for a very wide range of Prandtl numbers ($0.0084 < \mathrm{Pr} < 1000$:

$$\mathrm{Nu}_L = \frac{hL}{k} = \frac{0.65\mathrm{Gr}^{0.25}\mathrm{Pr}^{0.5}}{(0.861+\mathrm{Pr})^{0.25}}. \tag{12.6.28}$$

In the range of $0.6 < \mathrm{Pr} < 10$, which does not include liquid metals or slags, the following simpler correlation has been proposed by numerous authors [3,5,23]:

$$\mathrm{Nu} = 0.56(\mathrm{Gr}\,\mathrm{Pr})^{0.25}. \tag{12.6.29}$$

For *turbulent natural convection to vertical plates*, Eckert and Jackson [19] developed the following correlation:

$$\mathrm{Nu}_x = \frac{0.0295\mathrm{Gr}^{0.4}\mathrm{Pr}^{7/15}}{(1+0.494\mathrm{Pr}^{2/3})^{2/5}}. \tag{12.6.30}$$

For gases ($\mathrm{Pr} = 0.7$–1), this correlation yields Nusselt number values close to the following simpler correlation by Gebhart, also for the turbulent regime of flow [24]:

$$\mathrm{Nu}_L = 0.02(\mathrm{Gr}\,\mathrm{Pr})^{0.4}. \tag{12.6.31}$$

Another correlation that has been proposed [5] for turbulent natural convection from gases to vertical plates shows the product $\mathrm{Gr}\,\mathrm{Pr}$ to the power of 0.333 instead of 0.4 as in the above correlations:

$$\mathrm{Nu}_x = 0.12(\mathrm{Gr}\,\mathrm{Pr})^{1/3}. \tag{12.6.32}$$

This correlation is very close to that recommended by Geiger and Poirier [23] for the range of $0.6 < \mathrm{Pr} < 10$:

$$\mathrm{Nu}_L = 0.13(\mathrm{Gr}\,\mathrm{Pr})^{1/3}. \tag{12.6.33}$$

Rohsenow et al. [5] noted that for the turbulent range of $10^{10} < \mathrm{Gr}\,\mathrm{Pr} < 10^{12}$, the calculated difference in the values of Nu for the two types of correlation (i.e., power exponent of 0.4 or 0.333) for a large number of experimental data was between +24% and −9%; the accuracy of the data is not sufficient to indicate which of the two expressions is preferable.

By integrating the correlations for the local Nu over the entire length of the plate, we find that the following correspondence applies between the average and local Nusselt numbers:

$$\text{For laminar flow, } (\mathrm{Gr\,Pr})^{0.25}: \quad \mathrm{Nu}_L = \frac{4}{3}\mathrm{Nu}_x,$$

$$\text{For turbulent flow, } (\mathrm{Gr\,Pr})^{0.40}: \quad \mathrm{Nu}_L = \frac{5}{6}\mathrm{Nu}_x,$$

$$\text{For turbulent flow, } (\mathrm{Gr\,Pr})^{0.333}: \quad \mathrm{Nu}_L = \mathrm{Nu}_x.$$

12.6.5. Natural Convection for Other Geometries

The available correlations for heat transfer by natural convection to other geometries are of a similar form to those discussed above for vertical plates. For laminar boundary layers ($\mathrm{Gr\,Pr} < 10^9$), Rohsenow et al. [5] recommended the following correlation:

$$\mathrm{Nu}_L = a(\mathrm{Gr\,Pr})^{0.25}, \tag{12.6.35}$$

where the constant a is a function of the geometry of the system and Prandtl number. For the low Pr range of gases (Pr = 0.6–1), a is nearly independent of Pr and, on the basis of the available correlations, is related to the geometry of the system as shown in the following tabulation:

Geometry of system	a
Horizontal cylinder, L = diameter	0.47
Sphere, L = diameter	0.49
Horizontal plate facing upward (downward if cooled), L = width	0.54
Horizontal plate facing downward (upward if cooled), L = width	0.27

Similarly, in the turbulent regime of natural convection ($\mathrm{Gr\,Pr} > 10^9$), Rohsenow et al. [5] recommended the following generalized correlation:

$$\mathrm{Nu}_L = b(\mathrm{Gr\,Pr})^{0.333}, \tag{12.6.36}$$

where, for gases b also depends on the geometry of the system, as shown in the following tabulation:

Geometry of system	b
Horizontal cylinder, L = diameter	0.10
Horizontal plate facing upward (or downward when plate is colder than fluid), L = width	0.14

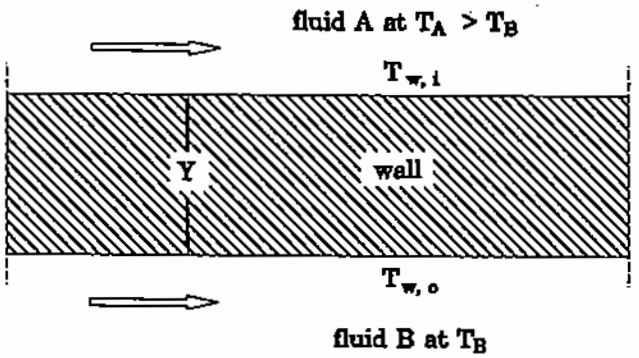

Figure 12.15. Heat transfer across the wall of a duct.

For natural convection to small spherical particles, the following correlation has been proposed [23]:

$$\mathrm{Nu} = 2 + 0.06\mathrm{Gr}^{1/4}\mathrm{Pr}^{1/3} \tag{12.6.37}$$

for the range of $\mathrm{Gr}^{1/4}\mathrm{Pr}^{1/3} < 200$. This range covers particles of the size encountered in fluid bed and flash reactors.

12.7. THE OVERALL HEAT TRANSFER COEFFICIENT

In §12.5, we defined the heat transfer coefficient as the constant of proportionality between the heat flux by convection and the driving force of the temperature difference between a fluid and a surface. In a similar way, it is convenient to define an *overall heat transfer coefficient* in systems which involve sequential conduction and convection of heat, such as heat transfer through furnace walls. For example, let us consider the transfer of heat across the walls of a rectangular duct (Fig. 12.15). Heat is transferred by convection from the fluid A to the inner surface of the duct wall; then by conduction across the wall thickness Y; and finally by convection from the outer surface of the duct to fluid B which is flowing around the duct.

Let us consider a location where the temperature of fluid A is T_A and the temperature of fluid B is T_B. The heat flux from fluid A to fluid B is then expressed as follows:

$$q_y = \frac{Q}{A} = h_A(T_A - T_{w,i}) = \frac{k_w}{Y}(T_{w,i} - T_{w,o}) = h_B(T_{w,o} - T_B), \tag{12.7.1}$$

where q_y is the heat flow Q per area A; h_A and h_B are the heat transfer coefficients by convection in fluids A and B; k_w is the thermal conductivity of the wall; $T_{w,i}$ and $T_{w,o}$ are the inside and outside wall temperatures.

Equation (12.7.1) is very similar to (10.7.10) which was presented earlier for conduction through a composite wall. By eliminating algebraically the intermediate temperatures $T_{w,i}$ and $T_{w,o}$, (12.7.1) can be rewritten as follows:

$$q_y = \left(\frac{1}{\frac{1}{h_A} + \frac{Y}{k_w} + \frac{1}{h_B}}\right)(T_A - T_B) = h_{ov}(T_A - T_B). \tag{12.7.2}$$

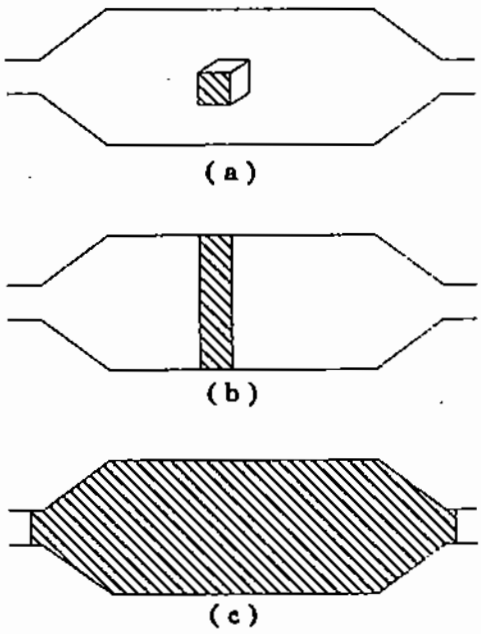

Figure 12.16. Thermal energy balance on (*a*) an infinitesimal volume element, (*b*) a section element, and (*c*) the entire volume of the vessel.

The term in the first parenthesis of the above equation is defined as the **overall heat transfer coefficient** and in the last term is denoted by h_{ov}:

$$h_{ov} = \frac{1}{\frac{1}{h_A} + \frac{Y}{k_w} + \frac{1}{h_B}}. \tag{12.7.3}$$

It can be seen that in analogy to Ohm's law, the individual coefficients, h_A, h_B, and k_w/Y may be regarded as conductances, i.e., the reciprocal of resistances; thus, the total resistance to heat flow is the sum of the individual resistances.

The above equation was derived for steady state conditions and also for heat transfer across a planar surface, so that the heat transfer area A does not change with y. In a cylindrical duct or pipe, the surface area for heat transfer does increase with distance from the center. As illustrated earlier, for conduction through a composite cylindrical wall, this geometrical effect is accounted for by the following modification of (12.7.3) for a cylindrical conduit:

$$\frac{1}{h_{ov,o}d_o} = \frac{1}{h_A d_o} + \frac{\ln(d_o/d_i)}{2k_w} + \frac{1}{h_B d_i}, \tag{12.7.4}$$

where d_o and d_i are the outside and inside diameters of the pipe wall, respectively, and the calculated overall coefficient, $h_{ov,o}$, is to be used in conjunction with the outside surface area of the conduit.

12.8. THE OVERALL THERMAL ENERGY BALANCE

At the beginning of this chapter, we obtained the differential equations for convective heat transfer by establishing an energy balance over an infinitesimal volume element (Fig. 12.16a). As discussed earlier, this method provides detailed information on the temperature and

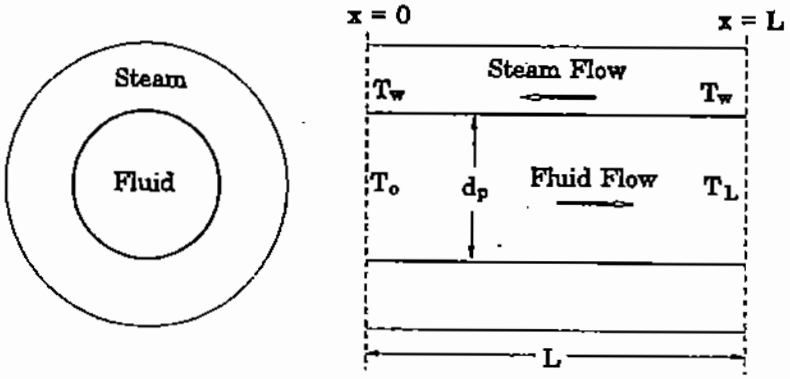

Figure 12.17. Counter-current flow heat exchanger.

velocity profiles in a fluid system. In this section, we shall discuss the *overall thermal energy balance* in which the control volume is chosen to extend over the entire cross section of the system and is of infinitesimal width only in one direction, usually the direction of the fluid flow (Fig. 12.16b).

The technique of overall thermal energy balance is analogous to the overall mechanical energy balance which was discussed in Chapter 8. It is much simpler than the differential thermal energy balance but requires additional information in the form of the heat transfer correlations which were discussed in this chapter.

12.8.1. Thermal Energy Balance in a Pipe

Let us consider a fluid of specific heat C_p flowing through a pipe at a mass flux G (dimensions M t^{-1} L^{-2}) at steady state conditions. The pipe is heated externally (e.g., by steam) to a uniform temperature T_w. The inlet temperature of the fluid into the pipe, at point 1, is T_0 and the heat transfer coefficient, h, from the pipe wall to the fluid, is assumed to be constant throughout the pipe.

It is required to develop an equation relating the temperature of the fluid to distance from the inlet point and, also, an expression for the total amount of heat transferred to the fluid over a length L of the pipe. With reference to Fig. 12.17, the control volume for this problem is chosen to be a section of the pipe of diameter d_p and length dx. Assuming that the conduction of heat in the fluid in the x-direction is negligible, the heat balance over the cylindrical section of length dx is:

$$\dot{m}C_p dT = h(\pi d_p dx)(T_w - T), \tag{12.8.1.}$$

where $\dot{m}$ is the mass flow rate (e.g., kg s^{-1}); dT is the temperature increase of fluid over length dx; C_p is the specific heat capacity of the fluid; T_w is the wall temperature.

This is a first-order differential equation which must be solved for the following boundary condition:

$$T = T_0 \text{ at } x = 0.$$

By integrating (12.8.1) between $x = 0$ and x, we obtain

$$\ln \frac{T_w - T_0}{T_w - T} = \left(\frac{\pi d_p h}{\dot{m}C_p}\right) x, \tag{12.8.2.}$$

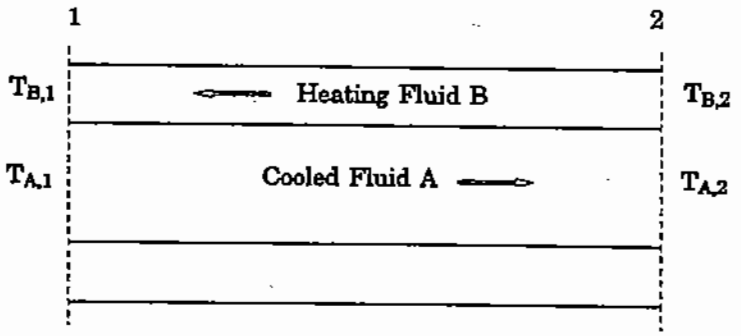

Figure 12.18. Counter-current flow heat exchanger.

and therefore

$$T = T_w - (T_w - T_0)\, e^{-(\pi d_p h/\dot{m}C_p)x}. \tag{12.8.3}$$

It can be seen that the temperature of the fluid approaches the temperature of the wall asymptotically with distance travelled through the pipe; the larger the heat transfer coefficient, the faster is the approach of T to T_w.

The total rate of heat transfer between the wall and the fluid over the distance L is expressed as follows:

$$Q = \dot{m}C_p(T_L - T_0), \tag{12.8.4}$$

where T_L is the temperature of the fluid at distance L from the entrance of the pipe. Combining (12.8.2) and (12.8.4) and rearranging, we obtain

$$Q = h(\pi d_p L)\left[\frac{(T_w - T_0) - (T_w - T_L)}{\ln\left(\frac{T_w - T_0}{T_w - T_L}\right)}\right], \tag{12.8.5}$$

where the first parenthesis represents the surface area of pipe wall over the length L.

12.8.2. The Logarithmic Mean Temperature Difference

The quantity in the brackets of (12.8.5) is defined as the logarithmic mean of the final $(T_w - T_L)$ and the initial $(T_w - T_0)$ temperature differences. The abbreviated notation of this "mean" driving force for heat transfer is shown in the following expression of (12.8.5):

$$Q = hA\Delta T_{LM}, \tag{12.8.6}$$

where A is the area available for heat transfer.

The logarithmic mean temperature difference is very useful in heat exchanger calculations where the temperatures of the fluid and the wall are varying with distance. As an example, let us consider heat transfer in the counter-current flow of two fluids through a heat exchanger (Fig. 12.18). In this case, the lower temperature fluid A enters the heat exchanger at point 1 and temperature $T_{A,1}$ and leaves at the other end at temperature $T_{A,2}$. The heating fluid B enters at point 2, at temperature $T_{B,2}$ and leaves at 1 and temperature $T_{B,1}$. If we assume that the heat exchanger is well insulated and the heat losses to the environment are negligible, the overall thermal energy balance yields:

heat gained by fluid A = heat lost by fluid B, i.e.,

$$\dot{m}_A C_{p,A}(T_{A,2} - T_{A,1}) = \dot{m}_B C_{p,B}(T_{B,1} - T_{B,2}). \tag{12.8.7}$$

In heat exchanger tubes, the thermal conductivity of the tube is high and the wall thickness kept at a minimum. Therefore, the "resistance" due to conduction through the tube wall is negligible and the overall heat transfer coefficient can be expressed as follows:

$$\frac{1}{h_{ov}} = \frac{1}{h_A} + \frac{1}{h_B}, \tag{12.8.8}$$

where h_A and h_B are the heat transfer coefficients for convection in fluid A and fluid B. In analogy with (12.8.6), the rate of heat transfer in this case is expressed as

$$Q = h_{ov} A \Delta T_{LM}, \tag{12.8.9}$$

where the logarithmic mean is now defined by the following equation:

$$\Delta T_{LM} = \frac{(T_{B,1} - T_{A,1}) - (T_{B,2} - T_{A,2})}{\ln\left(\frac{T_{B,1} - T_{A,1}}{T_{B,2} - T_{A,2}}\right)}. \tag{12.8.10}$$

By introducing in (12.8.10) any set of hypothetical values of inlet and outlet temperatures, it can be shown that *counter-current* flow of the fluids A and B, that is when they are flowing in opposite directions, results in a higher logarithmic mean temperature than *co-current* flow.

REFERENCES

1. W.R. Rohsenow and H. Choi, *Heat, Mass and Momentum Transfer*, Prentice-Hall, New York (1961).
2. S. Ostrach, *National Adv. Comm. Aeronaut.*, Tech. Note 2635, Washington, DC (1952).
3. R.I.L. Guthrie, *Engineering in Process Metallurgy*, Clarendon Press, Oxford (1989).
4. E.R.G. Eckert and E. Soehngen, *USAF Tech. Rep. 5747*, Wright-Patterson AFB, Dayton, Ohio (1958).
5. W.P. Rohsenow, J.P. Garnett, and E.N. Ganic, eds., *Handbook of Heat Transfer Fundamentals*, McGraw-Hill, New York (1985).
6. F.W. Dittus and L.M.K. Boelter, *University Calif. Publ. Eng.*, **2**, 443 (1930).
7. R.N. Lyon, *Chem. Eng. Progr.*, **47**, 75 (1951).
8. H.A. Johnson, J.P. Hartnett, and W.J. Clabaugh, *Trans. ASME*, **76**, 509 (1954).
9. R.A. Seban and T.T. Shimazaki, *Trans. ASME*, **73**, 803–809 (1951).
10. C.O. Bennett and J.E. Myers, *Momentum, Heat and Mass Transfer*, 3rd ed., McGraw-Hill, New York (1982).
11. M. Jacob and W.M. Dow, *Trans. ASME*, **68**, 124 (1946).
12. G.C. Huang, *Heat Transfer*, **85**, 237, (1963).
13. M. Jacob and W.M. Dow, *Trans. ASME*, **68**, 124 (1946).
14. W.E. Ranz and W.R. Marshall, *Chem. Eng. Progr.*, **48**, 141–173 (1952).
15. E.R.G. Eckert and R.M. Drake, *Heat and Mass Transfer*, McGraw-Hill, New York (1959).
16. N. Frössling, *Gerlands Beitr. Geophys.*, **52**, 170 (1938).
17. E.R.G. Eckert and T.W. Jackson, *NACA Rep. 1015*, Washington, DC (1951).
18. F. Kreith and W.Z. Black, *Basic Heat Transfer*, Harper and Row, New York (1980).
19. L.C. Wait, *Heat Transfer*, **90**, 9 (1968).

20. N.P. Cheremisinoff, ed., *Handbook of Heat and Mass Transfer*, Vol. 1: *Heat Transfer Operations*, Gulf Publishing, Houston (1986).
21. G.H. Geiger and D.R. Poirier, *Transport Phenomena in Metallurgy*, Addison-Wesley, Reading, MA (1973).
22. E.R.G. Eckert, *Introduction to the Transfer of Heat and Mass*, McGraw-Hill, New York (1950).
23. FIDAP Program, Version 7, Fluid Dynamics International, Evanston, Illinois (1993).
24. B. Gebhart, *Heat Transfer*, McGraw-Hill, New York (1970).

THIRTEEN

Heat Transfer by Radiation

(77-191

All forms of matter can emit or absorb thermal energy in the form of radiation. The rate at which radiation is emitted from a body is proportional to the fourth power of its temperature. Therefore, radiation is the dominant mode of heat transfer in high-temperature processing systems, such as pyrometallurgical reactors. For example, radiation accounts largely for heat transfer from a luminous flame to a combustion chamber and for heat loss from an open port in a furnace.

Radiant energy may be considered to be transported either by photons or by electromagnetic waves. In modern physics, both of these concepts are used in a complementary fashion to explain various facets of radiation. For our purposes, it is sufficient to consider radiation as the transport of energy by means of electromagnetic waves travelling at the speed of light. The propagation velocity is related to the wavelength as follows:

$$c = \lambda \tilde{\nu}. \tag{13.1.1}$$

where λ is the wavelength and $\tilde{\nu}$ the frequency of propagation.

As shown in Fig. 13.1, the wavelength of electromagnetic radiation ranges from hundreds of kilometers for radio waves to less than one angstrom (1×10^{-9} m) for gamma and cosmic rays. The wavelength range of interest in heat transfer is in the visible and infrared ranges and extends from about 0.2 to 20 microns.

As in Chapters 10–12 on heat conduction and convection, we will use the symbol Q to represent heat transport rate (Q t^{-1}) and q to denote heat flux (Q t^{-1} L^{-2}).

13.1. BLACK-BODY RADIATION

A *black body* is defined as a surface which absorbs all the incident radiant energy. At a given wavelength, the energy emitted per unit surface area of a black body is called the *monochromatic emissive power*. It depends only on the temperature of the body, as expressed by *Planck's radiation law*:

$$W'_{B,\lambda} = \frac{C_1 \lambda^{-5}}{e^{C_2/\lambda T} - 1}, \tag{13.1.2}$$

where $W'_{B,\lambda}$ is the monochromatic emissive power (i.e., radiant energy flux per unit wavelength); C_1 is a constant = $2\pi hc^2$; C_2 is a constant = ch/k; c is the velocity of light; h is

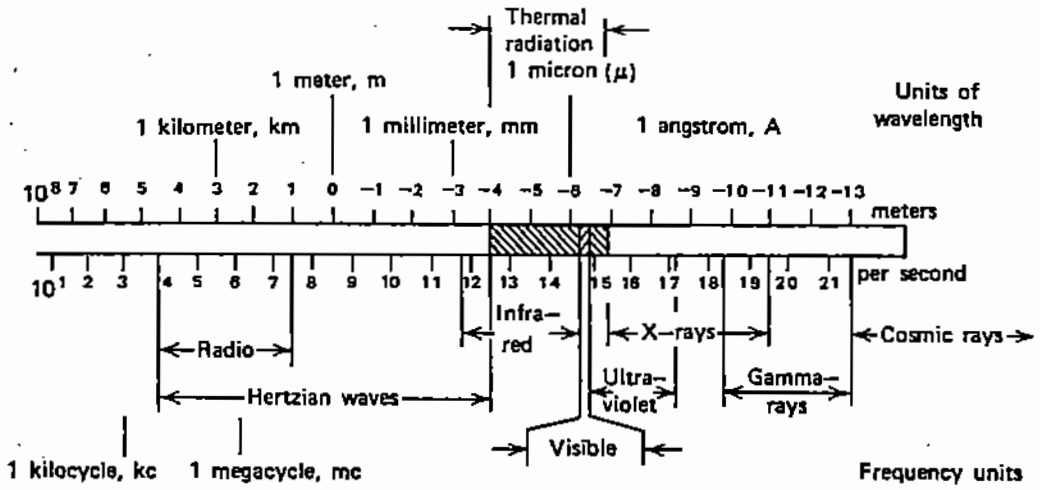

Figure 13.1. Electromagnetic wave spectrum.

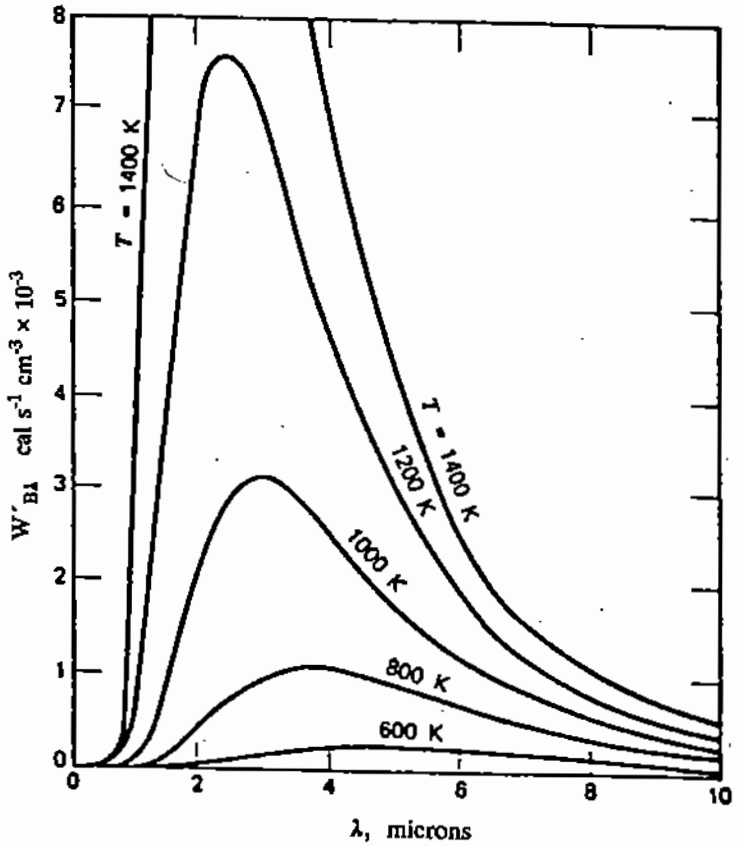

Figure 13.2. Monochromatic emissive power of a black body as a function of temperature and wavelength.

Planck's constant = 6.625×10^{-27} erg s; k is Boltzmann's constant = 1.381×10^{-16} erg K^{-1} [3].

Figure 13.2 is a plot of the monochromatic emissive power as a function of wavelength at different temperatures. It can be seen that these plots exhibit the following characteristics:

a. At a given wavelength, monochromatic radiation increases with increasing temperature.
b. At a given temperature, maximum radiation occurs at a particular wavelength (this explains why "red-hot" metal at 800°C appears to become "white-hot" when heated to 1100°C.
c. As the temperature increases, maximum emission occurs at progressively smaller wavelengths (this fact is utilized in the design of optical and electrooptical pyrometers for measuring temperatures).

By setting

$$\frac{dW'_{B,\lambda}}{d\lambda} = 0 \tag{13.1.3}$$

and differentiating the monochromatic emissive power (see (13.1.2)), we find that the wavelength at which maximum emission occurs is expressed by the following equation, called the *Wien displacement law*:

$$(\lambda T)_{\max} = \text{const} = 0.2898 \text{ cm K}. \tag{13.1.4}$$

The total rate of radiant energy emission per unit surface area (*total emissive power*) of a black body is obtained by integrating (13.1.2) over the entire spectrum of wavelengths:

$$W_B = \int_0^\infty W'_{B,\lambda} d\lambda = \int_0^\infty \left(\frac{C_1 \lambda^{-5}}{e^{C_2/\lambda T} - 1} \right) d\lambda. \tag{13.1.5}$$

The above equation has been integrated [1,2] to yield the following simple equation which is called the *Stefan–Boltzmann law of radiation*:

$$W_B = \sigma T^4, \tag{13.1.6}$$

where W_B is the total radiant energy flux (dimensions: $\mathrm{Q\,t^{-1}\,L^{-2}}$) at temperature T (in K); σ is called the *Stefan–Boltzmann radiation constant*, and its theoretical value is 5.669×10^{-8} $\mathrm{W\,K^{-4}\,m^{-2}}$ [3]. Experimental measurements are in close agreement with this number. The generally recommended value of σ for radiation calculations is (Table A2):

$$\begin{aligned}\sigma &= 5.73 \times 10^{-8}\,\mathrm{W\,K^{-4}\,m^{-2}} = 1.37 \times 10^{-12}\,\mathrm{cal\,s^{-1}\,K^{-4}\,cm^{-2}} \\ &= 0.173 \times 10^{-8}\,\mathrm{BTU\,h^{-1}\,R^{-4}\,ft^{-2}},\end{aligned}$$

where R represents degrees Rankin (see Table A1).

Example 13.1.1

The heating element of a laboratory furnace consists of a graphite slab heated electrically to 1000°C. If it is assumed that the graphite slab acts as a black body radiator, calculate the total emissive power of the heating element and the wavelength at which maximum radiation occurs.

On the basis of the Stefan–Boltzmann law of radiation (see (13.1.6)), we calculate

$$W_B = 1.37 \times 10^{-12} \times 1273^4 = 3.598 \text{ cal s}^{-1} \text{ cm}^{-2}.$$

Also, from the Wien displacement law (see (13.1.4)), the wavelength of maximum emission is

$$\lambda_{\max} = \frac{0.2898}{1273} = 0.000228\,\text{cm} = 2.28\,\text{microns}.$$

13.2. EMISSIVITY AND ABSORPTIVITY

We defined a black body as one that absorbs all the radiation reaching its surface. It may also be stated that the monochromatic emissive power of a black body is expressed by Planck's law (see (13.1.2)) and the total radiant energy flux by the Stefan–Boltzmann law (see (13.1.6)). However, most surfaces do not absorb all the incident radiation; also, the radiation emitted at a certain temperature and wavelength is less than predicted by the Planck law. The deviation of a surface from black-body behavior is expressed by means of its **monochromatic emissivity** which is defined as follows:

$$\varepsilon_\lambda = \frac{W'_\lambda}{W'_{B,\lambda}} = \frac{\text{m.c. emissive power of non-black body at } \lambda,\, T}{\text{m.c. emissive power of black body at } \lambda,\, T}. \tag{13.2.1}$$

Emissivity is a function of wavelength and may also depend on the temperature of a body and the angle of the emitted radiation. Theoretically, its value may range from unity to zero. Similarly, the **monochromatic absorptivity** of a body is defined as the fraction of incident radiation that is absorbed by the body:

$$\alpha_\lambda = \frac{\text{radiant energy absorbed by non-black body at } \lambda,\, T}{\text{incident radiant energy on non-black body at } \lambda,\, T}. \tag{13.2.2}$$

In general, the monochromatic emissivity of metals decreases with increasing wavelength while the reverse occurs with non-metals. Emissivity is not a unique property of a material but depends greatly on the condition of the surface. This is illustrated by Fig. 13.3 which shows that aluminum with "commercial" finish has a higher emissivity than polished aluminum. The variation of emissivity with wavelength for some non-metallic materials is shown in Fig. 13.4.

When the radiant energy absorbed and also emitted from a surface does not depend on orientation, i.e., the radiation is **diffuse**, the absorptivity and emissivity are equal:

$$\varepsilon_\lambda = \alpha_\lambda. \tag{13.2.3}$$

The above equation is called the *Kirchoff law*.

Bodies for which the emissive power is independent of direction are called *diffuse emitters*. We can also define the *directional absorptivity* of a surface as the ratio of radiant energy absorbed to the total radiant energy incident on the surface from a given direction. Similar considerations apply to the *directional reflectivity* of a surface. Figure 13.5 illustrates the difference between *specular* and *diffuse* emitters. In the case of a specular reflector, e.g., a mirror, the intensity of the reflected beam is zero except at a certain angle which is called the *specular* angle. On the other hand, for a diffuse reflector, the incident beam is reflected uniformly within the hemispherical space above the surface, irrespective of the angle of incidence.

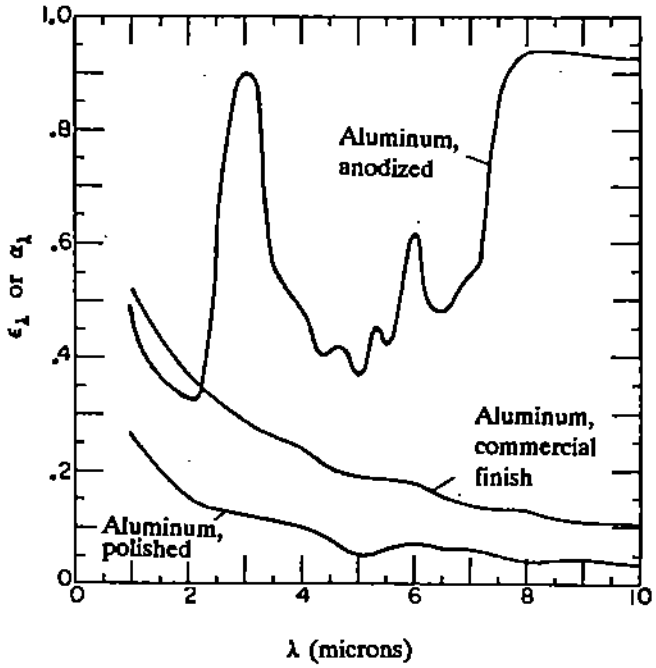

Figure 13.3. Typical emissivity and absorptivity distributions with wavelength for metallic surfaces.

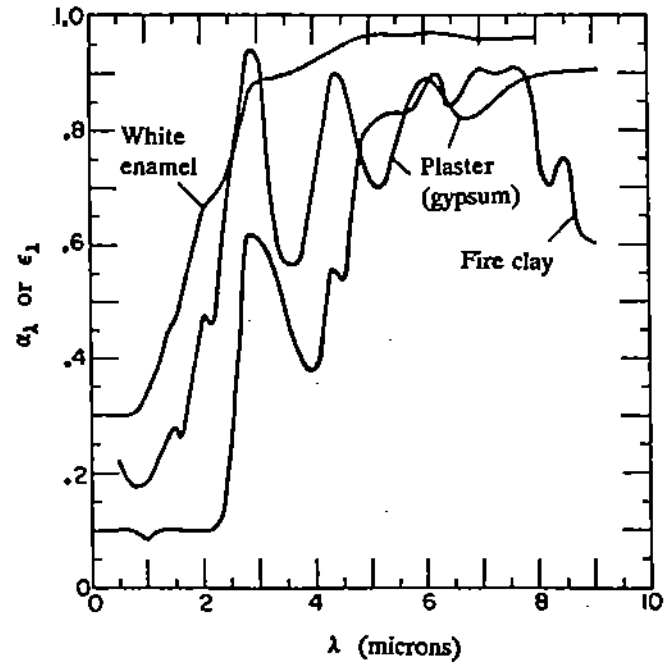

Figure 13.4. Typical emissivity and absorptivity distributions with wavelength for non-metallic surfaces.

Most real surfaces range between these two extremes. It may be said qualitatively that smooth, well-polished surfaces act as specular reflectors while rough surfaces are diffuse reflectors.

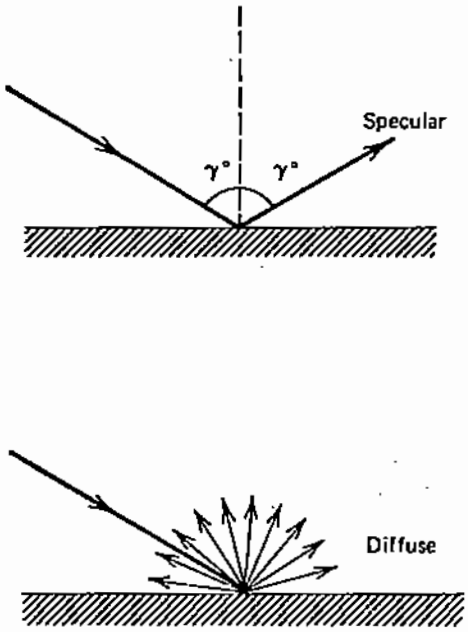

Figure 13.5. Illustration of specular and diffuse reflectance.

It is obvious from the definition of a black body that its emissivity and absorptivity are equal to unity:

$$\epsilon_{B,\lambda} = \alpha_{B,\lambda} = 1. \tag{13.2.4}$$

For a non-black body which does not transmit radiation (e.g., in contrast to glass which allows some radiation to be transmitted through it), the fraction of incident radiation that is not absorbed must be reflected away from the surface (e.g., a mirror reflects radiation). Therefore,

$$\rho_\lambda = 1 - \alpha_\lambda, \tag{13.2.5}$$

where ρ_λ is the monochromatic reflectivity of the surface. Most solids and inorganic melts are opaque and therefore do not transmit radiation. A high-temperature process where the transmission of radiation is important is the glass melting furnace. For transmitting materials

$$\rho_\lambda + \alpha_\lambda + \tau_\lambda = 1 \tag{13.2.6}$$

where τ_λ is the *transmittance* and depends both on the type of material and its thickness.

13.3. TOTAL RADIATION PROPERTIES

The total rate of radiant energy emitted from a surface is obtained by summing the monochromatic energy contributions over the entire spectrum of wavelengths:

$$W = \int_0^\infty W'_\lambda d_\lambda = \int_0^\infty \epsilon_\lambda W'_{B,\lambda} d_\lambda. \tag{13.3.1}$$

By combining (13.3.1) with (13.1.6), we obtain the following definition of the **total emissivity** of a surface:

$$\varepsilon = \frac{\int_0^\infty \varepsilon_\lambda W'_{B,\lambda} d\lambda}{\int_0^\infty W'_{B,\lambda} d\lambda} = \frac{\int_0^\infty \varepsilon_\lambda W'_{B,\lambda} d\lambda}{W_B} = \frac{\int_0^\infty \varepsilon_\lambda W'_{B,\lambda} d\lambda}{\sigma T_s^4}. \tag{13.3.2}$$

Introducing the definition of the total emissivity in (13.3.1), we obtain

$$W = \varepsilon \sigma T_s^4. \tag{13.3.3}$$

The total emissivity is a function of the material, its temperature and surface condition.

The **total absorptivity** is defined in a similar way as follows:

$$\alpha = \frac{\int_0^\infty \alpha_\lambda \, q_{i,\lambda} \, d\lambda}{\int_0^\infty q_{i,\lambda} \, d\lambda}, \tag{13.3.4}$$

where $q_{i,\lambda}$ is the monochromatic radiant energy flux arriving at a surface of absorptivity α.

It should be noted that while the total emissivity depends only on the properties of the emitting surface (type of material, roughness, temperature), the total absorptivity is also dependent on the spectral distribution of the incident radiation. Consequently, Kirchhoff's law on monochromatic emissivity and absorptivity (see (13.2.3)) cannot be generalized for the total radiation properties.

13.3.1. Definition of a Gray Body

There are many real surfaces which are not black bodies but exhibit a similar distribution of emissive power with wavelength, with the exception that the monochromatic energy flux is smaller than the corresponding black-body flux (Planck radiation law, see (13.1.2)), by a fixed ratio; in other words, their monochromatic emissivity and absorptivity remain constant with wavelength. Such surfaces are called *gray bodies*. The assumption that a surface behaves like a gray body is made frequently since it allows the use of total radiation properties which are more readily available in the literature than the monochromatic radiation properties. Many of the electrical non-conductors and semiconductors can be considered to belong to this class.

Example 13.3.1

The variation of monochromatic emissivity of a chromium plate with wavelength is as follows:

λ (microns)	0.9	2.0	3.5	5.0	8.0
ε_λ	0.73	0.64	0.54	0.49	0.41

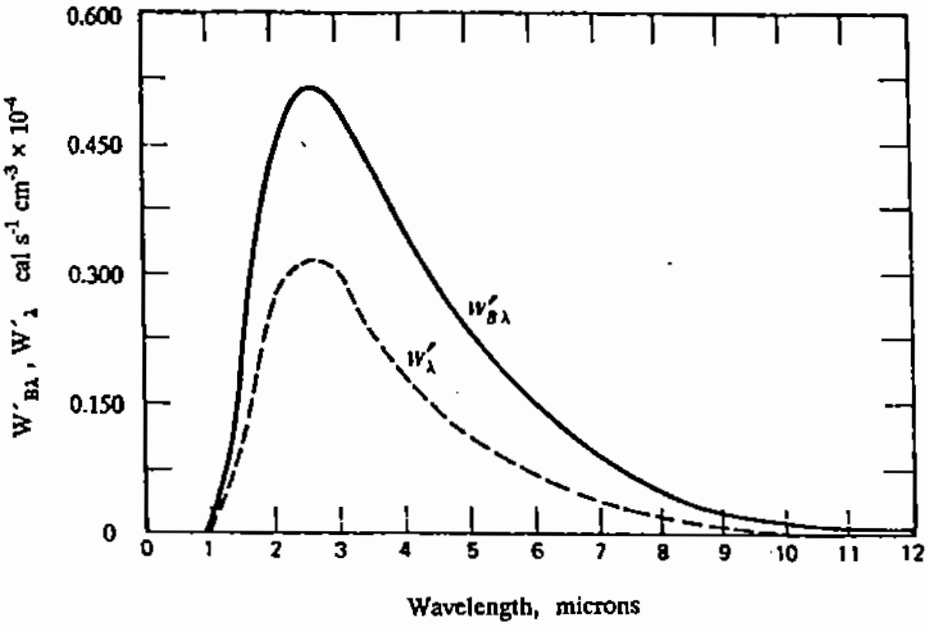

Figure 13.6. Comparison of monochromatic emissive power of a black and a gray body at 1100 K.

Calculate the total emissivity of this surface at 1100 K.

The monochromatic radiation from a black body, in the wavelength range under consideration, is calculated from (13.1.2) and is shown in Fig. 13.6. By multiplying the black body radiation by the above corresponding emissivities, we obtain the monochromatic emissive power of the chromium surface:

$$W'_\lambda = \varepsilon_\lambda W'_{B,\lambda},$$

which is also plotted in Fig. 13.6. Since the wavelength range of significant emission extends from 1 to 10 microns, the total radiant emissive power is

$$\int_{\lambda=1\mu}^{\lambda=10\mu} \varepsilon_\lambda W'_{B,\lambda} d\lambda.$$

This integral is represented by the area under the W_λ plot of Fig. 13.6 between limits $1 < \lambda < 10$ and is found to have the value of 1.06 cal s^{-1} cm^{-2}. Finally, by using the definition of the total emissivity (see (13.3.2)) we obtain

$$\varepsilon = \frac{1.06}{1.37 \times 10^{-12} \times 1100^4} = 0.53.$$

13.3.2. Values of Total Emissivity

A tabulation of the total emissivities of a number of materials is presented in Table 13.1; for a more extensive tabulation of radiative properties, the reader is referred to Siegel and Howell [2]. In general, clean, highly polished metallic surfaces have very low emissivities which can be increased by coating or the formation of oxide films. The emissivity of metallic surfaces increases with temperature, partly due to the fact that the monochromatic emissivity

of metals decreases with increasing wavelength. Nonmetallic materials are characterized by high emissivities in the infrared portion of the spectrum.

Table 13.1 shows that there is considerable variation in the total emissivity of some materials, even over a narrow range of temperature. The reason for this is that it is very difficult to characterize fully the roughness of different surfaces prepared by different investigators. Caution should be exercised in using emissivity data, particularly in the low emissivity range, for calculations where a high degree of accuracy is required.

Example 13.3.2

Compare the heat losses by radiation and convection per unit area from the top surface of a horizontal steel slab at 200 and 1200°C. It may be assumed that the emissivity of the steel slab at both temperatures is 0.6 and the temperature of the atmosphere above the plate (T_a) is 20°C.

The radiant flux is obtained from the Stefan–Boltzmann radiation law (see (13.1.6)) for the given value of emissivity:

$$\begin{aligned}
\text{at } 200^\circ\text{C},\ q_r &= W = \varepsilon\sigma(T_s^4 - T_a^4) \\
&= 0.6 \times 1.37 \times 10^{-12} \times (473^4 - 293^4) = 0.035 \text{ cal s}^{-1}\text{ cm}^{-2} \\
\text{at } 1200^\circ\text{C},\ q_r &= 0.6 \times 1.37 \times 10^{-12} \times (1473^4 - 293^4) \\
&= 3.86 \text{ cal s}^{-1}\text{ cm}^{-2}.
\end{aligned}$$

The convective loss can be calculated from the heat convection equation (Chapter 12):

$$q_c = h(T_s - T_a). \tag{13.3.5}$$

In this case, the heat transfer coefficient h may be computed from the following empirical equation for heat transfer to air from an upward facing horizontal plate:

$$h = 5 \times 10^{-5}(T_s - T_a)^{0.25}, \tag{13.3.6}$$

where all units are in the metric system. By combining the above two equations, we obtain the heat loss by convection:

$$\text{at } 200^\circ\text{C},\ q_c = 5 \times 10^{-5} \times (200 - 20)^{1.25} = 0.033 \text{ cal s}^{-1}\text{ cm}^{-2},$$

$$\text{at } 1200^\circ\text{C},\ q_c = 5 \times 10^{-5} \times (1200 - 20)^{1.25} = 0.346 \text{ cal s}^{-1}\text{ cm}^{-2}.$$

The above calculations show that at 200°C the radiative and convective losses are comparable, while at 1200°C the radiative loss is nearly ten times greater.

13.4. RADIANT HEAT TRANSFER BETWEEN BLACK-BODY SURFACES

Up to this point we have considered the special case where a single surface either emits or absorbs radiant energy from the environment. However, in an enclosure consisting of a number of surfaces, the *net* radiation emitted by one surface depends not only on the temperature and emissivity of that surface but also on the radiation received from all other surfaces in the enclosure. Thus, the radiant energy/time emitted by surface *1* and intercepted

Table 13.1. Total Emissivities of Various Surfaces

Surface	Temperature, °C	Emissivity[a]
Aluminum		
bright foil	20	0.04
polished plate	100	0.09
heavily oxidized	100–540	0.20–0.33
Chromium, polished	20–1100	0.08–0.40
Copper		
polished	20–260	0.04–0.05
black oxidized	30–600	0.78
molten copper	1080–1280	0.16–0.13
Iron		
casted and heated	880–1000	0.60–0.70
wrought, polished	40–250	0.28
steel sheet, oxidized	20	0.66
oxidized at 600°	200–600	0.64–0.78
Iron oxide	200–1200	0.85–0.89
Steel plate, rough surface	20–370	0.94–0.97
Molten surfaces		
copper	1080–1280	0.16–0.13
iron for casting	1300–1400	0.29
steel	1500–1600	0.42–0.53
Lead		
polished	30–300	0.06–0.08
rough, unoxidized	40	0.40
Silver, polished	100	0.02–0.05
Tantalum filament	1300–3000	0.19–0.31
Thorium oxide	270–830	0.58–0.21
Commercial tin-plated sheet	100	0.05
Tungsten filament	25–3300	0.032–0.35
Zinc, comm. grade,		
polished	220–320	0.045–0.053
heated in air at 400°	400	0.11
galvanized sheet	100	0.21
Alumina (99.5–85% Al_2O_3; 0–12% SiO_2; 0–1 Fe_2O_3), 100–10 grain size	1000–1600	0.50–0.18
Alumina-silica (80–58% Al_2O_3, 16–18SiO_2, 0.4Fe_2O_3)	1000–1600	0.61–0.43
Fireclay brick	1000	0.75
Carbon		
filament	1000–1400	0.53
rough plate	100–500	0.77–0.72
Silicon carbide (87%SiC; 2.3 g cm^{-3})	1000–1400	0.92–0.82
Glass (pyrex, lead, and soda)	250–550	0.95–0.85
Magnesite brick	1000	0.38
Quartz, fused	20	0.93

[a]Temperatures and emissivities appearing in pairs and separated by dashes correspond and can be interpolated linearly.

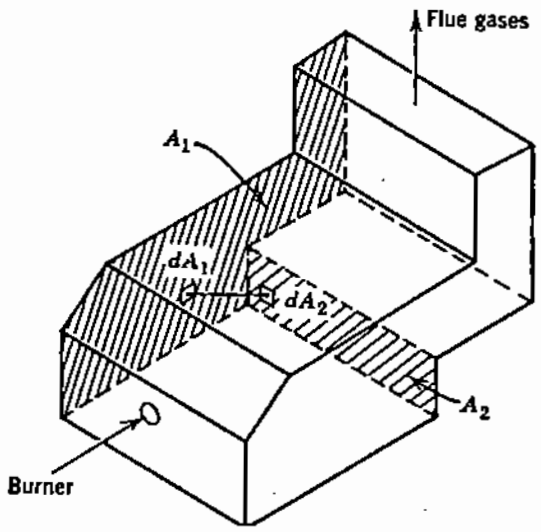

Figure 13.7. Illustration of radiation surfaces in a furnace enclosure.

by surface 2 will be denoted by $Q_{1\to 2}$ or, for short, Q_{12}. The same notation will be used for radiant energy fluxes (e.g., $q_{12}, q_{21}, \ldots$) and for the view factors to be discussed in the next section.

13.4.1. Geometric View Factors

In order to calculate the exchange of radiant energy between surfaces, it is convenient to consider a fully enclosed system for which all radiant energy emitted from a given surface can be accounted for. If the system under consideration is not enclosed physically, we may "construct" imaginary surfaces so as to complete the enclosure. For example, in the case of an open window in a furnace, where all the incident radiation is lost from the enclosure (i.e., there is negligible back radiation from the environment), it may be assumed that the open window corresponds to a black body surface at zero absolute temperature.

Let us now consider an enclosure consisting of n surfaces (Fig. 13.7) and assume that the radiation flux within the enclosure is diffuse, that is, it has no angular dependence. If A_1 and A_2 are two of the surfaces in this enclosure, the **geometric view factor** between them, F_{12}, is defined as *the fraction of radiation emitted by surface A_1 and intercepted by surface A_2*; the first subscript represents the emitting surface and the second the intercepting. In radiant heat transfer equations, the emitted energy is shown as a positive term and the incident energy as negative.

Stating the above definition in more general terms, the view factor, F_{kj}, between two surfaces A_k and A_j in an enclosure, represents the fraction of radiation emitted by surface A_k and intercepted by surface A_j. The geometric view factors depend only on the geometry of the system and are not affected either by the temperature or the emissivity of the surfaces, provided that the assumption of diffuse radiation is satisfied.

For a mathematical definition of the view factor, let us consider two surfaces, A_1 and A_2 located at a distance r apart in an enclosure (Fig. 13.8); each surface emits radiation over the entire hemisphere above it. Let us now consider the infinitesimal area elements dA_1 and dA_2 on the two surfaces; if the angles formed by the connecting line with the normals on the two surfaces, n_1 and n_2, are β_1 and β_2, respectively, it can be shown by

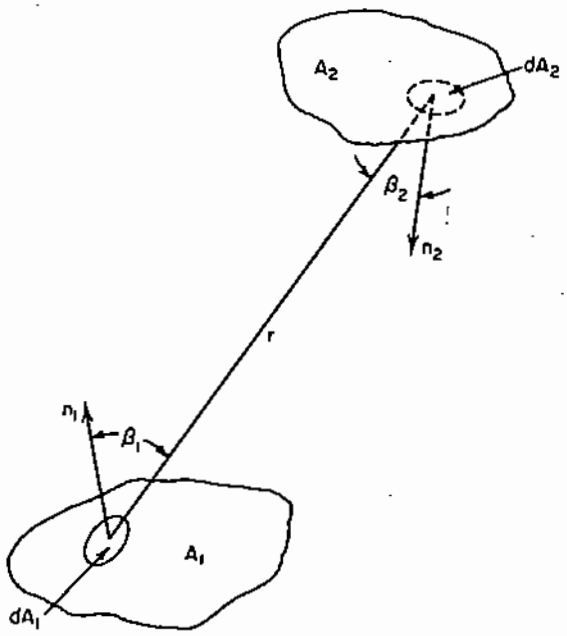

Figure 13.8. View factor between two infinitesimal surfaces separated by distance r.

solid geometry that the fraction of the hemispherical radiation emitted by surface *1* and intercepted by surface 2 is represented by the following equation:

$$F_{A_1 \to A_2} = \frac{1}{A_1} \int_0^{A_1} \int_0^{A_2} \frac{\cos\beta_1 \cos\beta_2}{\pi r^2} \, dA_1 \, dA_2. \tag{13.4.1}$$

A similar equation is derived for the reverse situation:

$$F_{A_2 \to A_1} = \frac{1}{A_2} \int_0^{A_1} \int_0^{A_2} \frac{\cos\beta_1 \cos\beta_2}{\pi r^2} \, dA_1 \, dA_2. \tag{13.4.2}$$

Comparison of (13.4.1) and (13.4.2) shows that the following *reciprocity rule* applies to view factors:

$$A_1 F_{1 \to 2} = A_2 F_{2 \to 1}, \tag{13.4.3}$$

or in more general form:

$$A_i F_{ij} = A_j F_{ji}. \tag{13.4.4}$$

The reciprocity rule may also be proved by the following reasoning: Consider two black-body surfaces in an enclosure in which all other surfaces are also black and at absolute zero temperature (therefore, $q = 0$); thus, the amount of radiation emitted from surface *1* and intercepted by surface *2* is expressed as

$$Q_{1 \to 2} = \sigma A_1 F_{12} T_1^4. \tag{13.4.5}$$

Also, the amount of radiation from surface 2 intercepted by surface *1* is

$$Q_{2 \to 1} = \sigma A_2 F_{21} T_2^4. \tag{13.4.6}$$

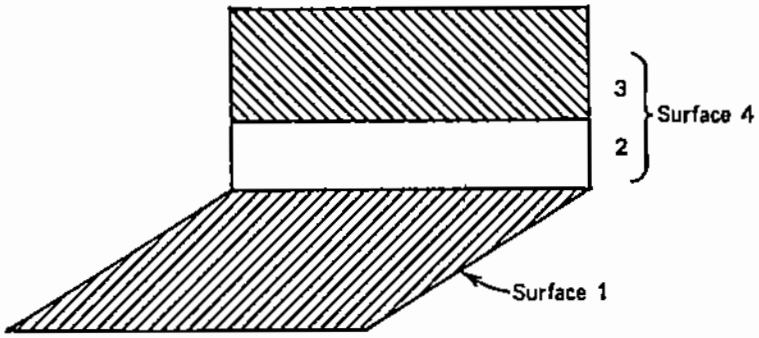

Figure 13.9. Perpendicular rectangles in a furnace enclosure.

Therefore, the *net* heat transfer by radiation from surface *1* to surface *2* is

$$Q_{12} = \sigma A_1 F_{12} T_1^4 - \sigma A_2 F_{21} T_2^4. \tag{13.4.7}$$

The above equation is true for all values of T_1 and T_2. Obviously, when $T_1 = T_2$ the net transfer of radiation between the two surfaces must be zero, and (13.4.4) yields the required proof:

$$A_1 F_{12} = A_2 F_{21}. \tag{13.4.8}$$

Considering the definitions of the radiation enclosure and of the view factor, we can conclude that all radiation emitted from one surface, A_i, must be intercepted by some or all of the other surfaces in the enclosure. Therefore, we may write

$$\sum_{j=1}^{n} F_{kj} = 1, \tag{13.4.9}$$

where k is any one of the n surfaces in the enclosure.

13.4.2. View Factor Calculations

As discussed earlier, view factors are calculated using the principles of solid geometry. Fortunately, the view factors for many geometric configurations have been worked out and published in the literature [2,5]. In this section, we shall present some of these formulae and describe a method for using view factors available in the literature to compute the view factors for other configurations. This technique is called "view factor algebra."

As an illustration, consider the geometric configuration of Fig. 13.9. In this case, surface *4* is equal to surface *2* plus surface *3*. Mathematical formulae are available for the view factors between the perpendicular surfaces *1* and *2* and also between surface *1* and *4*. However, we need to find the view factor between the surfaces *1* and *3*. Consideration of the geometry of the system (Fig. 13.9) shows that the following relationship must be true:

$$A_1 F_{14} = A_1 F_{12} + A_1 F_{13}.$$

Therefore, we can obtain the value of the unknown F_{13} by subtracting the known values of F_{14} and F_{12}:

$$F_{13} = F_{14} - F_{12}.$$

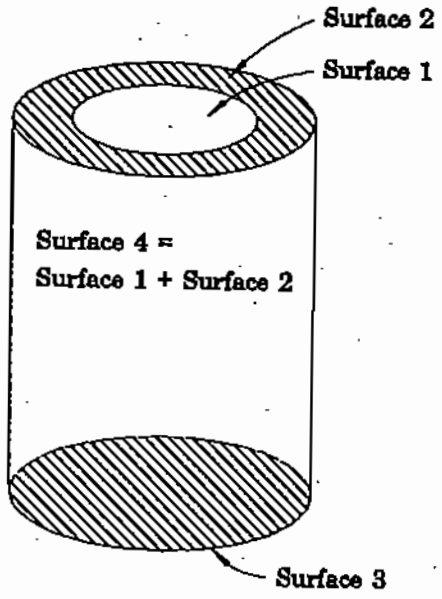

Figure 13.10. Parallel disks in a furnace enclosure.

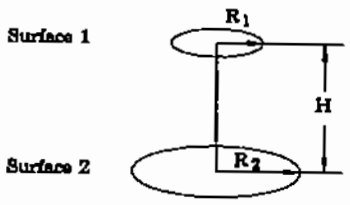

$$F_{12} = \frac{1}{2}\left[a - \sqrt{a^2 - 4\left(\frac{b}{c}\right)^2}\right]$$

where:

$$b = \frac{R_1}{H}, \quad c = \frac{R_2}{H}, \quad a = 1 + (1 + b^2)\frac{1}{c^2}$$

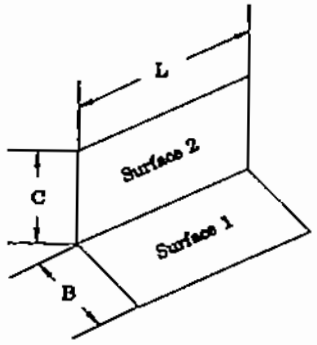

$$F_{12} = \frac{1}{\pi}\left[\tan^{-1}\left(\frac{1}{b}\right) + \frac{b}{2}\ln\frac{b^2(a+1)}{a(b^2+1)} - \frac{b}{\sqrt{a}}\tan^{-1}\left(\frac{b}{\sqrt{a}}\right)\right]$$

where:

$$b = \frac{B}{L}, \quad c = \frac{C}{L}, \quad a = b^2 + c^2$$

Figure 13.11. Examples of derived formulae for view factors between surfaces.

Another example of the use of this technique is presented in Fig. 13.10; the view factor between the bottom disk *3* and the top ring *2* is obtained by subtracting the known view

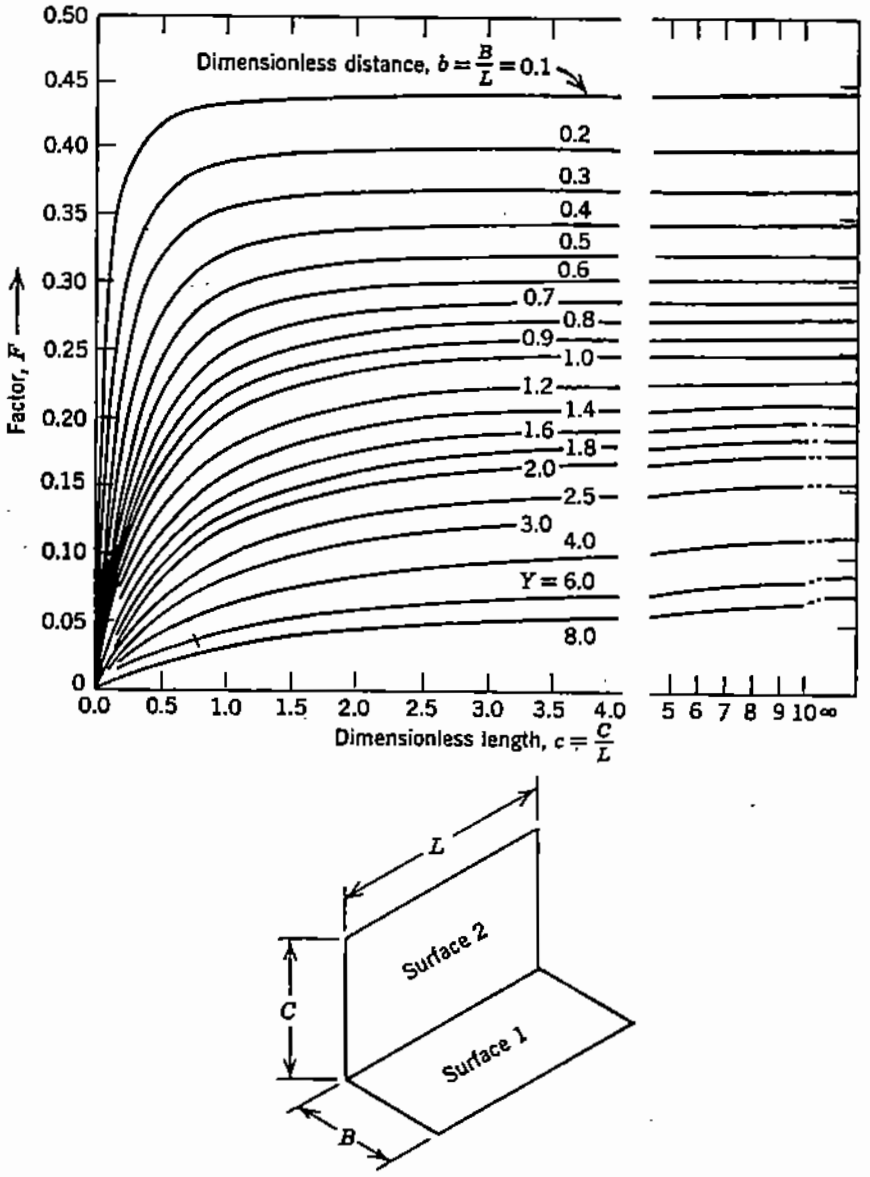

Figure 13.12. Calculated view factors between two perpendicular rectangles.

factors for disk-to-disk radiation:

$$F_{32} = F_{34} - F_{31}.$$

Examples of the formulae derived for the geometric factors between perpendicular rectangles and between parallel disks are shown in Fig. 13.11. Calculated values of the view factors between perpendicular rectangles are plotted in Fig. 13.12.

13.4.3. Radiation Within a Black-Body Enclosure

Consider an enclosure (Fig. 13.13) which is divided into n isothermal black-body surfaces, $A_1, A_2, \ldots, A_n$, maintained at temperatures $T_1, T_2, \ldots, T_n$, respectively. The *net* radiation

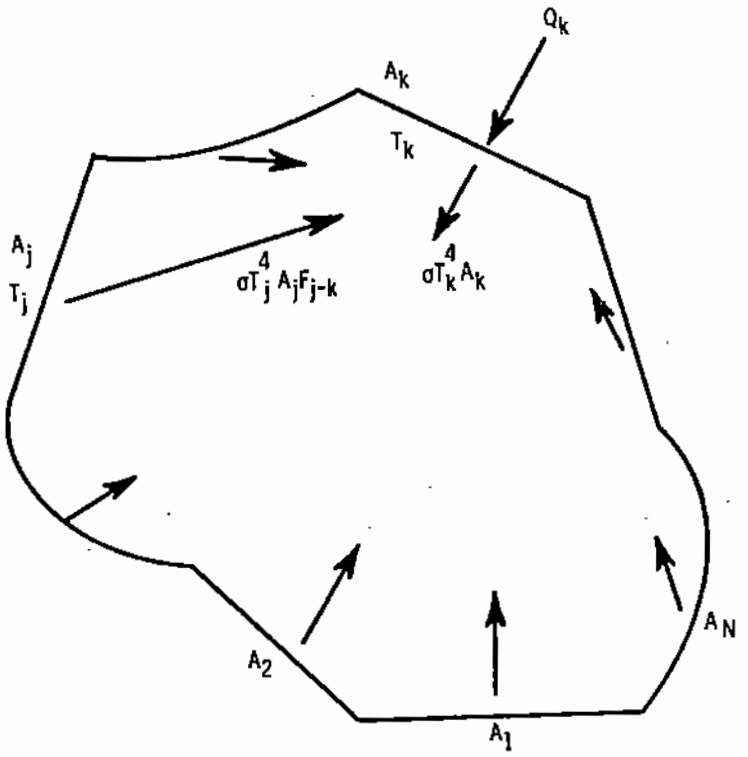

Figure 13.13. Black-body enclosure of n isothermal surfaces.

from surface A_k is the emission from the surface k minus the sum of the incident radiation from all other surfaces j:

$$Q_k = \sigma A_k T_k^4 - \sigma A_k \sum_{j=1}^{n} F_{kj} T_j^4. \tag{13.4.10}$$

By using (13.4.9), we can rewrite the above equation as a generalized rate equation for radiant heat transfer between black-body surfaces in an enclosure:

$$\frac{Q_k}{A_k} = q_k = \sigma \sum_{j=1}^{n} F_{kj} \left(T_k^4 - T_j^4\right). \tag{13.4.11}$$

It should be noted that the sum of the view factors includes the self-view factor F_{kk}, that is the radiation received from the surface itself. This is possible only when the isothermal surface k is concave, e.g., in the case of a concave roof of a furnace, or when it is assumed to consist of more than one planar surface.

Equations (13.4.10) and (13.4.11) are used in radiation problems to determine either the required heat input to a particular surface, Q_k, or the temperature of a surface on the basis of the known fluxes and temperatures at the other surfaces of the enclosure. For example, let us consider a black-body enclosure consisting of n surfaces; the temperature is specified at $(n-1)$ surfaces and the net input radiant flux is specified at the remaining surface, A_k.

It is required to determine the temperature at that surface, T_k. By subtracting the self-view function of radiation $\sigma F_{kk} T^4$ from the sum in (13.4.11) and solving for T_k, we obtain

$$T_k^4 = \frac{(q_k/\sigma) + \sum_{j=1,\neq k} F_{kj} T_j^4}{1 - F_{kk}}. \tag{13.4.12}$$

One of the most common situations encountered in furnace enclosures is that one surface may be considered as a radiation *source* (e.g., flame, arc, heating elements) and another as a radiation *sink* (e.g., molten bath surface, metal strip in an annealing furnace). In comparison to these two types of surfaces, the radiant heat emitted or absorbed from all other surfaces may be assumed to be negligible; such surfaces are usually lined with refractory insulation and the heat losses by conduction through the wall may be small in comparison to the source-to-sink radiation level in the furnace.

Under these conditions, a furnace enclosure may be assumed to consist of a "source" surface, a "sink" surface, and a number of "zero-flux" surfaces which re-radiate (i.e., reflect) to the enclosure nearly all of the incident radiation.

If we designate these three types of surfaces by A_1 for the source, A_2 for the sink, and A_R for the "zero-flux" surfaces, we have for a black-body enclosure

$$Q_{1R} = F_{1R}\sigma A_1(T_1^4 - T_R^4) = Q_{R2} = F_{R2}\sigma A_R(T_R^4 - T_2^4), \tag{13.4.13}$$

where Q_{1R} is the radiation from the source surface *1* intercepted by surface R and Q_{R2} the re-radiation from surface R to the sink surface *2*. The reciprocity rule yields

$$F_{R2}A_R = F_{2R}A_2. \tag{13.4.14}$$

Substituting from (13.4.14) into (13.4.13) and solving for T_R, we obtain

$$T_R^4 = \frac{F_{1R}A_1T_1^4 + F_{2R}A_2T_2^4}{F_{1R}A_1 + F_{2R}A_2}. \tag{13.4.15}$$

Of course, part of the radiation leaving A_1 is intercepted directly by A_2; therefore, the net flux between A_1 and A_2 consists of two terms:

$$Q_{12,\text{net}} = F_{12}\sigma A_1(T_1^4 - T_2^4) + F_{1R}\sigma A_1(T_1^4 - T_R^4). \tag{13.4.16}$$

If the temperatures T_1 and T_2 are specified, T_R can be calculated from (13.4.15); this value is then used in (13.4.16) to yield the required net heat input, $Q_{12,\text{net}}$, to the source surface.

The use of the above equations is illustrated in the following examples.

Example 13.4.1

The enclosure of an annealing furnace can be divided into three radiating surfaces at temperature $T_1 = 1500$ K, $T_2 = 1000$ K, and $T_3 = 600$ K, respectively. Assuming black-body conditions, calculate the radiant heat flux from surface *1*, if the view factors are

$$F_{11} = 0.15, \quad F_{12} = 0.25, \quad F_{13} = 0.6.$$

To solve this problem, we use (13.4.11):

$$q_1 = 1.37 \times 10^{-12} \left[1500^4 - 0.15 \times 1500^4 - 0.25 \times 1000^4 - 0.6 \times 600^4\right]$$
$$= 5.446 \text{ cal s}^{-1} \text{ cm}^{-2}.$$

Example 13.4.2

The following conditions are specified at the four black surfaces of an enclosure:

$$\text{at } A_1,\ T_1 = 2000 \text{ K}, \quad \text{at } A_2,\ q_2 = 0,$$
$$\text{at } A_3,\ T_3 = 1000 \text{ K}, \quad \text{at } A_4,\ T_4 = 293 \text{ K}.$$

The zero flux specified at surface 2 signifies a condition of "perfect insulation" behind this surface. Surface *4* is obviously a window or other opening to the atmosphere. The calculated view factors are given as

$$F_{21} = 0.2,\ F_{22} = 0.15,\ F_{23} = 0.4, F_{24} = 0.25,$$
$$F_{41} = 0.5,\ F_{42} = 0.2,\ F_{43} = 0.3.$$

It is required to calculate the net heat flux by radiation at the surface *4*.
We may proceed by calculating T_2 from (13.4.12):

$$T_2^4 = \frac{0.2 \times 2000^4 + 0.4 \times 1000^4 + 0.25 \times 293^4}{1 - 0.15} \quad T_2 = 1435 \text{ K}.$$

The net flux at surface *4* is then computed by using (13.4.11):

$$q_4 = 1.37 \times 10^{-12}[293^4 - (0.5 \times 2000^4 + 0.2 \times 1435^4 + 0.3 \times 1000^4)] = -12.52 \text{ cal s}^{-1} \text{ cm}^{-2}.$$

The negative sign indicates that the radiation received at surface *4* is greater than the radiation emitted. In this case, the net radiant flux at surface *4* represents a heat loss by radiation through a furnace port. It is also interesting to note that surface 2, which has a zero net flux, nevertheless contributes to the net flux to surface *4*.

13.5. RADIATION BETWEEN GRAY-BODY SURFACES

As discussed earlier, in contrast to black bodies where the emissivity is assumed to be unity, part of the incident radiation on real surfaces is absorbed and part is reflected. In order to develop the equation for radiant heat transfer in this case, let us make the following simplifying assumptions:

a. The surfaces are gray-body so that emissivity and absorptivity are equal and independent of wavelength.
b. The incident, emitted and reflected radiation are independent of direction.
c. The radiating surfaces are isothermal and the radiant flux is uniform along each surface.

Despite these simplifying assumptions, the radiative exchange within an enclosure of real surfaces is very complex: Radiation leaves a surface, travels to other surfaces and part of it is reflected many times before it is absorbed totally. Since it is not possible to "follow"

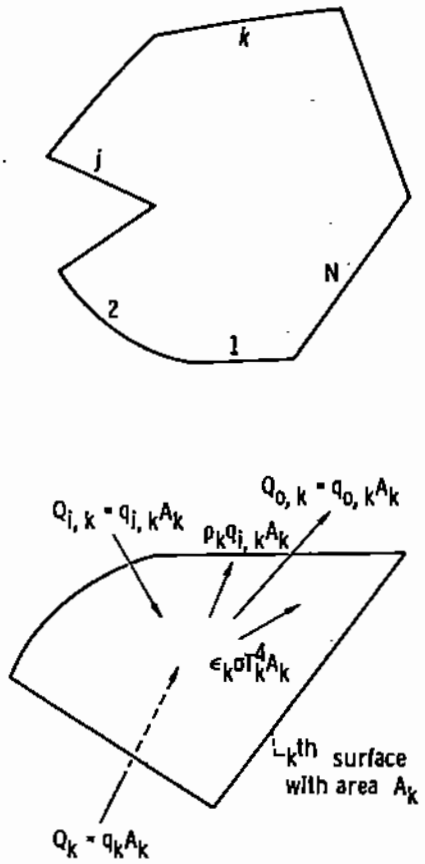

Figure 13.14. Illustration of enclosure of n surfaces (top) and of fluxes entering or leaving surface k (bottom).

the beams of radiation, it is convenient to describe quantitatively radiant heat transfer by means of the *net radiation method*, originally proposed by Hottel [7].

Let us consider an enclosure of n surfaces in an enclosure (Fig. 13.14). The bottom part of Fig. 13.14 shows the various fluxes entering or leaving the surface k of area A_k in the enclosure. The *net* heat to surface k, Q_k, can be expressed as follows:

$$Q_k = A_k q_k = A_k(q_{k,o} - q_{k,i}), \tag{13.5.1}$$

where $q_{k,o}$ represents the total radiation leaving the surface k ("outgoing" radiation) and is called the **radiosity** of the surface k. The radiosity consists of two terms: the radiation emitted directly from surface k, according to the Stefan–Boltzmann law, and the reflected radiation received by surface k from all other surfaces in the enclosure:

$$q_{k,o} = \epsilon_k \sigma T_k^4 + \rho_k q_{k,i}, \tag{13.5.2}$$

where ρ_k is the reflectivity of surface k and $q_{k,i}$, represents the *incident* (i.e.,"incoming") radiation on surface A_k from all other surfaces in the enclosure. As discussed earlier (see (13.2.5)), for opaque, gray surfaces,

$$\rho_k = 1 - \alpha_k = 1 - \epsilon_k. \tag{13.5.3}$$

Therefore, (13.5.2) can be written as

$$q_{k,o} = \varepsilon_k \sigma T_k^4 + (1 - \varepsilon_k) q_{k,i}. \tag{13.5.4}$$

The incident radiation on surface k, $q_{k,i}$, is equal to the sum of radiations received at surface k from all other surfaces in the enclosure:

$$A_k q_{k,i} = F_{1k} A_1 q_{1,o} + F_{2k} A_2 q_{2,0} + F_{3k} A_3 q_{3,o} + \ldots + F_{kk} A_k q_{k,o} + \ldots + F_{jk} A_j q_{j,o}. \tag{13.5.5}$$

However, the reciprocity rule for geometric factors (see (13.4.3)) yields

$$F_{1k} A_1 = F_{k1} A_k; \;\; F_{2k} A_2 = F_{k2} A_k; \;\ldots\ldots; \; F_{kj} A_j = F_{jk} A_k.$$

Therefore, (13.5.5) can be written so that the only area appearing in all terms on both sides of the equation is A_k:

$$A_k q_{k,i} = F_{k1} A_k q_{1,o} + F_{k2} A_k q_{2,o} + F_{k3} A_k q_{3,o} + \ldots + F_{kk} A_k q_{k,o} + \ldots + F_{kj} A_k q_{j,o}, \tag{13.5.6}$$

or

$$q_{k,i} = \sum_{j=1}^{n} F_{kj} q_{j,o}. \tag{13.5.7}$$

We now have two equations ((13.5.4) and (13.5.7)) for $q_{k,i}$. By combining them, we eliminate $q_{k,i}$ and obtain two equations for the *net* heat radiation from surface A_k:

$$q_k = \frac{\varepsilon_k}{1 - \varepsilon_k} \left(\sigma T_k^4 - q_{k,o} \right), \tag{13.5.8}$$

and

$$q_k = q_{k,o} - \sum_{j=1}^{n} F_{kj} q_{j,o}. \tag{13.5.9}$$

It can be seen that (13.5.8) and (13.5.9) can be written for each of the n surfaces in the enclosure. This will result in $2n$ equations with $2n$ unknowns; the radiosities q_0 from each surface will amount to n of the unknowns, while the remaining n unknowns will consist of various q and T, depending on the boundary conditions of the problem.

For example, for a gray-body enclosure of three surfaces, (13.5.8) yields the following three equations:

$$\begin{aligned} q_{1,o} &= \varepsilon_1 \sigma T_1^4 + (1 - \varepsilon_1)(F_{11} q_{1,o} + F_{12} q_{2,o} + F_{13} q_{3,o}), \\ q_{2,o} &= \varepsilon_2 \sigma T_2^4 + (1 - \varepsilon_2)(F_{21} q_{1,o} + F_{22} q_{2,o} + F_{23} q_{3,o}), \\ q_{3,o} &= \varepsilon_3 \sigma T_3^4 + (1 - \varepsilon_3)(F_{31} q_{1,o} + F_{32} q_{2,o} + F_{33} q_{3,o}). \end{aligned} \tag{13.5.10}$$

This system of equations can be solved easily by means of matrix algebra, as illustrated in the following example.

Example 13.5.1

An experimental furnace has the approximate geometry of a vertical cylinder. If the enclosure is assumed to consist of the three isothermal surfaces A_1, A_2, and A_3, calculate the net

heat flux at each surface for the following conditions: $A_1 = 3\ \text{m}^2$, $A_2 = 3\ \text{m}^2$, $A_3 = 12\ \text{m}^2$ (cylindrical wall), $T_1 = 1400$ K, $T_2 = 900$ K, $T_3 = 300$ K; $\varepsilon_1 = 0.8$, $\varepsilon_2 = 0.4$, $\varepsilon_3 = 0.7$; $F_{11} = 0$, $F_{22} = 0$, and $F_{12} = 0.38$.

Using the reciprocity rule (see (13.4.4)) and (13.4.9), we can calculate the remaining view factors:

$$F_{13} = 1 - F_{12} - F_{11} = 0.62, \quad F_{23} = 1 - F_{21} - F_{22} = 0.62,$$
$$F_{31} = F_{13}\frac{A_1}{A_3} = 0.65 \times \frac{3}{12} = 0.155$$
$$F_{32} = 0.155, \quad F_{33} = 1 - F_{31} - F_{32} = 0.69.$$

13.5.10

Substituting the numerical values of emissivities, temperatures, and view factors in (13.4.20), we have three equations and three unknowns, $q_{1,0}$, $q_{2,0}$, and $q_{3,0}$. By collecting all the unknown radiosities on the right-hand side of the equation and grouping the $q_{1,0}$, $q_{2,0}$, and $q_{3,0}$ terms in three terms, we obtain:

$$\begin{aligned}
\varepsilon_1\sigma T_1^4 &= [1 - (1-\varepsilon_1)F_{11}]q_{1,o} - (1-\varepsilon_1)F_{12}q_{2,o} - (1-\varepsilon_1)F_{13}q_{3,o},\\
\varepsilon_2\sigma T_2^4 &= -(1-\varepsilon_2)F_{21}q_{1,o} + [1 - (1-\varepsilon_2)F_{22}]q_{2,o} - (1-\varepsilon_2)F_{23}q_{3,o},\\
\varepsilon_3\sigma T_3^4 &= -(1-\varepsilon_3)F_{31}q_{1,o} - (1-\varepsilon_3)F_{32}q_{2,o} + [1 - (1-\varepsilon_3)F_{33}]q_{3,o}.
\end{aligned} \tag{13.5.11}$$

This problem in matrix algebra can be solved using the matrix solution facility of the Lotus 1-2-3 [10], or a similar spreadsheet program, as follows. The system of equations (13.5.11) can be expressed in matrix form as

$$\boldsymbol{A} = \boldsymbol{C}\,\boldsymbol{X},$$

where $\boldsymbol{A}$ represents the known terms on the left-hand side of (13.5.11), $\boldsymbol{C}$ the coefficients of the unknown radiosities and $\boldsymbol{X}$ the three unknown radiosities. The coefficients $\boldsymbol{A}$ and $\boldsymbol{C}$ are computed from the known emissivities, temperatures and view factors and are entered in cells B14-B16 and C14-E16, respectively (Fig. 13.15). The Data, Matrix, Invert facility of the LOTUS 123 program is then used to invert the coefficients $\boldsymbol{C}$ and place the results of the inversion in cells C18-E20. We now use the Data, Matrix, Multiply facility of LOTUS 123 to multiply the coefficients $\boldsymbol{A}$ by the inverted coefficients $\boldsymbol{C}$:

$$\boldsymbol{X} = \frac{1}{\boldsymbol{C}} \times \boldsymbol{A},$$

and yield the values of the three unknown radiosities (cells G14-G16, Fig. 13.15). The net heat flux at each of the three surfaces is thus calculated to be:

$$q_1 = 4.3705,\ q_2 = 1.4955,\ q_3 = 0.3749,\ \text{all in cal}\,\text{s}^{-1}\,\text{cm}^{-2}.$$

	A	B	C	D	E	F	G
1							
2		Stefan-Boltzmann constant:			1.37E-12		
3			Surf. 1	Surf.2	Surf.3		
4		Area, m2	3	3	12		
5		Temp., K	1400	900	400		
6		Emissivity	0.8	0.4	0.7		
7		Calculated				Sum of F	
8		View factors, F:				for A1, etc.	
9		11, 12, 13	0	0.38	0.62	1	
10		21, 22, 23	0.38	0	0.62	1	
11		31, 32, 33	0.155	0.155	0.69	1	
12						Calc'd radiosities:	
13	Temp, K	A coeff't's		C coeff't's			cal/(s cm2)
14	1400	4.2103936	1	-0.076	-0.124	$q_{1,o}$:	4.370543
15	900	0.7190856	-0.228	1	-0.372	$q_{2,o}$:	1.495501
16	400	0.0280576	-0.0465	-0.0465	0.793	$q_{3,o}$:	0.374932
17			Inverted C coeff't's:				
18			1.029375	0.087628	0.202068		
19			0.262886	1.044678	0.531170		
20			0.075775	0.066396	1.304029		

Figure 13.15. Lotus 1-2-3 screen after solution of matrix problem of Example 13.4.3.

Example 13.5.2

Derive an equation for the radiant heat transfer between two infinite parallel plates at temperatures T_1 and T_2 respectively, when $T_1 > T_2$.

Since all radiation leaving plate *1* will reach plate 2, $F_{12} = F_{21} = 1$. Therefore, (13.5.8)–(13.5.9) are expressed as follows for plate *1*:

$$q_1 = \frac{\varepsilon_1}{1-\varepsilon_1}\left(\sigma T_1^4 - q_{1,o}\right), \tag{13.5.12}$$

$$q_1 = q_{1,o} - q_{2,o}, \tag{13.5.13}$$

and for plate 2:

$$q_2 = \frac{\varepsilon_2}{1-\varepsilon_2}\left(\sigma T_2^4 - q_{2,o}\right), \tag{13.5.14}$$

$$q_2 = q_{2,o} - q_{1,o}. \tag{13.5.15}$$

Inspection of (13.5.13) and (13.5.15) shows that in this case $q_1 = -q_2$, i.e., all heat added externally to surface *1* is removed at surface 2. Solving (13.5.12) for $q_{1,o}$ and (13.5.14) for $q_{2,o}$, we obtain:

$$q_{1,o} = \sigma T_1^4 - \frac{(1-\varepsilon_1)}{\varepsilon_1} q_1, \tag{13.5.16}$$

and

$$q_{2,o} = \sigma T_2^4 - \frac{(1-\varepsilon_2)}{\varepsilon_2} q_2 = \sigma T_2^4 + \frac{(1-\varepsilon_2)}{\varepsilon_2} q_1. \tag{13.5.17}$$

We can now substitute for $q_{1,o}$ and $q_{2,o}$ in (13.5.13) to obtain the following expression for q_1 and q_2:

$$q_1 = -q_2 = \frac{\sigma(T_1^4 - T_2^4)}{\frac{1}{\varepsilon_1} + \frac{1}{\varepsilon_2} - 1}. \tag{13.5.18}$$

In a similar way, it can be shown that the radiant heat transfer between the shells of two concentric spheres is expressed as follows:

$$Q_1 = \frac{A_1\sigma(T_1^4 - T_2^4)}{\frac{1}{\varepsilon_1} + \frac{A_1}{A_2}\left(\frac{1}{\varepsilon_2} - 1\right)}, \tag{13.5.19}$$

where A_1 is the source and A_2 the sink surface.

13.6. RADIATION THROUGH EMITTING AND ABSORBING MEDIA

In the preceding sections, we discussed radiation between surfaces separated by a medium that does not absorb or emit radiation. This assumption is justified for systems under vacuum or when the intervening medium consists of monatomic or symmetrical diatomic gases, such as helium, argon, nitrogen, oxygen and hydrogen.

However, when the radiation enclosure contains complex molecules, such as CO_2, H_2O, hydrocarbons, or fine particles, as in the case of luminous flames and flash reactors, the furnace atmosphere participates in the radiation process.

Radiant heat transfer calculations in such media are more complex because the emission and absorption characteristics of gases are strongly dependent on temperature and wavelength. In this section, we shall describe the basic concepts and some approximate methods for calculating radiant heat transfer in emitting and absorbing media.

13.6.1. Radiation Between a Surface and a Gray Gas

Let us consider a gray-body enclosure at temperature T_s which contains a gray gas at a higher temperature T_g. Experimental studies have shown that the net radiant flux received at the surface of the enclosure from the gas may be expressed as

$$q_R = \varepsilon_s'\sigma(\varepsilon_g T_g^4 - \alpha_{g,s} T_s^4), \tag{13.6.1}$$

where ε_s' is defined as the effective emissivity of the solid and is approximated by

$$\varepsilon_s' = \frac{\varepsilon_s + 1}{2}, \tag{13.6.2}$$

and ε_s is surface emissivity, ε_g is effective gas emissivity, and $\alpha_{g,s}$ is effective gas absorptivity.

The value of the gas emissivity depends on the temperature, pressure and gas composition of the system, as well as the width or other characteristic length, L, of the enclosure. Values of ε_g have been determined experimentally and typical examples are shown in Fig. 13.16 for water vapor and Fig. 13.17 for CO_2 [6]. In these plots, the parameters $p_{H_2O}L$, etc. are the product of the partial pressure of the radiating gas and the characteristic length

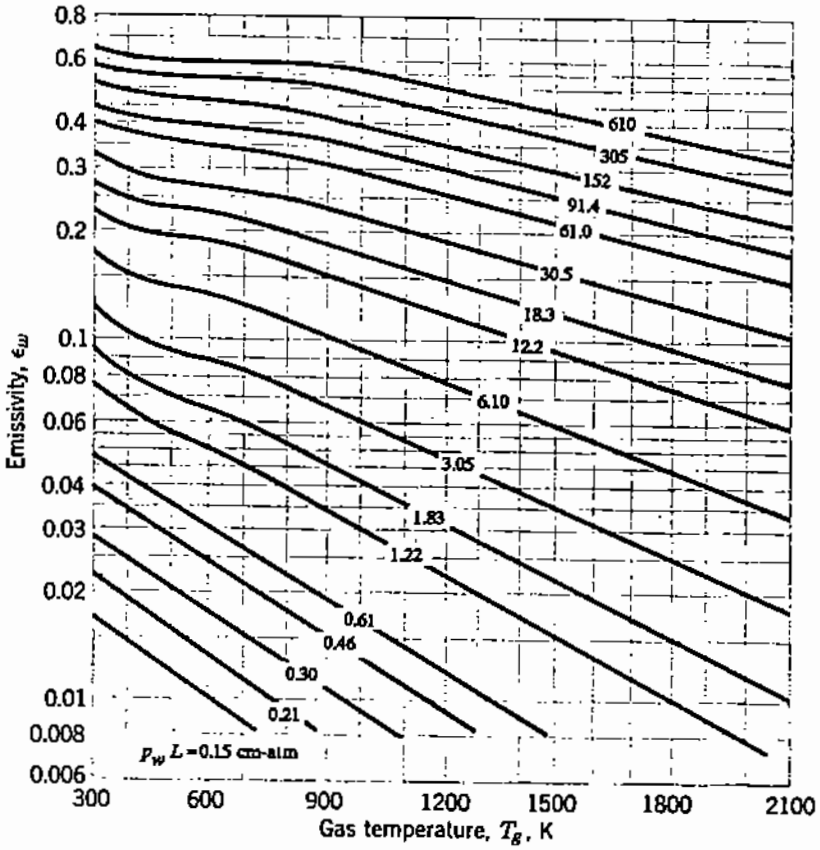

Figure 13.16. Emissivity of water vapor mixed with non-radiating gases at 1 atm total pressure as a function of temperature (after [1]).

of the enclosure. The characteristic length of some typical enclosures is shown in Table 13.2.

The values of ε_g shown in Figs. 13.16–13.17 apply for system pressure near one atmosphere. For other values of total pressure, the values of ε_g from these plots must be multiplied by the pressure correction factor which is plotted in Fig. 13.18 for H_2O-containing atmospheres and in Fig. 13.19 for CO_2 atmospheres [1]:

$$\varepsilon_{g,p} = C_w \varepsilon_g \text{ or } \varepsilon_{g,p} = C_c \varepsilon_g. \tag{13.6.3}$$

In the case of gas mixtures, e.g., a combustion gas containing both CO_2 and H_2O, the appropriate emissivities are not simply additive and a further correction is required. For example, Fig. 13.20 [4] shows the experimentally developed correction factor for a mixture of these two gases. In this case, the overall emissivity of the gas mixture is calculated as follows:

$$\varepsilon_{\text{tot}} = \varepsilon_{g,CO_2} + \varepsilon_{g,H_2O} - \Delta\varepsilon, \tag{13.6.4}$$

where $\Delta\varepsilon$ is the correction factor for the mixture.

Once the emissivity of the gas atmosphere, ε_g, has been determined according to the above procedure, the effective absorptivity of a CO_2- and H_2O-containing gas can be calculated by means of the following empirical correlation:

$$\alpha_{g,s} = \varepsilon_g \left(\frac{T_g}{T_s}\right)^{0.65}. \tag{13.6.5}$$

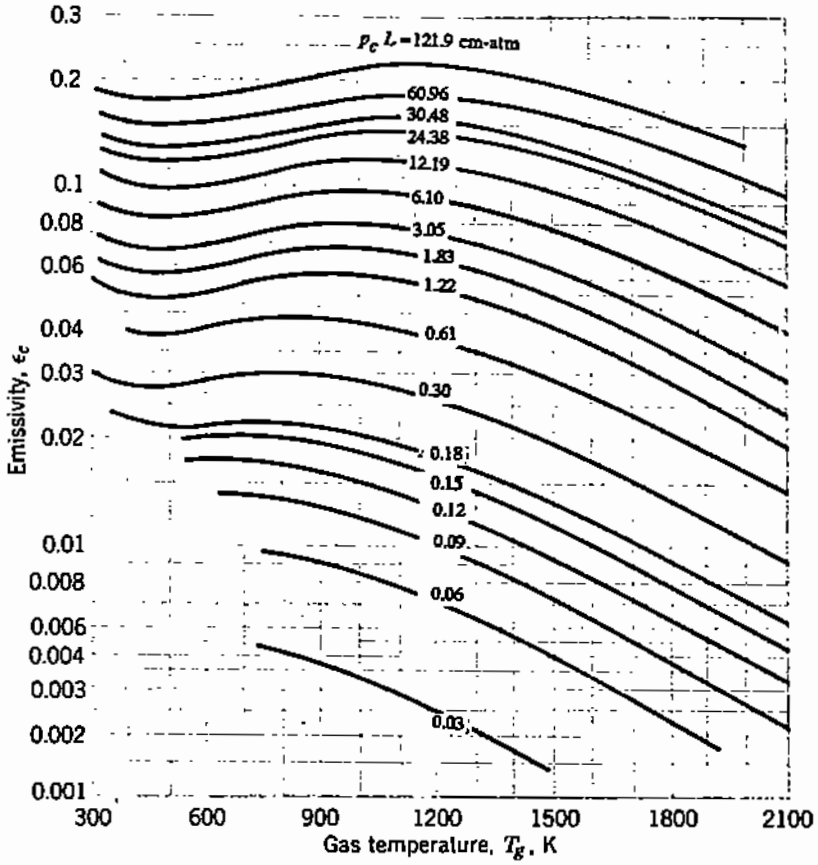

Figure 13.17. Emissivity of carbon dioxide mixed with non-radiating gases at 1 atm total pressure as a function of temperature (after [1]).

Table 13.2. Characteristic Length for Some Enclosures

Shape of enclosure	Characteristic length
Sphere	0.6 × diameter
Short cylinder ($h = d$)	0.6 × diameter
Long cylinder	0.9 × diameter
Rectangle	1.06 × length of short side
Other shapes	0.75 × volume/surface

Example 13.6.1

The exhaust gases from a furnace contain 10% CO_2 and 13% H_2O. The gases, at 1100°C and atmospheric pressure, flow through a cylindrical ceramic duct (2.66 m I.D., 20 m long) the wall of which is at 300°C. Calculate the radiant heat flux at the wall if the surface emissivity is 0.8.

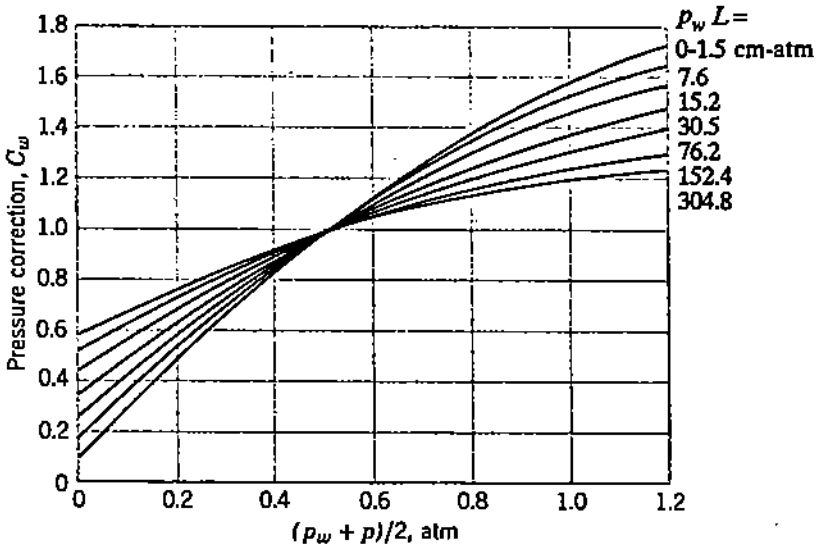

Figure 13.18. Correction factor for the effect of pressures other than 1 atm on the emissivity of water vapor atmospheres (after [1]).

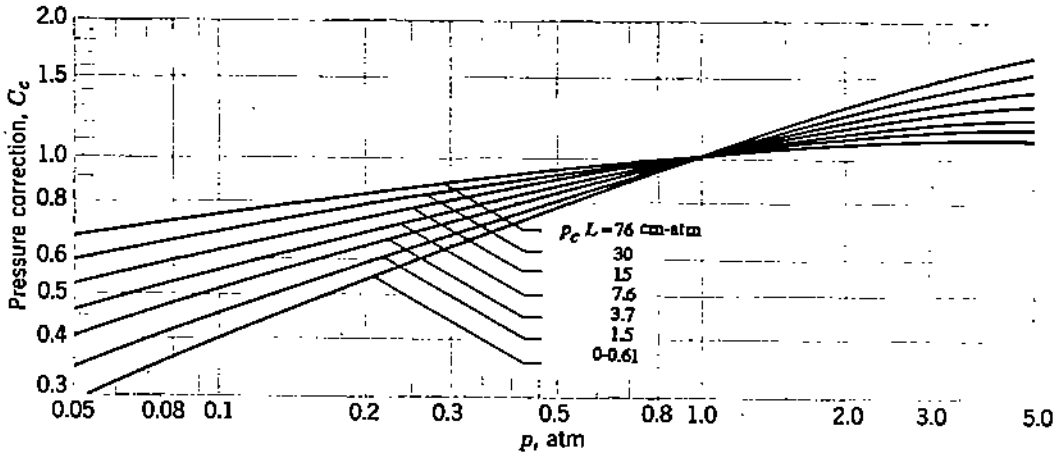

Figure 13.19. Correction factor for the effect of pressures other than 1 atm on the emissivity of CO_2 atmospheres (after [1]).

We first calculate the effective emissivity of the surface from (13.6.2):

$$\varepsilon_s' = \frac{0.8 + 1}{2} = 0.9.$$

Also, from Table 13.2, the characteristic length of the duct is $L = 0.9\times$ diameter = 2.4 m. For $p_{CO_2}L = (1 \times 0.1) \times 2.4 = 0.24$, we obtain from Fig. 13.17: $\varepsilon_g = 0.13$; since the system is at 1 atmosphere, there is no pressure correction to be made. Similarly, for $p_{H_2O}L = (1 \times 0.13) \times 2.4 = 0.312$, we obtain from Fig. 13.16: $\varepsilon_g = 0.18$. Finally, Fig. 13.20 shows that the correction for the superimposed radiation of CO_2 and H_2O is

$$\Delta\varepsilon = 0.045.$$

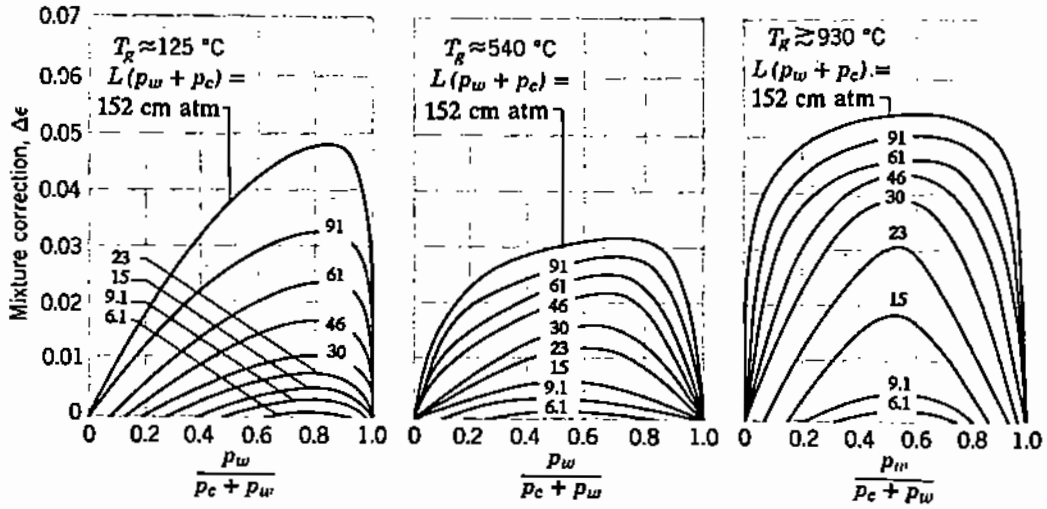

Figure 13.20. Correction factor for emissivity of superimposed radiation from CO_2 (p_c) and H_2O (p_w) atmospheres (after [1]).

Therefore, the total gas emissivity is

$$\varepsilon_{\text{mix}} = \varepsilon_{CO_2} + \varepsilon_{H_2O} - \Delta\varepsilon = 0.13 + 0.18 - 0.045 = 0.265.$$

By means of the empirical correlation (13.4.5), we can now calculate the effective absorptivity of the gas:

$$\alpha_{g,s} = \varepsilon_g \left(\frac{T_g}{T_s}\right)^{0.65} = 0.265 \left(\frac{1373}{573}\right)^{0.65} = 0.47.$$

We now have the numerical values of all the parameters in (13.6.1). Solving, we obtain

$$q_R = 0.9 \times 1.37 \times 10^{-12}(0.265 \times 1373^4 - 0.47 \times 573^4) = 1.10 \text{ cal s}^{-1} \text{ cm}^{-2}.$$

13.6.2. Radiation from a Cloud of Particles

We will conclude this chapter with a brief discussion of the emissivity of luminous flames and clouds of particles. On the basis of work by Hottel and Broughton on the monochromatic emissivity of luminous flames [9] and the theory of probability, Haslam and Hottel [5] derived the following equation for the emissivity of a cloud of particles of known concentration and particle size:

$$\varepsilon_c = 1 - e^{-\varepsilon_p n_p L A_p}, \tag{13.6.6}$$

where ε_c is the emissivity of a cloud of particles; ε_p is the surface emissivity of a particle; n_p is the number of particles per unit volume of cloud, m^{-3}; L is the thickness of the cloud, m; A_p is the average cross-sectional area of the particle (e.g., for spherical particles of diameter d_p, $\pi d_p^2/4$), m^2.

If the particles in the cloud are not uniform in size, the surface mean diameter is used to calculate the particle area:

$$A = \frac{\pi d_s^2}{4} = \frac{\pi}{4}\left(\frac{\sum^n n_i d_i^2}{\sum^n n_i}\right). \tag{13.6.7}$$

Example 13.6.2

Copper concentrates are charged with oxygen-enriched air (35700 N m^3 per hour) in a flash smelting reactor (6.0 m diameter) at the rate of 61 tons per hour. The average particle size is 70 microns and the particle density and emissivity are 5.5 g cm^{-3} and 0.8, respectively. Calculate the particle "cloud" emissivity at 1000°C.

We first calculate the ratio of concentrate to air at 1000°C: $61\times10^6/(35700\times1273/273)$ = 366 g of particles per m^3 of reactor space. Also, we calculate the number of particles per gram of concentrate, on the assumption that all particles are spheres of 70 microns diameter:

$$\begin{aligned}\text{Number of particles/g} &= (\text{cm}^3/\text{g}) \times (\text{number of particles/cm}^3)\\ &= (1/5.5) \times [1/(\pi \times 0.007^3/6) = 1.01 \times 10^6.\end{aligned}$$

Therefore, the number of particles per m^3 of reactor space is

$$n_p = 366 \times 1.01 \times 10^6 = 3.7 \times 10^8.$$

The cross-sectional area of a particle is calculated to be 3.85×10^{-9} m^2. We now can calculate the particle "cloud" emissivity from (13.6.6):

$$\varepsilon_c = 1 - e^{-0.8\times3.7\times10^8\times6\times3.85\times10^{-9}} = 0.9989.$$

It can be seen that in this case the contribution of the particles to the emissivity of the gas phase is very high. In an experimental reactor of 0.15 m diameter and at the same particle "loading," the cloud emissivity would be only 0.16.

REFERENCES

1. M. Jacob, *Heat Transfer*, Vols. 1 and 2, Wiley, New York (1944).
2. R. Siegel and J.R. Howell, *Thermal Radiation Heat Transfer*, McGraw-Hill, New York (1972).
3. Perry, *Chemical Engineers' Handbook*, 6th ed., McGraw-Hill, New York (1984).
4. A. Guerrieri, in *Perry's Chemical Engineers' Handbook*, 4th ed., pp 10–43, McGraw-Hill, New York (1963).
5. R.T. Haslam and H.C. Hottel, *Trans. ASME*, **50**, 9 (1928).
6. W.P. Rohsenow, J.P. Garnett, and E.N. Ganic, eds., *Handbook of Heat Transfer Fundamentals*, McGraw-Hill, New York (1985).
7. H.C. Hottel, "Radiant Heat Transmission," in *Heat Transmission*, ed. McAdams, McGraw-Hill, New York (1954).
8. H.C. Hottel and R.B. Egbert, *Trans. AIChE*, **38**, 531 (1942).
9. H.C. Hottel and F.P. Broughton, *Ind. Eng. Chem.*, **4**, 166 (1932).
10. Lotus 1-2-3 Computer Program, Lotus Development Corporation, Cambridge, MA.

FOURTEEN

Mass Diffusivity: Steady State Diffusion

Most processes used for producing metals and other inorganic materials involve the transfer of matter between phases. Some examples are:

a. In steel refining, two immiscible liquids, metal and slag (a silicate solution) are brought in contact with the objective of transferring the impurities from the metal, such as silicon, manganese, and phosphorus, to the slag phase.
b. In the formation of titanium oxide films on a silicon substrate, by chemical vapor deposition, an organometallic compound of titanium in vapor form flows through a reactor where it is decomposed thermally to form a thin TiO_2 film on the substrate.
c. In the "in-situ" mining of uranium and some other metals, an aqueous solution is piped through boreholes into the ore deposit and the metal is transferred by leaching from the ore to the solution. In the surface plant, the metal is transferred once more by chemical interaction between the aqueous solution and an organic reagent (ion exchange or solvent extraction).

When two or more phases are brought into intimate contact in a closed system, mass is transported between them until *thermodynamic equilibrium* has been established (Chapter 18); that is, when the *chemical potential* of any component is the same in all phases of the system. Therefore, on the basis of thermodynamic equilibrium data, such as free energies and activity coefficients, we can predict the endpoint of a particular chemical reaction or physicochemical phenomenon, such as dissolution, vaporization, and so forth.

However, in the design and operation of processes, it is also necessary to know the **rate** at which equilibrium can be approached under certain operating conditions. The rate of approach to equilibrium depends both on the **chemical kinetics** of the particular reaction (Chapter 18) and on the **mass transfer** rate of reactants and products to and from the reaction zone. Transport of materials to the reaction zone takes place by two mechanisms:

a. There is a movement of molecules (or atoms, or ions depending on the particular system) due to the tendency of chemical species to move from a region of a high chemical potential to a lower one; i.e., from a region of high concentration to one of lower concentration. This mechanism is called **diffusion** and will be discussed in this chapter and Chapter 15.
b. In fluid systems, mass can also be transported by means of the fluid elements as they move about, i.e., by **convection**. The combination of diffusion and convection in fluid systems is called **mass transfer** and will be discussed in Chapters 16 and 17. An example of mass transfer is the transport of oxygen atoms through the boundary layer enveloping a burning particle of coal: It is affected partly by the thickness of the boundary layer, which depends on

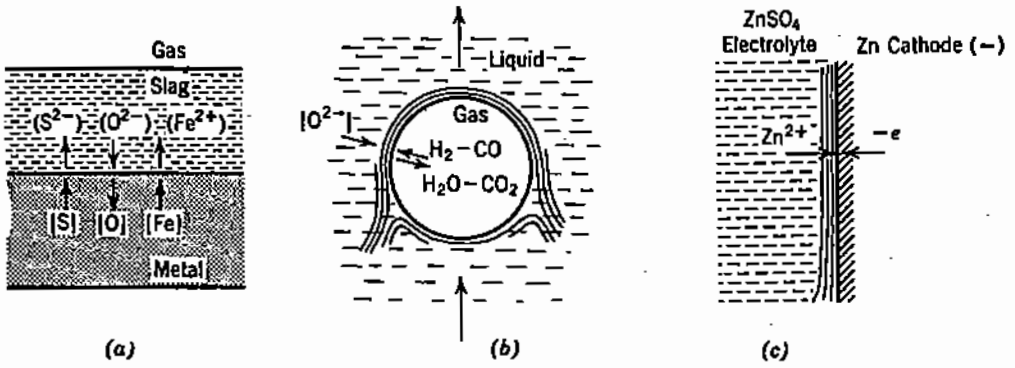

Figure 14.1. Examples of mass transfer phenomena: a) Desulphurization of iron, b) reacting gas bubble in deoxidation of anode copper, c) electrowinning of zinc.

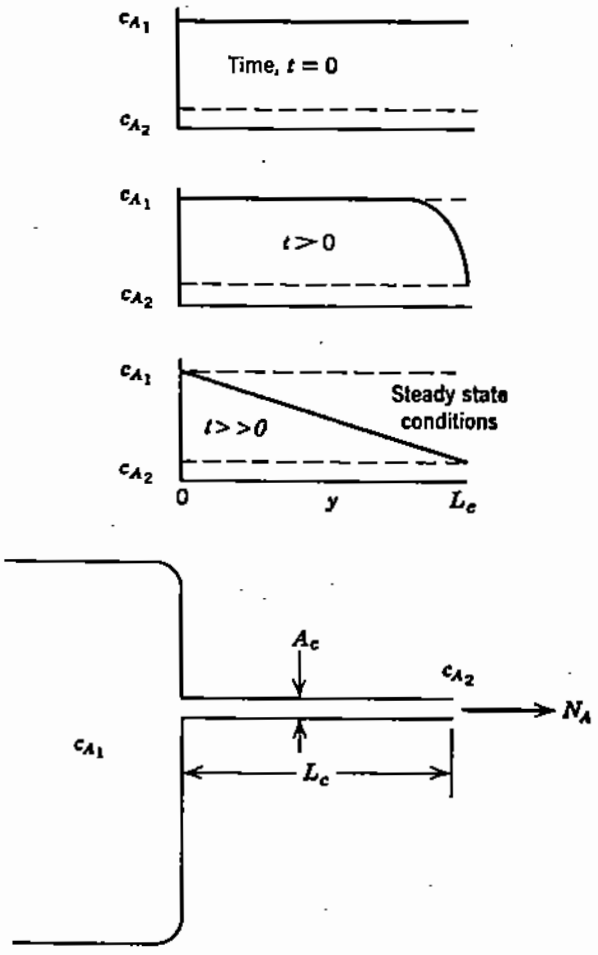

Figure 14.2. Concentration profiles for diffusion through a capillary as a function of time.

the flow conditions around the particle, and partly by the molecular diffusion of oxygen molecules through the carbon dioxide film around the particle. Figure 14.1 is an illustration of some examples of mass transfer between phases.

14.1. THE CONCEPT OF MASS DIFFUSIVITY

Materials consist of chemical species (molecules, atoms, ions). The rate at which a chemical species diffuses from a higher to a lower concentration region depends on its **mass diffusivity**. This is a property that depends both on the species and the medium through which it diffuses; in the following discussion, we will represent the mass diffusivity by the symbol D_{AB}, where the subscript A denotes the diffusing species A and B denotes the medium through which it diffuses.

To illustrate the phenomenon of diffusion, let us consider a large reservoir containing air plus a small amount of argon gas at atmospheric pressure. A capillary tube of length L_c is attached to the reservoir (Fig. 14.2). At the beginning of the experiment, the outer end of the capillary is sealed so that the concentration of argon in the reservoir and along the length of the capillary is uniform. However, at time $t = 0$, the seal at the end of the capillary is broken. Since the concentration of argon in the reservoir, $c_{A,1}$, is larger than the natural concentration of argon in the atmosphere around the reservoir, $c_{A,2}$, argon molecules will start moving through the capillary by diffusion.

Figure 14.2 shows that shortly after the capillary seal is broken, the concentration of argon decreases asymptotically near the outer end of tube. With time, the argon concentration closer to the reservoir is affected. Finally, after a period sufficiently long to reach steady state conditions, a linear concentration profile is established along the length of the capillary. If we now measure the rate at which argon molecules exit through the open end of the capillary, we find that their rate of diffusion through the tube can be expressed as follows:

$$\frac{n_A}{t} = \frac{\text{number of gram moles of argon transferred}}{\text{time}} \propto A_c \frac{(c_{A1} - c_{A2})}{L_c}, \tag{14.1.1}$$

where c_{A1} and c_{A2} is the concentration of argon molecules at the two ends of the capillary, in gram moles per unit volume; A_c is the cross-sectional area of the capillary passage.

It is noted that in the above equation, and throughout the discussion of mass transfer, we use the quantity of *gram moles* to represent the number of transferred *molecules*. It is of course much easier to measure the weight or volume of a certain amount of material than attempt to count molecules; the result is the same, since one gram mole of any chemical species, i.e., its molecular weight expressed in grams, contains the same number of molecules (Avogadro number, Table A2, Appendix A).

The proportionality constant in the above phenomenological relationship has been defined as the **mass diffusivity**, or **diffusion coefficient**, of component A in component B. By introducing this constant in (14.1.1), we can express the **molar flux** of argon, i.e., the molar rate per unit cross-sectional area of the capillary, as follows:

$$N_A = \frac{n_A}{tA_c} = D_{AB} \frac{(c_{A1} - c_{A2})}{L_c}, \tag{14.1.2}$$

where D_{AB} is the diffusion coefficient of species A (in this case, argon) in species B (in this case, air); N_A is the molar flux of diffusing species A (e.g., mol s^{-1} cm^{-2}).

Since, at steady state, the concentration profile along the length of the capillary is linear, every infinitesimal segment of the concentration gradient is represented by the same relationship. Therefore, (14.1.2) can be expressed in differential form:

$$N_{A,y} = -D_{AB}\frac{dc_A}{dy}, \tag{14.1.3}$$

where $N_{A,y}$ denotes the molar flux diffusing in the y-direction (in this case, the direction of the capillary). Equation (14.1.3) is commonly referred to as **Fick's first law of diffusion.** The minus sign in (14.1.3) expresses the fact that diffusion always occurs from a region of higher concentration to a lower one ($y_1 - y_2 = -dy$).

In the above equation, the concentration of the diffusing species is expressed in **molar** terms, i.e., g moles cm^{-3} (for short: mol cm^{-3}) or kg moles m^{-3} (for short: kmol m^{-3}). For example, we know from the ideal gas law that the volume of 1 kg mole (abbreviated to 1 kmol) of any ideal gas at 1 atmosphere and 0°C (273 K) is 22.4 m^3. Therefore, the concentration of the gas under these conditions is 1/22.4 kmol m^{-3}. The symbol c_A will be used in this text to denote molar concentration.

In some problems, it is preferable to express concentration in **mass** terms, e.g., kg m^{-3} in the SI system. For example, the concentration of pure water at room temperature, i.e., its density, is approximately 1000 kg m^{-3} (1 g cm^{-3} in the metric system). The Greek letter ρ, which we have used throughout this text to denote density, will be used to denote mass concentration, since the two terms are synonymous.

Let us now use (14.1.3) to derive the units of mass diffusivity, or diffusion coefficient. First we note that the units of the mass dimension (M) in the molar flux $N_{A,x}$, on the left-hand side of (14.1.3), and in the concentration differential, on the right, must always be the same; therefore, they cancel out and do not affect either the dimensions or the units of the diffusion coefficient. By substituting the dimensions of mass flux (M t^{-1} L^{-2}) and concentration gradient (M L^{-3} L^{-1}) in (14.1.3), we conclude that the dimensions of diffusivity are L^2 t^{-1}. Therefore, its units are m^2 s^{-1} in the SI system and cm^2 s^{-1} in the metric system.

In the above example, we considered diffusion only in the x-direction. In the general case of three-dimensional diffusion, Fick's first law of diffusion would be expressed as follows for a binary system:

$$N_{A,x} + N_{A,y} + N_{A,z} = -\left(D_{AB}\frac{\partial c_A}{\partial x} + D_{AB}\frac{\partial c_A}{\partial y} + D_{AB}\frac{\partial c_A}{\partial z}\right), \tag{14.1.4}$$

and for a system of constant diffusivity in all three dimensions (isotropic diffusion), in vector notation,

$$N_A = -D_{AB}\nabla c_A. \tag{14.1.5}$$

14.2. ANALOGY OF DIFFUSION TO MOMENTUM AND HEAT TRANSFER

The reader will recall that in Chapters 3 and 11 we introduced the concepts of kinematic viscosity, ν, and thermal diffusivity, α, which have the same dimensions as the diffusion coefficient, i.e., L^2 t^{-1}. We also showed that, for constant fluid properties, the following analogy exists between the equations describing momentum and heat transfer:

Newton's law of viscosity:

$$\tau_{y,x} = -\nu \frac{\partial(\rho u_x)}{\partial y}; \tag{3.1.4}$$

Fourier's law of heat conduction:

$$q_y = -\alpha \frac{\partial(\rho C_p T)}{\partial y}. \tag{10.4.1}$$

We now note that there is a clear analogy between the above two relationships and Fick's first law for diffusion (see (14.1.4), diffusion in y-direction):

$$N_{A,y} = -D_{AB} \frac{\partial c_A}{\partial y}. \tag{14.1.3}$$

It can be seen that all three equations express a proportionality between a flux (momentum, heat, mass) and a gradient (velocity, temperature, concentration) which is the driving force for transport of kinetic energy, or thermal energy, or matter. The proportionality constant for momentum transfer is the momentum diffusivity, ν; for heat conduction, the thermal diffusivity, α; and for mass transfer the molecular diffusivity, D_{AB}. The analogy between the three laws was illustrated in Table 1.1 (Chapter 1).

14.3. CONCENTRATION OF MIXTURES AND SOLUTIONS

The *molar concentration* of a mixture or solution is equal to the sum of the molar concentrations of all species in the mixture:

$$c = c_A + c_B + c_C + \ldots = \sum_{i=1}^{n} c_i. \tag{14.3.1}$$

The *mass density*, or simply density, of a mixture or solution is the sum of the mass concentrations of all species in the mixture:

$$\rho = \rho_A + \rho_B + \rho_C + \ldots = \sum_{i=1}^{n} \rho_i. \tag{14.3.2}$$

It is also useful to define the *mole fraction* of a species A in a mixture as follows:

$$X_A = \frac{c_A}{c} = \frac{c_A}{\sum_{i=1}^{n} c_i}, \tag{14.3.3}$$

and therefore,

$$\sum_{i=1}^{n} X_i = 1. \tag{14.3.4}$$

Finally, the *mass fraction* of species A is defined as

$$X'_A = \frac{\rho_A}{\rho} = \frac{\rho_A}{\sum_{i=1}^{n} \rho_i}, \tag{14.3.5}$$

and therefore,

$$\sum_{i=1}^{n} X_i' = 1. \tag{14.3.6}$$

The molar and mass fractions of species A are related as follows:

$$X_A' = \frac{X_A M_A}{M_{\text{ave}}}, \tag{14.3.7}$$

where M_A and M_{ave} are the molecular weights of component A and of the solution or mixture, respectively.

Fick's law of diffusion (see (14.1.4)) is expressed as follows in terms of the molar fraction of the component A diffusing in the y-direction:

$$N_{A,y} = -D_{ABC} \frac{\partial X_A}{\partial y}, \tag{14.3.8}$$

and in terms of the mass fractional concentration:

$$N_{A,y}' = -D_{AB\rho} \frac{\partial X_A'}{\partial y}, \tag{14.3.9}$$

where $N_{A,y}'$ is the mass flux of component A in the y-direction.

14.4. VALUES OF MASS DIFFUSIVITIES OF MATERIALS

Values of the molecular diffusivity vary widely from phase to phase and from material to material. Table 14.1 [1,2] lists typical values of the diffusivities of gas, liquid and solid systems. In general, the diffusivity of gases is four to five orders of magnitude larger than for liquids and 8 to 30 orders of magnitude greater than that of solids.

Table 14.1 also shows that the variation in the coefficients of diffusion in different molten metals is less than one order of magnitude. The diffusivity of alcohol in water has been included in this tabulation for comparison with a low-temperature system of general interest.

It can also be seen that the measured diffusivities in slags are considerably lower than in metallic melts, with the exception of Fe in high-iron slags of the type encountered in non-ferrous smelting. Finally, diffusion coefficients in solids are usually less than 10^{-5} cm^2 s^{-1} and at room temperature can be as low as 10^{-30} cm^2 s^{-1} [1,2].

14.4.1. Factors Affecting the Diffusivity of Gases

At low to moderate pressures (< 10 atm), gas diffusivity is not affected by concentration. On the basis of the kinetic theory of gases, the diffusivity of gases should be proportional to the 1.5 power of the absolute temperature and inversely proportional to the pressure of the system. However, experimental studies suggest that the temperature coefficient is closer to 1.75. The best available correlation, based on nearly 340 experimental data on the gases listed in Table 14.2 and a number of organic vapors, is by Fuller, Schettler and Giddings [4] (P is in atm):

$$D_{AB} = \frac{0.001 T^{1.75}}{P(V_A^{1/3} + V_B^{1/3})^2} \left(\frac{1}{M_A} + \frac{1}{M_B}\right)^{1/2}, \tag{14.4.1}$$

Table 14.1. Diffusivities of Some Gases, Liquids, and Solids

System	Temperature, °C	$D_{A\text{-}B}$, $cm^2\ s^{-1}$
Gases:		
H_2O in N_2	25	0.26
H_2O in O_2	450	1.3
CO_2 in O_2	500	0.9
H_2 in O_2	25	0.7
H_2 in O_2	500	4.2
H_2 in H_2O	500	5.15
H_2 in H_2O	900	11.4
Aqueous solutions:		
NaCl in water	25	1.48×10^{-5}
Ethyl alcohol in water	25	1.28×10^{-5}
Sucrose in water	25	0.56×10^{-5}
Molten metals:		
Pb in lead melt	343	2.5×10^{-5}
Ag in silver melt	1060	3.22×10^{-5}
Cu in Cu-S melt (19.8% S)	1160	7.49×10^{-5}
Cu in Cu-S melt (19.8% S)	1256	10.10×10^{-5}
Fe in Fe-S (33.5%S)	1152	5.22×10^{-5}
Fe in 2.5% C iron	1400	9.0×10^{-5}
C in 3.5% C iron	1550	6.0×10^{-5}
Molten salts:		
Na in molten NaCl	906	14.2×10^{-5}
Molten slags:		
Cu in 39%CaO, 21%Al_2O_3, 40% SiO_2	1400	0.067×10^{-5}
Si in 40%CaO, 20%Al_2O_3, 40% SiO_2	1430	0.01×10^{-5}
O in 40%CaO, 20%Al_2O_3, 40%SiO_2	1430	0.4×10^{-5}
Fe in 43%CaO, 22%Al_2O_3, 35% SiO_2	1500	0.35×10^{-5}
Fe in 61% FeO, 39% SiO_2	1275	9.6×10^{-5}
Solids:		
Al in copper	20	1.3×10^{-30}
Bi in lead	20	1.1×10^{-16}
Sn in iron	900	8.3×10^{-11}
C in iron	800	2.7×10^{-8}
C in iron	1000	32.7×10^{-8}

Table 14.2. Diffusion Volumes of Simple Molecules of Gases [4]

Element or compound	Diffusion volume	Element or compound	Diffusion volume
H_2	7.07	CO_2	26.9
D_2	6.70	N_2O	35.9
He	2.88	NH_3	14.9
N_2	17.9	(CCl_2F_2)	114.8
Ar	16.1	(SF_6)	69.7
CO	18.9	O_2	16.6
CO_2	26.9	Air	20.1
CH_4	24.4	Ne	5.59
H_2O	12.7	Kr	22.8
Cl_2	37.7	(Xe)	37.9
Br_2	67.2	SO_2	41.1

Parentheses indicate that the correlation was based on only a few data.

Atomic and structural diffusion volume elements			
C	16.5	Cl	19.5
H	1.98	S	17.0
O	5.48	Aromatic or hetero-	
(N)	5.69	cyclic rings	–20.2

where the molecular diffusivity is expressed in $cm^2\ s^{-1}$, V_A and V_B are the **diffusion volumes** of molecules A and B, and M_A and M_B are their respective molecular weights.

The diffusion volumes shown in Table 14.2 are derived semi-empirically to provide the "best fit" of the available experimental data to (14.4.1). The diffusion volumes of organic molecules can be calculated by adding the atomic and structural diffusion volume elements shown at the bottom of Table 14.2; for example the diffusion volume of CH_4 is calculated to be 24.4.

The diffusion volumes have the same units and are of the same order of magnitude as the **molar volumes** of elements and compounds, i.e., the ratio M_A/ρ_A, where ρ_A is the density of substance A at its boiling point and atmospheric pressure. For example, the diffusion volume of H_2 is 7.07 (Table 14.2) while its molar volume is calculated [5] to be 28.4; for heavier gases, the diffusion volumes and molecular volumes are very close (e.g., for SO_2, 41.1 vs. 44.7). For metallic vapors, in the absence of information on their diffusion volumes, it is recommended to use their molar volumes (Table 14.3) in (14.4.1).

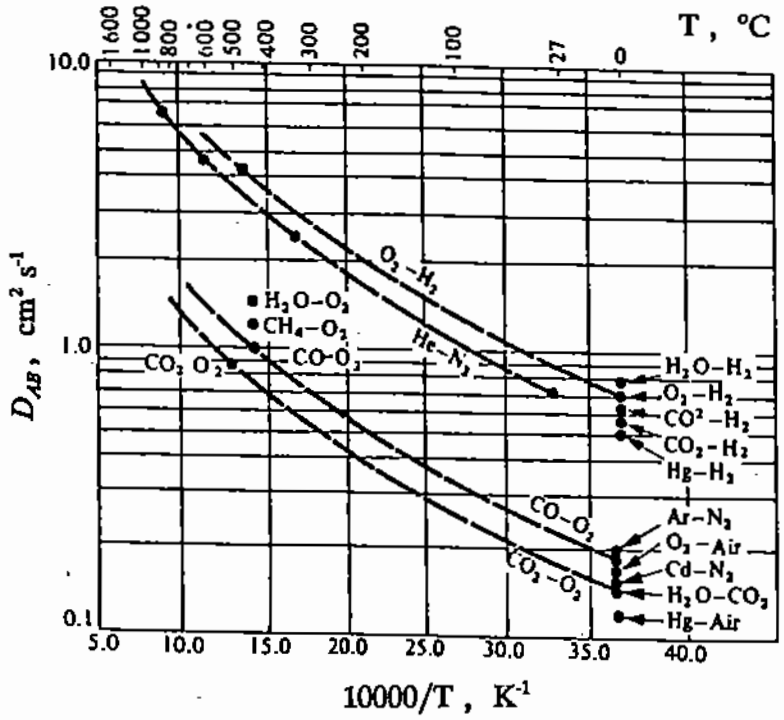

Figure 14.3. Diffusivities of some binary gas mixtures [3].

The diffusivities of some binary gas mixtures commonly used in materials processing are shown in Fig. 14.3 [3].

Example 14.4.1

An argon atmosphere is maintained over an iron melt at 1600°C. Calculate the diffusivity of iron vapor in argon using the correlation of (14.4.1), the diffusion volume of argon (Table 14.2) and the molecular volume of iron (M_{Fe}/ρ_{Fe}, etc.) from Table 14.3.

Substituting numerical values in (14.4.1), we obtain

$$D_{Fe-Ar} = \frac{0.001 \times 1873^{1.75}}{1 \times (7.1^{1/3} + 16.1^{1/3})^2} \times \left(\frac{1}{55.85} + \frac{1}{39.95}\right)^{0.5} = 5.59 \text{ cm}^2 \text{ s}^{-1}.$$

0.05 x 10^{-7}

14.4.2. Factors Affecting the Diffusivity of Liquids

Figures 14.4 and 14.5 show that diffusion coefficients in liquids vary with concentration and temperature. In most cases, the concentration dependence of diffusivity is nonlinear, especially for non-ideal solutions such as the ethanol–water system and most slag and metal systems. As in the case of viscosity, the dependence of liquid diffusivity to temperature is expressed by means of an Arrhenius type of equation

$$D_T = D_0 e^{-E_d/RT}. \tag{14.4.2}$$

where D_0 is the diffusivity at some reference temperature and E_d the temperature coefficient, or apparent activation energy for diffusivity. However, it is evident that diffusivity is

Table 14.3. Molar Volumes of Metal Vapors

Element or compound	Melting point (°C)	Boiling point (°C)	Molar volume $cm^3\ mol^{-1}$
Ag	960.8	1950	10.3
Al	660	2056	10.0
Bi	271	1450	21.3
Cd	321	767	13.0
Co	1493	2900	6.6
Cu	1083	2300	7.1
Fe	1535	3000	7.1
Hg	–38.9	357	14.8
In	156.4	1450	15.7
K	63.7	760	45.5
Li	186	1336	13.1
Mg	651	1110	14.0
Na	97.9	880	23.7
Ni	1453	2900	6.6
Pb	327.4	1620	18.3
Sb	630.5	1380	18.2
Sn	231.9	2260	20.6
Zn	419.5	907	9.2

proportional to the mobility of the liquid molecules while the inverse is true for viscosity; this is accounted for by the minus sign in (14.4.2).

Typical values of E_d for molten salts and liquid metal solutions range from 4-16 kcal mol^{-1} [3]. For slags, the fluidity of which increases rapidly with temperature, the apparent activation energy has been found to range between 20 and 95 kcal mol^{-1} [3].

As in the case of liquid viscosities and thermal conductivities, our present understanding of diffusion in the liquid state is inadequate to allow the prediction of diffusion coefficients on the basis of the molecular properties of the system. However, some models of the liquid state have been proposed which relate the diffusivity to some other physical property of the system [6,7].

14.4.3. Factors affecting the Diffusivity of Solids

Similarly to liquids, the molecular diffusivity in solids depends on the concentration of the diffusing species and is also strongly temperature-dependent. Activation energies range from 10 to 100 kcal per gram mole. Diffusion in some solids can be very nonisotropic. A particular case of anisotropy is in *grain boundary diffusion* where diffusion proceeds much faster at the interfaces between adjacent grains than through the grains. For example, Fig.

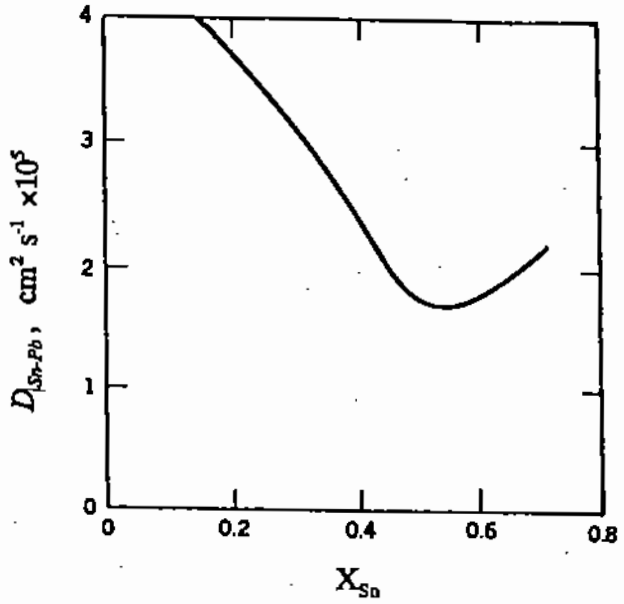

Figure 14.4. Effect of concentration on diffusivity of tin in liquid lead at 510°C [14].

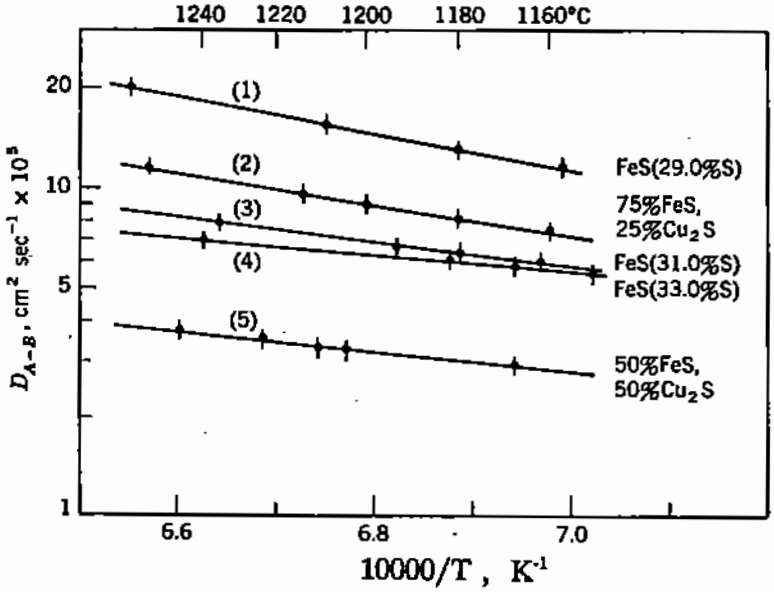

Figure 14.5. Self-diffusion coefficient of Fe in molten matte [15].

14.6 [3] shows that the diffusivity of interstitial carbon in iron at 1000–1200°C is in the order of 10^{-5} to 10^{-4}; in contrast, Fig. 14.7 [3] shows that the diffusivity of Si and Al atoms through iron, in the same temperature range, is much lower. In general, it is not possible to specify a unique diffusion coefficient for a solid without also specifying the structure of the material.

14.5. EFFECT OF NET DIFFUSION VELOCITY

Equation (14.1.4) expresses the mass flux of component A in a two-component (binary), motionless system. However, since diffusion is the physical movement of a chemical species,

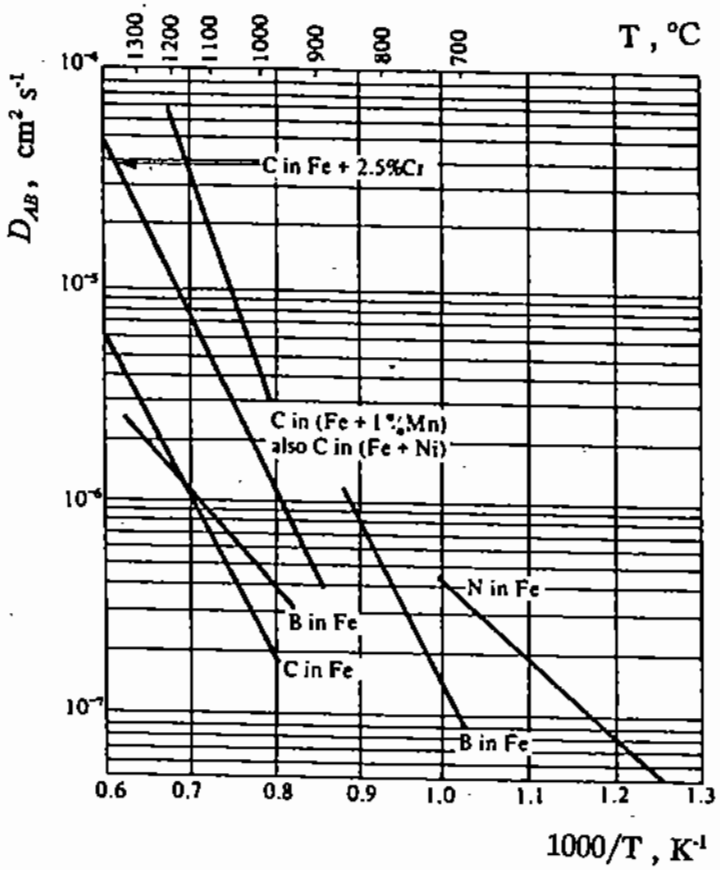

Figure 14.6. Interdiffusion coefficients of interstitial elements through ferrous materials [3].

there may be a resulting *bulk flow*, unless each molecule diffusing away from a particular location is replaced by molecules of the same volume diffusing towards that location.

To visualize the bulk flow due to diffusion, let us express the molar flux of the diffusing component A, N_A, in terms of a diffusion velocity, u_A^* (dimensions L t^{-1}) as follows:

$$N_A = c_A u_A^*. \tag{14.5.1}$$

It can be seen that both the diffusion velocity and the molar flux have a direction. Thus, if species A and B are diffusing toward opposite directions, one flux will be positive and the other negative. The net bulk flow of the mixture, due solely to diffusion, is obtained by adding up the molar fluxes of the contained species:

$$u^* = \frac{N_{\text{total}}}{c} = \frac{N_A + N_B}{c}. \tag{14.5.2}$$

In the presence of such a net bulk flow due to diffusion, the molar flux of component A, *past a fixed point in space*, will be equal to the molar flux due to diffusion, as expressed by Fick's law of diffusion (see (14.1.3),) *plus* the amount of component A carried along in the net bulk flow:

$$N_{A,y} = -D_{AB} c \frac{\partial X_A}{\partial y} + N_{\text{total}} X_A = -D_{AB} c \frac{\partial X_A}{\partial y} + (N_A + N_B) X_A, \tag{14.5.3}$$

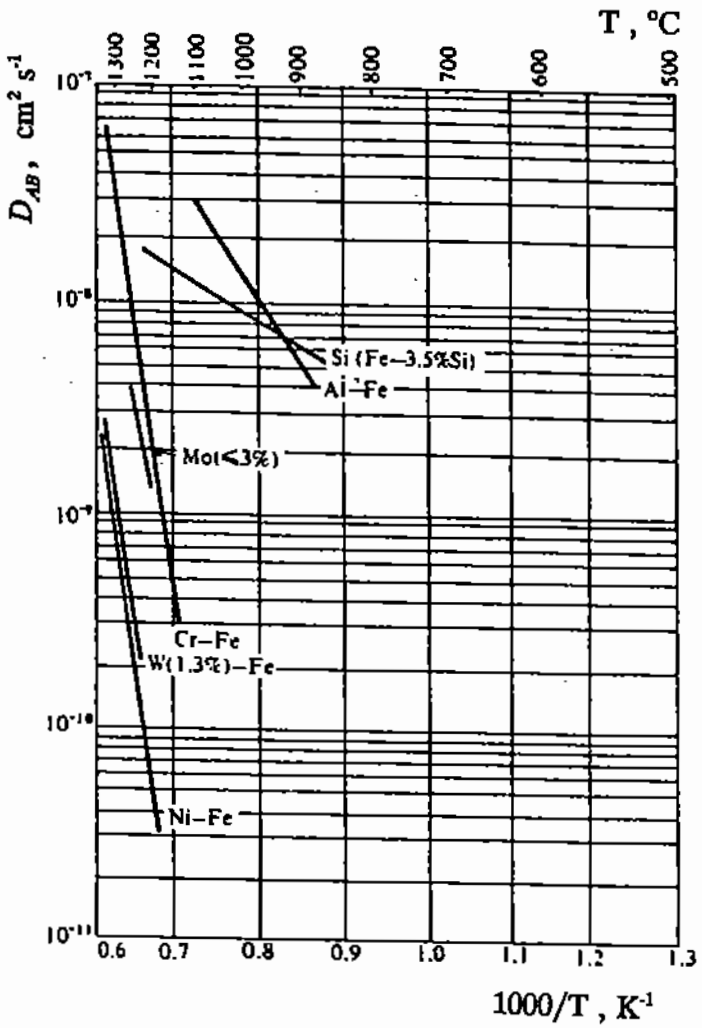

Figure 14.7. Interdiffusion coefficients in ferrous materials [3].

and in vector notation:

$$N_A = -cD_{AB}\nabla X_A + (N_A + N_B)X_A. \tag{14.5.4}$$

Similarly, the mass flux is expressed as follows:

$$N'_{A,x} = -D_{AB}\rho\frac{\partial X'_A}{\partial y} + (N'_A + N'_B)X'_A. \tag{14.5.5}$$

The above equations represent the general statement of Fick's law of diffusion over the whole concentration range in a binary system. In the case of very low concentrations of A, the net bulk flow terms in (14.5.3)–(14.5.5) are negligible. The same is true in the case of equimolar counter-diffusion in a binary system, where

$$N_A = -N_B.$$

In order to distinguish between the molar flux due to diffusion (i.e., Fick's law, see (14.1.3)) and that due to diffusion plus net bulk flow (i.e., see (14.5.3)), we will use the

respective symbols N_A and N_A^* (some authors use J_A^* for the combined molar flux). Therefore,

$$N_A^* = N_A + (N_A + N_B)X_A = N_A + cu^*X_A \tag{14.5.6}$$

where u^* is defined by (14.5.2).

14.6. DIFFUSION IN MULTICOMPONENT SYSTEMS

As noted above, the discussion in §14.5 referred to binary systems. Multicomponent diffusion systems are more complex. For example, the diffusion coefficients in such systems may depend both on the nature of the diffusing species and on the fluxes of the other species contained in the mixture. For gases, it is normally assumed that the diffusivity is independent of composition. On the basis of this assumption, diffusion in a multicomponent gas system of n components is described by the *Stefan–Maxwell equation* [8]:

$$\frac{dX_i}{dy} = \sum_{j=1}^{n} \frac{c_i c_j}{c^2 D_{ij}} \left(\frac{N_j}{c_j} - \frac{N_i}{c_i} \right). \tag{14.6.1}$$

For the case of diffusion of component i, at low concentration and diffusing into a homogeneous mixture, the N_j fluxes can be considered to be negligible and (14.6.1) reduces to

$$\frac{dX_i}{dy} = -\frac{N_i}{c} \sum_{j=1,\, j\neq i}^{n} \frac{X_j}{D_{ij}}. \tag{14.6.2}$$

If we define the diffusivity of component i in the mixture m as

$$D_{im} = -\frac{N_i}{c} \left(\frac{dX_i}{dy} \right)^{-1}, \tag{14.6.3}$$

we obtain the following expression for D_{im}:

$$D_{im} = \left(\sum_{j=1,\, j\neq i}^{n} \frac{X_j}{D_{ij}} \right)^{-1}. \tag{14.6.4}$$

Diffusion in multicomponent liquids is even more complex and it is usually necessary to resort to experimental measurements of the diffusion coefficient for a particular system.

14.7. STEADY-STATE UNIDIRECTIONAL DIFFUSION

In this section we shall discuss the use of Fick's law for formulating and solving simple diffusion problems. As in the case of momentum and heat transfer, we start by considering an appropriate infinitesimal element in a material B through which are diffusing molecules of the species A (Fig. 14.8). The mass balance for the diffusing species is stated as follows:

$$\begin{aligned} &\text{accumulation of } A \text{ in element} \\ &\quad = \text{rate of diffusion in} - \text{rate of diffusion out} \\ &\quad + \text{rate of generation of } A \text{ in element.} \end{aligned} \tag{14.7.1}$$

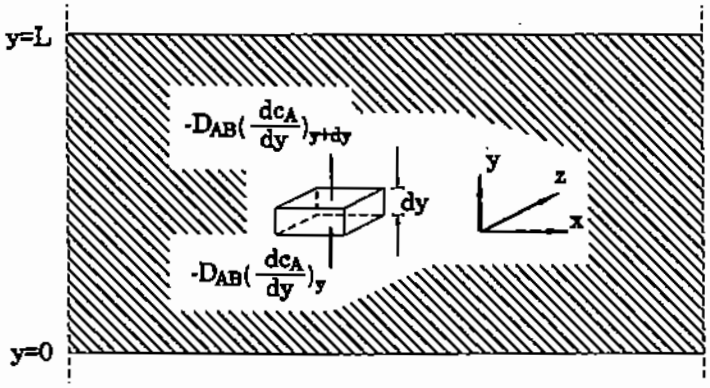

Figure 14.8. Diffusion in and out of an infinitesimal volume element.

For generality, we have included in the above statement a term for the generation (or consumption) of A within the element by chemical reaction. Problems of this nature are encountered in some systems and will be discussed later.

Under steady-state conditions, which we shall consider in this section, the accumulation (or depletion) term in the above mass balance is zero. Also, in the absence of a homogeneous chemical reaction, (14.7.1) can be expressed mathematically as follows, for unidirectional diffusion of A in the y-direction:

$$\frac{dN_A}{dy} = 0. \tag{14.7.2}$$

If the net bulk flow due to diffusion through the element is negligible, we can substitute for N_A in the above equation from Fick's law (see (14.1.3)) to obtain the following second-order differential equation:

$$\frac{d^2c_A}{dy^2} = 0. \tag{14.7.3}$$

The boundary conditions required for the solution of such an equation depend on the physical and chemical characteristics of the system and may take the following forms:

a. The concentration is specified at the boundary surfaces.
b. The mass flux, i.e., some function of the concentration gradient, is specified at the boundary surfaces.
c. In the case of composite media, the relationships between the mass fluxes and the concentrations are specified at the interfaces between two adjacent media.

The above formulation allows us to incorporate the effect of any chemical reactions in the mathematical statement of the problem. For example, a homogeneous reaction, i.e., one that takes place throughout the volume of the control element (Chapter 18), would appear as an additional term in (14.7.3); while a heterogeneous reaction, occurring at a boundary surface, would appear as a boundary condition.

The reader will note the similarity between the above procedure and that used earlier for the solution of heat conduction problems. However, the formulation and solution of diffusion problems can be more complex because of the following important differences from heat conduction:

a. If the diffusing species is present in large concentrations, the diffusion process may result in bulk motion within a fluid system, as discussed earlier.

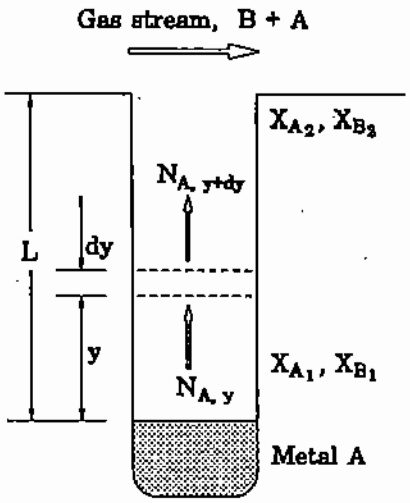

Figure 14.9. Diffusion of a vapor through a stagnant gas in a tube.

b. In the case of diffusion in mixtures of species, it may be necessary to set up several equations, one for each diffusing species.
c. In non-ideal diffusion systems, the concentration may affect molecular diffusivity more strongly than temperature affects thermal diffusivity.

Despite these important differences, the techniques developed for the solution of heat conduction problems can frequently be applied to diffusion by making certain simplifying assumptions.

14.7.1. Diffusion Through a Stagnant Fluid

Let us consider the vaporization of a liquid metal A contained in the bottom of a narrow tube and the entrainment of the vapor in a gas stream B flowing over the top of the tube (Fig. 14.9). The whole system is isothermal and convection through the length of the tube may be considered to be negligible. The vapor pressure at the surface of the liquid metal is much lower than the system pressure and all mass transport to the gas stream occurs by diffusion.

Following the procedure described above, we can formulate this problem by selecting the control volume to be a cylindrical section of height dy (Fig. 14.9). The material balance for this volume element yields

$$\frac{dN_A}{dy} = 0. \tag{14.7.4}$$

Also, from the general (14.5.3), the molar flux in this case is expressed as follows:

$$N_A = -cD_{AB}\frac{dX_A}{dy} + X_A(N_A + N_B). \tag{14.7.5}$$

At steady state, molecules of A move away from the evaporating surface while species B remains stationary. Therefore, $N_B = 0$ and (14.7.5) can be rearranged to yield

$$N_A = -\frac{cD_{AB}}{1 - X_A}\frac{dX_A}{dy}. \tag{14.7.6}$$

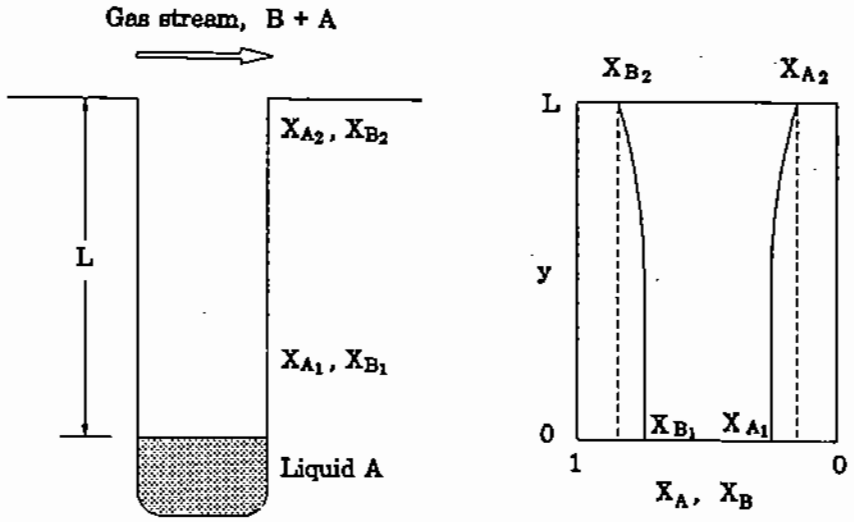

Figure 14.10. Steady-state concentration profile of species A diffusing in "stagnant" species B.

By combining (14.7.4) and (14.7.6), we obtain

$$\frac{d}{dy}\left(-\frac{cD_{AB}}{1-X_A}\frac{dX_A}{dy}\right)=0. \tag{14.7.7}$$

and for constant molar density, c, and diffusivity, D_{AB},

$$\frac{d}{dy}\left(-\frac{1}{1-X_A}\frac{dX_A}{dy}\right)=0. \tag{14.7.8}$$

The above equation can be integrated for the following boundary conditions:

$$X_A = X_{A,0} \text{ at } y=0 \text{ and } X_A = X_{A,L} \text{ at } y=L,$$

to yield the following solution:

$$\frac{1-X_A}{1-X_{A,0}}=\left(\frac{1-X_{A,L}}{1-X_{A,0}}\right)^{y/L}. \tag{14.7.9}$$

The concentration profile of species B can also be determined from this equation since for a binary system

$$X_B = 1-X_A. \tag{14.7.10}$$

Figure 14.10 shows a typical plot of X_A and X_B against the dimensionless distance from the surface of the liquid metal, y/L. The reader may question the fact that, earlier, we specified that the net flux of B is zero while we now show that a concentration gradient exists in the species B; the answer is that due to the diffusion of A, there is a net upward flow which would result in convective transfer of the species B. In other words, the diffusion of B downwards, due to the concentration gradient shown in Figure 14.10, is in balance

with the convective transfer of B caused by the upward diffusion of species A; as a result, the net molar flux of B is zero.

In many diffusion problems, it is required to determine the net flux of the diffusing species, rather than its concentration profile. For steady state conditions and in the absence of chemical reaction, N_A is independent of y; therefore,

$$N_A = N_{A,0} = N_{A,L}.$$

From the above equation and (14.7.6), we obtain

$$\frac{N_{A,0}}{cD_{AB}}\,dy = -\frac{dX_A}{1-X_A}, \tag{14.7.11}$$

which can be integrated for the boundary conditions of this problem to yield

$$N_{A,0} = \frac{cD_{AB}}{L}\ln\left(\frac{1-X_{A,L}}{1-X_{A,0}}\right), \tag{14.7.12}$$

which may also be expressed as

$$N_{A,0} = \frac{cD_{AB}}{L}\ln\frac{X_{B,L}}{X_{B,0}}. \tag{14.7.13}$$

14.7.2. Diffusion Through Porous Media

In the processing of materials, there are situations where one is interested in the diffusion of a fluid through porous solids. Examples are the reduction of oxides or the oxidation of sulfides, gas phase alloying, drying and so forth. The **porosity** of a solid body can be estimated from its bulk density, i.e., mass/outer volume, as follows:

$$\text{porosity: } \varepsilon = 1 - \frac{\text{bulk density}}{\text{density of element or compound}}. \tag{14.7.14}$$

It is generally considered that diffusion of gases in a porous material occurs either by ordinary gas diffusion through the pores of the medium or by *Knudsen diffusion*. Ordinary diffusion occurs when the pores are much larger than the *mean free path* of the gas molecules, i.e., the distance that a molecule travels between collisions with other molecules.

Ordinary diffusion through a porous medium is treated in the same way as molecular diffusion in "the open" with the exception that the cross-sectional area available for diffusion is decreased, because of the presence of the solid interstices between pores; also, the length of the path is increased because of the tortuous path that must be followed by the gas molecules through the interconnected pores. Therefore, the same equations can be used as for diffusion in the open but the molecular diffusivity is replaced by the **effective diffusivity** which accounts for the above geometric effects and is defined as follows:

$$\text{Effective diffusivity of } A \text{ in } B = D_{\text{eff}} = \frac{D_{AB}\,\varepsilon}{\tau}, \tag{14.7.15}$$

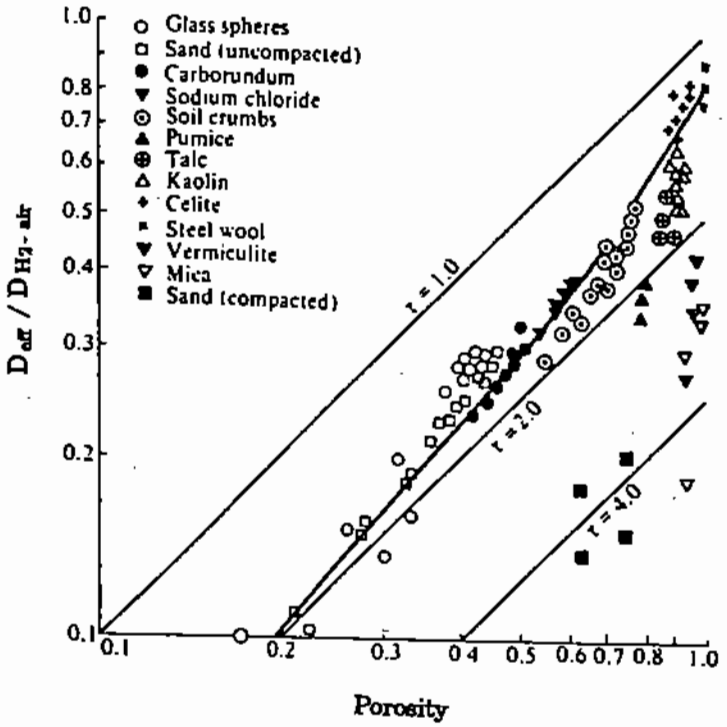

Figure 14.11. Effective diffusivity of hydrogen in air in various non-consolidated porous media [8].

where the porosity, ε, accounts for the decreased area available for diffusion and the **tortuosity**, τ, accounts for the longer path to be followed by the diffusing molecules.

In practice, the porosity of a material may range from 0.2 to 1 and the tortuosity from 1 to 10. Figure 14.11 [8] shows how the ratio D_{eff}/D_{AB} varies with porosity for the diffusion of hydrogen in air, through a number of loose (non-consolidated) materials.

At very low gas pressures, or when the pore size is very small, there is a higher probability that the gas molecules will collide with the walls of the pore than with each other and the mass flux of molecules through the pore is expressed as follows:

$$N_A = -\frac{2\overline{u}_g\, r\, c}{3}\frac{dX_A}{dy}, \tag{14.7.16}$$

where r is the pore radius and $\overline{u}_g$ is the average velocity of the gas molecules expressed by

$$\overline{u}_g = \left(\frac{8RT}{\pi M_g}\right)^{1/2}, \tag{14.7.17}$$

where M_g is the molecular weight of the gas, and R is the universal gas constant, as defined in Table A2 (Appendix).

By combining (14.7.16) and (14.7.17), we obtain the definition of the **Knudsen diffusion coefficient**:

$$D_K = 9700 r \left(\frac{T}{M_g}\right)^{1/2}. \tag{14.7.18}$$

As in the case of ordinary diffusion, Knudsen diffusion is also affected by the porosity of the material and the tortuosity of the pores; therefore, the *effective* Knudsen diffusion coefficient is expressed as follows:

$$\text{Effective Knudsen diffusivity} = D_{K,e} = \frac{D_K \epsilon}{\tau}. \tag{14.7.19}$$

In practice, the micropore radius has been found to range from 16 to 200 angstroms and the tortuosity factor in micropore media from 1 to 10 [8].

14.7.3. Logarithmic Mean Concentration

In mass transfer, in analogy to the heat convection problems discussed in Chapter 12, it is frequently convenient to use the logarithmic mean "driving force." The logarithmic mean of the two concentrations $X_{B,1}$ and $X_{B,2}$ is defined similarly to (12.8.10) as

$$X_{B,LM} = \frac{X_{B,2} - X_{B,1}}{\ln \frac{X_{B,2}}{X_{B,1}}}. \tag{14.7.20}$$

By introducing the definition of $X_{B,LM}$ in (14.7.13) (§14.7.1), we obtain

$$N_{A,0} = \frac{cD_{A-B}}{X_{B,LM}} \frac{(X_{B,2} - X_{B,1})}{L}, \tag{14.7.21}$$

which may also be written as

$$N_{A,0} = \frac{cD_{A-B}}{X_{B,LM}} \frac{(X_{A,1} - X_{A,2})}{L}. \tag{14.7.22}$$

In very dilute binary systems where $X_{A,1}$ and $X_{A,2}$ are very low,

$$X_{B,2} \approx X_{B,1} \approx 1,$$

and therefore

$$X_{B,LM} \approx 1.$$

Under these conditions, (14.7.22) shows that the molar flux $N_{A,0}$ will be proportional to $(X_{A,1} - X_{A,2})/L$, which may be called the *driving force for diffusion.* On the other hand, for increasing values of $X_{A,1}$, the term $X_{B,LM}$ will become progressively lower than unity; thus any increase in $X_{A,1}$ will result in a larger than linear increase of $N_{A,0}$. The presence of the logarithmic mean term in (14.7.22) provides for the "net bulk flow" effect of diffusion, which was described earlier.

Expressions similar to (14.7.22) are frequently used in the so-called film theories of mass transfer, where it is assumed that the resistance to the diffusion process can be attributed to a thin stagnant film of a certain thickness. In earlier diffusion studies, the effect of $X_{B,LM}$ on the mass flux was neglected. The following example shows that such an omission may not be justifiable under certain conditions.

Example 14.7.1

The rate of decomposition of a layer of calcium carbonate placed in an oven tray is controlled by the mass transfer of carbon dioxide between the surface of the layer and the atmospheric air above it. As a very rough approximation, this process may be represented by the diffusion of CO_2 through a 0.1-cm-thick stagnant film gas. It may be assumed that the molar density of the gas film is constant at 1.4×10^{-5} mol cm^{-3}, the diffusivity of CO_2 in air is 2.0 cm^2 s^{-1}, and there is no accumulation of CO_2 in the oven atmosphere above the stagnant film (i.e., $X_{A,2} \approx 0$, or $X_{B,2} \approx 1$). We need to calculate the variation in the molar flux of CO_2 with concentration of CO_2 at the solid/gas interface. By substituting the given numerical values in (14.7.20) and (14.7.22) we obtain

Concentration of CO_2 at solid/gas interface, $X_{A,1}$	Logarithmic mean of air concentration across film, $X_{B,L}$	N_{CO_2}, mol s^{-1} cm^{-2}
0.01	0.995	2.8×10^{-6}
0.10	0.949	29.5×10^{-6}
0.50	0.721	194×10^{-6}
0.90	0.391	645×10^{-6}
0.99	0.215	1289×10^{-6}

This tabulation shows that the "net bulk flow" effect, represented by the logarithmic mean $X_{B,LM}$, increases rapidly as the mole fraction of the diffusing species approaches unity. This theoretical prediction is supported by practical experience. For instance, in the use of the oxygen-acetylene torch for cutting metals, the use of high-purity oxygen has been found to increase the efficiency of the cutting torch.

14.7.4. Diffusion and Chemical Reaction in a Stagnant Film

As an example of simultaneous diffusion and homogeneous chemical reaction, let us consider a case where molten metal contained in the bottom of a narrow tube is volatilized and the vapor reacts with a component of the gas phase over the liquid surface (Fig. 14.12). For example, this situation occurs in the industrial practice of purifying selenium by boiling the impure liquid in a retort and oxidizing the vapor with air to SeO_2.

If we assume that reaction occurs only in the gas phase above the liquid, the problem may be formulated by considering that diffusion and chemical reaction take place in a stagnant film of thickness δ. Under steady state conditions, the mathematical statement of the material balance equation (see (14.7.1)) for species A is

$$\frac{d}{dy}(N_{A,y}) + \dot{r}_A = 0, \tag{14.7.23}$$

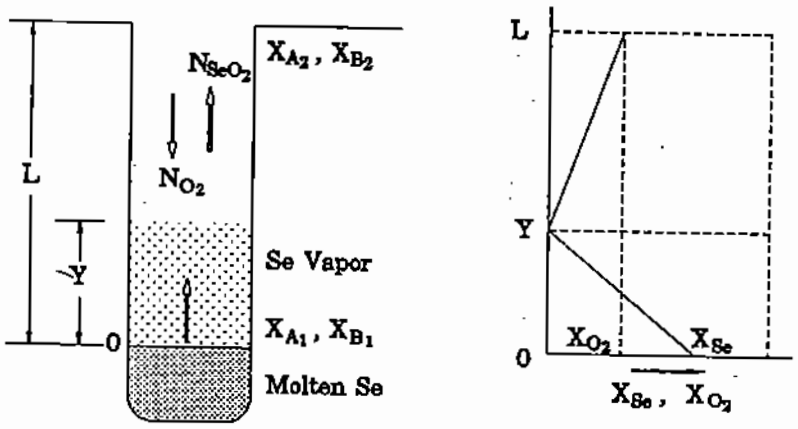

Figure 14.12. Diffusion and homogeneous reaction of selenium vapor and oxygen in a nitrogen atmosphere.

and for species B:

$$\frac{d}{dy}(N_{B,y}) + \dot{r}_B = 0, \tag{14.7.24}$$

where $\dot{r}_A$ and $\dot{r}_B$ represent the rates of reaction of species A and B and have the units of moles/time/unit volume.

Before we proceed further, it is necessary to express $\dot{r}_A$ and $\dot{r}_B$ in terms of the concentration of A and B. Let us assume that in this case, the reaction between A and B is a second-order irreversible reaction (Chapter 18) of the form

$$A + B \rightarrow AB.$$

Therefore,

$$\dot{r}_A = \dot{r}_B = k_r c^2 X_A X_B, \tag{14.7.25}$$

where X_A and X_B are the mole fractions of species A and B, and k_r is the reaction rate constant for the second-order reaction (Chapter 18).

To simplify the problem further, we shall assume that the system is isothermal and that the diffusing species A and B are at a low enough concentration so that the effect of net bulk flow is negligible (i.e., $N_i^* = N_i$). By substituting for $\dot{r}_A$, $\dot{r}_B$ from (14.7.25) into (14.7.23) and (14.7.24) and expressing $N_{A,y}$ and $N_{B,y}$ by the concentration gradients of A and B, we obtain

$$-cD_{A-g}\frac{d^2X_A}{dy^2} + k_r c^2 X_A X_B = 0, \tag{14.7.26}$$

and

$$-cD_{B-g}\frac{d^2X_B}{dy^2} + k_r c^2 X_A X_B = 0, \tag{14.7.27}$$

where D_{A-g} and D_{B-g} are the diffusivities of species A and B in the gas phase over the liquid.

Equations (14.7.26) and (14.7.27) are a system of coupled nonlinear differential equations, the solution of which would require a numerical method of solution. However, an analytical solution can be obtained for the case where the rate of the chemical reaction between A and B is much higher than the respective rates of diffusion of A and B to the

reaction zone; i.e., when the A molecules react with B as soon as they are transported by diffusion to the reaction zone, where their concentration becomes zero (plane Y, Fig. 14.12).

Under these conditions, there is no chemical reaction at any other location than $y = Y$ and (14.7.26)–(14.7.27) simplify to

$$\frac{d^2X_A}{dy^2} = 0 \text{ for } 0 \leq y \leq Y, \tag{14.7.28}$$

$$\frac{d^2X_B}{dy^2} = 0 \text{ for } Y \leq y \leq L. \tag{14.7.29}$$

The boundary conditions are:

$$X_A = X_{A,1} \text{ at } y = 0, \tag{14.7.30}$$

$$X_B = X_{B,1} \text{ at } y = L, \tag{14.7.31}$$

$$X_A = X_B = 0 \text{ at } y = Y. \tag{14.7.32}$$

Finally, the location of Y is specified by the fact that at that plane the molar fluxes of A and B must be at the required stoichiometric ratio for the reaction; in the present case of equimolar reaction of A and B, at steady conditions we have at $y = Y$, $N_A = N_B$, i.e.,

$$D_{A-g}\left(\frac{X_{A,1} - X_{A,Y}}{Y}\right) = D_{B-g}\left(\frac{X_{B,1} - X_{B,Y}}{L - Y}\right), \tag{14.7.33}$$

where, from (14.7.32), $X_{A,Y} = X_{B,Y} = 0$. Solving (14.7.33) for Y, we obtain

$$Y = \frac{L}{1 + \left(\frac{D_{B-g}X_{B,1}}{D_{A-g}X_{A,1}}\right)}. \tag{14.7.34}$$

Differential equations (14.7.28)–(14.7.29) and boundary conditions (14.7.30)–(14.7.32) (with Y as defined by (14.7.34)) represent the complete statement of the problem. Equations (14.7.28)–(14.7.29) can be integrated to yield

$$X_A = X_{A,1}\left(\frac{Y - y}{Y}\right), \tag{14.7.35}$$

and

$$X_B = X_{B,1}\left(\frac{y - Y}{L - Y}\right), \tag{14.7.36}$$

where Y is expressed by (14.7.34). The net molar flux of A from the liquid surface (i.e., at $y = 0$) is expressed by

$$N_{A,0} = cD_{A-g}\left(\frac{X_{A,1} - X_{A,Y}}{Y}\right). \tag{14.7.37}$$

Substituting for Y from (14.7.34) and considering that $X_{A,Y} = 0$ at $y = Y$ (see (14.7.32)), we obtain

$$N_{A,0} = \frac{cD_{A-g}X_{A,1}}{L}\left(1 + \frac{D_{B-g}X_{B,1}}{D_{A-g}X_{A,1}}\right). \tag{14.7.38}$$

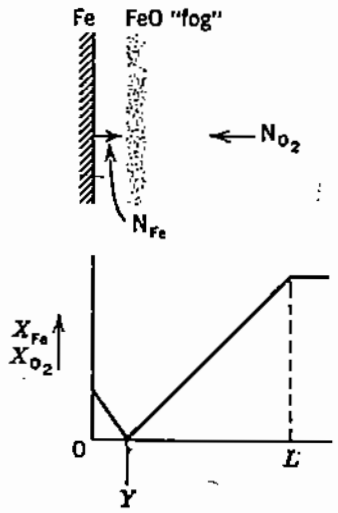

Figure 14.13. Iron vapor and oxygen concentration profiles in the formation of iron oxide.

It is interesting to note that (14.7.22), which was derived in §14.7.3 for a nonreacting system and low concentrations of A (i.e., $X_{B,LM} \approx 1$), yields the following expression which is equivalent to (14.7.38):

$$N_{A,0} = \frac{cD_{A-g}X_{A,1}}{L}. \tag{14.7.39}$$

Comparison of (14.7.38) and (14.7.39) shows that the effect of a homogeneous chemical reaction which consumes the species A is to increase its rate of mass transfer from the liquid surface. This line of reasoning was followed by Turkdogan, Grieveson, and Darken [9] to explain their experimental finding that the rate of vaporization of a number of metals increased greatly with oxygen concentration in the atmosphere above the liquid surface. Figure 14.13 is a schematic diagram of the countercurrent molar flux of iron vapor and oxygen towards the reaction plane, $y = Y$, where they react to form a "fog" of iron oxide particles [10].

Figure 14.14 [9] compares the observed rate of vaporization of a number of metals with the theoretical prediction by Turkdogan et al., as a function of the oxygen partial pressure. It can be seen that over a certain range of oxygen concentration, the rate of vaporization of iron is proportional to the mole fraction of oxygen in the gas phase, as predicted by (14.7.38). The abrupt decrease in the vaporization rate shown by the vertical dotted lines in Fig. 14.14 was most likely due to the formation of an iron oxide layer on the surface of the melt.

Example 14.7.2

At 1600°C, the vapor pressure of iron is 0.057 mm Hg [11] and the diffusivity of iron vapor in an argon atmosphere is estimated at 5.6 $cm^2\ s^{-1}$. Use the Langmuir equation (see (14.7.40)) to calculate the maximum possible rate of vaporization of iron vapor from the surface of an iron melt. Compare this value with the maximum vaporization rate of 0.88×10^{-4} kmol $s^{-1}\ m^{-2}$ determined experimentally by Turkdogan et al. [10]. Calculate the molar fraction of iron vapor and its concentration, c_{Fe}, next to the surface of the melt and

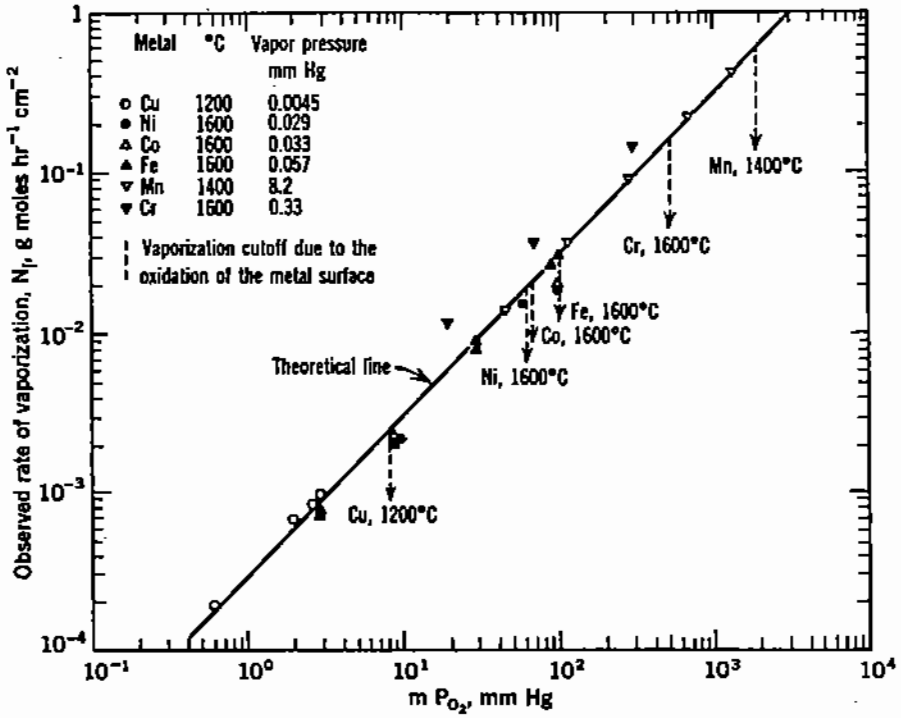

Figure 14.14. Calculated and experimental rates of vaporization of metals as a function of the partial pressure of oxygen in the atmosphere [9].

the thickness of the iron vaporization zone, Y (Fig. 14.13), if an argon-oxygen atmosphere is maintained over the melt ($P = 1$ atm).

The Langmuir equation predicts the maximum rate of vaporization under vacuum:

$$N_{i,\max} = \frac{p_i}{\sqrt{2\pi RTM_i}}, \tag{14.7.40}$$

where p_i is the vapor pressure of material i at absolute temperature T; M_i is the molecular weight of material i; R is the universal gas constant (= 8.314×10^3 J kmol^{-1} K^{-1}, Table A2).

In order to use the Langmuir equation, we express the vapor pressure of iron, p_{Fe} in SI units as

$$p_{\mathrm{Fe}} = \frac{0.057}{760} \times 1.013 \times 10^5 = 7.6 \text{ Newtons m}^{-2},$$

and substituting numerical values in (14.7.40), we calculate ($M_{\mathrm{Fe}} = 55.85$ g mol^{-1}):

$$N_{\mathrm{Fe},\max} = \frac{7.6}{\sqrt{2\pi \times 8.314 \times 10^3 \times 1873 \times 55.85}} = 1.03 \times 10^{-4} \text{ kmol s}^{-1}\text{m}^{-2}.$$

It can be seen that the theoretically predicted value of the molar flux of iron is in fairly good agreement with the experimental value of $N_{\mathrm{Fe},\max} = 0.88 \times 10^{-4}$ kmol s^{-1} m^{-2}. We now introduce the experimental value of N_{Fe} in the following form of (14.7.37):

$$Y = \frac{cD_{\mathrm{Fe}-A}\,(X_{\mathrm{Fe},s} - X_{\mathrm{Fe},Y})}{N_{\mathrm{Fe},\max}}, \tag{14.7.41}$$

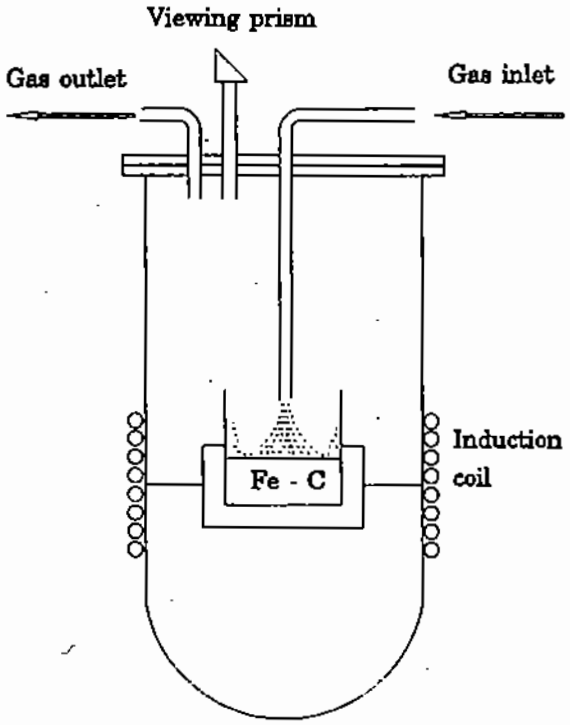

Figure 14.15. Schematic diagram of apparatus used for reaction between a CO/CO_2 gas jet and a Fe–C melt.

where $X_{Fe,s}$ is the fractional concentration of iron vapor at the melt surface (= 0.057 mm Hg/760 mm Hg = 7.5×10^{-5}), $X_{Fe,Y} = 0$ and c, the molar density of the atmosphere above the melt, is calculated from the ideal gas law:

$$c = \frac{P}{RT} = \frac{1.013 \times 10^5}{8.314 \times 10^3 \times 1873} = 6.5 \times 10^{-3} \text{ kmol m}^{-3}. \tag{14.7.42}$$

By substituting numerical values in (14.7.41), we calculate the thickness of the vaporization layer between the melt surface and the reaction "interface" Y to be

$$Y = \frac{6.5 \times 10^{-3} \times 5.6 \times 10^{-4} \times 7.5 \times 10^{-5}}{0.88 \times 10^{-4}} = 3.1 \times 10^{-6} \text{ m} \equiv 3.1 \text{ microns}.$$

Example 14.7.3

In a study of the decarburization of iron-carbon melts [12], an 80-g melt, maintained at 1580°C in a 3.18-cm-diameter crucible, was decarburized by directing a stream of CO–CO_2 gas against the surface of the melt, at an estimated velocity of about 200 cm s^{-1} (Fig. 14.15). The observed initial rates of decarburization are shown in Fig. 14.16 as a function of the concentration of CO_2 in the impinging jet. Determine whether the reaction is controlled by diffusion through a gas film over the melt surface (D_{CO_2-CO} at 1580°C = 3.47 cm^2 s^{-1}).

In this case, the diffusing species is CO_2, which reacts at the surface of the melt with carbon in the metal to produce CO:

(14.7.43)

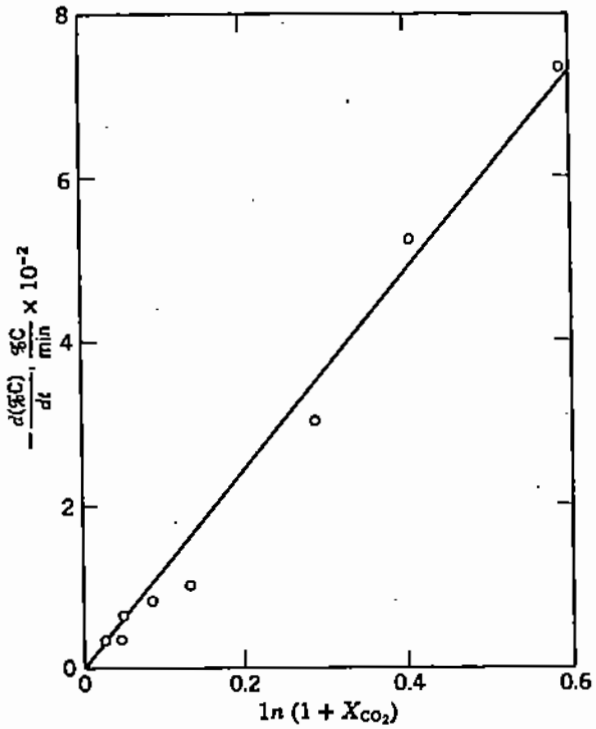

Figure 14.16. Initial rate of decarburization as a function of CO_2 concentration [12].

Therefore,

$$N_{CO} = -2N_{CO_2}. \tag{14.7.44}$$

It can be seen that in this case, diffusion is not equimolar and there is a net bulk flow due to diffusion. The corresponding form of (14.7.5) is

$$N_{CO_2} = -cD_{CO_2-CO}\frac{dX_{CO_2}}{dy} + X_{CO_2}(N_{CO_2} + N_{CO}). \tag{14.7.45}$$

By substituting for CO from (14.7.44), collecting the N_{CO_2} terms on one side of (14.7.45)and integrating dX_{CO_2} for boundary conditions

$$X_{CO_2} = X_{CO_2,e}$$

(equilibrium concentration for reaction (14.7.43) at melt surface, Chapter 18) at $y = 0$, and

$$X_{CO_2} = X_{CO_2,b}$$

(bulk concentration of CO_2 in impinging gas jet), we obtain the following expression for the decarburization rate:

$$N_{CO_2} = -\frac{cD_{CO_2-CO}}{Y}\ln\left(\frac{1 + X_{CO_2,b}}{1 + X_{CO_2,e}}\right). \tag{14.7.46}$$

From thermodynamic data (Chapter 18), we find that $X_{CO_2,e}$, the equilibrium mole fraction of CO_2 at reaction surface, may be assumed to be near zero at concentrations in the melt above 0.5% C. The molar density of the gas is calculated from the ideal gas law:

$$c = \frac{\rho}{M} = \frac{P}{RT} = \frac{1\,\text{atm}}{82.05\,\frac{\text{cm}^3\,\text{atm}}{\text{mol K}} \times 1853\,\text{K}} = 6.58 \times 10^{-6}\ \text{mol cm}^{-3}.$$

Also the ratio $N_{CO_2}/\ln(1 + X_{CO_2})$ can be estimated by converting the slope of the linear plot of Fig. 14.16 (0.122×10^{-2} min^{-1}) to moles of C (= moles of CO_2) reacted per second and dividing by the surface area of the melt (7.92 cm^2):

$$\frac{N_{CO_2}}{\ln(1 + X_{CO_2})} = \frac{0.122 \times 10^{-2}}{60} \times \frac{80}{12} \times \frac{1}{7.92} = 1.71 \times 10^{-5}\ \text{mol CO}_2\,\text{s}^{-1}\,\text{cm}^{-2}.$$

By substituting these numerical values in (14.7.46), we compute the thickness of the hypothetical stagnant film:

$$Y = \frac{6.57 \times 10^{-6} \times 3.47}{1.71 \times 10^{-5}} = 1.33\ \text{cm}.$$

Therefore, for the reaction to be controlled by gaseous diffusion, the thickness of the "stagnant" film should be about 1.33 cm. This value is highly unlikely for the present experimental system where a 200 cm s^{-1} gas jet is directed against the surface. It must therefore be concluded that the rate of decarburization is controlled by some other phenomenon, such as the chemical reaction rate at the surface of the melt, or the transport of carbon atoms from the bulk of the Fe–C melt to the reaction surface.

REFERENCES

1. L. Yang and G. Derge, in: *Physical Chemistry of Process Metallurgy*, ed. P. St. Pierre, Wiley-Interscience, New York, p. 503 (1961).
2. J.F. Elliott and M. Gleiser, *Thermochemistry for Steelmaking*, Vol. I; J.F. Elliot, M. Gleiser, and V. Ramakrishna, *Thermochemistry for Steelmaking*, Vol. 2, Addison-Wesley, Reading, MA (1963).
3. G.H. Geiger and D.R. Poirier, *Transport Phenomena in Metallurgy*, Addison-Wesley, Reading, MA (1973).
4. E.N. Fuller, P.D. Schettler, and J.C. Giddings, *Indust. and Eng. Chem.*, **58**, 19 (1966).
5. *Perry's Chemical Engineer's Handbook*, 6th ed., McGraw-Hill, New York (1984).
6. R.C. Reid, J.M. Prausnitz, and B.E. Poling, *The Properties of Gases and Liquids*, McGraw-Hill, New York (1986).
7. R.B. Bird, W.E. Stewart, and E.N. Lightfoot, *Transport Phenomena*, Wiley. New York (1960).
8. L.N. Shatterfield and T.K. Sherwood, *The Role of Diffusion in Catalysis*, Addison-Wesley, Reading, MA (1963).
9. E.T. Turkdogan, P. Grieveson, and L.S. Darken, *J. Phys. Chem.*, **67**, 1647 (1963).
10. E.T. Turkdogan, P. Grieveson, and L.S. Darken, *J. Metals* (July 1962).
11. G.R. Zellars, S.L. Payne, J.P. Morris, and R.L. Kipp, *Trans. AIME*, **215**, 185 (1959).
12. J.H. Swisher and E.T. Turkdogan, *Trans. AIME*, **239**, 602 (1967).
13. J. Szekely and N.J. Themelis, *Rate Phenomena in Process Metallurgy*, Wiley, New York (1971).
14. L. Yang, S. Kado, and G. Derge, in: *Phys. Chem. Proc. Met.*, ed. G.R. St. Pierre, Vol. 535, Wiley-Interscience, New York (1961).
15. K. Niwa, M. Shimoji, S. Kado, Y. Watanabe, and T. Yokohawa, *Trans. AIME*, **209**, 96 (1957).

FIFTEEN

Unsteady State Diffusion

In Chapter 14, we discussed the concept of mass diffusivity and used Fick's first law of diffusion to solve problems of unidirectional steady-state diffusion. In this chapter, a similar approach will be used to develop the differential equations for the general case of three-dimensional, unsteady-state diffusion.

15.1. THE DIFFERENTIAL EQUATIONS OF DIFFUSION

As we did earlier in developing the equations of motion (Chapter 5) and the differential thermal energy balance (Chapter 11), let us consider an infinitesimal cubical element of volume $dx \cdot dy \cdot dz$ in a material B of overall concentration, or density, c (Fig. 15.1). Molecules of a species A are being transferred through this volume element either by diffusion or, in the case of fluids, by net bulk flow. Also, in the general case, some molecules of A are either consumed or generated within the differential element by means of chemical reaction. The material energy balance for molecules A within this element is stated as follows:

rate of accumulation of A in element
= rate of net transfer by diffusion
+ rate of net transfer by convection
+ rate of generation of A in element.

The *net* transfer rate signifies the difference between input and output molar flux of A, by diffusion and by bulk flow, with reference to a fixed coordinate system. Mathematically, the above statement is expressed as follows:

$$\frac{\partial c_A}{\partial t}\,dx\,dy\,dz = (N_{A,x} - N_{A,x+dx})\,dy\,dz + (N_{A,y} - N_{A,y+dy})\,dx\,dz + (N_{A,z} - N_{A,z+dz})\,dx\,dy + \dot{r}_A\,dx\,dy\,dz, \tag{15.1.1}$$

where $\dot{r}_A$ is the rate of chemical reaction per unit volume of the material and the second subscript of N_A signifies location. As demonstrated in Chapter 5 for the continuity equation which is of similar form, this equation can be rearranged as follows:

$$\frac{\partial c_A}{\partial t} = -\left[\frac{\partial N_A}{\partial X} + \frac{\partial N_A}{\partial y} + \frac{\partial N_A}{\partial z}\right] + \dot{r}_A, \tag{15.1.2}$$

or in vector notation:

$$\frac{\partial c_A}{\partial t} = -\nabla N_A + \dot{r}_A. \tag{15.1.3}$$

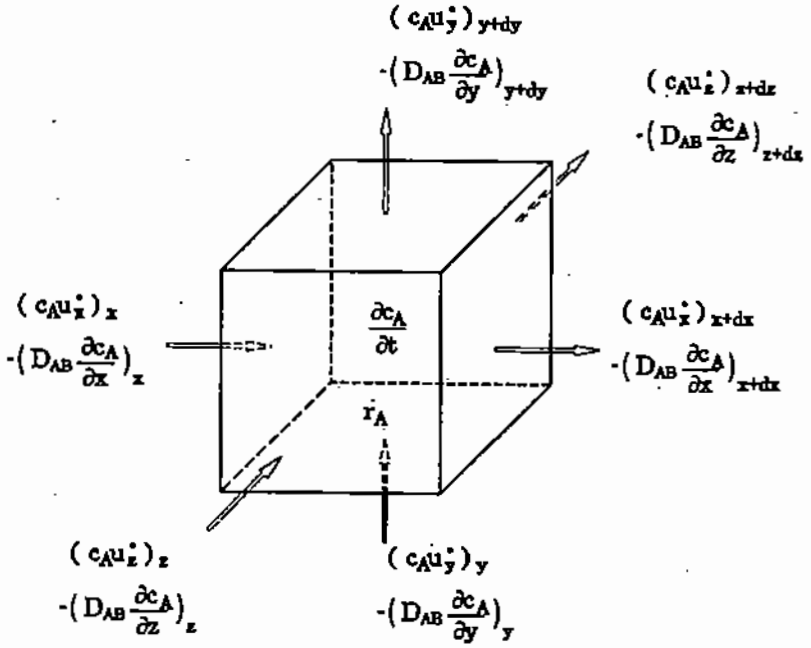

Figure 15.1. Material balance in a cubical element.

For diffusion of A through component B, we can substitute for N_A in the above equation from (14.5.4) (Chapter 14)

$$N_A = -cD_{AB}\nabla X_A + X_A(N_A + N_B). \tag{15.1.4}$$

to obtain:

$$\frac{\partial c_A}{\partial t} = \nabla\left[cD_{AB}\nabla X_A\right] - \nabla\left[X_A(N_A + N_B)\right] + \dot{r}_A. \tag{15.1.5}$$

Also, by definition (Chapter 14),

$$c_A = cX_A, \tag{15.1.6}$$

where c is the molar concentration of the mixture (see (14.3.3)), and

$$\frac{N_A + N_B}{c} = u^*, \tag{15.1.7}$$

where u^* is the *net diffusion velocity* of the mixture as defined in Chapter 14 (see (14.5.2)). By introducing these definitions in (15.1.5), we obtain

$$\frac{\partial cX_A}{\partial t} = \nabla\left[cD_{AB}\nabla X_A\right] - \nabla\left[cX_A u^*\right] + \dot{r}_A. \tag{15.1.8}$$

The velocity term u^* in (15.1.8) represents the net bulk flow due to diffusion as discussed in Chapter 14. The analytical solution of the general (15.1.8) is very difficult. However, certain simplifying assumptions can be made to allow for such a solution in special cases. Thus, for a material of *constant density*, (15.1.8) is expressed as follows:

$$\begin{aligned}\frac{\partial X_A}{\partial t} = &\left[\frac{\partial}{\partial x}\left(D_{AB}\frac{\partial X_A}{\partial x}\right) + \frac{\partial}{\partial y}\left(D_{AB}\frac{\partial X_A}{\partial y}\right) + \frac{\partial}{\partial z}\left(D_{AB}\frac{\partial X_A}{\partial z}\right)\right] \\ &- \left[u_x^*\frac{\partial X_A}{\partial x} + u_y^*\frac{\partial X_A}{\partial y} + u_z^*\frac{\partial X_A}{\partial z}\right] + \frac{\dot{r}_A}{c},\end{aligned} \tag{15.1.9}$$

where u_x^*, u_y^*, and u_z^* represent the components of the molar average velocity in the x-, y-, and z-directions. By moving the negative term of (15.1.9) to the left side, we can use the definition of the substantial time derivative of X_A, i.e.,

$$\frac{\partial X_A}{\partial t} + u_x^* \frac{\partial X_A}{\partial x} + u_y^* \frac{\partial X_A}{\partial y} + u_z^* \frac{\partial X_A}{\partial z} = \frac{DX_A}{Dt},$$

and express (15.1.9) as

$$\frac{DX_A}{Dt} = \frac{\partial}{\partial x}\left(D_{AB}\frac{\partial X_A}{\partial x}\right) + \frac{\partial}{\partial y}\left(D_{AB}\frac{\partial X_A}{\partial y}\right) + \frac{\partial}{\partial z}\left(D_{AB}\frac{\partial X_A}{\partial z}\right) + \frac{\dot{r}_A}{c}. \quad (15.1.10)$$

At *negligible net bulk flow due to diffusion*, that is at low concentration of the diffusing species or equimolar diffusion, the velocity components in the above equation are zero. Also, if the diffusivity does not change appreciably with concentration, (15.1.9) yields:

$$\frac{\partial X_A}{\partial t} = D_{AB}\left(\frac{\partial^2 X_A}{\partial x^2} + \frac{\partial^2 X_A}{\partial y^2} + \frac{\partial^2 X_A}{\partial z^2}\right) + \frac{\dot{r}_A}{c}. \quad (15.1.11)$$

In the *absence of chemical reaction*, (15.1.11) simplifies further to what is called *Fick's second law of diffusion*:

$$\frac{\partial X_A}{\partial t} = D_{AB}\left(\frac{\partial^2 X_A}{\partial x^2} + \frac{\partial^2 X_A}{\partial y^2} + \frac{\partial^2 X_A}{\partial z^2}\right). \quad (15.1.12)$$

In cylindrical coordinates, the equivalent form of (15.1.9), for constant diffusivity is

$$\begin{aligned}&\frac{\partial X_A}{\partial t} + u_r^* \frac{\partial X_A}{\partial r} + \frac{u_\theta^*}{r}\frac{\partial X_A}{\partial \theta} + u_z^* \frac{\partial X_A}{\partial z}\\ &\quad = D_{AB}\left(\frac{\partial^2 X_A}{\partial r^2} + \frac{1}{r}\frac{\partial X_A}{\partial r} + \frac{1}{r^2}\frac{\partial^2 X_A}{\partial \theta^2} + \frac{\partial^2 X_A}{\partial z^2}\right) + \frac{\dot{r}_A}{c},\end{aligned} \quad (15.1.13)$$

where the coordinates r, θ, and z are as defined in Chapter 11 (Fig. 11.2). For cylindrical symmetry and negligible bulk flow, the above equation reduces to

$$\frac{\partial X_A}{\partial t} = D_{AB}\left(\frac{\partial^2 X_A}{\partial r^2} + \frac{1}{r}\frac{\partial X_A}{\partial r} + \frac{\partial^2 X_A}{\partial z^2}\right) + \frac{\dot{r}_A}{c}. \quad (15.1.14)$$

The equivalent form of (15.1.9) and (15.1.13) in spherical coordinates is as follows:

$$\begin{aligned}&\frac{\partial X_A}{\partial t} + u_r^* \frac{\partial X_A}{\partial r} + \frac{u_\theta^*}{r}\frac{\partial X_A}{\partial \theta} + \frac{u_\theta^*}{r\sin\theta}\frac{\partial X_A}{\partial \phi}\\ &\quad = D_{AB}\left[\frac{1}{r^2}\frac{\partial}{\partial r}\left(r^2\frac{\partial X_A}{\partial r}\right) + \frac{1}{r^2\sin\theta}\frac{\partial}{\partial \theta}\left(\sin\theta\frac{\partial X_A}{\partial \theta}\right) + \frac{1}{r^2\sin^2\theta}\frac{\partial^2 X_A}{\partial \phi^2}\right] + \frac{\dot{r}_A}{c},\end{aligned} \quad (15.1.15)$$

where the coordinates r, θ, and ϕ are as defined in Chapter 11 (Fig. 11.3). For spherical symmetry and negligible bulk flow, (15.1.15) reduces to

$$\frac{\partial X_A}{\partial t} = D_{AB}\left(\frac{\partial^2 X_A}{\partial r^2} + \frac{2}{r}\frac{\partial X_A}{\partial r}\right) + \frac{\dot{r}_A}{c}. \quad (15.1.16)$$

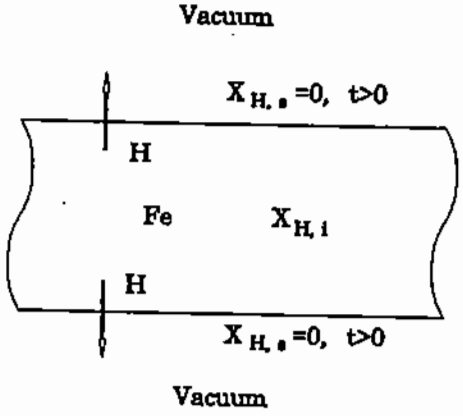

Figure 15.2. Removal of hydrogen from a steel plate under vacuum.

The reader may note that the equations for mass transfer in the absence of net bulk flow effects (i.e., when $u^* = 0$) are similar to the equations for unsteady state conduction presented in Chapter 11. Therefore, some of the techniques presented for the solution of heat conduction problems can also be applied to mass transfer. However, when bulk flow effects are involved, the mass transfer equations are not fully analogous to those presented for combined heat conduction and heat convection in Chapter 12. The difference is that in heat transfer the velocities are due to external forces or to buoyancy phenomena; while in the case of mass transfer, bulk flow may also be caused by the diffusion process.

In the following sections of this chapter, we shall examine the application of the above equations in solving engineering problems, under conditions where mass transfer by diffusion is predominant; i.e., when the diffusing species is at a low concentration and the net bulk flow is negligible. The reverse situation will be discussed in Chapter 16 on mass transfer by convection.

15.2. DIFFUSION IN A PLATE OF FINITE THICKNESS

Let us consider a steel plate of thickness L (Fig. 15.2) which contains hydrogen at an initial concentration, $X_{H,i}$. It is required to decrease the average hydrogen content of the metal by heating the plate at 650°C under vacuum. We shall assume that the plate is preheated uniformly to this temperature and that at time $t = 0$, it is subjected to vacuum. Under vacuum, the concentration of hydrogen at the upper and lower surfaces of the plate becomes $X_{H,s} = 0$. We need to develop a relationship between the time of vacuum treatment and the change in the average concentration of hydrogen throughout the plate.

In the absence of bulk flow effects and chemical reaction and assuming unidirectional diffusion of hydrogen from the bulk of the plate to its upper and lower surfaces, we obtain from (15.1.12)

$$\frac{\partial X_H}{\partial t} = D_{\mathrm{H-Fe}} \frac{\partial^2 X_H}{\partial y^2}. \tag{15.2.1}$$

The boundary conditions in this case are:

$$X_H = X_{H,i} \text{ at } t = 0, \tag{15.2.2}$$

$$X_H = 0 \text{ at } y = 0 \text{ and } y = L. \tag{15.2.3}$$

Equation (15.2.1) is of the same form as (11.2.1) for unsteady state conduction (Chapter 11). Carslaw and Jaeger [1] derived an analytical solution of (11.2.1) in the form of the product of a trigonometric and an exponential series; in terms of the differential (15.2.1) and its boundary conditions, this solution is expressed as follows:

$$\frac{X_H}{X_{H,i}} = \frac{4}{\pi} \sum_{n=0}^{\infty} \frac{1}{2n+1} \sin \frac{(2n+1)\pi y}{L} e^{-D_{H-Fe}(2n+1)^2\pi^2 t/L^2}. \tag{15.2.4}$$

Since the average concentration of hydrogen in the plate, at any time, is expressed by

$$X_{H,ave} = \frac{1}{L} \int_0^L X_H \, dy, \tag{15.2.5}$$

(15.2.4) and (15.2.5) can be combined and integrated to yield

$$\frac{X_{H,ave}}{X_{H,i}} = \frac{8}{\pi^2} \sum_{n=0}^{\infty} \frac{1}{(2n+1)^2} e^{-D_{H-Fe}(2n+1)^2\pi^2 t/L^2}. \tag{15.2.6}$$

Example 15.2.1

Calculate the time required to decrease the hydrogen content of a 1.22-cm thick steel plate from 0.5 ppm (parts per million) to an average of 0.25 ppm by heating it under vacuum at 400°C. The diffusivity of hydrogen in iron has been reported to be 1.66×10^{-9} at 10°C, 11.4×10^{-9} at 50°C, and 124×10^{-9} $cm^2 s^{-1}$ at 100°C. Extrapolate these data on the basis of an Arrhenius-type of relationship of diffusivity to temperature (see (14.4.2)) to estimate the diffusivity of hydrogen atoms in steel at 400°C.

From a linear regression analysis of the given diffusivity data for hydrogen in iron, using the Lotus 1-2-3 **Data Regression** facility, we establish the following equation for D_{H-Fe}:

$$\ln D_{H-Fe} = -2.46 - \frac{5052}{T}.$$

From this equation, the value of D_{H-Fe} at 673 K is estimated at 4.7×10^{-5} cm^2 s^{-1}. By using (15.2.6) for the given ratio of

$$\frac{X_{H,ave}}{X_{H,i}} = \frac{0.25}{0.50} = 0.5,$$

and introducing numerical values for the first five terms ($n = 0 \ldots 4$) of (15.2.6) in a spreadsheet program such as Lotus 1-2-3, we calculate the required time, t, to be 1557 seconds.

In the above example, we can also obtain an approximate solution by using graphical solutions which have been developed from the differential equations for unsteady-state conduction (Chapter 11) but apply equally well for unsteady-state diffusion. In these plots (Fig. 15.3), the dimensionless temperature on the y-axis is replaced by the dimensionless concentration ratio $(X_{ave} - X_e)/(X_i - X_e)$, where X_e represents the "equilibrium" or final attainable concentration of the component A in the material after infinite time of diffusion.

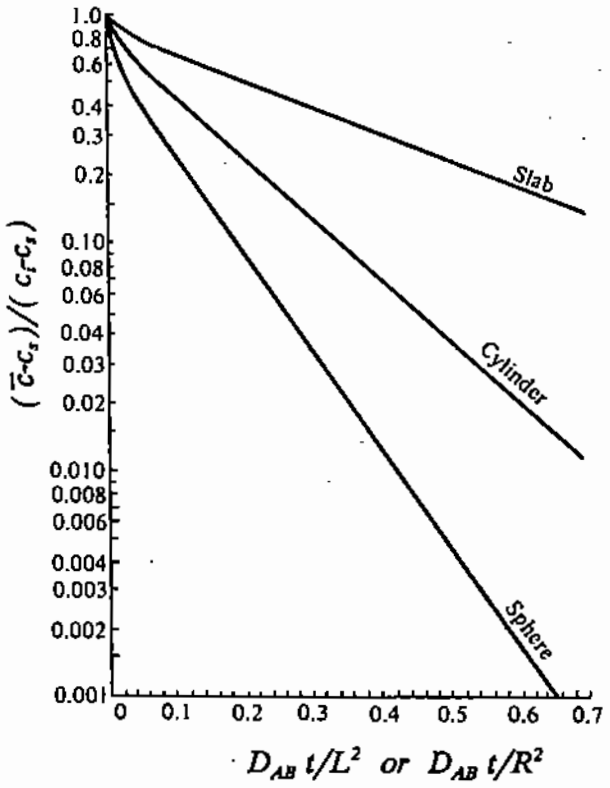

Figure 15.3. Dimensionless average concentration vs. time for slabs of thickness $2L$ and spheres and cylinders of radius R [3].

As in the case of thermal diffusion (Chapter 11), the x-axis represents the dimensionless time of diffusion of component A, expressed by the group $D_{AB}t/L^2$.

Figure 15.3 [3] shows three such plots of the fractional change in the dimensionless concentration vs. dimensionless time for slabs of thickness $2L$ and spheres and cylinders of radius R [4]. Another form of graphical representation of such data is in the form of the fractional degree of diffusion of species A out of medium B as a function of the dimensionless time elapsed since time $t = 0$. For example, Fig. 15.4 is such a plot of the diffusion of a species A out of a spherical particle [2]; m_t is the amount of A diffused out of a sphere over a time period t and m_i is the initial amount of A in the sphere at time 0.

15.3. DIFFUSION IN A SEMI-INFINITE MEDIUM

As in the case of heat conduction problems (Chapter 11), the unsteady state diffusion equations for semi-infinite media can be applied to systems of finite dimensions, provided that the diffusion times are relatively short. Also, since the solutions of the diffusion equation for infinite or semi-infinite media are relatively simple, they can be used as convenient asymptotes for checking out part of the numerical solutions of more complex mathematical models.

In this section we shall examine the following cases of diffusion in semi-infinite media:

a. Unsteady state diffusion at low concentration of the diffusing species and at constant diffusivity.
b. As in item a, but with variable diffusivity.
c. Unsteady state diffusion in a two-phase system.

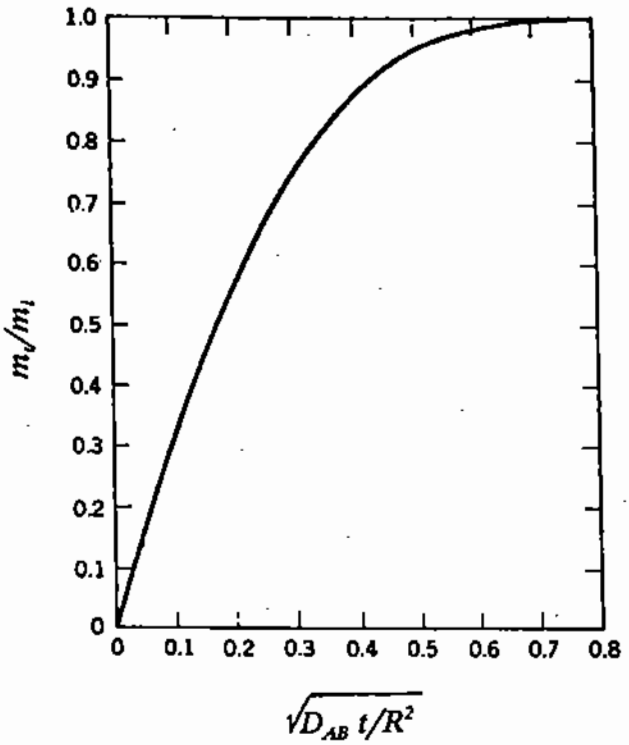

Figure 15.4. Fractional degree of diffusion of species A as a function of dimensionless time for a sphere of radius R.

15.3.1. Unsteady State Diffusion at Constant Diffusivity

Let us consider a semi-infinite medium extending from $y = 0$ to $y = \infty$. Initially, the mole fraction of the diffusing species A in the medium is X_i; at time $t > 0$, the mole fraction at the surface plane $y = 0$ is maintained at X_s. For unidirectional mass transfer, the diffusion (15.1.12) simplifies to

$$\frac{\partial X}{\partial t} = D_{AB}\frac{\partial^2 X}{\partial y^2} \quad \text{for } 0 \leq y \leq \infty, \tag{15.3.1}$$

where D_{AB} is the diffusion coefficient of A in B and X_A is the mole fraction of A. The boundary conditions are (see (11.2.15)):

$$X = X_i \text{ at } t = 0, \tag{15.3.2}$$

$$X = X_i \text{ at } y \to \infty, \tag{15.3.3}$$

$$X = X_s \text{ at } y = 0 \text{ and } t > 0. \tag{15.3.4}$$

The solution of this system of equations is analogous to the equivalent heat conduction problem discussed in §11.2.1:

$$X - X_i = (X_s - X_i)\,\text{erfc}\,\frac{y}{2\sqrt{D_{AB}t}}. \tag{15.3.5}$$

The molar flux of diffusing species A is therefore expressed as

$$N_A = -cD_{AB}\left(\frac{\partial X}{\partial y}\right)_{y=0} = c(X_s - X_i)\left(\frac{D_{AB}}{\pi t}\right)^{1/2}. \tag{15.3.6}$$

The mean value of the flux over a certain time interval t_e is given by

$$N_{A,\text{ave}} = \frac{1}{t_e}\int_0^{t_e} N_A\,dt = 2c(X_s - X_i)\left(\frac{D_{AB}}{\pi t_e}\right)^{1/2}. \tag{15.3.7}$$

Equation (15.3.6) may be used in experimental determinations of diffusion coefficients, by measuring the molar flux of the diffusing species as a function of time (e.g., in gas diffusivity measurements in liquids or solids, where the change in pressure can be recorded). A plot of the experimentally measured values of N_A against $t^{-1/2}$ then yields a straight line of slope $c(X_s - X_i)(D_{AB}/\pi)^{1/2}$.

Another method used frequently to measure diffusivities in liquids consists of filling a capillary tube with the liquid solution and then immersing the open upper end of the tube in a solution of higher concentration of the diffusing species A. After a given time interval, the capillary is withdrawn and its contents are analyzed. Let us assume that the initial concentration of A in the capillary was X_i and that the concentration of A in the bulk of the melt is maintained constant at X_b throughout the experiment. After a time interval t_e, a length L of the capillary is analyzed and found to have an average concentration X_{ave}. From (15.3.7), the total quantity of A that has diffused into the capillary in time t_e is

$$N_A t_e A_c = 2c(X_b - X_i)\left(\frac{D_{AB}t_e}{\pi}\right)^{1/2} A_c, \tag{15.3.8}$$

where A_c is the cross-sectional area of the capillary passage.

By equating this quantity to the change in the amount of species A contained in the capillary passage of length L, before and after diffusion, we obtain:

$$2c(X_b - X_i)\left(\frac{D_{AB}t_e}{\pi}\right)^{1/2} A_c = c(X_{\text{ave}} - X_i)LA_c, \tag{15.3.9}$$

and

$$\frac{X_{\text{ave}} - X_i}{X_b - X_i} = \frac{2}{L}\left(\frac{D_{AB}t_e}{\pi}\right)^{1/2}. \tag{15.3.10}$$

The diffusivity, D_{AB}, is then calculated by inserting the experimentally determined values in (15.3.10).

15.3.2. Unsteady State Diffusion at Variable Diffusivity

For systems where the diffusion coefficient is concentration-dependent, the differential equation for diffusion is expressed by

$$\frac{\partial(cX_A)}{\partial t} = \frac{\partial}{\partial y}\left[D_{AB}\frac{\partial(cX_A)}{\partial y}\right], \tag{15.3.11}$$

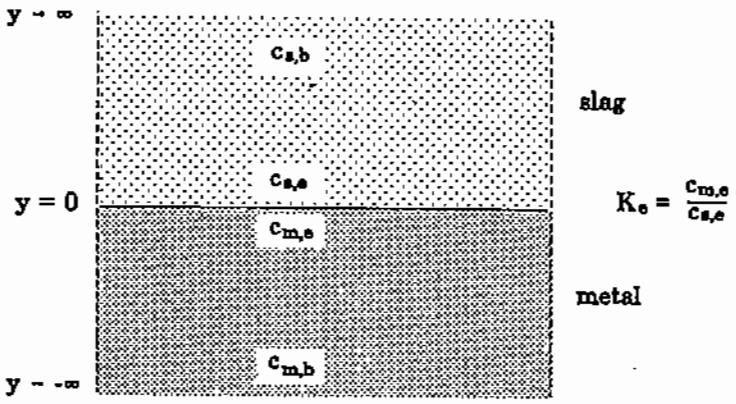

Figure 15.5. Unsteady state diffusion in a liquid–liquid system.

where D_{AB} is a known function of concentration, $f(cX)$. This equation can be solved by means of the finite difference technique which was discussed in Chapter 11 for unsteady-state heat conduction or by other numerical methods.

15.3.3. Unsteady State Diffusion in a Two-Phase System

Let us consider a reaction system of two semi-infinite media consisting of two immiscible stagnant liquids, e.g., the slag and metal layers in a furnace. As illustrated in Fig. 15.5, the upper slag phase is considered to extend from $y = 0$ to $y = \infty$, and the metal phase from $y = 0$ to $y = -\infty$. Let us assume that species A diffuses through the metal layer and at the metal-slag interface undergoes a chemical reaction through which it is transferred to the slag phase:

$$[A] \rightleftharpoons (A).$$

The species (A) must now diffuse away from the interface through the slag layer. Because of the high temperature of the system, the rate of the chemical reaction at the interface is very fast and the overall rate of removal of A from the metal depends solely on the rates of diffusion of A through metal and slag.

At time $t = 0$, the bulk concentration of the diffusing species A is assumed to be uniform at $c_{s,b}$ and $c_{m,b}$ in the slag and metal phases respectively. At the interface, the concentrations of the diffusing species A in the two phases are at *chemical equilibrium* (Chapter 18) which is expressed by

$$K_e = \frac{c_{m,e}}{c_{s,e}}, \tag{15.3.12}$$

where K_e is called the distribution coefficient of A, and the subscript e denotes equilibrium conditions. In the absence of bulk flow effects, Fick's second law of diffusion is expressed as follows for each of the two phases:

$$\frac{\partial c_s}{\partial t} = D_{A-s}\frac{\partial^2 c_s}{\partial y^2} \quad \text{for } 0 \le y \le \infty, \tag{15.3.13}$$

$$\frac{\partial c_m}{\partial t} = D_{A-m}\frac{\partial^2 c_m}{\partial y^2} \quad \text{for } 0 \ge y \ge -\infty. \tag{15.3.14}$$

Four of the boundary conditions express the initial concentrations in the two phases and also the concentrations at far away from the slag-metal interface:

$$c_s = c_{s,b} \text{ at } t = 0 \text{ and all } y, \tag{15.3.15}$$

$$c_m = c_{m,b} \text{ at } t = 0 \text{ and all } y, \tag{15.3.16}$$

$$c_s \to c_{s,b} \text{ at } y \to \infty, \tag{15.3.17}$$

$$c_m \to c_{m,b} \text{ at } y \to -\infty. \tag{15.3.18}$$

The remaining two boundary conditions express the equilibrium at the reaction interface and the fact that the rate at which the diffusing species A leaves the metal phase must be equal to the rate that it enters the slag phase:

$$\frac{c_{s,e}}{c_{m,e}} = K_e \text{ at } y = 0,\ t > 0, \tag{15.3.19}$$

$$D_{A-s}\frac{\partial c_s}{\partial y} = D_{A-m}\frac{\partial c_m}{\partial y} \text{ at } y = 0,\ t > 0, \tag{15.3.20}$$

Using a mathematical technique which was described in Chapter 11, the analytical solution of the above system of equations is expressed in the form of the following complementary error functions:

$$c_s = C_1 + C_2 \operatorname{erfc} \frac{y}{2\sqrt{D_{A-s}t}} \text{ for } 0 \le y \le \infty, \tag{15.3.21}$$

$$c_m = C_3 + C_4 \operatorname{erfc} \frac{|y|}{2\sqrt{D_{A-m}t}} \text{ for } 0 \ge y \ge -\infty, \tag{15.3.22}$$

where C_1, C_2, C_3, and C_4 are integration constants the values of which must be determined from the boundary conditions.

On the basis of the stated boundary conditions, at $t = 0$ the value of the complementary error function is 0 (see (11.2.5), Chapter 11) and the first two integration constants are obtained from (15.3.21) and (15.3.22):

$$C_1 = c_{s,b}, \quad C_3 = c_{m,b}.$$

The other two constants must be estimated from the boundary conditions of (15.3.19) and (15.3.20). At the interface ($y = 0$), the complementary error function is equal to 1 (see (11.2.5), Chapter 11) and (15.3.21) and (15.3.22) yield

$$c_s = c_{s,b} + C_2, \tag{15.3.23}$$

$$c_m = c_{m,b} + C_4. \tag{15.3.24}$$

On the basis of the assumption of equilibrium at the interface (see (15.3.19)), (15.3.23) and (15.3.24) can be combined as follows:

$$\frac{C_{m,b} + C_4}{c_{s,b} + C_2} = K_e. \tag{15.3.25}$$

Finally, by differentiating (15.3.21) and (15.3.22) with respect to y (Chapter 11) and substituting in the boundary condition expressed by (15.3.20), we obtain a second equation between C_2 and C_4:

$$D_{A-s}\left(-\frac{C_2}{(\pi D_{A-S}t)^{1/2}}\right) = D_{A-m}\left(-\frac{C_4}{(\pi D_{A-m}t)^{1/2}}\right), \tag{15.3.26}$$

and after simplifying (15.3.26),

$$C_4 = C_2\left(\frac{D_{A-s}}{D_{A-m}}\right)^{1/2}. \tag{15.3.27}$$

Solving (15.3.25) and (15.3.27) for the integration constants C_2 and C_4 we obtain

$$C_2 = \frac{K_e c_{s,b} - c_{m,b}}{\left(\frac{D_{A,s}}{D_{A,m}}\right)^{1/2} - K_e}, \tag{15.3.28}$$

$$C_4 = \frac{K_e c_{s,b} - c_{m,b}}{1 - K_e\left(\frac{D_{A,m}}{D_{A,s}}\right)^{1/2}}, \tag{15.3.29}$$

Therefore, the concentrations (15.3.21) and (15.3.22) can now be written in their full form:

$$c_s = c_{s,b} + \frac{K_e c_{s,b} - c_{m,b}}{\left(\frac{D_{A,s}}{D_{A,m}}\right)^{1/2} - K_e}\,\text{erfc}\,\frac{y}{2\sqrt{D_{A-s}t}} \quad \text{for } 0 \le y \le \infty, \tag{15.3.30}$$

$$c_m = c_{m,b} + \frac{K_e c_{s,b} - c_{m,b}}{1 - K_e\left(\frac{D_{A,m}}{D_{A,s}}\right)^{1/2}}\,\text{erfc}\,\frac{|y|}{2\sqrt{D_{A-m}t}} \quad \text{for } 0 \ge y \ge -\infty. \tag{15.3.31}$$

The flux of the diffusing species A across the interface is expressed by

$$N_{A-s} = N_{A-m} = -D_{A-s}\frac{\partial c_s}{\partial y} = -D_{A-m}\frac{\partial c_m}{\partial y} \text{ at } y = 0. \tag{15.3.32}$$

Therefore, by differentiation of (15.3.30) and (15.3.31) we obtain the following equations for the respective mass fluxes at the interface between the two phases:

$$N_{A,s} = -\left(\frac{D_{A,s}}{\pi t}\right)^{1/2}\frac{K_e c_{s,b} - c_{m,b}}{\left(\frac{D_{A,s}}{D_{A,m}}\right)^{1/2} - K_e}, \tag{15.3.33}$$

$$N_{A,m} = -\left(\frac{D_{A,m}}{\pi t}\right)^{1/2}\frac{K_e c_{s,b} - c_{m,b}}{1 - K_e\left(\frac{D_{A,m}}{D_{A,s}}\right)^{1/2}}. \tag{15.3.34}$$

REFERENCES

1. H.S. Carslaw and J.C. Jaeger, *Conduction of Heat in Solids*, Clarendon Press, Oxford (1959).
2. J. Crank, *Mathematics of Diffusion*, Oxford Press, New York (1956).
3. G.H. Geiger and D.R. Poirier, *Transport Phenomena in Metallurgy*, Addison-Wesley, Reading, MA (1973).
4. R.B. Bird, W.E. Stewart, and E.N. Lightfoot, *Transport Phenomena*, Wiley, New York (1960).
5. T.K. Sherwood, R.L. Pigford, and C.R. Wilke, *Mass Transfer*, McGraw-Hill, New York (1975).
6. R.I.L. Guthrie, *Engineering in Process Metallurgy*, Clarendon Press, Oxford (1989).
7. J. Szekely and N.J. Themelis, *Rate Phenomena in Process Metallurgy*, Wiley, New York (1971).

SIXTEEN

Mass Transfer by Convection

In Chapter 15, we examined problems where the predominant mode of mass transfer was by diffusion. In **convective** mass transfer, which occurs only in fluids or fluidized solids, the bulk motion of the fluid plays a major role in the transfer of the diffusing species between two or more phases.

As in the case of heat convection (Chapter 12), when the flow field is imposed by external forces, mass transfer is said to occur by means of **forced convection**. Examples of this are flow systems under pressure or electromagnetic forces.

In the second group of convective mass transfer problems, bulk flow is due to internal buoyancy forces within the fluid system. This phenomenon is called **natural convection** and the density differences that cause it may be due to either concentration or temperature gradients in the fluid.

Similarly to other transport phenomena (Chapters 5 and 11), the formulation of the mass convection equation is based on a material balance of the diffusing component A over an infinitesimal volume element $dx \cdot dy \cdot dz$ (Fig. 16.1). The resulting differential equation is nearly the same as that developed in Chapter 15 for diffusion:

$$\frac{\partial c X_A}{\partial t} = \nabla \cdot [c D_{AB} \nabla X_A] - \nabla \cdot [c X_A \boldsymbol{u}] + \dot{r}_A. \qquad (16.1.1)$$

The only difference between (15.1.8) and (16.1.1) is that the velocity term $\boldsymbol{u}^*$ in (15.1.8) represented the *net bulk flow due to diffusion* (Chapter 14) while the term $\boldsymbol{u}$ in the above equation represents the diffusion velocity $\boldsymbol{u}^*$ plus the *flow due to externally imposed forces* such as pressure and gravity gradients. It is obvious that in the case of forced or natural convection these externally imposed velocities are predominant.

In many problems of forced convection, the fluid flow and mass transfer equations can be considered separately; thus we may first determine the velocity distribution in the flow field and then use it in the appropriate form of the differential mass balance equation. Problems in natural convection are more complex because the fluid flow and mass transfer equations are coupled and must be solved simultaneously.

The analogy between heat and mass transfer, which has already been mentioned, can be utilized frequently to obtain the solution of a mass transfer problem from the corresponding equations for heat transfer by convection, and vice versa. Exceptions to this rule are problems

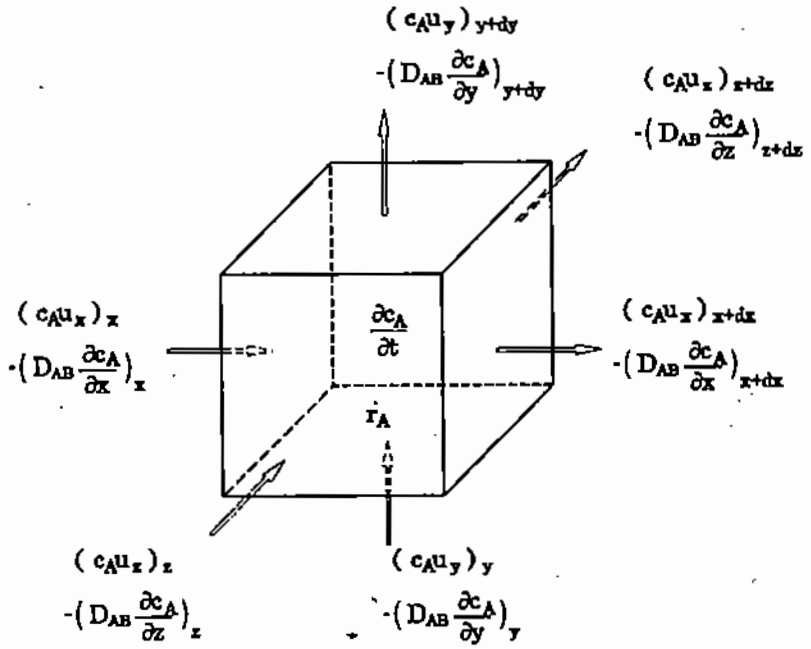

Figure 16.1. Control volume element for mass transfer by diffusion and convection.

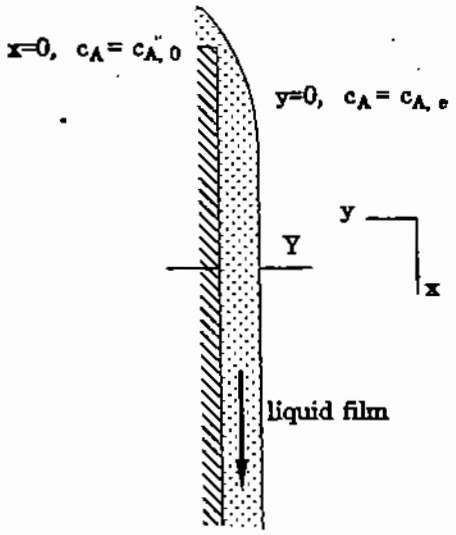

Figure 16.2. Mass transfer from a gas to a falling film in laminar flow.

involving chemical reaction or when the net bulk flow due to diffusion is large enough to modify the velocity profile.

16.1. FORCED CONVECTION IN LAMINAR FLOW

Let us consider the absorption of a species A diffusing from a gas phase into a laminar film of liquid B flowing downward (x-direction) on a vertical wall (Fig. 16.2). It is assumed that the rate of mass transfer of A through the gas phase and its rate of absorption in the liquid surface are very high so that the concentration of A at the surface of the film is maintained

at the saturation, or equilibrium, concentration, $c_{A,e}$. If the initial concentration (i.e., at the top of the wall, $x = 0$) of A in the liquid is $c_{A,0}$, the problem is to develop an expression for the concentration profile of A, as the film moves downwards. Problems of this type occur in absorption or desorption processes, such as the removal of sulfur dioxide from plant exhaust gases by caustic solutions.

If we assume that the laminar flow in the film is fully developed, that is, the film thickness and the velocity profile are constant with vertical distance down the wall, the conservation of A can be expressed by (16.1.1), which in this case simplifies to

$$u_x \frac{\partial c_A}{\partial x} = D_{AB} \frac{\partial^2 c_A}{\partial y^2} \text{ for } 0 \leq y \leq Y, \tag{16.1.2}$$

where y is the axis perpendicular to the direction of flow and Y is the thickness of the film (Fig. 16.2). It can be seen that for unidirectional flow, as implied by the assumption of fully developed laminar flow in the x-direction, the y- and z-components of velocity in (16.1.1) have been neglected.

The boundary conditions for (16.1.2) are

$$c_A = c_{A,0} \text{ at } x = 0 \text{ and } 0 \leq y \leq Y, \tag{16.1.3}$$

$$c_A = c_{A,e} \text{ at } y = 0 \text{ and all } x, \tag{16.1.4}$$

where $y = 0$ denotes the outer edge of the film in contact with the gas phase and Y is the full thickness of the falling film. Also, the fact that A cannot diffuse into the wall is expressed by the following equation:

$$\frac{\partial c_A}{\partial y} = 0 \text{ at } y = Y \text{ and all } x. \tag{16.1.5}$$

Before we can proceed with the solution of (16.1.2), we must obtain an expression for the velocity profile in the film. In the discussion on falling films in Chapter 4, it was shown that the velocity profile in the liquid film is parabolic:

$$u_x = u_{\max} \left[1 - \left(\frac{y}{Y}\right)^2\right], \tag{16.1.6}$$

where $u_{\max}$ denotes the maximum velocity:

$$u_{\max} = \frac{\rho g Y^2}{2\mu}. \tag{16.1.7}$$

The *average* velocity of the fluid is:

$$\overline{u} = \frac{1}{Y} \int_0^Y u \, dy = \frac{\dot{v}}{Y}, \tag{16.1.8}$$

where $\dot{v}$ is the volumetric flow rate of liquid per unit width of the wall.

By combining (16.1.2) and (16.1.6) we obtain:

$$u_{\max}\left(1-\left(\frac{y}{Y}\right)^2\right)\frac{\partial c_A}{\partial x}=D_{AB}\frac{\partial^2 c_A}{\partial y^2}. \tag{16.1.9}$$

Pigford [7] derived the following solution of (16.1.9) for the boundary conditions (16.1.3)–(16.1.5):

$$\begin{aligned}\frac{c_{A,e}-\bar{c}_{A,x}}{c_{A,e}-\bar{c}_{A,0}} =& 0.061+0.7857e^{-5.213\tau}+0.1001e^{-39.318\tau}\\ &+0.03599e^{-105.64\tau}+0.01811e^{-204.75\tau},\end{aligned} \tag{16.1.10}$$

where $c_{A,e}$ is the equilibrium concentration of A in the liquid and $\bar{c}_{A,0}$ and $\bar{c}_{A,x}$ are the average concentrations of A across the film at $x=0$ and at distance x down the wall, i.e.,

$$\bar{c}_{A,x}=\frac{1}{Y}\int_0^Y c_A\,dy \quad \text{at } x, \tag{16.1.11}$$

and τ represents dimensionless time, which we encountered earlier (Chapter 15) for diffusion:

$$\tau=\frac{D_{AB}t}{Y^2}. \tag{16.1.12}$$

In this case, the time of contact t between the gas and liquid phases is equal to the distance travelled by the fluid, x, divided by the surface velocity, i.e., the maximum velocity of the fluid film, $u_{\max}$. Therefore, since for laminar flow in a film $u_{\max}=\frac{3}{2}\bar{u}$,

$$\tau=\frac{D_{AB}}{Y^2}\frac{x}{u_{\max}}=\frac{D_{AB}}{Y^2}\frac{x}{1.5\bar{u}}. \tag{16.1.13}$$

It should be noted that (16.1.10) contains the constant 0.061 which is not shown in previous publications of this equation (e.g., [3,4,5]) including the 1944 paper by Johnstone and Pigford [6]. If the equation is to include only the first four terms of the series, as shown above and in earlier publications [3–6], this constant is necessary to satisfy the initial condition of $(c_{A,e}-\bar{c}_{A,0})/(c_{A,e}-\bar{c}_{A,0})=1$, at $x^*=0$. A plot of (16.1.10) is shown in Fig. 16.3.

16.2. FORCED CONVECTION IN A LAMINAR BOUNDARY LAYER

We will now consider the problem of mass transfer from a flat surface (e.g., by sublimation or evaporation) to an incompressible fluid flowing over the plate (Fig. 16.4). The bulk fluid velocity is u_b, and the concentration of the diffusing species A in the bulk fluid, $c_{A,b}$. Let us also assume that, at the surface of the plate, the concentration of A is maintained at the saturation concentration, $c_{A,s}$. The problem is to develop an equation for the concentration profile of A in the fluid above the surface. An example of this situation is the transfer of water vapor from a wet surface to the air flow above it.

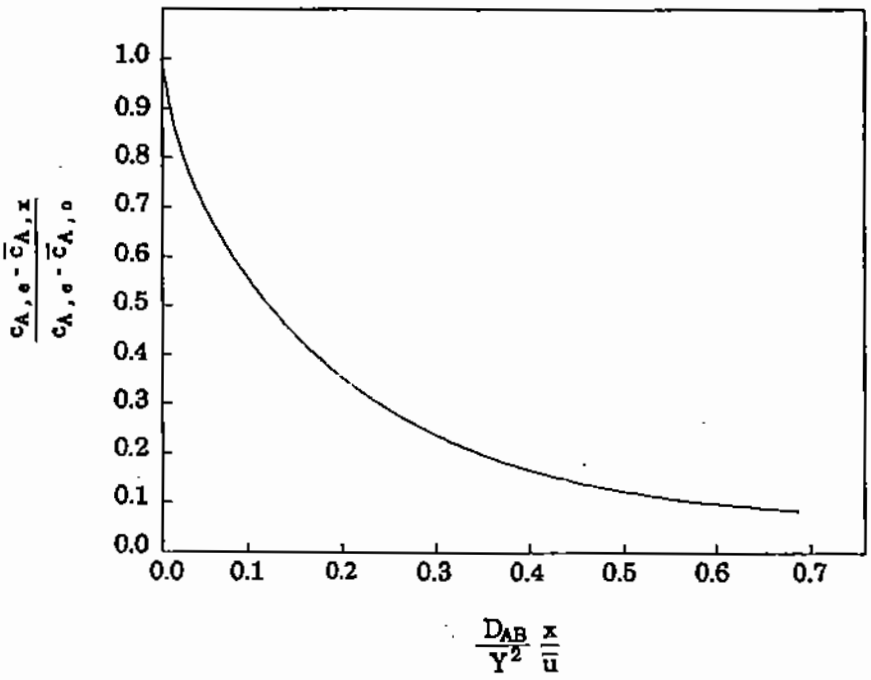

Figure 16.3. Graphical representation of Pigford equation.

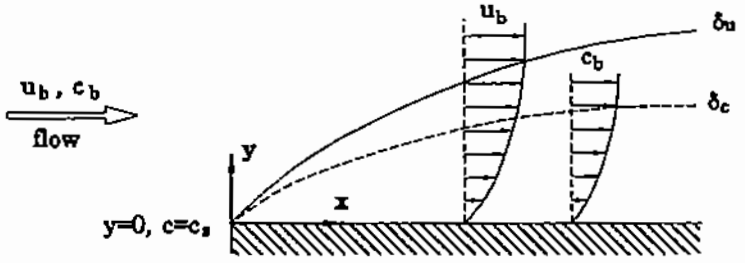

Figure 16.4. Velocity and concentration boundary layers in laminar flow along a flat plate.

16.2.1. The Concentration Boundary Layer

In physical terms, the situation depicted in Fig. 16.4 can be visualized as follows: The fluid near the plate is retarded because of viscous momentum transfer, and a region is formed where the fluid velocity is lower than in the bulk stream. As discussed in Chapter 6 on fluid flow, this region is called the **velocity boundary layer.** Also, in Chapter 12, we described how in heat transfer the retardation of the fluid close to the surface leads to the formation of a **thermal boundary layer.**

In a similar way, we can visualize a film of fluid next to the surface in which the concentration differs from that in the bulk stream; this region is called the **concentration boundary layer** (or *diffusion boundary layer*). As discussed in Chapters 6 and 12, the equation of continuity for the two-dimensional flow in this boundary layer is expressed as follows:

$$\frac{\partial u_x}{\partial x} + \frac{\partial u_y}{\partial y} = 0, \tag{16.2.1}$$

while the equation of motion is

$$u_x \frac{\partial u_x}{\partial x} + u_y \frac{\partial u_x}{\partial y} = \frac{\mu}{\rho} \frac{\partial^2 u_x}{\partial y^2}. \tag{16.2.2}$$

The boundary conditions for the above equations are:

$$u_x = 0,\ u_y = 0 \text{ at } y = 0 \text{ (plate surface)},$$

$$u_x = u_b,\ u_y = 0 \text{ at } y \to \infty \text{ (away from plate surface)},$$

$$u_x = u_b, u_y = 0 \text{ at } x = 0 \text{ for all } y. \tag{16.2.3}$$

The equation of conservation for the diffusing species A can be obtained from (16.1.1), on the basis of the following assumptions:

a. There is no chemical reaction ($\dot{r}_A = 0$).
b. The z-component of velocity is neglected (two-dimensional flow).
c. Diffusion in the x-direction is negligible in comparison with the transport of mass by bulk of the fluid, i.e.,

$$u_x \frac{\partial c_A}{\partial x} \gg D_{AB} \frac{\partial^2 c_A}{\partial x^2}.$$

Accordingly, (16.1.1) simplifies to:

$$u_x \frac{\partial c_A}{\partial x} + u_y \frac{\partial c_A}{\partial y} = D_{AB} \frac{\partial^2 c_A}{\partial y^2}. \tag{16.2.4}$$

The velocity boundary conditions for this equation are the same as for the equations of motion (see (16.2.3)). The concentration boundary conditions are

$$c_A = c_{A,s} \text{ at } y = 0,\ \ c_A = c_{A,b} \text{ at } y \to \infty,\ \ c_A = c_{A,b} \text{ at } x = 0. \tag{16.2.5}$$

The method of solving these equations is identical to that discussed in Chapter 12 for heat transfer by forced convection through a thermal boundary layer: The analytical solution for the velocity profile in a boundary layer was developed in Chapter 6 (§6.2.1) and is expressed by the following equation:

$$\frac{u_x}{u_b} = f(\eta) = \frac{3}{2}\eta - \frac{1}{2}\eta^3, \tag{16.2.6}$$

where

$$\eta = \frac{y}{\delta_x} = \frac{y}{4.64\sqrt{\nu x/u_b}} \tag{16.2.7},$$

and δ_x is the thickness of the boundary layer as a function of distance x from the leading edge of the plate. In order to solve the mass balance of (16.2.4), we first define a dimensionless concentration as follows:

$$\widetilde{c} = \frac{c_{A,s} - c_A}{c_{A,s} - c_{A,b}}. \tag{16.2.8}$$

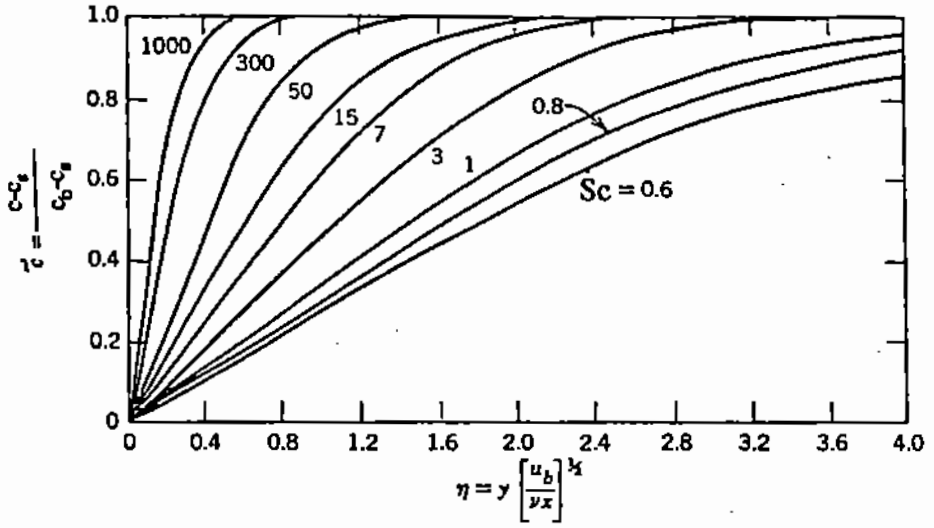

Figure 16.5. Dimensionless concentration profiles in the laminar boundary layer along a flat plate.

By introducing the variable $\tilde{c}$ and the transform variable η in (16.2.4), we obtain

$$\frac{d^2\tilde{c}}{d\eta^2} + \frac{1}{2}\,\mathrm{Sc}\, f(\eta)\,\frac{d\tilde{c}}{d\eta} = 0, \tag{16.2.9}$$

where Sc is a dimensionless group called the **Schmidt number** which will be discussed in the following section:

$$\mathrm{Sc} = \frac{\nu}{D_{AB}} = \frac{\mu}{\rho D_{AB}}. \tag{16.2.10}$$

The boundary conditions of 16.2.5 are now transformed to dimensionless form:

$$\tilde{c} = 0 \text{ at } \eta = 0, \tag{16.2.11}$$

$$\tilde{c} = 1 \text{ at } \eta \to \infty. \tag{16.2.12}$$

The solution of (16.2.9) for these boundary conditions is shown in graphical form in Fig. 16.5 as a function of the Schmidt number.

16.2.2. The Schmidt Dimensionless Number

As shown by (16.2.10), the Schmidt number represents the ratio of the momentum diffusivity to the mass diffusivity of a particular fluid. It corresponds to the Prandtl number for heat transfer by convection (Chapter 12). When the Schmidt number is near unity, as it is for some gases, the velocity and concentration boundary layers coincide and the equations for the dimensionless velocity and concentration profiles are identical.

For high values of the Schmidt number, as in the case of all liquids, the ability of the fluid to transmit momentum is much greater than its diffusivity, and consequently the velocity boundary layer is thicker than the concentration boundary layer.

The effect of Schmidt number on the concentration profiles in the boundary layer is illustrated in Fig. 16.5. Comparison of this graph with the equivalent plots of the dimensionless temperature profiles in the boundary layer (Chapter 12, Fig. 12.6) shows that the

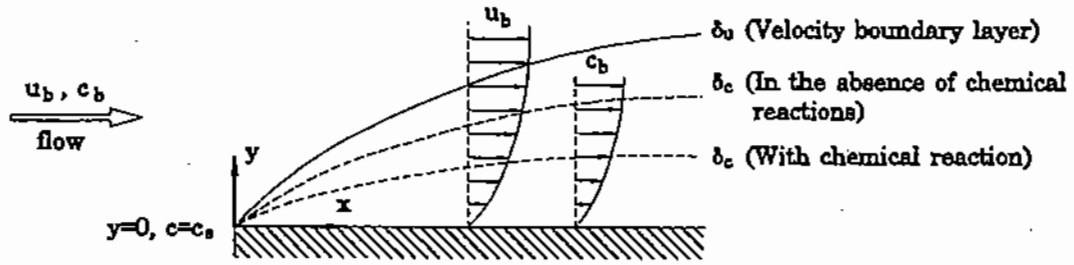

Figure 16.6. Effect of homogeneous chemical reaction on the concentration boundary layer.

two plots are identical; i.e., the Schmidt number in mass transfer has the same significance as the Prandtl number in heat transfer by convection.

For gases, both the Schmidt and the Prandtl numbers are close to unity. For viscous, low-conductivity fluids, such as slags or molten glass, the Prandtl number is in the order of 10–1000, while for molten metals it is much less than unity. The Schmidt number is high for all liquids, including molten metals and slags.

16.2.3. Mass Transfer with Chemical Reaction

Let us consider a system where a fluid flows over a flat plate. Species A diffuses from the plate into the fluid stream, where it reacts with the stream according to the following rate equation:

$$\dot{r} = -k_r c_A^n, \tag{16.2.13}$$

where $\dot{r}_A$ is the rate of the homogeneous chemical reaction (Chapter 18); k_r is the specific rate constant; n is the order of the chemical reaction (Chapter 18).

For an incompressible fluid and for low concentration of the diffusing species, this problem is analogous to that discussed in §16.2.1. Thus, the fluid flow equations are identical to (16.2.1) and (16.2.2), while the conservation of A is expressed by

$$u_x \frac{\partial c_A}{\partial x} + u_y \frac{\partial c_A}{\partial y} = D_{AB} \frac{\partial^2 c_A}{\partial y^2} - k_r c_A^n. \tag{16.2.14}$$

The boundary conditions are similar to (16.2.3) and (16.2.5). The solution of this system of equations is described in the literature [3]. As illustrated in Fig. 16.6, the effect of the chemical reaction is to narrow the concentration boundary layer and thus increase the rate of mass transfer from the plate.

16.3. NATURAL CONVECTION IN A LAMINAR BOUNDARY LAYER

In the absence of chemical reaction and for low concentrations of the diffusing species, the equations for mass transfer by natural convection are analogous to the corresponding heat transfer equations, as discussed in Chapter 12.

As noted earlier, natural convection occurs under the influence of buoyancy forces which may be due to either concentration or temperature gradients. For instance, let us consider the transfer of diffusing species A from a vertical wall immersed in a liquid bath (Fig. 16.7); the fractional molar concentration of A at the plate surface is $X_{A,s}$ and in

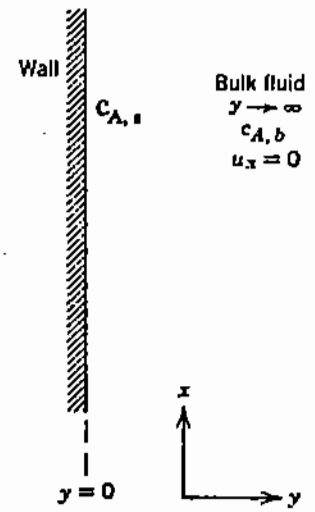

Figure 16.7. Mass transfer by natural convection at a vertical wall.

the bulk of the fluid, $X_{A,b}$. The formulation of this problem is almost identical to the corresponding case of heat transfer case discussed in Chapter 12:

$$\text{equation of continuity:} \quad \frac{\partial u_x}{\partial x} + \frac{\partial u_y}{\partial y} = 0, \tag{16.3.1}$$

$$\text{equation of motion:} \quad u_x \frac{\partial u_x}{\partial x} + u_y \frac{\partial u_x}{\partial y} = \nu \frac{\partial^2 u_x}{\partial y^2} + g_x \beta' (X_{A,s} - X_{A,y}), \tag{16.3.2}$$

where g_x is the component of the acceleration due to gravity in the x-direction; β' is the coefficient of density change of fluid with X_A (see (16.3.7)); $X_{A,y}$ is the fractional concentration of A at distance y perpendicularly from the plate surface.

The material balance equation for species A is as follows:

$$u_x \frac{\partial X_A}{\partial x} + u_y \frac{\partial X_A}{\partial y} = D_{AB} \frac{\partial^2 X_A}{\partial y^2}. \tag{16.3.3}$$

The boundary conditions for (16.3.1)–(16.3.3) are

$$u_x = u_y = 0 \text{ at } y = 0, \quad u_x = 0 \text{ at } y \to \infty,$$

$$X_{A,y} = X_{A,s} \text{ at } y = 0, \quad X_{A,y} = X_{A,b} \text{ at } y \to \infty,$$

$$X_A = X_{A,b} \text{ at } x = 0 \text{ for all } y. \tag{16.3.4}$$

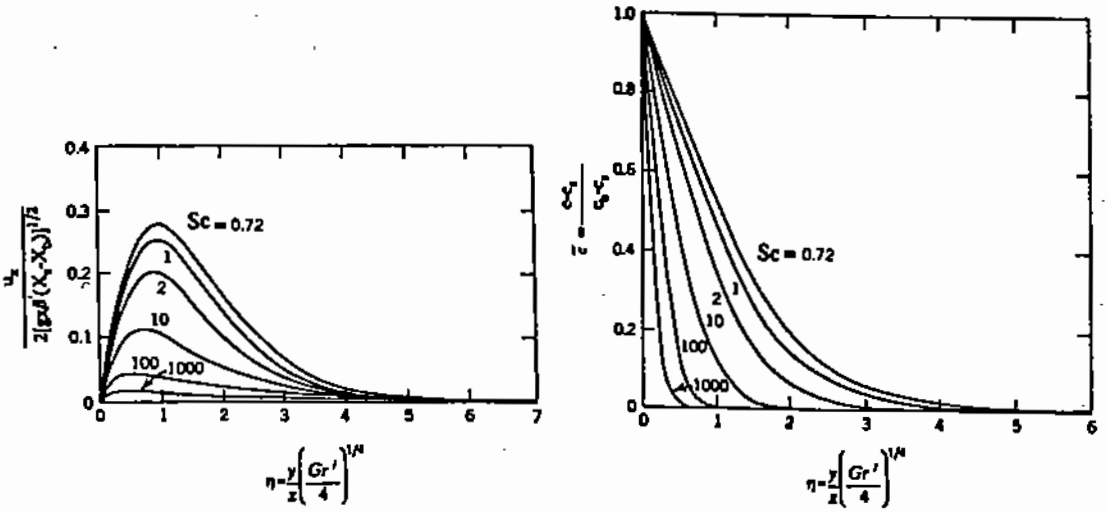

Figure 16.8. Dimensionless velocity and concentration profiles for laminar natural convection along a vertical wall.

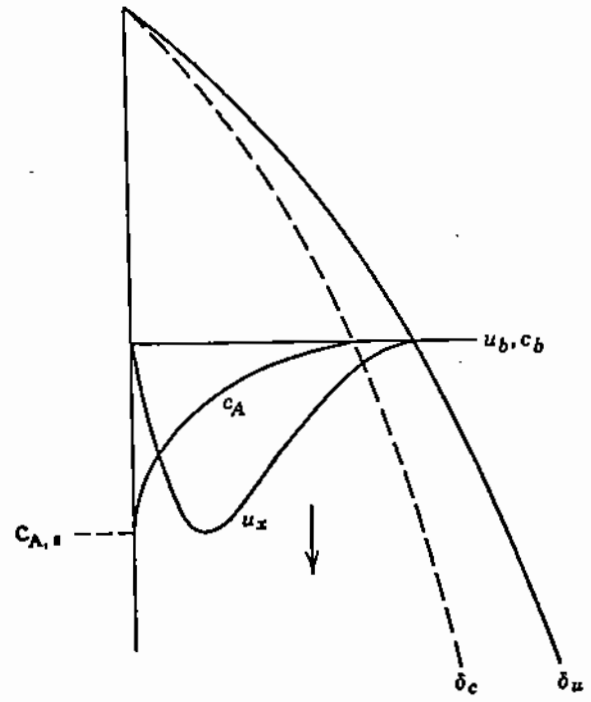

Figure 16.9. Velocity and concentration boundary layers for a dissolving surface (e.g., a copper anode).

The solution of this system of equations is derived in the same way as for the corresponding case of heat transfer by natural convection (Chapter 12). The resultant velocity and concentration profiles are plotted in Fig. 16.8 as a function of the dimensionless distance parameter:

$$\eta = \frac{y}{x}\left(\frac{\mathrm{Gr}'}{4}\right)^{1/4}, \tag{16.3.5}$$

where Gr' is the dimensionless *concentration Grashof number* to be described shortly.

These plots are identical to the plots of heat transfer by natural convection (Figs. 12.8 and 12.9) with the exception that the dimensionless Prandtl number ($\mathrm{Pr} = C_p\mu/k$) has been replaced by the Schmidt number ($\mathrm{Sc} = \mu/\rho D_{AB}$); also, the dimensionless temperature gradients have been replaced by the dimensionless concentration gradients which are now causing the buoyancy forces in the liquid. The concentration Grashof number is defined as follows:

$$\mathrm{Gr}' = \frac{gx^3\beta'(X_s - X_b)}{\nu^2}, \tag{16.3.6}$$

where

$$\beta' = \frac{1}{\rho}\left(\frac{\partial\rho}{\partial X_A}\right)_T \tag{16.3.7}$$

is the fractional change of density of the fluid with mole fraction of A, and X_s and X_b are the mole fractions of A at the surface and in the bulk fluid; x is the distance from the leading edge of the surface.

Figure 16.9 shows the velocity and concentration profiles and also the respective boundary layers for the case where X_s is higher than X_b; for example, this case exists in the anodic dissolution of copper from a vertical anode plate. Figure 16.9 would be reversed in the opposite case of electrodeposition of copper on a vertical cathode plate, where X_s is lower than X_b.

It can be seen that the Schmidt numbers in Figs. 16.5 and 16.8 are in the range of $\mathrm{Sc} > 0.72$. As noted earlier, the Schmidt numbers for gases are in the order of unity, while for liquids they are much higher. Therefore, the concentration (or "diffusion") boundary layer for liquids is much smaller than the corresponding velocity boundary layer (Fig. 16.9). An important result of this behavior is that a slight convective motion in a liquid can produce a large increase in the rate of mass transfer.

REFERENCES

1. J. Tallmadge, *AIChE J.*, **11**, 1153 (1965).
2. R.B. Bird, W.E. Stewart, and E.N. Lightfoot, *Transport Phenomena*, Wiley, New York (1975).
3. T.K. Sherwood, R.L. Pigford, and C.R. Wilke, *Mass Transfer*, McGraw-Hill, New York (1975).
4. N.P. Cheremisinoff, ed., *Handbook of Heat and Mass Transfer*, Vol. 2: *Mass Transfer and Reactor Design*, Gulf Publishing, Houston (1986).
5. J. Szekely and N.J. Themelis, *Rate Phenomena in Process Metallurgy*, Wiley, New York (1971).
6. H.F. Johnstone and R.L. Pigford, *Trans. AIChE*, **38**, 25 (1942).
7. R.L. Pigford, PhD Thesis, University of Illinois (1941).

SEVENTEEN

Mass Transfer Models and Correlations

In Chapter 16, we examined methods of formulating and solving problems of convective mass transfer in the laminar region of flow. It was shown that the solution of the differential equations of motion and diffusion can yield the concentration profiles of the diffusing species in a system.

In many mass transfer problems, we do not need detailed information on the concentration profiles in the system, but only a reliable estimate of the mass transfer between a fluid and a solid surface, or between two fluids. In principle, this can be done by first establishing the concentration profile near the interface between the two phases and then using it to calculate the mass flux, by an equation of the type shown in Chapter 15:

$$N_{A,y} = -cD_{AB}\frac{\partial X_A}{\partial y} + X_A(N_{A,y} + N_{B,y}), \tag{17.1.1}$$

where c is the molar density of fluid, and $N_{A,y}$ and $N_{B,y}$ are the molar fluxes of components A and B in the y-direction.

However, in many cases this procedure is not practical, because of the geometric complexity of the system or for other reasons. It is then necessary to use published information on similar systems or carry out experiments, in order to determine the rate of mass transfer. This is particularly the case for turbulent systems, where the velocity and concentration profiles cannot be determined from first principles.

17.1. THE CONCEPT OF THE MASS TRANSFER COEFFICIENT

In order to provide a rational framework for the development of semi-empirical mass transfer correlations, the concept of the *mass transfer coefficient* has been introduced. Let us consider a fluid flowing past a surface (Fig. 17.1) where the concentration of the diffusing species A is $c_{A,s}$ at the surface and $c_{A,b}$ in the bulk fluid. If the molar flux between the surface and the bulk fluid is N_A, the mass transfer coefficient is defined by the following equation:

$$N_A = k_d(c_{A,s} - c_{A,b}). \tag{17.1.2}$$

Equation (17.1.2) states that the mass flux between the surface and the bulk fluid is proportional to the concentration difference between the surface and the bulk of fluid; the constant of proportionality, k_d, is defined as the **mass transfer coefficient**. Inspection of (17.1.2) shows that the mass transfer coefficient, k_d, has the following dimensions:

$$k_d = \frac{\text{molar flux}}{\text{molar concentration}} = \frac{\text{mass flux}}{\text{mass concentration}} = \frac{\text{M t}^{-1}\,\text{L}^{-2}}{\text{M L}^{-3}} = \text{L t}^{-1}.$$

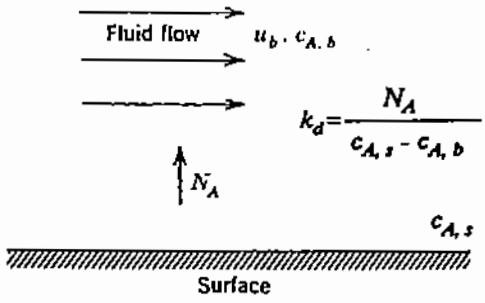

Figure 17.1. Definition of the mass transfer coefficient

It can be seen that the dimensions of k_d are the same as those of the ratio of molecular diffusivity divided by the thickness of an assumed boundary layer($L^2\ t^{-1}/L$). In effect, the mass transfer coefficient is a composite measure of the mass diffusion coefficient and the thickness of the boundary layer, through which species A must diffuse in order to reach the bulk fluid.

As in the case of the heat transfer coefficient (Chapter 12), we may use the analogy with Ohm's law and regard the concentration difference as a potential, the mass flux as electric current and the mass transfer coefficient as the conductance, that is, the reciprocal of resistance.

17.2. ANALYTICAL CORRELATIONS OF THE MASS TRANSFER COEFFICIENT

As would be expected from theory, the mass transfer coefficient depends on geometry, fluid velocity, properties of the fluid and concentration. For unsteady state situations, the mass transfer coefficient may also depend on time.

Values of mass transfer coefficients may be obtained either experimentally or from empirical or semi-empirical correlations established by others. When analytical solutions are available for the concentration profile in a system, such correlations can be based on first principles, as illustrated in the following cases.

17.2.1. Laminar Forced Convection over a Flat Plate

This problem was discussed in Chapter 16 (§16.2.1) for laminar flow and the calculated concentration profiles were shown in Fig. 16.5 as a function of Schmidt number and the group $y(u_b/\nu x)^{1/2}$. From this analytical correlation and the definition of the mass transfer coefficient (see (17.1.2)), it can be shown that, for laminar flow and low concentration of the diffusing species, k_d can be expressed as follows:

$$\frac{k_{d,x}x}{D_{AB}} = 0.332\left(\frac{xu_b\rho}{\mu}\right)^{1/2}\left(\frac{\mu}{\rho D_{AB}}\right)^{1/3}, \qquad (17.2.1)$$

where $k_{d,x}$ is the local mass transfer coefficient at location x and u_b is the bulk velocity of the fluid in the x-direction.

The dimensionless group on the left-hand side of this equation is called the **Sherwood number** and is analogous to the Nusselt number for heat transfer (Chapter 12). The groups in the parentheses on the right-hand side of the equation will be recognized by the reader

as the **Reynolds** and **Schmidt** numbers, both of which were introduced earlier (Table 2.1). Therefore, (17.2.1) may also be written as follows:

$$\mathrm{Sh}_x = 0.332\mathrm{Re}_x^{1/2}\mathrm{Sc}^{1/3}, \tag{17.2.2}$$

where Sh_x and Re_x represent the local Sherwood and Reynolds numbers at location x. In general, the Sherwood number is defined as

$$\mathrm{Sh} = \frac{k_d}{D_{AB}/L} = \frac{k_d L}{D_{AB}}, \tag{17.2.3}$$

where L is the characteristic length of the system.

We can now obtain the mean value of the mass transfer coefficient, and hence of the Sherwood number, by performing the following integration over the entire length L of the diffusing surface:

$$\begin{aligned} k_{d,\mathrm{ave}} =& \frac{1}{L}\int_0^L k_{d,x}\,dx = \frac{1}{L}\int_0^L 0.332\frac{D_{AB}}{x}\left(\frac{xu_b\rho}{\mu}\right)^{1/2}\left(\frac{\mu}{\rho D_{AB}}\right)^{1/3} dx \\ =& 0.664\frac{D_{AB}}{L}\left(\frac{Lu_b\rho}{\mu}\right)^{1/2}\left(\frac{\mu}{\rho D_{AB}}\right)^{1/3}, \end{aligned} \tag{17.2.4}$$

and therefore

$$\mathrm{Sh}_{\mathrm{ave}} = \frac{1}{L}\int_0^L \mathrm{Sh}_x\,dx = 0.664\mathrm{Re}^{1/2}\mathrm{Sc}^{1/3}, \tag{17.2.5}$$

where Sh_{ave} is the average Sherwood number over the length L.

17.2.2. Natural Convection from a Vertical Plate

Mass transfer by natural convection from a vertical plate in the laminar region was discussed in Chapter 16 and the computed concentration profiles were shown in Fig. 16.8. By introducing the definition of the mass transfer coefficient in the boundary layer equations (§16.3) and calculating the first and second derivatives, the analytical results can be expressed in the form of the following correlation for the local Sherwood for mass transfer from a vertical plate by natural convection:

$$\mathrm{Sh}_x = \left(\frac{\mathrm{Gr}'_x}{4}\right)^{1/4}\frac{0.902\mathrm{Sc}^{1/2}}{(0.861+\mathrm{Sc})^{1/4}}, \tag{17.2.6}$$

where Gr'_x is the concentration Grashof number for mass transfer at distance x from the leading edge of the plate.

17.3. MODELS OF MASS TRANSFER

The mass transfer correlations presented in §17.2 were derived from the rigorous formulation and solutions of the differential equations of continuity, motion, and diffusion for the particular problem. A less rigorous but more convenient approach is to represent the actual

system by a simplified mathematical model. Such model equations generally contain some parameters which must be either measured experimentally or estimated.

17.3.1. The Stagnant Film Model

To illustrate the use of the **film model**, let us consider the case of fluid flowing past a solid surface. The concentration of the diffusing species is $c_{A,s}$ at the surface, and $c_{A,b}$ in the bulk of the fluid. Instead of attempting to solve the equations of fluid flow, which in many instances may be impossible, we shall "idealize" the system by assuming that all resistance to mass transfer is confined to a stagnant layer of thickness δ adjacent to the surface. Therefore, the concentration at the outer edge of this film is $c_{A,b}$.

The problem is now reduced to steady state diffusion through a stagnant film of thickness δ caused by a concentration difference of $c_{A,s} - c_{A,b}$. This problem was solved in Chapter 14 to yield the following equation of the molar flux of A:

$$N_{A,y} = \frac{cD_{A-B}}{\delta} \frac{(X_{A,s} - X_{A,b})}{X_{B,LM}}, \tag{17.3.1}$$

where c is the molar density of the fluid; $X_{A,s}$ and $X_{A,b}$ are the mole fractions of A at surface and at the outer edge of the film; $X_{B,LM}$ is the logarithmic mean of the initial and final mole fractions of component B ($X_B = 1 - X_A$), as defined in Chapter 14 (see (14.7.14)).

Equation (17.3.1) can also be expressed in terms of the molar concentrations of A and B as follows:

$$N_{A,y} = \frac{cD_{AB}}{\delta c_{B,LM}} (c_{A,s} - c_{A,b}), \tag{17.3.2}$$

where $c_{B,LM}$ is the logarithmic mean concentration of species B.

Comparison of the above equation with the definition of the mass transfer coefficient (see (17.1.2)) shows that

$$k_d \equiv \frac{cD_{AB}}{\delta c_{B,LM}}. \tag{17.3.3}$$

When $c_{A,s}$ and $c_{A,b} \ll c$, i.e., at low concentrations of the diffusing species A, we have

$$c \approx c_{B,LM},$$

and therefore,

$$k_d = \frac{D_{AB}}{\delta}. \tag{17.3.4}$$

It may appear that (17.3.3) and (17.3.4) offer a direct way of evaluating k_d. However, this is not true because the thickness of the conceptual film, δ, is a function of the same parameters as the mass transfer coefficient: velocity and properties of the fluid, geometry, concentration levels, and so forth. Nevertheless, the stagnant film model is useful in that it

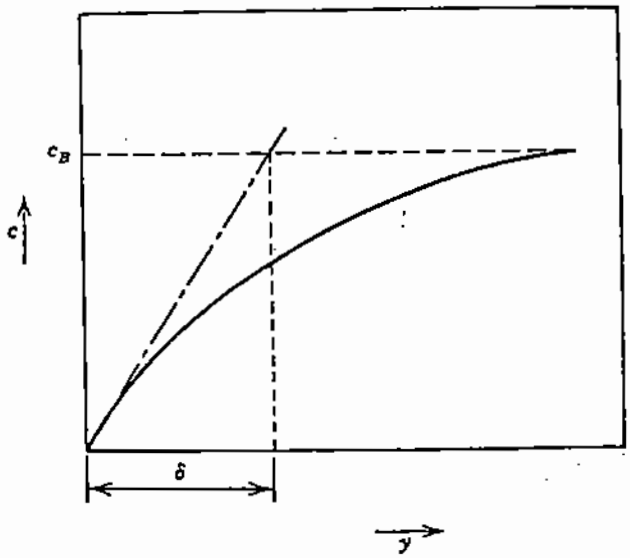

Figure 17.2. Film model for mass transfer.

provides a simple physical picture of resistance to convective mass transfer which can be used as a basis for correlating mass transfer coefficients.

For instance, Fig. 17.2 depicts the concentration profile next to the cathode in an electroplating cell. The tangent of this plot at a point near the surface intersects the horizontal line representing the concentration of the bulk electrolyte at a distance δ from the cathode surface.

This conceptual film of thickness δ is often called the *diffusion layer*. For laminar forced convection of a liquid past a flat surface, the thickness of this film has been expressed as follows [1]:

$$\delta = 3\left(\frac{L}{u_b}\right)^{1/2}\left(\frac{\mu}{\rho}\right)^{1/6} D_{AB}^{1/3}, \tag{17.3.5}$$

where L is the distance from the edge of the electrode in the direction of liquid flow; u_b is the velocity of the bulk flow parallel to the surface; D_{AB} is the diffusivity coefficient of diffusing ions in the electrolyte.

Under the same conditions but in turbulent flow, the thickness of the diffusion layer can be expressed [1] by

$$\delta = \frac{L^{0.1}}{u_b^{0.9}}\left(\frac{\mu}{\rho}\right)^{17/30} D_{AB}^{1/3} = L\,\mathrm{Re}^{-0.9}\,\mathrm{Sc}^{-0.333}. \tag{17.3.6}$$

It can be seen that in the case of turbulent flow the local mass transfer coefficient is much less dependent on position, L, than in laminar flow.

17.3.2. The Surface Renewal Model for Mass Transfer

There are some cases when mass transfer occurs as diffusion through a genuinely stagnant film, such as a capillary tube, a membrane, or a porous medium. More frequently, the assumption of a stagnant film is an idealization of a fairly complex flow situation.

An alternative, and in many cases more satisfactory, model for mass transfer is the **surface renewal model** also known as the Higbie model [2]. This model postulates that

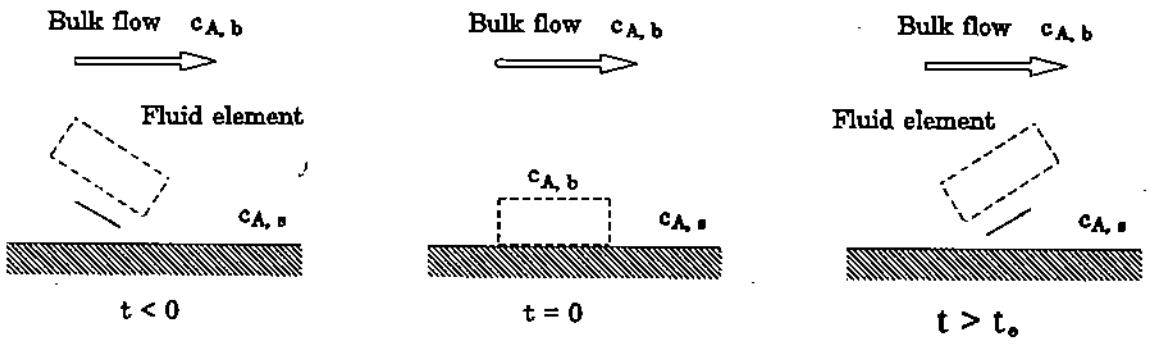

Figure 17.3. Surface renewal model.

a fluid element comes in contact with the surface for a certain time period, during which unsteady state diffusion occurs between the fluid element and the surface. At the end of this time period, the fluid element is swept away from the surface and replaced by a new element from the bulk. While these assumptions may appear at first sight to be unrealistic, the surface renewal model has found many applications in materials processing.

Let us consider a turbulent fluid stream flowing over a surface (Fig. 17.3); the concentration of the diffusing species at the surface is $c_{A,s}$ and the concentration in the bulk of the fluid is $c_{A,b}$. The model equations are expressed by assuming that for a very short time of contact between the surface and a fluid element, the latter is semi-infinite in thickness; in other words, the contact time is so short that the concentration gradient in the element does not reach the side of the element away from the surface.

Under these conditions, and for low concentrations of the diffusing species so that the bulk flow due to diffusion is negligible, the diffusion equation in the fluid element is

$$\frac{\partial c_A}{\partial t} = D_{AB}\frac{\partial^2 A}{\partial y^2} \text{ for } 0 < y < \infty \text{ and } 0 < t < t_e, \tag{17.3.7}$$

where the time interval t_e is the contact time, i.e., the *residence time* of the fluid element at the surface. The boundary conditions are

$$c_A = c_{A,s} \text{ at } y = 0, \tag{17.3.8}$$

$$c_A = c_{A,b} \text{ at } y \to \infty, \tag{17.3.9}$$

$$c_A = c_{A,b} \text{ at } t = 0. \tag{17.3.10}$$

The solution of this system of equations was discussed in Chapter 15 and provides the concentration profile in dimensionless form:

$$\frac{c_A - c_{A,b}}{c_{A,s} - c_{A,b}} = \text{erfc}\,\frac{y}{2\sqrt{D_{AB}t}}. \tag{17.3.11}$$

Also, the molar flux of A crossing the plane $y = 0$ is expressed by the concentration gradient (see (15.3.6), Chapter 15):

$$N_A = -D_{AB}\left(\frac{\partial c_A}{\partial y}\right)_{y=0} = (c_{A,s} - c_{A,b})\left(\frac{D_{AB}}{\pi t}\right)^{1/2}. \tag{17.3.12}$$

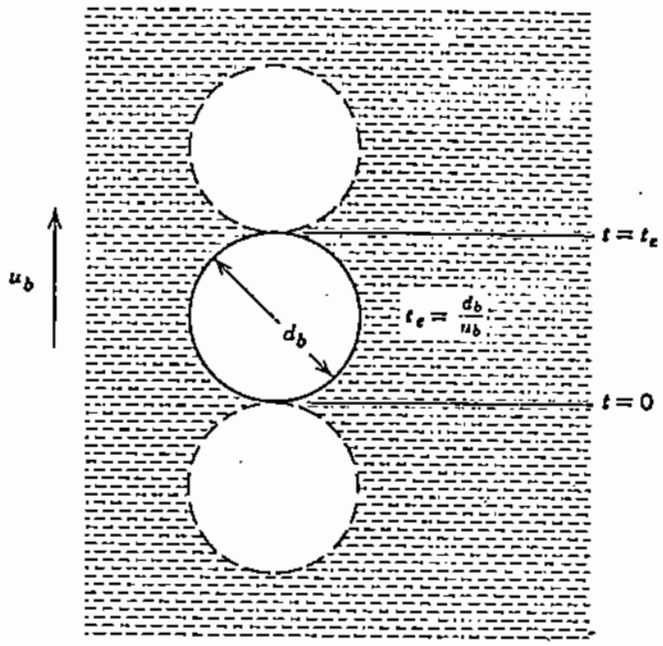

Figure 17.4. Surface renewal model for bubble rising in a liquid.

The average value of the molar flux over the time interval t_e is (see (15.3.7), Chapter 15):

$$N_{A,\text{ave}} = \frac{1}{t_e}\int_0^{t_e} N_A\,dt = 2(c_{A,0} - c_{A,b})\left(\frac{D_{AB}}{\pi t_e}\right)^{1/2}. \tag{17.3.13}$$

Comparison of (17.3.13) with the definition of the mass transfer coefficient (see (17.1.2)) shows that, for low concentrations of the diffusing substance, the mass transfer coefficient can be expressed as follows:

$$k_d = 2\left(\frac{D_{AB}}{\pi t_e}\right)^{1/2}. \tag{17.3.14}$$

We can see that the most important parameter of the surface renewal model is the contact time, t_e. In most cases, the value of t_e must be deduced from experimental measurements of the mass flux. However, there are some practical situations where t_e can be estimated directly and then be used to calculate k_d from (17.3.14).

For instance, in the case of a bubble rising in a liquid, the contact time between the bubble and a fluid element in its path starts when the fluid element touches the top of the bubble and ends when it reaches the bottom (Fig. 17.4); this time interval is calculated from

$$t_e = \frac{d_b}{u_b}, \tag{17.3.15}$$

where d_b and u_b are the bubble diameter and velocity, respectively. Since the rising velocity of bubbles in liquids is well established, the surface renewal model provides a convenient way for estimating the mass transfer coefficient.

The same model can be used for problems where a large bubble passes across the interface of two immiscible liquids (e.g., metal-slag) or the surface of a liquid reacting with

the gas above it. In this case, the bubble disrupts the interface and therefore "renews" the fluid elements at that location. Despite the difficulty of estimating accurately the surface area "disrupted" by the passage of the bubble, this model offers a convenient tool for the calculation of mass transfer rates, as illustrated in the following example.

Example 17.3.1

The surface of a molten steel bath, of bulk concentration 0.03% oxygen by weight, is in contact with the atmospheric air. The surface layer is saturated with oxygen at a concentration of 0.16% oxygen by weight. The surface is disrupted by carbon monoxide bubbles rising through the metal to the surface at a frequency of 1200 bubbles per second per m^2 of surface area; the surface area disrupted by each rising bubble is estimated at about 15 cm^2. The diffusivity of oxygen in the metal may be taken as 1.2×10^{-4} cm^2 s^{-1}, and the density of steel is 7.1 g cm^{-3}.

Assuming that the oxygen transfer process to the melt can be represented by the surface-renewal model, calculate: a) The mass transfer coefficient, b) the mean mass flux of oxygen to the surface.

a. The average contact time can be estimated from the frequency of bubbles per square meter and the area "renewed" per bubble:

$$t_e = \frac{10000\,\text{cm}^2}{1200\,\text{bubbles}\,\text{s}^{-1} \times 15\,\text{cm}^2\,\text{per bubble}} = 0.555\,\text{s}.$$

The mass transfer coefficient is then calculated from (17.3.14):

$$k_d = 2\left(\frac{D_{AB}}{\pi t_e}\right)^{1/2} = 1.66 \times 10^{-2}\ \text{cm}^2\,\text{s}^{-1}. \tag{17.3.16}$$

b. The average mass flux of oxygen at the surface is

$$N_{A,\text{ave}} = k_d \rho (X'_s - X'_b), \tag{17.3.17}$$

where ρ is the density of steel; X'_s and X'_b are the mass fractions of oxygen in the surface layer and in the bulk fluid. Therefore,

$$N'_{A,\text{ave}} = 1.66 \times 10^{-2} \times 7.1 \times (0.0016 - 0.0003) = 1.53 \times 10^{-4}\ \text{g}\,\text{s}^{-1}\,\text{cm}^{-2}.$$

It is interesting to estimate the equivalent "film thickness" from the stagnant film model (see (17.3.4)):

$$\delta = \frac{D_{AB}}{k_d} = \frac{1.2 \times 10^{-4}}{1.66 \times 10^{-2}} = 0.007\,\text{cm} = 70\,\text{microns}.$$

17.4. MASS TRANSFER CORRELATIONS

Values of mass transfer coefficients can be obtained either by direct measurement or by means of existing semi-empirical correlations. Such correlations are usually presented in terms of the dimensionless numbers discussed earlier. Some of the important correlations in materials processing are described in the following sections.

As in the case of heat convection (Chapter 12), when the temperature of a fluid property in a mass or heat transfer correlation is not specified, the property should be calculated at the **mean film temperature** which is defined as the average of the bulk flow temperature of the fluid and the temperature at the surface:

$$T_{\text{film}} = \frac{(T_{\text{bulk}} + T_{\text{surface}})}{2}.$$

Some correlations are based on a limited number of experimental data; therefore, their validity is limited to the particular geometry and to the range of Reynolds (or Grashof) and Schmidt numbers covered in the original study. Consequently, great care must be exercised if such correlations are extrapolated beyond the range studied, or if they are used for systems much different than those in which they were obtained.

Mass transfer correlations are usually expressed in the form of $\text{Sh} = f(\text{Re}, \text{Sc})$, for forced convection and $\text{Sh} = f(\text{Gr}', \text{Sc})$, for natural convection. In general, there are many more correlations available for fluid–solid systems than for gas–liquid and liquid–liquid systems, especially at high temperatures.

17.4.1. Mass Transfer to Spherical Particles

As in the case of heat transfer (§12.6.3), mass transfer to spheres varies with location and the maximum value is attained at the foremost point of the sphere with respect to flow. However, the following correlations refer to the *average* value of the mass transfer coefficient over the entire surface of a sphere.

One of the earliest studies on the subject of mass transfer was by Frössling [3], who determined the evaporation of various liquid droplets and the sublimation of naphthalene spheres in a hot air stream. The data covered particle Reynolds numbers from 2 to 1300. Frössling showed theoretically that the Nusselt number was proportional to $\text{Re}^{1/2}$ and the experimental results confirmed this. Experimental work with different liquid systems resulted in the value of the exponent of the Schmidt number equal to 1/3. The final equation for mass transfer was

$$\text{Sh} = 2 + 0.552\text{Re}_p^{0.50}\text{Sc}^{0.333}, \tag{17.4.1}$$

where the Reynolds number is calculated at the relative velocity between the bulk fluid velocity and the velocity of the particle.

One of the best known works on simultaneous heat and mass transfer is by Ranz and Marshall [4], who determined the evaporation of water and benzene drops in air. Their experimental results for mass transfer were correlated by the following equation:

$$\text{Sh} = 2 + 0.60\text{Re}_p^{0.50}\text{Sc}^{0.333}. \tag{17.4.2}$$

The above equation is of the same form as the Ranz–Marshall equation for heat convection to spherical particles (Chapter 12).

The droplet size in the case of the Ranz and Marshall experiments was in the order of about 0.1 cm. However, the validity of this correlation has been confirmed for much larger particles by Evnochides and Thodos [5], who measured the evaporation rates from spheres 3.5 to 5 cm in diameter impregnated with water or nitrobenzene, and by other investigators.

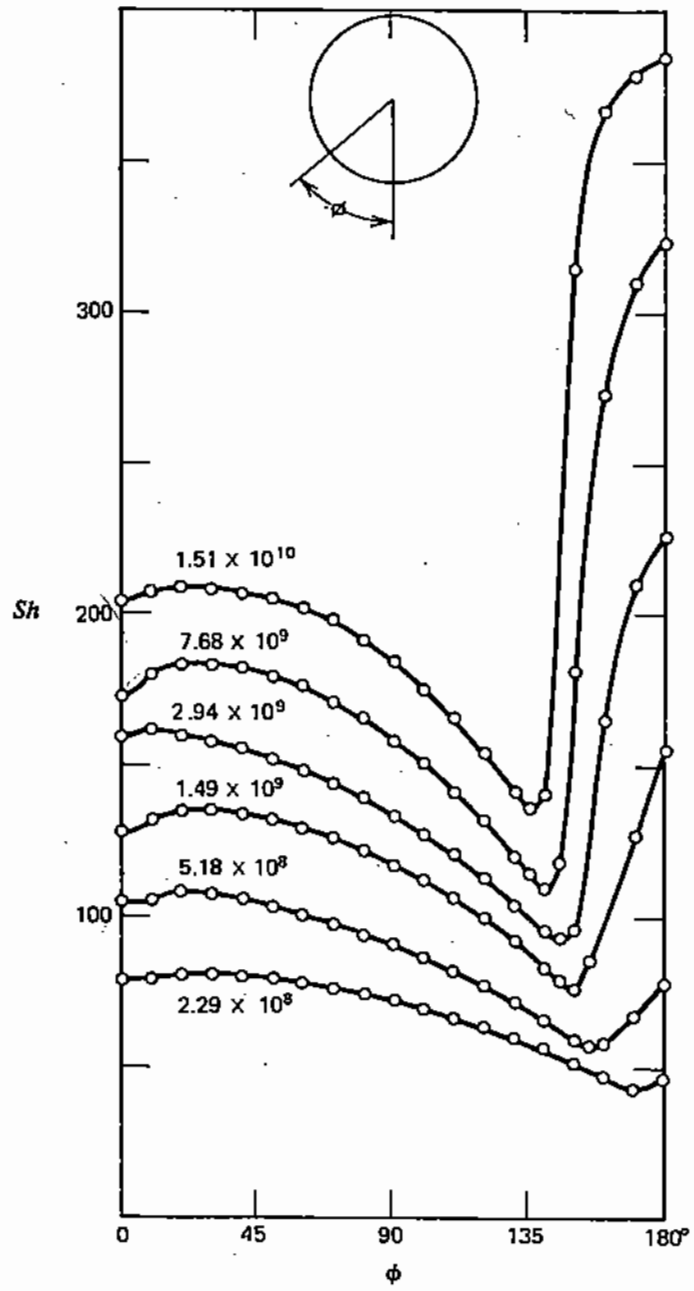

Figure 17.5. Variation of local mass transfer coefficient with location on a sphere at various Gr' Sc values [6].

Equation (17.4.2) is now generally used for estimating the heat and mass transfer to spherical particles by convection.

An interesting study of mass transfer by natural convection to spherical particles has been conducted by Schutz [6]. By making use of the fact that the limiting current in electrodeposition is proportional to the mass transfer coefficient, this author measured local and overall mass transfer rates to spherical cathodes immersed in a $CuSO_4$–H_2SO_4 electrolyte. The variation of the mass flux, as expressed by the Sherwood number, with location on the

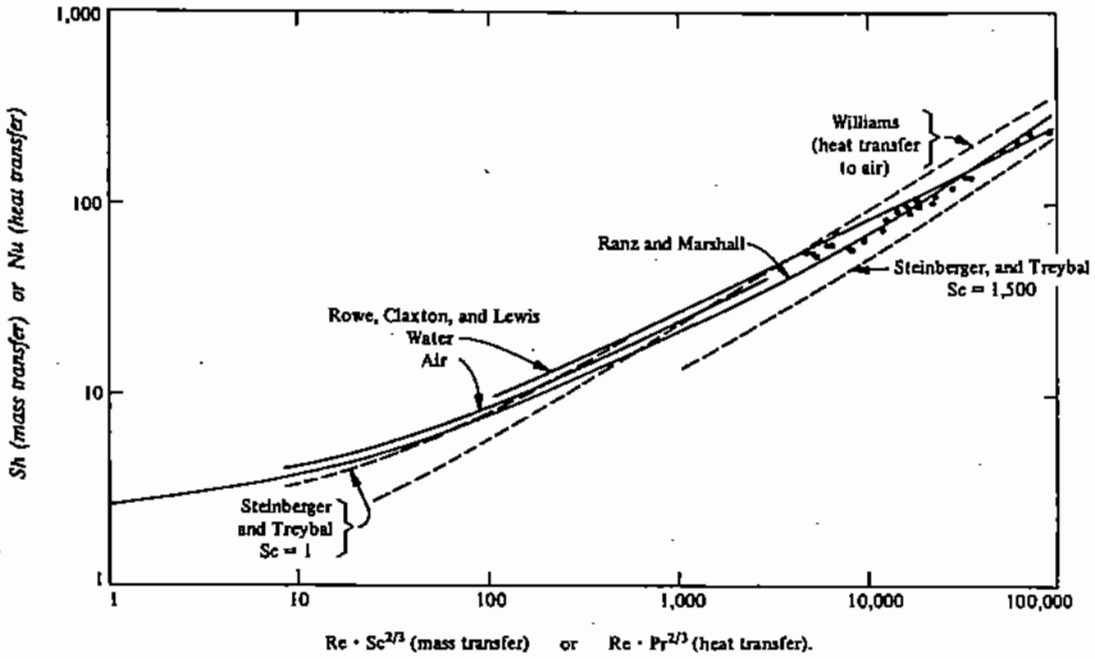

Figure 17.6. Graphical representation of correlations for heat and mass transfer to spherical particles [21].

surface of the sphere is shown in Fig. 17.5 at different values of the $Gr' Sc$ group. The overall mass transfer coefficient to the sphere was represented by the following correlation:

$$Sh_{Re=0} = 2 + 0.59(Gr' Sc)^{1/4}. \tag{17.4.3}$$

The above equation is very similar to the Wilke [7] correlation for natural convection from flat plates, to be presented in the next section.

In the case of mass transfer by combined natural and forced convection to a spherical particle, Steinberger and Treybal [8] proposed the following correlation:

$$Sh = Sh_{Re=0} + 0.347(Re\, Sc^{1/2})^{0.62}, \tag{17.4.4}$$

where Sh is the Sherwood number for mass transfer in the presence of combined natural and forced convection; $Sh_{Re} = 0$ is the Sherwood number for mass transfer under natural convection only (i.e., at $Re = 0$) and is expressed as follows:

$$Sh_{Re=0} = 2 + 0.569(Gr' Sc)^{0.25} \text{ for } Gr' Sc < 10^8, \tag{17.4.5}$$

and

$$Sh_{Re=0} = 2 + 0.0254(Gr' Sc)^{1/2} Sc^{0.244} \text{ for } Gr' Sc > 10^8. \tag{17.4.6}$$

The Steinberger and Treybal correlation is based on a large number of experimental data including those by Frössling [3] and Ranz and Marshall [4] and encompasses both gas and liquid systems of Schmidt numbers in the range of 0.6–3000 and Reynolds numbers in the range of 1–30,000.

Figure 17.6 [21] presents in graphical form a number of correlations for mass transfer by forced convection to spherical particles. As is shown in Fig. 17.6, these plots also apply to heat transfer by replacing the Schmidt number on the x-axis by the Prandtl number. The analogy between mass and heat transfer is evident.

17.4.2. Mass Transfer to Vertical Plates by Natural Convection

The rate of mass transfer from vertical plates in natural convection can be calculated by means of the Wilke correlation [7]:

$$\mathrm{Sh} = 0.673(\mathrm{Gr}'\,\mathrm{Sc})^{0.25}, \tag{17.4.7}$$

which was based on data in the range of Schmidt number from 500 to 800,000 and in the range of Grashof number 10^4–10^9.

In Chapter 12 it was noted that for heat transfer by natural convection, the transition from laminar to turbulent flow occurs at

$$\mathrm{Gr}\,\mathrm{Sc} > 10^9.$$

Experiments by Ibl and Muller [9] on the electrodeposition of copper from copper sulphate solutions showed that the "diffusion layer" next to the cathode became turbulent at a higher value of the Grashof-Schmidt product:

$$\mathrm{Gr}'\,\mathrm{Sc} > 4 \times 10^{11}.$$

The Wilke correlation (see (17.4.7)) encompassed the range $4\times10^6 < \mathrm{Gr}'\,\mathrm{Sc} < 5\times10^{11}$ and therefore should be applicable only in the laminar flow. However, Fouad and Ibl [10] studied the electrodeposition of copper in the range $2 \times 10^{11} < \mathrm{Gr}'\,\mathrm{Sc} < 10^{13}$, which is in the turbulent regime, and developed the following correlation:

$$\mathrm{Sh} = 0.59(\mathrm{Gr}'\,\mathrm{Sc})^{0.26}. \tag{17.4.8}$$

It can be seen that this equation is very similar to the Wilke correlation. The data of other investigators are also in good agreement with (17.4.7), as illustrated in Fig. 17.7 [18].

Mass transfer in natural convection is very important in the operation of electrorefining cells, since it effectively determines the limiting current density and the current distribution across the electrodes. An illustration of the application of mass transfer correlations in the electrorefining of copper is presented in the following example.

Example 17.4.1

In an experiment on the electrodeposition of copper on a 7.62 cm high cathode (Fig. 17.8), from a solution containing 0.467 M $CuSO_4$ and 1.471 M H_2SO_4 (density $\rho_b = 1.165$ g cm^{-3}, viscosity $\mu_b = 1.61$ cP) at 18°C, it was found that the limiting current was 297 A m^{-2} ($= 29.7\times10^{-3}$ A cm^{-2}). In a copper electrolyte solution, the rate of electrodeposition is equal to two components of electron flow: the current conveyed by the diffusing copper ions plus the current due to the electron migration through the electrolyte. The second term is represented by the *transference number* of Cu^{++}, which is the fraction of current carried by the copper ions *in the absence of concentration gradients*, i.e., not by diffusion.

However, in order to increase the conductance of electrolytic solutions, an additional component is added, which does not participate in the electrode reactions and is called a *supporting electrolyte*, such as the H_2SO_4 used here. In this case, the transference number of Cu^{++}, t_{Cu+}, is only 0.015 and the transference number of H^+ ions, t_{H+}, is 0.75. If the deposition is limited by mass transfer between the electrolyte and the cathode, it is required

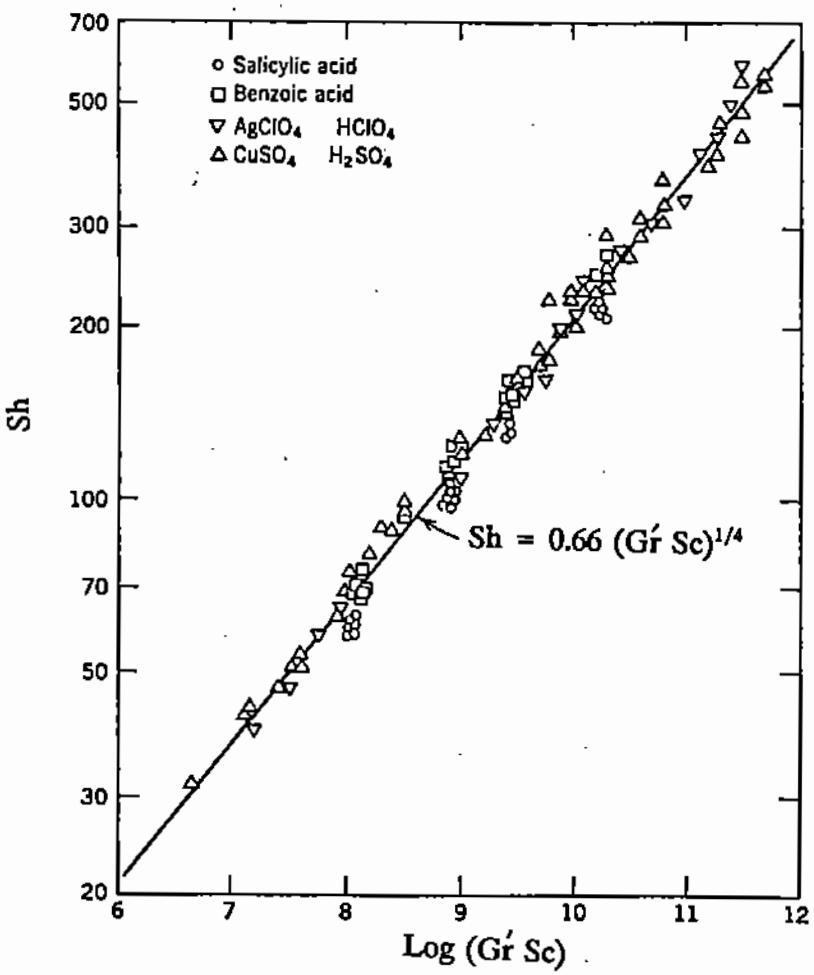

Figure 17.7. Correlation for mass transfer between a liquid and a vertical plate, in natural convection [18].

to calculate the mass transfer coefficient and compare with the value predicted from the Wilke correlation (see (17.4.7)).

The limiting current was determined experimentally by gradually increasing the potential across the anode and cathode and recording the current. The limiting current density is attained when further increase in potential has no effect on the current (Fig. 17.9). An energy balance on the copper ions diffusing through the boundary layer and depositing on the cathode yields the following equation for the mass transfer coefficient of copper ions:

$$k_{d,\mathrm{Cu}^{++}} = \frac{i(1 - t_{\mathrm{Cu}^{++}})}{nF(c_{\mathrm{Cu}^{++},b} - c_{\mathrm{Cu}^{++},s})}, \tag{17.4.9}$$

where i is the limiting current density; $t_{\mathrm{Cu}^{++}}$ is the transference number of copper ions; n is the valence of the deposited metal (in this case, Cu^{++}, $n = 2$); F is the Faraday number, 96500 coulomb; $c_{\mathrm{Cu}^{++},b}$ is the concentration of copper in electrolyte in bulk fluid (from given data, $c_{\mathrm{Cu}^{++},b} = 0.467$ moles per 1000 cm^3); $c_{\mathrm{Cu}^{++},s}$ is the concentration of copper in electrolyte at the cathode surface and, under limiting current conditions, can be assumed to be near zero; $D_{\mathrm{Cu}^{++}}$ is the diffusivity of cupric ions in the electrolyte and can be assumed

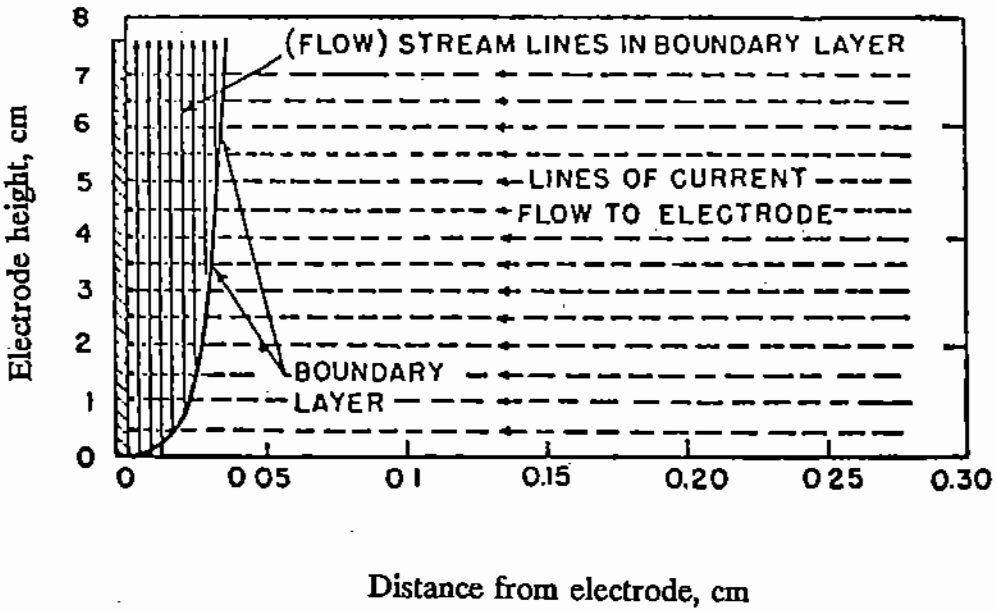

Figure 17.8. Concentration boundary layer due to electrodeposition and natural convection in an electrolytic cell.

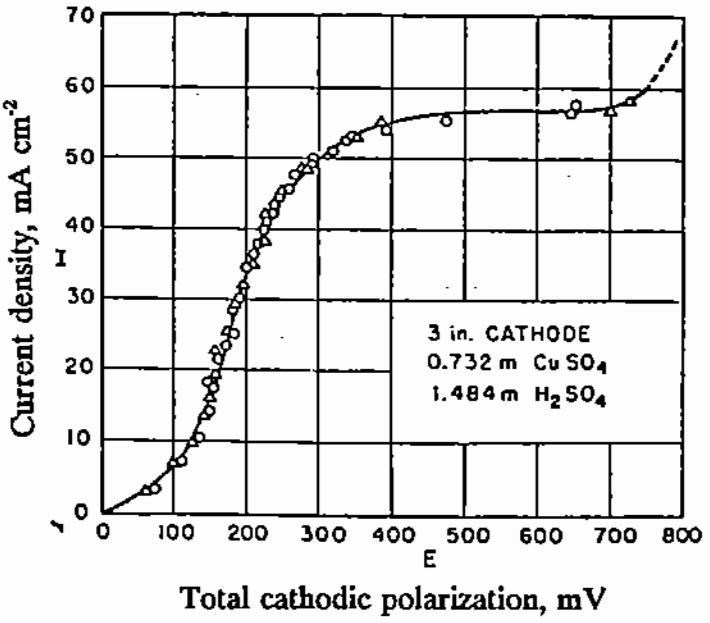

Figure 17.9. Limiting current density in the electrodeposition of copper [7].

to be equal to that of $CuSO_4$ in water ($= 0.461 \times 10^{-5}$ cm^2 s^{-1}); D_{H+} is the diffusivity of hydrogen ions in water ($= 1.6 \times 10^{-5}$ cm^2 s^{-1}).

Substituting numerical values in (17.4.9), we obtain the experimental value of the mass transfer coefficient:

$$k_{d,Cu++} = \frac{29.7 \times 10^{-3}(1 - 0.015)}{2 \times 96500 \times 0.467 \times 10^{-3}} = 0.325 \times 10^{-3} \text{ cm s}^{-1}.$$

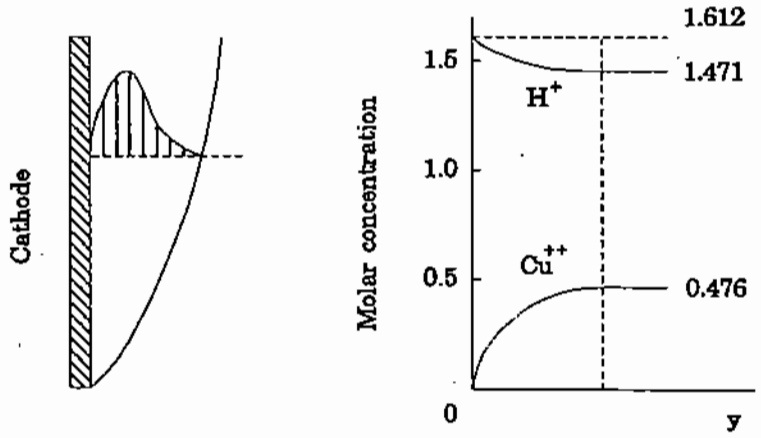

Figure 17.10. Concentration profiles of Cu^{++} and H^+ in the boundary layer next to a cathode plate.

Therefore, for $L = 7.62$ cm, the Sherwood number (see (17.2.3)) is

$$\mathrm{Sh} = \frac{0.325 \times 10^{-3} \times 7.62}{0.461 \times 10^{-5}} = 536.$$

In order to compare the experimental Sh with the Wilke correlation, we need to calculate the Grashof and Schmidt numbers for the system. The definition of the Grashof number (see (16.3.10)) can be written in a slightly modified form as

16.3.6

$$\mathrm{Gr}' = \frac{gL^3\rho_b^2}{\mu_b^2}\,\frac{(\rho_b - \rho_s)}{\rho_s}, \tag{17.4.10}$$

where ρ_b and ρ_s are the densities of the electrolyte in the bulk fluid and at the interface, respectively.

We now need to estimate the density of the solution at the interface. Figure 17.10 illustrates the concentration gradients of hydrogen ions and copper ions in the boundary layer next to the cathode: The copper ions migrate across the boundary later to the interface and their concentration decreases from $c_{\mathrm{Cu}^{++},b}$ to nearly zero at the interface. Electrical neutrality in the boundary layer is established by the formation of a hydrogen ion concentration gradient, as shown in Fig. 17.10. The diffusion of hydrogen ions away from the cathode surface, is in balance with the net bulk flow caused by the diffusion of copper ions towards the surface; therefore the net molar flux of hydrogen ions is zero. The reader may recall a similar situation discussed in §14.7.1 (diffusion through a stagnant film). The energy balance for the charge carried by the hydrogen ions is as follows:

$$nF\,k_{d,\mathrm{H}^+}(c_{\mathrm{H}^+,s} - c_{\mathrm{H}^+,b}) - it_{\mathrm{H}^+} = 0, \tag{17.4.11}$$

and therefore

$$k_{d,\mathrm{H}^+} = \frac{it_{\mathrm{H}^+}}{nF\left(c_{\mathrm{H}^+,s} - c_{\mathrm{H}^+,b}\right)}. \tag{17.4.12}$$

If we assume that the Wilke correlation (see (17.4.7)) is applicable, the mass transfer coefficients for $CuSO_4$ and H_2SO_4 must be proportional to their respective diffusivities in

the electrolyte to the power of 3/4 (since all other properties in the correlation are the same for both ions):

$$\frac{k_{d,\mathrm{Cu}^{++}}}{k_{d,\mathrm{H}^{+}}} = \left(\frac{D_{\mathrm{Cu}^{++}}}{D_{\mathrm{H}^{+}}}\right)^{3/4}. \tag{17.4.13}$$

By solving for the H^+ concentration from (17.4.9), (17.4.12), and (17.4.13), for $c_{\mathrm{Cu}^{++},b} = 0.467$ M and $c_{\mathrm{Cu}^{++},s} = 0$, we obtain

$$\left(c_{\mathrm{H}^{+},s} - c_{\mathrm{H}^{+},b}\right) = 0.467\left(\frac{0.461}{1.6}\right)^{3/4}\frac{0.75}{1-0.015} = 0.141\,\mathrm{M}.$$

Since the concentration of acid in the bulk solution has been given as 1.471 M, the concentration at the interface is $1.471 + 0.141 = 1.612$ M H_2SO_4. This molarity corresponds to a density of 1.08 g cm^{-3} [13]. Therefore, the density term in the Grashof number (see (17.4.10)) is

$$\left(\frac{\rho_b - \rho_s}{\rho_s}\right) = \frac{1.165 - 1.08}{1.08} = 0.079.$$

Using this value and introducing the other numerical values in (17.4.10), we obtain

$$\mathrm{Gr}' = \frac{0.079 \times 981 \times 7.62^3 \times 1.165^2}{0.161^2} = 1.79 \times 10^8.$$

Finally, as noted earlier, the Schmidt number is defined by

$$\mathrm{Sc} = \frac{\mu}{\rho D_{\mathrm{Cu}^{++}}} = \frac{0.0161}{1.165 \times 0.461 \times 10^{-5}} = 2998.$$

Substituting the calculated values of the Grashof and Schmidt numbers in the Wilke correlation (see (17.4.7)), we obtain

$$\mathrm{Sh} = 0.673(\mathrm{Gr}'\,\mathrm{Sc})^{0.25} = 0.673(1.79 \times 10^8 \times 2998)^{0.25} = 576.$$

It can be seen that the calculated value for the Sherwood number of 576 is in good agreement with the experimental value of 536.

17.4.3. Forced Convection over a Flat Plate

The following correlation has been recommended for forced convection over a horizontal flat plate in turbulent flow [14]:

$$\mathrm{Sh} = 0.037\,\mathrm{Re}^{0.8}\,\mathrm{Sc}^{0.333}. \tag{17.4.14}$$

This correlation was found to represent well experimental data on the deposition of metals [15] and the dissolution of carbon in iron melts [16].

An alternative to the Sherwood number for expressing the mass transfer coefficient is the *j factor for mass transfer*, j_d, which is defined as follows:

$$j_d = \frac{k_d}{u_b}\mathrm{Sc}^{2/3}, \tag{17.4.15}$$

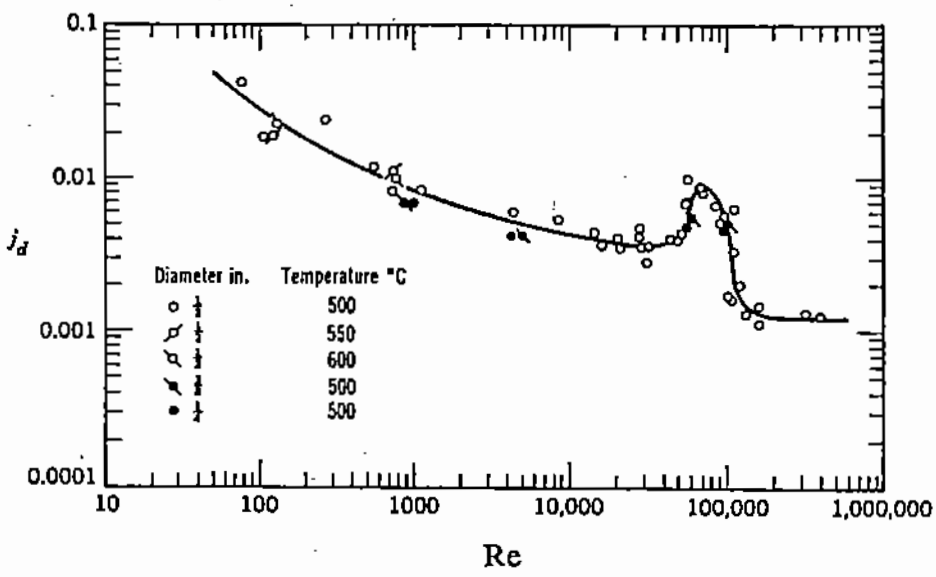

Figure 17.11. Mass transfer factor (j_d) vs. Reynolds number for the dissolution of uranium spheres in liquid cadmium [17].

where, as before, k_d is the mass transfer coefficient, u_b the fluid bulk velocity, and Sc the Schmidt number. Figure 17.11 is a plot of experimentally observed mass transfer factors, for the dissolution of uranium spheres in liquid cadmium, as a function of Reynolds number [17].

Example 17.4.2

Calculate the mass transfer rate from a uranium sphere (1.25-cm diameter) in a stream of liquid cadmium flowing at velocity of 2 m s^{-1}. At the system temperature of 500°C, the properties of the fluid are [17]: density of liquid cadmium, $\rho = 7.8$ g cm^{-3}; viscosity of liquid cadmium, $\mu = 1.84$ cP = 0.0184 g s^{-1} cm^{-1}; diffusivity of U atoms in liquid cadmium, $D_{U-Cd} = 1.6 \times 10^{-5}$ cm^2 s^{-1}:

$$\mathrm{Re} = \frac{d_p u \rho}{\mu} = \frac{1.25 \times 200 \times 7.8}{0.0184} = 106000.$$

From Fig. 17.8, we find that for Re = 106000, $j_d = 0.0016$. Also, the Schmidt number is

$$\mathrm{Sc} = \frac{\mu}{\rho D_{A-B}} = \frac{0.0184}{7.8 \times 1.6 \times 10^{-5}} = 147.$$

Finally, from the definition of j_d, we obtain

$$j_d = \frac{k_d}{u}\,\mathrm{Sc}^{2/3} = 0.0016 \text{ cm s}^{-1}, \quad \therefore\ k_d = 0.0115 \text{ cm s}^{-1}.$$

Example 17.4.3. Mass Transfer from a Rotating Cylinder

The following correlation has been proposed by Eisenberg et al. [18] for the rate of mass transfer from a cylinder rotating in a liquid bath:

$$\frac{k_d}{u_r} = 0.079\,\mathrm{Re}^{-0.3}\,\mathrm{Sc}^{-0.644}, \tag{17.4.16}$$

where k_d is the mass transfer coefficient between cylinder and liquid and u_r is the peripheral speed of rotation.

In an experiment by Olsson et al. [19], a 1.5-cm diameter by 5-cm long iron cylinder was rotated at a speed of 775 rpm in a melt of carbon-saturated iron, at 1275°C. The rate of dissolution, expressed as decrease of rod radius with time, was -5.57×10^{-3} cm s^{-1}. For the dissolution of Fe in C-saturated Fe, the Fe mass concentration driving force was estimated to be

$$\Delta X'_{\mathrm{Fe}} = 0.385.$$

Compare the experimental rate of dissolution with that predicted by the above correlation of Eisenberg et al. [18]. At 1275°C, the diffusivity of iron in the carbon-saturated melt, $D_{\mathrm{Fe-FeC}}$, can be assumed to be 9×10^{-5} cm^2 s^{-1} and the kinematic viscosity of the iron melt is 0.0141 cm^2 s^{-1}.

If it is assumed that the densities of the rod and melt are nearly equal, we have

$$-A\frac{dr}{dt} = k_d A \Delta X'_{\mathrm{Fe}},$$

where A is the surface area of rod in the melt, in cm^2, and dr/dt the rate of dissolution of the rod, in cm s^{-1}. Substituting numerical values, we obtain the experimental value of k_d:

$$k_{d,\mathrm{exp}} = \frac{-dr/dt}{\Delta X'_{\mathrm{Fe}}} = \frac{5.57 \times 10^{-3}}{0.385} = 0.0145 \text{ cm s}^{-1}.$$

The peripheral velocity is

$$u = \frac{\pi d(\mathrm{rpm})}{60} = \frac{3.14 \times 1.5 \times 775}{60} = 60.8 \text{ cm s}^{-1},$$

where d is the rod diameter. Therefore, the Reynolds number is

$$\mathrm{Re} = \frac{du}{\nu} = \frac{1.5 \times 60.8}{0.0141} = 6470,$$

and the Schmidt number

$$\mathrm{Sc} = \frac{\nu}{D_{\mathrm{Fe-FeC}}} = \frac{0.0141}{9 \times 10^{-5}} = 157.$$

By substituting the above numerical values in the Eisenberg correlation, we calculate the value of the mass transfer coefficient:

$$k_{d,\mathrm{calc}} = \frac{60.8 \times 0.079}{6470^{0.3} \times 157^{0.644}} = 0.0133 \text{ cm s}^{-1}.$$

It can be seen that in this case there is good agreement between the experimental and calculated values of k_d.

17.5. ADDITION OF PHASE RESISTANCES IN MASS TRANSFER

In the preceding discussion and examples on the use of mass transfer coefficients, we examined systems involving one fluid phase only, or systems where the resistance to mass

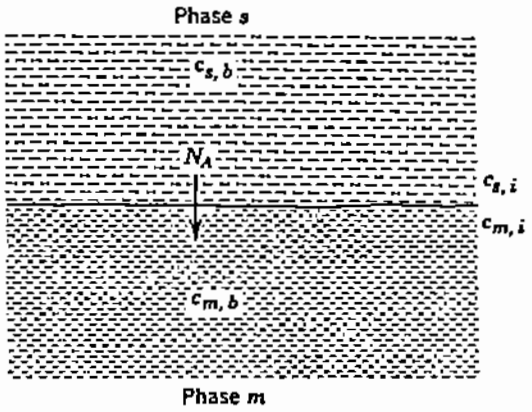

Figure 17.12. Mass transfer between two immiscible liquids.

transfer through a second fluid phase could be assumed negligible; for example, in the case of a bubble bursting through the liquid metal/air interface, it was tacitly assumed that the resistance to mass transfer through the gas phase was negligible in comparison to the liquid-phase resistance.

In this section we shall consider the problem of mass transfer between two immiscible fluids, which is in a way analogous to the development of an expression for the overall heat transfer coefficient (Chapter 12). The molar flux of diffusing species A between two immiscible fluids s and m (Fig. 17.12) can be expressed as

$$N_A = k_{d,s}(c_{s,b} - c_{s,i}) = k_{d,m}(c_{m,i} - c_{m,b}), \qquad (17.5.1\text{–}17.5.2)$$

where $k_{d,s}$ and $k_{d,m}$ are the mass transfer coefficients for diffusion of A in phases s and m, respectively; $c_{s,b}$ is the concentration of A in the bulk of phase s; $c_{m,b}$ is the concentration of A in the bulk of phase m; $c_{s,i}$ and $c_{m,i}$ are the concentrations of A at the interface and in phases s and m, respectively.

It may be assumed that chemical equilibrium (Chapter 18) prevails at the interface between the two phases, and therefore

$$\frac{c_{m,i}}{c_{s,i}} = K_e, \qquad (17.5.3)$$

where K_e is the equilibrium constant, or distribution coefficient for A, between the two phases s and m.

By introducing (17.5.3) in (17.5.1)–(17.5.2), we can eliminate the concentrations at the interface to obtain

$$N_A = \frac{K_e c_{s,b} - c_{m,b}}{\frac{K_e}{k_{d,s}} + \frac{1}{k_{d,m}}}. \qquad (17.5.4)$$

The numerator in this equation represents the **overall driving force** for mass transfer, and the denominator corresponds to the **overall resistance**.

It will be noted that this representation of the mass flux as the ratio of overall driving force to resistance is similar to the equivalent equation for heat flux presented in Chapter 12 (see (12.7.2)). However, there is a basic difference between the definitions of an overall mass transfer and an overall heat transfer coefficient: In the case of heat transfer, as for

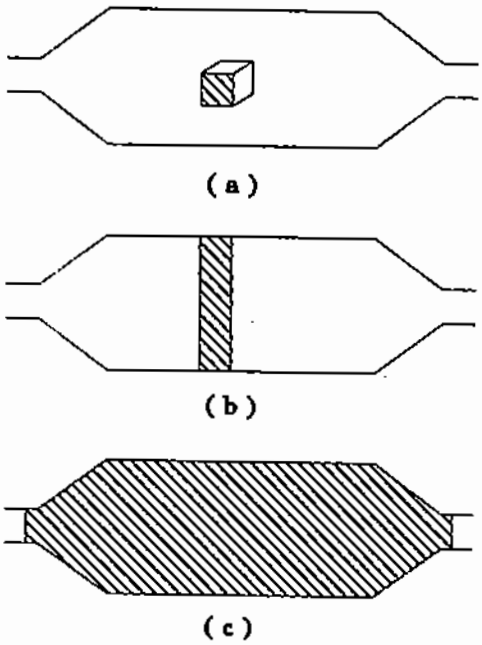

Figure 17.13. Material balance on (*a*) an infinitesimal volume element, (*b*) a section element, (*c*) the entire volume of the system.

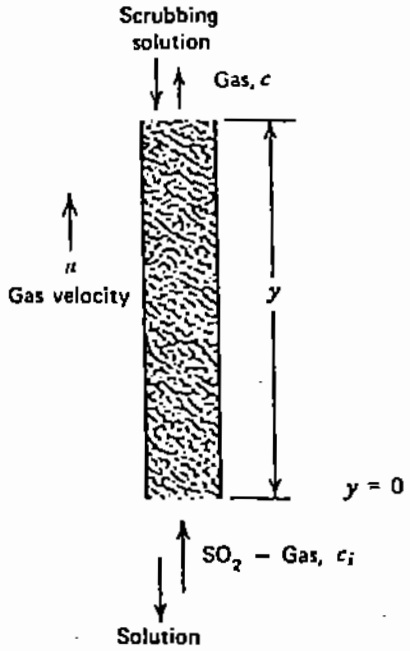

Figure 17.14. Absorption in a countercurrent-flow column.

example in a heat exchanger, the motion of the two fluids separated by the exchanger wall can be considered independently of each other. This is clearly not the case in interphase mass transfer where the two fluids are in direct contact, and the motion of one affects the other.

Consequently, the mass transfer coefficients $k_{d,s}$ and $k_{d,m}$ cannot be considered as truly independent parameters.

17.6. OVERALL MASS TRANSFER BALANCES

In Chapter 12, we showed that the formulation of convection problems can be based on the heat balance over an infinitesimal volume element or over a section element, which is of finite size except in one dimension (Fig. 17.13). The same reasoning applies to mass transfer problems. To illustrate, let us consider the removal of sulphur dioxide from a process gas by subjecting it to counter-current scrubbing with an alkaline solution in a packed column (Fig. 17.14).

The initial concentration of SO_2 in the gas is $c_{SO_2,0}$ and the concentration of SO_2 at equilibrium with the aqueous solution is $c_{SO_2,e}$. The mass transfer coefficient in the column is k_d, and the available *surface area for mass transfer per unit volume* of the column is a_v; the value of the latter depends on the type of gas/liquid contact system used in the column.

The material balance for sulphur dioxide over a section of the column of height dy can be stated as follows:

decrease in SO_2 in gas stream = rate of SO_2 transfer to liquid,

i.e.,

$$-A_c u_0 \frac{dc_{SO_2}}{dy} = A_c\, k_d\, a_v\, (c_{SO_2} - c_{SO_2,e}), \tag{17.6.1.}$$

where A_c is the cross-sectional area of the column and u_0 the *superficial velocity* of process gas through the column (i.e., gas flow rate/A_c).

The above first-order differential equation is integrated for the boundary condition $c = c_{SO_2,0}$, at $y = 0$ to yield the equation

$$\frac{(c_{SO_2} - c_{SO_2,e})}{(c_{SO_2,0} - c_{SO_2,e})} = e^{-k_d a_v y/u_0}, \tag{17.6.2}$$

where y is the distance from the entry point of gas into the column.

Similarly to the case of heat transfer (Chapter 12), the overall rate of mass transfer of SO_2 in the column is expressed by

$$\dot{m}_{SO_2} = k_d A (\Delta c)_{LM}, \tag{17.6.3}$$

where A is the total surface area available for mass transfer = $a_v\, L\, A_c$; L is the column height; $(\Delta c)_{LM}$ is called the *logarithmic mean* of the initial and final concentration "driving forces":

$$(\Delta c)_{LM} = \frac{(c_{SO_2,0} - c_{SO_2,e}) - (c_{SO_2,f} - c_{SO_2,e})}{\ln\left(\frac{c_{SO_2,0} - c_{SO_2,e}}{c_{SO_2,f} - c_{SO_2,e}}\right)}. \tag{17.6.4}$$

where $c_{SO_2,f}$ is the concentration of SO_2 in the exit gas.

Equations (17.6.3) and (17.6.4) are analogous to (12.8.9) and (12.8.10) which were developed in Chapter 12 for the equivalent heat transfer problem.

REFERENCES

1. K.J. Vetter, *Electrochemical Kinetics*, Academic Press, New York, p. 167 (1964).
2. R. Higbie, *Trans. AIChE*, **31**, 365 (1935).
3. N. Frössling, *Gerlands Beitr. Geophys.*, **52**, 170 (1938).
4. W.E. Ranz and W.R. Marshall, *Chem. Eng. Progr.*, **48**, 141, 173 (1952).
5. S. Evnochides and G. Thodos, *AIChE J.*, **7**, 78 (1961).
6. G. Schutz, *Intern. Heat and Mass Transfer*, **6**, 873 (1963).
7. C.R. Wilke, M. Eisenberg, and C.W. Tobias, *J. Electrochem. Soc.*, **100**, 513 (1953).
8. R.L. Steinberger and R.E. Treybal, *AIChE J.*, **6**, 327 (1960).
9. N. Ibl and R. Muller, *J. Electrochem. Soc.*, **105**, 346 (1958); **106**, 528 (1959).
10. M.G. Fouad and N. Ibl, *Electrochim. Acta*, **3**, 233 (1960).
11. C.R. Wilke, C.W. Tobias, and M. Eisenberg, *Chem. Eng. Progr.*, **49**, 663 (1953).
12. A.R. Gordon and A. Cole, *J. Phys. Chem.*, **40**, 733 (1936).
13. *Perry's Chemical Engineers' Handbook*, 6th ed., McGraw-Hill, New York (1984).
14. G.H. Geiger and D.R. Poirier, *Transport Phenomena in Metallurgy*, Addison-Wesley, New York (1973).
15. W.N. Gill, R.P. Vanek, R.V. Jelinek, and G.S. Grove, *AIChE J.*, **6**, 139 (1960).
16. M. Kosaka and S. Minowa, *J. Iron and Steel Inst.*, **8**, 393 (1968).
17. E.D. Traylor, L. Burris, and C.J. Geankoplis, *Ind. Eng. Chem. Fundamentals*, **4**, 119 (1965).
18. M. Eisenberg, C.W. Tobias, and C.R. Wilke, *Chem. Eng. Progr. Symp. Ser.*, **51**(16), 1 (1955).
19. R.G. Olsson, V. Koump, and T.F. Perzak, *Trans. AIME*, **233**, 1654 (1965).
20. R.I.L. Guthrie, *Engineering in Process Metallurgy*, Clarendon Press, Oxford (1989).
21. N.P. Cheremisinoff, ed., *Handbook of Heat and Mass Transfer*, Vol. 2: *Mass Transfer and Reactor Design*, Gulf Publishing, Houston (1986).

EIGHTEEN

Chemical Rate Phenomena

In Chapters 3–17, we discussed the theory and methodology of *momentum, heat and mass transfer*. Most processes used for the production of materials also involve *chemical or physicochemical transformations*, the rates of which may be controlling the overall processing rate. In this chapter, we will introduce the basic concepts of *chemical kinetics and thermodynamics* and formulate the rate equations for a reaction system which is controlled both by mass transfer and chemical reaction.

We have seen that in describing mass transfer rates there are certain rules that apply irrespective of the fluid or solid material involved. In the case of chemical kinetics, there is much more diversity to the point that almost each chemical rate coefficient is unique to a particular reaction system. However, there are certain common methods for dealing with chemical rate phenomena, as will be shown in this and the following chapters. For additional examples on the application of thermodynamics and kinetics in materials processing, the reader is referred to the textbook by Evans and De Jonghe on *The Production of Inorganic Materials* [1].

18.1. HOMOGENEOUS AND HETEROGENEOUS REACTIONS

Chemical reactions are classified in two broad classes: **Homogeneous** reactions, which involve only one phase (e.g., a gas or liquid solution), and **heterogeneous** reactions, which occur between a fluid and a solid or between two fluids separated by an interface. Single-phase reactions that require the presence of a catalytic surface (e.g., the formation of gaseous NH_3 from nitrogen and hydrogen gas), may be considered as quasi-heterogeneous reactions.

The rate of chemical reactions depends on the chemical nature and concentration of the reactants, the temperature and pressure of the system and, in the case of catalytic reactions, on the presence of catalysts. The rate of reaction of a component A is generally related to its concentration by means of the following material balance:

$$\begin{aligned} &\text{mass of } A \text{ reacted/time in reactor volume} \\ &= \quad \text{rate of reaction of } A \text{ (forward reaction)} \\ &\quad - \text{rate of generation of } A \text{ (reverse reaction)} \end{aligned} \tag{18.1.1}$$

It can be seen that when the rate of the reverse reaction is greater than that of the forward reaction, there will be accumulation rather than depletion of A molecules in the reactor volume.

18.1.1. Homogeneous Reactions

In homogeneous reactions, reaction occurs throughout the entire volume of the reacting mass. For an *irreversible* reaction of species A with species B (i.e., when the rate of the reverse reaction is negligible) in a closed vessel, the material balance of (18.1.1) is expressed mathematically as follows:

$$-V_r \frac{dc_A}{dt} = V_r\, k_{r,f}\, c_A^n, \tag{18.1.2}$$

where V_r is the reactor volume; c_A is the concentration of reacting species; $k_{r,f}$ is the *chemical rate coefficient* for the forward reaction.

The power exponent of concentration, n, is called the *order* of the reaction and usually has an integer value. When the rate depends only on the concentration of species A, the reaction is of the first order. If the rate is proportional to the product of the concentrations of reagents A and B, the reaction is of second-order.

Equation (18.1.2) shows that for homogeneous reactions the volume of the reactor, V_r, appears on both sides of the rate equation and therefore cancels out. Thus, the rate equation for a first-order *reversible reaction* may be written as

$$-\frac{dc_A}{dt} = k_{r,f} c_{A,b} - k_{r,r} c_{A,b}, \tag{18.1.3}$$

where $k_{r,f}$ and $k_{r,r}$ are the rate coefficients for the forward and reverse reactions, respectively.

In most reaction systems encountered in the processing of materials, the chemical rate coefficients cannot be calculated on theoretical grounds and are usually determined experimentally. It is therefore convenient to group the forward and reverse rate constants into a single rate coefficient, k_r, which represents the *net* rate of reaction of the species A. The potential for the reverse reaction (i.e., generation of A) is then accounted for by the value of the *equilibrium concentration* of the reacting component A as shown by the following equation for a first-order reaction:

$$-\frac{dc_A}{dt} = k_r(c_{A,b} - c_{A,e}), \tag{18.1.4}$$

where $c_{A,b}$ represents the actual concentration of A in the bulk of the fluid, and $c_{A,e}$ is its *equilibrium concentration*, which will be described in §18.2.

Dimensional analysis of (18.1.4) shows that the dimensions of the chemical rate coefficient for a homogeneous reaction, k_r, are t^{-1}. The form of (18.1.4) indicates that when the bulk concentration of the reacting species in the reactor, $c_{A,b}$, reaches the equilibrium concentration, $c_{A,e}$, the forward reaction (i.e., depletion of A) will be equal to the reverse reaction (i.e., formation of A); therefore, the net rate of reaction of A will be zero. At bulk concentrations of A in the reactor less than $c_{A,e}$, there will be formation rather than depletion of species A.

18.1.2. Heterogeneous Reactions

Heterogeneous reactions involve two or more phases and occur at the interface between a fluid and a solid (e.g., leaching of minerals) or between two immiscible fluids (e.g., gas absorption in a liquid). The majority of chemical reactions encountered in the processing of materials are first-order, heterogeneous reactions.

As noted in §18.1.1, homogeneous reactions occur throughout the entire volume of the reacting mass. Therefore, the dimensions of the rate coefficient, k_r, are $(L^3\ t^{-1})/L^3 = t^{-1}$. The rate of homogeneous reactions depends on the concentration, temperature and pressure of the reacting and product species. In addition to these parameters, the rate of heterogeneous reactions also depends on the surface or *interface area* available for reaction.

The rate equation for a first-order heterogeneous reaction in a closed vessel is expressed as follows:

$$-V_r \frac{dc_A}{dt} = A_r k_r (c_{A,b} - c_{A,e}), \tag{18.1.5}$$

where V_r is the volume of the reacting fluid and A_r the surface or interface area available for reaction. Inspection of (18.1.5) shows that the dimensions of the chemical rate coefficient of a heterogeneous reaction are $L\ t^{-1}$; i.e., they are the same as the dimensions of the *mass transfer coefficient* which was discussed in Chapter 17.

As in the case of mass transfer across an interface (Chapter 17), in many cases it is possible to calculate the surface area available for reaction, A_r, in a reactor of volume V_r; for example, in a pneumatic transport reactor where the gas-solids stream contains n_p spherical particles of diameter d_p per unit volume of stream, the surface area available for reaction per unit volume of reactor space is:

$$A_r = n_p A_p = n_p(\pi d_p^2). \tag{18.1.6}$$

In cases where it is difficult to calculate A_r directly, it is convenient to use the *specific surface area* per unit volume of the reactor which is defined by

$$a_v = \frac{A_r}{V_r}. \tag{18.1.7}$$

The specific surface area has the dimensions of L^{-1} and in some cases can be determined analytically. For example, in the case of gas injection in a liquid bath, an estimate can be made of the average bubble diameter, d_b, and then of the rising velocity, u_b, on the basis of a balance between buoyancy and drag forces (Chapter 8) or some other criterion; the average *residence time* of bubbles in the bath can then be calculated from

$$t_b = \frac{L}{u_b}, \tag{18.1.8}$$

where L is the distance between the point of injection and the surface of the bath. On the basis of the residence time of the bubbles in the bath, we can then calculate the total volume of gas in the bath (*gas hold-up*), at any instant of time, from the volumetric flow rate of gas injection, $\dot{v}$:

$$V_g = \dot{v}\, t_b. \tag{18.1.9}$$

The number of bubbles present in the bath, n_b, is then obtained by dividing V_g by the volume of a single bubble; and the total surface area of bubbles in the bath by multiplying n_b by the surface area of a single bubble:

$$A_r = n_b A_b = \frac{V_g}{(\pi d_b^3/6)} A_b = \frac{V_g}{(\pi d_b^3/6)}(\pi d_b^2) = V_g \frac{6}{d_b}. \tag{18.1.10}$$

Finally, the specific surface area of the gas-liquid suspension in the melt, a_v, is calculated by dividing A_r by the volume of the gas-liquid dispersion, V_r (see (18.1.7)).

It should be noted that the ratio $6/d_b$ in the last term of (18.1.10) represents the surface to volume ratio of a spherical or quasi-spherical bubble or particle of diameter d_b or d_p. Its form explains the very high transport and reaction rates encountered with fine particles.

In some cases, it is not possible to estimate A_r and V_r separately. The alternative is to express the available surface area in terms of the ratio a_v (see (18.1.7)), as in the following form of (18.1.5):

$$-\frac{dc_A}{dt} = \left(\frac{A_r}{V_r}\right) k_r(c_{A,b} - c_{A,e}) = a_v k_r(c_{A,b} - c_{A,e}). \tag{18.1.11}$$

For example, in a catalytic reaction, the surface area of platinum-coated ceramic shapes may be expressed in terms of m^2 per m^3 of packed reactor volume.

Frequently, there are reaction systems where it is impossible to differentiate even between a_v and k_r. For example, this may be the case in the analysis of rate data from a rotary kiln or a leaching tank. In such cases, it is sometimes convenient to group a_v and the heterogeneous rate coefficient k_r into a *volumetric rate coefficient*, k'_r, as shown in the following form of (18.1.11):

$$-\frac{dc_A}{dt} = (a_v k_r)(c_{A,b} - c_{A,e}) = k'_r(c_{A,b} - c_{A,e}). \tag{18.1.12}$$

It can be seen that through this device a heterogeneous reaction is treated as being homogeneous and the corresponding chemical rate constant, k'_r, has the dimensions t^{-1}.

The *overall rate of reaction* between two phases depends both on the rate of the chemical reaction and on the mass transfer rate of the reacting species between the bulk fluid and the reaction surface. Although chemical reaction and mass transfer are very different phenomena, they have a similar effect on the overall rate of the reaction. Also, as we will see in §18.3, in many cases their respective rate coefficients can be added to provide an *overall rate coefficient* for a particular reaction system.

The heterogeneous systems encountered in the processing of minerals and materials are:

- gas–solid (e.g., combustion of carbon, oxidation of sulfides, reduction of oxides)
- liquid–solid (e.g., leaching of minerals, electrodeposition of metals, surface coating, ion exchange)
- gas–liquid (e.g., oxidation of solutions, absorption)
- liquid–liquid (e.g., solvent extraction, slag-metal refining).

18.2. CHEMICAL THERMODYNAMICS

The quantitative description of chemical processes is based on *chemical thermodynamics*, which establish the feasibility of a particular reaction under certain conditions, and *chemical kinetics*, which determine the rate at which the reaction will proceed. In this section, we will present some of the basic concepts of thermodynamics which are essential for formulating and solving chemical processing problems.

18.2.1. Sensible Heat and Heat of Formation

Chemical processes are normally carried out at constant pressure. Under isobaric conditions, the total **enthalpy**, or total heat content, of a chemical species consists of

a. the *heat of formation* which will be discussed below,
b. the *sensible heat*, literally heat that can be sensed because it is associated with a temperature change and is expressed by

$$\int_0^T C_p \, dT,$$

where C_p is the *molar heat capacity* of the species in J mol^{-1} K^{-1}, i.e., its specific heat (Chapter 10) times its molecular weight ($C_p = C_p M$).
c. the *heat of transformation* associated with a particular physical change of the element, such as crystal transformation or change of phase (melting and evaporation), which is expressed in J mol^{-1} .

For convenience, the total enthalpies of all chemical species are tabulated with respect to a **reference temperature**, T_0, and at a **standard pressure**, p_0, which are usually taken to be 25°C (298.15 K) and 1 bar (0.9869 atm) or, in some texts, 1 atm. Therefore, the enthalpy, ΔH_i, of a chemical species i can be expressed as follows:

$$\Delta H_i = \Delta H_i^o + \int_{T_0}^{T} C_p \, dT + \sum (\Delta H_{\text{trans}}), \tag{18.2.1}$$

where ΔH_i^o is the total enthalpy of the species at T_0 and the last term of (18.2.1) represents the heat absorbed or released in transformations that have occurred between the reference temperature, T_0, and temperature T.

To illustrate these concepts, Fig. 18.1 [4] shows how the molar heat capacities of the elements nickel and silicon change with temperature and also with crystal transformation (λ *transition* for nickel), melting and evaporation. The change in total enthalpy with temperature is shown in Fig. 18.2 [4] for silicon.

When chemical elements react to form a compound, a certain amount of heat is released to the environment; in accordance with the *first law of thermodynamics* (the conservation of energy), this **heat of formation** of a compound is equal to the total enthalpy of the compound minus the total enthalpies of the reagent elements. The heat of formation is of the same nature as the heats of transformation of (18.2.1): Heat is stored in atoms and molecules in the form of kinetic or potential energy (energy of translation, rotation and oscillation).

For chemical compounds, the term ΔH_i^o in (18.2.1) is equal to the heat of formation of the compound at T_0:

$$\Delta H_i^o = \Delta H_f^o. \tag{18.2.2}$$

By definition, the heat of formation of the *elements* (e.g., H_2, O_2, Fe, and C) at 298.15 K and 1 bar (or 1 atm) is zero.

When elements and compounds react, they are rearranged to form new chemical species and heat may either be released or absorbed. Again in accordance with the first law of thermodynamics, the *heat of formation of the reaction*, or for short the **heat of reaction**, ΔH_{rx}, is equal to the sum of the total enthalpies of the products minus the total enthalpies of the reagents. For example, in the case of the reaction

$$bB + cC \rightleftharpoons dD + eE, \tag{18.2.3}$$

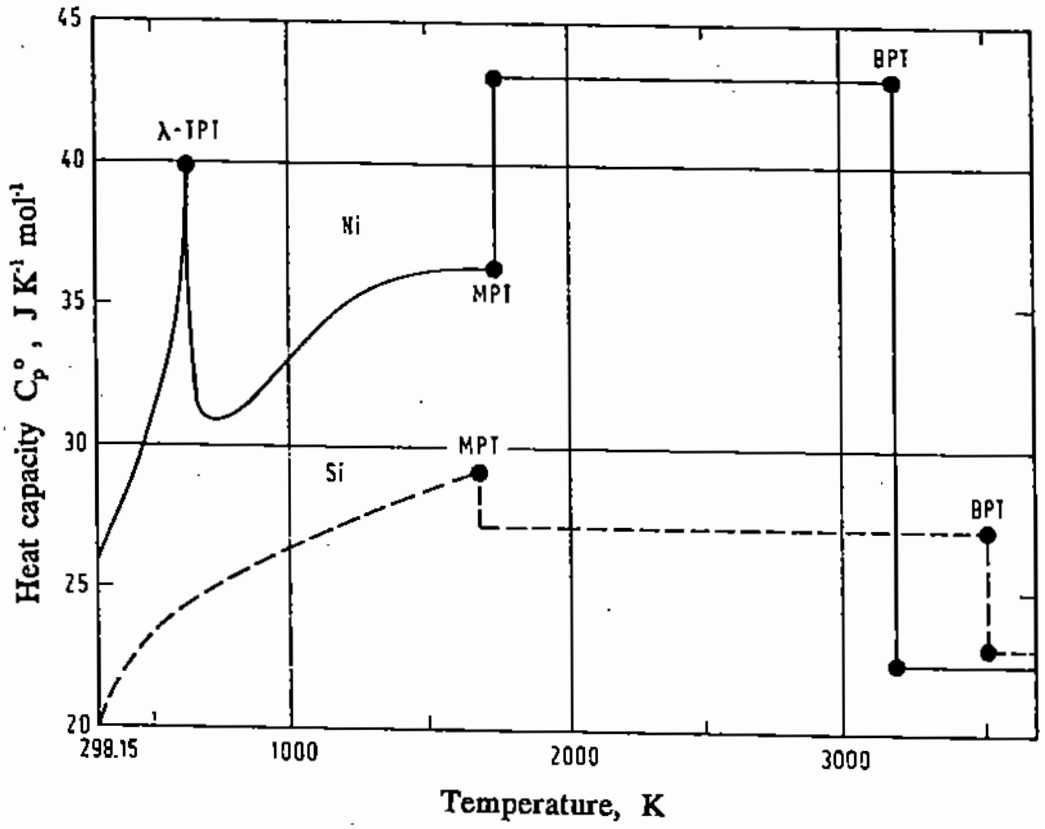

Figure 18.1. Heat capacities of Ni and Si at 1 bar as functions of temperature (λ-TPT = lambda transition point, MPT = melting point, BPT = boiling point; [4]).

the heat of reaction is expressed as follows:

$$\Delta H_{rx} = (d\Delta H_D + e\Delta H_E) - (b\Delta H_B + c\Delta H_C)\,, \tag{18.2.4}$$

where b, c, d, and e are the number of molecules or atoms of species B, C, D, and E involved in the reaction, and ΔH_B, ΔH_C, ΔH_D, and ΔH_E their respective total enthalpies at temperature T.

It is evident from (18.2.1), (18.2.2), and (18.2.4), that the same result is obtained if one sums up the total enthalpies of products (+) and reagents (–) at the reference temperature T_0 and then adds the sensible heat contents and any heats of transformation for all components between T_0 and T:

$$\Delta H_{rx} = (d\Delta H_D^\circ + e\Delta H_E^\circ) - (b\Delta H_B^\circ + c\Delta H_C^\circ) + \sum_{i=1}^{n} \left(\int_{T_0}^{T} C_p\, dT + \sum (\Delta H_{\text{trans}}) \right). \tag{18.2.5}$$

In *exothermic* reactions, heat is released and by convention the value of ΔH_{rx} is negative. On the other hand, reactions which absorb heat are called *endothermic* and have a positive ΔH_{rx}.

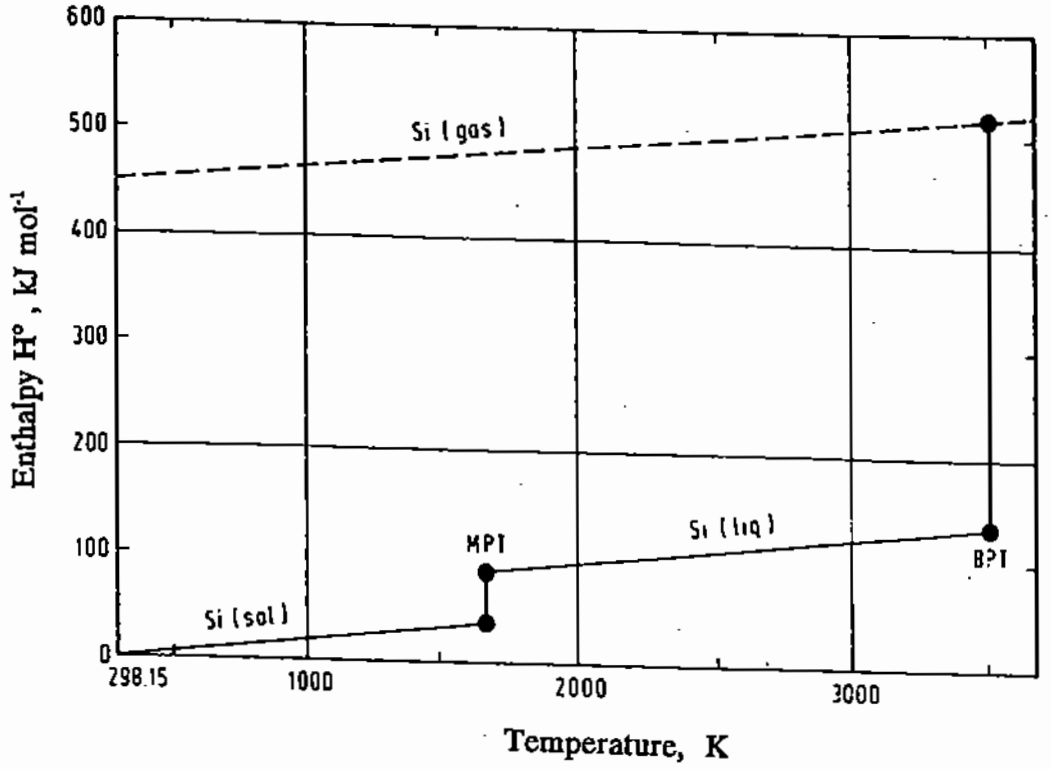

Figure 18.2. Enthalpy of solid, liquid and gaseous silicon as a function of temperature at 1 bar [4].

18.2.2. Gibbs Free Energy and Entropy

A very important concept in chemical thermodynamics is the **Gibbs free energy** of a species which is a function of its enthalpy and *entropy*:

$$G = H - TS. \tag{18.2.6}$$

The property of **entropy** has the dimensions of energy/temperature ($Q\,T^{-1}$) and derives from the *second law of thermodynamics* which states that *the total entropy change in a system resulting from any real process in the system is positive and approaches a limiting value of zero for any process that approaches reversibility*. The entropy of a *reversible process* is equal to the amount of heat absorbed during the process, divided by the temperature at which this heat was absorbed:

$$dS = \frac{dH}{T}.$$

In the above definitions, the word *reversible* denotes a process which is carried out under near-equilibrium conditions and, therefore, most efficiently; an example of this is the melting of a solid at its melting point. Since the heat content of a species is measured in small increments of one degree, the *total entropy* of a chemical species i at its equilibrium state, temperature T and standard pressure p_0 can be expressed as follows:

$$\Delta S_i = \Delta S_i^o + \int_{T_0}^{T} \frac{C_p\,dT}{T} + \sum \left(\frac{\Delta H_{\text{trans}}}{T_{\text{trans}}} \right), \tag{18.2.7}$$

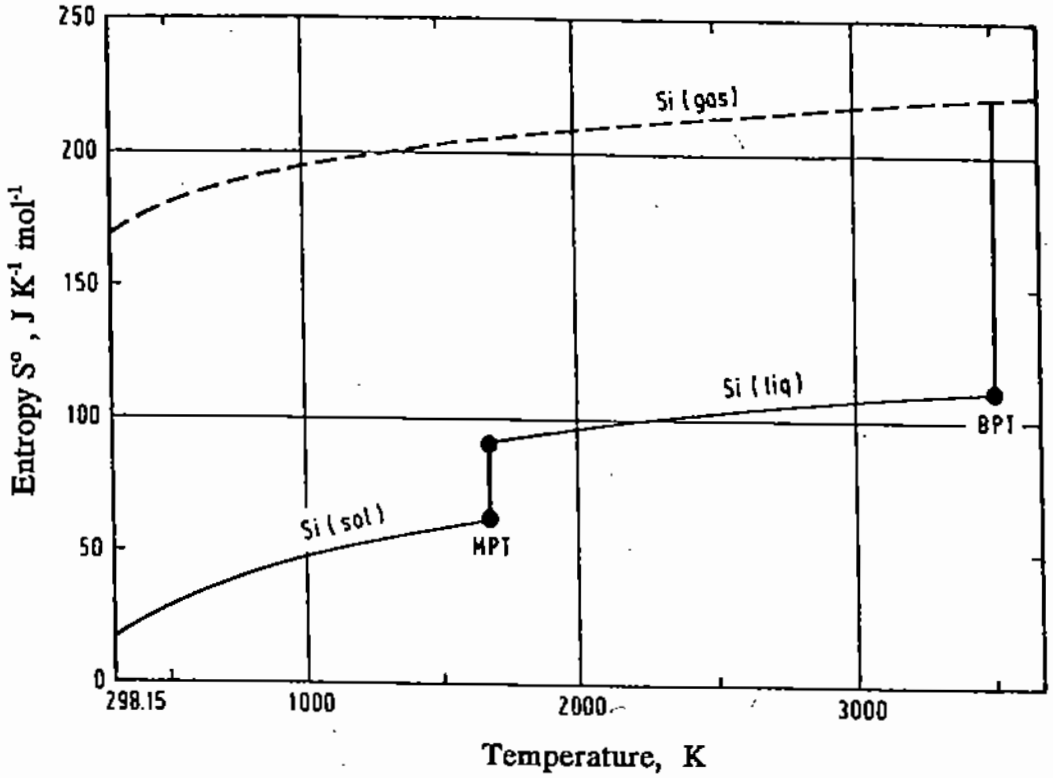

Figure 18.3. Entropy of solid, liquid and gaseous silicon as a function of temperature at 1 bar [4].

where ΔS_i^o refers to the entropy of the species at its *equilibrium state* and at temperature T_0 (298.15 K) and standard state pressure p_0 (1 bar or 1 atm); and T_{trans} are the temperatures of any transformation phenomena such as melting and evaporation that occur between T_0 and T.

Equation (18.2.7) applies down to temperatures of absolute zero by setting $\Delta S_i^o = 0$ and changing the lower limit of the integral from T_0 to 0. *At 0 K, the entropy of all crystalline elements and compounds is zero and for all other species it may be zero* ($\Delta S_{f,0} = 0$); this statement constitutes the *third law of thermodynamics*. The change of entropy with temperature is illustrated in Fig. 18.3 [4] for silicon at the standard pressure.

From the general definition of the Gibbs free energy (see (18.2.6)) we can now express the Gibbs free energy of a chemical species i at equilibrium in terms of its total enthalpy (see (18.2.5)) and total entropy (18.2.7) at temperature T and standard pressure p_0:

$$\Delta G_i^o = \Delta H_i^o - T\,\Delta S_i^o. \tag{18.2.8}$$

The heat capacities, enthalpies, entropies, and Gibbs free energies of chemical species at their *equilibrium state* and at the standard pressure of 1 bar (0.9869 atm), or 1 atm, are published in thermodynamic tables as a function of temperature T above the reference temperature T_0 (298.15 K) [2–4]. The term *equilibrium state* will be discussed in the following section.

The most inclusive and up to date compilation of thermochemical data is by Barin [4] which is also available in computer files. A very useful, and "user-friendly," tool for

computing heats of formation and for many other thermodynamic calculations is the HSC computer program developed by Outokumpu Research [5].

18.2.3. Actual and Equilibrium Gibbs Free Energy

To visualize better the following discussion, let us consider that all components of the reaction of (18.2.3) are in gaseous form:

$$bB + cC \rightleftharpoons dD + eE, \tag{18.2.3}$$

where b, c, d, and e are the number of molecules or atoms of species B, C, D, and E involved in the reaction.

The Gibbs free energy of this reaction is a function of the chemical species and number of moles of the reagents and products and the temperature and pressure of the system in which the reaction takes place. However, it is evident that the effects of temperature and pressure on the Gibbs free energy of the reaction are manifested through the energy levels of the reagents and products. Therefore, the Gibbs free energy of a reaction can be expressed solely as a function of the number of moles involved in the reaction and their respective levels of Gibbs free energy.

On the basis of the law of conservation of energy, we can state that

$$\begin{aligned} &\text{Gibbs free energy of reagents} \\ &\quad + \text{Gibbs free energy of reaction} \\ &\quad = \text{Gibbs free energy of products,} \end{aligned}$$

which leads to an equation similar to (18.2.4) for the heat of reaction:

$$\Delta G_{rx} = [(d\Delta G_D + e\Delta G_E) - (b\Delta G_B + c\Delta G_C)]. \tag{18.2.9}$$

Let us now divide the **actual** Gibbs free energy of a chemical species i at temperature T and *actual* partial pressure $p_{i,a}$ into two components:

- an **equilibrium** (or *standard*) component of the Gibbs free energy which corresponds to the *equilibrium pressure* of the species at the *standard state*, $p_{i,o}$.
- a **relative** component of the Gibbs free energy which represents the effect of the difference between the *equilibrium pressure* and the *actual partial pressure* of the species, i.e.,

$$\Delta G_{i,\text{rel}} = \Delta G_i^o - \Delta G_i, \tag{18.2.10}$$

where ΔG_i^o, ΔG_i, and $\Delta G_{i,\text{rel}}$ denote the equilibrium, actual, and relative Gibbs free energies of species i.

Both the *equilibrium* and *actual* pressures refer to the *thermodynamically effective* partial pressure of a gas species; in most thermodynamic texts the effective pressure is called **fugacity** (from the greek $\phi\upsilon\gamma\eta$, lit. capacity to flee). Fugacity has the same units as pressure. For ideal gases, fugacity is equal to the partial pressure of the gas; all gases approach ideal-gas behavior as the pressure is reduced.

At pressures less than 5 atmospheres and temperatures over 700 K, gases and vapors exhibit near ideal behavior [8]. However, at higher pressures and lower temperatures, there

can be deviations from ideality due to attraction forces between the gas molecules and the finite volume occupied by the molecules; under such conditions, the effective partial pressure of a gas can be lower than its actual pressure. For example, at 473 K and 10 atm pressure, the effective pressure of H_2O vapor is 95% of the actual pressure; at 473 K and 1 atm, the effective pressure is 99.9% of the actual [8].

Let us now define the **activity** of an ideal gas i as the dimensionless ratio of the partial pressure of the species divided by the standard state pressure:

$$a = \frac{p_i}{p_0}. \tag{18.2.11}$$

Generally, the standard state pressure is selected to be

$$p_0 = 1\,\text{bar (or 1 atm)},$$

and for pure condensed phases

$$a = 1.$$

In the case of non-ideal gas behavior we introduce the **activity coefficient**, γ, in (18.2.11):

$$a = \gamma_i \frac{p_i}{p_0}. \tag{18.2.12}$$

For gaseous species, the activity coefficient accounts for any deviation from ideal gas behavior. Therefore, in the above example of water vapor at 473 K, the value of γ_{H_2O} is 0.999 at 1 atm and 0.95 at 10 atm. As noted above, γ can be assumed to be unity for gases at moderate to low pressures and this applies to all examples in this chapter.

We now need a relationship between the actual and equilibrium Gibbs free energies (see (18.2.10)), temperature and pressure. The reader will recall that an exponential "Arrhenius-type" of equation has been found to represent well the relationship of the *mobility* of liquid molecules, such as fluidity (1/viscosity, Chapter 3) and diffusivity (Chapter 14) to temperature:

$$\frac{1/\mu_T}{1/\mu_o} = e^{-E_\mu/RT}, \tag{3.2.16}$$

$$\frac{D_{AB,T}}{D_{AB,o}} = e^{-E_d/RT}, \tag{14.4.2}$$

where the constants E_μ and E_d are called the *activation energies* of the respective phenomena. The same relationship exists between the chemical rate coefficient of reactions and their temperature and activation energy (see (18.3.11), §18.3):

$$\frac{k_{r,T}}{k_{r,o}} = e^{-E_a/RT}. \tag{18.3.11}$$

The same exponential relationship also applies to the effect of temperature on the vapor pressures of liquids and to other natural phenomena and is derived from mathematical statistics (extreme value distribution). It is therefore not surprising that the actual and equilibrium pressures of a gaseous species i are related to the standard pressure and temperature

of the system, and to the corresponding Gibbs free energy levels, by a similar exponential relationship:

$$\frac{p_{i,a}}{p_o} = e^{-\Delta G_i/RT} \text{ and } \frac{p_{i,o}}{p_o} = e^{-\Delta G_i^o/RT}. \tag{18.2.13}$$

By replacing the pressure ratios in the above relationships by the definition of activity (18.2.11), we obtain

$$\Delta G_i = -RT \ln a_i, \tag{18.2.14}$$

and

$$\Delta G_i^o = -RT \ln a_{i,o}. \tag{18.2.15}$$

Therefore, the relative component of the Gibbs free energy (see (18.2.10)) can be expressed as follows:

$$\Delta G_{i,\text{rel}} = \Delta G_i^o - \Delta G_i = -RT \ln a_{i,o} + RT \ln a_i. \tag{18.2.16}$$

We now have an expression for the actual Gibbs free energy of a chemical species as a function of its equilibrium free energy at T and p_o, its activity at equilibrium ($a_{i,o}$, $p_{i,o}$), and its actual activity (a_i, p_i) at temperature T.

Let us now apply the same reasoning to the chemical reaction of (18.2.3). As discussed earlier (see (18.2.9)), the actual Gibbs free energy of this reaction is equal to the net sum of the actual Gibbs free energies of the components of the reaction:

$$\Delta G_{rx} = (d\Delta G_D + e\Delta G_E) - (b\Delta G_B + c\Delta G_C). \tag{18.2.17}$$

By replacing the total Gibbs free energy terms by the corresponding activity terms from (18.2.14), we obtain

$$\Delta G_{rx} = -RT \ln \left(\frac{a_D^d a_E^e}{a_B^b a_C^c} \right)_{\text{actual}}. \tag{18.2.18}$$

The corresponding equations for the equilibrium components of the Gibbs free energy for the same reaction are:

$$\Delta G_{rx}^o = (d\Delta G_D^o + e\Delta G_E^o) - (b\Delta G_B^o + c\Delta G_C^o)$$

$$\Delta G_{rx}^o = -RT \ln \left(\frac{a_D^d a_E^e}{a_B^b a_C^c} \right)_{\text{equil}}. \tag{18.2.19}$$

On the basis of the (18.2.18) and (18.2.19) and (18.2.16), the *relative* Gibbs free energy of this reaction may now be expressed as follows:

$$\begin{aligned} \Delta G_{rx,\text{rel}} = \Delta G_{rx}^o - \Delta G_{rx} &= -RT \ln \left(\frac{a_D^d a_E^e}{a_B^b a_C^c} \right)_{\text{equil}} \\ &+ RT \ln \left(\frac{a_D^d a_E^e}{a_B^b a_C^c} \right)_{\text{actual}}. \end{aligned} \tag{18.2.20}$$

where the first group of activities are at equilibrium and the second at actual conditions.

18.2.4. Equilibrium Constant of a Reaction

When the relative Gibbs free energy of a reaction system is zero, there is no "driving force" for the reaction to proceed either to the right or to the left; therefore, the reaction system

is said to be **at equilibrium**. However, by definition, the equilibrium or standard Gibbs free energy of a compound or reaction, ΔG^o_{rx}, at a specified temperature T is constant; therefore, the group of activities at equilibrium in (18.2.19) must also be constant:

$$\left(\frac{a_D^d a_E^e}{a_B^b a_C^c}\right)_{\text{equil}} = K_e. \tag{18.2.21}$$

By substituting from (18.2.21) into (18.2.19) we obtain

$$\Delta G^o_{rx} = -RT \ln K_e, \tag{18.2.22}$$

where K_e is called the **equilibrium constant** for the reaction of (18.2.3), at temperature T and $p_o = 1$ bar (or 1 atm).

The group of *actual* activities in (18.2.25) is a *nonequilibrium* function, K_{n-e}, which is of the same form as K_e:

$$\left(\frac{a_D^d a_E^e}{a_B^b a_C^c}\right)_{\text{actual}} = K_{n-e}. \tag{18.2.23}$$

By introducing the terms K_e and K_{n-e} in (18.2.20) we obtain

$$\Delta G_{rx,\text{rel}} = -RT \ln K_e + RT \ln K_{n-e}. \tag{18.2.24}$$

Equation (18.2.24) shows that for any reaction, when $K_{n-e} = K_e$, $\Delta G_{rx,\text{rel}} = 0$, and the system is at equilibrium; when $K_{n-e} < K_e$, $\Delta G_{rx,\text{rel}} < 0$, the spontaneous reaction is to the right of the chemical equation; when $K_{n-e} > K_e$, $\Delta G_{rx,\text{rel}} > 0$, the reaction is to the left. Therefore, the criterion for equilibrium depends both on the value of the equilibrium constant and the value of the actual ratio of activities in the system. It must also be kept in mind that K_{n-e}, unlike K_e, is *not* a constant and can be controlled during the design and operation of a process.

Example 18.2.1

At the reaction temperature of about 1600 K, magnesium vapor is produced by the following reaction of dolomite-ferrosilicon briquettes [9]:

$$2(\text{CaO} \cdot \text{MgO})\,(\text{s}) + \text{Fe}_x\text{Si(s)} = 2\text{Mg(g)} + 2\text{CaO} \cdot \text{SiO}_2\text{(s)} + x\text{Fe}\,(\text{s}),$$

where (s) denotes solid components, and (g) gaseous components.

The HSC program [5] computes the ΔG^o_{rx} of this reaction at 1600 K to be +37.1 kcal mol^{-1} and the equilibrium constant 8.58×10^{-6}. As will be shown in the next section, the activity of solids is equal to 1; therefore, $a_{\text{Mg}} = (8.58 \times 10^{-6})^{1/2} = 2.93 \times 10^{-3}$ and $p_{\text{Mg}} = 2.93 \times 10^{-3}$ atm. Therefore, it is not practical to produce Mg by this reaction at atmospheric pressure. However, by carrying out the reaction under reduced pressure, the partial pressure of magnesium vapor over the reaction surface can be reduced to 1×10^{-3} atm, i.e., lower than the equilibrium pressure ($K_{n-e} < K_e$); therefore, the reaction becomes feasible.

18.2.5. Calculation of Equilibrium Concentrations

As discussed in §18.2.3–18.2.4, the standard free energy of formation of a reaction, ΔG^o_{rx}, is obtained by adding up the standard Gibbs free energies of the products and subtracting the

standard Gibbs free energies of the reagents (e.g., see (18.2.19)). The equilibrium constant is then calculated from (18.2.22) and used to determine the ratio of the activities at equilibrium (see (18.2.21)).

For gases, the standard state pressure (p_o) is usually taken to be 1 bar = 0.9869 atm (e.g., Barin [4] and HSC program [5]) or 1 atm (e.g., see [2]). In either case, the activity of a non-ideal gas is expressed by

$$a_i = \gamma_i \frac{p_i}{p_0}, \tag{18.2.12}$$

and for ideal gases

$$a_i = \frac{p_i}{p_0}. \tag{18.2.11}$$

The activity of pure condensed states is

$$a_i = 1. \tag{18.2.25}$$

For liquid solutions, the activity of component A is equal to its mole fraction (Chapter 14) in the solution multiplied by its **activity coefficient** in the solution:

$$a_i = \gamma_i X_i. \tag{18.2.26}$$

The value of the activity coefficient, γ_i, depends on the nature of species i and its interaction with the other species in the solution. At very high concentrations of the solvent, the activity coefficient is close to unity and the activity of a solute may be assumed to be equal to its molar fraction in the solution (*Raoult's law*). The value of γ for solutions can be estimated from thermodynamic rules or from semi-empirical correlations, as illustrated in the following example.

Example 18.2.2

Zinc vapor is recovered from a non-ferrous smelting slag (molten silicate solution) in an electric arc furnace at 1200°C. The chemical reaction between the slag surface and the CO–CO_2 atmosphere above it is expressed as follows:

$$\mathrm{ZnO\,(l) + CO\,(g) \rightleftharpoons Zn\,(g) + CO_2\,(g)}, \tag{18.2.27}$$

where the letter "l" signifies that ZnO is dissolved in the liquid slag and the letter "g" the gaseous components of the reaction. The slag contains 15% Zn by weight ($X^l_{\mathrm{Zn}} = 0.15$) which in this case corresponds to a molar fraction of $X_{\mathrm{ZnO}} = 0.07$. It is required to estimate the equilibrium concentration of zinc vapor as a function of the CO/CO_2 ratio in the furnace atmosphere.

The standard Gibbs free energy of this reaction is calculated from the free energies of the components (as in (18.2.19)):

$$\Delta G^o_{\mathrm{ZnO}\rightarrow\mathrm{Zn}} = \Delta G^o_{\mathrm{Zn}(g)} + \Delta G^o_{\mathrm{CO_2}} - \Delta G^o_{\mathrm{ZnO}} - \Delta G^o_{\mathrm{CO}}. \tag{18.2.28}$$

On the basis of this equation, the HSC program [5] computes the standard free energy of the reaction at 1473 K to be 13200 J/mole ZnO. The corresponding equilibrium constant

(see (18.2.22)) is 0.3399. At equilibrium, the activity of zinc is a function of the CO/CO_2 ratio, the activity of ZnO in the slag and the system temperature (see (18.2.21)):

$$a_{Zn,e} = 0.3399 a_{ZnO} \frac{a_{CO}}{a_{CO_2}}. \tag{18.2.29}$$

If we were concerned with the reduction of solid ZnO particles (e.g., zinc calcines), the activity of ZnO would be assumed to be unity. Therefore, from (18.2.29), the equilibrium activity of zinc vapor would be

$$a_{Zn} = \frac{p_{Zn,e}}{1\,\text{atm}} = 0.3399 \frac{a_{CO}}{a_{CO_2}} = 0.3399 \frac{p_{CO}}{p_{CO_2}} = 0.3399 \frac{X_{CO}}{X_{CO_2}}.$$

However, the activity of ZnO in molten slag depends on its molar fraction in the melt (X_{ZnO}) and the activity coefficient of ZnO, γ_{ZnO}. By correlating a number of experimental results, Battle and Hager [6] developed a correlation of γ_{ZnO} as a linear function of the concentrations of CaO, MgO, Al_2O_3, FeO, and Fe_2O_3 in the slag; let us assume that on the basis of this correlation, γ_{ZnO} is estimated to have the typical value of 2 [6]. Therefore,

$$a_{ZnO} = \gamma_{ZnO} X_{ZnO} = 2 \times 0.07 = 0.14, \tag{18.2.30}$$

and the equilibrium pressure of zinc vapor is calculated to be

$$\frac{p_{Zn,e}}{1\,\text{atm}} = 0.3399 \times 0.14 \times \frac{X_{CO}}{X_{CO_2}} = 0.0476 \frac{X_{CO}}{X_{CO_2}}. \tag{18.2.31}$$

For instance, if the CO/CO_2 ratio in the electric arc furnace is controlled (by means of the coal and air input rates) at 1, the partial pressure of Zn vapor in the gas cannot exceed 0.0476 atm; at higher Zn pressures, and therefore concentrations of Zn in the gas atmosphere above the slag, the reduction reaction would be reversed and some of the zinc vapor would be oxidized by CO_2 to ZnO.

Example 18.2.3

Estimate the rate of loss of MgO from a surface heated at 2000 K in vacuum. The decomposition reaction is expressed as follows:

$$MgO\,(s) = Mg\,(g) + 0.5O_2\,(g). \tag{18.2.32}$$

The standard Gibbs free energy of this reaction is computed [5] to be 76.53 kcal mol^{-1} and the corresponding $K_e = 4.08 \times 10^{-9}$ ($p_0 = 1$ atm). Therefore (see (18.2.21)),

$$K_e = \left(\frac{a_{Mg} a_{O_2}^{1/2}}{a_{MgO}} \right)_e, \tag{18.2.33}$$

and for $a_{MgO} = 1$,

$$K_e = 4.08 \times 10^{-9} = a_{Mg} a_{O_2}^{1/2} \equiv p_{Mg} p_{O_2}^{1/2}. \tag{18.2.34}$$

This is a *sublimation* reaction and the molar fluxes of the two elements leaving the reaction surface are in the ratio of 2 to 1:

$$\frac{N_{Mg}}{N_{O_2}} = 2. \tag{18.2.35}$$

Also, the mass flux of magnesium leaving the surface is controlled by sublimation and can be expressed by the *Knudsen equation* [9]:

$$N'_{Mg} = 44.4 p_{Mg} \left(\frac{M_{Mg}}{T}\right)^{1/2}, \tag{18.2.36}$$

where p_{Mg} is in atm and the mass flux in g s^{-1} cm^{-2}. The same equation applies to the sublimation of oxygen molecules; by converting the mass fluxes in the two sublimation equations to molar (division by M_{Mg} and M_{O_2}) and combining with (18.2.35), we obtain a second equation between p_{Mg} and p_{O_2}:

$$p_{Mg} = 2 p_{O_2} \left(\frac{M_{Mg}}{M_{O_2}}\right)^{1/2}. \tag{18.2.37}$$

We now have two equations ((18.2.34) and (18.2.37)) for the two unknown pressures of sublimation. By solving them, we find that $p_{O2} = 1.76 \times 10^{-6}$ atm. and $p_{Mg} = 3.07 \times 10^{-6}$ atm. Finally, the mass flux from the MgO surface is calculated from (18.2.36) to be N'_{Mg} $= 15 \times 10^{-6}$ g s^{-1} cm^{-2}.

Example 18.2.4

Examine whether it is feasible to produce aluminum by means of the hydrogen reduction of Al_2O_3 at 2000 K:

$$Al_2O_3\,(s) + 3H_2\,(g) = 3H_2O\,(g) + 2Al\,(l). \tag{18.2.38}$$

The equilibrium constant of this reaction at 2000 K is computed [5] to be 4.473×10^{-17}. Therefore, $K_e = (p_{H_2O}/p_{H_2})^{1/3} = (X_{H_2O}/X_{H_2})^{1/3}$, and $X_{H_2O}/X_{H_2} = 3.55 \times 10^{-6}$. This means that it will be necessary to recirculate a very large amount of hydrogen in order to remove a relatively minute amount of oxygen as H_2O.

18.2.6. Ellingham Diagrams

In Example 18.2.4 above, we examined the thermodynamic "ability" of hydrogen to remove oxygen from a metal oxide and produce metal, at a given temperature. This type of reaction is encountered with many metal oxides. It is therefore convenient to construct a thermodynamic diagram where the standard Gibbs free energy of each oxide is expressed *per mole of oxygen* and plotted against temperature. By plotting the free energies for all known oxides, including

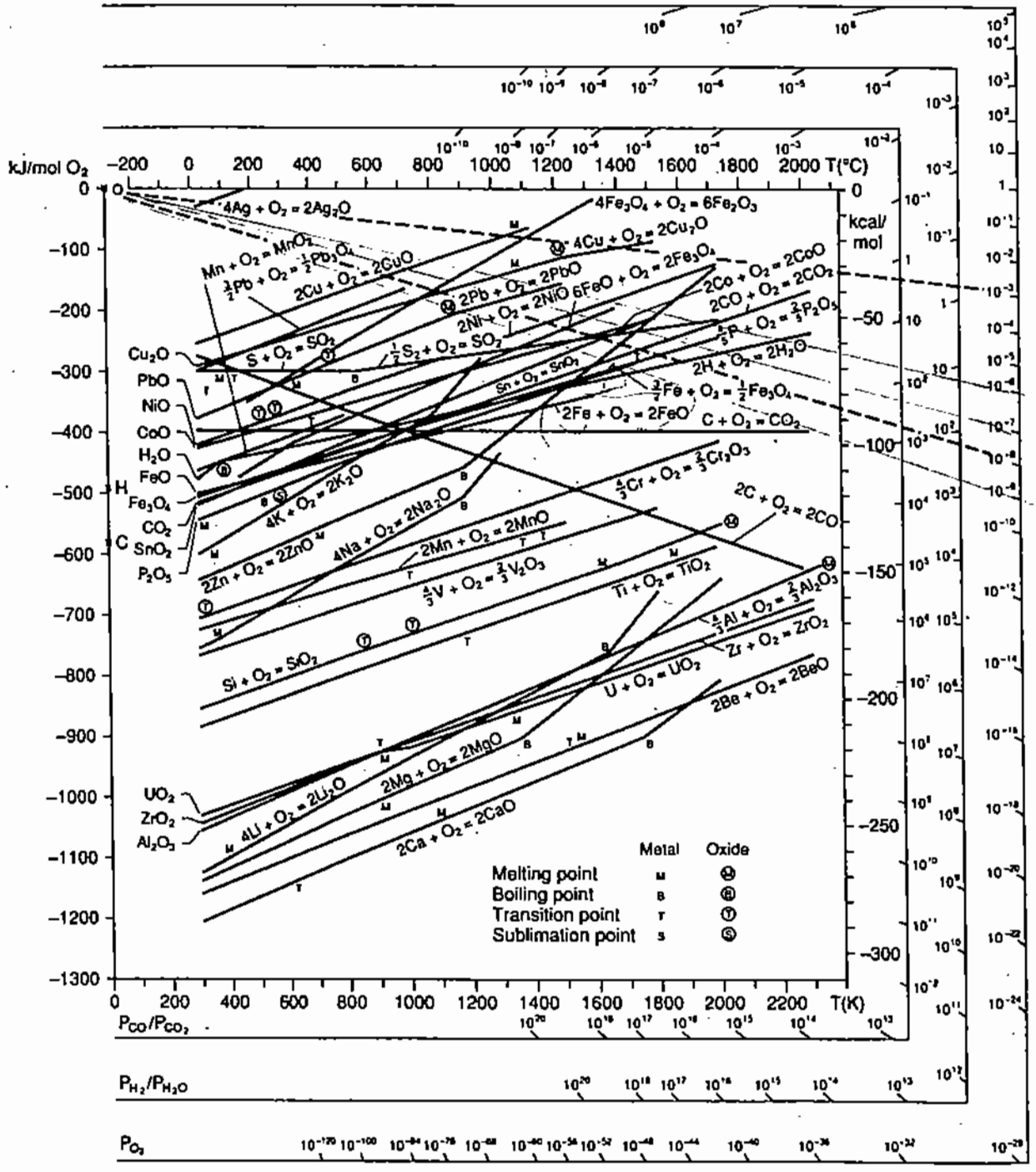

Figure 18.4. Ellingham diagram for oxides [1].

those of the reducing agents H_2, C, and CO on this plot, one can see the thermodynamic *relative reducibility* of any particular oxide.

This type of plot is very useful in the analysis of chemical reactions and is called the **Ellingham diagram**. Figure 18.4 [1] is such a diagram for oxides. For example, it tells us that an element which is lower down on the plot can reduce an oxide higher up.

In addition to the Gibbs free energies, Fig. 18.4 contains other useful information, by means of three nomographs. The outermost nomograph represents the partial pressure of oxygen at equilibrium with a metal oxide at a particular temperature. For example, the thermal decomposition of silver oxide can be presented as follows:

$$2Ag_2O\,(s) \rightleftharpoons 4Ag\,(s) + O_2(g)\,. \tag{18.2.39}$$

On the basis of the theory we presented earlier, the activities of silver oxide and silver are equal to 1. Therefore, from (18.2.22), the equilibrium pressure of O_2 at temperature T can be expressed as a function of the standard Gibbs free energy of the above reaction:

$$\frac{p_{O_2,e}}{p_0} = K_e = e^{-\Delta G^\circ_{rx}/RT}, \tag{18.2.40}$$

where p_o is the standard state pressure. The equilibrium pressure of oxygen in a particular oxygen-containing system is also called the **oxygen potential** of the system. Let us now consider the dashed line joining the origin of the y-axis with the oxygen potential of 10^{-3} on the $\ln p_{O_2}$ nomograph of Fig. 18.4 [1]. Consideration of (18.2.40) shows that this line represents the function $RT \ln p_{O_2}$ at $p_{O_2} = 10^{-3}$, i.e., the standard Gibbs free energy for decomposition. Therefore, the point where such a line intersects the standard Gibbs free energy plot for a particular oxide signifies the temperature at which the oxide will start decomposing spontaneously to metal and oxygen; for example, at $p_{O_2} = 10^{-3}$, Ag_2O will start decomposing at about 70°C (Fig. 18.4).

Of course, the use of vacuum for reducing metal oxides is not a practical means in most cases. Reduction of metal oxides is usually carried out by means of a *displacement reaction* where oxygen atoms of one oxide react with another element to form a new oxide. The displacing element can be either another metal, or more often hydrogen to form H_2O, carbon to form CO, and CO to form CO_2.

Let us now extrapolate the free energy lines for reactions

$$2H_2 + O_2 = 2H_2O \tag{18.2.41}$$

and

$$2CO + O_2 = 2CO_2 \tag{18.2.42}$$

in Fig. 18.4 to the y-axis (points H and C, respectively). The p_{H_2}/p_{H_2O} and p_{CO}/p_{CO_2} nomograph scales of Fig. 18.4 represent logarithmic ranges of values of these ratios and correspond to the values of the O_2 nomograph, according to the standard Gibbs free energies of the respective reactions of (18.2.41)–(18.2.42); therefore, they are on the same basis as all other plots in Fig. 18.4. For example, let us draw a line between the value of $p_{H_2}/p_{H_2O} = 1$ on the H-nomograph and the point H on the y-axis. All oxides (e.g., Cu, Ni, Pb, etc.) that have plots above this line can be reduced at this H_2/H_2O ratio. To reduce oxides with plots below the line, we need to use more hydrogen, i.e., to decrease the *oxygen potential* in the reaction system.

Similar diagrams to Fig. 18.4 have been constructed for many other reaction systems, such as sulfides, sulfates, carbonates, halides, carbides and silicates [1,9].

Example 18.2.5

Calculate the degree of decomposition of pure nitrogen tetroxide according to reaction

$$N_2O_4(g) \rightleftharpoons 2NO_2(g) \tag{18.2.43}$$

over the temperature range of 200–400 K and at pressures of 0.1, 1, and 10 atmospheres [15].

We first obtain from thermodynamic tables [4] the values of the equilibrium constant for this reaction in the range of 200–400 K. Then, on the basis of the stoichiometry of the reaction, for one mole of reagent we obtain the following tabulation:

	Initial number of moles	Number of moles at equilibrium	Mole fraction at equilibrium
N_2O_4	1	$1-f$	$(1-f)/(1+f)$
NO_2	0	$2f$	$2f/(1+f)$
Total	1	$1+f$	1

The fraction of N_2O_4 reacted, f, is related to the equilibrium constant, K_e, by (18.2.21) as follows:

$$K_e = \frac{a_{NO_2}^2}{a_{N_2O_4}} = \frac{(X_{NO_2}p/p_0)^2}{X_{N_2O_4}p/p_0} = \frac{[2f/(1+f)p/p_0]^2}{(1-f)/(1+f)p/p_0} = \frac{4f^2}{(1-f^2)}p/p_0. \tag{18.2.44}$$

Therefore, f is related to K_e by the following expression:

$$f = \left(\frac{K_e p_0/p}{1+K_e p_0/p}\right)^{1/2}. \tag{18.2.45}$$

Figure 18.5 [15] shows the results of the above calculation in graphical form. It can be seen that the degree of N_2O_4 decomposition is decreased with increasing pressure; this is due to the fact that two moles of product are formed for each mole of reactant (see (18.2.43)).

18.3. MASS TRANSFER AND CHEMICAL REACTION

As a first example of heterogeneous reactions, we will consider the reaction between a solid particle and the gas atmosphere around it. For example, this type of reaction is commonly encountered in metal reduction processes, such as the direct reduction of partly reduced iron oxide (FeO) by hydrogen at 900°C:

$$FeO\,(s) + H_2\,(g) \rightleftharpoons Fe\,(s) + H_2O\,(g). \tag{18.3.1}$$

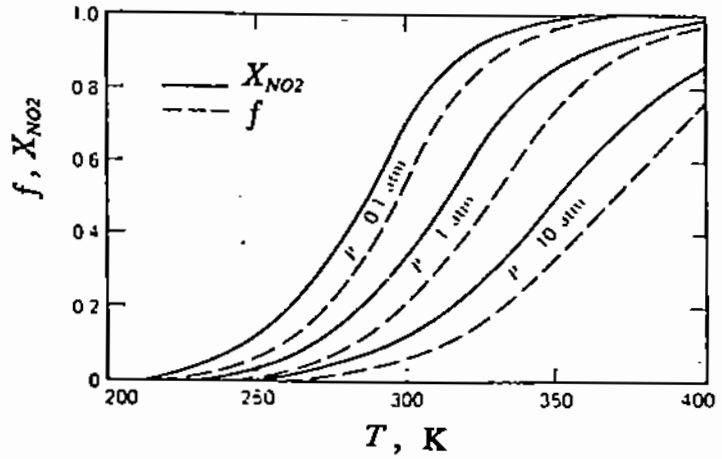

Figure 18.5. Effect of pressure on degree of decomposition of N_2O_4 and molar fraction of NO_2 at equilibrium.

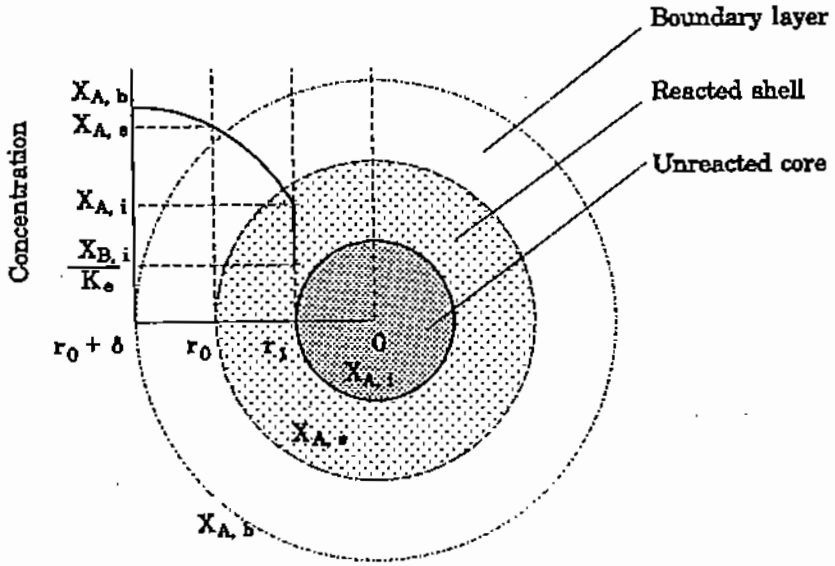

Figure 18.6. Concentration profile of reacting species *A* through boundary layer and sectioned, semi-reacted sphere.

This reaction proceeds through the following "steps" (Fig. 18.6):

a. diffusion of H_2 through the gaseous boundary layer around the particle;
b. diffusion of H_2 through the reduced porous shell;
c. reduction of FeO to Fe at the interface between the oxidized shell and the unreacted core;
d. diffusion of the product H_2O through the reduced shell;
e. diffusion of the product H_2O through the gaseous boundary layer.

It can be seen that "steps" a and e are in fact one process, the counter-diffusion of H_2 and H_2O through the boundary layer. Also, steps b and d are the counter-diffusion of H_2 and H_2O through the reacted shell. Therefore, the five "steps" listed above can be regrouped into the following three basic processes:

a. mass transfer through the gaseous boundary layer;

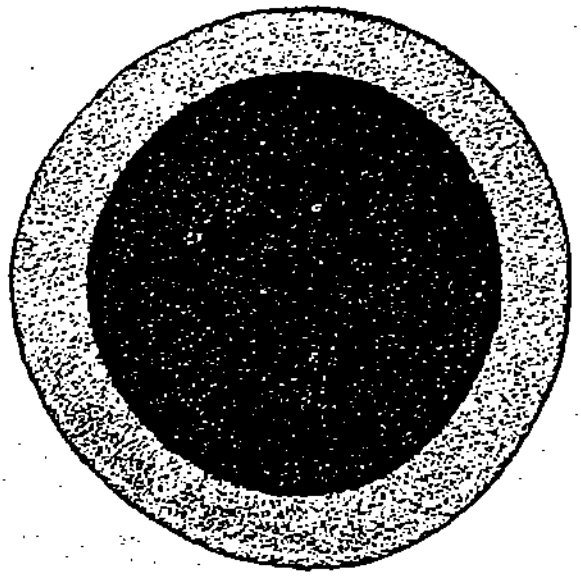

Figure 18.7. Photograph of partly reduced copper oxide sphere showing outer shell of metallic copper.

b. diffusion through the reacted shell;
c. chemical reaction at the interface.

It is evident that a molecule or atom of the reacting species, in this case hydrogen, must pass through all three processes. Therefore, the overall rate of reaction, i.e., the number of molecules reacted per unit time, must be equal to the rate of each of these processes. The situation is similar to the problem of heat transfer by conduction through a composite medium (Chapter 10) or diffusion through the interface between two immiscible fluids (Chapter 17).

In this particular example, one molecule of hydrogen diffuses inward for each molecule of H_2O diffusing in the opposite direction. Therefore, this is a case of equimolar diffusion and, as discussed in §14.5, the *net bulk flow due to diffusion* is zero; the rate of molar flux, N_{H_2}, and molar flow, $\dot{m}_{H_2}$, of H_2 through the boundary layer can be expressed as follows:

$$N_{H_2} = -N_{H_2O} = k_d\, c\, (X_{H_2,b} - X_{H_2,s}), \tag{18.3.2}$$

and therefore,

$$\dot{m}_{H_2} = 4\pi r_0^2 N_{H_2} = 4\pi r_0^2 k_d\, c\, (X_{H_2,b} - X_{H_2,s}), \tag{18.3.3}$$

where the subscript b denotes the concentration of H_2 in the bulk gas around the particle and the subscript s the concentration of H_2 at the surface of the particle.

From diffusion theory (Chapter 14), the molar flow of the reagent H_2 through the reacted shell is related to time and distance as follows:

$$\dot{m}_{H_2} = 4\pi r^2 D_{\text{eff}}\, c \left(\frac{\partial X_{H_2}}{\partial r}\right)_{r,t}, \tag{18.3.4}$$

where $4\pi r^2$ is the diffusion area; D_{eff} is the effective diffusivity of hydrogen through reacted shell around unreacted core; r is the distance from the particle center; t is the reaction time.

As discussed in Chapter 14, the effective diffusivity of a gas through a porous medium is lower than the molecular diffusivity, because only the pores of the reacted shell (Fig.

18.7) are available for diffusion; also, the diffusing species may have to follow a tortuous path through these pores. The effective diffusivity can be related to the molecular diffusivity of the species in free space by means of the following expression (Chapter 14):

$$D_{\text{eff}} = D_{AB}\frac{\varepsilon}{\tau}, \tag{14.7.15}$$

where ε is the porosity of the reacted solid and τ is the "tortuosity" factor representing the increase in length of the diffusion path through the interconnected pores.

The porosity may range from 0 to over 0.5 and the tortuosity from 1 to over 10. For example, in the case of iron oxides reduced at 750°C, the porosity was found to be about 50% and the pore sizes ranged from 0.2–0.5 microns [6]; the experimentally determined values of porosity, tortuosity and diffusivity for hydrogen diffusing through reduced iron are shown in the following tabulation by Olson and McKewan [11]:

Temp. °C	D_{H_2}	Porosity	Tortuosity	D_{eff,H_2}
800	8.28	0.54	3.07	1.46
900	9.59	0.54	2.36	2.20
1000	13.3	0.44	2.25	2.63

The decrease of tortuosity at higher temperatures was explained by the formation of larger pores by recrystallization due to sintering. The *decrease* of porosity at 1000°C may be due to shrinking of the outer diameter of the particle, caused by the increased mobility of the reduced iron atoms at higher temperatures.

As the reaction interface moves towards the center of the particle, the effective cross-sectional area for diffusion through the reacted shell is constantly changing. However, since the diffusion velocity (Chapter 14) of gas through the reacted shell is much faster than the rate of advance of the reaction interface, we can assume that the interface radius, r, is constant with time over short periods of time (quasi-steady state conditions). Thus, the partial differential of the molar fraction in (18.3.4) may be assumed to be a total differential with respect to r and integrated for the boundary condition of $X_{H_2} = X_{H_2,s}$ at $r = r_0$ and $X_{H_2} = X_{H_2,i}$ at $r = r_i$, to yield

$$\dot{m}_{H_2} = \frac{4\pi r_0 r_i}{(r_0 - r_i)} D_{\text{eff}}\, c\,(X_{H_2,s} - X_{H_2,i}), \tag{18.3.5}$$

where r_0 is the radius of the particle and r_i the radius of the interface between reacted and unreacted zones.

When hydrogen molecules reach the reaction interface, at $r = r_i$, they react with FeO to produce metallic iron. As discussed in §18.1, the rate of the chemical reaction can be expressed as follows:

$$\dot{m}_{H_2} = k_r(4\pi r_i^2)\, c(X_{H_2,i} - X_{H_2,e}). \tag{18.3.6}$$

where k_r is the chemical rate coefficient and $X_{H_2,e}$ the equilibrium concentration of hydrogen at the reaction interface.

The equilibrium concentration of H_2 at the reaction interface is calculated from the standard free energy of formation of the reaction, as discussed in §18.2:

$$\Delta G^o_{FeO\rightarrow Fe} = (\Delta G^o_{Fe} + \Delta G^o_{H_2O}) - (\Delta G^o_{FeO} + \Delta G^o_{H_2}). \tag{18.3.7}$$

In this case, the activities of the FeO and Fe solids can be assumed to be unity; therefore, the equilibrium concentration of hydrogen at the interface is related to the H_2O concentration at the interface and to the equilibrium constant, K_e, as follows:

$$K_e = \frac{X_{H_2O,i}}{X_{H_2,e}}, \tag{18.3.8}$$

or

$$X_{H_2,e} = \frac{X_{H_2O,i}}{K_e}, \tag{18.3.9}$$

and by substituting for $X_{H_2,e}$ in (18.3.6):

$$\dot{m}_{H_2} = k_r(4\pi r_i^2)\, c \left(X_{H_2,i} - \frac{X_{H_2O,i}}{K_e}\right). \tag{18.3.10}$$

The effect of temperature on the chemical rate coefficient is usually expressed by means of an Arrhenius-type equation:

$$k_{r,T} = k_{r,o} e^{-E_a/RT}, \tag{18.3.11}$$

where $k_{r,o}$ is the rate constant at some reference temperature T_o, and E_a is the "activation energy," or, in more practical terms the *temperature coefficient* of the reaction. For example, in the case of $FeCl_2$ reduction by hydrogen, the activation energy in the temperature range of 500–630°C was estimated, from the rate of advance of the reaction interface (Fig. 18.8 [7]), to be 27500 cal/mol^{-1}.

Returning to (18.3.10), it is noted that the concentration of the product gas at the interface, $X_{H_2O,i}$, depends on the rate of diffusion of H_2O away from the interface, first through the reacted layer and then through the boundary layer. These phenomena are also represented by (18.3.5) and (18.3.3), respectively, with the exception that the hydrogen concentrations are replaced by the appropriate H_2O concentrations:

$$\dot{m}_{H_2O} = \frac{4\pi r_0 r_i}{(r_0 - r_i)} D_{eff}\, c\, (X_{H_2O,i} - X_{H_2O,s}), \tag{18.3.12}$$

and

$$\dot{m}_{H_2O} = 4\pi r_0^2 k_d\, c\, (X_{H_2O,s} - X_{H_2O,b}). \tag{18.3.13}$$

Let us now compare the five rate equations which represent the overall movement of hydrogen in and out of the reacting particle, either in the form of H_2 or H_2O: (18.3.3), (18.3.5), (18.3.10), (18.3.12) and (18.3.13). We see that all five rate steps are functions of a concentration difference which may be considered as the driving force for each step.

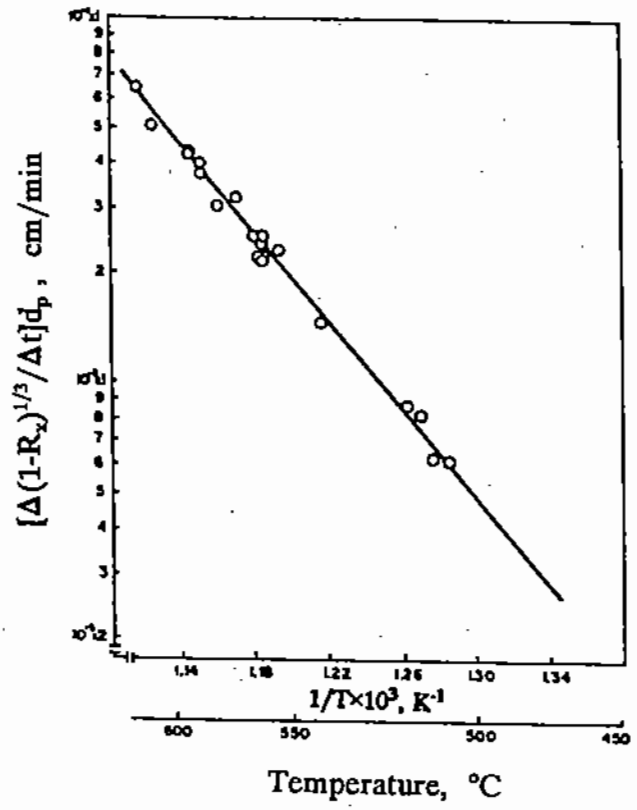

Figure 18.8. Arrhenius-type plot of chemical rate coefficient for reduction of $FeCl_2$ spheres by hydrogen.

In an actual experimental or industrial reaction system, the "intermediate" concentrations of hydrogen at the particle surface, $X_{H_2,s}$, and at the reaction interface, $X_{H_2,i}$, are not known. However, the bulk concentrations of H_2 and H_2O can be estimated easily. It is therefore convenient to express the overall rate of the reaction in terms of the difference between these two concentrations. The reader will recall that a similar approach was used in expressing the heat flux across a composite medium involving both conduction and convection (Chapter 10), and the mass flux between two fluid phases (Chapter 17).

Accordingly, by algebraic manipulation of (18.3.2), (18.3.5), (18.3.10), (18.3.12) and (18.3.13), we can eliminate the intermediate concentrations at the reaction interface and at the surface of the particle and obtain the following expression for $\dot{m}_{H_2}$ solely as a function of the bulk concentrations of H_2 and H_2O:

$$\dot{m}_{H_2} = 4\pi r_0^2\, c \left(x_{H_2,b} - \frac{X_{H_2O,b}}{K_e} \right) \left(\frac{1}{\frac{1}{k_d}\left(1+\frac{1}{K_e}\right) + \frac{(r_o - r_i)}{(r_i/r_o) D_{eff}}\left(1+\frac{1}{K_e}\right) + \frac{1}{(r_i/r_o)^2 k_r}} \right). \tag{18.3.14}$$

Inspection of (18.3.14) shows that the last bracket represents the *overall rate coefficient*, k_{ov}, for the reaction and is equal to the inverse of the sum of the individual "resistances" to the five rate states; therefore:

$$\frac{1}{k_{ov}} = \frac{1}{k_d}\left(1+\frac{1}{K_e}\right) + \frac{(r_o - r_i)}{(r_i/r_o) D_{eff}}\left(1+\frac{1}{K_e}\right) + \frac{1}{(r_i/r_o)^2 k_r}. \tag{18.3.15}$$

For a system of planar geometry, i.e., when the reaction interface does not change with degree of reaction, the above equation simplifies to

$$\frac{1}{k_{ov}} = \frac{1}{k_d}\left(1+\frac{1}{K_e}\right) + \frac{\Delta Y}{D_{eff}}\left(1+\frac{1}{K_e}\right) + \frac{1}{k_r}, \qquad (18.3.16)$$

where ΔY is the thickness of the reacted layer. If, in addition, the reaction is favored thermodynamically (i.e., for high values of K_e) (18.3.16) simplifies further to:

$$\frac{1}{k_{ov}} = \frac{1}{k_d} + \frac{\Delta Y}{D_{A,eff}} + \frac{1}{k_r}. \qquad (18.3.17)$$

It can be seen that (18.3.15)–(18.3.17) for the overall rate coefficient are analogous to the equations for the overall heat transfer (Chapter 12) and mass transfer (Chapter 17) coefficients.

In Chapter 19, we will discuss some applications of the above rate equations. For additional information on gas–solid reactions, the reader is referred to Szekely et al. [12], Kunii and Levenspiel [13], and Smoot and Smith [14].

REFERENCES

1. J.W. Evans and L.C. De Jonghe, *The Production of Inorganic Materials*, Macmillan Publishing, New York (1991).
2. R.H. Perry and D. Green, eds., *Perry's Chemical Engineer's Handbook*, 6th ed., McGraw-Hill, New York (1984).
3. R.C. Weast and M.J. Astle, editors, *Handbook of Chemistry and Physics*, 60th ed., CRC Press, Boca Raton, FL (1979).
4. I. Barin, in collaboration with F. Sauert, E. Schulze-Rhonohof, and W. Shu Sheng, *Thermochemical Data of Pure Substances*, Parts I and II, VCH Press, Weinheim D-6940, Germany (1989).
5. A. Roine, *Outokumpu HSC Chemistry for Windows*, Outokumpu Research Company, Pori, Finland (1993).
6. T.P. Battle and J.P.Hager, *Metallurgical Transactions B*, **21B**, 501–510 (1990).
7. J.C. Yannopoulos and N.J. Themelis, *Can. J. Chem. Eng.*, **43**, 173-177 (1965).
8. H.H. Kellogg, *Thermodynamics and Chemical Equilibrium*, Lecture Notes, Columbia University (1988).
9. O. Kubaschewski and C,B. Alcock, *Metallurgical Thermochemistry*, Pergamon Press, Oxford (1979).
10. T. Rosenqvist, *Principles of Extractive Metallurgy*, McGraw-Hill, New York (1974).
11. R.G. Olsson and W.M. McKewan, *Trans. AIME*, **236**, 1518–1522 (1966).
12. J. Szekely, J.W. Evans, and H.Y. Sohn, *Gas-Solid Reactions*, Academic Press, New York (1976).
13. D. Kunii and O. Levenspiel, *Fluidization Engineering*, Wiley, New York (1969).
14. L.D. Smoot and P.J. Smith, *Coal Combustion and Gasification*, Plenum Press, New York (1985).
15. S.I. Sandler, *Chemical and Engineering Thermodynamics*, Wiley, New York (1989).
16. B.G. Kyle, *Chemical and Process Thermodynamics*, Prentice-Hall, Englewood Cliffs, NJ (1984).

NINETEEN

Applications of Rate Phenomena Theory

In this chapter, we will discuss problems which involve simultaneous transport and chemical phenomena.

19.1. COMBUSTION OF CARBON PARTICLES

One of the most important reactions for producing energy is the combustion of coal particles with oxygen. The major constituent of coal is carbon and the combustion reaction is expressed by:

$$\mathrm{C(s) + O_2\,(g) \rightleftharpoons CO_2\,(g)}. \tag{19.1.1}$$

On the basis of experimental work (Fig. 19.1, [1]), the following equation has been proposed for the chemical rate of combustion of anthracite particles (73% C) in oxygen-containing atmospheres:

$$N'_{\mathrm{C}} = 20.4e^{-19000/RT}\, c\,(X_{\mathrm{O_2},s} - X_{\mathrm{O_2},c}) = k_{r,\mathrm{C}}\, c\,(X_{\mathrm{O_2},s} - X_{\mathrm{O_2},c}), \tag{19.1.2}$$

where N'_C is the mass flux of combusted carbon, in g carbon $\mathrm{s^{-1}\ cm^{-2}}$, $X_{\mathrm{O_2},s}$ and $X_{\mathrm{O_2},e}$ are the mole fractions of the reagent at the reaction surface and at equilibrium, T is the reaction temperature and the activation energy is expressed in cal $\mathrm{mol^{-1}}$ ($R = 1.987$ cal $\mathrm{mol^{-1}\ K^{-1}}$).

It is required to estimate the relative magnitudes of the rate coefficients for mass transfer through the boundary layer and for chemical reaction during the combustion of anthracite particles of assumed spherical shape; also, the time required for complete combustion in air of a 0.1-cm diameter particle at 1300 K.

It is noted from (19.1.2) that the chemical rate coefficient $k_{r,\mathrm{C}}$ is expressed in terms of grams of carbon reacted and, therefore, must be converted to the units of the gaseous rate coefficients that were discussed in §18.3 (Chapter 18). It can be assumed that the ash content in the anthracite does not form a "reacted shell" around the unreacted core of the particle; therefore, the resistance to diffusion through the reacted layer (§18.3) is negligible.

Since we have no information on the relative velocity between particle and air, we will assume the "worst case" of mass transfer of $\mathrm{O_2}$ through the boundary layer, i.e., Re = 0; therefore, from the Ranz–Marshall correlation (see (17.4.2)), Sh=2 and the corresponding mass transfer coefficient of $\mathrm{O_2}$ through the $\mathrm{CO_2}$ boundary layer around the particle is

$$k_d = \mathrm{Sh}\frac{D_{\mathrm{O_2-CO_2}}}{d_p} = 2 \times \frac{1.6}{d_p} = \frac{3.2}{d_p}\ \mathrm{cm\,s^{-1}}, \tag{19.1.3}$$

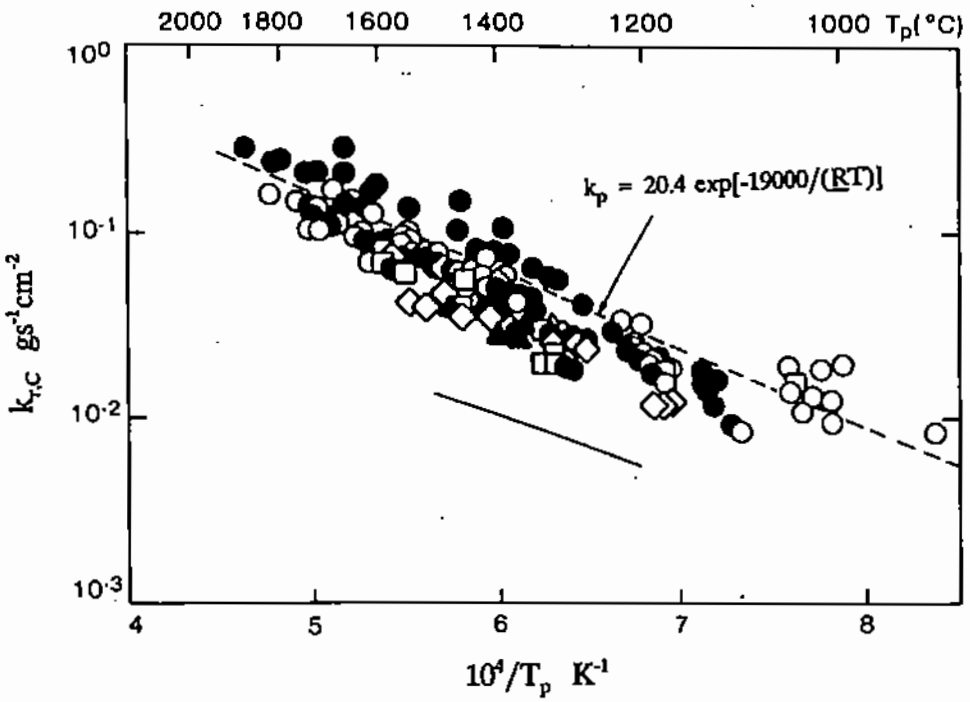

Figure 19.1. Combustion rate data for anthracites and semi-anthracites [11].

where d_p ($=2r_p$) is the particle diameter in cm and the diffusivity of oxygen in CO_2 (Fig. 14.3) is 1.6 cm^2 s^{-1}. Therefore, at the beginning of the reaction when the particle diameter is 0.1 cm, $k_d = 32$ cm s^{-1}.

The equations for molar flux of O_2 through the boundary layer and reacting at the surface of the anthracite particle are of the same form as (18.3.2) and (18.3.10) (Chapter 18):

$$\dot{m}_{O_2} = A_p N_{O_2} = (4\pi r_p^2) k_d\, c\, (X_{O_2,b} - X_{O_2,s}), \tag{19.1.4}$$

$$\dot{m}_{O_2} = A_p N_{O_2} = (4\pi r_p^2) k_r\, c\, (X_{O_2,s} - X_{O_2,e}). \tag{19.1.5}$$

The thermodynamic tables [5] show that the equilibrium constant for combustion of carbon by oxygen at 1300 K is 8.3×10^{15}. Therefore, the equilibrium concentration of O_2 at the interface (see (19.1.5)) is negligible. By combining (19.1.4) and (19.1.5), we can express the "intermediate" concentration of O_2 at the reaction surface as follows:

$$X_{O_2,s} = \frac{k_d}{k_d + k_r} X_{O_2,b}. \tag{19.1.6}$$

The overall rate coefficient of the combustion reaction is defined by an equation of the same form as (18.3.12) (Chapter 18):

$$\dot{m}_{O_2} = (4\pi r_p^2) k_{ov}\, c\, X_{O_2,b}, \tag{19.1.7}$$

where, in this case

$$\frac{1}{k_{ov}} = \frac{1}{k_d} + \frac{1}{k_r}. \tag{19.1.8}$$

Let us now convert the chemical rate coefficient of (19.1.2) to the same units as k_d and k_r. To do so we make use of the unit equation (Chapter 2):

$$\frac{\cancel{g\,C}}{s\ cm^2} \times \frac{mol\ C}{\cancel{g\,C}} \times \frac{mol\ O_2}{mol\ C} \times \frac{cm^3 O_2\ (T,P)}{mol\ O_2} = \frac{cm}{s}.$$

$$k_{r,C} \times \frac{1}{12} \times \frac{1}{1} \times \frac{22400 \times 1300}{273} = k_r. \tag{19.1.9}$$

From (19.1.2), we calculate the value of $k_{r,C}$ at 1300 K to be 0.013 g carbon s^{-1} cm^{-2}; the equivalent value of the gas-phase chemical rate coefficient k_r is calculated from the unit equation (see (19.1.9)) to be

$$k_r = 116\ cm/s$$

The difference between the values of $k_{r,C}$ and k_r reflects the large difference between the molar density of carbon in the anthracite and the molar density of the gas phase. It should be noted that $k_{r,C}$ can also be expressed in the "velocity" units of cm s^{-1}, i.e., rate of advance of the reaction interface towards the center, by dividing it by the density of carbon in the anthracite, i.e., $k_{r,C}/\rho_C$ ($\rho_C = 1.7$ g cm^{-3}).

It can be seen that the chemical rate coefficient k_r is not a function of particle diameter, while k_d is inversely proportional to the diameter. During most of the reaction, the rate of combustion depends mostly on mass transfer but towards completion (e.g., at $d_p < 0.01$ cm, $k_d > 320$ cm/s), control will revert to the chemical reaction unless the temperature increases further.

From (19.1.8), we may now calculate the value of the overall rate coefficient:

$$\frac{1}{k_{ov}} = \frac{d_p}{3.2} + \frac{1}{116}. \tag{19.1.10}$$

To estimate the time for complete combustion, we set up the material balance of *oxygen transferred = carbon consumed*:

$$\dot{m}_C\, dt = (4\pi r_p^2)\, k_{ov}\, c\, X_{O_2,b}\, dt = (4\pi r_p^2)\, dr\, \frac{\rho_C}{M_C}, \tag{19.1.11}$$

where $\dot{m}_C$ is the molar rate of oxidized carbon and is equal to the molar flux of reacting oxygen (see (19.1.1)); ρ_C is the apparent density of carbon in the anthracite particles, and M_C is the molecular weight of carbon.

For chemical control (i.e., at relatively high k_d and $k_{ov} \approx k_r$), the last two terms of (19.1.11) are integrated readily to yield the time for complete combustion of a particle of initial size $r_{p,0}$:

$$t_{comb,r} = \frac{r_{p,0}(\rho_C/M_C)}{k_r\, c\, X_{O_2,b}}, \tag{19.1.12}$$

and by substituting numerical values (X_{O_2} in air = 0.21):

$$t_{comb,r} = \frac{0.05 \times (1.7/12)}{116 \times \frac{1}{22400} \times \frac{273}{1300} \times 0.21} = 31\ s.$$

For diffusion control, $k_{ov} \approx k_d$, which is inversely proportional to r_p, as explained earlier. If we substitute for k_d from (19.1.3) in (19.1.11) and integrate for the time of complete combustion, we find that it is now proportional to the *square* of the particle radius:

$$t_{\text{comb},d} = \frac{r_{p,0}^2(\rho_C/M_C)}{2D_{O_2-CO_2}\, c X_{O_2,b}}, \tag{19.1.13}$$

and by substituting numerical values:

$$t_{\text{comb},d} = \frac{0.05^2 \times (1.7/12)}{2 \times 1.6 \times \frac{1}{22400} \times \frac{273}{1300} \times 0.21} = 56 \text{ s}.$$

Of course, a differential equation can be set up which includes both coefficients and integrated for $r_{p,0} > r_p > 0$ to yield a more accurate estimate of the overall time for combustion.

It is interesting to note that a correlation of a very large number of experimental data on the time for complete combustion of various types of coal particles in air shows a dependence on the square of the particle diameter (Fig. 19.2, [2]). This indicates that the reaction is usually controlled by mass transfer (see (19.1.13)).

19.2. CALCINATION OF LIMESTONE

The production of lime by calcination of limestone is by far the largest application of a high temperature reaction; it is carried out in rotary kilns (Fig. 19.3) and other types of furnaces to process annually nearly three billion tons of limestone and meet the world's needs for cement. The calcination reaction is as follows:

$$CaCO_3\,(s) \rightleftharpoons CaO\,(s) + CO_2\,(g), \tag{19.2.1}$$

where (g) indicates that CO_2 is in gaseous form and (s) solid state.

The equilibrium Gibbs free energy of formation of this reaction, at $p_o = 1$ bar, can be expressed as a function of temperature by means of the following equation [3]:

$$\Delta G^o_{rx} = 182837 + 13.402T\ln T - 251.059T \text{ J mol}^{-1}. \tag{19.2.2}$$

From this equation and (18.2.22), which relates the equilibrium constant of a reaction to its free energy of formation, we obtain the following correlation between the equilibrium constant and the temperature of the reaction:

$$\ln K_e = -\frac{21990}{T} - 1.6119\ln T + 30.196. \tag{19.2.3}$$

In this case, the activities of the solid phases CaO and $CaCO_3$ may be assumed to be unity and the activity of the gaseous phase is equal to the decomposition pressure of $CaCO_3$ divided by the standard state pressure (Chapter 18):

$$a_{CO_2} \approx \frac{p_{CO_2}}{p_o}. \tag{19.2.4}$$

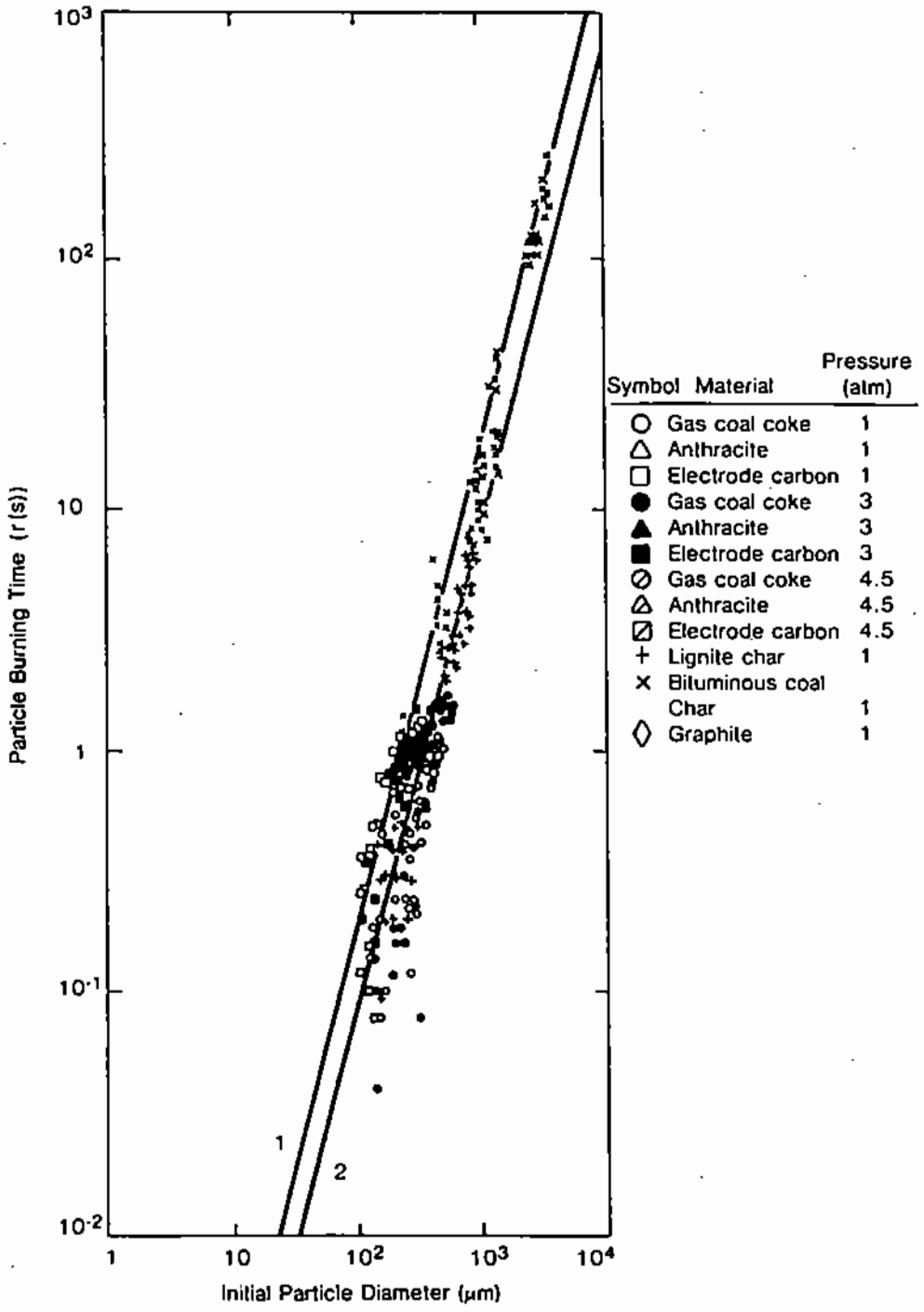

Figure 19.2. Time for complete combustion of carbon particles vs. particle size. [12].

Therefore, the partial pressure of CO_2 at equilibrium with $CaCO_3$ is numerically equal to the equilibrium constant of (19.2.3):

$$p_{CO_2,e} \approx K_c p_o, \tag{19.2.5}$$

where $p_{CO_2,e}$ is expressed in bars (1 bar = 10^6 dynes/cm^2 = 0.987 atm).

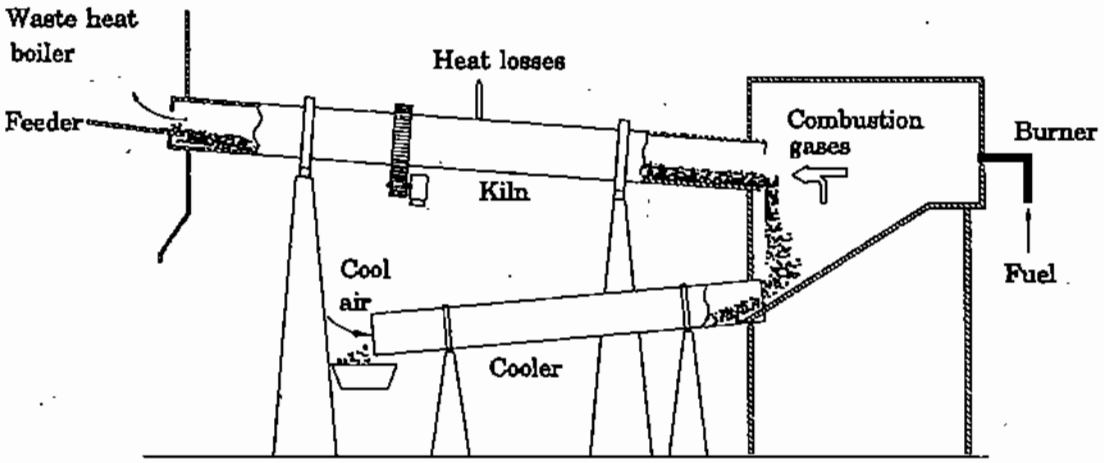

Figure 19.3. Schematic diagram of rotary kiln for calcining limestone to CaO.

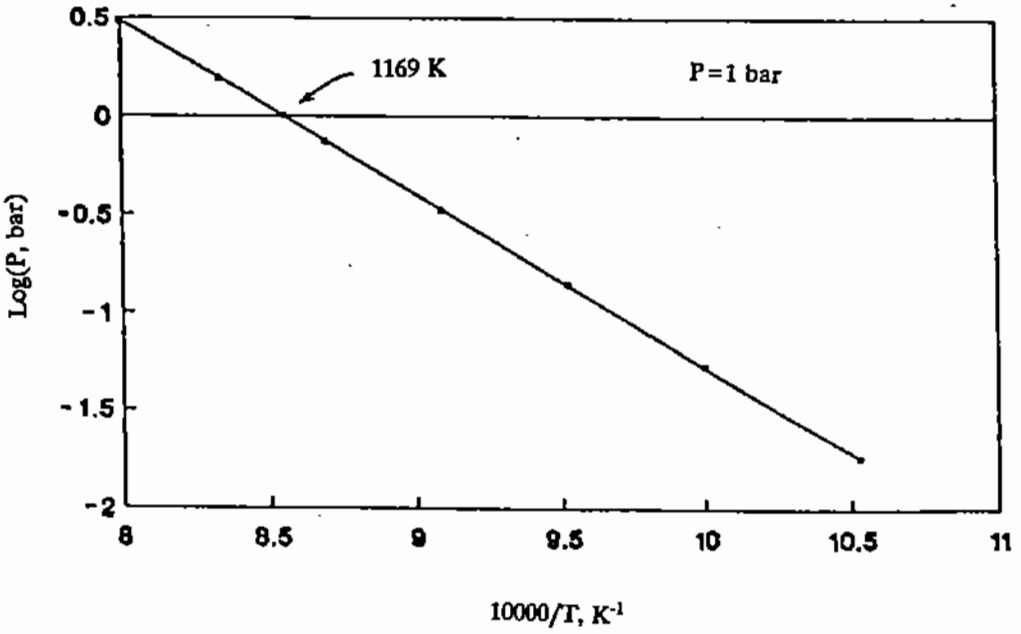

Figure 19.4. Decomposition pressure of calcium carbonate as a function of temperature.

Figure 19.4 [3] shows the effect of temperature on the decomposition pressure of $CaCO_3$ to CO_2. It can be seen that at about 1170 K, this pressure becomes greater than one atmosphere. On the basis of this information, we can bring about the decomposition of the calcium carbonate in two ways:

a. We can select a reactor temperature above 1170 K for calcining limestone. Decomposition will proceed much as in the case of boiling water in a pot which is heated to above 100°C.

b. An alternative means of attaining decomposition, at temperatures lower than 1170 K, is to decrease the bulk concentration of CO_2 in the reactor by providing a flow of air, or any other gas with the exception of carbon dioxide, over the decomposing limestone. As long as the actual partial pressure of

CO_2 in the exit gas stream from the reactor is less than the equilibrium pressure of decomposition of $CaCO_3$ at the reaction temperature, limestone will decompose to CaO; this case is similar to the evaporation of water from a pond to the atmosphere above it. The same effect can be obtained by reducing the atmospheric pressure in the reactor by means of a vacuum pump.

As a limestone particle starts to decompose, the reaction proceeds inward leaving behind a layer of porous CaO. The reaction interface is the boundary between CaO and $CaCO_3$. This type of reaction is called **topochemical** or *shrinking core* reaction and is similar to the reduction of metal oxides which was discussed in Chapter 18 (Figs. 18.6 and 18.7).

The decomposed $CaCO_3$ shell has a relatively high porosity and a low effective thermal conductivity (in range 0.001–0.0015 cal s^{-1} cm^{-1} $°C^{-1}$) and acts as a thermal barrier. Also, the decomposition reaction is *endothermic* and, therefore, heat must be transferred from the environment to the reaction interface through this barrier.

Turkdogan et al. [4] studied the calcination of limestone spheres (0.18–4.15 cm diameter) in a furnace under controlled conditions. Thermocouples were embedded at the surface and in the body of the spheres and the temperature profile was measured during the decomposition reaction. Figure 19.5 shows the temperature record for one of their experiments. In this case, a limestone sphere (4.15-cm in diameter) was pre-heated to 800°C in a CO_2 atmosphere and then lowered into a hotter zone of the furnace which was maintained at 1332°C and atmospheric pressure.

During an initial period, the pellet surface reached the furnace temperature while the unreacted core increased to only 905°C. After this period, the surface and core temperatures remained essentially constant until calcination was complete; then the center temperature increased to the level of the furnace temperature (Fig. 19.5).

Experiments with spheres of various sizes showed the same behavior: the core temperature (T_i) was always in the range of 883-907°C, which is close to the equilibrium temperature for decomposition of limestone at atmospheric pressure (896°C). In the following section, we will examine the reasons for this behavior.

19.2.1. Reaction Mechanism and Rate Control

In calculations of the reaction rate of solid particles, such as the calcination of limestone particles, it is convenient to assume that the reacting particles have a spherical shape. The progress, or degree, of the reaction is expressed in terms of the fractional transformation of the particle, R_x (e.g., at 100% reaction, $R_x = 1$). For a topochemical reaction, the ratio of the radius of the unreacted core, r, to the initial radius of the particle, r_0, is related geometrically to the *fractional degree of reaction*, R_x, as follows:

$$R_x = 1 - \left(\frac{r}{r_0}\right)^3 \quad \text{or} \quad r = r_0(1 - R_x)^{1/3}. \tag{19.2.6}$$

Therefore, the thickness of the reacted layer can be expressed as follows:

$$r_0 - r = r_0\left[1 - (1 - R_x)^{1/3}\right]. \tag{19.2.7}$$

As we have noted earlier, the rate of a gas-solid reaction can be affected either by gas diffusion or by chemical reaction at the interface. However, in the case of the Turkdogan experiments [4], the sustained large temperature difference between surface and core

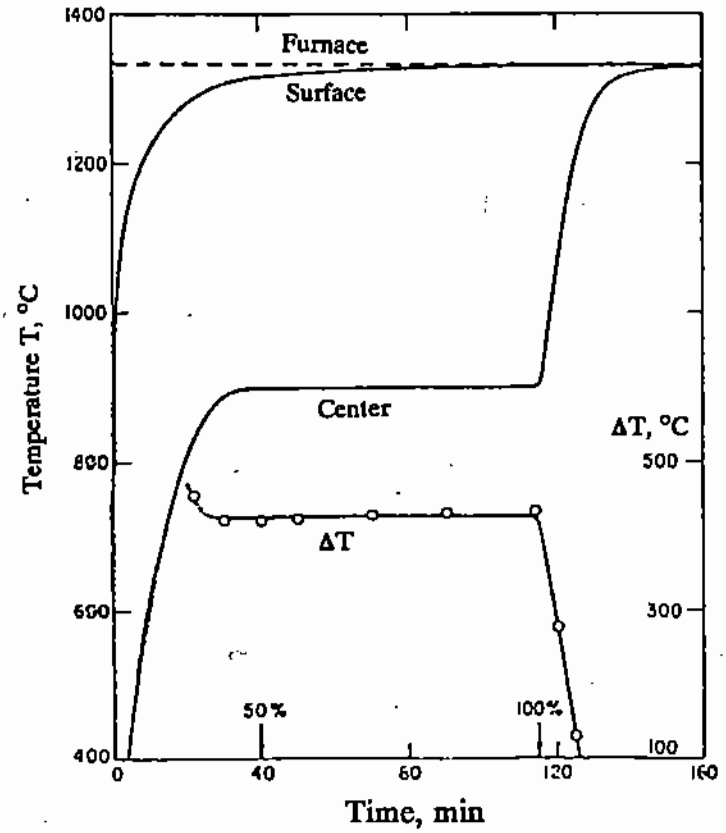

Figure 19.5. Temperatures measured during calcination of $CaCO_3$ spheres (4.15 cm diameter) in argon (1 atm, furnace temp. = 1332°C; [4]).

temperatures during decomposition shows that the diffusion and reaction phenomena are relatively fast in comparison to the *rate of heat conduction* from the surface to the core of the particle; accordingly, the overall heat of reaction is controlled by heat conduction.

This can be expressed mathematically by equating the rate of heat transfer by conduction through the calcined shell to the rate of absorption of the endothermic heat of calcination:

$$4\pi r^2 k_e \frac{dT}{dr} = \Delta H_d^o \frac{d(n_{CaCO_3})}{dt}, \tag{19.2.8}$$

where ΔH_d^o is the heat of decomposition reaction in J mole^{-1}; n_{CaCO_3} is the number of moles reacted; k_e is the effective thermal conductivity of reacted shell.

From the geometry of the situation, we can also state that, over a time interval dt, the number of decomposed $CaCO_3$ moles is equal to the volume of reacted shell times the molar density of $CaCO_3$ in the limestone:

$$d(n_{CaCO_3}) = (4\pi r^2 dr) c_{CaCO_3}, \tag{19.2.9}$$

where c_{CaCO_3} is the molar density of $CaCO_3$ in the unreacted pellet in moles cm^{-3}. Let us now substitute for n_{CaCO_3}, from (19.2.9), into (19.2.8) and for r by R_x (see (19.2.6)). By assuming that a steady-state temperature profile is established across the reacted shell

much faster than the rate of interface advance (i.e., quasi-steady state heat conduction), we can integrate for R_x as a function of time, t, to obtain the following correlation:

$$t = \frac{\Delta H c_{CaCO_3} r_0^2}{6k_c(T_s - T_i)} \left[1 - 3(1 - R_x)^{2/3} + 2(1 - R_x)\right]. \tag{19.2.10}$$

From the above equation, the time required for complete calcination of the particle (i.e., $r = 0$, $R_x = 1$) is

$$t_f = \frac{\Delta H c_{CaCO_3} r_0^2}{6k_c(T_s - T_i)}. \tag{19.2.11}$$

If we now divide the actual time of calcination, t, by the time required for complete calcination, (t_f, for $R_x = 1$), we obtain the dimensionless time ratio τ as a function of the degree of reaction, R_x:

$$\frac{t}{t_f} = \tau = 1 - 3(1 - R_x)^{2/3} + 2(1 - R_x). \tag{19.2.12}$$

It should be noted that the above equation was obtained for a constant surface temperature (T_s). However, as noted earlier, in the Turkdogan experiments [4], a certain amount of time passed before the limestone particles reached a steady-state surface temperature (Fig. 19.5). By analysis of these data, Kellogg [3] calculated the value of this initial period (t_i/t_f) to be approximately 0.145 for all tests. This time correction was then introduced in (19.2.10) and the following correlation was obtained for time required for reaction as a function of r_o and the difference between surface and decomposition temperatures:

$$t = \frac{1.26 \times 10^5 r_0^2}{(T_s - T_i)} \left[0.145 + \left(1 - 3(1 - R_x)^{2/3} + 2(1 - R_x)\right)\right]. \tag{19.2.13}$$

Equation (19.2.13) was solved for $R_x = 0.99$ (i.e., at 99% decomposition) and T_i = 896°C, for particles ranging from 0.018 to 3 cm in diameter and T_s values in range 1050–1200°C. Some of the results are shown in graphical form in Fig. 19.6. For example, at a surface temperature of 1200°C, a 2-cm sphere requires about 500 seconds to decompose fully; at 1050°C, the required reaction time is nearly double.

It should be noted that in a different reaction system, where the overall rate of reaction is controlled by *diffusion* through the reacted layer, τ can be expressed by an equation identical to (19.2.12); also, the controlling rate equations will be of similar form to the other equations shown above. However, in that case, the driving force is the *concentration gradient* across the reacted shell and the effective thermal conductivity is replaced by the *effective diffusivity* of the reagent. This case was developed in a pioneering textbook by Levenspiel [5].

19.3. REDUCTION OF IRON OXIDE: CONSTANT RATE OF INTERFACE ADVANCE

In certain gas–solid and liquid–solid reactions, the rate of chemical reaction at the interface is much slower than the other rate phenomena; therefore, it controls the rate of overall

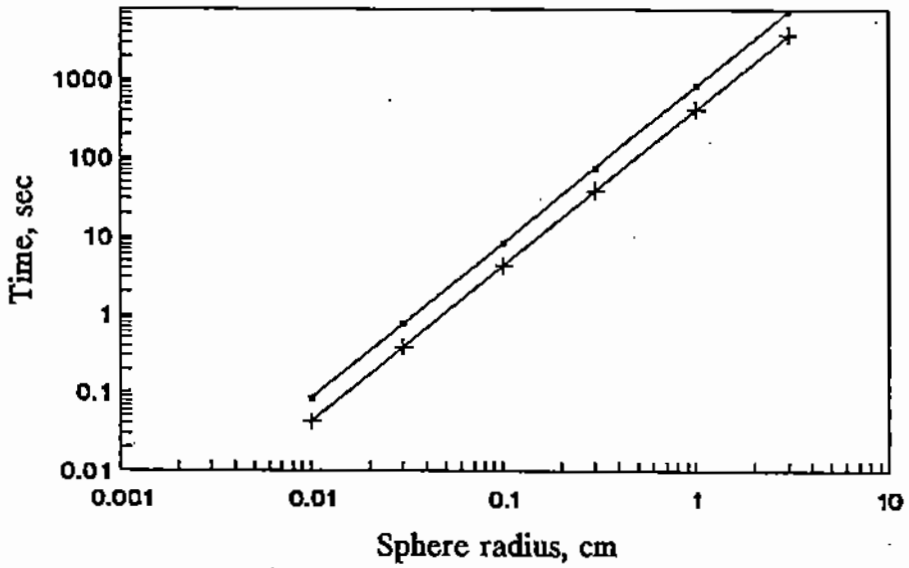

Figure 19.6. Time required for 99% decomposition of $CaCO_3$ spheres of various sizes at 1050°C (upper curve) and 1200°C (lower curve, [3]).

reaction. Under these conditions, the overall rate of reaction $A + B = C + D$ is expressed by the chemical rate equation (Chapter 18):

$$\dot{m}_A = \dot{m}_B = k_r(4\pi r_i^2)\, c\,(X_{A,b} - X_{A,e}), \tag{19.3.1}$$

where A is the gas species reacting with solid species B, $X_{A,b}$ and $X_{A,e}$ the bulk and equilibrium concentrations of A, and $\dot{m}_B$ the number of moles of B reacting per unit time:

$$\dot{m}_B = \frac{(4\pi r_i^2\, dr)c_{B,s}}{dt}, \tag{19.3.2}$$

where $c_{B,s}$ denotes the molar density of B in the unreacted solid. By combining (19.3.1) and (19.3.2) and noting that the interface area $4\pi r_i^2$ appears on both sides of the equation, we obtain:

$$c_{B,s}\,\frac{dr}{dt} = k_r\, c\,(X_{A,b} - X_{A,i}). \tag{19.3.3}$$

Equation (19.3.3) shows that the rate of interface advance, dr/dt, of a chemically-controlled reaction is constant; or, alternatively, that the reaction interface advances towards the center of the reacting particle *linearly with time*.

As discussed in §19.2, the radius of the reaction interface can be related to the fractional degree of reaction, R_x, of the particle. Thus, at the beginning of reaction when $r_i = r_0$, $R_x = 0$; also, at complete reaction, i.e., at $R_x = 1$, $r_i = 0$. In between the two extremes,

$$R_x = 1 - \left(\frac{r_i}{r_0}\right)^3, \tag{19.3.4}$$

where r_0 is the initial radius of the particle.

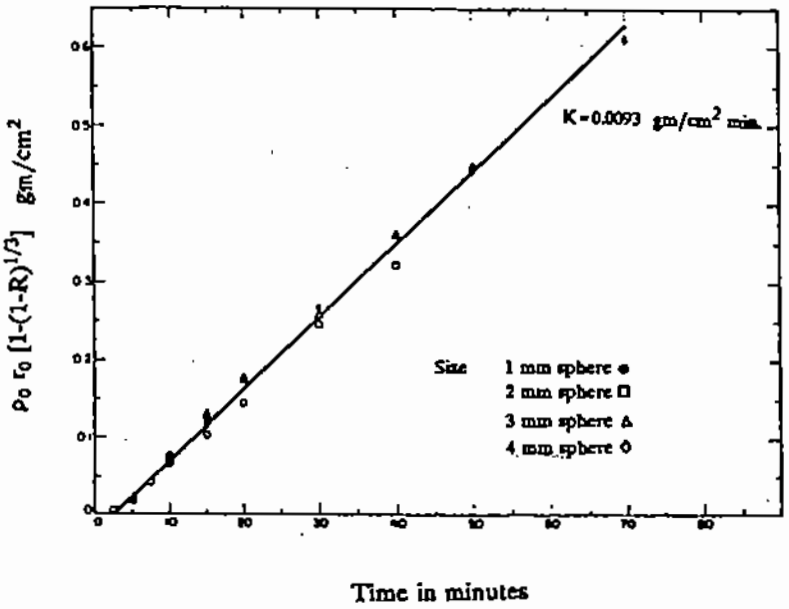

Figure 19.7. Rate data for reduction of iron oxide particles (ρ_0 is the density of unreduced oxide) [6].

Thus, for a chemically controlled reaction, the dimensionless time of reaction, τ, required to effect a certain degree of reaction, R_x, can be expressed as follows:

$$\frac{t}{t_f} = \tau = 1 - (1 - R_x)^{1/3}, \tag{19.3.5}$$

where t_f is the time required for complete reaction of the particle.

The linear advance of the reaction interface with time for such reactions denotes that the time required for a certain degree of reaction is proportional to the particle diameter. An example of this type of reaction is the reduction of iron oxides by hydrogen or carbon monoxide. As illustrated by the typical reduction data plotted in Fig. 19.7 for iron oxide particles of different sizes reduced in hydrogen atmospheres [6], a plot of the experimental results in the form of the function $[1 - (1 - R_x)^{1/3}]$ against time yields a straight line. The slopes of these lines are a function of particle size and temperature.

McKewan was the first researcher to recognize that the interface advance of iron reduction was constant with particle size (Fig. 19.7, [6]). On the assumption of constant rate of interface advance and by providing an Arrhenius-type correction for the temperature effect, a very large number of iron reduction data by hydrogen were correlated by means of the graph shown in Fig. 19.8 [7]. This plot shows that despite the differences in types of iron oxides included in this correlation, the time of reduction increases proportionally with particle diameter.

On the same plot (Fig. 19.8) are shown some experimental data for iron reduction by carbon monoxide. The nearly four-fold decrease in reduction rate is a chemical phenomenon which has not yet been explained.

In experimental studies of gas–solid reaction rates, a single particle of the solid is usually suspended in a flowing stream of the reagent gas. In such cases, in order to minimize the effect of mass transfer through the gaseous boundary layer around the particle, it is necessary

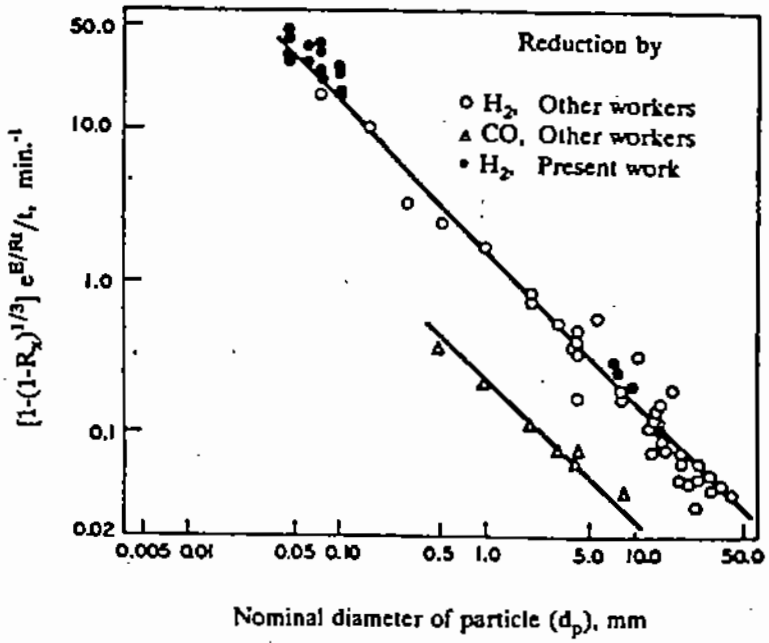

Figure 19.8. Reduction rate data for iron oxides reduced in hydrogen and carbon monoxide [7].

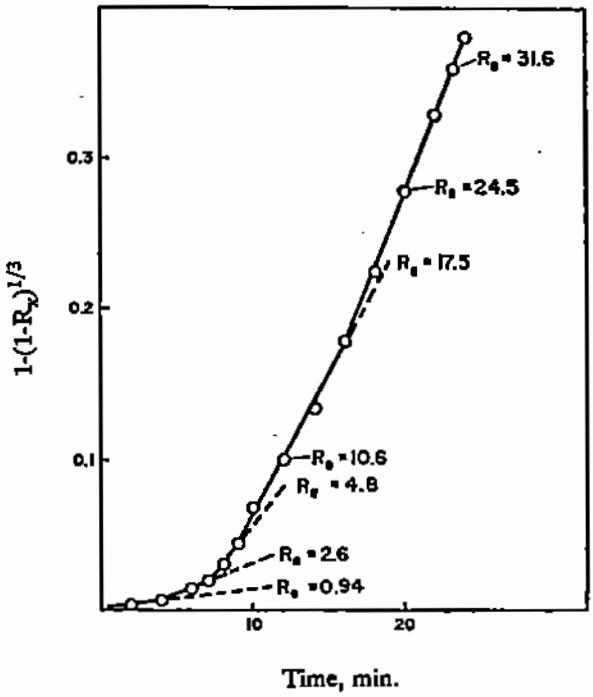

Figure 19.9. Effect of Reynolds number on rate of reduction of $FeCl_2$ particle [8].

to maintain an adequate flow of gas. This is illustrated in Fig. 19.9 [8] which shows that the rate of reduction of a 0.78 cm sphere of $FeCl_2$ particle (slope of plot in Fig. 19.9) increased as the flow velocity of the reducing gas (hydrogen) was increased. At particle Reynolds numbers above 25, there was no further noticeable effect of the gas flow around the particle.

This may indicate that beyond Re > 25 the rate of reduction was controlled by chemical reaction at the interface.

19.4. REFINING OF METALS BY GAS INJECTION

In some metal refining processes, an inert gas is injected at the bottom of the molten metal. As the gas bubbles ascend to the surface of the melt, they produce a mixing action and they promote the removal of unwanted impurities from the metal. Examples are the removal of antimony from lead (lead softening), the Argon Oxygen Decarburization (AOD) process for the refining of stainless steel, and the degassing of liquid steel under vacuum.

Let us consider the *argon degassing* of liquid steel in a ladle. Argon gas is injected into the molten bath by means of a porous refractory plug located at the bottom of the ladle (Fig. 19.10) while the surface of the melt is subjected to a vacuum of about 1300 Pa. In the example shown in Fig. 19.10, hydrogen (4–8 ppm), nitrogen (40–70 ppm) and oxygen (200–600 ppm) are to be reduced to levels of 1–2, 20–30, and 0–50 ppm, respectively. Part of the gas removal takes place as the argon bubbles rise through the melt and part by evaporation at the surface of the metal bath.

In order to quantify the rate of surface evaporation, it is reasonable to assume that as each argon bubble breaks through the surface (Fig. 19.11), it brings to the surface a new element of molten steel. These fluid elements are assumed to remain on the surface a finite time interval, which depends on the rate of arrival of another gas bubble at the same location of the liquid/gas interface. For example, if bubbles arrive at a certain location at the rate of one bubble every two seconds, then the finite time interval at the surface may be assumed to be equal to 2 seconds, and the rate of surface renewal of the surface is equal to 0.5 s^{-1}.

In contrast to gases dissolving in aqueous solutions, which maintain their molecular state, dissolved gases in metals are in atomic form. For example, as dissolved hydrogen reaches the surface of the melt, the atoms must recombine to molecules before evaporation can occur:

$$2[\mathrm{H}]_s \rightarrow \mathrm{H}_2, \tag{19.4.1}$$

where the brackets indicate that hydrogen is dissolved in the metal in atomic form and the subscript s indicates the concentration of hydrogen at the surface of the melt.

Because of the vacuum above the melt, it can be safely assumed that the removal of hydrogen gas is not controlled by gaseous diffusion. Also, the rate of the chemical combination of the hydrogen atoms to molecular hydrogen at the surface of the melt is very high, and $X'_{H,s} \doteq 0$. Therefore, in this case, the overall rate of hydrogen removal is controlled by mass transfer from the bulk of the melt, where the concentration of hydrogen is $c_{H,b}$, to the surface of the bath, where $c_{H,s}$ can be assumed to be zero. Adopting the surface renewal model which was described earlier (§17.3.2), we can express the mass flux of hydrogen atoms to the surface as follows:

$$N'_{\mathrm{H}} = k_d \rho_s (X'_{H,b} - X'_{H,s}) = 2\sqrt{\frac{D_{\mathrm{H-Fe}}}{\pi t_e}}\, \rho_s X'_{H,b}, \tag{19.4.2}$$

where $D_{\mathrm{H-Fe}}$ is the diffusivity of hydrogen through liquid iron and t_e is the residence time of an element on the surface, or the inverse of the surface renewal rate.

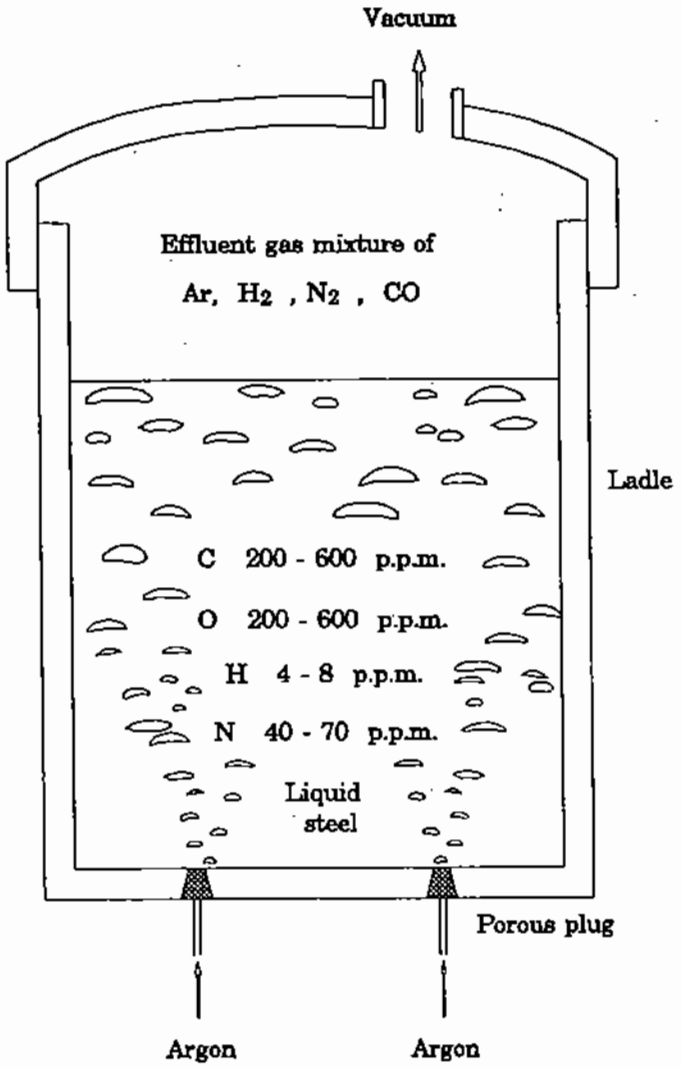

Figure 19.10. Removal of impurities from steel by vacuum degassing.

By inserting the values of $D_{\mathrm{H-Fe}} = 90 \times 10^{-5}$ cm^2 s^{-1}, $t_e = 2$ s, $X'_{H,b} = 8$ ppm = 8×10^{-6} and steel density = $\rho_s = 7.3$ g cm^{-3} in (19.4.2), we obtain:

$$N'_{\mathrm{H}} = 2 \times \left(\frac{90 \times 10^{-5}}{\pi \times 2}\right)^{0.5} \times 7.3 \times 8 \times 10^{-6} = 1.40 \times 10^{-6}\, g\,\mathrm{H\,s^{-1}\,cm^{-2}}.$$

Example 19.4.1

Molten iron at 1500°C containing 0.01% oxygen by weight is brought in contact with liquid slag containing 30% FeO by weight. If the equilibrium constant, or *partition coefficient*, for oxygen atoms between slag of this activity and metal, for reaction

$$(\mathrm{FeO})_s \rightleftharpoons [\mathrm{Fe}]_m + [\mathrm{O}]_m$$

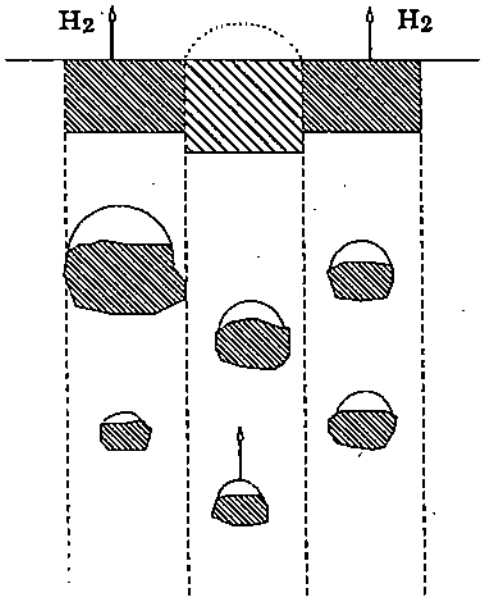

Figure 19.11. Flotation of metal droplets by bubbles rising through melt.

is

$$K_e = \frac{[\mathrm{O}]}{(\mathrm{FeO})_s} = 3.3 \times 10^{-3},$$

estimate the relative importance of the slag phase and metal phase resistances to mass transfer.

As discussed in §17.5 (see (17.5.4)), the respective mass transfer resistances for the two phases are

$$\frac{K_e}{k_{d,s}} \text{ and } \frac{1}{k_{d,m}}.$$

or

$$\frac{3.3 \times 10^{-3}}{k_{d,s}} \text{ and } \frac{1}{k_{d,m}}.$$

It can be seen that the mass transfer coefficients in the slag and metal phase are "weighted" by the value of the equilibrium constant between the two phases. Therefore, even when the rate of chemical reaction at the interface is not controlling, as it is not in this case, the chemical equilibrium constant can have a major influence on the rate controlling phenomena. For example, in this case, the overall transfer between slag and metal may be controlled by the resistance in the metal phase, despite the fact that the diffusion and mass transfer coefficients in the metal are greater than in the slag.

19.5. FLASH REDUCTION OF ZINC CALCINE PARTICLES

In a proposed process for zinc production, zinc calcines (58% ZnO, 22% $ZnO{\cdot}Fe_2O_3$, balance SiO_2, CaO) are reduced with coal and oxygen in a flash reactor similar to the Outokumpu

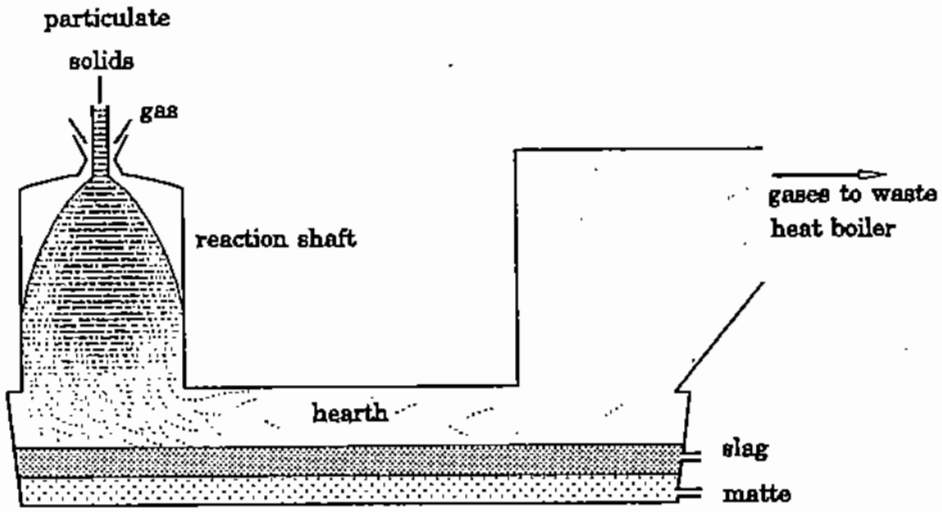

Figure 19.12. Outokumpu flash smelting reactor.

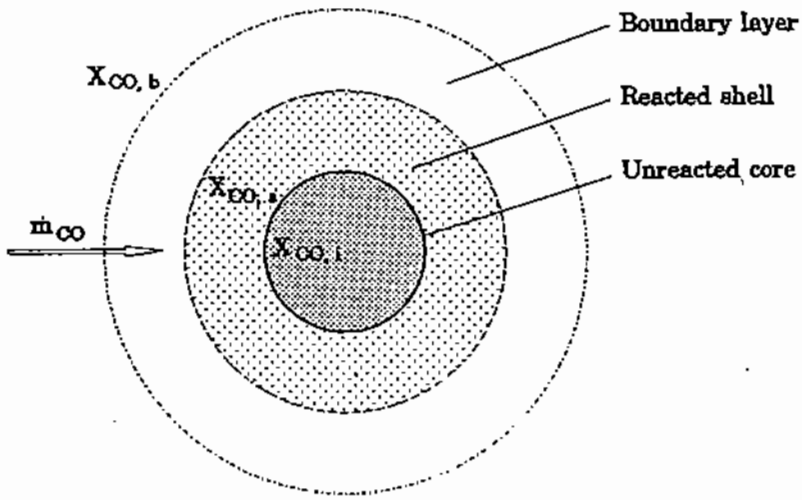

Figure 19.13. Schematic representation of rate determining steps for solid reduction.

process for copper production (Fig. 19.12). The objective is to produce an environmentally acceptable silicate slag, to be discarded, and zinc vapor, to be collected in a zinc condenser.

The reducing agent is carbon monoxide and is produced in the reaction shaft by the partial oxidation of the inlet coal particles by the O_2 in the inlet gas. Carbon monoxide then reacts with ZnO in the calcine particles to produce carbon dioxide, which back-reacts with carbon to regenerate CO and zinc vapor. The principal reaction is the production of zinc vapor:

$$\mathrm{ZnO\,(s) + CO\,(g) \rightleftharpoons Zn\,(g) + CO_2\,(g)}. \tag{19.5.1}$$

The partial zinc pressure in the process gas will be controlled at less than 0.2 atm. The above reaction is endothermic and the equilibrium constant increases rapidly with temperature [10]:

$$K_e = \frac{p_{CO_2}}{p_{CO}} \frac{p_{Zn}}{a_{ZnO}} \equiv e^{(-42550+26.7T)/RT}. \tag{19.5.2}$$

A simplified phase diagram for the equilibria of zinc and iron reduction with carbon monoxide is shown in Fig. 19.14 [13]. It shows the CO_2/CO equilibrium ratio as a function of temperature for the zinc oxide reduction, at different partial pressures of zinc.

In this section, we will examine the development of a mathematical model of the gas-solid rate phenomena in the cylindrical flash reduction shaft of this process (Fig. 19.12); for simplicity, this model will be unidimensional, i.e., the velocity, temperature and concentration of the gas-solids stream will be assumed to be uniform in the radial direction.

19.5.1. Mass Transfer Through Boundary Layer

As shown by (19.5.1), two gas molecules are produced for each molecule of CO diffusing inward through the boundary layer:

$$N_{CO} = -N_{CO_2} = -N_{Zn},$$

$$\text{net bulk flow} = N_{CO} - N_{CO_2} - N_{Zn} = -N_{CO}. \tag{19.5.3}$$

Therefore, in this case there is a net bulk flow (Chapter 14) against the flux of the diffusing CO:

$$N_{CO} = -D_{CO}\, c \frac{dX_{CO}}{dr} - X_{CO} N_{CO}. \tag{19.5.4}$$

By separating the N_{CO} terms and integrating across the boundary layer thickness δ, i.e., for $X_{CO} = X_{CO,s}$ at $r = r_s$ (surface of particle) and $X_{CO} = X_{CO,b}$ at $r = r_s + \delta$, we obtain:

$$N_{CO} = \frac{D_{CO}}{\delta}\, c \ln \frac{1 + X_{CO,b}}{1 + X_{CO,s}} = k_d\, c \ln \frac{1 + X_{CO,b}}{1 + X_{CO,s}}, \tag{19.5.5}$$

where c is the molar gas concentration and k_d is the mass transfer coefficient and can be represented by the Ranz–Marshall equation (see (17.4.2)):

$$\mathrm{Sh} = 2 + 0.6\mathrm{Re}^{1/2}\mathrm{Sc}^{1/3}. \tag{17.4.2}$$

The corresponding molar flow of CO is obtained by multiplying N_{CO} by the particle surface:

$$\dot{m}_{CO} = 4\pi r_s^2\, k_d\, c \ln \frac{1 + X_{CO,b}}{1 + X_{CO,s}}. \tag{19.5.6}$$

19.5.2. Diffusion Through Reacted Layer

We now need an expression for the rate of diffusion through the reacted layer. To simplify this presentation, let us assume that the iron oxide content of the calcines is not reduced appreciably and remains as a porous shell around the unreacted core (Fig. 19.13). The molar flow of CO diffusing through this layer is expressed by an equation similar to (18.3.5) and also to (19.5.6), since we still have to deal with a net bulk flow:

$$\dot{m}_{CO} = \frac{4\pi r_s r_i}{(r_s - r_i)}\, D_{eff}'\, c \ln \frac{1 + X_{CO,s}}{1 + X_{CO,i}}, \tag{19.5.7}$$

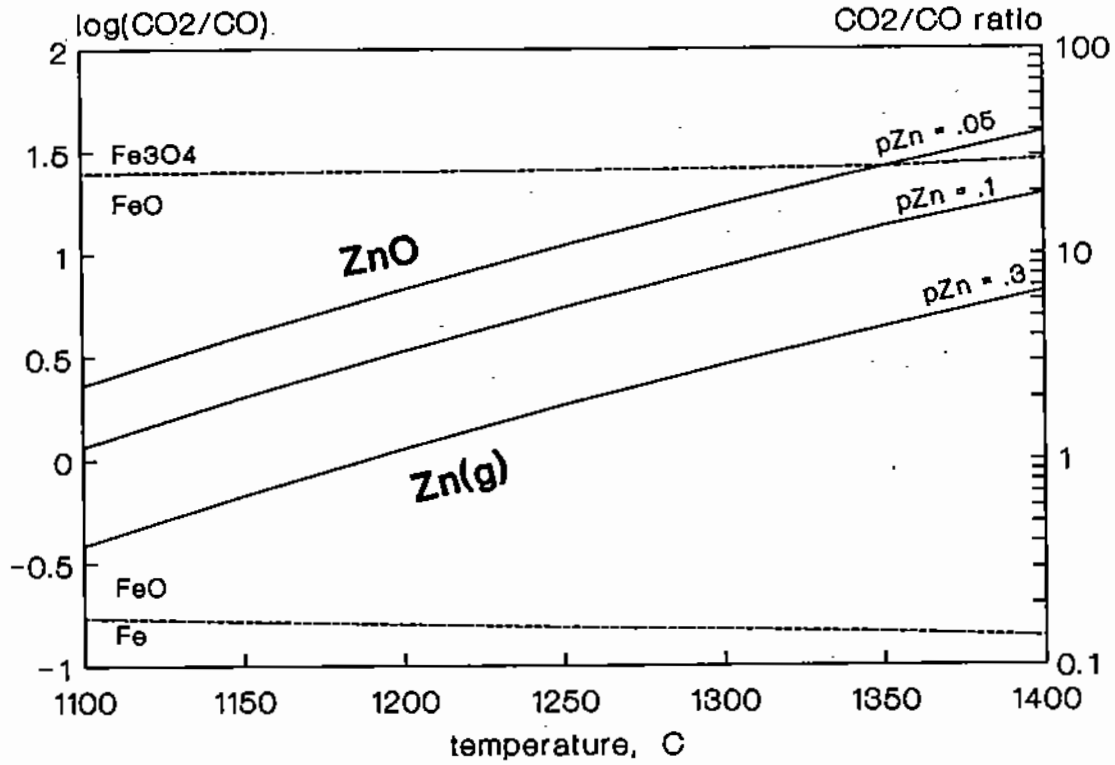

Figure 19.14. Phase diagram for zinc and iron reduction by carbon monoxide.

where $X_{\mathrm{CO},i}$ is the mole fraction of CO at the reaction interface, $r = r_i$, and the effective diffusivity (see (14.7.15)) can be expressed [13] as follows:

$$D_{\mathrm{eff}} = \frac{\varepsilon}{\tau} D_{\mathrm{CO}} = \frac{0.5}{4} D_{\mathrm{CO}} = 0.125 D_{\mathrm{CO}}, \tag{19.5.8}$$

where ε is the porosity and τ the tortuosity of the reacted shell (§18.3).

By merging (19.5.6) and (19.5.7) we can eliminate the intermediate molar fraction of $X_{\mathrm{CO},s}$ at the surface and combine the diffusion coefficients through the boundary layer and the reacted layer into one *combined diffusion coefficient*:

$$\dot{m}_{\mathrm{CO}} = 4\pi r_s^2 k_{\mathrm{diff}} c \ln \frac{1 + X_{\mathrm{CO},b}}{1 + X_{\mathrm{CO},i}}, \tag{19.5.9}$$

where

$$\frac{1}{k_{\mathrm{diff}}} = \frac{1}{k_d} + \frac{r_s}{r_i} \frac{(r_s - r_i)}{D_{\mathrm{eff}}}. \tag{19.5.10}$$

19.5.3. Chemical Reaction at Interface

The following correlation has been found [15–17] to represent the chemical rate coefficient, k_r, of zinc oxide reduction by CO in the range of 800–1200°C:

$$k_r = \frac{N_{\mathrm{CO}}}{c(X_{\mathrm{CO},i} - X_{\mathrm{CO},e})} = 3.55 \times 10^{-3} e^{-17700/RT}, \tag{19.5.11}$$

where N_{CO} is expressed in mol s^{-1} cm^{-2}. Therefore, the corresponding molar rate of CO reaction at the interface is

$$\dot{m}_{CO} = 4\pi r_i^2 \times 3.55 \times 10^{-3}\, e^{-17700/RT}\, c(X_{CO,i} - X_{CO,e}). \tag{19.5.12}$$

It is now necessary to determine the equilibrium concentration of CO at the reaction interface. This can be done by relating $X_{CO,e}$ to $X_{CO_2,i}$ by means of K_e and then developing the diffusion equations relating $X_{CO_2,i}$ to $X_{CO_2,b}$ (§18.3). However, there is an alternative method: Let us assume that for every 1 mole of CO reaching the reaction interface, a fraction z reacts with ZnO to form z moles of CO_2 and z moles of zinc vapor (chemical reaction of (19.5.1)), thus leaving $(1 - z)$ moles of unreacted CO. Therefore, the total amount of gas after reaction is $(1 + z)$ moles for every z mole of CO reacted; accordingly, at equilibrium conditions (i.e., when the diffusion of Zn (g) and CO_2 away from the interface is relatively slow) and for $a_{ZnO,s} = 1$ we have

$$K_e = \frac{\frac{z}{(1+z)}\,\frac{z}{(1+z)}}{(1-z)/(1+z)}, \tag{19.5.13}$$

and by solving for z:

$$z = \left(\frac{K_e}{1 + K_e}\right)^{1/2}. \tag{19.5.14}$$

From the value of the fraction z of CO reacted we can calculate the value of $X_{CO,e}$ $(= (1 - z)/(1 + z))$. On the basis of (19.5.14) for z and using the values of K_e from the free energy for zinc oxide reduction reaction [4], the equilibrium concentration of CO at the reaction interface, $X_{CO,e}$ has been calculated as a function of temperature and is shown in the following tabulation [13]. It can be seen that the effect of temperature on $X_{CO,e}$ is significant.

T, °C	K_e	$X_{CO,e}$	T, °C	K_e	$X_{CO,e}$
900	0.007	0.842	1150	0.202	0.418
1000	0.033	0.698	1200	0.340	0.330
1050	0.063	0.608	1250	0.552	0.253
1100	0.115	0.513	1300	0.867	0.189

19.5.4. Overall Rate Coefficient

We now have expressions for the rate of the two diffusion steps and the reaction step. The two rate coefficients (see (19.5.9) and (19.5.12)) can be combined into a single algebraic

expression, as was done in §18.3, by approximating the logarithmic functions of the diffusion rate equation (19.5.9) by the first two terms of a series expansion:

$$\begin{aligned}\ln\frac{1+X_{\mathrm{CO},b}}{1+X_{\mathrm{CO},i}} &= \frac{X_{\mathrm{CO},b}-X_{\mathrm{CO},i}}{1+X_{\mathrm{CO},b}} + 0.5\,\frac{X_{\mathrm{CO},b}^2 - X_{\mathrm{CO},i}^2}{(1+X_{\mathrm{CO},b})} + \dots \\ &= (X_{\mathrm{CO},b}-X_{\mathrm{CO},i})\left(\frac{1+0.5X_{\mathrm{CO},b}+0.5X_{\mathrm{CO},i}}{1+X_{\mathrm{CO},b}}\right) + \dots\end{aligned} \tag{19.5.15}$$

The second term in parentheses in (19.5.15) represents the effect of net bulk flow on the diffusion of CO. It shows that this effect is negligible when $X_{\mathrm{CO},i}$ is close in value to $X_{\mathrm{CO},b}$; also, that the adverse effect of the net bulk flow on CO diffusion is at a maximum when $X_{\mathrm{CO},i}$ is at its minimum value (i.e., in this case, $X_{\mathrm{CO},i} = X_{\mathrm{CO},e}$). Therefore, it is reasonable to use the following modified expression of diffusion rate equation (19.5.9):

$$\dot{m}_{\mathrm{CO}} = 4\pi r_s^2\, k'_{\mathrm{diff}}\, c\,(X_{\mathrm{CO},b} - X_{\mathrm{CO},i})\,, \tag{19.5.16}$$

where k'_{diff} is the combined diffusion coefficient (i.e., k_{diff}, (19.5.10), *corrected for the effect of net bulk flow due to diffusion* (see (19.5.15)):

$$k'_{\mathrm{diff}} = \left(\frac{1}{k_d} + \frac{r_s}{r_i}\,\frac{(r_s - r_i)}{D_{\mathrm{eff}}}\right)^{-1}\left(\frac{1+0.5X_{\mathrm{CO},b}+0.5X_{\mathrm{CO},e}}{1+X_{\mathrm{CO},b}}\right). \tag{19.5.17}$$

The form of this equation now allows us to merge it with the chemical reaction rate of (19.5.12) into a single rate equation where the concentration driving force is $X_{\mathrm{CO},b} - X_{\mathrm{CO},e}$:

$$\dot{m}_{\mathrm{CO}} = 4\pi r_s^2\, k_{\mathrm{ov}}\, c\,(X_{\mathrm{CO},b} - X_{\mathrm{CO},e})\,, \tag{19.5.18}$$

and the *overall rate coefficient*, k_{ov}, for the reduction of ZnO by CO is defined by

$$\frac{1}{k_{\mathrm{ov}}} = \frac{1}{k'_{\mathrm{diff}}} + \left(\frac{1}{3.55\times 10^{-3}\, e^{-17700/RT}}\right)\frac{r_s^2}{r_i^2}. \tag{19.5.19}$$

The rate of reaction of the carbon particles with oxygen is computed by the rate equation presented in §19.1. Comparison of the rate coefficient of carbon combustion, and also that of the Boudouard reaction for regeneration of CO, with (19.5.11) for the reduction of ZnO shows that the latter is much slower; therefore there is ample carbon monoxide in the gas-solids stream for zinc reduction.

19.5.5. Gas and Particle Velocities

The gas-jet stream entering at the top of the reactor under isothermal conditions and "free" expansion, i.e., in the absence of the reactor walls, would expand at an angle of about 22°. In order to determine the rate of expansion in non-isothermal flow in a confined space, it is necessary to solve the equations of motion in turbulent flow, as discussed in Chapter 7. However, for this simplified unidimensional model we can assume that the jet cone expands at the angle of 22° plus an additional amount due to the volume expansion with increasing

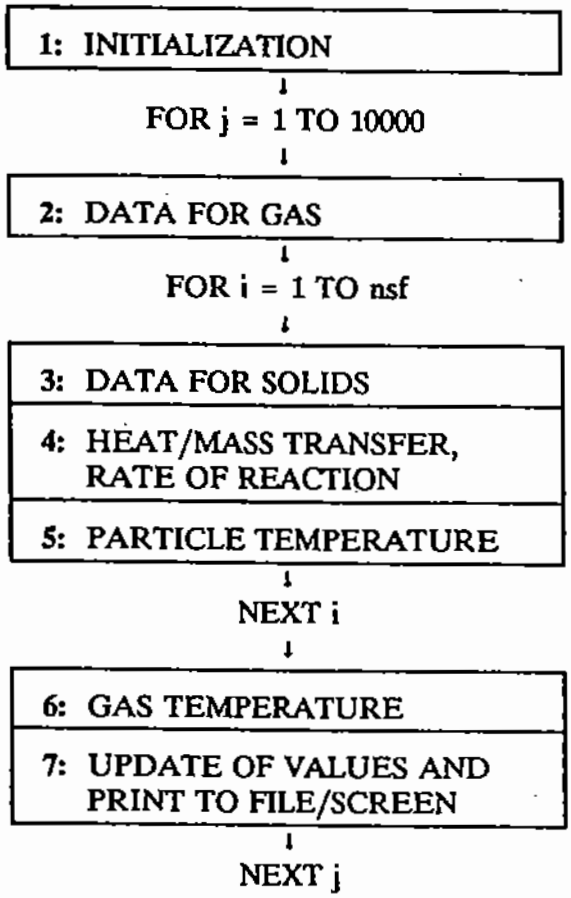

Figure 19.15. Schematic flowsheet of the computer program.

temperature; accordingly, the diameter of the gas/particle stream at distance x below the point of entry is:

$$d_{c,x} = (d_{c,0} + 2x\tan 22°)\left(\frac{\dot{v}_x}{\dot{v}_0}\right)^{1/3} = (d_{c,0} + 2x\tan 22°)\left(\frac{T_x}{T_0}\right)^{1/3}, \qquad (19.5.20)$$

where $d_{c,0}$ and $d_{c,x}$ are the diameters of the gas/solid cone at the entry point and at distance x below it, and $\dot{v}_0$ and $\dot{v}_x$ the volumetric flow rates at T_0 and T_x.

The particle size distribution is divided into a convenient number of size fractions. The particle velocity relative to the gas is calculated from the Stokes equation for terminal velocity (see (8.6.9)). This value is used for calculating the heat and mass transfer coefficients to particles. The sum of the particle and gas velocities is used to calculate the residence time of a particle in a finite distance increment Δx.

19.5.6. Heat and Mass Transfer Coefficients

The convective heat transfer coefficient between the turbulent gas flow and the reactor wall, h_{gw}, may be calculated from a correlation of the type $\mathrm{Nu} = f(\mathrm{Re}, \mathrm{Pr})$ for turbulent flow through a pipe (Chapter 12, see (12.6.3)). For a small experimental flash reactor, the following correlation was found to apply [14]:

$$\mathrm{Nu} = 0.117\mathrm{Re}^{0.8}\mathrm{Pr}^{1/3}. \qquad (19.5.21)$$

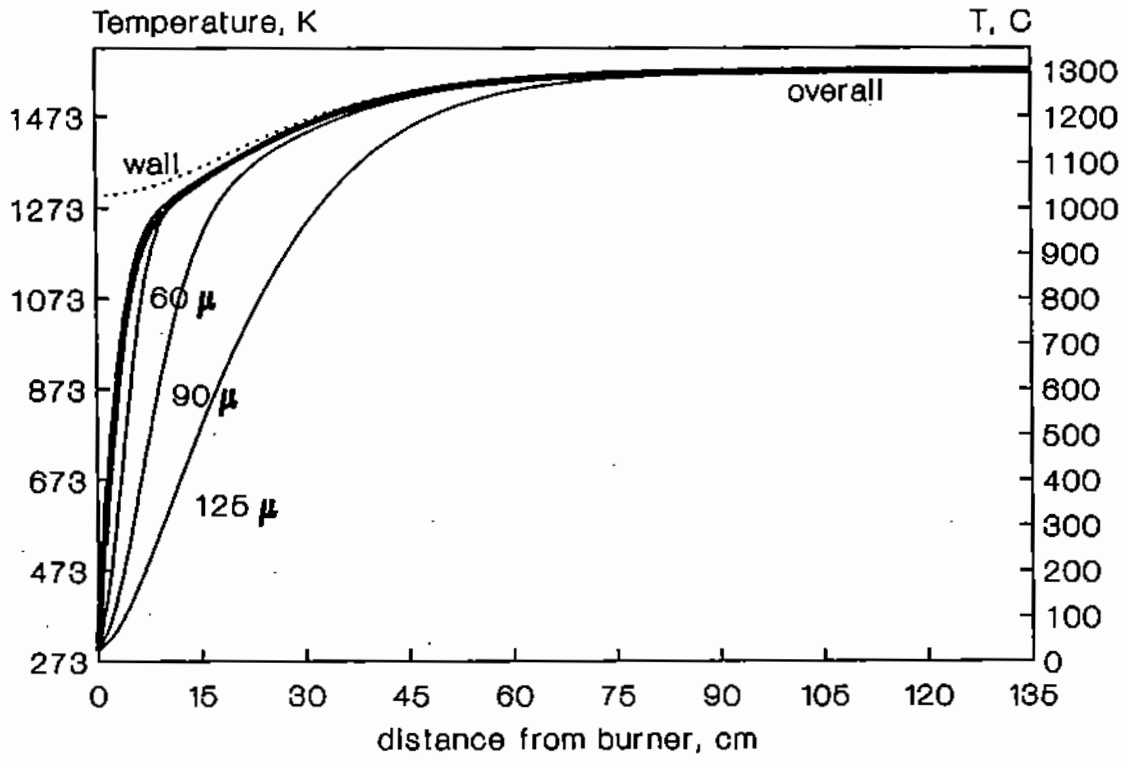

Figure 19.16. Computed temperature axial profile for various particle sizes.

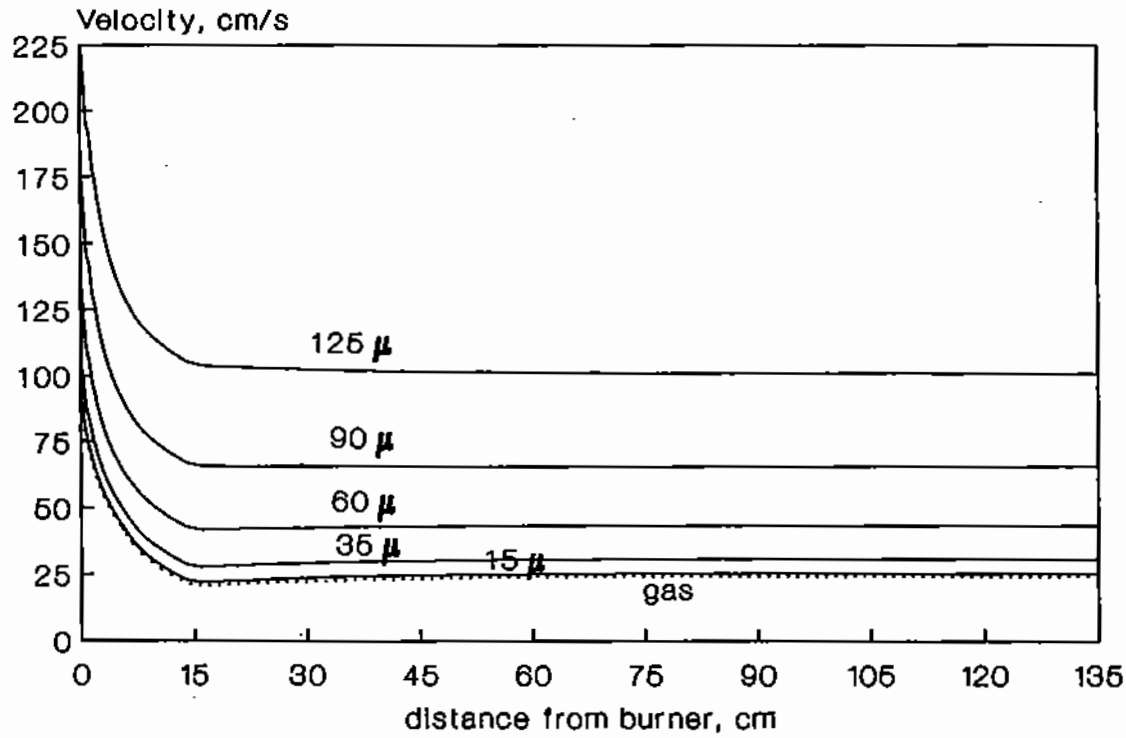

Figure 19.17. Computed particle and gas velocity axial profiles.

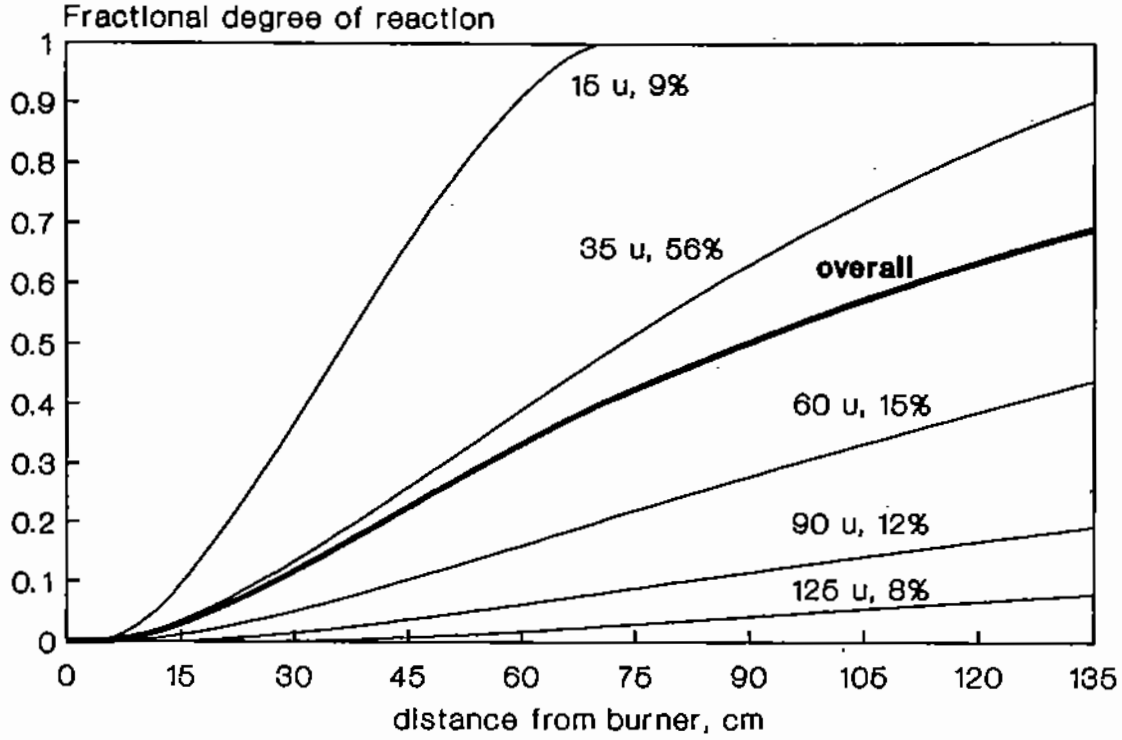

Figure 19.18. Computed fractional degree of reduction of zinc calcine particles (wt%).

The convective heat transfer coefficient between particle and gas can be calculated from the Ranz–Marshall correlation (Chapter 12, see (12.~~7~~6)):

6.18 (12.6.18)

$$\mathrm{Nu}_p = \frac{h_{pg} d_p}{k_{\mathrm{gas}}} = 2 + 0.6\mathrm{Re}_p^{1/2}\mathrm{Pr}^{1/3}, \tag{19.5.22}$$

where k_{gas} denotes the thermal conductivity of the gas, Re_p is the Reynolds number for particles and Pr the Prandtl number, as defined in Chapter 12 and Table 2.1.

The mass transfer coefficient between particles and gas, k_d, is calculated from the Ranz–Marshall equivalent correlation for mass transfer (Chapter 17, see (17.4.2)).

19.5.7. Particle and Gas Temperatures

The particle temperature change with time is calculated by equating the heat accumulation within a particle of size fraction i to the convective (Chapter 12) and radiant (Chapter 13) heat transfer from the environment minus the endothermic heat of reduction. Since the volume/surface ratio of the particle is $d_p/6$ this balance is expressed as follows:

$$\begin{aligned}\frac{d_p \rho_p C_{p,p}}{6}\frac{\Delta T_p}{\Delta t} =& h_{pg}(T_g - T_p) + \varepsilon_p \sigma \varepsilon_g \left(T_g^4 - \left(\frac{T_g}{T_p}\right)^{0.65} T_p^4\right) \\ &+ \frac{\varepsilon_w + 1}{2}\sigma\left(T_w^4 - T_p^4\right) - \frac{\dot{m}_{\mathrm{CO}}}{4\pi r_s^2}\Delta H_{rx},\end{aligned} \tag{19.5.23}$$

where h_{pg} denotes the convective heat transfer coefficient between particle and gas, σ is the Stefan–Boltzmann constant, ε_w, ε_p, and ε_g are the emissivities of the wall, particle, and

gas, and ΔH_{rx} is the heat of reaction. The time increment Δt corresponds to the distance increment Δx as discussed earlier.

The gas temperature is computed from a similar balance on the heat accumulation in a cylindrical "slice" of reactor volume of width equal to the finite element Δx. This accumulation is equal to the convective and radiant heat transfer rates from all particles inside the "slice" plus the convective and radiant heat transfer through the *periphery* of the "slice," i.e., the area $\pi d_c\,\Delta x$, plus the chemical heats of combustion (C and CO with input oxygen):

$$\rho_g c_{p,g}\frac{\Delta T_g}{\Delta t} = \sum_{i=1}^{n} nA_p\left[h_{pg}(T_g - T_p) - \varepsilon_p\sigma\varepsilon_g\left(T_g^4 - \left(\frac{T_g}{T_p}\right)^{0.65}T_p^4\right)\right] + \frac{4}{d_{\text{shaft}}}\left[h_{gw}(T_w - T_g) + \frac{\varepsilon_w + 1}{2}\sigma(T_w^4 - T_g^4)\right] - \frac{\Delta R_{x,\text{comb}}}{\Delta t}\,c\Delta H_{\text{comb}}, \tag{19.5.24}$$

where h_{gw} denotes the heat transfer coefficient between gas and reactor wall and ΔH_{comb} and $\Delta R_{x,\text{comb}}/\Delta t$ are the heat and rate of combustion, respectively. The number and size fractions of particles in the "slice" are computed from the ratio of solids and gas feed rates to the reactor, corrected for volume expansion due to temperature and chemical reaction.

19.5.8. Numerical Solution

We can now proceed to solve the three principal equations, i.e., the molar flow rate of CO for reduction (see (19.5.18)), particle temperature (see (19.5.23)) and gas temperature (see (19.5.24)). These equations are coupled and cannot be solved analytically. However, a numerical solution can be obtained readily by expressing these equations in computer language, e.g., using the program BASICA, entering property and system values, initial and boundary conditions and selecting appropriate distance and time increments.

A schematic flow sheet of the computer program is shown in Fig. 19.15. After initialization, the program proceeds iteratively to calculate values of ΔT_p, ΔT_g, ΔR_x, etc. for each finite increment of distance and time, starting from the point of entry. Thus, it provides axial velocity, temperature and concentration profiles as well as degree of reaction attained within a certain length of reactor. Some typical results in the reduction of zinc calcines, computed for a small experimental flash reactor, are shown in Figs. 19.16–19.18 [13].

REFERENCES

1. L.D. Smoot and P.J. Smith, *Coal Combustion and Gasification*, Plenum Press, New York (1985).
2. R.H. Essenhigh, "Fundamentals of Coal Combustion," in: *Chemistry of Coal Utilization*, ed. M.A. Elliott, Wiley, New York (1981).
3. H.H. Kellogg, *Elements of Pyrometallurgy*, Lecture Notes, Columbia University (1989).
4. E.T. Turkdogan et al., *Trans. Soc. Min. Eng., AIME*, 9–21 (1973).
5. O. Levenspiel, *Chemical Reaction Engineering*, Wiley, New York (1961).
6. W.M. McKewan, *Trans. AIME*, **212**, 791–793 (1958).
7. N.J. Themelis and W.H. Gauvin, *Trans. Met. Soc. AIME*, **290**, 290–300 (1963).
8. J.C. Yannopoulos and N.J. Themelis, *Can. J. Chem. Eng.*, **43**, 173–177 (1965).
9. R.G. Olsson and W.M. McKewan, *Trans. AIME*, **236**, 1518–1522 (1966).
10. I. Barin, in collaboration with F. Sauert, E. Schulze-Rhonohof, and W. Shu Sheng, *Thermochemical Data of Pure Substances*, Parts I and II, VCH Press, Weinheim D-6940, Germany (1989).

11. A. Roine, *Outokumpu HSC Chemistry for Windows*, Outokumpu Research Company, Pori, Finland (1993).
12. J. Szekely and N.J. Themelis, *Rate Phenomena in Process Metallurgy*, Wiley, New York (1971).
13. E.M. Weenink, PhD Thesis, Columbia University (1992).
14. Li Wu Ebenfelt, PhD Thesis, Columbia University, New York (1991).
15. E.C. Truesdale and R.K. Waring, *Trans. AIME*, **159**, 97–109 (1944).
16. C.E. Gugger and F.S. Manning, *Metall. Trans.*, **2**, 3083–3090 (1971).
17. G. Bjorling, PhD Thesis, Royal Institute of Technology, Sweden (1955).
18. J.M. Smith, *Chemical Engineering Kinetics*, McGraw-Hill, New York (1981).

TWENTY

Flow Behavior in Chemical Reactors

We will conclude our discussion of chemical rate phenomena with an introduction to batch and continuous flow reactors and some examples of the effect of flow behavior on reactor performance. For further reading on this subject, the reader is referred to *Chemical Reaction Engineering* by Levenspiel [1], *Chemical Reactor Analysis and Design* by Froment and Bischoff [2] and *Elements of Chemical Reaction Engineering* by Fogler [3].

Chemical reactors can be classified into two broad classes: **Batch reactors** in which materials are charged, reacted over a period of time and then discharged; and **continuous flow reactors**, where reagents are fed continuously at one point and products are withdrawn continuously or semicontinuously at another. Both types of reactors may involve a number of stages, such as heating, reacting, cooling and so forth.

In batch reactors, the separation of these processing stages takes place in the same space but at a different *time*; in continuous flow reactors the various "stages" occur simultaneously but are separated *in space* (Fig. 20.1). In both types, it is important to establish the *residence time* of materials in a particular stage of the processing sequence. Also, the temperature and concentration profiles in a reactor have a major effect on its performance.

In a batch reactor, all elements of fluid have the same residence time. In a continuous flow reactor, parts of the fluid may move through the system slower than others, as in the case of laminar flow through a tube (Chapter 4). The average residence time of all fluid or fluidized elements can be calculated by dividing the volume of materials in the reactor by their volumetric flow rate in and out of the reactor:

$$t_{\text{ave}} = \frac{\text{active reactor volume}}{\text{volumetric rate of fluid flow}} = \frac{V_r}{\dot{v}}. \tag{20.1.1}$$

The variation of actual residence times from the calculated average, that is the *distribution of residence times*, is an important characteristic of the reactor and influences appreciably its performance. A continuous flow reactor in which all fluid elements have the same residence time is called a **plug flow reactor**.

At the other end of the spectrum of continuous flow reactors, is the **back-mixed**, or *perfectly mixed* reactor: material fed at one point is very rapidly mixed throughout the volume of the reactor. This type of reactor is also referred to in the literature as a *continuous-stirred tank reactor* (CSTR).

When the velocity profiles in a reactor can be established on the basis of fluid flow theory, the distribution of residence times of fluid elements in the reactor are easily calculated. In the absence of such information, engineers have developed the concepts of continuous flow reactors which will be introduced in this chapter.

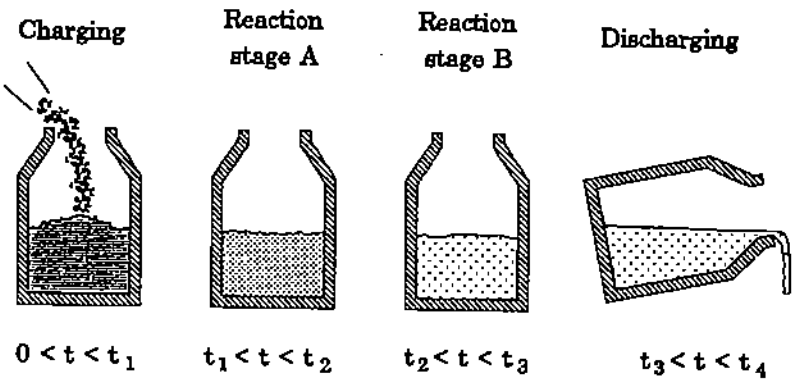

(a) Batch reactor

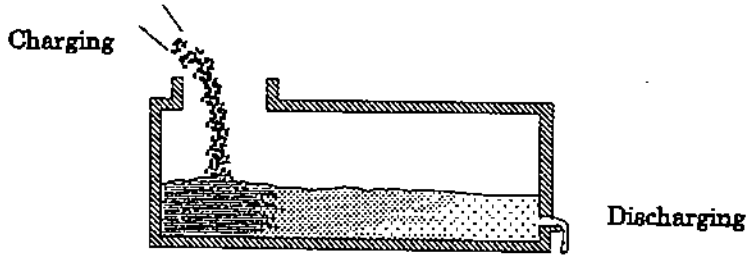

(b) Continuous flow reactor

Figure 20.1. Batch and continuous flow reactors.

20.1. TRACER TECHNIQUES: STEP INPUT

The residence time distribution of a fluid flowing through a vessel can be determined by means of tracer tests. Basically, these involve the addition of a tracer (e.g., dye, radioactive material, chemical substance) into the stream entering the vessel, and then measuring its concentration in the exit stream. The principal tracer techniques are:

a. Continuous addition of tracer to the inlet stream, starting at a certain instant of time (*step input*).
b. Addition of a finite quantity of tracer over a very short time interval in comparison with the average residence time of fluid in the vessel (*pulse input*).

To illustrate the step-input technique, let us consider a reactor vessel through which there is a continuous flow of materials. At time $t = 0$, we start adding a tracer into the inlet stream to the reactor, at a rate which is maintained constant throughout the experiment. At the same instant, we start sampling the exit stream and plotting the exit concentration of tracer as a function of time.

The results can be plotted in dimensionless, and thus more general, form by using the variables F for the *dimensionless concentration* and τ, for the *dimensionless time*:

$$F = \frac{c}{c_i}, \quad \tau = \frac{t}{t_{\text{ave}}},$$

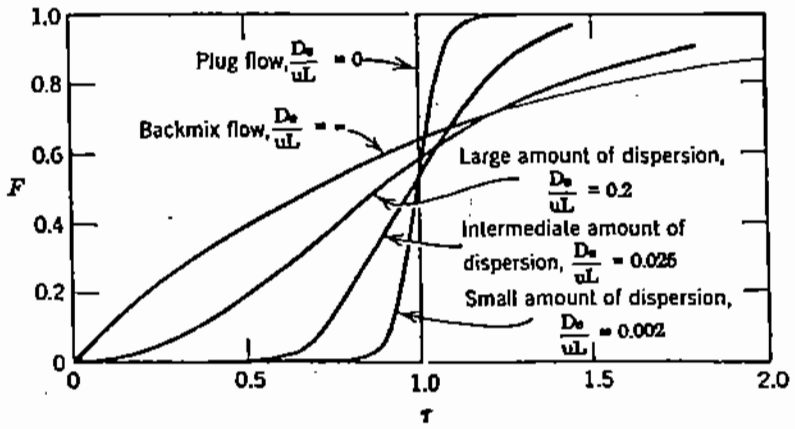

Figure 20.2. F-diagrams for plug flow, perfect mixing, and intermediate degrees of mixing.

where c_i is the concentration of tracer in the inlet stream; c is the concentration of tracer in exit stream at time t; t_{ave} is the mean residence time of fluid in the vessel.

A plot of F against τ is called the **F-diagram** (or *F curve*) for the system. The value of F represents the concentration in the exit stream as a fraction of the inlet concentration of tracer. The common characteristic of these diagrams is that at time zero the value of F is also zero, while for large values of t/t_{ave}, F approaches unity. This, of course, reflects the fact that after a sufficiently long period of time all the fluid originally in the vessel (i.e., before the step input at $t = 0$) is replaced by "new" fluid having the inlet tracer concentration.

The shape of the F-diagram varies considerably between different reactors and can provide useful information as to the flow characteristics in a vessel. The principal types of flow are described below.

20.1.1. Plug Flow Reactors

In *plug flow*, or *piston flow*, all fluid elements travel through the vessel at nearly the same velocity and do not intermix during their passage through the reactor. In this type of reactor, a "step" change introduced in the tracer concentration at the inlet at time $\tau = 0$ (i.e., $t = 0$), is reproduced exactly at the exit at time $\tau = 1$ (i.e., $t = t_{ave}$). Thus, the tracer arrives at the exit point at the "expected time," which indicates that there is no spread of residence times and that all fluid elements spend the same length of time in the vessel (Fig. 20.2, "plug flow").

Although the ideal of plug flow cannot be attained exactly, the flow of fluids through long packed beds or the motion of material through a cement or iron reduction rotary kiln (Fig. 20.3) are close approximations.

20.1.2. Perfectly Mixed Flow

In *back-mixed* (or *perfectly mixed flow*), the tracer introduced at the inlet is dispersed instantaneously and uniformly throughout the system. Therefore, the tracer appears at the exit shortly after it has been introduced into the inlet stream, but the approach to the value of $F = 1$ is comparatively slow. At any given time the tracer concentration in the exit stream is the same as that in the vessel. This behavior indicates that a fraction of the material

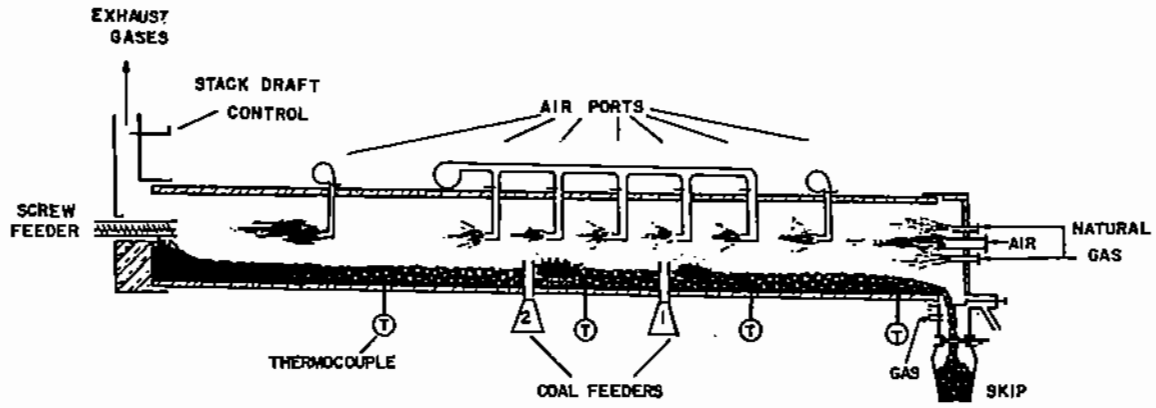

Figure 20.3. Rotary kiln used for iron reduction.

remains in the vessel for periods much longer than t_{ave}, while other parts of the stream pass through it very rapidly.

For perfect mixing conditions, and in the absence of chemical reaction, the material balance on the tracer element A yields:

rate of change of concentration of A in vessel
= rate of input of tracer in inlet stream
− rate of outlet of tracer in exit stream,

which mathematically is expressed as follows:

$$V_r \frac{dc}{dt} = \dot{v}c_i - \dot{v}c, \tag{20.1.2}$$

where V_r is the volume of fluid in the vessel; $\dot{v}$ is the volumetric rate of flow; c_i is the inlet concentration of tracer in the stream to the reactor; c is the concentration of tracer in the exit stream.

It can be seen that (20.1.2) has the form of a first-order rate equation. By integrating it, we obtain the following equation for the F-diagram of back mixed flow (Fig. 20.2, "backmix flow"):

$$c_t = c_i(1 - e^{-t\dot{v}/V_r}) = c_i(1 - e^{-t/t_{ave}}), \tag{20.1.3}$$

or in dimensionless form:

$$F_\tau = \frac{c_t}{c_i} = 1 - e^{-t/t_{ave}} = 1 - e^{-\tau}. \tag{20.1.4}$$

The idealized concept of perfect mixing may be applied as a good approximation to some reactors, such as mechanically agitated leaching cells.

20.1.3. Plug Flow with Axial Mixing

As noted above, Fig. 20.2 shows the representative F-diagrams for plug and perfectly mixed flows. However, the flow in most vessels falls somewhere between these two extremes. Some intermediate cases are also shown in Fig. 20.2. It can be seen that in such cases the

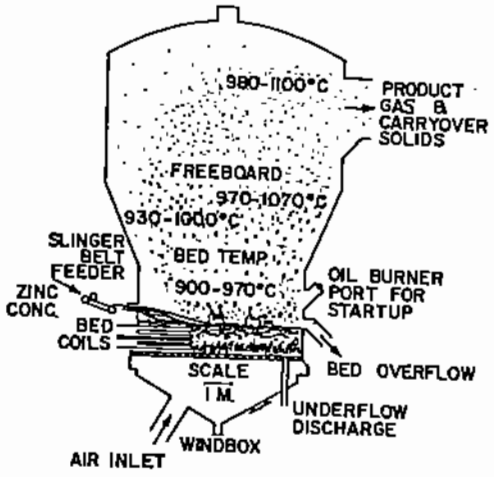

Figure 20.4. Zinc fluid bed roaster.

tracer front arrives at the exit point earlier than $\tau = 1$; then there is a rapid increase in the value of F, which reaches unity at $\tau > 1$.

An example of such a reactor is the fluid bed roaster used in the oxidation (roasting) of zinc sulfides (Fig. 20.4). Although fluid beds are regarded as well-mixed reactors, the results of a radioactive tracer have shown (Fig. 20.5, [6]) that some of the solid particles moved through the bed in plug flow. In Fig. 20.4, at $t = 0$, the concentrate feed was switched to concentrates containing some radioactive zinc. After a few hours, the feed was changed back to "normal" concentrates; the plot of Fig. 20.5 shows the combined F-diagrams for both of these step-changes in the feed stream for three tests.

20.1.4. Dead Volume Region

In some cases, there can be inactive or *dead volume* zones within a reactor. Because of that, the bulk of the fluid spends less time in the vessel than is indicated by the calculated average residence time. This type of behavior indicates inefficient use of the reactor volume and should be minimized in practice.

In practical situations, dead volume zones may occur due to eddies trapped at sharp corners, especially when material is introduced or withdrawn through a small port in a large vessel, e.g., a taphole in a metallurgical furnace (Fig. 20.6), or due to large variations in fluid viscosity caused by temperature gradients.

20.2. TRACER TECHNIQUES: PULSE INPUT

An alternative tracer technique, which is used more frequently than the step-input, is the **pulse input** method. In this case, we introduce at the inlet end of the reactor a mass m_{tr} of tracer "instantaneously," i.e., over a time period which is very small in comparison with t_{ave}.

As in the previous case, the concentration of the tracer is measured with time in the exit stream and the results are plotted in the form of the dimensionless exit concentration:

$$C = \frac{c}{m_{tr}/V_r}, \tag{20.2.1}$$

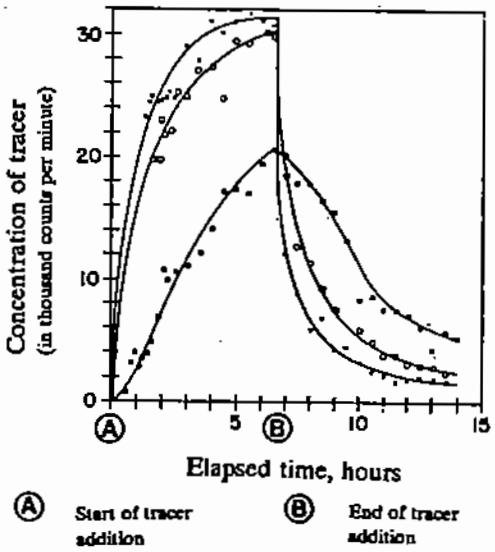

Figure 20.5. Results of F-tracer test in a zinc fluid bed roaster.

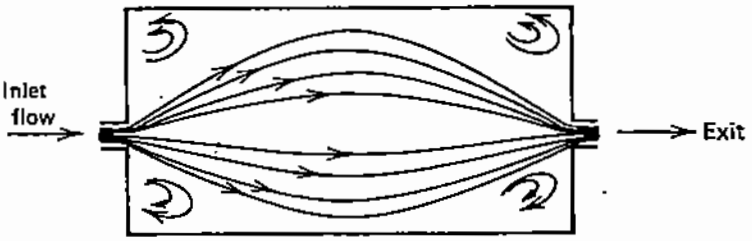

Figure 20.6. Streamlines in a vessel containing dead-volume regions.

where $m_{t\tau}$ is the mass of injected tracer; V_τ is the volume of fluid in the vessel.

The denominator of (20.2.1) represents the average concentration that the tracer would reach if it were mixed instantaneously with the contents of the vessel. In cases where $m_{t\tau}$ cannot be determined accurately (e.g., in radioactive tracer tests), the average concentration of the tracer can be estimated from the weighted average of the exit concentrations during the entire test.

The results of pulse input tracer tests are plotted in the form of the dimensionless concentration C against dimensionless time ($\tau = t/t_{\text{ave}}$). These curves are usually called **C-diagrams** and some representative plots, corresponding to the F-diagrams of Fig. 20.2, are shown in Figs. 20.7–20.10. Comparison of the F- and C-diagrams shows that the latter follow a more distinctive pattern than the F-diagrams for the various types of flow behavior; for this reason, the C-diagrams are more useful for the characterization of flow systems.

The area under each C curve is equal to unity, since all the tracer introduced at the inlet must eventually leave the system, i.e.,

$$\int_0^\infty C\, d\tau \equiv 1. \tag{20.2.2}$$

In the idealized case of *plug flow*, the fluid element containing the tracer material will not mix with the rest of the fluid as it travels toward the exit of the vessel (Fig. 20.7). For a

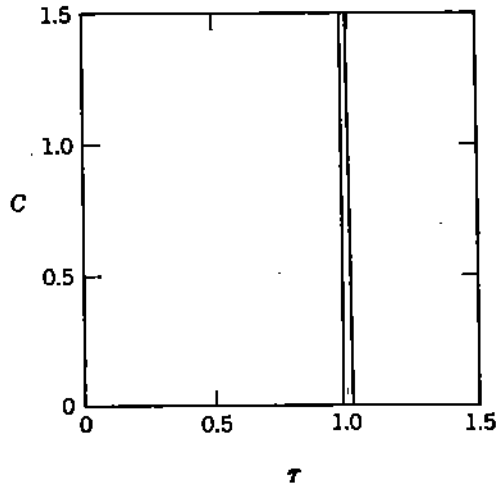

Figure 20.7. C-diagram for pulse-input tracer test in plug flow vessel.

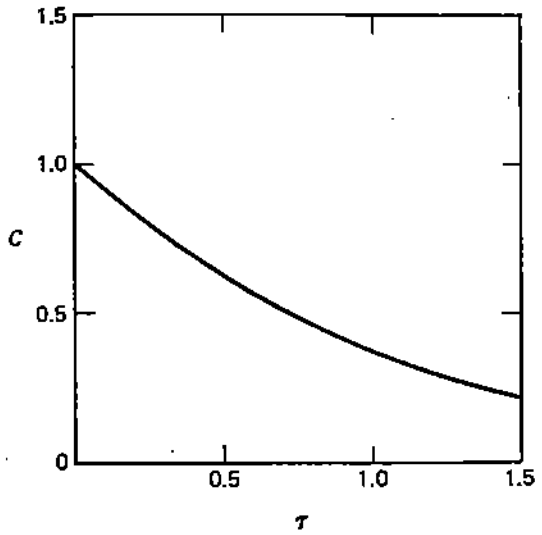

Figure 20.8. C-diagram for perfectly mixed flow.

back-mixed system, the C-diagram has an initial value of unity and then decreases gradually to zero (Fig. 20.8).

Following the reasoning which led to (20.1.3)–(20.1.5)) for the F-diagram from a step-input tracer, we can readily show that the C curve is described by the following exponential decay equation:

$$C_t = \frac{c}{m_{tr}/V_r} = e^{-t/(V_r/\dot{v})} = e^{-t/t_{ave}}, \tag{20.2.3}$$

or in dimensionless form:

$$C_\tau = e^{-\tau}, \tag{20.2.4}$$

where

$$C_\tau = \frac{c_t}{m_{tr}/V_r} \text{ and } \tau = \frac{t}{t_{ave}}.$$

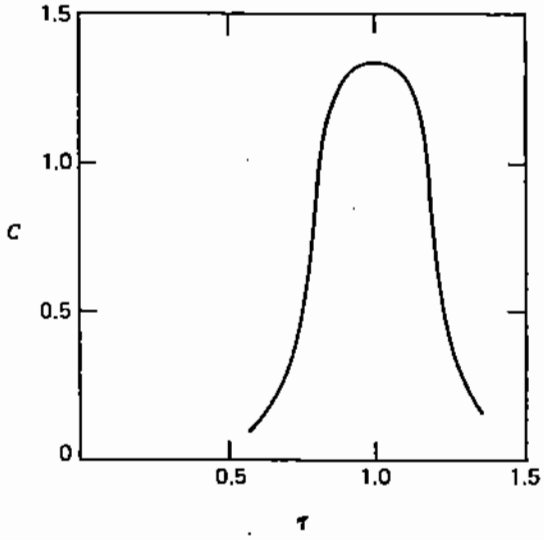

Figure 20.9. C-diagram for plug flow with axial mixing.

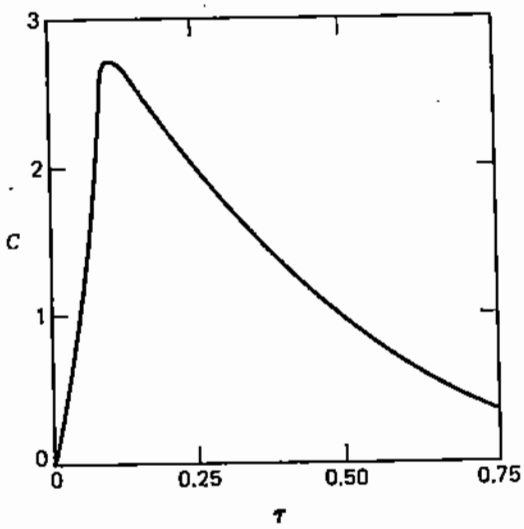

Figure 20.10. C-diagram for plug flow with some axial mixing, in presence of dead volume region.

Comparison of this equation with (20.1.5) shows that the C curve is in fact a derivative of the F curve. It can be shown that this is a general rule which is valid regardless of the flow pattern. Therefore, we may write

$$C_\tau = \frac{dF_\tau}{d\tau}. \tag{20.2.5}$$

In the case of plug flow with a small amount of axial mixing, the C curve exhibits a maximum peak at $\tau = 1$ (Fig. 20.9). The spread of the curve about the median $\tau = 1$ can be used to describe quantitatively the mixing conditions in the system, as will be discussed shortly.

The presence of a dead volume region (Fig. 20.10, §20.4) is indicated by a maximum in the C curve, occurring at $\tau < 1$; at that peak, $C > 1$. The value of C and the location

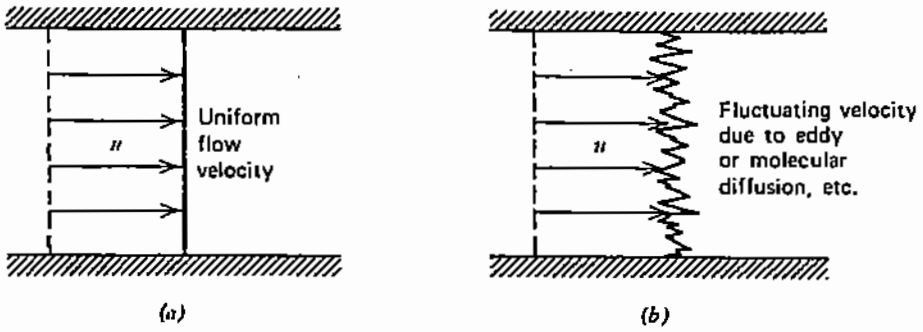

Figure 20.11. Velocity profiles in the case of (*a*) plug flow and (*b*) plug flow with axial mixing (dispersion model).

of this peak on the time axis can be used to estimate the extent of the dead volume zone in a vessel (§20.4).

20.3. QUANTITATIVE EVALUATION OF TRACER RESULTS

In order to characterize quantitatively the mixing conditions in a reactor, it is necessary to develop a mathematical model and then adjust the parameters of the model until it matches the experimental results satisfactorily. The numerical values of these parameters may then serve as a quantitative measure of the mixing conditions in the vessel.

20.3.1. The Eddy Diffusion Dispersion Model

The **dispersion model** is based on the assumption that mixing is brought about by *eddy diffusion* in the fluid (Fig. 20.11), a concept which was also discussed in Chapter 7 on turbulent flow. It is assumed that the dispersion of the tracer material in the fluid follows the laws of diffusion and that the mass flux is proportional to the concentration gradient. The constant of proportionality is called the **eddy diffusivity** and is not a molecular property of the fluid, but depends both on the fluid and a number of other parameters in the particular reactor.

According to this model, the rate of dispersion of the tracer in a continuous flow system, in the absence of chemical reaction, is expressed by an equation similar to (15.1.8) derived in Chapter 15 for describing diffusion in the presence of net bulk flow:

$$\frac{\partial c}{\partial t} = D_e \frac{\partial^2 c}{\partial x^2} - u \frac{\partial c}{\partial x} \quad \text{for } 0 < x < L, \tag{20.3.1}$$

where D_e is the eddy diffusivity; u is the velocity in the direction of the flow; L is the length of the reactor; x is the distance along the reactor in the direction of the flow.

The boundary conditions required for the solution of (20.3.1) depend on the method of introducing the tracer. For the pulse input technique, the boundary conditions are:

$$\int_0^\infty c\dot{v}\, dt = m_{tr} \quad \text{at } x = L, \tag{20.3.2}$$

$$\frac{\partial c}{\partial x} = 0 \quad \text{at } x = 0,\ x = L, \tag{20.3.3}$$

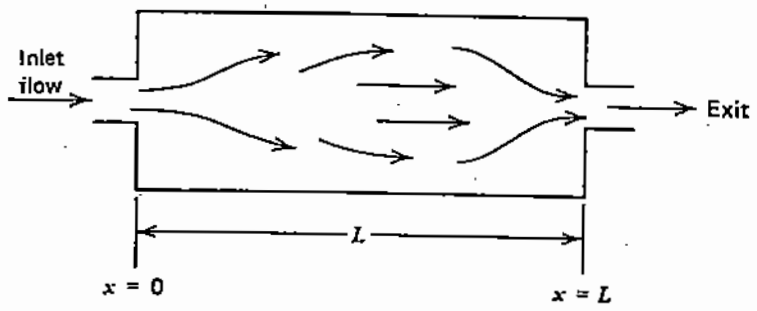

Figure 20.12. Schematic representation of closed-end vessel.

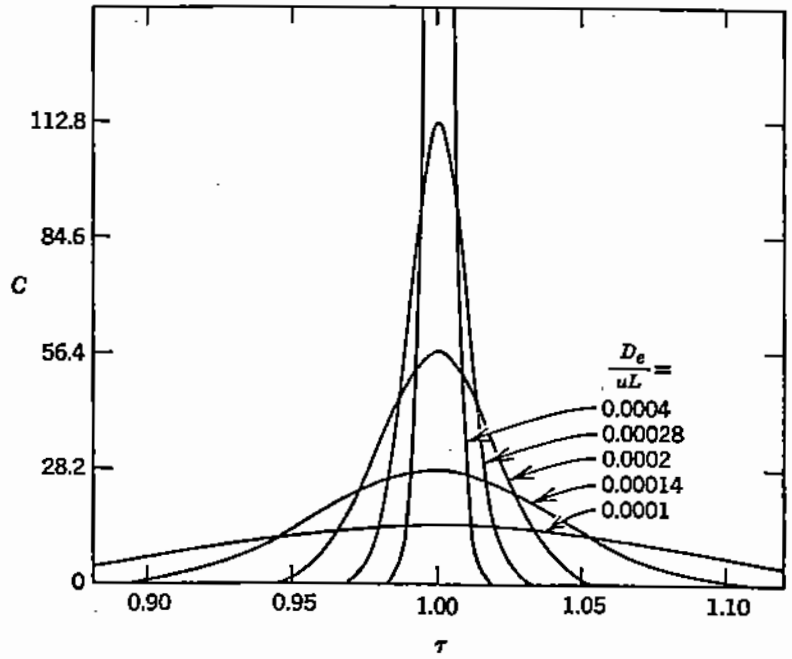

Figure 20.13. Calculated C-diagrams for low values of $\mathrm{Le} = D_e/uL$ [1].

where $\dot{v}$ is the volumetric flow rate through the reactor.

Equation (20.3.3) states that at the end walls of the reactor ($x = 0$, $x = L$) the concentration gradient is zero, i.e., there is no eddy diffusion past the walls (Fig. 20.12). For small values of D_e/uL, the spreading tracer curve does not change much in shape as it passes through the measuring point. Under these conditions, equation 20.3.1 can be solved analytically [1] to yield the following symmetrical C-diagram:

$$C_\tau = \frac{c}{m_{t\tau}/V_r} = \frac{1}{2\sqrt{\pi(D_e/uL)}}\, e^{-(1-\tau)^2/[4(D_e/uL)]}. \tag{20.3.4}$$

Equation (20.3.4) shows that, according to the dispersion model, the tracer concentration against time is a unique function of the dimensionless parameter D_e/uL. This group is equivalent to the inverse of the dimensionless *Peclet number for mass transfer* (Chapter 17):

$$\mathrm{Pe} = \frac{uL}{D_{AB}}, \tag{20.3.5}$$

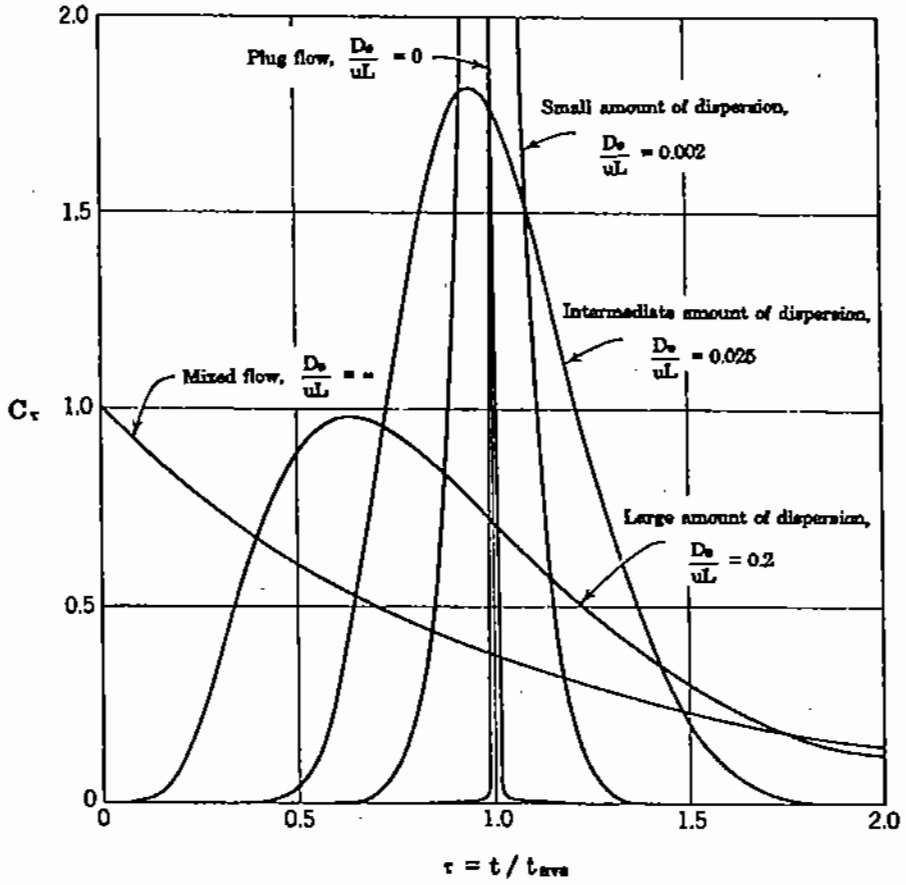

Figure 20.14. Computed C-diagrams for flow ranging from perfectly mixed to plug flow [1].

and, for convenience, will be referred to in this text as the *Levenspiel number* (Le), in honor of the chemical engineer [1] who contributed so much to the study of mixing phenomena in reactors.

The C-diagrams represented by (20.3.4) are shown for various values of Le in Fig. 20.13. The Levenspiel number represents the ratio of material transferred by eddy diffusion to that transferred by bulk flow. For small values of Le, the transfer of mass by mixing, i.e., by eddy diffusion, is negligible in comparison to that by bulk flow and, therefore, the system approaches the conditions in a plug flow reactor. At progressively increasing values of D_e/uL, the flow approaches that of a perfectly mixed reactor.

For large degrees of dispersion, (20.3.1) must be solved by numerical techniques. Figure 20.14 shows the computed C-diagrams [1] for Levenspiel numbers ranging from zero (plug flow) to infinity (perfectly mixed flow). It can be seen that for large values of D_e/uL the curves tend to the pattern for perfectly mixed flow; at very low values a sharp peak appears at τ which characterizes plug flow.

As illustrated by Figs. 20.13 and 20.14 the shape of the C-diagrams is highly sensitive to the value of the Levenspiel number. Therefore, these plots provide a satisfactory method for computing eddy diffusivities from experimental tracer tests.

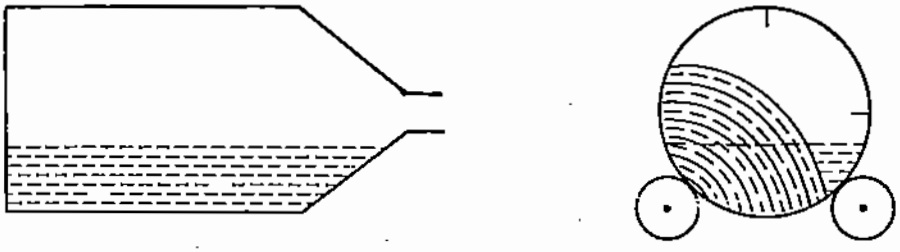

Figure 20.15. Section of rotary reactor for batch precipitation of tellurium.

The Levenspiel number for a particular flow may be calculated by direct comparison of an experimental curve to a series of C-diagrams (e.g., Figs. 20.13–20.14) or by using the following expression for the variance of the experimental data [1]:

$$\sigma^2 = 2\mathrm{Le} + 2\mathrm{Le}^2(1 - \mathrm{e}^{-1/\mathrm{Le}}), \tag{20.3.6}$$

where σ^2 is the statistical variance, or square of standard deviation of the spread of the concentration around the mean residence time:

$$\sigma^2 = \frac{\int_0^\infty c(t - t_{\mathrm{mean}})^2\, dt}{\int_0^\infty c\, dt}. \tag{20.3.7}$$

For small deviations from plug flow, the dispersion is symmetrical about the mean and can be represented by the normal Gaussian distribution:

$$C_\tau = \frac{1}{2\sqrt{\pi(D_e/uL)}}\, e^{-(1-\tau)^2/[4(D_e/uL)]}. \tag{20.3.8}$$

Figure 20.14 shows that for large values of the group D_e/uL the curves tend to the pattern for backmix flow; at very low values, a sharp peak appears at $\tau = 1$, which characterizes plug flow (Fig. 20.7).

Example 20.3.1

In the electrolytic refining of copper, the impurities in the copper anodes are recovered in the form of "slimes." It has been determined experimentally that tellurium (Te) can be separated by pressure leaching of the slimes in a basic solution followed by the following displacement reaction by copper when sulfuric acid is added to the basic solution:

$$\mathrm{Te(OH)_6} + 5\mathrm{Cu^0} + 3\mathrm{H_2SO_4} \rightleftharpoons \mathrm{Cu_2Te} + 3\mathrm{CuSO_4} + 6\mathrm{H_2O}.$$

In this reaction, the metallic copper is in the form of metal shot brought into contact with the pressure leach solution. It is required to design a reactor to process 3 $\mathrm{m^3\ h^{-1}}$ of solution containing 10 g/liter (10 $\mathrm{kg\ m^{-3}}$) of tellurium.

The rate of the tellurium precipitation reaction was studied in the rotary drum reactor shown in Fig. 20.15 [7]. In batch operation, the experimental results showed that the optimum operating conditions were as follows: Temperature: 103°C; copper shot diameter: 0.3 cm; pH: 2; speed of rotation: 10 rpm; reactor loading (volume of bath/volume of

reactor): 50%; volume of copper shot/volume of solution: 0.35. Under these conditions, the copper telluride formation is a first-order heterogeneous reaction and its rate is expressed as follows:

$$V_{\text{sol}} \frac{dc_{\text{Te}}}{dt} = -k_r A_s (c_{\text{Te}} - c_{\text{Te},e}), \tag{20.3.9}$$

where V_{sol} is the volume of solution in the reactor, A_s the total surface area of copper shot in the reactor (interfacial area for reaction) and c_{Te} and $c_{\text{Te},e}$ are the actual and equilibrium concentrations of tellurium in the solution. However, examination of the free energy of the above chemical reaction at the stated pH and temperature showed that the reaction is practically irreversible and therefore $c_{\text{Te},e}$ can be assumed to be zero.

It is required to calculate and compare the required volumes of a) a batch reactor, which is loaded and unloaded at specified time intervals and b) a continuous flow reactor, which is charged and discharged continuously.

Solution. It should be noted that the chemical rate constant of this heterogeneous reaction, k_r, has the dimensions of L t^{-1} (Chapter 18). However, in this situation, where the amount of shot present per unit volume of reaction is relatively constant, it is convenient to consider the reaction as a quasi-homogeneous reaction and assign to it a modified rate constant which incorporates the relationship of "surface area for reaction" to "volume of reacting mixture," as follows (§18.1):

$$\frac{dc_{\text{Te}}}{dt} = -k_r'(c_{\text{Te}} - c_{\text{Te},e}), \tag{20.3.10}$$

where

$$k_r' = k_r \frac{A_s}{V_{\text{sol}}}.$$

It can be seen that the dimensions of k_r' are t^{-1}, as would be expected for a homogeneous reaction.

As was mentioned in §18.1, the device of "transforming" a heterogeneous reaction to a quasi-homogeneous one is used frequently in interpreting chemical reaction data, in situations where the values of k_r and A_s cannot be estimated separately but the product $k_r A_s/V$ can be measured experimentally. However, caution should be exercised in reporting or scaling up such experimental data: The area/volume ratio must be reproducible in order for the modified rate constant to be meaningful.

a. **Design of batch reactor:** Fig. 20.16 is a plot of the rate data obtained in an experimental batch reactor for the optimum conditions. By plotting the decrease in c_{Te} with time in semilogarithmic form, we obtain from the slope of this plot the value of k_r' = 3.1 h^{-1}. First, we have to make a decision as to what will be the final concentration of the tellurium remaining in solution after reaction: The semilogarithmic form of Fig. 20.16 shows that it will take just as much reaction time to reduce the tellurium concentration from the initial 10 g/liter of solution to 1 g/liter, as from 1 to 0.1 g/liter.

In some cases, it may be necessary to recover as much as possible of the contained metal from the solution, either for economic or environmental reasons. However, in this case, the "stripped" solution is recirculated to the electrorefining plant so that we do not need to go to a very low concentration. By choosing a final concentration of tellurium of $c_{\text{Te},f}$ = 1 g/liter, we calculate from the integrated (20.3.10):

$$\frac{c_{\text{Te},f}}{c_{\text{Te},i}} = e^{-k_r t_f}, \text{ i.e., } \frac{1}{10} = e^{-3.1 t_f}. \tag{20.3.11}$$

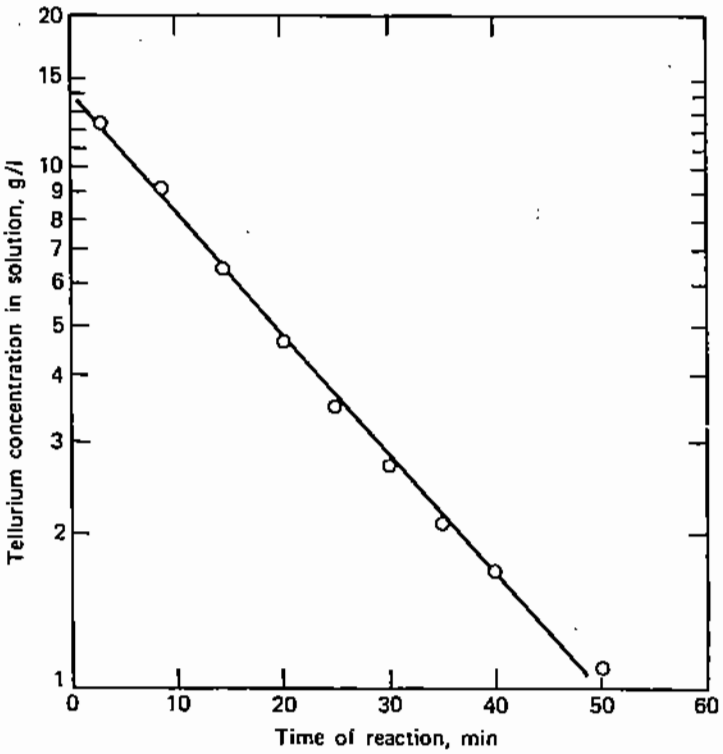

Figure 20.16. Rate of precipitation of Cu_2Te in rotary batch reactor [3].

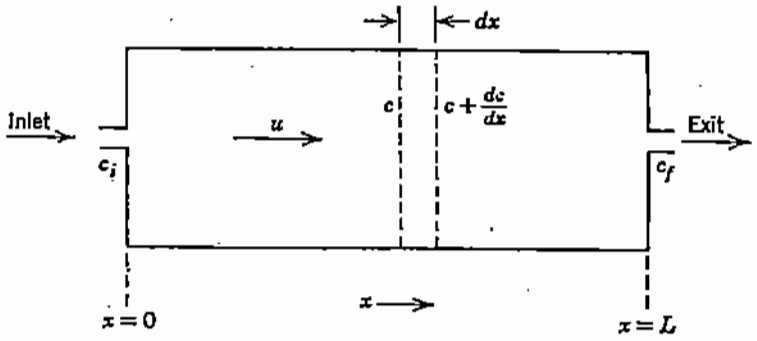

Figure 20.17. Material balance across a differential section of a reactor.

Solving the above equation we obtain $t_f = 0.75$ h. If we now assume that the time required to unload and reload the batch reactor is 0.5 hour per cycle, the volume of solution to be treated per cycle is

$$3\,\frac{\text{m}^2}{\text{h}} \times \frac{\text{time per cycle}}{\text{operating time per cycle}} = 3 \times \frac{(0.75 + 0.50)}{0.75} = 5\ \text{m}^3.$$

Therefore, the batch reactor must contain 5 cubic meters of solution. Maintaining the same ratio of copper shot to solution (0.35/1) and the same reactor loading as in the experimental tests (50%), we calculate that the required total volume of the batch reactor is

$$V_{\text{reactor}} = \left(5\ \text{m}^3\ \text{of solution} + 0.35 \times 5\ \text{m}^3\ \text{of coppershot}\right) \times \frac{100}{50} = 13.5\ \text{m}^3.$$

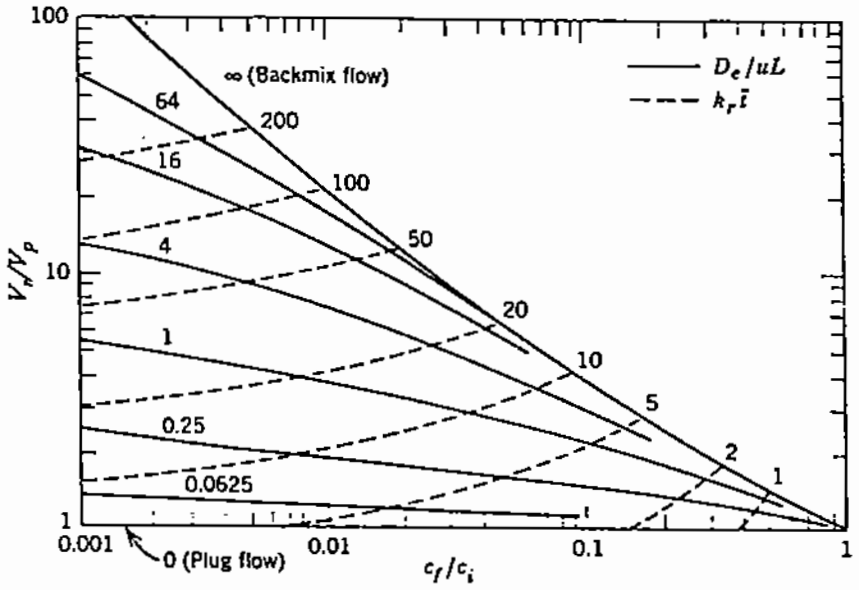

Figure 20.18. Required volume of a real reactor (V_r) expressed as a multiple of the volume of plug flow reactor (V_p) to attain same degree of reaction [1].

b. **Design of continuous flow reactor**: According to the diffusion model (§20.3.1), the mass balance for the tracer across a differential element dx of the length of a continuous flow reactor (Fig. 20.17) can be stated as follows:

rate of accumulation = net mass transfer by eddy diffusion
− net mass transfer by bulk flow
− rate of consumption by chemical reaction.

Mathematically, this statement is expressed by the following modification of (20.3.1):

$$\frac{dc}{dt} = D_e \frac{d^2c}{dx^2} - u\frac{dc}{dx} - k_r' c \text{ for } 0 < x < L, \tag{20.3.12}$$

where k_r' is the chemical rate coefficient and L the length of the reactor. The boundary conditions are:

$$uc_i = uc - D_e \frac{dc}{dx} \text{ at } x = 0; \quad \frac{dc}{dx} = 0 \text{ at } x = L. \tag{20.3.13}$$

The solution of the above differential equation is shown in graphical form in Fig. 20.18 [1]. In this plot, the y-axis, V_r/V_p, is the ratio of the required volume of a mixed-regime reactor at eddy diffusion D_e to that of a plug flow reactor, for the same degree of reaction. Evidently, as the degree of mixing increases, the concentration driving force for reaction along the length of the reactor decreases and a longer residence time is required to attain a certain degree of reaction.

In a perfectly mixed reactor, the concentration along the length of the reactor is equal to the concentration of the exit stream; therefore, the reactor volume required to attain a certain degree of conversion is substantially larger than in the case of plug flow. This is illustrated in Fig. 20.19 [1] which is a plot of the inverse rate of reaction per unit volume as a function of the degree of conversion; the shaded areas represent the dimensionless times

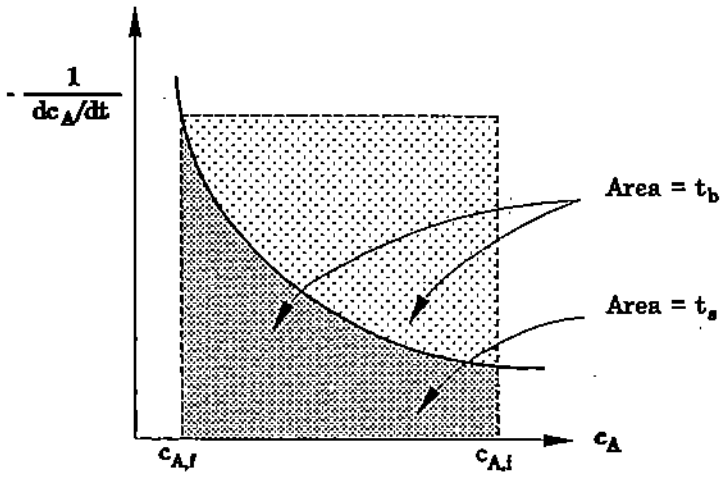

Figure 20.19. Comparison of residence times required in plug-flow (t_s) and back-mix reactor (t_b) for any reaction kinetics ($c_{A,i}$, $c_{A,f}$: initial and final concentration of reacting species).

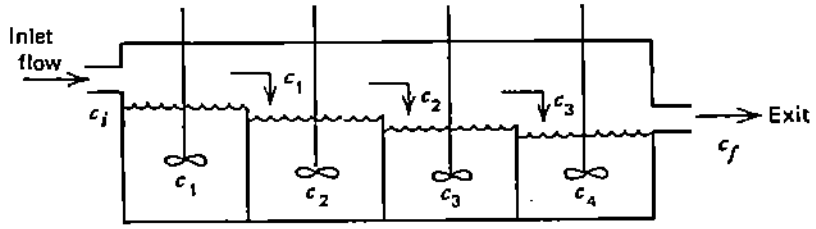

Figure 20.20. Schematic diagram of reactor consisting of a series of back-mixed flow cells.

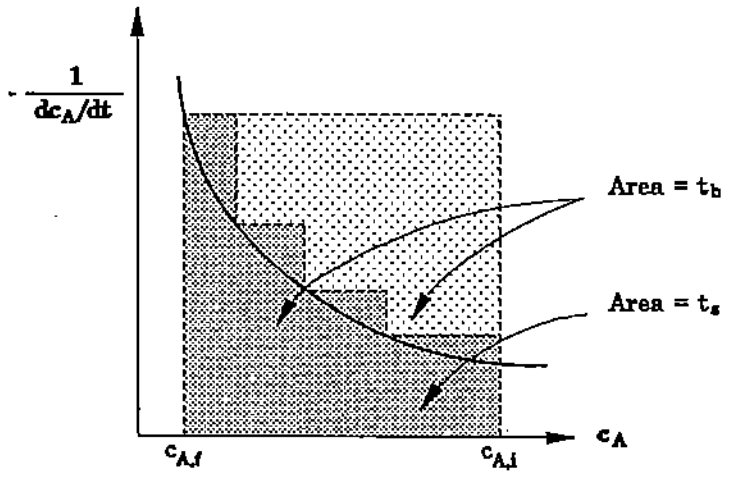

Figure 20.21. Comparison of residence times required in four cells in series (t_s) and in back-mix reactor (t_b) for any reaction kinetics.

required in a plug-flow and in a perfectly-mixed reactor for the reaction to proceed from the inlet fractional concentration $X_{A,i}$ to the final, $X_{A,f}$.

One way to approach plug flow is by using a larger number of small reactor cells in series so that the exit fluid from the first becomes the feed material to the second, and so

on (Fig. 20.20). The effect of this arrangement is illustrated in Fig. 20.21, which is similar to Fig. 20.19 and compares the relative volume of a back-mixed reactor with the volume of four reactor cells in series. This arrangement of reactors in series is used routinely in aqueous and organic liquid reactions but is not very practical for pyrometallurgical systems.

Returning to the generalized plot of Fig. 20.18, the x-axis, c_f/c_i, represents the required degree of conversion; the solid lines represent different degrees of eddy diffusion (expressed by the Levenspiel number); and the dotted lines represent the product of the chemical rate coefficient and the required residence time for a particular reaction.

With reference to our example, in order to determine the size of the continuous precipitation reactor it is necessary to estimate the value of the eddy diffusivity in such a system. It was relatively simple to construct [7] a plexiglass model of the proposed reactor (projected length to diameter ratio = 5) and load it with the prescribed quantity of copper shot per volume of solution, as determined in the batch reactor tests. A water flow was used to simulate the tellurium solution in the projected continuous flow reactor. The water model was rotated at the prescribed speed and a tracer pulse was introduced. Comparison of the obtained concentration curve with the calculated curves of Fig. 20.14 showed that the Levenspiel number of the model was

$$\frac{D_e}{uL} = 0.18.$$

Now from Fig. 20.18, at the intersection of the required degree of conversion and Le = 0.18, we obtain

$$k'_r t_{\text{ave}} \approx 3.1.$$

Therefore, since $k'_r = 3.1\ \text{h}^{-1}$, the required residence time in a continuous flow reactor under these mixing conditions is approximately 1 hour. Of course, in the case of the continuous flow reactor we do not have to allow for loading time, etc. Therefore, the required "bath" volume of the projected continuous flow reactor is calculated to be

$$3\,\frac{\text{m}^3}{\text{h}} \times \frac{\text{residence time in mixed flow reactor}}{\text{residence time in plug flow (or batch)}} = 3 \times \frac{1}{0.75} = 4\,\text{m}^3.$$

Finally, by allowing for the volume of the copper shot (0.35 m^3/m^3 solution) and the 50% loading of the reactor, the total reactor volume is $4 \times 1.35 \times 2 = 10.8\,\text{m}^3$. For the projected length/diameter ratio of 5, the calculated inside dimensions of the reactor would be about 1.4 I.D. × 7 m long.

20.3.2. Use of Dispersion Model in a Batch Reactor

The dispersion model is not limited to continuous flow systems, but may also be used to describe mixing in batch reactors, in cases where the mixing mechanism is due to small eddies rather than to an overall bulk, circulatory motion. A representative case is the open

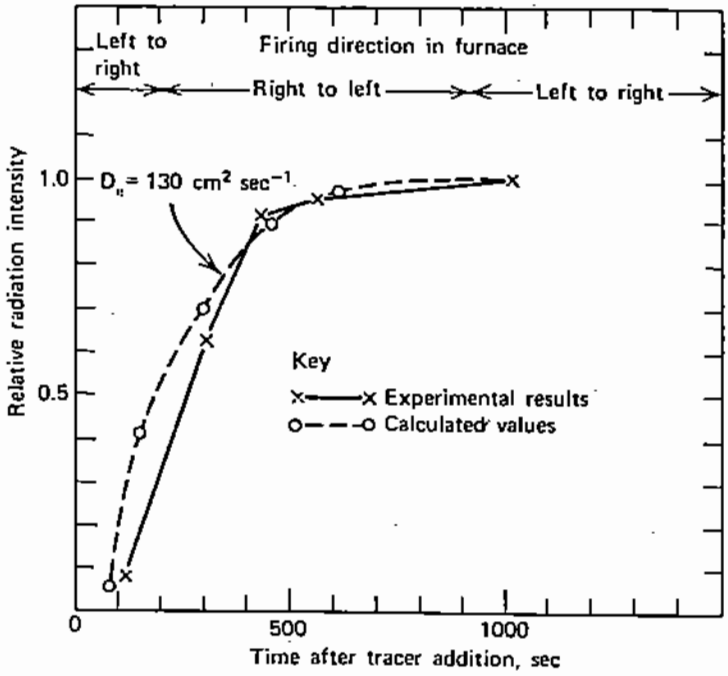

Figure 20.22. Comparison of experimental tracer results in an open hearth furnace for steelmaking with projection of dispersion model, for $D_e = 130$ cm^2/s [4].

hearth furnace for steelmaking, where metal mixing is brought about by natural convection currents and by the action of carbon monoxide bubbles as they rise through the bath.

For example, in a study of mixing in an open hearth bath [4], a small amount of radioactive gold was introduced through the center door of the furnace and metal samples were obtained periodically through the side doors. The samples were analyzed for radioactivity and a typical set of experimental data of tracer concentration against time are shown in Fig. 20.22 (solid line). If it is assumed that the eddy diffusion is unidirectional from the center of the furnace, at $x = 0$, and that the furnace extends from $-L > 0 > L$, i.e., the furnace length is $2L$, the eddy diffusion may be represented by

$$\frac{\partial c}{\partial t} = D_e \frac{\partial^2 c}{\partial x^2} \quad \text{for} \quad -L < x < L. \tag{20.3.14}$$

This equation may be regarded as a special case of (20.3.1), where the bulk flow term, $u\,\partial c/\partial x$, is zero. Its boundary conditions are $c = 0$ at $x = 0$ and $t = 0$, and

$$\frac{\partial c}{\partial y} = 0 \quad \text{at } x = L, \; x = -L \tag{20.3.15}$$

Comparison of (20.3.14) with (15.2.1), which was used in Chapter 15 to determine the diffusion of hydrogen atoms through a steel plate, shows that they are identical but their boundary conditions are different. Equation (20.3.14) was solved by Szekely (4) in the form of an exponential series equation. Various values of eddy diffusivity, D_e, were introduced into this

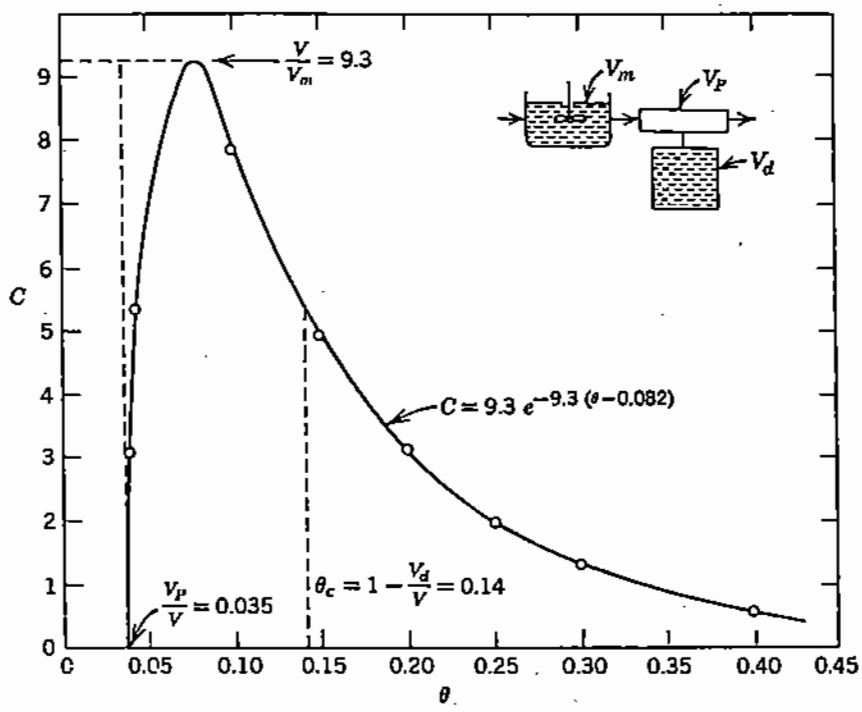

Figure 20.23. Analysis of C-diagram obtained from tracer test in a copper reverberatory furnace.

equation and the corresponding plots of c against t were constructed. By comparing each of these plots with the experimental data of Fig. 20.22, (4) Szekely concluded that the eddy diffusivity in the metal bath was about 130 $cm^2\ s^{-1}$. This high value was due to the reaction of carbon with oxygen in the steel. There is spontaneous formation of carbon monoxide bubbles throughout the molten metal ("carbon boil" conditions); as the bubbles rise to the furnace, they impart energy to the liquid and result in intensive mixing.

20.4. MIXED MODEL

The **mixed model**, assumes that the reactor volume may be divided into fractions in each of which there exists a simple well-defined flow pattern. The flow patterns that are most commonly used are: plug flow volume (V_p), backmix flow volume (V_m), and dead volume (V_d). This represents the portion of the liquid in the bath that is moving so slowly that it may be assumed to be stagnant. According to the definition by Levenspiel [1], the cut-off point between "active" and "stagnant" fluid may be taken as material that stays in the vessel for a period greater than twice the mean residence time.

A simple representation of such mixed models is shown in the insert of Fig. 20.23; the plug flow and backmix flow regions are in series, while the dead volume region is in parallel. The usefulness of the mixed model lies in the fact that the experimentally determined C-diagram for a particular system can be analyzed to determine the relative volumes of plug flow, back-mix flow, and dead volume regions. In this manner, the flow conditions in the system can be described quantitatively and compared with C-diagrams obtained after necessary operational changes (e.g., changes in flow, geometry, introduction of dams or agitators).

As an illustration of the use of this model, let us consider the experimentally determined C-diagram of Fig. 20.23. The tracer material first appears at the exit of the vessel at time t_p. Dividing t_p by the calculated average residence time of fluid in the vessel, we obtain the fraction of reactor volume which can be assumed to be in plug flow:

$$\tau_p = \frac{t_p}{t_{\text{ave}}} = \frac{V_p}{V}, \tag{20.4.1}$$

where V_p is the volume of fluid in plug flow and V is the total volume of fluid in the reactor.

Figure 20.23 also shows that the maximum tracer concentration is observed at time $t/t_{\text{ave}} < 1$ and has a value

$$C_{\max} = \frac{c_{\max}}{m_{tr}/V} > 1, \tag{20.4.2}$$

where $c_{\max}$ is the peak concentration of tracer at the exit.

This behavior indicates the presence of dead volume regions in the vessel. To determine the fraction of dead volume, we must first calculate the actual mean residence time of liquid in the reactor from the following statistical definition:

$$\tau_{\text{mean}} = \frac{\text{actual mean residence time}}{\text{calculated mean residence time}(= V/\dot{v})} = \frac{t_{\text{mean}}}{t_{\text{ave}}}. \tag{20.4.3}$$

It is obvious that the actual mean residence time will differ from the calculated dimensionless mean (i.e., reactor volume/volumetric flow rate) only in the presence of dead volume regions. It can be readily shown that the following relationship applies:

$$\frac{V_d}{V} = 1 - \tau_{\text{mean}}, \tag{20.4.4}$$

where V_d is the volume of the dead volume region in the vessel. Equation (20.4.4) shows that in the absence of dead volume ($V_d = 0$),

$$t_{\text{mean}} = t_{\text{ave}}.$$

From the values of the plug flow volume (see (20.4.1)) and the dead volume region (see (20.4.4)), we can calculate the volume of the back-mixed region from the equation

$$V_p + V_m + V_d = V\,, \tag{20.4.5}$$

which states that the sum of the plug flow, dead volume, and backed-mix volumes must be equal to the total volume of fluid in the vessel.

The back-mix flow volume may also be determined from the value of the maximum concentration, which, as shown in (20.4.2) is greater than unity. The lesser the degree of mixing in the vessel, the higher will be the value of the peak concentration. The following relationship applies for a mixed model:

$$C_{\max} = \frac{V}{V_m}. \tag{20.4.6}$$

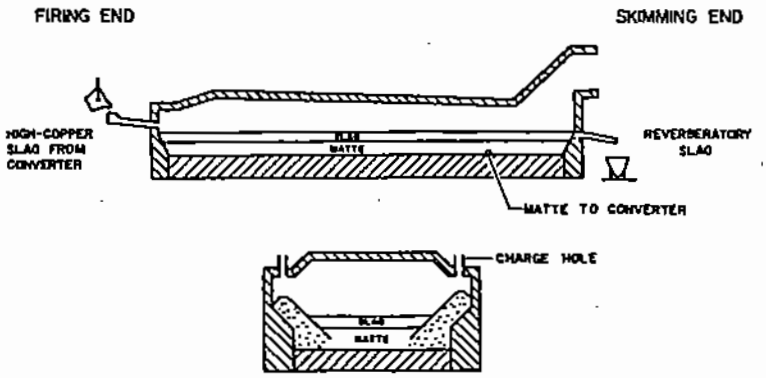

Figure 20.24. Schematic diagram of a reverberatory furnace; converter slag is charged at the left end and "clean" slag is tapped at the other end.

A "reliability" test for a mixed model is to compute the value of V_m from (20.4.6) and see whether it matches the value obtained by difference from the computed V_p and V_d values (see (20.4.5)). The use of the mixed model is illustrated in the following example.

Example 20.4.1. Flow in a Copper Reverberatory Smelting Furnace

Copper concentrates are smelted in a reverberatory furnace to form two liquids phases, a sulfide matte and an iron silicate slag (Fig. 20.24). The matte is tapped and subsequently converted to metallic copper in a converter, while the reverberatory slag is skimmed and discarded. Molten slag from the converting operation is returned intermittently to the reverberatory furnace in order to recover most of its copper content.

In an investigation of methods for decreasing the copper losses in slag, a small amount of radioactive copper was introduced in a ladle of converter slag, before pouring the slag into the reverberatory furnace. Slag samples were then obtained from the skimmed slag and analyzed for radioactivity. The results are shown in the form of a dimensionless C-diagram shown earlier in Fig. 20.23. We wish to represent the flow in the furnace by means of the mixed model and calculate the values of the plug flow, perfect mixing, and dead volume regions. The calculated average residence time of the slag in the furnace is 30 hours.

We start by using (20.4.3) to calculate the actual mean residence time of slag in the furnace:

$$\tau_{\text{mean}} = \frac{C_1\tau_1 + C_2\tau_2 + C_3\tau_3 + \dots}{C_1 + C_2 + C_3 \dots} = 0.14,$$

where C_1 is the dimensionless concentration in the exit stream at time τ_1, and so forth, as obtained from the C-diagram of Fig. 20.23. Therefore, from (20.4.4) we have

$$\frac{V_d}{V} = 1 - 0.14 = 0.86.$$

Also, from (20.4.1) and Fig. 20.23, we obtain

$$\frac{V_p}{V} = \tau_p = 0.035.$$

Finally, (20.4.5) yields the backmix flow volume in the furnace:

$$\frac{V_m}{V} = 1 - \frac{V_p}{V} - \frac{V_d}{V} = 1 - 0.035 - 0.86 = 0.105.$$

The reliability of the model may be checked by also evaluating V_m/V by the alternative method of using the value of the peak concentration (see (20.4.6)):

$$\frac{V}{V_m} = C_{\max} = 9.3 \quad \therefore \quad \frac{V_m}{V} = 0.108,$$

which is in good agreement with the previous value of 0.105.

REFERENCES

1. O. Levenspiel, *Chemical Reaction Engineering*, 2nd ed., Wiley, New York (1972).
2. G.F. Froment and K.B. Bischoff, *Chemical Reactor Analysis and Design*, Wiley, New York (1979).
3. H.S. Fogler, *Elements of Chemical Reaction Engineering*, 2nd ed., Prentice Hall, Englewood Cliffs (1992).
4. J. Szekely, *J. Iron Steel Inst.*; **202**, 505 (1964)
5. F.L. Bishop, *Am. Ceram. Soc. Bull.*, **29**, 99 (1951).
6. N.J. Themelis and G.M. Freeman, *J. Metals*, 52–57, (August 1984).
7. P.H. Jennings, N.J. Themelis, and E.S. Stratigakos, *Can. Metall. Quart.*, **8**, 281 (1969).

APPENDIX A

Table A1. Conversion of Various Units of Measurement to SI Units (Adapted from ASTM Standard for Metric Practice, Publ. E380-86)

To convert from:	to:	multiply by:
Acceleration		
ft s^{-2}	m s^{-2}	3.048×10^{-1}
Angle		
degree	radian	1.745×10^{-2}
Area		
cm^2	m^2	1.000×10^{-4}
hectare	m^2	1.000×10^{4}
acre	m^2	4.047×10^{3}
ft^2	m^2	9.290×10^{-2}
Density or Concentration		
g cm^{-3}	kg m^{-3}	1.000×10^{3}
lb ft^{-3}	kg m^{-3}	1.602×10^{1}
Diffusivity (mass, momentum, thermal)		
cm^2 s^{-1}	m^2 s^{-1}	1.000×10^{-4}
ft^2 h^{-1}	m^2 s^{-1}	2.581×10^{-5}
Electricity		
Faraday	C (Coulomb)	9.649×10^{4}
Energy (work)		
Newton meter	J (Joule)	1.000
calorie	J	4.187
erg, g cm^2 s^{-2}	J	1.000×10^{-7}
British thermal unit	J	1.055×10^{3}
ft lb force	J	1.356
ft poundal	J	4.214×10^{-2}
Energy Flux		
cal s^{-1} cm^{-2}	W m^{-2}	4.187×10^{4}
BTU h^{-1} ft^{-2}	W m^{-2}	3.155
Force		
g force	g cm s^{-2}	9.807×10^{2}
kg m s^{-2}	N (Newton)	1.000
kg force	N	9.807
dyne, g cm s^{-2}	N	1.000×10^{-5}
lb force	N	4.448
poundal	N	1.383×10^{-1}

cont'd

Heat Capacity		
cal g^{-1} °C^{-1}	J kg^{-1} K^{-1}	4.187×10^3
BTU lb^{-1} °F^{-1}	J kg^{-1} K^{-1}	4.187×10^3
Heat Conductivity		
cal s^{-1} cm^{-1} °C^{-1}	W m^{-1} K^{-1}	4.187×10^2
BTU h^{-1} ft^{-1} °F^{-1}	W m^{-1} K^{-1}	1.731
Length		
angstrom (Å)	m	1.000×10^{-10}
micron	m	1.000×10^{-6}
centimeter	m	1.000×10^{-2}
foot	m	3.048×10^{-1}
inch	m	2.540×10^{-2}
mil	m	2.540×10^{-5}
mile (US)	m	1.609×10^3
yard	m	9.144×10^{-1}
Mass		
g	kg	1.000×10^{-3}
gram mole	kilomole	1.000×10^{-3}
ounce (avoirdupois)	kg	2.835×10^{-2}
ounce (troy)	kg	3.110×10^{-2}
pound	kg	4.536×10^{-1}
ton (metric)	kg	1.000×10^3
ton (US)	kg	9.072×10^2
ton (long, 2240 lb)	kg	1.016×10^3
Mass Flow Rate (mass/unit time)		
lb h^{-1}	kg s^{-1}	1.260×10^{-4}
ton h^{-1} (metric)	kg s^{-1}	2.778×10^{-1}
ton h^{-1} (US)	kg s^{-1}	2.520×10^{-1}
Power		
Joule s^{-1}	W	1.000
volt ampere	W	1.000
cal s^{-1}	W	4.187
kilocalorie s^{-1}	W	4.187×10^3
BTU h^{-1}	W	2.931×10^{-1}
horsepower (550 ft lb force s^{-1})	W	7.457×10^2
Pressure or Shear Stress		
Newton m^{-2}	Pa (Pascal)	1.000
bar	Pa	1.000×10^5
atmosphere, standard	Pa	1.013×10^5
cm of mercury, 0°C	Pa	1.333×10^3
cm of water, 4°C	Pa	9.806×10^1
lb force ft^{-2}	Pa	4.788×10^1
lb force in^{-2}	Pa	6.895×10^3

cont'd

Temperature		
degree Celsius	K	$T_K = T_C + 273.15$
degree Fahrenheit	C	$T_C = (T_F - 32)/1.8$
degree Fahrenheit	K	$T_K = (T_F + 459.67)/1.8$
degree Rankin	K	$T_K = T_R/1.8$
Torque		
dyne cm	N m	1.000×10^{-7}
Velocity		
ft s^{-1}	m s^{-1}	3.048×10^{-1}
km h^{-1}	m s^{-1}	2.778×10^{-1}
miles h^{-1}	m s^{-1}	4.470×10^{-1}
Viscosity		
centipoise	Pa s	1.000×10^{-3}
centistokes	m^2 s^{-1}	1.000×10^{-6}
poise	Pa s	1.000×10^{-1}
lb ft^{-1} h^{-1}	Pa s	4.134×10^{-4}
Stokes	m^2 s^{-1}	1.000×10^{-4}
Volume		
cm^3	m^3	1.000×10^{-6}
liter	m^3	1.000×10^{-3}
barrel (42 gallons)	m^3	1.590×10^{-1}
ft^3	m^3	2.832×10^{-2}
gallon	m^3	3.785×10^{-3}
ounce	m^3	2.957×10^{-5}
quart	m^3	9.464×10^{-4}

Table A2. Important Physical Constants

Quantity	Symbol	Value	Units
Universal gas constant	R	1.987	cal mol^{-1} K^{-1}
		8.314×10^3	J $kmol^{-1}$ K^{-1}
		8.205×10^1	cm^3 atm mol^{-1} K^{-1}
		1.545×10^3	ft lb_f lb–mol^{-1} R^{-1}
Standard acceleration due to gravity	g	9.807×10^2	cm s^{-2}
		9.807	m s^{-2}
		3.217×10^1	ft s^{-2}
Avogadro's number	N_A	6.023×10^{23}	molecules mol^{-1}
Boltzmann's constant	k	1.381×10^{-23}	J K^{-1}
Planck's constant	h	6.625×10^{-34}	J s
Stefan-Boltzmann radiation constant	σ	5.73×10^{-8}	W m^{-2} K^{-4}
		1.37×10^{-12}	cal s^{-1} cm^{-2} K^{-4}
		0.173×10^{-8}	BTU h^{-1} ft^{-2} R^{-4}
Velocity of light	c	2.998×10^{10}	cm s^{-1}
		2.998×10^8	m s^{-1}
Melting point of H_2O	T_{mp}	273.15	K
Ideal gas volume of 1 kmol at 1 atm, 273.15 K		22.4	m^3
Faraday constant	F	9.649×10^4	Coulomb (mol equiv)$^{-1}$

NOMENCLATURE

a: chemical activity of a species (Chapter 18), —
a_v: specific surface area per unit volume of reaction system, L^{-1}
A: area (surface, interface, cross-section), L^2
A_c: cross-sectional area of conduit, L^2
A_p: cross-sectional area of particle, L^2
A_r: surface or interface area available for reaction, L^2
Bi: Biot number (Table 2.1), —
c: velocity of light, Lt^{-1}
$\tilde{c}$: dimensionless concentration, —
c: molar concentration (density) of fluid, ML^{-3}
c_A: molar concentration of species A, ML^{-3}
$c_{A,b}$, $c_{A,s}$, $c_{A,e}$: bulk, surface and equilibrium concentrations of species A, ML^{-3}
$\overline{c}_{A,x}$: average concentration of species A across film at location x, ML^{-3}
$c_{A,LM}$: logarithmic mean concentration of species A, ML^{-3}
C_d: dimensionless drag coefficient, —
C_p, C_v: specific heat at constant pressure and volume, respectively, $QM^{-1}T^{-1}$
C_p: molar heat capacity (Chapter 18), $QM^{-1}T^{-1}$
C_o, C_v: orifice, venturi coefficients (Chapter 8), —
d_b: bubble diameter, L
d_h: hydraulic mean diameter (Chapter 8), L
d_j: jet diameter, L
d_o, d_i: outside and inside diameters of pipe, L
d_p: pipe diameter, particle diameter, L
D_e: eddy diffusivity, L^2t^{-1}
D_{eff}: effective diffusivity of species A, L^2t^{-1}
$D_{k,\text{eff}}$: effective Knudsen diffusivity, L^2t^{-1}
D_{AB}: diffusivity of species A in species B, L^2t^{-1}
Df/Dt: substantial time derivative of function f (Chapter 5)
e: roughness of surface (Table 8.1), L
E_a: activation energy (or temperature coefficient) of reaction, QM^{-1}
E_d: temperature coefficient for diffusivity, QM^{-1}
E_μ: temperature coefficient for fluidity (1/viscosity), QM^{-1}
f', f'': first and second differentials of function f
f_{fr}: friction factor, —

F, F_x, F_y, F_z: force vector and its components, MLt^{-2}
F_d, F_{fr}: drag force, frictional force, MLt^{-2}
F_g: gravity force, MLt^{-2}
F_{kj}: geometric view factor between two surfaces A_k and A_j in an enclosure (Chapter 13), —
F: Faraday number (Table A2)
F: dimensionless concentration (Chapter 20), —
Fo: Fourier number (Table 2.1), —
g, g_x, g_y, g_z: acceleration due to gravity vector and its components, Lt^{-2}
G: mass flux of fluid ($=\rho u$), $ML^{-2}t^{-1}$
G: Gibbs free energy (Chapter 18), QM^{-1}
Gr: Grashof number (Table 2.1), —
Gr′: concentration Grashof number (Table 2.1), —
h: heat transfer coefficient, $QL^{-2}t^{-1}T^{-1}$
h_{ov}: overall heat transfer coefficient, $QL^{-2}t^{-1}T^{-1}$
h_{pg}: heat transfer coefficient between particle and gas, $QL^{-2}t^{-1}T^{-1}$
h: Planck's constant (Table A2, Chapter 13)
H: height of liquid level, height of vessel, L
i, j, k: unit vectors in the x, y, and z directions, respectively (Chapter 6), —
j_d: mass transfer factor (Chapter 17), Lt^{-1}
k: turbulent energy per unit mass of fluid (Chapter 7), L^2t^{-2}
k: thermal conductivity of a material, $QL^{-1}t^{-1}T^{-1}$
k: Boltzmann's constant (Table A2, Chapter 13)
$k-\varepsilon$: turbulence model (Chapter 7)
k_c, k_e: friction loss coefficient for contraction or expansion (Chapter 8), —
k_d: mass transfer coefficient, Lt^{-1}
$k_{d,s}$, $k_{d,m}$: mass transfer coefficients through phases s and m, Lt^{-1}
k_{diff}: combined diffusion coefficient (Chapter 19), Lt^{-1}
$k_{d,x}$: local mass transfer coefficient at location x, Lt^{-1}
k_{ov}: overall rate coefficient, Lt^{-1}
k_r: chemical rate coefficient, heterogeneous reaction, Lt^{-1}
k_r: chemical rate coefficient, homogeneous reaction, t^{-1}
k_r': volumetric rate coefficient, quasi-homogeneous reaction, t^{-1}
$k_{r,o}$: chemical rate coefficient at reference temperature T_0, Lt^{-1}
$k_{r,T}$: chemical rate coefficient at temperature T, Lt^{-1}
K_e: equilibrium constant, —
K_e: distribution coefficient between two phases (Chapter 15), —
K_v: viscosity modulus (Chapter 3), —
l_m: mixing length (Chapter 7), L
L: characteristic length of flow system (Chapter 7), L
L: distance between two points, length of vessel, L

$\dot{m}$: mass flow rate, Mt^{-1}
m_{tr}: mass of tracer injected (Chapter 20), M
M: molecular weight, M
Ma: Mach number (Table 2.1), —
M_i: molecular weight of species i, M
n: order of chemical reaction (Chapter 18), —
n_b: number of bubbles in the bath (Chapter 18), —
n_p: number of particles per unit volume of cloud (Chapter 13), L^{-3}
n_A: number of moles of species A, M
$\dot{n}_A$: number of moles of species A per unit time, Mt^{-1}
N_A, N_B: molar flux of diffusing species A and B, $\mathrm{ML}^{-2}\mathrm{t}^{-1}$
$N_{A,\mathrm{ave}}$: average value of molar flux of A, $\mathrm{ML}^{-2}\mathrm{t}^{-1}$
$N_{i,\mathrm{max}}$: maximum molar flux of species i, $\mathrm{ML}^{-2}\mathrm{t}^{-1}$
N_A^*: molar flux by diffusion and net bulk flow, $\mathrm{ML}^{-2}\mathrm{t}^{-1}$
N'_A: mass flux of species A, $\mathrm{ML}^{-2}\mathrm{t}^{-1}$
$N'_{A,x}$: mass flux of species A in the x direction, $\mathrm{ML}^{-2}\mathrm{t}^{-1}$
Nu: Nusselt number (Table 2.1), —
Nu_x: average value of Nu at distance x from leading edge, —
$\overline{\mathrm{Nu}}$: average value of Nusselt number over a surface, —
p_i : partial pressure of species i, $\mathrm{ML}^{-1}\mathrm{t}^{-2}$
p_0: standard pressure of species i (Chapter 18), $\mathrm{ML}^{-1}\mathrm{t}^{-2}$
P: pressure, $\mathrm{ML}^{-1}\mathrm{t}^{-2}$
P': fluctuating component of pressure, $\mathrm{ML}^{-1}\mathrm{t}^{-2}$
$\overline{P}$: time-averaged pressure, $\mathrm{ML}^{-1}\mathrm{t}^{-2}$
P_c: critical pressure (Chapter 3), $\mathrm{ML}^{-1}\mathrm{t}^{-2}$
Pe: Peclet number (Table 2.1), —
Pr: Prandtl number (Table 2.1), —
q_x: heat flux in direction x, $\mathrm{QL}^{-2}\mathrm{t}^{-1}$
q_{cond}, q_{conv}, q_{rad}: heat flux by conduction, convection, radiation, $\mathrm{QL}^{-2}\mathrm{t}^{-1}$
$q_{i,\lambda}$: monochromatic radiant energy flux (Chapter 13), $\mathrm{QL}^{-2}\mathrm{t}^{-1}$
$q_{k,i}$: incident radiation on surface A_k (Chapter 13), $\mathrm{QL}^{-2}\mathrm{t}^{-1}$
$q_{k,o}$: radiosity of surface k (Chapter 13), $\mathrm{QL}^{-2}\mathrm{t}^{-1}$
$\dot{q}$: rate of heat generation per unit volume of the material, $\mathrm{QL}^{-3}\mathrm{t}^{-1}$
Q: rate of heat transfer, Qt^{-1}
r: distance from center of cylinder, sphere, L
r_b: outer radius of boundary layer around sphere (Chapter 12), L
r_i, r_o: inner and outer radius of hollow cylinder, sphere, L
r_p: radius of pipe, spherical particle, L
$\dot{r}_A$: rate of homogeneous reaction of species A, $\mathrm{ML}^{-3}\mathrm{t}^{-1}$
R: universal gas constant (Table A2), $\mathrm{QM}^{-1}\mathrm{T}^{-1}$

Re: Reynolds number, —
Re_p: particle Reynolds number, —
Re_x: Reynolds number at distance x from entry point, —
R_m: ratio of mass of gas entrained to mass of cylinder (Chapter 6), —
R_x: fractional degree of reaction, —
S: entropy, $\mathrm{QM^{-1}T^{-1}}$
Sc: Schmidt number (Table 2.1), —
Sh: Sherwood number (Table 2.1), —
Sh_x: local Sherwood number at distance x from leading edge, —
t: time, t
t_{ave}: mean residence time of fluid in vessel (Chapter 20), t
t_e: time interval, t
t_f: time for complete reaction, t
T: temperature, T
T_a: temperature of atmosphere, T
T_b: bulk temperature of fluid, T
T_s: surface temperature, T
T_c: critical temperature (Chapter 3), T
T_{film}: mean film temperature, T
T_i: initial temperature, T
T_0, T_Y: temperature at $y = 0$ and $y = Y$, respectively, T
T_0: reference temperature, T
T_{trans}: temperature of transformation phenomenon (Chapter 18), T
T_w: temperature of wall, T
$\boldsymbol{u}$, u_x, u_y, u_z: velocity vector and its components, $\mathrm{Lt^{-1}}$
u_{ave}: average flow velocity, $\mathrm{Lt^{-1}}$
u_b: bulk or "free stream" velocity of fluid, $\mathrm{Lt^{-1}}$
u_b: bubble velocity (Chapter 17), $\mathrm{Lt^{-1}}$
u_{max}: maximum fluid velocity, $\mathrm{Lt^{-1}}$
u_o: superficial velocity of fluid through vessel, $\mathrm{Lt^{-1}}$
u_p: relative velocity between particle and bulk velocity of fluid (Chapter 8), $\mathrm{Lt^{-1}}$
u_r: i.e., peripheral velocity (Chapter 17), radial velocity, $\mathrm{Lt^{-1}}$
u_s: velocity of sound in the fluid, $\mathrm{Lt^{-1}}$
u_t: terminal velocity of bubble or particle (Chapter 8), $\mathrm{Lt^{-1}}$
u^*: velocity due to net bulk flow, $\mathrm{Lt^{-1}}$
$\overline{u}$: average velocity of fluid, $\mathrm{Lt^{-1}}$
u'_x: fluctuating component of velocity, $\mathrm{Lt^{-1}}$
u_θ: tangential velocity, $\mathrm{Lt^{-1}}$
$\dot{v}$: volumetric flow rate, $\mathrm{L^3t^{-1}}$
$V = 1/\rho$: specific volume of the gas (Chapter 9), $\mathrm{L^3\,M^{-1}}$

V: volume, L^3
V_d: dead flow volume (Chapter 20), L^3
V_m: backmix flow volume (Chapter 20), L^3
V_p: plug flow volume (Chapter 20), L^3
V_r: reactor volume, L^3
V_A, V_B: diffusion volumes of molecules A and B (Chapter 14), L^3M^{-1}
W: width of plate, vessel, L
W_{fr}: work done by fluid to overcome friction, ML^2t^{-2}
W_m: mechanical work done by fluid, ML^2t^{-2}
W'_{fr}: work done to overcome friction per unit mass of fluid, L^2t^{-2}
$W'_{fr,c}$: contraction energy loss per unit mass of fluid, L^2t^{-2}
$W'_{fr,e}$: expansion energy loss per unit mass of fluid, L^2t^{-2}
W'_m: mechanical work done per unit mass of fluid, L^2t^{-2}
W_B: radiant energy flux (Chapter 13), $QL^{-2}t^{-1}$
$W'_{B,\lambda}$: monochromatic emissive power of black body (Chapter 13), $QL^{-3}t^{-1}$
W'_λ: monochromatic emissive power of non-black body (Chapter 13), $QL^{-3}t^{-1}$
x: distance from origin in x direction, L
X_A: mole fraction of species A in a mixture, —
$X_{A,0}$, $X_{A,L}$: mole fraction of species A at location $y = 0$, $y = L$, —
$X_{A,b}$, $X_{A,s}$: mole fraction of A in bulk fluid and at surface, —
$X_{A,LM}$: logarithmic mean concentration of species A, —
X'_A: mass fraction of species A, —
y: distance from origin in direction y, L
Y: thickness of plate or wall, L
z: distance from origin in direction z, L
Z, Z_0, Z_1: liquid depth, initial depth, depth at level I, L

Greek Symbols

$\alpha = k/\rho C_p$: thermal diffusivity of conducting medium, L^2t^{-1}
α: gas fraction in "plume" rising above point of injection (Chapter 7), —
α: total absorptivity (Chapter 13), —
α_λ: monochromatic absorptivity (Chapter 13), —
$\alpha_{g,s}$: effective absorptivity of gas (Chapter 13), —
β: dimensionless length (Chapter 11), —
β: volume coefficient of thermal expansion, T^{-1}
β': coefficient of density change of fluid with concentration, —
$\gamma = C_p/C_v$: ratio of heat capacity of gas at constant pressure to that at constant volume (Chapter 9), —
γ: activity coefficient in non-ideal solution (Chapter 18), —

δ: boundary layer thickness, L

δ_x: boundary layer thickness at location x, L

δ^*: displacement thickness of boundary layer, L

$(\Delta c)_{LM}$: logarithmic mean molar concentration difference, ML^{-3}

Δx: finite element of distance, L

$\Delta G_{i,a}$, ΔG_i^o, $\Delta G_{i,\text{rel}}$: actual, equilibrium, and relative Gibbs free energies of species i, QM^{-1}

ΔG_i^o: Gibbs free energy of chemical species i at equilibrium at temperature T and standard pressure p_0 (Chapter 18), QM^{-1}

ΔH_d^o: heat of decomposition reaction at equilibrium, QM^{-1}

ΔH_f^o: heat of formation of compound at equilibrium, QM^{-1}

ΔH_i^o: total enthalpy of the species at equilibrium, QM^{-1}

ΔH_{rx}: heat of reaction, QM^{-1}

ΔH_{trans}: heat of transformation, QM^{-1}

ΔP: finite pressure difference, $ML^{-1}t^{-2}$

$\Delta S_{i,T}$, $\Delta S_{i,o}^o$: total entropy of species i at its equilibrium state at T and at reference temperature T_0, $QM^{-1}T^{-1}$

ΔT: finite temperature difference, T

$(\Delta T)_{LM}$: logarithmic mean temperature difference, T

ΔY: finite element of thickness, L

$\Delta\varepsilon$: emissivity correction factor for mixture of gases, —

$\Delta\tau$: finite difference of dimensionless time, —

ε: energy parameter for interaction between molecules (Chapter 3), $ML^2t^{-2}\text{molecule}^{-1}$

ε: rate of dissipation of turbulent energy (Chapter 7), L^2t^{-3}

ε: total emissivity, —

ε: porosity of solid body (Chapter 14), —

ε_c: emissivity of cloud of particles, —

ε_g: effective emissivity of gas, —

ε_p, ε_s: emissivity of particle, surface, —

ε_λ: monochromatic emissivity (Chapter 7), —

ε_s': effective emissivity of solid, —

θ: angle from reference plane on sphere or cylinder, in radians

θ: dimensionless temperature (Chapter 11), —

θ_m: dimensionless temperature at grid point m (Chapter 11), —

θ_m^*: dimensionless temperature at m after time interval $\Delta\tau$ (Chapter 11), T

λ: wavelength, L

$\lambda_{\max}$: wavelength of maximum emission at temperature T, L

μ: molecular viscosity, $ML^{-1}t^{-1}$

μ_e: eddy viscosity, $ML^{-1}t^{-1}$

μ_{mix}: viscosity of gas mixture, $ML^{-1}t^{-1}$

μ_o: viscosity at reference temperature T_o, $ML^{-1}t^{-1}$

μ_t: turbulent viscosity, $ML^{-1}t^{-1}$
ν: momentum diffusivity or kinematic viscosity, L^2t^{-1}
ν_t: turbulent momentum diffusivity, L^2t^{-1}
$\widetilde{\nu}$: frequency of propagation (Chapter 13), t^{-1}
ρ: density of the fluid, ML^{-3}
ρ_b, ρ_s: density of fluid in bulk fluid and at surface, ML^{-3}
ρ_g: density of gas, ML^{-3}
ρ_o: density of fluid at reference temperature T_o, ML^{-3}
ρ_k: reflectivity of surface k (Chapter 13), —
ρ_λ: monochromatic reflectivity of surface (Chapter 13), —
σ: Stefan–Boltzmann radiation constant (Table A2, Chapter 13), $QL^{-2}t^{-1}T^{-4}$
σ^2: statistical variance, —
σ_c: collision diameter (Chapter 3), L
τ: dimensionless time (Chapter 11), —
τ: tortuosity (Chapter 14), —
τ_o: shear stress at wall of conduit, $ML^{-1}t^{-2}$
$\tau_{y,x}$: shear stress at plane y due to flow in direction x, $ML^{-1}t^{-2}$
$\tau'_{y,x}$: turbulent component of shear stress $\tau_{y,x}$, $ML^{-1}t^{-2}$
τ_λ: transmittance at wavelength λ (Chapter 13), —
ϕ: angle from reference plane, degrees
$\phi(x, y, z)$: velocity potential (Chapter 6), L^2t^{-1}
ψ: stream function (Chapter 6), L^2t^{-1}
Ω: degree of rotation of fluid element (Chapter 6), t^{-1}
Ω_μ: collision integral (Chapter 3), —
ω_x, ω_y, ω_z: angular velocity about the x, y, and z axes, t^{-1}

INDEX

D

E

F

G

H

N

O

P

R

S

T

U

V

W

Z